THE EUROPEAN
PHYSICAL JOURNAL C

Review

B, *D* and *K* decays[*]

G. Buchalla[17,b], T.K. Komatsubara[43,b], F. Muheim[55,a,b], L. Silvestrini[4,b], M. Artuso[1], D.M. Asner[2], P. Ball[3], E. Baracchini[4], G. Bell[5], M. Beneke[6], J. Berryhill[7], A. Bevan[8], I.I. Bigi[9], M. Blanke[10,19], Ch. Bobeth[11], M. Bona[12], F. Borzumati[13,14], T. Browder[15], T. Buanes[16], O. Buchmüller[18], A.J. Buras[19], S. Burdin[20], D.G. Cassel[21], R. Cavanaugh[22], M. Ciuchini[23], P. Colangelo[24], G. Crosetti[25], A. Dedes[3], F. De Fazio[24], S. Descotes-Genon[26], J. Dickens[27], Z. Doležal[28], S. Dürr[29], U. Egede[30], C. Eggel[31,32], G. Eigen[16], S. Fajfer[33], Th. Feldmann[34], R. Ferrandes[24], P. Gambino[35], T. Gershon[36], V. Gibson[27], M. Giorgi[37], V.V. Gligorov[38], B. Golob[39], A. Golutvin[18,40], Y. Grossman[41], D. Guadagnoli[19], U. Haisch[42], M. Hazumi[43], S. Heinemeyer[44], G. Hiller[11], D. Hitlin[45], T. Huber[6], T. Hurth[18,46], T. Iijima[47], A. Ishikawa[48], G. Isidori[49,50], S. Jäger[18], A. Khodjamirian[34], P. Koppenburg[30], T. Lagouri[28], U. Langenegger[31], C. Lazzeroni[27], A. Lenz[51], V. Lubicz[23], W. Lucha[52], H. Mahlke[21], D. Melikhov[53], F. Mescia[50], M. Misiak[54], M. Nakao[43], J. Napolitano[56], N. Nikitin[57], U. Nierste[5], K. Oide[43], Y. Okada[43], P. Paradisi[19], F. Parodi[58], M. Patel[18], A.A. Petrov[59], T.N. Pham[60], M. Pierini[18], S. Playfer[55], G. Polesello[61], A. Policicchio[25], A. Poschenrieder[19], P. Raimondi[50], S. Recksiegel[19], P. Řezníček[28], A. Robert[62], J.L. Rosner[63], G. Ruggiero[18], A. Sarti[50], O. Schneider[64], F. Schwab[65], S. Simula[23], S. Sivoklokov[57], P. Slavich[18,66], C. Smith[67], M. Smizanska[68], A. Soni[69], T. Speer[42], P. Spradlin[38], M. Spranger[19], A. Starodumov[31], B. Stech[70], A. Stocchi[71], S. Stone[1], C. Tarantino[23], F. Teubert[18], S. T'Jampens[12], K. Toms[57], K. Trabelsi[43], S. Trine[5], S. Uhlig[19], V. Vagnoni[72], J.J. van Hunen[64], G. Weiglein[3], A. Weiler[21], G. Wilkinson[38], Y. Xie[55], M. Yamauchi[43], G. Zhu[73], J. Zupan[33], R. Zwicky[3]

[1]Syracuse University, Syracuse, NY, USA
[2]Carleton University, Ottawa, Canada
[3]Durham University, IPPP, Durham, UK
[4]Università di Roma La Sapienza and INFN, Rome, Italy
[5]Universität Karlsruhe, Karlsruhe, Germany
[6]RWTH Aachen, Aachen, Germany
[7]Fermi National Accelerator Laboratory, Batavia, IL, USA
[8]Queen Mary, University of London, London, UK
[9]University of Notre Dame, Notre Dame, IN, USA
[10]Max-Planck-Institut für Physik, München, Germany
[11]Institut für Physik, Universität Dortmund, Dortmund, Germany
[12]LAPP, Université de Savoie, IN2P3-CNRS, Annecy-le-Vieux, France
[13]ICTP, Trieste, Italy
[14]National Central University, Chung-li, Taiwan
[15]University of Hawaii at Manoa, Honolulu, HI, USA
[16]University of Bergen, Bergen, Norway
[17]Ludwig-Maximilians-Universität München, München, Germany
[18]CERN, Geneva, Switzerland
[19]Technische Universität München, Garching, Germany
[20]The University of Liverpool, Liverpool, UK
[21]Cornell University, Ithaca, NY, USA
[22]University of Florida, Gainesville, FL, USA
[23]Università di Roma Tre and INFN, Rome, Italy
[24]INFN, Bari, Italy
[25]Università di Calabria and INFN Cosenza, Cosenza, Italy
[26]LPT, CNRS/Université de Paris-Sud 11, Orsay, France
[27]University of Cambridge, Cambridge, UK
[28]IPNP, Charles University in Prague, Prague, Czech Republic
[29]NIC, FZ Jülich and DESY Zeuthen, Jülich, Germany
[30]Imperial College, London, UK
[31]ETH, Zürich, Switzerland
[32]PSI, Villigen, Switzerland
[33]Ljubljana University and Jozef Stefan Institute, Ljubljana, Slovenia
[34]Universität Siegen, Siegen, Germany
[35]Università di Torino and INFN, Torino, Italy
[36]University of Warwick, Coventry, UK

[37]Università di Pisa, SNS and INFN, Pisa, Italy
[38]University of Oxford, Oxford, UK
[39]University of Ljubljana, Ljubljana, Slovenia
[40]ITEP, Moscow, Russia
[41]Technion, Haifa, Israel
[42]Universität Zürich, Zürich, Switzerland
[43]KEK and Graduate University for Advanced Studies (Sokendai), Tsukuba, Japan
[44]IFCA, Santander, Spain
[45]CalTech, Pasadena, CA, USA
[46]SLAC, Stanford, CA, USA
[47]Nagoya University, Nagoya, Japan
[48]Saga University, Saga, Japan
[49]SNS and INFN, Pisa, Italy
[50]INFN, LNF, Frascati, Italy
[51]Universität Regensburg, Regensburg, Germany
[52]Institut für Hochenergiephysik, Österreichische Akademie der Wissenschaften, Wien, Austria
[53]Nuclear Physics Institute, Moscow State University, Moscow, Russia
[54]Warsaw University, Warsaw, Poland
[55]University of Edinburgh, Edinburgh, UK
[56]Rensselaer Polytechnic Institute, Troy, NY, USA
[57]Skobeltsin Institute of Nuclear Physics, Lomonosov Moscow State University, Moscow, Russia
[58]Università di Genova and INFN, Genova, Italy
[59]Wayne State University, Detroit, MI, USA
[60]Ecole Polytechnique, CNRS, Palaiseau, France
[61]Università di Pavia and INFN, Pavia, Italy
[62]Université de Clermont-Ferrand, Clermont-Ferrand, France
[63]Enrico Fermi Institute, University of Chicago, Chicago, IL, USA
[64]Ecole Polytechnique Fédérale de Lausanne (EPFL), Lausanne, Switzerland
[65]Universitat Autonoma de Barcelona, IFAE, Barcelona, Spain
[66]LAPTH, Annecy-le-Vieux, France
[67]Universität Bern, Bern, Switzerland
[68]Lancaster University, Lancaster, UK
[69]Brookhaven National Laboratory, Upton, NY, USA
[70]Universität Heidelberg, Heidelberg, Germany
[71]LAL, IN2P3-CNRS and Université de Paris-Sud, Orsay, France
[72]Università di Bologna and INFN, Bologna, Italy
[73]Universität Hamburg, Hamburg, Germany

Abstract The present report documents the results of Working Group 2: B, D and K decays, of the workshop on Flavor in the Era of the LHC, held at CERN from November 2005 through March 2007.

With the advent of the LHC, we will be able to probe New Physics (NP) up to energy scales almost one order of magnitude larger than it has been possible with present accelerator facilities. While direct detection of new particles will be the main avenue to establish the presence of NP at the LHC, indirect searches will provide precious complementary information, since most probably it will not be possible to measure the full spectrum of new particles and their couplings through direct production. In particular, precision measurements and computations in the realm of flavor physics are expected to play a key role in constraining the unknown parameters of the Lagrangian of any NP model emerging from direct searches at the LHC.

The aim of Working Group 2 was twofold: on the one hand, to provide a coherent up-to-date picture of the status of flavor physics before the start of the LHC; on the other hand, to initiate activities on the path towards integrating information on NP from high-p_T and flavor data.

This report is organized as follows: in Sect. 1, we give an overview of NP models, focusing on a few examples that have been discussed in some detail during the workshop, with a short description of the available computational tools for flavor observables in NP models. Section 2 contains a concise discussion of the main theoretical problem in flavor physics: the evaluation of the relevant hadronic matrix elements for weak decays. Section 3 contains a detailed discussion of NP effects in a set of flavor observables that we identified as "benchmark channels" for NP searches. The experimental prospects for flavor physics at future facilities are discussed in Sect. 4. Finally, Sect. 5 contains some assess-

ments on the work done at the workshop and the prospects for future developments.

Contents

[a] e-mail: f.muheim@ed.ac.uk

[b] Convenors

1 New physics scenarios[1]

1.1 Overview

The Standard Model (SM) of electroweak and strong interactions describes with an impressive accuracy all experimental data on particle physics up to energies of the order of the electroweak scale. On the other hand, we know that the SM should be viewed as an effective theory valid up to a scale $\Lambda \sim M_W$, since, among many other things, the SM does not contain a suitable candidate of dark matter and it does not account for gravitational interactions. Viewing the SM as an effective theory, however, poses a series of theoretical questions. First of all, the quadratic sensitivity of the electroweak scale on the cutoff calls for a low value of Λ, in order to avoid excessive fine tuning. Second, several of the higher-dimensional operators which appear in the SM effective Lagrangian violate the accidental symmetries of the SM. Therefore, their coefficients must be highly suppressed in order not to clash with the experimental data, in particular in the flavor sector. Unless additional suppression mechanisms are present in the fundamental theory, a cutoff around the electroweak scale is thus phenomenologically not acceptable since it generates higher-dimensional operators with large coefficients.

We are facing a formidable task: formulating a natural extension of the SM with a cutoff close to the electroweak scale and with a very strong suppression of additional sources of flavor and CP violation. While the simplest supersymmetric extensions of the SM with minimal flavor and CP violation, such as Minimal Supergravity (MSUGRA) models, seem to be the phenomenologically most viable NP options, it is fair to say that a fully consistent model of SUSY breaking has not been put forward yet. On the other hand, alternative solutions of the hierarchy problem based on extra dimensions have recently become very popular, although they have not yet been tested at the same level of accuracy as the Minimal Supersymmetric Standard Model (MSSM). Waiting for the LHC to discover new particles and shed some light on these fundamental problems, we should consider a range of NP models as wide as possible, in order to be ready to interpret the NP signals that will show up in the near future.

In the following paragraphs, we discuss how flavor and CP violation beyond the SM can be analysed on general grounds in a model-independent way. We then specialize to a few popular extensions of the SM, such as SUSY and little Higgs models, and present their most relevant aspects in view of our subsequent discussion of NP effects in flavor physics.

[1] Section coordinators: A.J. Buras, S. Heinemeyer, G. Isidori, Y. Okada, F. Parodi, L. Silvestrini.

1.2 Model-independent approaches

1.2.1 General considerations

In most extensions of the Standard Model (SM), the new degrees of freedom that modify the ultraviolet behavior of the theory appear only around or above the electroweak scale ($v \approx 174$ GeV). As long as we are interested in processes occurring below this scale (such as B, D and K decays), we can integrate out the new degrees of freedom and describe the new-physics effects—in full generality—by means of an Effective Field Theory (EFT) approach. The SM Lagrangian becomes the renormalizable part of a more general local Lagrangian which includes an infinite tower of higher-dimensional operators constructed in terms of SM fields and suppressed by inverse powers of a scale $\Lambda_{NP} > v$.

This general bottom-up approach allows us to analyse all realistic extensions of the SM in terms of a limited number of parameters (the coefficients of the higher-dimensional operators). The disadvantage of this strategy is that it does not allow us to establish correlations of New Physics (NP) effects at low and high energies (the scale Λ_{NP} defines the cut-off of the EFT). The number of correlations among different low-energy observables is also very limited, unless some restrictive assumptions about the structure of the EFT are employed.

The generic EFT approach is somehow the opposite of the standard top-down strategy towards NP, where a given theory—and a specific set of parameters—are employed to evaluate possible deviations from the SM. The top-down approach usually allows us to establish several correlations, both at low energies and between low- and high-energy observables. However, the price to pay is the loss of generality. This is quite a high price given our limited knowledge about the physics above the electroweak scale.

An interesting compromise between these two extreme strategies is obtained by implementing specific symmetry restrictions on the EFT. The extra constraints increase the number of correlations in low-energy observables. The experimental tests of such correlations allow us to test/establish general features of the NP model (possibly valid both at low and high energies). In particular, B, D and K decays are extremely useful in determining the flavor-symmetry breaking pattern of the NP model. The EFT approaches based on the Minimal Flavor Violation (MFV) hypothesis and its variations (MFV at large $\tan \beta$, n-MFV, ...) have exactly this goal.

In Sect. 1.2.2, we illustrate some of the main conclusions about NP effects in the flavor sector derived so far within general EFT approaches. In Sect. 1.2.3, we analyse in more detail the MFV hypothesis, discussing: (i) the general formulation and the general consequences of this hypothesis; (ii) the possible strategies to verify or falsify the MFV assumption from low-energy data; (iii) the implementation of the MFV hypothesis in more explicit beyond-the-SM frameworks, such as the Minimal Supersymmetric SM (MSSM) or Grand Unified Theories (GUTs).

1.2.2 Generic EFT approaches and the flavor problem

The NP contributions to the higher-dimensional operators of the EFT should naturally induce large effects in processes which are not mediated by tree-level SM amplitudes, such as meson–antimeson mixing ($\Delta F = 2$ amplitudes) or flavor-changing neutral-current (FCNC) rare decays. Up to now there is no evidence of deviations from the SM in these processes, and this implies severe bounds on the effective scale of various dimension-six operators. For instance, the good agreement between SM expectations and experimental determinations of K^0–$\bar{K}^0$ mixing leads to bounds above 10^4 TeV for the effective scale of $\Delta S = 2$ operators, i.e. well above the few TeV range suggested by a natural stabilization of the electroweak-symmetry breaking mechanism. Similar bounds are obtained for the scale of operators contributing to lepton-flavor violating (LFV) transitions in the lepton sector, such as $\mu \to e\gamma$.

The apparent contradiction between these two determinations of Λ is a manifestation of what in many specific frameworks (supersymmetry, technicolour, etc.) goes under the name of *flavor problem*: if we insist on the theoretical prejudice that new physics has to emerge in the TeV region, we have to conclude that the new theory possesses a highly nongeneric flavor structure. Interestingly enough, this structure has not been clearly identified yet, mainly because the SM (the low-energy limit of the new theory), does not possess an exact flavor symmetry. Within a model-independent approach, we should try to deduce this structure from data, using the experimental information on FCNC transitions to constrain its form.

1.2.2.1 Bounds on $\Delta F = 2$ operators   In most realistic NP models, we can safely neglect NP effects in all cases where the corresponding effective operator is generated at the tree-level within the SM. This general assumption implies that the experimental determination of γ and $|V_{ub}|$ via tree-level processes (see Fig. 1) is free from the contamination of NP contributions. The comparison of the experimental data on meson–antimeson mixing amplitudes (both magnitudes and phases) with the theoretical SM expectations (obtained by means of the tree-level determination of the CKM matrix) allows us to derive some of the most stringent constraints on NP models.

In a wide class of beyond-the-SM scenarios, we expect sizable and uncorrelated deviations from the SM in the various $\Delta F = 2$ amplitudes.[2] As discussed by several authors [2–6], in this case, NP effects can be parameterized in

---

[2]As discussed for instance in Ref. [1], there is a rather general limit where NP effects in $\Delta F = 2$ amplitudes are expected to be the dom-
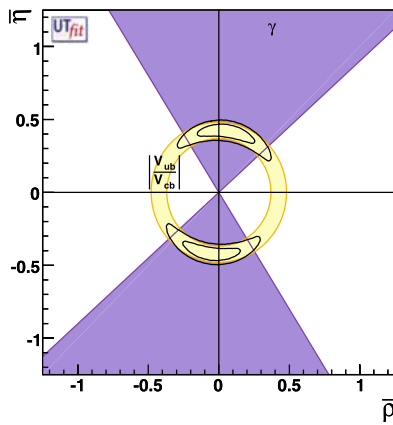
Fig. 1 Constraints on the $\bar{\rho}-\bar{\eta}$ plane using tree-level observables only, from Ref. [7] (see also Ref. [8])

terms of the shift induced in the $B_q-\bar{B}_q$ mixing frequencies ($q=d,s$) and in the corresponding CPV phases,

$$\frac{\langle B_q|H_{\text{eff}}^{\text{full}}|\bar{B}_q\rangle}{\langle B_q|H_{\text{eff}}^{\text{SM}}|\bar{B}_q\rangle} = C_{B_q}e^{2i\phi_{B_q}} = r_q^2 e^{2i\theta_q}, \qquad (1)$$

and similarly for the neutral kaon system. The two equivalent parameterizations [(C_{B_q}, ϕ_{B_q}) or (r_q, θ_q)] have been shown to facilitate the interpretation of the results of the UTfit [7] and CKMfitter [8] collaborations for the B_d case, shown in Fig. 2.

The main conclusions that can be drawn form the present analyses of new-physics effects in $\Delta F = 2$ amplitudes can be summarized as follows:

– In all the three accessible short-distance amplitudes ($K^0-\bar{K}^0$, $B_d-\bar{B}_d$ and $B_s-\bar{B}_s$), the magnitude of the new-physics amplitude cannot exceed, in size, the SM short-distance contribution. The latter is suppressed both by the GIM mechanism and by the hierarchical structure of the CKM matrix (V):

$$\mathcal{A}_{\text{SM}}^{\Delta F=2} \sim \frac{G_F^2 M_W^2}{2\pi^2}\left(V_{ti}^* V_{tj}\right)^2 \langle \bar{M}|\left(\bar{Q}_L^i \gamma^\mu Q_L^j\right)^2|M\rangle. \quad (2)$$

Therefore, new-physics models with TeV-scale flavored degrees of freedom and $\mathcal{O}(1)$ flavor-mixing couplings are essentially ruled out. To quantify this statement, we report here the results of the recent analysis of Ref. [9]. Writing

$$\mathcal{A}_{\text{NP}}^{\Delta F=2} \sim \frac{C_{ij}^k}{\Lambda^2} \langle \bar{M}|\left(\bar{Q}^i \Gamma^k Q^j\right)^2|M\rangle, \qquad (3)$$

inant deviations from the SM in the flavor sector. This happens under the following two general assumptions: (i) the effective scale of NP is substantially higher than the electroweak scale; (ii) the dimensionless effective couplings ruling $\Delta F = 2$ transitions can be expressed as the square of the corresponding $\Delta F = 1$ coupling, without extra suppression factors.

where Γ^k is a generic Dirac and colour structure (see Ref. [9] for details), one has[3]

$$\Lambda > \begin{cases} 2 \times 10^5 \text{ TeV} \times |C_{12}^4|^{1/2}, \\ 2 \times 10^3 \text{ TeV} \times |C_{13}^4|^{1/2}, \\ 3 \times 10^2 \text{ TeV} \times |C_{23}^4|^{1/2}. \end{cases}$$

– As clearly shown in Fig. 3, in the $B_d-\bar{B}_d$ case, there is still room for a new-physics contribution up to the SM one. However, this is possible only if the new-physics contribution is aligned in phase with respect to the SM amplitude (ϕ_d^{NP} close to zero). Similar, but tighter, constraints hold also for the new physics contribution to the $K^0-\bar{K}^0$ amplitude.

– Contrary to $B_d-\bar{B}_d$ and $K^0-\bar{K}^0$ amplitudes, at present there is only a very loose bound on the CPV phase of the $B_s-\bar{B}_s$ mixing amplitude. This leaves open the possibility of observing a large $\mathcal{A}_{\text{CP}}(B_s \to J/\Psi\phi)$ at LHCb, which would be a clear signal of physics beyond the SM.

As we will discuss in the following, the first two items listed above find a natural explanation within the so-called hypothesis of Minimal Flavor Violation.

1.2.3 Minimal flavor violation

A very reasonable, although quite pessimistic, solution to the flavor problem is the so-called Minimal Flavor Violation (MFV) hypothesis. Under this assumption, which will be formalized in detail below, flavor-violating interactions are linked to the known structure of Yukawa couplings also beyond the SM. As a result, nonstandard contributions in FCNC transitions turn out to be suppressed to a level consistent with experiments even for $\Lambda \sim$ few TeV. One of the most interesting aspects of the MFV hypothesis is that it can naturally be implemented within the EFT approach to NP [10]. The effective theories based on this symmetry principle allow us to establish unambiguous correlations among NP effects in various rare decays. These falsifiable predictions are the key ingredients to identify in a model-independent way which are the irreducible sources of flavor symmetry breaking.

1.2.3.1 The MFV hypothesis The pure gauge sector of the SM is invariant under a large symmetry group of flavor transformations: $\mathcal{G}_{\text{SM}} = \mathcal{G}_q \otimes \mathcal{G}_\ell \otimes U(1)^5$, where

$$\begin{aligned} \mathcal{G}_q &= SU(3)_{Q_L} \otimes SU(3)_{U_R} \otimes SU(3)_{D_R}, \\ \mathcal{G}_\ell &= SU(3)_{L_L} \otimes SU(3)_{E_R}, \end{aligned} \qquad (4)$$

[3]The choice $\Gamma^4 = P_L \otimes P_R$ gives the most stringent constraints. Constraints from other operators are up to one order of magnitude weaker.

314

Eur. Phys. J. C (2008) 57: 309–492

Fig. 2 Constraints on the effective parameters encoding NP effects in the B_d–$\bar{B}_d$ mixing amplitude (magnitude and phase) obtained by the UTfit [7] (*left*) and CKMfitter [8] (*right*) collaborations
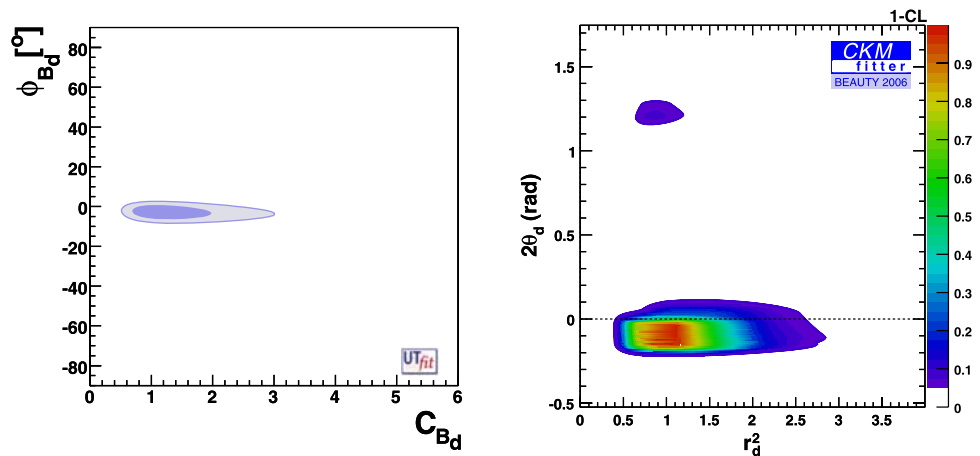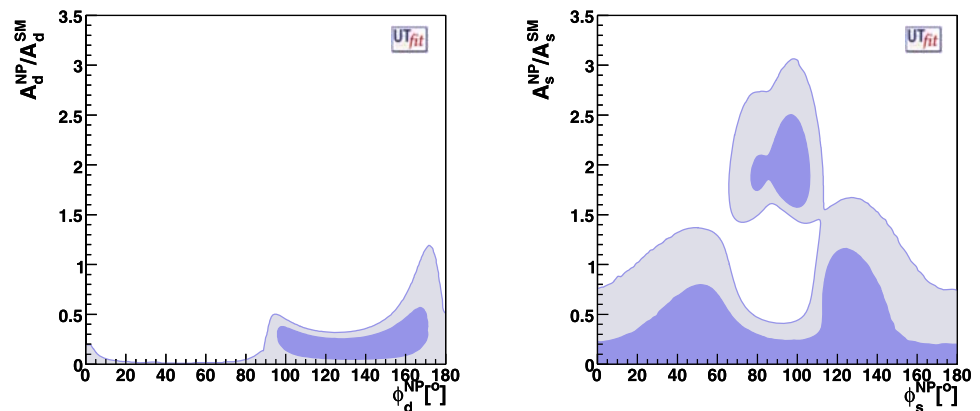
Fig. 3 Constraints on the absolute value and phase (normalized to the SM) of the new physics amplitude in B_d–$\bar{B}_d$ and B_s–$\bar{B}_s$ mixing from Ref. [9]

and three of the five $U(1)$ charges can be identified with baryon number, lepton number and hypercharge [11]. This large group and, particularly the $SU(3)$ subgroups controlling flavor-changing transitions, is explicitly broken by the Yukawa interaction

$$\mathcal{L}_Y = \bar{Q}_L Y_D D_R H + \bar{Q}_L Y_U U_R H_c + \bar{L}_L Y_E E_R H + \text{h.c.} \quad (5)$$

Since $\mathcal{G}_{SM}$ is already broken within the SM, it would not be consistent to impose it as an exact symmetry beyond the SM: even if absent a the tree-level, the breaking of $\mathcal{G}_{SM}$ would reappear at the quantum level because of the Yukawa interaction. The most restrictive hypothesis we can make to *protect* in a consistent way flavor mixing in the quark sector is to assume that Y_D and Y_U are the only sources of $\mathcal{G}_q$ breaking also beyond the SM. To implement and interpret this hypothesis in a consistent way, we can assume that $\mathcal{G}_q$ is indeed a good symmetry, promoting $Y_{U,D}$ to be nondynamical fields (spurions) with nontrivial transformation properties under this symmetry:

$$Y_U \sim (3, \bar{3}, 1)_{\mathcal{G}_q}, \qquad Y_D \sim (3, 1, \bar{3})_{\mathcal{G}_q}. \quad (6)$$

If the breaking of the symmetry occurs at very high energy scales—well above the TeV region where the new de-

grees of freedom necessary to stabilize the Higgs sector should appear—at low energies we would only be sensitive to the background values of the Y, i.e. to the ordinary SM Yukawa couplings. Employing the effective-theory language, we then define that an effective theory satisfies the criterion of Minimal Flavor Violation in the quark sector if all higher-dimensional operators constructed from SM and Y fields are invariant under CP and (formally) under the flavor group $\mathcal{G}_q$ [10].

According to this criterion, one should in principle consider operators with arbitrary powers of the (dimensionless) Yukawa fields. However, a strong simplification arises by the observation that all the eigenvalues of the Yukawa matrices are small, but for the top one, and that the off-diagonal elements of the CKM matrix (V_{ij}) are very suppressed. Using the $\mathcal{G}_q$ symmetry, we can rotate the background values of the auxiliary fields Y such that

$$Y_D = \lambda_d, \qquad Y_U = V^\dagger \lambda_u, \quad (7)$$

where λ are diagonal matrices and V is the CKM matrix. It is then easy to realize that, similarly to the pure SM case, the leading coupling ruling all FCNC transitions with external

down-type quarks is:

$$(\lambda_{\mathrm{FC}})_{ij} = \begin{cases} (Y_U Y_U^\dagger)_{ij} \approx \lambda_t^2 V_{3i}^* V_{3j}, & i \neq j, \\ 0, & i = j. \end{cases} \qquad (8)$$

The number of relevant dimension-6 effective operators is then strongly reduced (representative examples are reported in Table 1, while the complete list can be found in Ref. [10]).

1.2.3.2 Universal UT and MFV bounds on the effective operators As originally pointed out in Ref. [12], within the MFV framework several of the constraints used to determine the CKM matrix (and in particular the unitarity triangle) are not affected by NP. In this framework, NP effects are negligible not only in tree-level processes but also in a few clean observables sensitive to loop effects, such as the time-dependent CPV asymmetry in $B_d \to J/\Psi K_{L,S}$. Indeed the structure of the basic flavor-changing coupling in (8) implies that the weak CPV phase of B_d–$\bar{B}_d$ mixing is $\arg[(V_{td} V_{tb}^*)^2]$, exactly as in the SM. The determination of the unitarity triangle using only these clean observables (denoted Universal Unitarity Triangle) is shown in Fig. 4.[4] This construction provides a natural (a posteriori) justification of why no NP effects have been observed in the quark sector: by construction, most of the clean observables measured at B factories are insensitive to NP effects in this framework.

In Table 1, we report a few representative examples of the bounds on the higher-dimensional operators in the MFV framework. As can be noted, the built-in CKM suppression leads to bounds on the effective scale of new physics not far from the TeV region. These bounds are very similar to the bounds on flavor-conserving operators derived by precision electroweak tests. This observation reinforces the conclusion that a deeper study of rare decays is definitely needed in order to clarify the flavor problem: the experimental precision on the clean FCNC observables required to obtain bounds more stringent than those derived from precision electroweak tests (and possibly discover new physics) is typically in the 1–10% range.

Although the MFV seems to be a natural solution to the flavor problem, it should be stressed that we are still very far from having proved the validity of this hypothesis from data. A proof of the MFV hypothesis can be achieved only with a positive evidence of physics beyond the SM exhibiting the flavor pattern (link between $s \to d$, $b \to d$ and $b \to s$ transitions) predicted by the MFV assumption.

---

[4]The UUT as originally proposed in Ref. [12] includes $\Delta M_{B_d}/\Delta M_{B_s}$ and is therefore valid only in models of CMFV (see Sect. 1.2.3.3). On the other hand, removing $\Delta M_{B_d}/\Delta M_{B_s}$ from the analysis gives a UUT that is valid in any MFV scenario.

1.2.3.3 Comparison with other approaches (CMFV & n-MFV) The idea that the CKM matrix rules the strength of FCNC transitions also beyond the SM has become a very popular concept in the recent literature and has been implemented and discussed in several works (see e.g. Refs. [12–16]).

It is worth stressing that the CKM matrix represents only one part of the problem: a key role in determining the structure of FCNCs is also played by quark masses, or by the Yukawa eigenvalues. In this respect, the MFV criterion illustrated above provides the maximal protection of FCNCs (or the minimal violation of flavor symmetry), since the full structure of Yukawa matrices is preserved. At the same time, this criterion is based on a renormalization-group-invariant symmetry argument. Therefore, it can be implemented independently of any specific hypothesis about the dynamics of the new-physics framework. The only two assumptions are: (i) the flavor symmetry and the sources of its breaking; (ii) the number of light degrees of freedom of the theory (identified with the SM fields in the minimal case).

This model-independent structure does not hold in most of the alternative definitions of MFV models that can be found in the literature. For instance, the definition of Ref. [16] (denoted constrained MFV, or CMFV) contains the additional requirement that the effective FCNC operators playing a significant role within the SM are the only relevant ones also beyond the SM. This condition is realized within weakly coupled theories at the TeV scale with only one light Higgs doublet, such as the model with universal extra dimensions analysed in Ref. [17], or the MSSM with small $\tan\beta$ and small μ term. However, it does not hold in other frameworks, such as technicolour models, or the MSSM with large $\tan\beta$ and/or large μ term (see Sect. 1.2.3.6), whose low-energy phenomenology could still be described using the general MFV criterion discussed in Sect. 1.2.3.1.

Since we are still far from having proved the validity of the MFV hypothesis from data, specific less restrictive symmetry assumptions about the flavor-structure of NP can also be considered. Next-to-minimal MFV frameworks have recently been discussed in Refs. [18, 19]. As shown in Ref. [19], a convenient way to systematically analyse the possible deviations from the MFV ansatz is to introduce additional spurions of the $\mathcal{G}_{\mathrm{SM}}$ group.

1.2.3.4 MFV at large $\tan\beta$ If the Yukawa Lagrangian contains only one Higgs field, as in (5), it necessarily breaks both $\mathcal{G}_q$ and two of the $U(1)$ subgroups of $\mathcal{G}_{\mathrm{SM}}$. In models with more than one Higgs doublet, the breaking mechanisms of $\mathcal{G}_q$ and the $U(1)$ symmetries can be decoupled, allowing a different overall normalization of the $Y_{U,D}$ spurions with respect to the SM case.

A particularly interesting scenario is the two-Higgs-doublet model where the two Higgses are coupled separately

316

Eur. Phys. J. C (2008) 57: 309–492

Fig. 4 Fit of the CKM unitarity triangle within the SM (*left*) and in generic extensions of the SM satisfying the MFV hypothesis (*right*) [7]
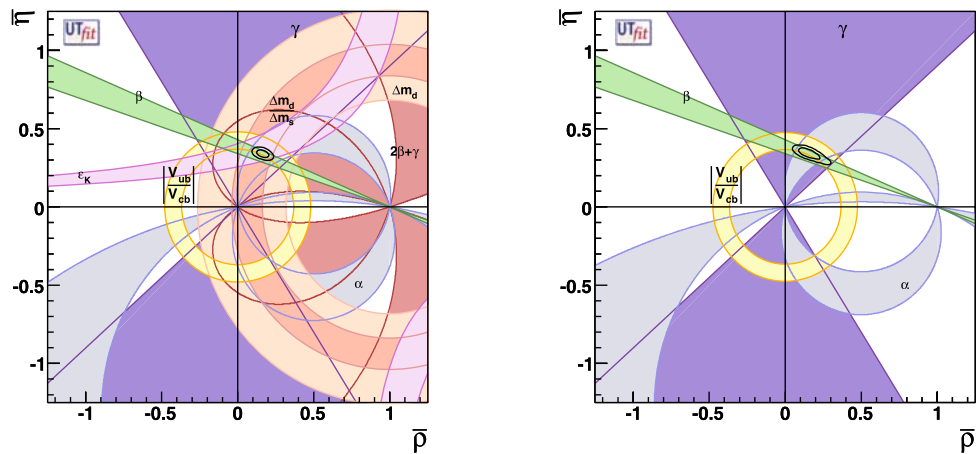

Table 1 95% C.L. bounds on the scale of representative dimension-six operators in the MFV scenario. The constraints are obtained on the single operator, with coefficient $\pm 1/\Lambda^2$ (+ or − denote constructive or destructive interference with the SM amplitude)

MFV dim-6 operator	Main observables	Λ [TeV]	
$\frac{1}{2}(\bar{Q}_L Y_U Y_U^\dagger \gamma_\mu Q_L)^2$	ϵ_K, Δm_{B_d}, Δm_{B_s}	5.9 [+]	8.8 [−]
$eH^\dagger(\bar{D}_R Y_D^\dagger Y_U Y_U^\dagger \sigma_{\mu\nu} Q_L)F_{\mu\nu}$	$B \to X_s \gamma$	5.0 [+]	9.0 [−]
$(\bar{Q}_L Y_U Y_U^\dagger \gamma_\mu Q_L)(\bar{L}_L \gamma_\mu L_L)$	$B \to (X)\ell\bar{\ell}$, $K \to \pi\nu\bar{\nu}$, $(\pi)\ell\bar{\ell}$	3.7 [+]	3.2 [−]
$(\bar{Q}_L Y_U Y_U^\dagger \gamma_\mu Q_L)(H^\dagger i D_\mu H)$	$B \to (X)\ell\bar{\ell}$, $K \to \pi\nu\bar{\nu}$, $(\pi)\ell\bar{\ell}$	2.0 [+]	2.0 [−]

to up- and down-type quarks:

$$\mathcal{L}_{Y_0} = \bar{Q}_L Y_D D_R H_D + \bar{Q}_L Y_U U_R H_U + \bar{L}_L Y_E E_R H_D + \text{h.c.}$$
(9)

This Lagrangian is invariant under a $U(1)$ symmetry, denoted $U(1)_{\text{PQ}}$, whose only charged fields are D_R and E_R (charge +1) and H_D (charge −1). The U_{PQ} symmetry prevents tree-level FCNCs and implies that $Y_{U,D}$ are the only sources of $\mathcal{G}_q$ breaking appearing in the Yukawa interaction (similar to the one-Higgs-doublet scenario). Coherently with the MFV hypothesis, in order to protect the good agreement between data and SM in FCNCs and $\Delta F = 2$ amplitudes, we assume that $Y_{U,D}$ are the only relevant sources of $\mathcal{G}_q$ breaking appearing in all the low-energy effective operators. This is sufficient to ensure that flavor-mixing is still governed by the CKM matrix and naturally guarantees a good agreement with present data in the $\Delta F = 2$ sector. However, the extra symmetry of the Yukawa interaction allows us to change the overall normalization of $Y_{U,D}$ with interesting phenomenological consequences in specific rare modes.

The normalization of the Yukawa couplings is controlled by $\tan\beta = \langle H_U \rangle / \langle H_D \rangle$. For $\tan\beta \gg 1$, the smallness of the b quark and τ lepton masses can be attributed to the smallness of $1/\tan\beta$ rather than to the corresponding Yukawa couplings. As a result, for $\tan\beta \gg 1$, we cannot anymore neglect the down-type Yukawa coupling. In this scenario, the

determination of the effective low-energy Hamiltonian relevant to FCNC processes involves the following three steps:

– Construction of the gauge-invariant basis of dimension-six operators (suppressed by Λ^{-2}) in terms of SM fields and two Higgs doublets.
– Breaking of $SU(2) \times U(1)_Y$ and integration of the $\mathcal{O}(M_H^2)$ heavy Higgs fields.
– Integration of the $\mathcal{O}(M_W^2)$ SM degrees of freedom (top quark and electroweak gauge bosons).

These steps are well separated if we assume the scale hierarchy $\Lambda \gg M_H \gg M_W$. On the other hand, if $\Lambda \sim M_H$, the first two steps can be joined, resembling the one-Higgs-doublet scenario discussed before. The only difference is that now, at large $\tan\beta$, Y_D is not negligible, and this requires to enlarge the basis of effective dimension-six operators. From the phenomenological point of view, this implies the breaking of the strong MFV link between K- and B-physics FCNC amplitudes occurring in the one-Higgs-doublet case [10].

A more substantial modification of the one-Higgs-doublet case occurs if we allow sizable sources of $U(1)_{\text{PQ}}$ breaking. It should be pointed out that the $U(1)_{\text{PQ}}$ symmetry cannot be exact: it has to be broken at least in the scalar potential in order to avoid the presence of a massless pseudoscalar Higgs. Even if the breaking of $U(1)_{\text{PQ}}$ and $\mathcal{G}_q$ are decoupled, the presence of $U(1)_{\text{PQ}}$ breaking sources can have important

implications on the structure of the Yukawa interaction. We can indeed consider new dimension-four operators such as

$$\epsilon \bar{Q}_L Y_D D_R (H_U)^c \quad \text{or} \quad \epsilon \bar{Q}_L Y_U Y_U^\dagger Y_D D_R (H_U)^c, \quad (10)$$

where ϵ denotes a generic $\mathcal{G}_q$-invariant $U(1)_{\mathrm{PQ}}$-breaking source. Even if $\epsilon \ll 1$, the product $\epsilon \times \tan\beta$ can be $\mathcal{O}(1)$, inducing $\mathcal{O}(1)$ nondecoupling corrections to $\mathcal{L}_{Y_0}$. As discussed in specific supersymmetric scenarios, for $\epsilon \tan\beta = \mathcal{O}(1)$, the $U(1)_{\mathrm{PQ}}$-breaking terms induce $\mathcal{O}(1)$ corrections to the down-type Yukawa couplings [20], the CKM matrix elements [21] and the charged-Higgs couplings [22–24]. Moreover, sizable FCNC couplings of the down-type quarks to the heavy neutral Higgs fields are allowed [25–30]. All these effects can be taken into account to all orders with a proper re-diagonalization of the effective Yukawa interaction [10].

Since the b-quark Yukawa coupling becomes $\mathcal{O}(1)$, the large-$\tan\beta$ regime is particularly interesting for helicity-suppressed observables in B physics. One of the clearest phenomenological consequences is a suppression (typically in the 10–50% range) of the $B \to \ell\nu$ decay rate with respect to its SM expectation [31]. Potentially measurable effects in the 10–30% range are expected also in $B \to X_s\gamma$ and ΔM_{B_s}. The most striking signature could arise from the rare decays $B_{s,d} \to \ell^+\ell^-$, whose rates could be enhanced over the SM expectations by more than one order of magnitude. An enhancement of both $B_s \to \ell^+\ell^-$ and $B_d \to \ell^+\ell^-$ respecting the MFV relation $\Gamma(B_s \to \ell^+\ell^-)/\Gamma(B_d \to \ell^+\ell^-) \approx |V_{ts}/V_{td}|^2$ would be an unambiguous signature of MFV at large $\tan\beta$.

Within the EFT approach where all the heavy degrees of freedom except the Higgs fields are integrated out, we cannot establish many other correlations among the helicity-suppressed B-physics observables. However, the scenario becomes quite predictive within a more ambitious EFT: the MSSM with MFV (see Sect. 1.2.3.6). As recently discussed in Refs. [32–34], in the MFV-MSSM with large $\tan\beta$ and heavy squarks, interesting correlations can be established among all the B-physics observables mentioned above and several flavor-conserving observables (both at low and high energies). In particular, while compatible with present B-physics constraints, this scenario can naturally resolve the long-standing $(g-2)_\mu$ anomaly and explain in a natural way why the lightest Higgs boson has not been observed yet. The predictivity, the high-sensitivity to various B-physics observables and the natural compatibility with existing data make this scenario a very interesting benchmark for correlated studies of low- and high-energy data (see Sect. 5).

1.2.3.5 MFV in grand unified theories Once we accept the idea that flavor dynamics obeys an MFV principle, at least in the quark sector, it is interesting to ask if and how this is compatible with Grand Unified Theories (GUTs),

where quarks and leptons sit in the same representations of a unified gauge group. This question has recently been addressed in Ref. [35], considering the exemplifying case of $SU(5)_{\mathrm{gauge}}$.

Within $SU(5)_{\mathrm{gauge}}$, the down-type singlet quarks (D_R^i) and the lepton doublets (L_L^i) belong to the $\bar{\mathbf{5}}$ representation; the quark doublet (Q_L^i), the up-type (U_R^i) and lepton singlets (E_R^i) belong to the $\mathbf{10}$ representation, and finally the right-handed neutrinos (ν_R^i) are singlets. In this framework, the largest group of flavor transformation commuting with the gauge group is $\mathcal{G}_{\mathrm{GUT}} = SU(3)_{\bar{5}} \times SU(3)_{10} \times SU(3)_1$, which is smaller than the direct product of the quark and lepton flavor groups compatible with the SM gauge sector: $\mathcal{G}_q \times \mathcal{G}_l$. We should therefore expect some violations of the MFV predictions, either in the quark sector, or in the lepton sector, or in both (a review of the MFV predictions for the lepton sector [36] can be found in the Chapter *Flavor physics of leptons and dipole moments* of this volume).

A phenomenologically acceptable description of the low-energy fermion mass matrices requires the introduction of at least four irreducible sources of $\mathcal{G}_{\mathrm{GUT}}$ breaking. From this point of view the situation is apparently similar to the nonunified case: the four $\mathcal{G}_{\mathrm{GUT}}$ spurions can be put in one-to-one correspondence with the low-energy spurions $Y_{U,D,E}$ plus the neutrino Yukawa coupling Y_ν (which is the only low-energy spurion in the neutrino sector assuming an approximately degenerate heavy ν_R spectrum). However, the smaller flavor group does not allow the diagonalization of Y_D and Y_E (which transform in the same way under $\mathcal{G}_{\mathrm{GUT}}$) in the same basis. As a result, two additional mixing matrices can appear in the expressions for flavor changing rates [35]. The hierarchical texture of the new mixing matrices is known since they reduce to the identity matrix in the limit $Y_E^T = Y_D$. Taking into account this fact and analysing the structure of the allowed higher-dimensional operators, a number of reasonably firm phenomenological consequences can be deduced [35]:

– There is a well-defined limit in which the standard MFV scenario for the quark sector is fully recovered: $|Y_\nu| \ll 1$ and small $\tan\beta$. The upper bound on the neutrino Yukawa couplings implies an upper bound on the heavy neutrino masses (M_ν). In the limit of a degenerate heavy neutrino spectrum, this bound is about 10^{12} GeV. For $M_\nu \sim 10^{12}$ GeV and small $\tan\beta$, deviations from the standard MFV pattern can be expected in rare K decays but not in B physics.[5] Ignoring fine-tuned scenarios, $M_\nu \gg 10^{12}$ GeV

---

[5]The conclusion that K decays are the most sensitive probes of possible deviations from the strict MFV ansatz follows from the strong suppression of the $s \to d$ short-distance amplitude in the SM [$V_{td}V_{ts}^* = \mathcal{O}(10^{-4})$] and goes beyond the hypothesis of an underlying GUT. This is the reason why $K \to \pi\nu\bar{\nu}$ decays, which are the best probes of $s \to d$, $\Delta F = 1$ short-distance amplitudes, play a key role in any extension of the SM containing nonminimal sources of flavor symmetry breaking.

318

Eur. Phys. J. C (2008) 57: 309–492

is excluded by the present constraints on quark FCNC transitions. Independently from the value of M_ν, deviations from the standard MFV pattern can appear both in K and in B physics for $\tan\beta \gtrsim m_t/m_b$.

– Contrary to the non-GUT MFV framework for the lepton sector, the rate for $\mu \to e\gamma$ and other LFV decays cannot be arbitrarily suppressed by lowering the mass of the heavy ν_R. This fact can easily be understood by noting that the GUT group allows also M_ν-independent contributions to LFV decays proportional to the quark Yukawa couplings. The latter become competitive for $M_\nu \lesssim 10^{12}$ GeV, and their contribution is such that for $\Lambda \lesssim 10$ TeV, the $\mu \to e\gamma$ rate is above 10^{-13} (i.e. within the reach of MEG [37]).

– Within this framework, improved experimental searches on $\tau \to \mu\gamma$ and $\tau \to e\gamma$ are a key tool: they are the best observables to discriminate the relative size of the non-GUT MFV contributions with respect to the GUT ones. In particular, if the quark-induced terms turn out to be dominant, the $\mathcal{B}(\tau \to \mu\gamma)/\mathcal{B}(\mu \to e\gamma)$ ratio could reach values of $\mathcal{O}(10^{-4})$, allowing $\tau \to \mu\gamma$ to be just below the present exclusion bounds.

1.2.3.6 The MFV hypothesis in the MSSM A detailed discussion of the so-called Minimal Supersymmetric extension of the SM will be presented in Sect. 1.3. Here we limit ourselves to analyse how the MFV hypothesis can be implemented in this framework and to briefly summarize its main implications.

It is first worth to recall that the adjective *minimal* in the MSSM acronyms refers to the particle content of the model and not to its flavor structure. In general, the MSSM contains a huge number of free parameters, and most of them are related to the flavor structure of the model (sfermion masses and trilinear couplings). Since the new degrees of freedom (in particular the squark fields) have well-defined transformation properties under the quark-flavor

to express the squark mass terms and the trilinear quark–squark–Higgs couplings as follows [10, 38]:

$$\tilde{m}_{Q_L}^2 = \tilde{m}^2\big(a_1\mathbb{1} + b_1 Y_U Y_U^\dagger + b_2 Y_D Y_D^\dagger + b_3 Y_D Y_D^\dagger Y_U Y_U^\dagger$$
$$+ b_4 Y_U Y_U^\dagger Y_D Y_D^\dagger + \cdots\big), \tag{11}$$

$$\tilde{m}_{U_R}^2 = \tilde{m}^2\big(a_2\mathbb{1} + b_5 Y_U^\dagger Y_U + \cdots\big), \tag{12}$$

$$\tilde{m}_{D_R}^2 = \tilde{m}^2\big(a_3\mathbb{1} + b_6 Y_D^\dagger Y_D + \cdots\big), \tag{13}$$

$$A_U = A\big(a_4\mathbb{1} + b_7 Y_D Y_D^\dagger + \cdots\big)Y_U, \tag{14}$$

$$A_D = A\big(a_5\mathbb{1} + b_8 Y_U Y_U^\dagger + \cdots\big)Y_D, \tag{15}$$

where the dimensionful parameters $\tilde{m}$ and A set the overall scale of the soft-breaking terms. In (11)–(15), we have explicitly shown all independent flavor structures which cannot be absorbed into a redefinition of the leading terms (up to tiny contributions quadratic in the Yukawas of the first two families). When $\tan\beta$ is not too large and the bottom Yukawa coupling is small, the terms quadratic in Y_D can be dropped.

In a bottom-up approach, the dimensionless coefficients a_i and b_i in (11)–(15) should be considered as free parameters of the model. Note that this structure is renormalization-group invariant: the values of a_i and b_i change according to the Renormalization Group (RG) flow, but the general structure of (11)–(15) is unchanged. This is not the case if the b_i are set to zero (corresponding to the so-called hypothesis of flavor universality). If this hypothesis is set as initial condition at some high-energy scale M, then nonvanishing $b_i \sim (1/4\pi)^2 \ln M^2/\tilde{m}^2$ are generated by the RG evolution. This is for instance what happens in models with gauge-mediated supersymmetry breaking [39–41], where the scale M is identified with the mass of the hypothetical messenger particles.

Using the soft terms in (11)–(15), the physical 6×6 squark-mass matrices, after electroweak symmetry breaking, are given by

$$\tilde{M}_U^2 = \begin{pmatrix} \tilde{m}_{Q_L}^2 + Y_U Y_U^\dagger v_U^2 + \left(\frac{1}{2} - \frac{2}{3}s_W^2\right)M_Z^2\cos 2\beta & (A_U - \mu Y_U \cot\beta)v_U \\ (A_U - \mu Y_U \cot\beta)^\dagger v_U & \tilde{m}_{U_R}^2 + Y_U^\dagger Y_U v_U^2 + \frac{2}{3}s_W^2 M_Z^2\cos 2\beta \end{pmatrix},$$

$$\tilde{M}_D^2 = \begin{pmatrix} \tilde{m}_{Q_L}^2 + Y_D Y_D^\dagger v_D^2 - \left(\frac{1}{2} - \frac{1}{3}s_W^2\right)M_Z^2\cos 2\beta & (A_D - \mu Y_D \tan\beta)v_D \\ (A_D - \mu Y_D \tan\beta)^\dagger v_D & \tilde{m}_{D_R}^2 + Y_D^\dagger Y_D v_D^2 - \frac{1}{3}s_W^2 M_Z^2\cos 2\beta \end{pmatrix},$$

$$\tag{16}$$

group $\mathcal{G}_q$, the MFV hypothesis can easily be implemented in this framework following the general rules outlined in Sect. 1.2.3.1: we need to consider all possible interactions compatible with (i) softly-broken supersymmetry; (ii) the breaking of $\mathcal{G}_q$ via the spurion fields $Y_{U,D}$. This allows one

where μ is the higgsino mass parameter, and $v_{U,D} = \langle H_{U,D}\rangle$ ($\tan\beta = v_U/v_D$). The eigenvalues of these mass matrices are not degenerate; however, the mass splittings are tightly constrained by the specific (Yukawa-type) symmetry-breaking pattern.

Eur. Phys. J. C (2008) 57: 309–492

319

If we are interested only in low-energy processes, we can integrate out the supersymmetric particles at one loop and project this theory into the general EFT discussed in the previous sections. In this case, the coefficients of the dimension-six effective operators written in terms of SM and Higgs fields (see Table 1) are computable in terms of the supersymmetric soft-breaking parameters. We stress that if $\tan\beta \gg 1$ (see Sect. 1.2.3.4) and/or if μ is large enough [42], the relevant operators thus obtained go beyond the restricted basis of the CMFV scenario [16]. The typical effective scale suppressing these operators (assuming an overall coefficient $1/\Lambda^2$) is

$$\Lambda \sim 4\pi\tilde{m}. \tag{17}$$

Looking at the bounds in Table 1, we then conclude that if MFV holds, the present bounds on FCNCs do not exclude squarks in the few hundred GeV mass range, i.e. well within the LHC reach.

It is finally worth recalling that the integration of the supersymmetric degrees of freedom may also lead to sizable modifications of the renormalizable operators and, in particular, of the effective Yukawa interactions. As a result, in an effective field theory with supersymmetric degrees of freedom, the relations between $Y_{U,D}$ and the physical quark masses and CKM angles are potentially modified. As already pointed out in Sect. 1.2.3.4, this effect is particularly relevant in the large $\tan\beta$ regime.

1.3 SUSY models

1.3.1 FCNC and SUSY

The generation of fermion masses and mixings ("flavor problem") gives rise to the first important distinction among theories of new physics beyond the electroweak Standard Model.

One may conceive a kind of new physics that is completely "flavor blind", i.e. new interactions that have nothing to do with the flavor structure. To provide an example of such a situation, consider a scheme where flavor arises at a very large scale (for instance the Planck mass) while new physics is represented by a supersymmetric extension of the SM with supersymmetry broken at a much lower scale and with the SUSY breaking transmitted to the observable sector by flavor-blind gauge interactions. In this case, one may think that the new physics does not cause any major change to the original flavor structure of the SM, namely that the pattern of fermion masses and mixings is compatible with the numerous and demanding tests of flavor changing neutral currents.

Alternatively, one can conceive a new physics that is entangled with the flavor problem. As an example, consider a technicolour scheme where fermion masses and mixings

arise through the exchange of new gauge bosons which mix together ordinary and technifermions. Here we expect (correctly enough) new physics to have potential problems in accommodating the usual fermion spectrum with the adequate suppression of FCNC. As another example of new physics that is not flavor blind, take a more conventional SUSY model which is derived from a spontaneously broken $N = 1$ supergravity and where the SUSY breaking information is conveyed to the ordinary sector of the theory through gravitational interactions. In this case, we may expect that the scale at which flavor arises and the scale of SUSY breaking are not so different and possibly the mechanism of SUSY breaking and transmission itself is flavor-dependent. Under these circumstances, we may expect a potential flavor problem to arise, namely that SUSY contributions to FCNC processes are too large.

The potentiality of probing SUSY in FCNC phenomena was readily realized when the era of SUSY phenomenology started in the early 80's [43, 44]. In particular, the major implication that the scalar partners of quarks of the same electric charge but belonging to different generations had to share a remarkably high mass degeneracy was emphasized.

Throughout the large amount of work in the past decades, it became clearer and clearer that generically talking of the implications of low-energy SUSY on FCNC may be rather misleading. We have a minimal SUSY extension of the SM, the so-called Constrained Minimal Supersymmetric Standard Model (CMSSM), where the FCNC contributions can be computed in terms of a very limited set of unknown new SUSY parameters. Remarkably enough, this minimal model succeeds to pass all FCNC tests unscathed. To be sure, it is possible to severely constrain the SUSY parameter space, for instance using $b \to s\gamma$ in a way that is complementary to what is achieved by direct SUSY searches at colliders.

However, the CMSSM is by no means equivalent to low-energy SUSY. A first sharp distinction concerns the mechanism of SUSY breaking and transmission to the observable sector that is chosen. As we mentioned above, in models with gauge-mediated SUSY breaking (GMSB models [39, 40, 45–68]), it may be possible to avoid the FCNC threat "ab initio" (notice that this is not an automatic feature of this class of models, but it depends on the specific choice of the sector that transmits the SUSY breaking information, the so-called messenger sector). The other more "canonical" class of SUSY theories that was mentioned above has gravitational messengers and a very large scale at which SUSY breaking occurs.

In this brief discussion, we focus only on this class of gravity-mediated SUSY breaking models. Even sticking to this more limited choice, we have a variety of options with very different implications for the flavor problem: first, there exists an interesting large class of SUSY realizations where

320

Eur. Phys. J. C (2008) 57: 309–492

the customary R-parity (which is invoked to suppress proton decay) is replaced by other discrete symmetries which allow either baryon or lepton violating terms in the superpotential. But, even sticking to the more orthodox view of imposing R-parity, we are still left with a large variety of extensions of the MSSM at low energy. The point is that low-energy SUSY "feels" the new physics at the superlarge scale at which supergravity (i.e. local supersymmetry) broke down. In the past years, we have witnessed an increasing interest in supergravity realizations without the so-called flavor universality of the terms which break SUSY explicitly. Another class of low-energy SUSY realizations, which differ from the MSSM in the FCNC sector, is obtained from SUSY-GUT's. The interactions involving superheavy particles in the energy range between the GUT and the Planck scale bear important implications for the amount and kind of FCNC that we expect at low energy [69–71].

1.3.2 FCNC in SUSY without R-parity

It is well known that in the SM case, the imposition of gauge symmetry and the usual gauge assignment of the 15 elementary fermions of each family lead to the automatic conservation of baryon and lepton numbers (this is true at any order in perturbation theory).

On the contrary, imposing in addition to the usual $SU(3) \otimes SU(2) \otimes U(1)$ gauge symmetry an $N = 1$ global SUSY does not prevent the appearance of terms which explicitly break B or L [72, 73]. Indeed, the superpotential reads:

$$
\begin{aligned}
W = {}& h^U Q H_U u^c + h^D Q H_D d^c + h^L L H_D e^c + \mu H_U H_D \\
& + \mu' H_U L + \lambda''_{ijk} u_i^c d_j^c d_k^c + \lambda'_{ijk} Q_i L_j d_k^c \\
& + \lambda_{ijk} L_i L_j e_k^c,
\end{aligned}
\tag{18}
$$

where the chiral matter superfields Q, u^c, d^c, L, e^c, H_U and H_D transform under the above gauge symmetry as:

$$
\begin{aligned}
& Q \equiv (3, 2, 1/6); \qquad u^c \equiv (\bar{3}, 1, -2/3); \\
& d^c \equiv (\bar{3}, 1, 1/3); \\
& L \equiv (1, 2, -1/2); \qquad e^c \equiv (1, 1, 1); \\
& H_U \equiv (1, 2, 1/2); \qquad H_D \equiv (1, 2, -1/2).
\end{aligned}
\tag{19}
$$

The couplings h^U, h^D, h^L are 3×3 matrices in the generation space; i, j and k are generation indices. Using the product of λ' and λ'' couplings, it is immediate to construct four-fermion operators leading to proton decay through the exchange of a squark. Even if one allows for the existence of λ' and λ'' couplings only involving the heaviest generation, one can show that the bound on the product $\lambda' \times \lambda''$ of these couplings is very severe (of $O(10^{-7})$) [74].

A solution is that there exists a discrete symmetry, B-parity [75–79], which forbids the B-violating terms proportional to λ'' in (18). In that case, it is still possible to produce sizable effects in FC processes. Two general features of these R-parity violating contributions are:

1. Complete loss of any correlation to the CKM elements. For instance, in the above example, the couplings λ' and λ have nothing to do with the usual angles V_{tb} and V_{ts} which appear in $b \to s l^+ l^-$ in the SM.
2. Loss of correlation among different FCNC processes, which are tightly correlated in the SM. For instance, in our example, $b \to d l^+ l^-$ would depend on λ' and λ parameters which are different from those appearing in B_d–$\bar{B}_d$ mixing.

In this context, it is difficult to make predictions given the arbitrariness of the large number of λ and λ' parameters. There exist bounds on each individual coupling (i.e. assuming that all the other L violating couplings are zero) [80, 81].

Obviously, the most practical way of avoiding any threat of B- and L-violating operators is to forbid all such terms in (18). This is achieved by imposing the usual R matter parity. This quantum number is +1 for every ordinary particle and −1 for SUSY partners. We now turn to FCNC in the framework of low-energy SUSY with R parity.

1.3.3 FCNC in SUSY with R parity—CMSSM framework

Even when R parity is imposed the FCNC challenge is not over. It is true that in this case, analogously to what happens in the SM, no tree level FCNC contributions arise. However, it is well known that this is a necessary but not sufficient condition to consider the FCNC problem overcome. The loop contributions to FCNC in the SM exhibit the presence of the GIM mechanism, and we have to make sure that in the SUSY case with R parity, some analog of the GIM mechanism is active.

To give a qualitative idea of what we mean by an effective super-GIM mechanism, let us consider the following simplified situation where the main features emerge clearly. Consider the SM box diagram responsible for K^0–$\bar{K}^0$ mixing and take only two generations, i.e. only the up and charm quarks run in the loop. In this case, the GIM mechanism yields a suppression factor of $O((m_c^2 - m_u^2)/M_W^2)$. If we replace the W boson and the up quarks in the loop with their SUSY partners and we take, for simplicity, all SUSY masses of the same order, we obtain a super-GIM factor which looks like the GIM one with the masses of the superparticles instead of those of the corresponding particles. The problem is that the up and charm squarks have masses which are much larger than those of the corresponding quarks. Hence the super-GIM factor tends to be of $O(1)$ instead of being

$O(10^{-3})$ as it is in the SM case. To obtain this small number we would need a high degeneracy between the mass of the charm and up squarks. It is difficult to think that such a degeneracy may be accidental. After all, since we invoked SUSY for a naturalness problem (the gauge hierarchy issue), we should avoid invoking a fine-tuning to solve its problems! Then one can turn to some symmetry reason. For instance, just sticking to this simple example that we are considering, one may think that the main bulk of the charm and up squark masses is the same, i.e. the mechanism of SUSY breaking should have some universality in providing the mass to these two squarks with the same electric charge. Another possibility one may envisage is that the masses of the squarks are quite high, say above few TeV's. Then even if they are not so degenerate in mass, the overall factor in front of the four-fermion operator responsible for the kaon mixing becomes smaller and smaller (it decreases quadratically with the mass of the squarks), and, consequently, one can respect the experimental result. We see from this simple example that the issue of FCNC may be closely linked to the crucial problem of how we break SUSY.

We now turn to some more quantitative considerations. We start by discussing the different degrees of concern that FCNC raise according to the specific low-energy SUSY realization one has in mind. In this section, we will consider FCNC in the CMSSM realizations. In Sect. 1.3.4, we will deal with CP-violating FCNC phenomena in the same context. After discussing these aspects in the CMSSM, we will provide bounds from FCNC and CP violation in a generic SUSY extension of the SM (Sect. 1.3.5).

Obviously the reference frame for any discussion in a specific SUSY scheme is the MSSM. Although the name seems to indicate a well-defined particle model, we can identify at least two quite different classes of low-energy SUSY models. First, we have the CMSSM, the minimal SUSY extension of the SM (i.e. with the smallest needed number of superfields) with R-parity, radiative breaking of the electroweak symmetry, universality of the soft breaking terms and simplifying relations at the GUT scale among SUSY parameters. In this *constrained* version, the MSSM exhibits only four free parameters in addition to those of the SM and is an example of a SUSY model with MFV. Moreover, some authors impose specific relations between the two parameters A and B that appear in the trilinear and bilinear scalar terms of the soft breaking sector, further reducing the number of SUSY free parameters to three. Then, all SUSY masses are just functions of these few independent parameters, and, hence, many relations among them exist.

In SUSY, there are five classes of one-loop diagrams that contribute to FCNC and CP-violating processes. They are distinguished according to the virtual particles running in the loop: W and up-quarks, charged Higgs and up-quarks, charginos and up-squarks, neutralinos and down-squarks, gluinos and down-squarks. It turns out that, in this *constrained* version of the MSSM, at low or moderate $\tan\beta$, the charged Higgs and chargino exchanges yield the dominant SUSY contributions, while at large $\tan\beta$, Higgs-mediated effects become dominant.

Obviously this very minimal version of the MSSM can be very predictive. The most powerful constraint on this minimal model in the FCNC context comes from $b \to s\gamma$ [23, 82–84]. For large values of $\tan\beta$, strong constraints are also obtained from the upper bound on $B_s \to \mu^+\mu^-$, from ΔM_s and from $B(B \to \tau\nu)$ [27–30, 32, 85]. No observable deviations from the SM predictions in other FCNC processes are expected, given the present experimental and theoretical uncertainties.

It should be kept in mind that the above stringent results strictly depend not only on the minimality of the model in terms of the superfields that are introduced but also on the "boundary" conditions that are chosen. All the low-energy SUSY masses are computed in terms of the four SUSY parameters at the Planck scale M_{Pl} through the RG evolution. If one relaxes this tight constraint on the relation of the low-energy quantities and treats the masses of the SUSY particles as independent parameters, then much more freedom is gained. This holds true even in the MSSM with MFV at small or moderate $\tan\beta$: sizable SUSY effects can be present both in meson–anti-meson mixing and in rare decays [86], in particular for light stop and charginos.

Moreover, flavor universality is by no means a prediction of low-energy SUSY. The absence of flavor universality of soft-breaking terms may result from radiative effects at the GUT scale or from effective supergravities derived from string theory. For instance, even starting with an exact universality of the soft breaking terms at the Planck scale, in a SUSY GUT scheme, one has to consider the running from this latter scale to the GUT scale. Due to the large value of the top Yukawa coupling and to the fact that quarks and lepton superfields are in common GUT multiplets, we may expect the tau slepton mass to be conspicuously different from that of the first two generation sleptons at the end of this RG running. This lack of universality at the GUT scale may lead to large violations of lepton flavor number yielding, for instance, $\mu \to e\gamma$ at a rate in the ball park of observability [87]. In the nonuniversal case, most FCNC processes receive sizable SUSY corrections, and indeed flavor physics poses strong constraints on the parameter space of SUSY models without MFV.

1.3.4 CP violation in the CMSSM

CP violation has a major potential to exhibit manifestations of physics beyond the SM. Indeed, it is quite a general feature that NP possesses new CP-violating phases in addition

322

Eur. Phys. J. C (2008) 57: 309–492

to the CKM phase (δ_{CKM}) or, even in those cases where this does not occur, δ_{CKM} shows up in interactions of the new particles, hence with potential departures from the SM expectations. Moreover, although the SM is able to account for the observed CP violation, the possibility of large NP contributions to CP violation in $b \rightarrow s$ transitions is still open (see Sect. 3.7 and Ref. [88] for recent reviews). The detection of CP violation in B_s mixing and the improvement of the measurements of CP asymmetries in $b \rightarrow s$ penguin decays will constitute a crucial test of the CKM picture within the SM. Again, on general grounds, we expect new physics to provide departures from the SM CKM scenario. A final remark on reasons that make us optimistic in having new physics playing a major role in CP violation concerns the matter–anti-matter asymmetry in the Universe. Starting from a baryon–anti-baryon symmetric Universe, the SM is unable to account for the observed baryon asymmetry. The presence of new CP-violating contributions when one goes beyond the SM looks crucial to produce an efficient mechanism for the generation of a satisfactory ΔB asymmetry.

The above considerations apply well to the new physics represented by low-energy supersymmetric extensions of the SM. Indeed, as we will see below, supersymmetry introduces CP-violating phases in addition to δ_{CKM}, and, even if one envisages particular situations where such extra-phases vanish, the phase δ_{CKM} itself leads to new CP-violating contributions in processes where SUSY particles are exchanged. CP violation in $b \rightarrow s$ transitions has a good potential to exhibit departures from the SM CKM picture in low-energy SUSY extensions, although, as we will discuss, the detectability of such deviations strongly depends on the regions of the SUSY parameter space under consideration.

In this section, we will deal with CP violation in the context of the CMSSM. In Sect. 1.3.5, we will discuss the CP issue in a model-independent approach.

In the CMSSM, two new "genuine" SUSY CP-violating phases are present. They originate from the SUSY parameters μ, M, A and B. The first of these parameters is the dimensionful coefficient of the $H_u H_d$ term of the superpotential. The remaining three parameters are present in the sector that softly breaks the $N = 1$ global SUSY. M denotes the common value of the gaugino masses, A is the trilinear scalar coupling, while B denotes the bilinear scalar coupling. In our notation, all these three parameters are dimensionful. The simplest way to see which combinations of the phases of these four parameters are physical [89] is to notice that for vanishing values of μ, M, A and B, the theory possesses two additional symmetries [90]. Indeed, letting B and μ vanish, a $U(1)$ Peccei–Quinn symmetry arises, which in particular rotates H_u and H_d. If M, A and B are set to zero, the Lagrangian acquires a continuous $U(1)$ R symmetry. Then we can consider μ, M, A and B as spurions which break the $U(1)_{PQ}$ and $U(1)_R$ symmetries. In this

way, the question concerning the number and nature of the meaningful phases translates into the problem of finding the independent combinations of the four parameters which are invariant under $U(1)_{PQ}$ and $U(1)_R$ and determining their independent phases. There are three such independent combinations, but only two of their phases are independent. We use here the commonly adopted choice:

$$\Phi_A = \arg(A^* M), \qquad \Phi_B = \arg(B^* M). \qquad (20)$$

The main constraints on Φ_A and Φ_B come from their contribution to the electric dipole moments of the neutron and of the electron. For instance, the effect of Φ_A and Φ_B on the electric and chromoelectric dipole moments of the light quarks (u, d, s) lead to a contribution to d_N^e of order

$$d_N^e \sim 2\left(\frac{100 \text{ GeV}}{\tilde{m}}\right)^2 \sin \Phi_{A,B} \times 10^{-23} \, e \, \text{cm}, \qquad (21)$$

where $\tilde{m}$ here denotes a common mass for squarks and gluinos. We refer the reader to the Chapter *Flavor physics of leptons and dipole moments* of this volume for a detailed discussion of the present status of constraints on SUSY from electric dipole moments. We just remark that the present experimental bounds imply that $\Phi_{A,B}$ should be at most of $\mathcal{O}(10^{-2})$, unless one pushes SUSY masses up to $\mathcal{O}(1 \text{ TeV})$.

In view of the previous considerations, most authors dealing with the CMSSM prefer to simply put Φ_A and Φ_B equal to zero. Actually, one may argue in favor of this choice by considering the soft breaking sector of the MSSM as resulting from SUSY breaking mechanisms which force Φ_A and Φ_B to vanish. For instance, it is conceivable that both A and M originate from the same source of $U(1)_R$ breaking. Since Φ_A "measures" the relative phase of A and M, in this case, it would "naturally" vanish. In some specific models, it has been shown [40] that through an analogous mechanism also Φ_B may vanish.

If $\Phi_A = \Phi_B = 0$, then the novelty of the CMSSM in CP-violating contributions merely arises from the presence of the CKM phase in loops with SUSY particles [89, 91–96]. The crucial point is that the usual GIM suppression, which plays a major role in evaluating ε and ε' in the SM, is replaced in the MSSM case by a super-GIM cancellation, which has the same "power" of suppression as the original GIM (see previous section). Again also in the MSSM, as it is the case in the SM, the smallness of ε and ε' is guaranteed not by the smallness of δ_{CKM} but rather by the small CKM angles and/or small Yukawa couplings. By the same token, we do not expect any significant departure of the MSSM from the SM predictions also concerning CP violation in B physics. As a matter of fact, given the large lower bounds on squark and gluino masses, one expects relatively tiny contributions of the SUSY loops in ε or ε' in comparison with the normal W loops of the SM. Let us be more

detailed on this point. In the MSSM, the gluino exchange contribution to FCNC is subleading with respect to chargino ($\chi^\pm$) and charged Higgs ($H^\pm$) exchanges. Hence, when dealing with CP-violating FCNC processes in the MSSM with $\Phi_A = \Phi_B = 0$, one can confine the analysis to $\chi^\pm$ and $H^\pm$ loops. If one takes all squarks to be degenerate in mass and heavier than ~ 200 GeV, then $\chi^\pm$–$\tilde{q}$ loops are obviously severely penalized with respect to the SM W–q loops (remember that at the vertices, the same CKM angles occur in both cases). The only chance to generate sizable contributions to CP-violating phenomena is for a light stop and chargino: in this case, sizable departures from the SM predictions are possible [86].

In conclusion, the situation concerning CP violation in the MSSM case with $\Phi_A = \Phi_B = 0$ and exact universality in the soft-breaking sector can be summarized in the following way: the MSSM does not lead to any significant deviation from the SM expectation for CP-violating phenomena as d_N^e, ε, ε' and CP violation in B physics; the only exception to this statement concerns a small portion of the MSSM parameter space where a very light $\tilde{t}$ and χ^+ are present.

1.3.5 Model-independent analysis of FCNC and CP violating processes in SUSY

Given a specific SUSY model, it is in principle possible to make a full computation of all the FCNC phenomena in that context. However, given the variety of options for low-energy SUSY which was mentioned above (even confining ourselves here to models with R matter parity), it is important to have a way to extract from the whole host of FCNC processes a set of upper limits on quantities that can be readily computed in any chosen SUSY frame.

A useful model-independent parameterization of FCNC effects is the so-called mass insertion (MI) approximation [97]. It concerns the most peculiar source of FCNC SUSY contributions that do not arise from the mere supersymmetrization of the FCNC in the SM. They originate from the FC couplings of gluinos and neutralinos to fermions and sfermions [98–100]. One chooses a basis for the fermion and sfermion states where all the couplings of these particles to neutral gauginos are flavor diagonal, while the FC is exhibited by the nondiagonality of the sfermion propagators. Denoting by Δ the off-diagonal terms in the sfermion mass matrices (i.e. the mass terms relating sfermions of the same electric charge but different flavor), the sfermion propagators can be expanded as a series in terms of $\delta = \Delta/\tilde{m}^2$, where $\tilde{m}$ is the average sfermion mass. As long as Δ is significantly smaller than $\tilde{m}^2$, we can just take the first term of this expansion, and then the experimental information concerning FCNC and CP-violating phenomena translates into upper bounds on these δ's [101–104].

Obviously the above mass insertion method presents the major advantage that one does not need the full diagonalization of the sfermion mass matrices to perform a test of the SUSY model under consideration in the FCNC sector. It is enough to compute ratios of the off-diagonal over the diagonal entries of the sfermion mass matrices and compare the results with the general bounds on the δ's that we provide here from all available experimental information.

There exist four different Δ mass insertions connecting flavors i and j along a sfermion propagator: $(\Delta_{ij})_{LL}$, $(\Delta_{ij})_{RR}$, $(\Delta_{ij})_{LR}$ and $(\Delta_{ij})_{RL}$. The indices L and R refer to the helicity of the fermion partners. Instead of the dimensionful quantities Δ, it is more useful to provide bounds making use of dimensionless quantities, δ, that are obtained dividing the mass insertions by an average sfermion mass.

The comparison of several flavor-changing processes to their experimental values can be used to bound the δ's in the different sectors [104–116]. In these analyses, it is customary to consider only the dominant contributions due to gluino exchange, which give a good approximation of the full amplitude, barring accidental cancellations. In the same spirit, the bounds are usually obtained taking only one nonvanishing MI at a time, neglecting the interference among MIs. This procedure is justified a posteriori by observing that the MI bounds have typically a strong hierarchy, making the destructive interference among different MIs very unlikely.

The effective Hamiltonians for $\Delta F = 1$ and $\Delta F = 2$ transitions including gluino contributions computed in the MI approximation can be found in the literature together with the formulae of several observables [104]. Even the full NLO calculation is available for the $\Delta F = 2$ effective Hamiltonian [117, 118]. See Refs. [111–113] for the calculation of $\tan\beta$-enhanced subleading terms for several B decays in the case of general flavor violation.

In our study, we use the phenomenological constraints collected in Table 2. In particular:

Sector 1–2 The measurements of ΔM_K, ε and ε'/ε are used to constrain the $(\delta_{12}^d)_{AB}$ with $(A, B) = (L, R)$. The first two measurements, ΔM_K and ε, respectively bound the real and imaginary parts of the product $(\delta_{12}^d)(\delta_{12}^d)$. In the case of ΔM_K, given the uncertainty coming from the long-distance contribution, we use the conservative range in Table 2. The measurement of ε'/ε, on the other hand, puts a bound on $\mathrm{Im}(\delta_{12}^d)$. This bound, however, is effective in the case of the LR MI only. Notice that, given the large hadronic uncertainties in the SM calculation of ε'/ε, we use the very loose bound on the SUSY contribution shown in Table 2. The bounds coming from the combined constraints are shown in Table 3. Notice that, here and in the other sectors, the bound on the RR MI is obtained in the presence of the radiatively-induced LL MI (see (11)). The product $(\delta_{12}^d)_{LL}(\delta_{12}^d)_{RR}$ generates left–right operators that

Table 2 Measurements and bounds used to constrain the hadronic δ^d's

Observable	Measurement/Bound	Ref.
Sector 1–2		
ΔM_K	$(0.0\text{–}5.3) \times 10^{-3}$ GeV	[119]
ε	$(2.232 \pm 0.007) \times 10^{-3}$	[119]
$|(\varepsilon'/\varepsilon)_{\mathrm{SUSY}}|$	$<2 \times 10^{-2}$	–
Sector 1–3		
ΔM_{B_d}	(0.507 ± 0.005) ps^{-1}	[389]
$\sin 2\beta$	0.675 ± 0.026	[389]
$\cos 2\beta$	> -0.4	[120]
Sector 2–3		
$BR(b \to (s+d)\gamma)(E_\gamma > 2.0 \text{ GeV})$	$(3.06 \pm 0.49) \times 10^{-4}$	[121]
$BR(b \to (s+d)\gamma)(E_\gamma > 1.8 \text{ GeV})$	$(3.51 \pm 0.43) \times 10^{-4}$	[122]
$BR(b \to s\gamma)(E_\gamma > 1.9 \text{ GeV})$	$(3.34 \pm 0.18 \pm 0.48) \times 10^{-4}$	[123]
$A_{\mathrm{CP}}(b \to s\gamma)$	0.004 ± 0.036	
$BR(b \to sl^+l^-)(0.04 \text{ GeV} < q^2 < 1 \text{ GeV})$	$(11.34 \pm 5.96) \times 10^{-7}$	[124, 125]
$BR(b \to sl^+l^-)(1 \text{ GeV} < q^2 < 6 \text{ GeV})$	$(15.9 \pm 4.9) \times 10^{-7}$	[124, 125]
$BR(b \to sl^+l^-)(14.4 \text{ GeV} < q^2 < 25 \text{ GeV})$	$(4.34 \pm 1.15) \times 10^{-7}$	[124, 125]
$A_{\mathrm{CP}}(b \to sl^+l^-)$	-0.22 ± 0.26	[119]
ΔM_{B_s}	(17.77 ± 0.12) ps^{-1}	[126]

Table 3 95% probability bounds on $|(\delta_{ij}^q)_{AB}|$ obtained for squark and gluino masses of 350 GeV. See the text for details

$|(\delta_{12}^d)_{LL,RR}|$	$|(\delta_{12}^d)_{LL=RR}|$	$|(\delta_{12}^d)_{LR}|$	$|(\delta_{12}^d)_{RL}|$
1×10^{-2}	2×10^{-4}	5×10^{-4}	5×10^{-4}
$|(\delta_{12}^u)_{LL,RR}|$	$|(\delta_{12}^u)_{LL=RR}|$	$|(\delta_{12}^u)_{LR}|$	$|(\delta_{12}^u)_{RL}|$
3×10^{-2}	2×10^{-3}	6×10^{-3}	6×10^{-3}
$|(\delta_{13}^d)_{LL,RR}|$	$|(\delta_{13}^d)_{LL=RR}|$	$|(\delta_{13}^d)_{LR}|$	$|(\delta_{13}^d)_{RL}|$
7×10^{-2}	5×10^{-3}	1×10^{-2}	1×10^{-2}
$|(\delta_{23}^d)_{LL}|$	$|(\delta_{23}^d)_{RR}|$	$|(\delta_{23}^d)_{LL=RR}|$	$|(\delta_{23}^d)_{LR,RL}|$
2×10^{-1}	7×10^{-1}	5×10^{-2}	5×10^{-3}

are enhanced both by the QCD evolution and by the matrix element (for kaons only). Therefore, the bounds on RR MIs are more stringent than the ones on LL MIs.

Sector 1–3 The measurements of ΔM_{B_d} and 2β respectively constrain the modulus and the phase of the mixing amplitude bounding the products $(\delta_{13}^d)(\delta_{13}^d)$. For the sake of simplicity, in Table 3, we show the bounds on the modulus of (δ_{13}^d) only.

Sector 2–3 This sector enjoys the largest number of constraints. The recent measurement of ΔM_{B_s} constrains the modulus of the mixing amplitude, thus bounding the products $|(\delta_{23}^d)(\delta_{23}^d)|$. Additional strong constraints come from $\Delta B = 1$ branching ratios, such as $b \to s\gamma$ and $b \to sl^+l^-$. Also for this sector, we present the bounds on the modulus of (δ_{23}^d) in Table 3.

All the bounds in Table 3 have been obtained by using the NLO expressions for the SM contributions and for SUSY where available. Hadronic matrix elements of $\Delta F = 2$ operators are taken from lattice calculations [127–130]. The values of the CKM parameters $\bar\rho$ and $\bar\eta$ are taken from the UTfit analysis in the presence of arbitrary loop-mediated NP contributions [7]. This conservative choice allows us to decouple the determination of SUSY parameters from the CKM matrix. For $b \to s\gamma$, we use NLO expressions with the value of the charm quark mass suggested by the recent NNLO calculation [376]. For the chromomagnetic contribution to ε'/ε, we have used the matrix element as estimated in Ref. [131]. The 95% probability bounds are computed using the statistical method described in Refs. [107, 132].

Concerning the dependence on the SUSY parameters, the bounds mainly depend on the gluino mass and on the "average squark mass". A mild dependence on $\tan\beta$ is introduced by the presence of double MIs $(\delta_{ij}^d)_{LL}(\delta_{jj}^d)_{LR}$ in chromomagnetic operators. This dependence however becomes siz-

able only for very large values of $\tan\beta$. Approximately, all bounds scale as squark and gluino masses.

1.4 Nonsupersymmetric extensions of the Standard Model

In this section, we briefly describe two most popular non-supersymmetric extensions of the SM, paying particular attention to the flavor structure of these models. These are Little Higgs models and a model with one universal extra dimension.

1.4.1 Little Higgs models

1.4.1.1 Little hierarchy problem and Little Higgs models The SM is in excellent agreement with the results of particle physics experiments, in particular with the electroweak (EW) precision measurements, thus suggesting that the SM cutoff scale is at least as large as 10 TeV. Having such a relatively high cutoff, however, the SM requires an unsatisfactory fine-tuning to yield a correct ($\approx 10^2$ GeV) scale for the squared Higgs mass, whose corrections are quadratic and therefore highly sensitive to the cutoff. This "little hierarchy problem" has been one of the main motivations to elaborate models of physics beyond the SM. While Supersymmetry is at present the leading candidate, different proposals have been formulated more recently. Among them, Little Higgs models play an important role, being perturbatively computable up to about 10 TeV and with a rather small number of parameters, although their predictivity can be weakened by a certain sensitivity to the unknown UV-completion of these models (see below).

In Little Higgs models [133], the Higgs is naturally light as it is identified with a Nambu–Goldstone boson (NGB) of a spontaneously broken global symmetry. An exact NGB, however, would have only derivative interactions. Gauge and Yukawa interactions of the Higgs have to be incorporated. This can be done without generating quadratically divergent one-loop contributions to the Higgs mass, through the so-called *collective symmetry breaking*.

In the following, we restrict ourselves to product-group Little Higgs models in order not to complicate the presentation. The idea of collective symmetry breaking has also been applied to simple-group models [134, 135], however the implementation is somewhat different there. (Product-group) Little Higgs models are based on a global symmetry group G, like $G = G'^N$ in the case of moose-type models [133, 136] or $G = SU(5)$ in the case of the Littlest Higgs, that is spontaneously broken to a subgroup $H \subset G$ by the vacuum condensate of a nonlinear sigma model field Σ. A subgroup of G is gauged, which contains at least two $SU(2) \times U(1)$ factors or larger groups containing such factors. The gauge group is then broken to the SM gauge group $SU(2)_L \times U(1)_Y$ by the vacuum expectation value (vev)

of Σ. The potential for the Higgs field is generated radiatively, making thus the scale of the EW symmetry breaking $v \simeq 246$ GeV a loop factor smaller than the scale f, where the breaking $G \to H$ takes place.

In order to allow for a Higgs potential being generated radiatively, interaction terms explicitly breaking the global symmetry group G have to be included as well. However, these interactions have to preserve enough of the global symmetry to prevent the Higgs potential from quadratically divergent radiative contributions. Only when two or more of the corresponding coupling constants are nonvanishing, radiative corrections are allowed. In particular, only at two or higher loop level, quadratically divergent contributions appear, but these are safely small due to the loop factor in front. This mechanism is referred to as the collective symmetry breaking.

1.4.1.2 The Littlest Higgs The most economical, in matter content, Little Higgs model is the Littlest Higgs (LH) [137], where the global group $SU(5)$ is spontaneously broken into $SO(5)$ at the scale $f \approx \mathcal{O}(1$ TeV$)$ and the EW sector of the SM is embedded in an $SU(5)/SO(5)$ nonlinear sigma model. Gauge and Yukawa Higgs interactions are introduced by gauging the subgroup of $SU(5)$: $[SU(2) \times U(1)]_1 \times [SU(2) \times U(1)]_2$, with gauge couplings respectively equal to g_1, g'_1, g_2, g'_2. The key feature for the realization of collective SB is that the two gauge factors commute with a different $SU(3)$ global symmetry subgroup of $SU(5)$, which prevents the Higgs from becoming massive when the couplings of one of the two gauge factors vanish. Consequently, quadratic corrections to the squared Higgs mass involve two couplings and cannot appear at one-loop. In the LH model, the new particles appearing at the TeV scale are the heavy gauge bosons ($W_H^\pm, Z_H, A_H$), the heavy top (T) and the scalar triplet Φ.

In the LH model, significant corrections to EW observables come from tree-level heavy gauge boson contributions and the triplet vev which breaks the custodial $SU(2)$ symmetry. Consequently, EW precision tests are satisfied only for quite large values of the NP scale $f \geq (2–3)$ TeV [138, 139] that are unable to solve the little hierarchy problem. Since the LH model belongs to the class of models with Constrained Minimal Flavor Violation (CMFV) [12], the contributions of the new particles to FCNC processes turn out to be at most (10–20)% [140–146].

1.4.1.3 T-parity Motivated by reconciling the LH model with EW precision tests, Cheng and Low [147, 148] proposed to enlarge the symmetry structure of the theory by introducing a discrete symmetry called T-parity. T-parity acts as an automorphism which exchanges the $[SU(2) \times U(1)]_1$ and $[SU(2) \times U(1)]_2$ gauge factors. The invariance of the theory under this automorphism implies $g_1 = g_2$ and $g'_1 =$

326

Eur. Phys. J. C (2008) 57: 309–492

g_2'. Furthermore, T-parity explicitly forbids the tree-level contributions of heavy gauge bosons and the interactions that induced the triplet vev. The custodial $SU(2)$ symmetry is restored and the compatibility with ew precision data is obtained already for smaller values of the NP scale, $f \geq 500$ GeV [149]. Another important consequence is that particle fields are T-even or T-odd under T-parity. The SM particles and the heavy top T_+ are T-even, while the heavy gauge bosons $W_H^\pm$, Z_H, A_H and the scalar triplet Φ are T-odd. Additional T-odd particles are required by T-parity: the odd heavy top T_- and the so-called mirror fermions, i.e., fermions corresponding to the SM ones but with opposite T-parity and $\mathcal{O}(1$ TeV) mass [150].

1.4.1.4 New flavor interactions in LHT Mirror fermions are characterized by new flavor interactions with SM fermions and heavy gauge bosons, which involve two new unitary mixing matrices, in the quark sector, analogous to the CKM matrix V_{CKM} [151, 152]. They are V_{Hd} and V_{Hu}, respectively involved when the SM quark is of down- or up-type, and satisfying $V_{Hu}^\dagger V_{Hd} = V_{CKM}$ [153]. Similarly, two new mixing matrices $V_{H\ell}$ and $V_{H\nu}$ appear in the lepton sector and are respectively involved when the SM lepton is charged or a neutrino and related to the PMNS matrix [154–156] through $V_{H\nu}^\dagger V_{H\ell} = V_{PMNS}^\dagger$. Both V_{Hd} and $V_{H\ell}$ contain 3 angles, like V_{CKM} and V_{PMNS}, but 3 (non-Majorana) phases [157], i.e. two more phases than the SM matrices, that cannot be rotated away in this case.

Therefore, V_{Hd} can be parameterized as

As the LHT model, in contrast to the LH model without T-parity, does not belong to the Minimal Flavor Violation (MFV) class of models, significant effects in flavor-violating observables both in the quark and in the lepton sector are possible. This becomes evident if one looks at the contributions of mirror fermions to the short distance functions X, Y and Z that govern rare and CP-violating K and B decays. For example, the mirror fermion contribution to be added to the SM one in the X function has the following structure [158]:

$$\frac{1}{\lambda_t^{(i)}}\left[\xi_2^{(i)} F(m_{H1}, m_{H2}) + \xi_3^{(i)} F(m_{H1}, m_{H3})\right], \qquad (25)$$

where the unitarity condition $\sum_{j=1}^3 \xi_j^{(i)} = 0$ has been used, F denotes a function of mirror fermion masses m_{Hj} ($j = 1, 2, 3$), and $\lambda_t^{(i)}$ are the well-known combinations of CKM elements with $i = K, d, s$ standing for K, B_d and B_s systems, respectively.

It is important to note that mirror fermion contributions are enhanced by a factor $1/\lambda_t^{(i)}$ and are different for K, B_d and B_s systems, thus breaking universality. As $\lambda_t^{(K)} \simeq 4 \times 10^{-4}$, whereas $\lambda_t^{(d)} \simeq 1 \times 10^{-2}$ and $\lambda_t^{(s)} \simeq 4 \times 10^{-2}$, the deviation from the SM prediction in the K system is found to be by more than an order of magnitude larger than in the B_d system and even by two orders of magnitude larger than in the B_s system. Analogous statements are valid for the Y and Z functions.

$$V_{Hd} = \begin{pmatrix} c_{12}^d c_{13}^d & s_{12}^d c_{13}^d e^{-i\delta_{12}^d} & s_{13}^d e^{-i\delta_{13}^d} \\ -s_{12}^d c_{23}^d e^{i\delta_{12}^d} - c_{12}^d s_{23}^d s_{13}^d e^{i(\delta_{13}^d - \delta_{23}^d)} & c_{12}^d c_{23}^d - s_{12}^d s_{23}^d s_{13}^d e^{i(\delta_{13}^d - \delta_{12}^d - \delta_{23}^d)} & s_{23}^d c_{13}^d e^{-i\delta_{23}^d} \\ s_{12}^d s_{23}^d e^{i(\delta_{12}^d + \delta_{23}^d)} - c_{12}^d c_{23}^d s_{13}^d e^{i\delta_{13}^d} & -c_{12}^d s_{23}^d e^{i\delta_{23}^d} - s_{12}^d c_{23}^d s_{13}^d e^{i(\delta_{13}^d - \delta_{12}^d)} & c_{23}^d c_{13}^d \end{pmatrix}, \qquad (22)$$

and a similar parameterization applies to $V_{H\ell}$.

The new flavor violating interactions involving mirror fermions contain the following combinations of elements of the mixing matrices:

$$\xi_i^{(K)} = V_{Hd}^{*is} V_{Hd}^{id}, \qquad \xi_i^{(d)} = V_{Hd}^{*ib} V_{Hd}^{id},$$
$$\xi_i^{(s)} = V_{Hd}^{*ib} V_{Hd}^{is} \quad (i = 1, 2, 3) \qquad (23)$$

in the quark sector, respectively for K, B_d and B_s systems, and

$$\chi_i^{(\mu e)} = V_{H\ell}^{*ie} V_{H\ell}^{i\mu}, \qquad \chi_i^{(\tau e)} = V_{H\ell}^{*ie} V_{H\ell}^{i\tau},$$
$$\chi_i^{(\tau \mu)} = V_{H\ell}^{*i\mu} V_{H\ell}^{i\tau} \qquad (24)$$

that enter the leptonic transitions $\mu \to e$, $\tau \to e$ and $\tau \to \mu$, respectively.

Other LHT peculiarities are the rather small number of new particles and parameters (the SB scale f, the parameter x_L describing T_+ mass and interactions, the mirror fermion masses and V_{Hd} and $V_{H\ell}$ parameters) and the absence of new operators in addition to the SM ones. On the other hand, one has to recall that Little Higgs models are low-energy nonlinear sigma models whose unknown UV-completion introduces a theoretical uncertainty reflected by a logarithmically enhanced cut-off dependence [142, 158] in $\Delta F = 1$ processes that receive contributions from Z-penguin and box diagrams. See [142, 158] for a detailed discussion of this issue.

1.4.1.5 Phenomenological results We conclude this section with a summary of the main results found in recent LHT phenomenological studies [153, 158–161].

In the quark sector [153, 158, 159], the most evident departures from the SM predictions are found for CP-violating observables that are strongly suppressed in the SM. These are the branching ratio for $K_L \rightarrow \pi^0 \nu \bar{\nu}$ and the CP-asymmetry $S_{\psi\phi}$ that can be enhanced by an order of magnitude relative to the SM predictions. Large departures from SM expectations are also possible for $Br(K_L \rightarrow \pi^0 \ell^+ \ell^-)$ and $Br(K^+ \rightarrow \pi^+ \nu \bar{\nu})$ and the semileptonic CP-asymmetry A_{SL}^s that can be enhanced by an order of magnitude. The branching ratios for $B_{s,d} \rightarrow \mu^+ \mu^-$ and $B \rightarrow X_{s,d} \nu \bar{\nu}$, instead, are modified by at most 50% and 35%, respectively, and the effects of new electroweak penguins in $B \rightarrow \pi K$ are small, in agreement with the recent data. The new physics effects in $B \rightarrow X_{s,d} \gamma$ and $B \rightarrow X_{s,d} \ell^+ \ell^-$ turn out to be below 5% and 15%, respectively, so that agreement with the data can easily be obtained. Small but still significant effects have been found in $B_{s,d}$ mass differences. In particular, a 7% suppression of ΔM_s is possible, thus improving the compatibility with the recent experimental measurement [126, 162].

The possible discrepancy between the values of $\sin 2\beta$ following directly from $A_{\mathrm{CP}}(B_d \rightarrow \psi K_S)$ and indirectly from the usual analysis of the unitarity triangle involving $\Delta M_{d,s}$ and $|V_{ub}/V_{cb}|$ can be cured within the LHT model thanks to a new phase $\varphi_{B_d} \simeq -5°$.

The universality of NP effects, characteristic for MFV models, can be largely broken, in particular between K and $B_{s,d}$ systems. In particular, sizable departures from MFV relations between $\Delta M_{s,d}$ and $Br(B_{s,d} \rightarrow \mu^+ \mu^-)$ and between $S_{\psi K_S}$ and the $K \rightarrow \pi \nu \bar{\nu}$ decay rates are possible. Similar results have been recently obtained in a model with Z'-contributions [163].

More recently, the most interesting lepton flavor violating decays have also been studied [160, 161]. These are $\ell_i \rightarrow \ell_j \gamma$ analysed in [160, 161], and $\tau \rightarrow \mu P$ (with $P = \pi, \eta, \eta'$), $\mu^- \rightarrow e^- e^+ e^-$, the six three-body decays $\tau^- \rightarrow \ell_i^- \ell_j^+ \ell_k^-$, the rate for μ–e conversion in nuclei, and the K or B decays $K_{L,S} \rightarrow \mu e$, $K_{L,S} \rightarrow \pi^0 \mu e$, $B_{d,s} \rightarrow \mu e$, $B_{d,s} \rightarrow \tau e$ and $B_{d,s} \rightarrow \tau \mu$ are studied in [161]. It was found that essentially all the rates considered can reach or approach present experimental upper bounds [164]. In particular, in order to suppress the $\mu \rightarrow e \gamma$ and $\mu^- \rightarrow e^- e^+ e^-$ decay rates and the μ–e conversion rate below the experimental upper bounds, the $V_{H\ell}$ mixing matrix has to be rather hierarchical, unless mirror leptons are quasi-degenerate. One finds [161] that the pattern of the branching ratios for LFV processes differs significantly from the one encountered in supersymmetry [165–167]. This is welcome as the distinction between supersymmetry and LHT models will be nontrivial in high-energy collider experiments. Finally, the muon anomalous magnetic moment $(g-2)_\mu$ has also been considered [160, 161], finding the result $a_\mu^{\mathrm{LHT}} < 1.2 \times 10^{-10}$, even for the scale f as low as 500 GeV. This

value is roughly a factor 5 below the current experimental uncertainty, implying that the possible discrepancy between the SM prediction and the data cannot be solved in the LHT model.

1.4.2 Universal extra dimensions

Since the work of Kaluza and Klein [168, 169] models with more than three spatial dimensions often have been used to unify the forces of nature. More recently, inspired by string theory, extra-dimensional models have been proposed to explain the origin of the TeV scale [170–179].

A simple extension of the SM including additional space dimensions is the ACD model [180] with one universal extra dimension (UED). Here all the SM fields are democratically allowed to propagate in a flat extra dimension compactified on an orbifold S^1/Z_2 of size 10^{-18} m or smaller. In general UED models, there can also be contributions from terms residing at the boundaries. Generically, these terms would violate bounds from flavor and CP violation. To be consistent with experiment, we will assume the minimal scenario where these terms vanish at the cut-off scale. The only additional free parameter then compared to the SM is the compactification scale $1/R$. Thus, all the tree level masses of the KK particles and their interactions among themselves and with the SM particles can be described in terms of $1/R$ and the parameters of the SM. In the effective four-dimensional theory, there are, in addition to the ordinary SM particles, denoted as zero ($n = 0$) modes, corresponding infinite towers of KK modes ($n \geq 1$) with masses $m_{(n),\mathrm{KK}}^2 = m_0^2 + m_n^2$, where $m_n = n/R$, and m_0 is the mass of the zero mode.

A very important property of UEDs is the conservation of KK parity that implies the absence of tree level KK contributions to low-energy processes taking place at scales $\mu \leq 1/R$. Therefore the flavor-changing neutral current (FCNC) processes like particle–anti-particle mixing, rare K and B decays and radiative decays are of particular interest. Since these processes first appear at one-loop in the SM and are strongly suppressed, the one-loop contributions from the KK modes to them could in principle be important. Also, due to conservation of KK parity, the GIM mechanism significantly improves the convergence of the sum over KK modes and thus removes the sensitivity of the calculated branching ratios to the scale $M_s \gg 1/R$ at which the higher-dimensional theory becomes nonperturbative and at which the towers of the KK particles must be cut off in an appropriate way. Since the low-energy effective Hamiltonians are governed by local operators already present in the SM and the flavor and CP violation in this model is entirely governed by the SM Yukawas, the UED model belongs to the class of models with CMFV [10, 12]. This has automatically the following important consequence for the FCNC processes considered in [17, 181–183]: the impact of the KK modes on the

328

Eur. Phys. J. C (2008) 57: 309–492

processes in question amounts only to the modification of the Inami–Lim one-loop functions [184], i.e. each function which in the SM depends only on m_t now also becomes a function of $1/R$:

$$F(x_t, 1/R) = F_0(x_t) + \sum_{n=1}^{\infty} F_n(x_t, x_n),$$

$$x_t = \frac{m_t^2}{m_W^2}, \ x_n = \frac{m_n^2}{m_W^2}. \tag{26}$$

1.5 Tools for flavor physics and beyond

1.5.1 Tools for flavor physics

An increasing number of calculations of flavor (related) observables is appearing, including more and more refined approaches and methods. It is desirable to have these calculations in the form of computer codes at hand. This allows us to easily use the existing knowledge for checks of the parameters/models for a phenomenological/experimental analysis or to check an independent calculation.

As a first step in this direction, we present here a collection of computer codes connected to the evaluation of flavor related observables. (A different class of codes, namely fit codes for the CKM triangle, are presented later in Sect. 1.5.3.) Some of these codes are specialized to the evaluation of a certain restricted set of observables at either low or high energies (the inclusion of codes for high-energy observables is motivated by the idea of testing a parameter space from both sides, i.e. at flavor factories and at the LHC). Others tools are devoted to the evaluation of particle spectra including NMFV effects of the MSSM or the 2HDM. Some codes allow the (essentially) arbitrary calculation of one-loop corrections including flavor effects. Finally tools are included that facilitate the hand-over of flavor

parameters and observables. Following the general idea of providing the existing knowledge to the community, only codes that either are already publicly available or will become available in the near future are included. In order to be useful for the high-energy physics community, it is mandatory that the codes provide a minimum of user friendliness and support.

As a second step, it would be desirable to connect different codes (working in the same model) to each other. This could go along the lines of the SUSY Les Houches Accord [185, 186], i.e. to define a common language, a common set of input parameters. It would require the continuous effort of the various authors of the codes to comply with these definitions. Another, possibly simpler approach is to implement the tools as sub-routines, called by a master code that takes care of the correct definition of the input parameters. This is discussed in more detail in Sect. 1.5.2. It will facilitate the use of the codes also for nonexperts.

An overview of the available codes is given in Table 4. To give a better idea of the properties of each code, we also provide a list summarizing the authors, a short description, the models included, the input and output options, as well as the available literature:

1. no name

   Authors: M. Ciuchini et al. [107, 116, 187]
   Description: calculation of K–$\bar{K}$ mixing, $B_{(s)}$–$\bar{B}_{(s)}$ mixing, $b \to s\gamma$, $b \to sl^+l^-$
   Models: NMFV MSSM
   Input: electroweak-scale soft SUSY-breaking parameters
   Output: see Description, no special format
   Availability: available from the authors in the near future

Table 4 Overview about codes for the evaluation of flavor related observables; av. $\equiv$ availability: $+$ = available, o = planned

Name	Short description	av.
1. no name	K–$\bar{K}$ mixing, $B_{(s)}$–$\bar{B}_{(s)}$ mixing, $b \to s\gamma$, $b \to sl^+l^-$ in NMFV MSSM	o
2. no name	B physics observables in the MFV MSSM	$+$
3. no name	rare B and K decays in/beyond SM	o
4. SusyBSG	$B \to X_s\gamma$ in MSSM with MFV	$+$
5. no name	FCNC observables in MSSM	o
6. no name	FC Higgs/top decays in 2HDM I/II	o
7. no name	squark/gluino production at LO for NMFV MSSM	$+$
8. FeynHiggs	Higgs phenomenology in (NMFV) MSSM	$+$
9. FCHDECAY	FCNC Higgs decays in NMFV MSSM	$+$
10. FeynArts/FormCalc	(arbitrary) one-loop corrections in NMFV MSSM	$+$
11. SLHALib2	read/write SLHA2 data, i.e. NMFV/RPV/CPV MSSM, NMSSM	$+$
12. SoftSUSY	NMFV MSSM parameters from GUT scale input	$+$
13. SPheno	NMFV MSSM parameters from GUT scale input	$+$

2. no name

   Authors: G. Isidori, P. Paradisi [32]
   Description: calculation of *B*-physics observables
   Models: MFV MSSM
   Input: electroweak-scale soft SUSY-breaking parameters
   Output: see Description, no special format
   Availability: available from the authors upon request

3. no name

   Authors: C. Bobeth, T. Ewerth, U. Haisch [188–190]
   Description: calculation of BR's, F/B asymmetries for rare *B* and *K* decays (in/exclusive)
   Models: SM, SUSY, CMFV
   Input: SM parameters, SUSY masses, scales
   Output: see Description, no special format
   Availability: available from the authors in the near future

4. SusyBSG

   Authors: G. Degrassi, P. Gambino, P. Slavich [191]
   Description: Fortran code for $B(B \rightarrow X_s \gamma)$
   Models: SM, MSSM with MFV
   Input: see manual (SLHA(2) compatible)
   Output: see Description, no special format
   Availability: cern.ch/slavich/susybsg/home.html, manual available

5. no name

   Authors: P. Chankowski, S. Jäger, J. Rosiek [192]
   Description: calculation of various FCNC observables in the MSSM (computes 2-, 3-, 4-point Greens functions that can be used as building blocks for various amplitudes)
   Models: MSSM
   Input: MSSM Lagrangian parameters in super CKM basis (as in SLHA2)
   Output: see Description, no special format
   Availability: available from the authors in the near future

6. no name

   Authors: S. Bejar, J. Guasch [193–195]
   Description: calculation of FC decays: $\phi \rightarrow tc$, $\phi \rightarrow bs$, $t \rightarrow c\phi$ ($\phi = h, H, A$)
   Models: 2HDM type I/II (with λ_5, λ_6)
   Input: similar to SLHA2 format
   Output: similar to SLHA2 format
   Availability: available from the authors in the near future

7. no name

   Authors: G. Bozzi, B. Fuks, M. Klasen
   Description: SUSY CKM matrix determination through squark- and gaugino production at LO
   Models: NMFV MSSM

   Input: MSSM spectrum as from SUSPECT (SLHA2 compliant)
   Output: cross section (and spin asymmetry, in case) as functions of CKM parameters
   Availability: from the authors upon request

8. FeynHiggs

   Authors: S. Heinemeyer, T. Hahn, W. Hollik, H. Rzehak, G. Weiglein [199–201]
   Description: Higgs phenomenology (masses, mixings, cross sections, decay widths)
   Models: (N)MFV MSSM, CPV MSSM
   Input: electroweak-scale soft SUSY-breaking parameters (SLHA(2) compatible)
   Output: Higgs masses, mixings, cross sections, decay widths (SLHA(2) output possible)
   Availability: www.feynhiggs.de, manual available

9. FCHDECAY

   Authors: S. Bejar, J. Guasch [196–198]
   Description: $BR(\phi \rightarrow bs, tc)$ ($\phi = h, H, A$), $BR(b \rightarrow s\gamma)$, masses, mixing matrices
   Models: NMFV MSSM
   Input: via SLHA2
   Output: via SLHA2
   Availability: fchdecay.googlepages.com, manual available

10. FeynArts/FormCalc

    Authors: T. Hahn [202–204]
    Description: Compute (essentially) arbitrary one-loop corrections
    Models: NMFV MSSM, CPV MSSM
    Input: Process definition
    Output: Fortran code to compute e.g. cross-sections can be linked with SLHALib2 to obtain data from other codes
    Availability: www.feynarts.de, www.feynarts.de/formcalc, manual available

11. SLHALib2

    Authors: T. Hahn [185, 205]
    Description: read/write SLHA2 data
    Models: NMFV MSSM, RPV MSSM, CPV MSSM, NMSSM
    Input: SLHA2 input file
    Output: SLHA2 output file in the SLHA2 record
    Availability: www.feynarts.de/slha, manual available

12. SoftSUSY

    Authors: B. Allanach [206]
    Description: evaluates NMFV MSSM parameters from GUT scale input

330

Eur. Phys. J. C (2008) 57: 309–492

Models: NMFV MSSM
Input: SLHA2 input file
Output: SLHA2 output file
Availability: hepforge.cedar.ac.uk/softsusy, manual available

13. `Spheno`

Authors: W. Porod [207]
Description: evaluates NMFV MSSM parameters from GUT scale input and some flavor obs.
Models: NMFV MSSM
Input: SLHA2 input file
Output: SLHA2 output file
Availability: ific.uv.es/~porod/SPheno.html, manual available

1.5.2 Combination of flavor physics and high-energy tools

It is desirable to connect different codes (e.g. working in the (N)MFV MSSM, as given in the previous subsection) to each other. Especially interesting is the combination of codes that provide the evaluation of (low-energy) flavor observables and others that deal with high-energy (high p_T) calculations for the same set of parameters. This combination would allow one to test the ((N)MFV MSSM) parameter space with the results from flavor experiments as well as from high-energy experiments such as ATLAS or CMS.

A relatively simple approach for the combination of different codes is their implementation as sub-routines, called by a "master code". This master code takes care of the correct definition of the input parameters for the various subroutines. This would enable e.g. experimentalists to test whether the parameter space under investigation is in agreement with various existing experimental results from both flavor and high-energy experiments.

A first attempt to develop such a "master code" has recently been started [208]. So far the flavor physics code (2) [32] and the more high-energy observable oriented code `FeynHiggs` [199–201] have been implemented as subroutines. The inclusion of further codes is foreseen in the near future (see [1122] for the latest developments).

The application and use of the master code would change once experimental data showing a deviation from the SM predictions is available. This can come either from the ongoing flavor experiments or latest (hopefully) from ATLAS and CMS. If such a "signal" appears at the LHC, it has to be determined to which model and to which parameters within a model it can correspond. Instead of checking parameter points (to be investigated experimentally) for their agreement with experimental data, now a scan over a chosen model could be performed. Using the master code with its subroutines, each scan point can be tested against the "signal", and preferred parameter regions can be obtained using

a χ^2 evaluation. It is obvious that the number of evaluated observables has to be as large as possible, i.e. the number of subroutines (implemented codes) should be as large as possible.

1.5.3 Fit tools

The analysis of the CKM matrix or the Unitarity Triangle (UT) requires to combine several measurements in a consistent way in order to bound the range of relevant parameters.

1.5.3.1 The UTfit package The first approach derives bounds on the parameters $\bar{\rho}$ and $\bar{\eta}$ determining the UT. The various observables, in particular ϵ_K, which parameterizes CP violation in the neutral kaon sector, the sides of the UT $|V_{ub}/V_{cb}|$, Δm_d, $\Delta m_d/\Delta m_s$ and the angles β, α and γ can be expressed as functions of $\bar{\rho}$ and $\bar{\eta}$, hence their measurements individually define probability regions in the $(\bar{\rho}, \bar{\eta})$ plane. Their combination can be achieved in a theoretically sound way in the framework of the Bayesian approach [132].

Each of the functions relates a constraint c_j (where c_j stands for ε_K, $|V_{ub}/V_{cb}|$, etc.) to $\bar{\rho}$ and $\bar{\eta}$ via a set of parameters $\mathbf{x}$, where $\mathbf{x} = \{x_1, x_2, \ldots, x_N\}$ stands for all experimentally determined or theoretically calculated quantities on which the various c_j depend,

$$c_j = c_j(\bar{\rho}, \bar{\eta}; \mathbf{x}). \tag{27}$$

The quantities c_j and $\mathbf{x}$ are affected by several uncertainties, which must be properly taken into account. The final p.d.f. obtained starting from a flat distribution of $\bar{\rho}$ and $\bar{\eta}$ is

$$f(\bar{\rho}, \bar{\eta}) \propto \int \prod_{j=1,M} f_j(\hat{c}_j | \bar{\rho}, \bar{\eta}, \mathbf{x}) \prod_{i=1,N} f_i(x_i) \, dx_i. \tag{28}$$

The integration can be done by Monte Carlo methods. There are several ways to implement a Monte Carlo integration, using different techniques to generate events.

The UTfit Collaboration has developed a software package, written in C++, that implements such a Bayesian Monte Carlo approach with the aim of performing the UT analysis. A considerable effort has been spent in order to achieve an optimal Monte Carlo generation efficiency. All the recent analyses published by the Collaboration are based on this package [7, 120, 209–211].

The UTfit code includes an interface to import job options from a set of configuration files, an interface for storing the relevant p.d.f.s inside ROOT histograms [212], tools for generating input quantities, the p.d.f.s of which cannot be expressed in simple analytical form but must be numerically defined—e.g. the current measurements of α and γ—and tools for plotting one-dimensional p.d.f.s and two-dimensional probability regions in the $(\bar{\rho}, \bar{\eta})$ plane. The

UTfit code can be easily re-adapted to solve any kind of statistical problem that can be formalized in a Bayesian inferential framework.

1.5.3.2 The CKMFitter package Another, somewhat different approach is followed by CKMFitter, an international group of experimental and theoretical particle physicists. Its goal is the phenomenology of the CKM matrix by performing a global analysis:

- within the SM, by quantifying the agreement between the data and the theory as a whole;
- within the SM, by achieving the best estimate of the theoretical parameters and the not yet measured observables;
- within an extended theoretical framework, e.g. SUSY, by searching for specific signs of new physics by quantifying the agreement between the data and the extended theory and by pinning down additional fundamental and free parameters of the extended theory.

The CKMfitter package is entirely based on the frequentest approach. The theoretical uncertainties are modeled as allowed ranges (Rfit approach) and no other a priori information is assumed where none is available. More detailed information is provided in Ref. [8] and on the CKMfitter website [213].

The source code of the CKMfitter package consists of more than 40,000 lines of Fortran code and 2000 lines of C++ code. It is publicly available on the CKMfitter website. Over the years, the fit problems became more and more complex, and the CPU time consumption increased. The global fit took about 20 hours (on one CPU). A year ago, it was decided to move to Mathematica [gain: analytical vs. numerical methods]: the global fit takes now 12 minutes. For the plots, we moved also from PAW with kumac macros to ROOT.

2 Weak decays of hadrons and QCD[6]

2.1 Overview

QCD interactions, both at short and long distances, necessarily modify the amplitudes of quark flavor processes. These interactions need to be computed sufficiently well in order to determine the parameters and mechanisms of quark flavor physics from the weak decays of hadrons observed in experiment. The standard framework is provided by the effective weak Hamiltonians

$$\mathcal{H}_{\text{eff}} \sim \sum_i C_i Q_i, \tag{29}$$

---

[6]Section coordinator: G. Buchalla.

based on the operator product expansion and the renormalization group method. The Wilson coefficients C_i include all relevant physics from the highest scales, such as the weak scale M_W or some new physics scale, down to the appropriate scale of a given process, such as m_b for B-meson decays. This part is theoretically well under control. Theoretical uncertainties are dominated by the hadronic matrix elements of local operators Q_i. Considerable efforts are therefore devoted to calculate, estimate, eliminate or at least constrain such hadronic quantities in flavor physics applications.

This section reviews the current status of theoretical methods to treat the strong interaction dynamics in weak decays of flavored mesons, with a particular emphasis on B physics. Specific aspects of D-meson physics will be discussed in Sect. 3.9, kaons will be considered in Sect. 3.8.

The theory of charmless two-body B decays and the concept of factorization are reviewed in Sect. 2.2. The status of higher-order perturbative QCD calculations in this field is described. Universal properties of electromagnetic radiative effects in two-body B decays, which influence precision studies and isospin relations, are also discussed here. Factorization in the heavy-quark limit simplifies the matrix elements of two-body hadronic B decays considerably. In this framework, certain nonperturbative input quantities, for instance B-meson transition form factors, are in general still required. QCD sum rules on the light cone (LCSR) provide a means to compute heavy-to-light form factors at large recoil ($B \rightarrow \pi$, $B \rightarrow K^*$, etc.). The results have applications for two-body hadronic as well as rare and radiative B-meson decays. This subject is treated in Sect. 2.3. Complementary information can be obtained from lattice QCD, a general approach based on first principles, to compute nonperturbative parameters of interest to quark flavor physics. Decay constants and form factors (at small recoil) are among the most important quantities. Uncertainties arise from the limitations of the practical implementations of lattice QCD. A critical discussion of this topic and a summary of results can be found in Sect. 2.4.

2.2 Charmless two-body B decays

2.2.1 Exclusive decays and factorization

The calculation of branching fractions and CP asymmetries for charmless two-body B decays is rather involved, due to the interplay of various short- and long-distance QCD effects. Most importantly, the hadronic matrix elements of the relevant effective Hamiltonian $\mathcal{H}_{\text{eff}}^{\Delta B=1}$ [214] cannot readily be calculated from first principles. The idea of factorization is to disentangle short-distance QCD dynamics from genuinely nonperturbative hadronic effects. In order to quantify the hadronic uncertainties resulting from this procedure we have to

– establish a factorization formula in quantum field theory,
– identify and estimate the relevant hadronic input parameters.

2.2.1.1 Basic concepts of factorization We consider generic charmless B decays into a pair of mesons, $B \to M_1 M_2$, where we may think of $B \to \pi\pi$ as a typical example. The operators Q_i in the weak Hamiltonian can be written as the local product of quark currents (and electro- or chromomagnetic field strength tensors), generically denoted as $J_i^{a,b}$. In naive factorization, one assumes that also on the hadronic level the matrix element can be written as a product,

$$C_i(\mu)\langle M_1 M_2|Q_i|B\rangle$$
$$\approx C_i(\mu)\langle M_1|J_i^a|B\rangle\langle M_2|J_i^b|0\rangle + (M_1 \leftrightarrow M_2), \qquad (30)$$

where $C_i(\mu)$ are Wilson coefficients, and the two matrix elements (if not zero) define the $B \to M$ form factor and the decay constant of M, respectively. The naive factorization formula (30) cannot be exact, because possible QCD interactions between M_2 and the other hadrons are neglected. On the technical level, this is reflected by an unmatched dependence on the factorization scale μ.

In order to better understand the internal dynamics in the $B \to M_1 M_2$ transition, it is useful to classify the external degrees of freedom according to their typical momentum scaling in the B-meson rest frame:

heavy b quark: $\quad p_b \simeq m_b(1, 0_\perp, 0)$,

constituents of M_1: $\quad p_{c1} \simeq u_i m_b/2(1, 0_\perp, +1)$,

soft spectators: $\quad p_s \sim \mathcal{O}(\Lambda)$,

constituents of M_2: $\quad p_{c2} \simeq v_i m_b/2(1, 0_\perp, -1)$,

where Λ is a typical hadronic scale of the order of a few 100 MeV. The index $\perp$ denotes the directions in the plane transverse to the two pion momenta, and u_i, v_i are momentum fractions satisfying $0 \leq u_i, v_i \leq 1$. Interactions of particles with momenta p_1 and p_2 imply internal virtualities of order $(p_1 \pm p_2)^2$. In Table 5, we summarize the situation for the possible interactions between the B-meson and pion constituents. We observe the emergence of two kinds of short-distance modes,

Table 5 External momentum configurations and their interactions in $B \to M_1 M_2$

	heavy	soft	coll$_1$	coll$_2$
heavy	–	heavy	hard	hard
soft	heavy	soft	hard-coll$_1$	hard-coll$_2$
coll$_1$	hard	hard-coll$_1$	coll$_1$	hard
coll$_2$	hard	hard-coll$_2$	hard	coll$_2$

– hard modes with invariant mass of order m_b,
– hard-collinear modes with energies of order $m_b/2$ and invariant mass of order $\sqrt{\Lambda m_b}$.

The systematic inclusion of these effects requires a simultaneous expansion in Λ/m_b and α_s. The leading term in the Λ/m_b expansion can be written as [215, 216]

$$\langle M_1 M_2|Q_i|B\rangle$$
$$= F^{BM_1} f_{M_2} \int dv\, T_i^{\mathrm{I}}(v)\phi_{M_2}(v) + (M_1 \leftrightarrow M_2)$$
$$+ \hat{f}_B f_{M_1} f_{M_2} \int d\omega\, du\, dv\, T_i^{\mathrm{II}}(u, v, \omega)$$
$$\times \phi_{B_+}(\omega)\phi_{M_1}(u)\phi_{M_2}(v). \qquad (31)$$

The functions ϕ_M and ϕ_{B_+} denote process-independent light-cone distribution amplitudes (LCDA) for light and heavy mesons, respectively, f_M, $\hat{f}_B$ are the corresponding decay constants, and F^{BM} is a $B \to M$ QCD form factor at $q^2 = 0$. These quantities constitute the hadronic input. The coefficient function T_i^{I} contains the effects of hard-vertex corrections as in Fig. 5(b). $T_i^{\mathrm{II}} = \mathcal{O}(\alpha_s)$ describes the hard and hard-collinear spectator interactions as in Fig. 5(c). The explicit scale dependence of the hard and hard-collinear short-distance functions T_i^{I}, T_i^{II} matches the one from the Wilson coefficients and the distribution amplitudes. The formula (31) holds for light flavor-nonsinglet pseudoscalars or longitudinally polarized vectors up to $1/m_b$ power corrections which do not, in general, factorize. Naive factorization, Fig. 5(a), is recovered in the limit $\alpha_s \to 0$ and $\Lambda/m_b \to 0$, in which T_i^{I} reduces to 1.

2.2.1.2 QCD factorization and soft-collinear effective theory (SCET) The factorization formula (31) can also be understood in the context of an effective theory for soft-collinear interactions (SCET), see for instance Refs. [217–219, 221]. Here the short-distance functions $T_i^{\mathrm{I,II}}$ arise as matching coefficients between QCD and the effective theory. The effective theory for $B \to M_1 M_2$ decays is constructed in two steps. As a consequence, the short-distance function T_i^{II} can be further factorized into a hard coefficient H_i^{II} and a hard-collinear jet function J:

$$T_i^{\mathrm{II}}(u, v, \omega) = \int dz\, H_i^{\mathrm{II}}(v, z) J(z, u, \omega). \qquad (32)$$

H_i^{II} and J comprise (respectively) the contributions associated with the hard scale $\mu_b \sim m_b$ and the hard-collinear scale $\mu_{\mathrm{hc}} \sim \sqrt{m_b \Lambda}$ from Feynman diagrams that do involve the spectator and cannot be absorbed into F^{BM}. The effective theory can be used to determine the hard-collinear contributions and to resume, if desired, parametrically large logarithms $\ln \mu_b/\mu_{\mathrm{hc}}$ by renormalization group methods. We emphasize that the theoretical basis for the (diagrammatic)
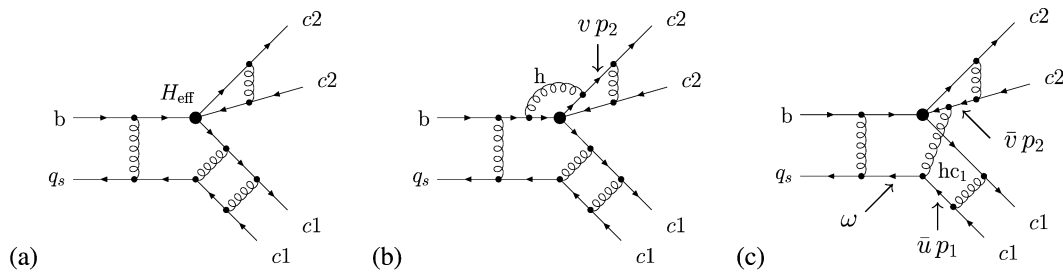
Fig. 5 Sample diagrams for QCD dynamics in $B \to M_1 M_2$ transition: (**a**) naive factorization, (**b**) vertex correction, sensitive to the momentum fraction v of collinear quarks inside the emitted pion, (**c**) spectator interactions, sensitive to the momenta of collinear quarks in both pions and of the soft spectator in the B-meson

factorization approach and SCET is *the same*. The factorization formula (31) was originally derived by a power-counting analysis of momentum regions of QCD Feynman diagrams and the resulting convolutions [215, 216]. However, in SCET the formulation of factorization proofs, the classification of power corrections of order Λ/m_b, the emergence of approximate symmetries, etc. may be more transparent [220, 221].

2.2.1.3 QCD factorization vs. "pQCD approach" The so-called "pQCD approach" [222] follows an alternative approach to understand the strong dynamics in charmless B-decays. In contrast to QCD factorization, where the B meson form factors as well as a certain class of power corrections are identified as "nonfactorizable" quantities of order $(\alpha_s)^0$, the pQCD approach describes all contributions to the hadronic matrix elements in terms of $\mathcal{O}(\alpha_s)$ hard-scattering kernels and nonperturbative wave functions. This is achieved by introducing additional infrared prescriptions which include an exponentiation of Sudakov logarithms and a phenomenological model for transverse momentum effects. The discussion of parametric and systematic theoretical uncertainties in the pQCD approach is more difficult, because a complete NLO (i.e. $\mathcal{O}(\alpha_s^2)$) analysis of nonfactorizable effects has not yet been performed and because independent information on the hadronic input functions is not available. We will therefore not attempt a detailed review here, but instead refer to a recent phenomenological analysis [223] for details.

2.2.2 Theoretical uncertainties

2.2.2.1 Status of perturbative calculations The calculation of the coefficient functions $T_i^{\mathrm{I,II}}$ in SCET involves the determination of perturbative matching coefficients as well as of anomalous dimensions for effective-theory operators. The matching coefficients at order α_s have been calculated in the original BBNS papers [215, 224]. The 1-loop jet function entering T_i^{II} has been determined in [225–228]. NLO results for the spectator scattering function at order α_s^2

have been reported in [229] and will be further discussed in Sect. 2.2.3 below. One important outcome of these investigations is that the perturbative expansion at the hard-collinear scale seems to be reasonably well behaved, and the uncertainty associated with the factorization-scale dependence is under control.

2.2.2.2 Hadronic input from nonperturbative methods Most of the theoretical information on B-meson form factors (at large recoil) and light-cone distribution amplitudes comes from the QCD sum rule approach, see Ref. [230] and references therein for a review. State-of-the-art predictions for decays into light pseudoscalars or vector mesons can be found in Refs. [231–233] and Sect. 2.3. Typically one finds (15–20)% uncertainties for form factors at $E = E_{\mathrm{max}}$ and the $1/u$ moment of distribution amplitudes. Recently, an alternative procedure has been proposed [234] (see also Refs. [235, 236]), where sum rules are derived *within* SCET at the hard-collinear scale. In particular, this approach allows us to separate the "soft" contribution to B-meson form factors, which is found to be dominating over the spectator-scattering term.

Information on the light-cone distribution amplitude of the B-meson is encoded in the phenomenologically relevant moments

$$\lambda_B^{-1} \equiv \langle \omega^{-1} \rangle_B \equiv \int_0^\infty \frac{d\omega}{\omega} \phi_B(\omega, \mu),$$

$$\sigma_B^{(n)} \langle \omega^{-1} \rangle_B \equiv \int_0^\infty \frac{d\omega}{\omega} \ln^n \left[\frac{\mu}{\omega} \right] \phi_B(\omega, \mu). \tag{33}$$

A recent OPE analysis [237] finds $\lambda_B^{-1} = (2.09 \pm 0.24)$ GeV^{-1} and $\sigma_B^{(1)} = 1.61 \pm 0.09$ at $\mu = 1$ GeV. Similar results, with somewhat larger uncertainties, have been obtained from sum rules in Ref. [238].

2.2.2.3 BBNS approach vs. BPRS approach So far, we have only considered the leading term in the $1/m_b$ expansion. Comparison with experimental data as well as (model-dependent) estimates show that for certain decay topologies,

power corrections may not be negligible. Different options for dealing with these (nonfactorizable) contributions lead to some ambiguity in the phenomenological analyses. The two main players are the "BBNS approach" [224, 239, 240] and the "BPRS approach" [221, 241]. A qualitative comparison of the different assumptions is given in Table 6. For more details, see Sect. 2.2.3, the original publications and the controversial discussion in [242].

The main obstacle in this context is the quantitative explanation of strong phases from final-state rescattering effects. The factorization formula predicts these phases to be either perturbative (and calculable) or power-suppressed. This qualitative picture has also been confirmed by a recent sum-rule analysis [243, 244]. However, a model-independent approach to calculate the genuinely nonperturbative rescattering effects is still lacking.

2.2.2.4 Flavor symmetries It is known for a long time (see for instance [245–247]) that approximate flavor symmetries in QCD can be used to relate branching fractions and CP asymmetries in different hadronic decay channels. In this way, the hadronic parameters can be directly extracted from experiment. For instance, in case of $B \to \pi\pi, \pi\rho, \rho\rho$ decays, the isospin analysis provides a powerful tool to constrain the CKM angle α in the SM (see Ref. [248] for a recent discussion). Isospin violation from the small quark mass difference $m_u - m_d$ and QED corrections are usually negligible. Still one has to keep in mind that long-distance radiative QED effects can be enhanced by large logarithms $\ln M_B/E_\gamma$ and compete with short-distance isospin violation from electroweak penguin operators in $\mathcal{H}_{\mathrm{eff}}$. For instance, it has recently been shown [249] (see Sect. 2.2.4 below) that the inclusion of soft photon radiation in charged $B \to \pi\pi, \pi K$ decays can give up to 5% corrections, depending on the experimental cuts. Including hadronic states with strange quarks, one can use flavor-$SU(3)$ to get even more constraints. In general, one expects corrections to the symmetry limit to be not larger than 30% (with the possible exception of potentially large differences in nonperturbative rescattering phases), see for instance the sum-rule analysis in [250]. In the long run, one should also aim to constrain first-order $SU(3)$ corrections directly from experimental data.

2.2.3 NNLO QCD corrections

NNLO QCD corrections to the heavy-quark expansion of hadronic matrix elements for two-body charmless hadronic B-decays can be phenomenologically relevant and are important to assess the validity and perturbative stability of the factorization framework. This section gives a concise account of available results and their phenomenological impact.

2.2.3.1 Hard and hard-collinear matching coefficients
The hard coefficients T_i^{I} and H_i^{II} introduced in Sect. 2.2.1 (see (31) and (32)) are found by matching the leading momentum dependence of (respectively) QCD four- and five-point functions with a Q_i insertion to operators in SCET$_{\mathrm{I}}$ given by products of a light (anti-)collinear quark bilinear and a heavy-light current. Schematically,

$$
\begin{aligned}
Q_i &= \int dt\, T_i^{\mathrm{I}}(t) \big[\bar{\chi}(tn_-)\chi(0)\big] \Big[C_{A0}\big[\bar{\xi}(0)h_v(0)\big] \\
&\quad + \frac{1}{m_b} \int ds\, C_{B1}(s)\big[\bar{\xi}(0)D_{\perp\mathrm{hc}1}(sn_+)h_v(0)\big]\Big] \\
&\quad + \frac{1}{m_b} \int dt\, ds\, H_i^{\mathrm{II}}(t,s)\big[\bar{\chi}(tn_-)\chi(0)\big] \\
&\quad \times \big[\bar{\xi}(0)D_{\perp\mathrm{hc}1}(sn_+)h_v(0)\big],
\end{aligned}
\tag{34}
$$

where certain Wilson lines and Dirac structures have been suppressed. The particular choice of heavy-light current in the first line is designed to reproduce the full QCD (not SCET) form factors; other choices of operator basis as, for instance, in the "SCET approach" [221], simply result in a reshuffling of contributions between the T_i^{I} and H_i^{II} terms. The product structure of either term together with the absence of soft-collinear interactions from the SCET$_{\mathrm{I}}$ Lagrangian at leading power suggests factorization of both terms' hadronic matrix elements into a light-cone distribution amplitude $\langle M_2|[\bar{\chi}\chi]|0\rangle \propto \phi_{M_2}$ and (respectively) the QCD form factor F^{BM_1} and a SCET$_{\mathrm{I}}$ nonlocal "form factor" $\Xi^{BM_1}(s)$ [251]. This expectation is indeed borne out by the finiteness of the convolutions, found in all available computations.

Table 6 Comparison of different phenomenological assumptions in BBNS and BPRS approaches

	BBNS	BPRS
Charm penguins	included in hard functions	left as complex fit parameter Δ_P
Spectator term	perturbative factorization	fit to data (two real-valued quantities ζ and ζ_J)
Ext. hadronic input	form factor and LCDA (different scenarios)	LCDA for light meson
Power corrections	model-dependent estimate (complex functions X_A and X_H)	part of systematic uncertainties

Eur. Phys. J. C (2008) 57: 309–492

335

The jet function J (see (32)) arises in matching the $B1$-type current from SCET_I onto SCET_{II} and is known to NLO [225–228]. This matching takes the form (in position space)

$$\int d^4x \, T\left(\mathcal{L}_{\text{SCET}_I}^{(1)}(x)[\bar{\xi}(0)D_{\perp hc1}(sn_+)h_v(0)]\right)$$

$$= \int dw \, dr \, J(s,r,w)[\bar{\xi}(rn_+)\xi(0)][\bar{q}_s(wn_-)h_v(0)], \tag{35}$$

where we again have suppressed Dirac structures and Wilson lines. Fourier transforming with respect to s, r, w results in $J(z,u,\omega)$ entering (31).

At leading power, all one-loop corrections to H_i^{II} and J and part of the two-loop contributions to T_i^{I} are now available. The current–current corrections to H_i^{II} for the $V - A \times V - A$ operators ($i = 1, 2$) have been found in Refs. [229, 252–254]. The imaginary parts of the corresponding two-loop contributions to T_i^{I} have been computed in Refs. [255, 256]. These are sufficient to obtain the topological tree amplitudes a_1 and a_2, involving the large Wilson coefficients $C_1 \sim 1.1$ and $C_2 \sim -0.2$ at NNLO up to an $\mathcal{O}(\alpha_s^2)$ correction to the real part of T_i^{I}. In particular, the imaginary part of $a_{1,2}$ is now fully known at $\mathcal{O}(\alpha_s^2)$. As it is first generated at $\mathcal{O}(\alpha_s)$, this represents a first step towards an NLO prediction of direct CP asymmetries in QCD factorization. Spectator-scattering corrections from the remaining $V - A \times V + A$ operators, as well as penguin contractions and magnetic penguin insertions, have been computed in Ref. [257]. Together they constitute the QCD penguin amplitudes a_4^p ($p = u, c$) and the colour-allowed and colour-suppressed electroweak penguin amplitudes $a_9^p \pm a_7^p$ and a_{10}^p, where the sign in front of a_7^p depends on the spins of the final-state mesons, and certain numerically enhanced power corrections ($a_{6,8}^p$, annihilation, etc.) are omitted (see, however, Sect. 2.2.3.2).

2.2.3.2 Phenomenological impact and final remarks

Numerical estimates of the a_i and their uncertainties require estimating $1/m_b$ corrections, some of which are "chirally enhanced" for pseudoscalars in the final state. Of these, the scalar penguin a_6^p, and its electroweak analog a_8^p, happen to factorize at $\mathcal{O}(\alpha_s)$. NNLO corrections are not known, and their factorization is an open question. Here we use the known $\mathcal{O}(\alpha_s)$ results. Annihilation and twist-3 spectator interactions do not factorize already at LO ($\mathcal{O}(\alpha_s)$). The former are not included in any a_i but enter the physical decay amplitudes. The latter have flavor structure identical to the a_i and are by convention included as estimates. For the colour-allowed and colour-suppressed tree amplitudes a_1 and a_2, we find

$$a_1(\pi\pi) = 1.015 + [0.025 + 0.012i]_{\text{V}} + [? + 0.027i]_{\text{VV}}$$

$$- \left[\frac{r_{\text{sp}}}{0.485}\right]\{[0.020]_{\text{LO}} + [0.034 + 0.029i]_{\text{HV}}$$

$$+ [0.012]_{\text{tw3}}\}$$

$$= 0.975^{+0.034}_{-0.072} + (0.010^{+0.025}_{-0.051})i, \tag{36}$$

$$a_2(\pi\pi) = 0.184 - [0.153 + 0.077i]_{\text{V}} + [? - 0.049i]_{\text{VV}}$$

$$+ \left[\frac{r_{\text{sp}}}{0.485}\right]\{[0.122]_{\text{LO}} + [0.050 + 0.053i]_{\text{HV}}$$

$$+ [0.071]_{\text{tw3}}\}$$

$$= 0.275^{+0.228}_{-0.135} + (-0.073^{+0.115}_{-0.082})i. \tag{37}$$

In each expression, the first line gives the form-factor (vertex) contribution, the second line the spectator-scattering contribution, and the third line their sum with an estimate of the theoretical uncertainties due to hadronic input parameters (form factors, LCDAs, quark masses), power corrections, and neglected higher-order perturbative corrections as explained in detail in Ref. [257], where also the input parameter ranges employed here are given. The first two lines in (36) and (37) are decomposed into the tree (naive factorization, α_s^0), one-loop (V), and two-loop (VV) vertex correction (the question marks denote unknown real parts of order α_s^2); tree (α_s, LO), one-loop (α_s^2, HV), and twist-3 power correction (tw3) to spectator scattering. The prefactor $r_{\text{sp}} = (9f_{M_1}\hat{f}_B)/(m_b F^{BM_1}\lambda_B)$ encapsulates the bulk of the hadronic uncertainties of the spectator-scattering term. Numerically, for a_1, the corrections are, both individually and in their sum, at the few-percent level such that a_1 is very close to 1 and to the naive-factorization result. On the other hand, individual corrections to a_2 are large, with a near cancellation between naive factorization and the one-loop vertex correction. a_2 is thus especially sensitive to spectator scattering and to higher-order vertex corrections. That these are all important is seen from the VV, LO, and HV numbers in (37).

Analogous expressions can be given for the remaining amplitude parameters $a_3^p \cdots a_{10}^p$ [257], except that no two-loop vertex corrections are known. Qualitatively, NNLO spectator-scattering corrections are as important for the leading-power, but small (electroweak) penguin amplitudes $a_{3,5,7,10}^p$ as they are for a_2 but are found to be small for the large electroweak penguin amplitude a_9^p. Corrections to the QCD penguin amplitude a_4^p are also small, in spite of the involvement of the large Wilson coefficient C_1. This is due to a numerical cancellation, which may be accidental. The scalar QCD and electroweak penguin amplitudes a_6^p and a_8^p are power suppressed but "chirally enhanced". NNLO corrections to them are currently unknown but might involve sizable contributions proportional to C_1, unless a similar

336

Eur. Phys. J. C (2008) 57: 309–492

numerical cancellation as in the case of a_4^p prevents this. This would be relevant for direct CP asymmetries in the πK system and elsewhere. For a more complete discussion, see Ref. [257].

A good fraction of NNLO corrections to the QCD factorization formula are now available. While the perturbation expansion is well behaved in all cases, some of these corrections turn out to be significant, particularly those to the colour-suppressed tree and (electroweak) penguin amplitudes. Further important corrections to the QCD and colour-suppressed EW penguin amplitudes proportional to C_1 may enter through the chirally-enhanced power corrections a_6^p and a_8^p, making their NNLO calculation an important goal.

2.2.4 QED corrections to hadronic B decays

2.2.4.1 Introduction The large amount of data collected so far at B factories has allowed one to reach a statistical accuracy on B decays into pairs of (pseudo)scalars at a level where electromagnetic effects cannot be neglected anymore [258, 259]. On the one hand, a correct simulation of the unavoidable emission of photons from charged particles has to be included in Monte Carlo programs in order to evaluate the correct efficiency. On the other hand, a clear definition of the effective cut on (soft) photon spectra is essential for a consistent comparison both between theory and experiments and between results from different experiments.

We discuss the theoretical and experimental treatment of radiative corrections in hadronic B decays. We present analytical expressions to describe the leading effects induced by both real and virtual (soft) photons in the generic process $H \to P_1 P_2(\gamma)$, where both H and $P_{1,2}$ are scalar or pseudoscalar particles. We then discuss the procedures to be adopted in experimental analyses for a clear definition of the observables.

2.2.4.2 The scalar QED calculation General properties of QED have been exploited in detail for most of the pure electroweak processes or in general for processes that can be fully treated in terms of perturbation theory. This is not the case of hadronic decays. However, due to the universal character of infrared QED singularities, it is possible to estimate the leading $\mathcal{O}(\alpha)$ contributions to these processes within scalar QED in the approximation of a point-like weak vertex.

The most convenient infrared-safe observable related to the process $B \to P_1 P_2$ is the photon inclusive width

$$
\begin{aligned}
\Gamma_{12}^{\text{incl}}\big(E^{\text{max}}\big) &= \Gamma(B \to P_1 P_2 + n\gamma)|_{\sum E_\gamma < E_\gamma^{\text{max}}} \\
&= \Gamma_{12} + \Gamma_{12+n\gamma}\big(E_\gamma^{\text{max}}\big),
\end{aligned}
\tag{38}
$$

namely, the width for the process $B \to P_1 P_2$ accompanied by any number of (undetected) photons with total missing

energy less than or equal to E^{max} in the B meson rest frame. The infrared cut-off E_γ^{max} can be the photon energy below which the state $|P_1 P_2\rangle$ cannot be distinguished from the state $|P_1 P_2 + n\gamma\rangle$; however, in principle, it can also be chosen to be a high reference scale (up to the kinematical limit). At any order in perturbation theory, we can decompose $\Gamma_{12}^{\text{incl}}$ in terms of two theoretical quantities: the so-called nonradiative width, Γ_{12}^0, and the corresponding energy-dependent e.m. correction factor $G_{12}(E_\gamma^{\text{max}})$,

$$
\Gamma_{12}^{\text{incl}}\big(E_\gamma^{\text{max}}\big) = \Gamma_{12}^0(\mu)\, G_{12}\big(E_\gamma^{\text{max}}, \mu\big).
\tag{39}
$$

In the limit $E_\gamma^{\text{max}} \ll M_B$, the electromagnetic correction factor can be reliably estimated within scalar QED. We define the nonradiative width $\Gamma_{12}^0(\mu)$ as

$$
\Gamma_{12}^0(\mu) = \frac{\beta}{16\pi M_B} \big|\mathcal{A}_{B \to P_1 P_2}(\mu)\big|^2,
\tag{40}
$$

$$
\beta^2 = \big[1 - (r_1 + r_2)^2\big]\big[1 - (r_1 - r_2)^2\big], \quad r_i = \frac{m_i}{M_B},
\tag{41}
$$

namely the tree-level rate expressed in terms of the renormalized (scale-dependent) weak coupling. Here the m_i refer to the masses of the light mesons in the final state, and M_B is the B-meson mass. The function $G_{12}(E_\gamma^{\text{max}}, \mu)$ can be written as

$$
\begin{aligned}
G_{12}(E, \mu) = 1 + \frac{\alpha}{\pi}\bigg[&b_{12} \ln\bigg(\frac{M_B^2}{4E^2}\bigg) + F_{12} \\
&+ \frac{1}{2} H_{12} + N_{12}(\mu) \bigg],
\end{aligned}
\tag{42}
$$

where H_{12} represents the finite term arising from virtual corrections, and F_{12} the energy-independent contribution generated by the real emission (here $E \equiv E_\gamma^{\text{max}}$):

$$
\begin{aligned}
\int_{E_\gamma < E} &\frac{d^3\vec{k}}{(2\pi)^3\, 2E_\gamma} \sum_{\text{spins}} \left|\frac{\mathcal{A}(B \to P_1 P_2 \gamma)}{\mathcal{A}(B \to P_1 P_2)}\right|^2 \\
&= \frac{\alpha}{\pi}\bigg[b_{12} \ln\bigg(\frac{m_\gamma^2}{4E^2}\bigg) + F_{12} + \mathcal{O}\bigg(\frac{E}{M_B}\bigg) \bigg].
\end{aligned}
\tag{43}
$$

As expected, after summing real and virtual corrections, the infrared logarithmic divergences cancel out in $G_{12}(E, \mu)$, giving rise to the universal $\ln(M_B/E_\gamma^{\text{max}})$ term. The scale dependence contained in $N_{12}(\mu)$ cancels out in the product $\Gamma_{12}^0 \times G_{12}$ due to the corresponding scale dependence of the weak coupling. For the explicit expressions of F_{12}, H_{12} and N_{12} and a more detailed discussion of the μ-dependence, we refer to [249]. The result thus obtained can be applied to both B and D decays.

We finally give the results for G_{+-} and G_{+0} in the limit $m_{1,2}$, $E \ll M_B$, which represents a convenient and very

good approximation:

$$G_{+-} = 1 - \frac{\alpha}{\pi} \left\{ \left[2 \ln \epsilon + 1 + \ln(1 - \delta^2) \right] \ln\left(\frac{4E^2}{M_B^2} \right) \right.$$
$$\left. - 4 \ln \epsilon + \frac{\pi^2}{3} + 1 + \mathcal{O}(\delta) \right\}, \qquad (44)$$

$$G_{+0} = 1 - \frac{\alpha}{\pi} \left\{ \left[\ln \epsilon + 1 + \ln(1 + \delta) \right] \ln\left(\frac{4E^2}{M_B^2} \right) \right.$$
$$\left. - 2 \ln \epsilon + \frac{\pi^2}{6} - 1 + \mathcal{O}(\delta) \right\}, \qquad (45)$$

where

$$\epsilon = \frac{m_1 + m_2}{2M_B}, \qquad \delta = \frac{m_1 - m_2}{m_1 + m_2}, \qquad (46)$$

with $12 = +-, +0$, respectively. This approximation also serves to clarify the physical relevance of the correction factors. The logarithmic terms as well as the Coulomb correction ($\sim \pi^2$) are model-independent well-defined effects. On the other hand, the remaining constant pieces (± 1) are not meaningful in the absence of the proper UV matching, but they are subdominant and numerically rather small.

2.2.4.3 Inclusion of final-state radiation effects in an experimental analysis We will discuss in particular the inclusion of final-state radiation in the analysis of rare B decays at B factories. In this kind of environment, the efficiency is estimated through Monte Carlo simulation where QED effects are taken into account using the PHOTOS simulation package [260]. The first issue is then to check if the performances of the entire event simulation chain are the ones expected from the theory. One can thus compare the simulated $G_{12}(E_\gamma^{max})$ function, as well as the energy and angular distribution of the generated photons (whose analytical expression can be found in [249]) and then, if needed, correct the distributions on which efficiency and parametrization of the fit variables are evaluated. Then particular care has to be taken in order to quote the results in such a way that radiation effects can be disentangled. In principle, it would be necessary to select B candidates with a specified maximum amount of $\mathcal{O}(100 \text{ MeV})$ photon energy in the final states, a quantity which is difficult to reconstruct in a B factory context. Instead, one could define the data sample selecting on an observed variable which can be clearly related to the maximum allowed energy for photons E_γ^{max}. The variable $\Delta E = E_B^* - \sqrt{s}/2$, where E_B^* is the reconstructed B candidate energy in the $e^+ e^-$ center of mass (CM) frame and $\sqrt{s}$ the total CM energy, is clearly suitable for this purpose. The ΔE window chosen for the analysis would then allow for the presence of radiated photons up to the chosen cut, providing the possibility of quoting results, e.g. on branching fractions, with a defined cut on the soft photon spectrum.

Once a result of this kind is obtained, it is easy to extract the weak couplings—which cannot be directly measured due to the intrinsic and unavoidable features of QED—employing the theoretical calculation explained in the previous section. This is very important, since the comparison between theoretical predictions and experiments can be done more efficiently in terms of weak couplings. Moreover, a meaningful comparison between different experiments can only be done in terms of weak couplings (nonradiative quantities) or in terms of inclusive widths employing the same infrared cutoff.

2.2.5 Outlook on future improvements

The improvement of our quantitative understanding of hadronic effects in charmless nonleptonic B-decays requires both experimental and theoretical efforts:

– Completion of the NNLO analyses for the factorizable vertex and hard-scattering contributions to reduce the perturbative uncertainties.
– Further improvement in hadronic input parameters (form factors, LCDA) by nonperturbative methods combined with experimental data on B- and D-meson decays.
– More systematic treatment of power-corrections.
– Better understanding of $SU(3)$-breaking effects in the analysis of B_s and $B_{u,d}$ decays.

In the future, the main limitations will probably be due to theoretical uncertainties in nonperturbative strong rescattering phases.

2.3 Light-cone QCD sum rules

2.3.1 Distribution amplitudes

Light-cone wave functions or distribution amplitudes (DA) are matrix elements defined near light-like separations connecting hadrons to their partonic constituents. They are widely used in hard exclusive processes with high momentum transfer [261], which are often dominated by light-like distances. Formally they appear in the light-cone operator product expansion (LCOPE) and can be seen as the analogue of matrix elements of local operators in the operator product expansion (OPE). The terms in the OPE are ordered according to the dimension of the operators, the terms in the LCOPE according to their twist, the dimension minus the spin. We shall discuss distribution amplitudes for light mesons, which are most relevant for the LHCb experiment.[7]

---

[7]There are of course other DA of interest. Baryon DA have recently been reviewed in [262], the photon DA is treated in [263], and a recent lecture on the B-meson DA can be found in [264].

We shall take the $K(495)$ and the $K^*(892)$ as representatives for the light pseudoscalar and vector mesons:[8]

$$\langle 0|\bar{q}(x)x_\mu\gamma^\mu\gamma_5[x,0]s(0)\big|K(q)\rangle$$

$$= if_K q \cdot x \int_0^1 du\, e^{-i\bar{u}q\cdot x}\phi_K(u) + O(x^2, m_K^2),$$

$$\langle 0|\bar{q}(x)x_\mu\gamma^\mu[x,0]s(0)\big|K^*(q,\lambda)\rangle$$

$$= \left(\varepsilon^{(\lambda)}\cdot x\right)f_{K^*}m_{K^*}\int_0^1 du\, e^{-i\bar{u}q\cdot x}\phi_K^\parallel(u) \qquad (47)$$

$$+ O\left(x^2, m_{K^*}^2\right),$$

$$\langle 0|\bar{q}(x)\sigma_{\mu\nu}[x,0]s(0)\big|K^*(q,\lambda)\rangle$$

$$= i\left(\varepsilon_\mu^{(\lambda)}q_\nu - \varepsilon_\nu^{(\lambda)}q_\mu\right)f_{K^*}^\perp(\mu)\int_0^1 du\, e^{-i\bar{u}q\cdot x}\phi_K^\perp(u)$$

$$+ O\left(x^2, m_{K^*}^2\right).$$

The vector x_μ is to be thought of as a vector close to the light-cone. The variable u ($\bar{u} \equiv 1 - u$) can be interpreted as the collinear momentum fraction carried by one of the constituent quarks in the meson. Corrections to the leading twist come from three sources: 1. other Dirac-structures (e.g. $\langle 0|\bar{q}(x)\gamma_5[x,0]s(0)|K(q)\rangle$), 2. higher Fock states (including an additional gluon) and 3. mass and light-cone corrections as indicated in the equations above.

The wave functions $\phi(u,\mu)$ are nonperturbative objects. Their asymptotic forms are known from perturbative QCD, $\phi(u,\mu)\overset{\mu\to\infty}{\to}6u\bar{u}$. Use of one-loop conformal symmetry of massless QCD is made by expanding in the eigenfunctions of the evolution kernel, the Gegenbauer polynomials $C_n^{3/2}$,

$$\phi(u,\mu) = 6u\bar{u}\left(1 + \sum_{n=1}^\infty \alpha_n(\mu)C_n^{3/2}(2u-1)\right), \qquad (48)$$

where the α_n are hadronic parameters, the Gegenbauer moments. If n is odd, they vanish for particles with definite G-parity, e.g. $\alpha_{2n+1}(\pi) = 0$. For the kaon, $\alpha_{2n+1}(K)\neq 0$, which contributes to $SU(3)$ breaking. In practice the expansion is truncated after a few terms. This is motivated by the fact that the hierarchy of anomalous dimensions $\gamma_{n+1} > \gamma_n > 0$ implies $|\alpha_{n+1}| < |\alpha_n|$ at a sufficiently high scale. From concrete calculations and fits it indeed appears that the hierarchy already sets in at typical hadronic scales ~ 1 GeV. Moreover, for smooth kernels, the higher Gegenbauer moments give small contributions upon convolution much like in the familiar case of the partial wave expansion in quantum mechanics.

A different method is to model the wave-functions by using experimental and theoretical constraints. In [279], a recursive relation between the Gegenbauer moments was proposed, which involves only two additional parameters. This constitutes an alternative tool especially in cases where the conformal expansion is converging slowly.

We shall not report on higher-twist contributions here but refer to the literature [277, 278]. It should also be mentioned that higher-twist effects can be rather prominent such as in the time-dependent CP asymmetry in $B \to K^*\gamma$ via soft gluon emission [265].

2.3.1.1 Decay constants The decay constants normalize the DA. For the pseudoscalars π and K, they are well known from experiment. The decay constants of the η and η' and in general their wave functions are more complicated due to η–η' mixing and the chiral anomaly and shall not be discussed here. For the vector particles, there are two decay constants, as seen from (47). The longitudinal decay constants can be taken from experiment. For instance, for ρ^0, ω and ϕ, they are taken from $V^0 \to e^+e^-$ and, for ρ^- and K^{*-}, from $\tau^- \to V^-\nu_\tau$. It is worth noting that the difference in f_{ρ^0} and f_{ρ^-} seems consistent with the expected size of isospin breaking, whereas some time ago, there seemed to be a slight tension [269].

For the transverse decay constants $f^\perp$, one has to rely on theory. QCD sum rules provide both longitudinal and transverse decay constants [233, 266]

$$f_\rho = (206 \pm 7)\text{ MeV},$$

$$f_\rho^\perp(1\text{ GeV}) = (165 \pm 9)\text{ MeV},$$

$$f_{K^*} = (222 \pm 8)\text{ MeV}, \qquad (49)$$

$$f_{K^*}^\perp(1\text{ GeV}) = (185 \pm 10)\text{ MeV}.$$

In lattice QCD, there exist two quenched calculations of the ratio of decay constants [267, 268], which are consistent with the sum-rule values above. Combining all these experimental, sum-rule and lattice results we get [270]

$$f_\rho = (216 \pm 2)\text{ MeV},$$

$$f_\rho^\perp(1\text{ GeV}) = (165 \pm 9)\text{ MeV},$$

$$f_\omega = (187 \pm 5)\text{ MeV},$$

$$f_\omega^\perp(1\text{ GeV}) = (151 \pm 9)\text{ MeV},$$

$$f_{K^*} = (220 \pm 5)\text{ MeV}, \qquad (50)$$

$$f_{K^*}^\perp(1\text{ GeV}) = (185 \pm 10)\text{ MeV},$$

$$f_\phi = (215 \pm 5)\text{ MeV},$$

$$f_\phi^\perp(1\text{ GeV}) = (186 \pm 9)\text{ MeV}.$$

---

[8]In the literature, sometimes another phase convention for the vector meson states is used, where $|V\rangle_{\text{other}} = i|V\rangle_{\text{here}}$.

Eur. Phys. J. C (2008) 57: 309–492

339

2.3.1.2 The first and second Gegenbauer moment As mentioned before, the first Gegenbauer moment vanishes for particles with definite G-parity. Intuitively the first Gegenbauer moment of the kaon is a measure of the average momentum fraction carried by the strange quark. Based on the constituent quark model, it is expected that $\alpha_1(K) > 0$. A negative value of this quantity [271] created some confusion and initiated reinvestigations. The sum rule used in that work is of the nondiagonal type and has a nonpositive definite spectral function, which makes the extraction of any kind of residue very unreliable. Later on, diagonal sum rules were used, and stable values were obtained [233, 272] ($\mu = 1$ GeV):

$$\alpha_1(K, \mu) = 0.06 \pm 0.03,$$
$$\alpha_1^{\|}(K^*, \mu) = 0.03 \pm 0.02, \qquad (51)$$
$$\alpha_1^{\perp}(K^*, \mu) = 0.04 \pm 0.03,$$

although with relatively large uncertainties. An interesting alternative method was suggested in [273], where the first Gegenbauer moment was related to a quark–gluon matrix element via the equation of motion. An alternative derivation and a completion for all cases was later given in [274]. The operator equation for the kaon is

$$\frac{9}{5}\alpha_1(K) = -\frac{m_s - m_q}{m_s + m_q} + 4\frac{m_s^2 - m_q^2}{m_K^2} - 8\kappa_4(K),$$

where the twist-4 matrix element κ_4 is defined as: $\langle 0|\bar{q}(gG_{\alpha\mu})i\gamma^\mu\gamma_5 s|K(q)\rangle = iq_\alpha f_K m_K^2 \kappa_4(K)$. Similar equations exist for the longitudinal and transverse case. It is worth stressing that those operator relations are completely general and it remains to determine the twist-4 matrix elements. Attempts to determine them from QCD sum rules [273, 274] turn out to be consistent with the determinations from diagonal sum rules (51) but cannot compete in terms of the accuracy. Later lattice QCD provided the first Gegenbauer moment for the kaon DA from domain-wall fermions [275] and Wilson fermions [276], whose values agree very well with the central value of $\alpha_1(K)$ in (51) but have significantly lower uncertainty.

The second Gegenbauer moment has also been determined from diagonal sum rules for the π and K [272, 277]:

$$\alpha_2(\pi, 1 \text{ GeV}) = 0.27 \pm 0.08, \qquad \frac{\alpha_2(K)}{\alpha_2(\pi)} = 1.05 \pm 0.15. \qquad (52)$$

It can be seen that the $SU(3)$ breaking in the second moment is presumably moderate. Values of α_2 for the vector mesons ρ, K^* and ϕ have recently been updated in [278].

2.3.2 Heavy-to-light form factors from LCSR

Light-cone sum rules (LCSR) were developed to improve on some of the shortcomings of three-point sum rules designed to describe meson-to-meson transition form factors. The problem is that for $B \to M$ transitions, where M is a light meson, higher-order matrix elements grow with m_b rendering the OPE nonconvergent. In the case $D \to M$, three-point sum rules and LCSR yield comparable results. A review of the framework of LCSR can be found in [230].

The form factors of V and A currents for B to light pseudoscalar and vector mesons are defined as ($q = p_B - p$)

$$\langle P(p)|\bar{q}\gamma_\mu b|\bar{B}(p_B)\rangle$$
$$= f_+(q^2)\left[(p_B + p)_\mu - \frac{m_B^2 - m_P^2}{q^2}q_\mu\right]$$
$$+ f_0(q^2)\frac{m_B^2 - m_P^2}{q^2}q_\mu, \qquad (53)$$

$$c_V\langle V(p, \varepsilon)|\bar{q}\gamma_\mu(1 - \gamma_5)b|\bar{B}(p_B)\rangle$$
$$= \frac{2V(q^2)}{m_B + m_V}\epsilon_{\mu\nu\rho\sigma}\varepsilon^{*\nu}p_B^\rho p^\sigma$$
$$- 2im_V A_0(q^2)\frac{\varepsilon^* \cdot q}{q^2}q_\mu$$
$$- i(m_B + m_V)A_1(q^2)\left[\varepsilon_\mu^* - \frac{\varepsilon^* \cdot q}{q^2}q_\mu\right]$$
$$+ iA_2(q^2)\frac{\varepsilon^* \cdot q}{m_B + m_V}\left[(p_B + p)_\mu - \frac{m_B^2 - m_V^2}{q^2}q_\mu\right]. \qquad (54)$$

The factor c_V accounts for the flavor content of particles: $c_V = \sqrt{2}$ for ρ^0, ω and $c_V = 1$ otherwise. The tensor form factors, relevant for $B \to V\gamma$ or $B \to P(V)l^+l^-$, are defined as

$$\langle P(p)|\bar{q}\sigma_{\mu\nu}q^\nu b|\bar{B}(p_B)\rangle$$
$$= \frac{if_T(q^2)}{m_B + m_P}[q^2(p + p_B)_\mu - (m_B^2 - m_P^2)q_\mu], \qquad (55)$$

$$c_V\langle V(p, \varepsilon)|\bar{q}\sigma_{\mu\nu}q^\nu(1 + \gamma_5)b|\bar{B}(p_B)\rangle$$
$$= 2iT_1(q^2)\epsilon_{\mu\nu\rho\sigma}\varepsilon^{*\nu}p_B^\rho p^\sigma$$
$$+ T_2(q^2)[(m_B^2 - m_V^2)\varepsilon_\mu^* - (\varepsilon^* \cdot q)(p_B + p)_\mu]$$
$$+ T_3(q^2)(\varepsilon^* \cdot q)\left[q_\mu - \frac{q^2}{m_B^2 - m_V^2}(p_B + p)_\mu\right], \qquad (56)$$

with $T_1(0) = T_2(0)$. Note that the tensor form factors depend on the renormalization scale μ of the matrix element. All form factors in (53)–(56) are positive, and $\epsilon^{0123} = -1$.

LCSR allow us to obtain the form factors from a suitable correlation function for virtualities of $0 < q^2 \lesssim 14$ GeV^2. The residue in the sum rule is of the type $(f_B f_+(q^2))_{SR}$. Using the second sum rule for $(f_B)_{SR}$ to the same accuracy, the form factor is obtained as $f_+ = (f_B f_+(q^2))_{SR}/(f_B)_{SR}$, where several uncertainties cancel. The final uncertainties of the sum-rule results for the form factors are around 10% and slightly more for the $B \to K$ transitions due to the additional uncertainty in the first Gegenbauer moment. The most recent and up-to-date calculation for $B \to M$ form factors, including twist-3 radiative corrections, can be found in [231, 232]. It is not obvious how the accuracy can be significantly improved by including further corrections. One interesting option would be to calculate NNLO QCD corrections, which could first be attempted in the large-β_0 limit.

Another interesting question is whether it is possible to extend the form factor calculations to the entire physical domain $0 < q^2 < (m_B - m_{P(V)})^2$. It has been advocated by Becirevic and Kaidalov [280] to write the form factor f_+ as a dispersion relation in q^2 with a lowest-lying pole term plus a contribution from multiparticle states, which in a minimal setup can be approximated by an effective pole term at higher mass:

$$f_+(q^2) = \frac{r_1}{1 - q^2/m_1^2} + \int_{(m_B + m_P)^2}^{\infty} ds \, \frac{\rho(s)}{s - q^2}$$
$$\to \frac{r_1}{1 - q^2/m_1^2} + \frac{r_2}{1 - q^2/m_{\text{fit}}^2}. \tag{57}$$

In the past, it has often been popular to adopt Vector Meson Dominance (VMD), i.e. to set $r_2 = 0$. BaBar measurements of semileptonic decay spectra with five bins in the q^2-distribution now strongly disfavor simple VMD [281]. Another important point is that the fits to the parametrization (57) allow us to reproduce the results from LCSR extremely well [231, 232]. The parametrization also passes a number of consistency tests. The soft pion point $f_0(m_B^2) = f_B/f_\pi$ can be attained upon extrapolation, leading to a B-meson decay constant of $f_B \approx 205$ MeV. This is well in the ballpark of expectations and consistent with the Belle measurement of $B \to \tau\nu$. Moreover the residue $(r_1)_{f_+} = (f_{B^*} g_{BB^*\pi})/(2m_{B^*})$, which is rather stable under the fits, agrees within ten percent with what is known from hadronic physics. Representative results are given in Table 7. More form factors can be found in (27) and Table 3 of [231] for $B \to \pi, K, \eta$ and in Table 8 of [232] for $B \to \rho, K^*, \phi, \omega$. It has to be emphasized that the $B \to K, K^*$ transitions have been evaluated before the progress in the $SU(3)$-breaking

was achieved. An update would be timely and will certainly be undertaken for such important cases as $B \to K^* l^+ l^-$. In particular, for the $B \to K^* \gamma$ decay rate in the SM, it was emphasized by [282, 283] that within the framework of QCD factorization, $T_1(0)_{SM-exp,QCDF} = 0.28 \pm 0.02$. An update of $SU(3)$-breaking effects yields $T_1(0) = 0.31 \pm 0.04$ [284], which seems reasonably consistent.

In certain decay channels, such as $B \to K^* l^+ l^-$, several form factors enter at the same time. Sometimes ratios of decay rates are needed, e.g. for the extraction of $|V_{td}/V_{ts}|$ from $B \to K^* \gamma$. Simply taking the uncertainties in the individual form factors and adding them linearly could be a drastic overestimate, since parametric uncertainties, such as those from m_b, might cancel in the quantities of interest. In the former case, no efforts have been undertaken. In the latter case, a consistent evaluation [266] leads to the form factor ratio $\xi \equiv T_1^{B \to K^*}(0)/T_1^{B \to \rho}(0) = 1.17 \pm 0.09$.

2.3.3 Comparison with heavy-to-light form factors from relativistic quark models

Quark models have been frequently used in the past to estimate hadronic quantities such as form factors. They may be applied to complicated processes hardly accessible to lattice calculations and they provide connections between different processes through the wave functions of the participating hadrons. Relativistic quark models are based on a simplified picture of QCD: below the chiral symmetry breaking scale $\mu_\chi \approx 1$ GeV, quarks are treated as particles of fixed mass interacting via a relativistic potential and hadron wave functions and masses are found as solutions of three-dimensional reductions of the Bethe–Salpeter equation. The structure of the confining potential is restricted by rigorous properties of QCD, such as heavy-quark symmetry for the heavy-quark sector [285, 286] and spontaneously broken chiral symmetry for the light-quark sector [287]. The values of the constituent-quark masses and the parameters of the potential are fixed by requiring that the spectrum of observed hadron states is well reproduced [288, 289].

Various versions of the quark model were applied to the description of weak properties of heavy hadrons (see e.g. [290–292]). For instance, the weak transition form factors are given in the quark model in [293] by relativistic double spectral representations in terms of the wave functions of initial and final hadrons and the double spectral density of the corresponding Feynman diagrams with massive quarks. This approach led to very successful predictions for D decays [294, 295]. Many results for various B and B_s decays

Table 7 Form factors from light-cone sum rules

$f_+^{B \to \pi}(0)$	$T_1^{B \to \rho}(0)$	$V^{B \to \rho}(0)$	$A_0^{B \to \rho}(0)$	$A_1^{B \to \rho}(0)$	$A_2^{B \to \rho}(0)$
0.258 ± 0.031	0.267 ± 0.023	0.323 ± 0.030	0.303 ± 0.029	0.242 ± 0.023	0.221 ± 0.023

Eur. Phys. J. C (2008) 57: 309–492

341

Table 8 Examples of form factors for $B \to \rho$ [$B_s \to K^*$] from the quark model [295]

$V(0)$	$A_1(0)$	$A_2(0)$	$A_0(0)$	$T_1(0)$	$T_3(0)$
0.31 [0.44]	0.26 [0.36]	0.24 [0.32]	0.29 [0.45]	0.27 [0.39]	0.19 [0. 27]

have been obtained [295–299], yielding an overall picture in agreement with other approaches, such as QCD sum rules. Table 8 gives examples of the results from [295]. A comparison between various quark models performed in [300] leads to a qualitative estimate of the overall uncertainty of some (10–15)%. The main limitation of the quark model approach is the difficulty to provide rigorous estimates of the systematic errors of the calculated hadron parameters. In this respect, quark models cannot compete with lattice gauge theory.

2.4 Lattice QCD

2.4.1 Recent results

In this section, we give a summary of recent lattice results relevant to flavor physics. The tables should be consulted with an eye on the systematics discussed in Sect. 2.4.2. For a more complete coverage, see the review talks on heavy flavor physics [301–303] and kaon physics [304–306] at the last few lattice conferences.

2.4.1.1 Decay constants
The axial-vector decay constants relevant to the $\pi \to \ell\nu$ leptonic decays

$$\langle 0|(\bar{d}\gamma_\mu\gamma_5 u)(x)|\pi(p)\rangle = if_\pi p_\mu e^{-ip\cdot x} \tag{58}$$

(and analogously for K, D, B mesons) may be evaluated on the lattice. Some recent results are collected in Table 9. The first column gives the statistical and systematic errors. The second column says whether the simulations are quenched ($N_f = 0$), or dynamical with a common m_{ud} mass only ($N_f = 2$), or with strange quark loops included ($N_f = 2 + 1$). The remaining columns indicate the light quark formulation in the sea and valence sectors and whether a continuum extrapolation has been attempted. To the quenched results, an extra 5% scale setting error should be added (see Sect. 2.4.2.1). Generally, the lattice results compare favorably to the recent experimental determinations (using the appropriate CKM element from another process) $f_D = 223(17)(03)$ MeV at CLEO [323], $f_{D_s} = 282(16)(7)$ MeV at CLEO [324], $f_{D_s} = 283(17)(16)$ MeV at BaBar [325] and $f_B = 229(^{+36}_{-31})(^{+34}_{-37})$ MeV at Belle [326]. One may also form the ratio $\sqrt{M_{D_s}} f_{D_s}/\sqrt{M_D} f_D$ to the result 1.30(12) implied by the CLEO and BaBar numbers.

2.4.1.2 Form factors
The vector form factors of semileptonic decays like $B \to \pi\ell\nu$ or $D \to K\ell\nu$ defined in (53) can be calculated in the range $q^2_{\min} < q^2 < q^2_{\max}$, where $q^2_{\max} = (M_B - M_\pi)^2$, $(M_D - M_K)^2$, respectively, while $q^2_{\min}$ is a soft bound (set by the cut-off effects and noise one considers tolerable). Often $f_+(0) = f_0(0)$ is used, and a parametrization is employed to extrapolate. Among the most popular are those of Bećirević–Kaidalov [280] and Ball–Zwicky [280, 281]:

$$f_+^{BK}(q^2) = \frac{f}{(1 - \tilde{q}^2)(1 - \alpha\tilde{q}^2)},$$

$$f_0^{BK}(q^2) = \frac{f}{1 - \tilde{q}^2/\beta}, \tag{59}$$

$$f_+^{BZ}(q^2) = \frac{f}{1 - \tilde{q}^2} + \frac{r\tilde{q}^2}{(1 - \tilde{q}^2)(1 - \alpha\tilde{q}^2)}, \tag{60}$$

where $\tilde{q}^2 = q^2/M_{B^*}^2$ (or $q^2/M_{D^*}^2$ for D-decays), with the parameters $f = f_+(0)$, α (BK, BZ) and r (BZ). The expression in (60) is equivalent to the approximate form in (57). Some recent results, with the same meaning of the columns as before, are given in Table 10. The definition of $\mathcal{F}$ is given in [333]. Earlier work on the $B \to \pi\ell\bar{\nu}$ form factors can be found in [336–339]. For $D \to K\ell\nu$ and $D \to \pi\ell\nu$, the q^2-dependence of the form factors has been traced out by the FNAL/MILC/+ Collaboration [332] and compared to experimental results by the BES [340] and FOCUS [341] Collaborations. For $B \to \pi\ell\nu$, the q^2-dependence, as determined by the HPQCD and FNAL/MILC/+ Collaborations, is in reasonable agreement [301]. For a generic comment why the form factor at $q^2 = 0$ is not always the best thing to ask for from the lattice, see Sect. 2.4.3.

2.4.1.3 Bag parameters
On the lattice, the SM bag parameters $B_K(\mu)$ and $B_B(\mu)$ for neutral kaon and B-meson mixing

$$\langle \bar{K}^0|(\bar{s}d)_{V-A}(\bar{s}d)_{V-A}|K^0\rangle = \frac{8}{3}M_K^2 f_K^2 B_K, \tag{61}$$

$$\langle \bar{B}_q^0|(\bar{b}q)_{V-A}(\bar{b}q)_{V-A}|B_q^0\rangle = \frac{8}{3}M_{B_q}^2 f_{B_q}^2 B_{B_q}$$

$$(q = d, s) \tag{62}$$

are extracted indirectly. The measured quantities are $f_B^2 B_B$ and f_B; then the ratio is taken to obtain the quoted B_B (similar for B_K). Therefore, it makes little sense to combine B_B

342

Eur. Phys. J. C (2008) 57: 309–492

Table 9 Decay constants from lattice QCD

$f_K/f_\pi = 1.24(2)$	$N_f = 2+1$	dom/dom	no	RBC/UKQCD [307]
$f_K/f_\pi = 1.218(2)(^{+11}_{-24})$	$N_f = 2+1$	stag/dom	no	NPLQCD [308]
$f_K/f_\pi = 1.208(2)(^{+07}_{-14})$	$N_f = 2+1$	stag/stag	yes	MILC [309]
$f_K/f_\pi = 1.189(7)$	$N_f = 2+1$	stag/stag	yes	HPQCD [310]
$f_{D_s} = 242(09)(10)$ MeV	$N_f = 0$	–/clov	yes	ALPHA [311]
$f_{D_s} = 240(5)(5)$ MeV	$N_f = 0$	–/clov	yes	RomeII [312]
$f_{D_s} = 249(03)(16)$ MeV	$N_f = 2+1$	stag/stag	yes	FNAL/MILC/+ [313]
$f_{D_s} = 238(11)(^{+07}_{-27})$ MeV	$N_f = 2$	clov/clov	yes	CP-PACS [301]
$f_{D_s} = 241(3)$ MeV	$N_f = 2+1$	stag/stag	yes	HPQCD [310]
$f_D = 232(7)(^{+6}_{-0})(53)$ MeV	$N_f = 0$	–/dom	no	RBC [314]
$f_D = 202(12)(^{+20}_{-25})$ MeV	$N_f = 2$	clov/clov	yes	CP-PACS [301]
$f_{D_s}/f_D = 1.05(2)(^{+0}_{-2})(6)$	$N_f = 0$	–/dom	no	RBC [314]
$f_{D_s}/f_D = 1.24(7)$	$N_f = 2+1$	stag/stag	yes	FNAL/MILC/+ [313]
$f_{D_s}/f_D = 1.162(9)$	$N_f = 2+1$	stag/stag	yes	HPQCD [310]
$f_{B_s} = 192(6)(4)$ MeV	$N_f = 0$	–/clov	yes	RomeII [312]
$f_{B_s} = 205(12)$ MeV	$N_f = 0$	–/clov	yes	ALPHA [315]
$f_{B_s} = 191(6)$ MeV	$N_f = 0$	–/clov	yes	ALPHA [316]
$f_{B_s} = 242(9)(51)$ MeV	$N_f = 2$	clov/clov	yes	CP-PACS [317]
$f_{B_s} = 217(6)(^{+37}_{-28})$ MeV	$N_f = 2$	stag/wils	yes	MILC [318]
$f_{B_s} = 260(7)(26)(8)$ MeV	$N_f = 2+1$	clov/clov	no	HPQCD [319]
$f_{B_s}/f_B = 1.179(18)(23)$	$N_f = 2$	clov/clov	yes	CP-PACS [317]
$f_{B_s}/f_B = 1.16(1)(3)(^{+4}_{-0})$	$N_f = 2$	stag/wils	yes	MILC [318]
$f_{B_s}/f_B = 1.13(3)(^{+17}_{-02})$	$N_f = 2$	clov/clov	no	JLQCD [320]
$f_{B_s}/f_B = 1.20(3)(1)$	$N_f = 2+1$	stag/stag	yes	HPQCD [321]
$f_{B_s}/f_B = 1.29(4)(6)$	$N_f = 2$	dom/dom	no	RBC [322]

from one group and f_B from another to come up with a lattice value for $f_B\sqrt{B_B}$. On the other hand,

$$\xi = \frac{f_{B_s}\sqrt{B_{B_s}}}{f_{B_d}\sqrt{B_{B_d}}} \qquad (63)$$

is benevolent from a lattice viewpoint, since it follows from the ratio of the same correlator with two different quark masses (in practice, an extrapolation $m_d \to m_d^{phys}$ is needed). Many systematic uncertainties cancel in such ratios, but the chiral extrapolation error is not reduced. It would make sense to quote the renormalization scheme and scale-independent quantity

$$\hat{B}_X = \lim_{\mu \to \infty} \alpha_s(\mu)^{2/\beta_0} \left[1 + \frac{\alpha_s}{4\pi} J_{N_f} + \cdots \right] B_X(\mu) \qquad (64)$$

with known J_{N_f}. From a perturbative viewpoint B_X and $\hat{B}_X$ are equivalent, but from a lattice perspective the latter is much better defined. Recent results for $B_K = B_K(2 \text{ GeV})$

and $B_B = B_B(m_b)$ are quoted in Table 11. Note that these values refer to bag parameters with spinor structure $VV + AA$ in the 4-fermion operator, as they appear in the SM.

2.4.1.4 BSM matrix elements There are several hadronic matrix elements for BSM operators available from the lattice. Kaon-mixing matrix elements with $VV - AA, SS + PP, SS - PP, TT$ spinor structure in the 4-fermion operator are found in [129, 130, 345, 353, 354], and $\langle \pi^0 | Q_\gamma^+ | K^0 \rangle$ is being addressed in [355]. In the literature, they go by the name of "SUSY matrix elements", but the idea is that only the (perturbatively calculated) Wilson coefficient refers to the specific BSM theory, while the (lattice-evaluated) matrix element is fully generic. Thanks to massless overlap fermions [356, 357] obeying the Ginsparg–Wilson relation [358] and hence enjoying a lattice analogue of chiral symmetry [359], it is now possible to avoid admixtures of operators with an unwanted chirality structure.

Table 10 Form factors from lattice QCD

$f_+^{K\to\pi}(0) = 0.960(5)(7)$	$N_f = 0$	–/clov	no	RomeI-Orsay [327]
$f_+^{K\to\pi}(0) = 0.952(6)$	$N_f = 2$	clov/clov	no	JLQCD [328]
$f_+^{K\to\pi}(0) = 0.968(9)(6)$	$N_f = 2$	dom/dom	no	RBC [329]
$f_+^{K\to\pi}(0) = 0.9680(16)$	$N_f = 2+1$	dom/dom	no	UKQCD/RBC [330]
$f_+^{K\to\pi}(0) = 0.962(6)(9)$	$N_f = 2+1$	stag/clov	no	FNAL/MILC/+ [331]
$f_+^{D\to\pi}(0) = 0.64(3)(6)$	$N_f = 2+1$	stag/stag	no	FNAL/MILC/+ [332]
$f_+^{D\to K}(0) = 0.73(3)(7)$	$N_f = 2+1$	stag/stag	no	FNAL/MILC/+ [332]
$f_+^{B\to\pi}(0) = 0.23(2)(3)$	$N_f = 2+1$	stag/stag	no	FNAL/MILC/+ [333]
$f_+^{B\to\pi}(0) = 0.31(5)(4)$	$N_f = 2+1$	stag/stag	yes	HPQCD [334]
$\mathcal{F}^{B\to D}(1) = 1.074(18)(16)$	$N_f = 2+1$	stag/stag	no	FNAL/MILC/+ [333]
$\mathcal{F}^{B\to D}(1) = 1.026(17)$	$N_f = 0$	–/clov	yes	RomeII [335]

Table 11 Bag parameters from lattice QCD

$B_K = 0.5746(061)(191)$	$N_f = 0$	–/dom	yes	CP-PACS [342]
$B_K = 0.55(7)$	$N_f = 0$	–/over	yes	MILC [343]
$\hat{B}_K = 0.96(10)$ [hat]	$N_f = 0$	–/wils	yes	Becirevic et al. [344]
$B_K = 0.563(21)(49)$	$N_f = 0$	–/dom	yes	RBC [345]
$B_K = 0.563(47)(07)$	$N_f = 0$	–/over	yes	BMW [129]
$\hat{B}_K = 0.789(46)$ [hat]	$N_f = 0$	–/twis	yes	ALPHA [346]
$B_K = 0.49(13)$	$N_f = 2$	clov/clov	no	UKQCD [347]
$B_K = 0.495(18)$	$N_f = 2$	dom/dom	no	RBC [348]
$B_K = 0.618(18)(135)$	$N_f = 2+1$	stag/stag	no	HPQCD/UKQCD [349]
$B_K = 0.557(12)(29)$	$N_f = 2+1$	dom/dom	no	RBC/UKQCD [350]
$B_{B_s} = 0.940(16)(22)$	$N_f = 0$	–/over	no	Orsay [351]
$B_B = 0.836(27)(^{+56}_{-62})$	$N_f = 2$	clov/clov	no	JLQCD [320]
$B_{B_s}/B_B = 1.017(16)(^{+56}_{-17})$	$N_f = 2$	clov/clov	no	JLQCD [320]
$B_{B_s}/B_B = 1.06(6)(4)$	$N_f = 2$	dom/dom	no	RBC [322]
$f_{B_s}\sqrt{\hat{B}_{B_s}} = 281(21)$ MeV	$N_f = 2+1$	stag/stag	no	HPQCD [352]
$\xi = 1.14(3)(^{+13}_{-02})$	$N_f = 2$	clov/clov	no	JLQCD [320]
$\xi = 1.33(8)(8)$	$N_f = 2$	dom/dom	no	RBC [322]

2.4.1.5 CKM matrix elements

In his Lattice 2005 write-up [301], Okamoto quantifies the magnitudes of all CKM matrix elements, except $|V_{td}|$, using *exclusively lattice results* (and experimental data, of course). They are collected in Table 12. The magnitudes $|V_{ud}|$, $|V_{ts}|$, $|V_{tb}|$ may be subsequently determined if one assumes unitarity of V_{CKM}. This gives $|V_{ud}|^{\text{SM}}_{\text{Lat05}} = 0.9743(3)$, $|V_{ts}|^{\text{SM}}_{\text{Lat05}} = 3.79(53) \times 10^{-2}$ and $|V_{tb}|^{\text{SM}}_{\text{Lat05}} = 0.9992(1)$.

2.4.2 Scale setting and systematic effects

2.4.2.1 Burning $N_f + 1$ observables in N_f flavor QCD

In a calculation with, say, a common ud and separate s, c quark masses, four observables must be used to set the lattice spacing and to adjust m_{ud}, m_s, m_c to their physical values (with m_{ud}, there is a practical problem, but this is immaterial to the present discussion). In general, $N_f + 1$ lattice observ-

Table 12 CKM matrix elements from lattice QCD

$|V_{us}|_{\text{Lat05}}$	$|V_{ub}|_{\text{Lat05}}$	$|V_{cd}|_{\text{Lat05}}$	$|V_{cs}|_{\text{Lat05}}$	$|V_{cb}|_{\text{Lat05}}$
0.2244(14)	$3.76(68) \times 10^{-3}$	0.245(22)	0.97(10)	$3.91(09)(34) \times 10^{-2}$

344

Eur. Phys. J. C (2008) 57: 309–492

ables cannot be used to make predictions, since LQCD establishes the connection

$$\begin{pmatrix} M_p \\ M_\pi \\ M_K \\ M_D \\ \underline{M_B} \end{pmatrix} \Longleftrightarrow \underbrace{\begin{pmatrix} \Lambda_{\mathrm{QCD}} \\ m_{ud} \\ m_s \\ m_c \\ \underline{m_b} \end{pmatrix}}_{\text{parameters}} + \underbrace{\begin{pmatrix} f_\pi \\ f_K, B_K \\ f_D, f_{D_s} \\ \dots \\ \overline{f_B, f_{B_s}} \\ B_B, B_{B_s} \end{pmatrix}}_{\text{predictions}}.$$

$\underbrace{}_{\text{experiment}}$

With infinitely precise data it would not matter which observables are sacrificed to specify the bare parameters in a given run (every observable depends a bit on each of the $N_f + 1$ parameters). In practice, the situation is different. To adjust the bare parameters in a controlled way, it is important to single out $N_f + 1$ observables that are easy to measure, do not show tremendous cut-off effects and depend strongly on one physical parameter but as weakly as possible on all other. By now it is clear that one should not use any broad resonance (e.g. the ρ), since this introduces large ambiguities [360].

Frequently, the Sommer radius r_0 [361] is used as an intermediate scale-setting quantity; e.g. the continuum limit is taken for $f_{B_s} r_0$. But the issue remains what physical distance should be identified with r_0. Typically, a quenched lattice study converts a value for $f_{B_s} r_0$ with specified statistical and systematic errors into an MeV result for f_{B_s}, assuming that r_0 is exactly 0.5 fm (the preferred value from charmonium spectroscopy), or exactly 0.47 fm (from the proton mass), or exactly 0.51 fm (from f_K). If one is interested in quenched QCD, any of these values is fine. However, if one intends to use the result for phenomenological purposes, it is more advisable to attribute a certain error to (r_0 MeV) itself. For instance, one might use $r_0 = 0.49(2)$ fm. This is where the suggestion to add an extra 5% scale-setting ambiguity to most quenched results comes from. In principle, such ambiguities persist in $N_f = 2 + 1$ QCD, but they get smaller as one moves towards realistic quark masses.

2.4.2.2 Perturbative versus nonperturbative renormalization On the lattice, there are two types of renormalization. Obviously, any operator which "runs" requires renormalization. For instance, when calculating a bag parameter, the lattice result is $B_X^{\mathrm{glue,ferm}}(a^{-1})$, where the superscript indicates the specific cut-off scheme defined by the gluon and fermion actions that have been used. In order to obtain an observable with a well-defined continuum limit, this object needs to be converted into a scheme where the pertinent scale μ is not linked to the cut-off a^{-1}. Consequently, the conversion factor in $B_X^{\overline{\mathrm{MS}}}(\mu) = C(\mu a) B_X^{\mathrm{glue,ferm}}(a^{-1})$ would diverge in the continuum limit, but this is immaterial, since $C(\mu a)$ is not an observable.

Besides, a finite renormalization is used for many quantities of interest. For instance, to measure f_π, one multiplies the point-like axial-vector current $A_\mu = \bar{d}\gamma_\mu\gamma_5 u$ with renormalization factor Z_A. Asymptotically (for large β), this factor behaves like $Z_A = 1 + \mathrm{const}/\beta + O(\beta^{-2})$. Accordingly, $Z_A(\beta)$ may be calculated either in weak coupling perturbation theory or nonperturbatively. For some actions, both avenues have been pursued, and sometimes it was found that within perturbation theory it is difficult to estimate the error (there may be big shifts when going from 1-loop to 2-loop, and/or all perturbative calculations of $Z_A(\beta)$ may differ significantly from the outcome of a nonperturbative determination). The results with $N_f = 2 + 1$ staggered quarks rely on perturbation theory, and some experts fear that some of the renormalization factors may be less precisely known than what is currently believed. On the other hand, one might argue that these actions involve UV-filtering ("link-fattening") and may be less prone to such uncertainties than unfiltered ("thin-link") actions. These issues are under active investigation.

2.4.2.3 Summary of extrapolations Lattice calculations are done in a euclidean box $L^3 \times T$ with a finite lattice spacing a. From a field-theoretic viewpoint only the $T \to \infty$ limit is needed to define particle properties (to locate the pole of an Euclidean Green's function and to extract the residue, the $t \to \infty$ behavior of the correlation function $C(t)$ needs to be studied). All other limits are taken subsequently in the physical observables. A summary of all extrapolations involved is:

(1) $T \to \infty$ or removal of excited states contamination (in practice, choosing $T \gg L$ is sufficient);
(2) $a \to 0$ or removal of discretization effects (at fixed $V = L^3$ and fixed $M_{\mathrm{had}}L$);
(3) $V \to \infty$ or removal of (spatial) finite-size effects (at fixed renormalized quark masses);
(4) $m_{ud} \to m_{ud}^{\mathrm{phys}}$ or chiral extrapolation;
(5) $m_b \to m_b^{\mathrm{phys}}$ or heavy-quark extrapolation/interpolation (not with Fermilab formulation).

Extrapolations 1–3 are standard in the sense that one knows how to control them. The chiral extrapolation is far from innocent, since it is not really justified to use chiral perturbation theory [362, 363] if one cannot clearly identify chiral logs in the data, and it is hard to tell such logs from lattice artifacts and finite-size effects. The entries with the smallest error bars among the $N_f = 2 + 1$ data quoted above stem from simulations with the staggered action. In such studies, the extrapolations 2 and 4 are performed by means of staggered chiral perturbation theory [364, 365], using a large number of fitting parameters. This makes it hard to judge whether the quoted error is realistic, but at least the "post

processing" is done in a field-theoretic framework (no modeling). The fifth point depends on the details of the heavy-quark formulation (NRQCD, HQET, Fermilab) employed, but eventually, with $a^{-1} \simeq 10$ GeV and higher, one could use a standard relativistic action.

2.4.2.4 Conceptual issues Besides these practical aspects, there might be conceptual issues regarding the theoretical validity of certain steps. In the past, the so-called quenched approximation has been used, where the functional determinant is neglected. While fundamentally uncontrolled, it seems to have little impact on the final result of a phenomenological study—as long as no flavor singlet quantity is measured, final-state interactions are not particularly important, and the long-distance physics involved does not exceed ~ 1 fm (i.e. for $M_\pi > 200$ MeV, which still is the case in present simulations). State-of-the-art calculations use the partially quenched framework [366–368], which, despite its name, is *not* a half-way extrapolation from quenched to unquenched. It amounts to having, besides $m_{ud}^{\mathrm{sea}} = m_{ud}^{\mathrm{val}}$, also data with $m_{ud}^{\mathrm{sea}} > m_{ud}^{\mathrm{val}}$, which typically stabilize the extrapolation to $m_{ud}^{\mathrm{sea}} = m_{ud}^{\mathrm{val}} = m_{ud}^{\mathrm{phys}}$. But even with the determinant included, things remain somewhat controversial. The rooting procedure with staggered quarks (to obtain $N_f = 2 + 1$, the square-root of $\det(D_{m_{ud}}^{\mathrm{st}})$ and the fourth-root of $\det(D_{m_s}^{\mathrm{st}})$ is taken) has been the subject of a lively debate. Much theoretical progress on understanding its basis has been achieved—for a summary see the plenary talks on this point at the last three lattice conferences [369–372].

2.4.3 Prospects of future error bars

Future progress on the precision of lattice calculations of QCD matrix elements will hopefully come from a variety of improvements, including a growth in computer power, the development of better algorithms, the construction of better interpolating fields, and the design of better relativistic and heavy quark actions. Some of these factors are easier to forecast than others. For instance, the amount of CPU power is a rather monotonic function of time (for the lattice community as a whole, not for an individual collaboration). By contrast, progress at the algorithmic frontier comes in evolutionary steps—we have just witnessed a dramatic improvement of full QCD hybrid Monte Carlo algorithms [373]. The last two points are somewhere in between; here, every collaboration has its own preferences, which are largely driven by the kind of physics it wants to address. Below, some estimates for future error bars on quantities relevant to flavor physics will be given, but it is important to keep in mind two caveats.

The first caveat is a reminder that the anticipated percentage errors quoted below belong to a rather restricted class of observables. In the foreseeable future, lattice methods can only be competitive for processes where the following conditions hold simultaneously:

– only one hadron in initial and/or final state,
– all hadrons stable (none near thresholds),
– all valence quarks in connected graphs,
– all momenta significantly below cut-off scale $2\pi/a$.

This is the case for the quantities discussed below, but it means that quick progress on other interesting quantities, such as $f^{B\to\rho}(q^2)$, is not likely.

The second caveat concerns the role of the theoretical uncertainties, as discussed in the previous paragraph. For instance, some of the estimates given below assume that certain (finite) renormalization (i.e. matching) factors will be known at the 2-loop level. Such calculations are tedious and rely on massive computer algebra (the lattice regularization reduces the full Lorentz symmetry, resulting in a proliferation of terms). Accordingly, future progress of such calculations is difficult to predict. In the same spirit, one should mention that in the predictions discussed below, it is assumed that for $M_\pi = (250-350)$ MeV, one is in a regime where chiral perturbation theory applies and can be used to further extrapolate the lattice data to the physical pion mass. In the unlikely event that for some specific process this is not the case, the corresponding prediction would undergo substantial revision.

With these caveats in mind, it is interesting to discuss the projected error bars as they are released by some lattice groups. For instance, MILC has a detailed "road-map" of their expected percentage errors (including statistical and theoretical uncertainties) for a number of matrix elements. They are collected in the following Table 13, which they kindly provide. By far the most ambitious plans are those of HPQCD. They have just released numbers for f_{D_s} and f_{D_s}/f_D with a claimed accuracy of 1.3% and 0.8%, respectively [310]. They plan on computing f_{B_s} and f_B as well as the $B \to \pi$ form factor at $q^2 \simeq 16$ GeV^2 to 4%. Finally, they envisage releasing the ratio f_{B_s}/f_B with 2% accuracy and ξ with 3% accuracy by the end of 2007.

In this context, it is worth pointing out that progress in other fields, in particular in experiment, has the potential to ease the task for the lattice community. For instance, quoting the vector form factor f_+ for semileptonic $B \to \pi\ell\nu$ decay at $q^2 = 0$ is not the best thing to ask for from the lattice,

Table 13 Prospects for lattice uncertainties (MILC Collab.). The $B \to \pi\ell\nu$ form factor is taken at $q^2 = 16$ GeV^2

	Lat'06	Lat'07	2–3 yrs.	5–10 yrs.
f_{D_s}, f_{B_s}	10	7	5	3–4
f_D, f_B	11	7–8	5	4
$f_B\sqrt{B_B}$	17	8–13	4–5	3–4
ξ	–	4	3	1–2
$(B, D) \to (K, \pi)\ell\nu$	11	8	6	4
$B \to (D, D^*)\ell\nu$	4	3	2	1

346

Eur. Phys. J. C (2008) 57: 309–492

since a long extrapolation is needed (see Sect. 2.4.1.2). Still, in the past, this was common practice, since there was very limited experimental information available. In the meantime, the situation has changed. Now, rather precise information on the shape of this form factor (via binned differential decay rate data $d\Gamma/dq^2$) is available, and only the absolute normalization is difficult to determine in experiment (see e.g. [374] for a detailed analysis). As a result, MILC and HPQCD give the future lattice precision attainable at $q^2 = 16$ GeV^2, i.e. at a momentum transfer which can be reached in the simulation.

3 New physics in benchmark channels

3.1 Radiative penguin decays[9]

The FCNC transitions $b \to s\gamma$ and $b \to d\gamma$ are among the most valuable probes of flavor physics. They place stringent constraints on a variety of NP models, in particular on those where the flavor-violating transition to a right-handed s- or d-quark is not suppressed, in contrast to the SM. Assuming the SM to be valid, the combination of these two processes offers a competitive way to extract the ratio of CKM matrix elements $|V_{td}/V_{ts}|$. This determination is complementary to the one from B mixing and to the one of the SM unitarity triangle based on the tree-level observables $|V_{ub}/V_{cb}|$ and the angle γ. Other interesting observables are the CP and isospin asymmetries and photon polarization. Radiative B decays are also characterized by the large impact of short-distance QCD corrections [375]. Considerable effort has gone into the calculation of these corrections, which are now approaching next-to-next-to-leading order (NNLO) accuracy [376–388]. On the experimental side, both exclusive and inclusive $b \to s\gamma$ branching ratios are known with good accuracy, $\sim$5% for $B \to K^*\gamma$ and $\sim$7% for $\bar{B} \to X_s\gamma$ [389], while the situation is less favorable for $b \to d\gamma$ transitions: measurements are only available for exclusive channels. Here, we shall discuss first the inclusive modes and then the exclusive ones. We shall begin with an overview of the current status of the SM calculations and later consider the situation for models of NP.

3.1.1 $\bar{B} \to X_{(s,d)}\gamma$ inclusive (theory)

The inclusive decay rate of the $\bar{B}$-meson ($\bar{B} = \bar{B}^0$ or B^-) is known to be well approximated by the perturbatively calculable partonic decay rate of the b-quark:

---

[9]Section coordinators: P. Gambino, A Golutvin.

$\Gamma(\bar{B} \to X_s\gamma)_{E_\gamma > E_0}$

$$= \Gamma\big(b \to X_s^{\text{parton}}\gamma\big)_{E_\gamma > E_0} + \mathcal{O}\left(\frac{\Lambda^2}{m_b^2}, \frac{\Lambda^2}{m_c^2}, \frac{\Lambda\alpha_s}{m_b}\right), \quad (65)$$

with $\Lambda \sim \Lambda_{\text{QCD}}$ and E_0 the photon energy cut in the $\bar{B}$-meson rest frame. The nonperturbative corrections on the r.h.s. of the above equation were analysed in Refs. [390–397]. There are also additional nonperturbative effects that become important when E_0 becomes too large ($E_0 \sim m_b/2 - \Lambda$) [398–400] or too small ($E_0 \ll m_b/2$) [401, 402].

It is convenient to consider the perturbative contribution first. At the leading order (LO), it is given by one-loop diagrams like the one in Fig. 6. Dressing this diagram with one or two virtual gluons gives examples of the next-to-leading order (NLO) and the NNLO diagrams, respectively. The gluon and light-quark bremsstrahlung must be included as well. The current experimental accuracy (see (67)) can be matched on the theoretical side only after including the NNLO QCD corrections [376].

At each order of the perturbative series in α_s, large logarithms $L = \ln M_W^2/m_b^2$ are resumed by employing a low-energy effective theory that arises after decoupling the top quark and the electroweak bosons. For example, the LO includes all $\alpha_s^n L^n$ terms, the NLO all $\alpha_s^n L^{n-1}$ terms, etc. Weak interaction vertices (operators) in this theory are either of dipole type ($\bar{s}\sigma^{\mu\nu}bF_{\mu\nu}$ and $\bar{s}\sigma^{\mu\nu}T^abG_{\mu\nu}^a$) or contain four quarks ($[\bar{s}\Gamma b][\bar{q}\Gamma'q]$). Coupling constants at these vertices (Wilson coefficients) are first evaluated at the electroweak renormalization scale $\mu_0 \sim m_t, M_W$ by solving the so-called *matching* conditions. Next, they are evolved down to the low-energy scale $\mu_b \sim m_b$ according to the effective theory renormalization group equations (RGE). The RGE are governed by the operator *mixing* under renormalization. Finally, one computes the *matrix elements* of the operators, which in the perturbative case amounts to calculating on-shell diagrams with single insertions of the effective theory vertices.

The NNLO matching and mixing are now completely known [377–381]. The same refers to those matrix elements that involve the photonic dipole operator alone [382–386]. Matrix elements involving other operators are known at the NNLO either in the so-called large-β_0 approximation [387] or in the formal $m_c \gg m_b/2$ limit [388]. The recently published NNLO estimate [376]

$$\mathcal{B}(\bar{B} \to X_s\gamma)_{E_\gamma > 1.6 \text{ GeV}} = (3.15 \pm 0.23) \times 10^{-4} \quad (66)$$

Fig. 6 Sample LO diagram for the $b \to s\gamma$ transition

Eur. Phys. J. C (2008) 57: 309–492

347
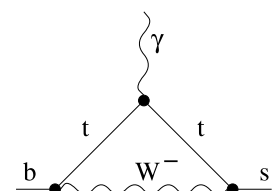
is based on this knowledge. The four types of uncertainties: nonperturbative (5%), parametric (3%), higher-order (3%) and m_c-interpolation ambiguity (3%) have been added in quadrature in (66) to obtain the total error. The main uncertainty is due to unknown $O(\alpha_s \Lambda/m_b)$ nonperturbative effects related to the matrix elements of four-quark operators (see [392]) for which no estimate exists. Similar effects related to dipole operators have been recently estimated in the vacuum insertion approximation [397].

As far as inclusive $b \to d\gamma$ decays are concerned, their measurement is quite challenging. Moreover, due to nonperturbative effects that are suppressed only by $\Lambda_{\mathrm{QCD}}/m_b$, their theoretical accuracy is not much better than in the exclusive case. On the other hand, the experimental prospects in the exclusive case are brighter.

3.1.2 $\bar{B} \to X_{(s,d)}\gamma$ inclusive (experiment)

3.1.2.1 Present status The inclusive $b \to s\gamma$ branching fraction has been measured by BaBar, Belle and CLEO using both a sum of exclusive modes and a fully inclusive method [122, 439, 444, 445]. The inclusive measurement utilizes the continuum subtraction technique using the off-resonance data sample. In order to suppress the continuum contribution, the BaBar measurement uses lepton tags. The analyses of Belle and CLEO are untagged, and their systematic errors are dominated by continuum subtraction. The accuracy of the BaBar measurement is limited by the subtraction of backgrounds from other B decays. The Belle measurement extends the minimum photon energy down to 1.8 GeV, which covers 95% of the entire photon spectrum. All $b \to s\gamma$ branching fractions measured by BaBar, Belle and CLEO using both exclusive and inclusive methods agree well, giving a new world average of [389]

$$\mathcal{B}(\bar{B} \to X_s\gamma)_{E_\gamma > 1.6 \text{ GeV}} = (3.55 \pm 0.30) \times 10^{-4}. \quad (67)$$

This is a bit high compared to the recent NNLO calculation in (66).

The published measurements are based on only a fraction of the available statistics, but improvements with the full data set will be limited by systematic errors: from the fragmentation of the hadronic X_s in the sum of exclusive modes and from the subtraction of backgrounds in the fully inclusive method. A new method measures the spectrum of photons recoiling against a sample of fully reconstructed decays of the other B. This is currently statistics limited but should eventually have lower systematic errors. A final accuracy of 5% on the inclusive $b \to s\gamma$ branching fraction looks achievable. As for the $b \to d\gamma$ inclusive branching fraction, the measurement using a sum of exclusive modes is under study and looks to be feasible with the full datasets from the B-factories. Preliminary results have appeared in [446].

We note that the $b \to s\gamma$ spectral shape also provides valuable information on the shape functions in B meson decays. This information has been used as an input in the extraction of V_{ub} from inclusive $b \to u\ell\nu$ decays [447, 448].

Measurements of the direct CP asymmetries, published for inclusive $b \to s\gamma$ by BaBar [449] and Belle [441], show no deviation from zero. All these measurements will be statistics limited at current B-factories and will not reach the sensitivity to probe the SM prediction.

3.1.2.2 Future prospects One would expect a substantial improvement of the experimental precision for inclusive measurements at future B-factories. Studies have been performed for SuperKEKB/Belle with 50 ab^{-1} data, assuming the existing Belle detector [839]. This is probably a reasonable assumption in many cases, since the expected improvements in the detector, especially in the calorimeter, would be just sufficient to compensate for the necessity to cope with the increased background.

For the measurements that are fully statistics dominated now, it is straightforward to extrapolate to a larger integrated luminosity. The error for the direct asymmetry measurement of $b \to s\gamma$ would be $\pm 0.009(\text{stat}) \pm 0.006(\text{syst})$ for 5 ab^{-1} or $\pm 0.003(\text{stat}) \pm 0.002(\text{syst}) \pm 0.003(\text{model})$ for 50 ab^{-1}. A small systematic error implies that kaon charge asymmetries are well under control. The size of the total error is still much larger than the SM estimate, but a few percent deviation from zero due to New Physics could be identified.

One would also expect a better measurement of the branching fraction of $B \to X_s\gamma$. Although the background level is more and more severe, it would be possible to lower the E_γ bound by 0.1 GeV with roughly twice more data, and it would be possible to measure the branching fraction for $E_\gamma > 1.5$ GeV with a few ab^{-1}. Beyond that, one may need to make use of the B-tag events or $\gamma \to e^+e^-$ conversion to suppress backgrounds from continuum and neutral hadrons. Another challenging measurement would be inclusive $b \to d\gamma$ to improve our knowledge on $|V_{td}/V_{ts}|$ besides the Δm_s measurement, since the one from exclusive $B \to \rho\gamma$ will hit the theory limit soon. The first signal may be measured with 5 ab^{-1} using the sum-of-exclusive method, with a total error of $\sim 25\%$, of which the systematic error would already be dominant.

3.1.3 Exclusive $b \to (s,d)\gamma$ transitions (theory)

Whereas the inclusive modes can be essentially computed perturbatively, the treatment of exclusive channels is more complicated. QCD factorization [282, 283, 403–406] has provided a consistent framework allowing one to write the

348

Eur. Phys. J. C (2008) 57: 309–492

relevant hadronic matrix elements as

$$\langle V\gamma|Q_i|B\rangle = \left[T_1^{B\to V}(0)T_i^{\mathrm{I}} \right.$$
$$\left. + \int_0^1 d\xi\, du\, T_i^{\mathrm{II}}(\xi,u)\phi_B(\xi)\phi_{2;V}^{\perp}(v) \right] \cdot \epsilon.$$
$$(68)$$

Here ϵ is the photon polarization four-vector, Q_i is one of the operators in the effective Hamiltonian for $b\to(s,d)\gamma$ transitions, $T_1^{B\to V}$ is a $B\to V$ transition form factor, and ϕ_B, $\phi_{2;V}^{\perp}$ are leading-twist light-cone distribution amplitudes of the B meson and the vector meson V, respectively. These quantities are universal nonperturbative objects and describe the long-distance dynamics of the matrix elements, which is factorized from the perturbative short-distance interactions included in the hard-scattering kernels T_i^{I} and T_i^{II} (see Sect. 2 for a more general discussion).

Equation (68) is sufficient to calculate observables that are of $O(1)$ in the heavy quark expansion, like $\mathcal{B}(B\to K^*\gamma)$. For $\mathcal{B}(B\to(\rho,\omega)\gamma)$, on the other hand, power-suppressed corrections play an important role, for instance weak annihilation, which is mediated by a tree-level diagram. In this case, the parametric suppression by one power of $1/m_b$ is alleviated by an enhancement factor $2\pi^2$ relative to the loop-suppressed contributions at leading order in $1/m_b$. Power-suppressed contributions also determine the time-dependent CP asymmetry in $B\to V\gamma$, see Refs. [265, 407–409], as well as isospin asymmetries [410]—all observables with a potentially large contribution from new physics. A more detailed analysis of power corrections in $B\to V\gamma$, including also B_s decays, was given in [270].

The nonperturbative quantities entering (68), i.e. $T_1^{B\to V}$ and the light-cone distribution amplitudes, at present are not provided by lattice, although this may change in the future. The most up-to-date predictions come from QCD sum rules on the light-cone, which are discussed in Sect. 2.3. In Ref. [266], the following result was obtained for the branching fraction ratio:

$$R \equiv \frac{\bar{\mathcal{B}}(B\to(\rho,\omega)\gamma)}{\bar{\mathcal{B}}(B\to K^*\gamma)}$$
$$= \frac{|V_{td}|^2}{|V_{ts}|^2}\big(0.75\pm0.11(\xi)$$
$$\pm 0.02\big(\mathrm{UT~param.}, O(1/m_b)\big)\big),$$
$$(69)$$

where $\xi \equiv T_1^{B\to K^*}(0)/T_1^{B\to\rho}(0) = 1.17\pm0.09$ (Sect. 2.3). The error of ξ is dominated by that of the tensor decay constants $f_{\rho,K^*}^{\perp}$, which currently are known to about 10% accuracy [266]; a new determination on the lattice is under way [411], which will help to reduce the error on ξ to ±0.05. Concerning (69), two remarks are in order. First,

the smallness of the $1/m_b$ correction are due to an accidental CKM suppression. Second, the $1/m_b$ corrections have a dependence on $|V_{td}/V_{ts}|$ as well, originating from a discrimination in the u- and c-loops. Equation (69) allows one to determine $|V_{td}/V_{ts}|$ from experimental data; at the time of writing (February 07), HFAG quotes $R_{\exp} = 0.028\pm0.005$, from which one finds $|V_{td}/V_{ts}|_{B\to V\gamma}^{\mathrm{HFAG}} = 0.192\pm0.014(\mathrm{th})\pm0.016(\exp)$, which agrees very well with the results from global fits [8, 120]. The branching ratios themselves carry a larger uncertainty, because the individual $T_1^{B\to V}$ are less accurately known than their ratio. The explicit results can be found in [270]. The isospin asymmetry in $B\to K^*\gamma$ was first studied in Ref. [410] and found to be very sensitive to penguin contributions; it was updated in [270] with the result

$$A_I(K^*) = \frac{\Gamma(\bar{B}^0\to\bar{K}^{*0}\gamma) - \Gamma(B^-\to K^{*-}\gamma)}{\Gamma(\bar{B}^0\to\bar{K}^{*0}\gamma) + \Gamma(B^-\to K^{*-}\gamma)}$$
$$= (5.4\pm1.4)\%;$$
$$(70)$$

the present (February 07) experimental result from HFAG [389] is $(3\pm4)\%$. The isospin asymmetry for $B\to\rho\gamma$ depends rather crucially on the angle γ [270]. The last observable in exclusive $B\to V\gamma$ transitions to be discussed here is the time-dependent CP asymmetry, which is sensitive to the photon polarization. Photons produced from the short-distance process $b\to(s,d)\gamma$ are predominantly left-polarized, with the ratio of right- to left-polarized photons given by the helicity suppression factor $m_{s,d}/m_b$. For $B\to K^*\gamma$, where direct CP violation is doubly CKM suppressed, the CP asymmetry is given by

$$A_{\mathrm{CP}}(t) = \frac{\Gamma(\bar{B}^0(t)\to\bar{K}^{*0}\gamma) - \Gamma(B^0(t)\to K^{*0}\gamma)}{\Gamma(\bar{B}^0(t)\to\bar{K}^{*0}\gamma) + \Gamma(B^0(t)\to K^{*0}\gamma)}$$
$$= C\cos(\Delta m_B t) + S\sin(\Delta m_B t)$$
$$(71)$$

with $S_{K^*\gamma} = -(2+O(\alpha_s))\sin(2\beta)m_s/m_b + \cdots \approx -3\%$ being the contribution induced by the electromagnetic dipole operator O_7. The dots denote additional contributions induced by $b\to s\gamma g$, which are not helicity suppressed but involve higher (three-particle) Fock states of the B and K^* mesons. The dominant contributions to the latter, due to c-quark loops, have been calculated in Ref. [265] from QCD sum rules on the light-cone in an expansion in inverse powers of the charm mass and updated for all other channels in [270]. A calculation of the charm-loop contribution without reference to a $1/m_c$ expansion is in preparation [412] and shows that there is a large strong phase. The u-quark loop contributions are essential for $b\to d$ transitions, since they are of the same CKM-order as the c-quark loops: a new method for their estimation was devised in [270], building on earlier ideas developed for $B\to\pi\pi$ [413]. In Table 14 we show the calculations of S for several channels.

Eur. Phys. J. C (2008) 57: 309–492

349

Table 14 Standard Model predictions of the time-dependent asymmetry S (see (71)) for exclusive $b \to (s, d)\gamma$ modes

$S_{V\gamma}$	$B \to \rho$	$B \to \omega$	$B \to K^*$	$B_s \to \bar{K}^*$	$B_s \to \phi$
in %	0.2 ± 1.6	0.1 ± 1.7	$-(2.3 \pm 1.6)$	0.3 ± 1.3	$-(0.1 \pm 0.1)$

Table 15 Branching fraction measurements at BaBar, Belle and CLEO for exclusive $b \to (s, d)\gamma$ modes

Decay	$B^+ \to K^{*+}\gamma$	$B^0 \to K^{*0}\gamma$	$B^+ \to \rho^+\gamma$	$B^0 \to \rho^0\gamma$	$B^0 \to \omega\gamma$
BR/10^{-6}	40.3 ± 2.6	40.1 ± 2.0	$0.88^{+0.28}_{-0.26}$	$0.93^{+0.19}_{-0.18}$	$0.46^{+0.20}_{-0.17}$

This class of observables is interesting, because any experimental signal much larger than 2% will constitute an unambiguous signal of NP. Scenarios beyond the SM that do modify S must include the possibility of a spin-flip on the internal line which removes the helicity suppression of γ_R. Examples include left–right symmetric models and non-MFV SUSY. To date the experimental result is $S_{\mathrm{HFAG}} = -(28 \pm 26)\%$.

3.1.4 Exclusive $b \to (s, d)\gamma$ transitions (experiment)

3.1.4.1 Present status
Many exclusive $b \to (s, d)\gamma$ modes have been studied by BaBar, Belle and CLEO. Results for several important channels are collected in Table 15 [389]. The results on the $B \to \rho\gamma$, $B \to \omega\gamma$ branching fractions are still statistics limited, but by the end of the B factories it is likely that the theoretical uncertainties will be the most significant factor.

Direct CP asymmetries have been published for $B \to K^*\gamma$ and $B \to K^+\phi\gamma$ decays [440, 450, 451]. The time-dependent CP asymmetry has been measured [442, 443, 452] using the technique of projecting the K_S vertex back to the beam axis for a large sample of $B \to K^{*0}\gamma \to K_S^0\pi^0\gamma$ and $B \to K_S^0\pi^0\gamma$ decays in the high $K\pi$-mass range. In the near future, similar measurements using other exclusive radiative decay modes such as $B^0 \to K_S^0\phi\gamma$, for which $\phi \to K^+K^-$ provides the B-decay vertex measurement, could provide similar constraints.

3.1.4.2 Future prospects at LHCb
A systematic study of CP violation in radiative penguin B decays will be performed at LHCb using a dedicated high-p_T photon trigger [453]. Due to small branching ratios of order 10^{-5}–10^{-6}, their reconstruction requires a drastic suppression of backgrounds from various sources, in particular combinatorial background from $b\bar{b}$ events, containing primary and secondary vertices and characterized by high charged and neutral multiplicities.

The background suppression exploits the generic properties of beauty production in pp collisions. The large mass of beauty hadrons results in hard transverse momentum spectra of secondary particles. The large lifetime, $\langle \beta\gamma c\tau \rangle \sim 5$ mm,

results in a good isolation of the B decay vertex and in the inconsistency of tracks of B-decay products with the reconstructed pp-collision vertex.

The selection procedure was optimized on the example of $B^0 \to K^{*0}\gamma \to K^+\pi^-\gamma$ decay [454], which LHCb considers as a control channel for the study of systematic errors common for radiative penguin decays. The selection cuts, based on using the two-body kinematics and various geometrical cuts on the primary and secondary vertices, were applied to 34 million fully simulated $b\bar{b}$ events. The invariant mass distribution for the selected events, shown in Fig. 7, corresponds to a data sample collected in 13 min of LHCb running at nominal luminosity of 2×10^{32} cm^{-2} s^{-1}. LHCb expects the yield for $B^0 \to K^{*0}\gamma$ decays to be 68k signal events per 2 fb^{-1} of accumulated data with background to signal ratio 0.60 ± 0.16. For $B_s \to \phi\gamma$ decays, the corresponding yield is estimated to be 11.5k with the background to signal ratio less than 0.55 at 90% C.L. The measurement of $B^0 \to K^{*0}\gamma$ decay looks also feasible at ATLAS [455].

Similar to $B^0 \to K_s^0\pi^0\gamma$ decays, the time-dependent CP-asymmetry sensitive to the photon polarization can also be measured in $B_s \to \phi\gamma$ decays, provided that the proper time resolution is sufficient to resolve B_s–$\bar{B}_s$ oscillations. The proper time resolution depends on the kinematics and topology of particular B_s candidates, mainly on the opening angle between kaons from ϕ decays. The sensitivity of this measurement is presently under study at LHCb.

For the future B-factory, scaling the error of the measured time-dependent CP violation asymmetry for the $B^0 \to K_s^0\pi^0\gamma$ channel, one would expect a statistical accuracy of about 0.1 at 5 ab^{-1} or 0.03 at 50 ab^{-1}.

Fig. 7 The invariant mass distribution for selected $B^0 \to K^{*0}\gamma$ candidates from a $b\bar{b}$ inclusive sample. The points indicate true $B^0 \to K^{*0}\gamma$ events, and the filled histogram represents combinatorial background

350

Eur. Phys. J. C (2008) 57: 309–492
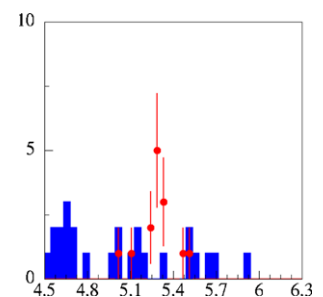
LHCb also studied the possibility to measure the photon polarization in the radiative decays of polarized beauty baryons, like $\Lambda_b \to \Lambda\gamma$, using the angular asymmetry between the Λ_b spin and the photon momentum combined with the $\Lambda^0 \to p\pi$ decay polarization [456–458].

3.1.5 New Physics calculations and tools

New Physics affects the matching conditions for the Wilson coefficients of the operators in the low-energy effective theory and may even induce sizable coefficients for operators that have negligible or vanishing coefficients in the SM. The theoretical accuracy of the predictions for radiative B decays in extensions of the SM is far from the accuracy achieved in the SM. Complete NLO matching conditions are available for the MSSM with Minimal Flavor Violation (MFV) and/or large $\tan\beta$, as well as for a class of nonsupersymmetric models [425] that includes Multi-Higgs-Doublet-Models and Left-Right symmetric (LR) models. The unknown NNLO contributions to the matching conditions beyond the SM are unlikely to be numerically relevant at present.

3.1.5.1 Summary of New Physics calculations Here is a brief summary of recent calculations and analyses in the most popular New Physics scenarios.

- *2HDMs* have been studied in full generality at NLO [83, 414, 415]. In the type-II 2HDM, $\mathcal{B}(\bar{B} \to X_s\gamma)$ places a strong bound on the mass of the charged Higgs boson, $M_{H^+} > 295$ GeV at 95% C.L., independently of the other 2HDM parameters [376]. This is much stronger than other available direct and indirect constraints on M_{H^+}.
- *MSSM*. The complete LO contributions in the MSSM have been known since the early nineties [416–423], but the NLO analysis is still incomplete to date. New sources of flavor violation generally arise in the MSSM, making a complete analysis quite complicated even at the LO [424]. While $\bar{B} \to X_s\gamma$ does place important constraints on the MSSM parameter space, they depend sensitively on the exact SUSY scenario and are hard to summarize because of the large number of parameters.
  - *MFV*. In the MFV scenario, the NLO QCD calculation of $\bar{B} \to X_s\gamma$ is now complete: the two-loop diagrams involving gluons were computed in [84, 425], and the two-loop diagrams involving gluinos were more recently computed in [426, 427]. Since weak interactions affect the squark and quark mass matrices in a different way, their simultaneous diagonalization is not RG-invariant and MFV can be imposed only at a certain renormalization scale. The results of [426, 427] therefore depend explicitly on the MFV scale, which is determined by the mechanism of SUSY breaking.
  - *Large* $\tan\beta$. In the limit of heavy superpartners, the Higgs sector of the MSSM is modified by nonde-coupling effects and can differ substantially from the type-II 2HDM. Large higher-order contributions to $\bar{B} \to X_s\gamma$ in that limit originate from terms enhanced by $\tan\beta$ factors and can be taken into account to all orders in an effective Lagrangian approach [10, 23, 24, 29, 428]. In fact, large $\tan\beta$ and logs of M_{susy}/M_W have been identified in [23] as dominant NLO QCD contributions in MFV with heavy squarks. Ref. [33] recently studied the $\tan\beta$-enhanced effects when MFV is valid at the GUT scale and additional flavor violation in the squark sector is generated by the RGE of the soft SUSY-breaking parameters down to the weak scale.
  - *Beyond MFV.* In the more general case of arbitrary flavor structure in the squark sector, experimental constraints on $b \to s$ transitions have been recently studied at LO [107, 108] and including $\tan\beta$-enhanced NLO effects [111–114]: radiative decays play a central role in these analyses, and the constraints are quite strong for some of the flavor-violating parameters (see however [429] for a scenario in which radiative corrections weaken the constraints).
- *Large extra dimensions*. In these models, the contribution to $\bar{B} \to X_s\gamma$ from the Kaluza–Klein excitations of the SM particles can induce bounds on the size of the additional dimension(s). This has been studied in Refs. [17, 430] for the case of flat extra dimensions and in Refs. [431–433] for the case of warped extra dimensions.
- *Little Higgs*. In these models, the Higgs boson is regarded as the pseudo-Goldstone boson of a global symmetry that is broken spontaneously at a scale much larger than the weak scale. The most extensively studied version of the model, the Littlest Higgs, predicts the existence of heavy vector bosons, scalars and quarks. The contribution to $\bar{B} \to X_s\gamma$ from these new particles has been studied in Refs. [142, 146] for the original Littlest Higgs model and in Ref. [159] for the model in which an additional T-parity and additional particles are introduced to preserve the $SU(2)$ custodial symmetry.
- *LR models*. The contributions of left–right-symmetric models to $\bar{B} \to X_s\gamma$ are known at the NLO [425], but no recent phenomenological analysis is available.

An alternative to the analysis of $\bar{B} \to X_s\gamma$ in different models consists in constraining the Wilson coefficients of the effective theory. This *model-independent approach* has been applied combining various B-decay modes and neglecting operators that do not contribute in the SM [434, 435]. While $\mathcal{B}(\bar{B} \to X_s\gamma)$ fixes only $|C_7(m_b)|$, the sign can be learned from $B \to X_s\ell^+\ell^-$ [188].

3.1.5.2 MSSM tools for $\bar{B} \to X_s\gamma$ Several public codes (see also Sect. 1.5) that determine the MSSM mass spec-

trum and other SUSY observables contain MSSM calculations of $\mathcal{B}(\bar{B} \to X_s\gamma)$ in various approximations. In `micrOMEGAs` [436], the SM part of the calculation is performed at NLO, while the MSSM contributions are implemented following [23]. The calculation in `SuSpect` [437] includes also the NLO gluon corrections to the chargino contributions from [84] in the case of light squarks. In contrast, `SPheno` [207] and `FeynHiggs` [204, 438] include the SUSY contributions only at LO, but they allow for a general flavor structure in the squark sector. A computer code for the NLO QCD calculation of $\mathcal{B}(\bar{B} \to X_s\gamma)$ in the MSSM with MFV [426, 427] has recently been published [191].

3.2 Electroweak penguin decays[10]

3.2.1 Introduction

In the SM, the electroweak penguin decays $b \to s(d)\ell^+\ell^-$ are only induced at the one-loop level, leading to small branching fractions and thus a rather high sensitivity to contributions from physics beyond the SM. On the partonic level, the main contribution to the decay rates comes from the semi-leptonic operators $\mathcal{O}_9$, $\mathcal{O}_{10}$ and from the electromagnetic dipole operator $\mathcal{O}_7^\gamma$ in the effective Hamiltonian for $|\Delta B| = |\Delta S(D)| = 1$ transitions [214]. Radiative corrections induce additional sensitivity to the current–current and strong penguin operators $\mathcal{O}_{1-6}$ and $\mathcal{O}_8^g$. Part of these effects are process-independent and can be absorbed into effective Wilson coefficients. In certain regions of phase-space and for particular exclusive and inclusive observables, hadronic uncertainties are under reasonable control, and the corresponding short-distance Wilson coefficients in and beyond the SM can be tested with sufficient accuracy.

Because of their small branching fractions, these decays are experimentally challenging. Their detection requires excellent triggering and identification of leptons, with low misidentification rates for hadrons. Combinatorial backgrounds from semileptonic B and D decays must be managed, and backgrounds from long-distance contributions, such as $B \to J/\psi X_s$, must be carefully vetoed. Once identified, their interpretation (particularly the angular distributions) requires disentangling the contributing hadronic final states. Most of these experimental problems can be managed by confining studies to the simplest exclusive decay modes. Leptonic states are restricted to e^+e^- and $\mu^+\mu^-$, and hadronic states are the simplest one- or two-particle varieties, typically K, K^*, ϕ, or Λ. More inclusive studies are significantly less sensitive but have the advantage of a simpler theoretical interpretation. Fortunately, measuring fully

---

[10]Section coordinators: Th. Feldmann, J. Berryhill.

reconstructed decays to final states with leptons (especially muons) is a strength of all future proposed B-physics experiments, hence all are capable of contributing to this topic in the LHC era.

3.2.2 Theory of electroweak penguin decays

3.2.2.1 Inclusive decays
The heavy quark expansion and the operator product expansion in the theory of inclusive $\bar{B} \to X_s\ell^+\ell^-$ decays allow one to calculate radiative QCD and QED corrections to the partonic decay rate and to parametrize and estimate power corrections to the hadronic matrix elements in a systematic way. The calculation of NNLO QCD corrections has (essentially) been completed recently [377, 379, 459–465]. These reduce the perturbative uncertainties below 10%. Also subleading $\Lambda_{\rm QCD}^2/m_c^2$ and $\Lambda_{\rm QCD}^2/m_b^2$, $\Lambda_{\rm QCD}^3/m_b^3$ corrections [390, 392, 466–470] as well as finite bremsstrahlung effects [471, 472] are available in the literature.

At this level of accuracy, QED effects become important, too. For instance, the scale ambiguity from $\alpha_{\rm em}(\mu)$ between $\mu = M_W$ and $\mu = m_b$ alone results in an uncertainty of about ±4%. QED corrections to the Wilson coefficients have been calculated in [465], and the results for the two-loop anomalous dimension matrices have been confirmed in [473]. QED bremsstrahlung contributions where the photon is collinear with one of the outgoing leptons are enhanced by $\ln(m_b^2/m_\ell^2)$. They disappear after integration over the whole available phase space but survive and remain numerically important when q^2 is restricted to either low or high values.

A numerical analysis [473], done under the assumption of perfect separation of electrons and energetic collinear photons, results in the following branching ratios integrated in the range $1~\text{GeV}^2 < m_{\ell\ell}^2 < 6~\text{GeV}^2$:

$$\mathcal{B}(\bar{B} \to X_s\mu^+\mu^-)$$
$$= \left[1.59 \pm 0.08_{\rm scale} \pm 0.06_{m_t} \pm 0.024_{C,m_c}\right.$$
$$\pm 0.015_{m_b} \pm 0.02_{\alpha_s(M_Z)}$$
$$\left.\pm 0.015_{\rm CKM} \pm 0.026_{\rm BR_{sl}}\right] \times 10^{-6}$$
$$= (1.59 \pm 0.11) \times 10^{-6}, \tag{72}$$

$$\mathcal{B}(\bar{B} \to X_s e^+e^-)$$
$$= \left[1.64 \pm 0.08_{\rm scale} \pm 0.06_{m_t} \pm 0.025_{C,m_c}\right.$$
$$\pm 0.015_{m_b} \pm 0.02_{\alpha_s(M_Z)}$$
$$\left.\pm 0.015_{\rm CKM} \pm 0.026_{\rm BR_{sl}}\right] \times 10^{-6}$$
$$= (1.64 \pm 0.11) \times 10^{-6}, \tag{73}$$

where the error includes the parametric and perturbative uncertainties only. For central values and error bars of the

352

Eur. Phys. J. C (2008) 57: 309–492

input parameters, see Table 1 of [473]. The electron and muon channels receive different contributions because of the $\ln(m_b^2/m_\ell^2)$ present in the bremsstrahlung corrections. The difference gets reduced when the BaBar and Belle angular cuts are included. One should also keep in mind that the contributions of the intermediate ψ and ψ' are assumed to be subtracted on the experimental side. Analogous results on the branching ratio in the high-$m_{\ell\ell}^2$ region and on the forward–backward asymmetry (FBA) are given in Ref. [474]. A numerical formula that gives the branching ratio for non-SM values of the relevant Wilson coefficients is given in (12) and (13) of Ref. [473].

The differential BR is sensitive to the interference of the Wilson coefficients C_7 and C_9. The FBA for the charged leptons is sensitive to the products $C_7 C_{10}$ and $C_9 C_{10}$. For instance, reversing the sign of C_7 makes the zero of the FBA disappear [434] and leads to an enhancement of the low-q^2 integrated BR:

$$\mathcal{B}(\bar{B} \to X_s \mu^+ \mu^-) = 3.11 \times 10^{-6},$$
$$\mathcal{B}(\bar{B} \to X_s e^+ e^-) = 3.19 \times 10^{-6}; \tag{74}$$

a similar value for that case has been found in [188].

3.2.2.2 Exclusive decays We focus on the theoretical description of $B \to K^* \ell^+ \ell^-$ decay as one of the phenomenologically most important examples. The double-differential spectrum may be parametrized as [475]

$$\frac{d^2\Gamma}{dq^2 \, d\cos\theta_\ell} = \frac{3}{8}\Big[(1 + \cos^2\theta_\ell)H_T(q^2) + 2\cos\theta_\ell H_A(q^2) + 2(1 - \cos^2\theta_\ell)H_L(q^2)\Big]. \tag{75}$$

Here, for $\bar{B}^0$ or B^- decays, θ_ℓ is the angle between the ℓ^+ and the B-meson 3-momentum in the $\ell^+\ell^-$ c.m.s.,[11] and $q^2 = m_{\ell\ell}^2$ is the invariant mass of the lepton pair. Alternatively, the functions $H_X(q^2)$ can be expressed in terms of transversity amplitudes [476, 477]

$$H_T(q^2) = |A_{\perp,L}|^2 + |A_{\perp,R}|^2 + |A_{\parallel,L}|^2 + |A_{\parallel,R}|^2, \tag{76}$$

$$H_L(q^2) = |A_{0,L}|^2 + |A_{0,R}|^2, \tag{77}$$

$$H_A(q^2) = 2\,\mathrm{Re}\big[A_{\parallel,R}A_{\perp,R}^* - A_{\parallel,L}A_{\perp,L}^*\big]. \tag{78}$$

If the invariant mass of the lepton pair is sufficiently below the charm threshold at $q^2 = 4m_c^2$ and above the real-photon pole at $q^2 = 0$, the transversity amplitudes can be estimated within the QCD factorization approach [283, 478, 479]:

$$A_{\perp,L/R} \simeq -A_{\parallel,L/R}$$
$$\simeq \sqrt{2}Nm_B\left(1 - \frac{q^2}{m_B^2}\right)\big[\mathcal{C}_9^\perp(q^2) \mp C_{10}\big]$$
$$\times \zeta_\perp(q^2), \tag{79}$$

$$A_{0,L/R} \simeq -\frac{Nm_B^2}{\sqrt{q^2}}\left(1 - \frac{q^2}{m_B^2}\right)\big[\mathcal{C}_9^\parallel(q^2) \mp C_{10}\big]\zeta_\parallel(q^2), \tag{80}$$

where the normalization factor N is defined in (3.7) in [476]. The functions $\mathcal{C}_{9,10}^\perp(q^2)$ can be calculated perturbatively in the heavy-quark limit, requiring $q^2 \lesssim \Lambda m_b \ll 4m_c^2$ [283, 478]. Large logarithms can be resumed using renormalization-group techniques in soft-collinear effective theory [479]. The form factors $\zeta_{\perp,\parallel}(q^2)$ have to be estimated from experimental data or theoretical models.[12] $1/m_b$ power corrections may be sizable and currently constitute a major source of theoretical uncertainty.

Similarly, in the region far above the charm resonances, the helicity amplitudes can be treated within heavy-quark effective theory, based on an expansion in Λ/m_b and $4m_c^2/q^2$ [480]. To first approximation one finds

$$A_{\perp,L/R} \simeq -\sqrt{2}Nm_B\left(1 - \frac{q^2}{m_B^2}\right)$$
$$\times \left[\mathcal{C}_9^{\mathrm{eff}}(q^2) + \frac{2m_b m_B}{q^2}C_7^{\mathrm{eff}} \mp C_{10}\right]m_B g(q^2), \tag{81}$$

$$A_{\parallel,L/R} \simeq -\sqrt{2}Nm_B\left[\mathcal{C}_9^{\mathrm{eff}}(q^2) + \frac{2m_b m_B}{q^2}C_7^{\mathrm{eff}} \mp C_{10}\right]$$
$$\times \frac{f(q^2)}{m_B}, \tag{82}$$

$$A_{0,L/R} \simeq -Nm_B\frac{m_B^2 - q^2}{2m_{K^*}\sqrt{q^2}}\left[\mathcal{C}_9^{\mathrm{eff}}(q^2) + \frac{2m_b}{m_B}C_7^{\mathrm{eff}} \mp C_{10}\right]$$
$$\times \frac{f(q^2) + (m_B^2 - q^2)a_+(q^2)}{m_B}. \tag{83}$$

Here $f(q^2), g(q^2), a_+(q^2)$ are the leading HQET form factors [480]. The effective "Wilson coefficients" C_9^{eff} are functions of the lepton invariant mass q^2 and combine short-distance dynamics encoded in Wilson coefficients and (nontrivial) long-distance dynamics at the scale m_b. In the naive

---

[11]Different sign conventions are used in the literature.

[12]The conventions to define the form factors $\zeta_{\perp,\parallel}$ in [479] are different from those of Ref. [478]. Therefore the explicit expressions for $\mathcal{C}_9^{\perp,\parallel}$ also differ.

factorization approximation, they are related to $\mathcal{C}_9^{\perp,\parallel}(q^2)$ via

$$
\mathcal{C}_9^{\perp}(q^2) \approx C_9(\mu) + Y(q^2, \mu) + \frac{2m_b m_B}{q^2} C_7^{\text{eff}}(\mu) + \cdots
$$
$$
= C_9^{\text{eff}}(q^2) + \frac{2m_b m_B}{q^2} C_7^{\text{eff}} + \cdots, \tag{84}
$$

$$
\mathcal{C}_9^{\parallel}(q^2) \approx C_9(\mu) + Y(q^2, \mu) + \frac{2m_b}{m_B} C_7^{\text{eff}}(\mu)
$$
$$
= C_9^{\text{eff}}(q^2) + \frac{2m_b}{m_B} C_7^{\text{eff}} + \cdots. \tag{85}
$$

(In the following, we will also use the notation $C_{9,10}(\mu = m_b) = A_{9,10}$ and $C_7^{\text{eff}}(\mu = m_b) = A_7$.)

It is to be stressed that the theoretical systematics in the kinematic regions $q^2 \ll 4m_c^2$ and $q^2 \gg 4m_c^2$ is quite different, due to the different short-distance effects to be accounted for in the calculation of $\mathcal{C}_9^{\perp,\parallel}(q^2)$ or $C_{7,9}^{\text{eff}}$, the independent hadronic form factors in SCET/HQET, and the different nature of (nonfactorizable) power corrections.

Experimentally, the dilepton invariant mass spectrum and the FBA are the observables of principal interest. Their theoretical expressions can be easily derived from (75). In particular, the FBA vanishes at q_0^2 if $\text{Re}[\mathcal{C}_9^{\perp}(q_0^2)] = 0$, which turns out to be very sensitive to the size and relative sign of the electroweak Wilson coefficients C_7 and C_9 [481, 482]. The theoretical predictions depend on the strategy to fix the hadronic input parameters and on the scheme to organize the perturbative expansion in QCD. The authors of [283, 478] fix the hadronic form factors from QCD sum rules [483] and calculate the short-distance coefficients in fixed-order perturbation theory. For the partially integrated branching fraction, they find

$$
\int_{1\,\text{GeV}^2}^{6\,\text{GeV}^2} dq^2 \frac{dBr[B^+ \to K^{*+}\ell^+\ell^-]}{dq^2}
$$
$$
= \left(\frac{\zeta_{\parallel}(4\,\text{GeV}^2)}{0.66}\right)^2 \times \left(3.33^{+0.40}_{-0.31}\right) \times 10^{-7}, \tag{86}
$$

where the leading dependence on one of the $B \to K^*$ form factors has been made explicit. For neutral B mesons, the result is about 10% smaller. The forward–backward asymmetry zero in this scheme comes out to be

$$
q_0^2[K^{*0}] = \left(4.36^{+0.33}_{-0.31}\right)\,\text{GeV}^2,
$$
$$
q_0^2[K^{*+}] = \left(4.15^{+0.27}_{-0.27}\right)\,\text{GeV}^2, \tag{87}
$$

with an additional uncertainty from power corrections estimated to be of order of 10%.

The authors of [479] fix the form factor $\zeta_{\perp}(0)$ by comparing the experimental results on $B \to K^*\gamma$ with the theoretical predictions at NLO at leading power and assuming a simple energy dependence of the form factor. Furthermore,

the leading perturbative logarithms in SCET are resumed. They get a somewhat smaller value for the partially integrated branching fraction[13]

$$
\int_{1\,\text{GeV}^2}^{7\,\text{GeV}^2} dq^2 \frac{dBr(B^+ \to K^{*+}\ell^+\ell^-)}{dq^2}
$$
$$
= \left(2.92^{+0.57}_{-0.50}|_{\zeta_{\parallel}} \,{}^{+0.30}_{-0.28}|_{\text{CKM}} \,{}^{+0.18}_{-0.20}\right) \times 10^{-7}, \tag{88}
$$

which is mainly due to a smaller default value for the $B \to K^*$ form factor $\zeta_{\parallel}$ taken from [232]. The forward–backward asymmetry zero now reads

$$
q_0^2 = \left(4.07^{+0.16}_{-0.13}\right)\,\text{GeV}^2, \tag{89}
$$

where the smaller parametric uncertainties compared to (87) are traced back to the renormalization-group improvement of the perturbative series and the different strategy to fix $\zeta_{\perp}(q^2)$. Isospin-breaking effects between charged and neutral B decays, and potentially large hadronic uncertainties from power corrections have not been specified in [479].

As has been pointed out in [484], the K^* meson is always observed through the resonant $B \to (K\pi)\ell^+\ell^-$ decay. Depending on the considered phase-space region in the Dalitz plot, this may induce further corrections to the position of the asymmetry zero. On the other hand, it allows for an analysis of angular distributions. Following Ref. [476], one can consider the polarization fractions

$$
F_L(q^2) = \frac{H_L(q^2)}{H_L(q^2) + H_T(q^2)},
$$
$$
F_T(q^2) = \frac{H_T(q^2)}{H_L(q^2) + H_T(q^2)} \tag{90}
$$

and the K^*-polarization parameter $\alpha_{K^*}(q^2) = 2F_L/F_T - 1$. Like the FBA, these observables have smaller hadronic uncertainties (for small values of q^2), as the hadronic form-factors cancel in the ratios to first approximation [476]. Introducing the angle θ_K of the K meson relative to the B-momentum in the K^* rest frame, the triple differential decay rate reads

$$
\frac{d^3\Gamma}{dq^2 \, d\cos\theta_l \, d\cos\theta_K}
$$
$$
= \left\{\frac{9}{8}F_L \cos^2\theta_K \sin^2\theta_\ell \right.
$$
$$
\left. + \frac{9}{32}(1 - F_L)\sin^2\theta_K\left(1 + \cos^2\theta_\ell\right)\right\}\frac{d\Gamma}{dq^2}
$$
$$
+ \frac{3}{4}\sin^2\theta_K \cos\theta_\ell\left(\frac{d\Gamma_F}{dq^2} - \frac{d\Gamma_B}{dq^2}\right). \tag{91}
$$

---

[13]Notice that the upper limit of integration in (88) is slightly larger than those in (86).

354

Eur. Phys. J. C (2008) 57: 309–492

Finally, the remaining angle, ϕ, between the decay planes of the lepton pair and K^* meson defines the distribution [476]

$$\frac{d^2\Gamma}{dq^2\,d\phi} = \frac{1}{2\pi}\left(1 + \frac{1}{2}(1 - F_L)A_T^{(2)}\cos 2\phi \right.$$
$$\left. + A_{\text{Im}}\sin 2\phi\right)\frac{d\Gamma}{dq^2}, \qquad (92)$$

where the asymmetry $A_T^{(2)}(q^2)$ is sensitive to new physics from right-handed currents, and the amplitude A_{Im} is sensitive to complex phases in the hadronic matrix elements. In the SM, the asymmetry $A_T^{(2)}$ and the amplitude A_{Im} are negligible at low q^2, so the measurement of either is a precision null test.

The differential decay rate for $B \to K\ell^+\ell^-$ can be found in [478]. Within the SM, the FB asymmetry in $B \to K\ell^+\ell^-$ is highly suppressed. At hadron colliders, also the decay modes $B_s \to \phi\ell^+\ell^-$ and $B_s \to \eta'\ell^+\ell^-$ can be studied. Their theoretical description is analogous to the $B \to K^*(K)$ case, but accurate numerical studies require better knowledge of the hadronic parameters entering the B_s and $\phi(\eta, \eta')$-meson wave functions.

Baryonic decay channels, $\Lambda_b \to \Lambda^0\ell^+\ell^-$, are theoretically less well understood. So far, they have only been discussed within the (naive) factorization approximation, based on symmetry relations and model estimates for the $\Lambda_b \to \Lambda^0$ form-factors (see, e.g., [485–487]). Besides the q^2 spectrum and the FBA, the baryonic $b \to s\ell^+\ell^-$ decays offer the possibility to study various asymmetry parameters and Λ^0 polarization effects, which exhibit a particular dependence on NP effects [488–494]. Also a possible initial Λ_b polarization can be accounted for [495].

3.2.2.3 Charmonium resonances in $b \to s\ell\ell$ The calculation of inclusive and exclusive observables in $b \to s\ell^+\ell^-$ decays is complicated by the presence of long-distance contributions related to intermediate $c\bar{c}$ pairs from the 4-quark operators in the effective Hamiltonian. The effect depends on the invariant mass q^2 of the lepton pair.

For the inclusive rate, the charm quarks can be integrated out perturbatively within an OPE based on an expansion in α_s and $(1/m_c, 1/m_b)$ (with the ratio m_c/m_b kept fixed). Below the charm threshold $q^2 \ll 4m_c^2$, the expansion in $1/m_c^2$ still converges, and the inclusive decay spectrum can be described in terms of a local OPE [392, 395, 396, 466, 496, 497]. Similarly, for exclusive decays, it is possible to integrate out the intermediate charm loops perturbatively, leading to nonlocal operators whose matrix elements can be further investigated using QCDF, SCET or (light-cone) sum rules, see the discussion in Sect. 2 and [265, 394] (for the case $q^2 = 0$).

Approaching the charm threshold at $q^2 \sim 4m_c^2$, the heavy-quark expansion breaks down, both in inclusive and exclusive decays. A pragmatic solution is to ignore the $c\bar{c}$ resonance region completely by introducing "appropriate" experimental cuts on q^2. Alternatively, one may attempt to model a few resonances explicitly (in practice the J/ψ and the $\psi(2S)$), see, e.g., [482] and references therein. However, this method bears the danger of double-counting when combined with the OPE result, which can be avoided by using dispersion relations for the electromagnetic vacuum polarization [498]. Still, nonfactorizable soft interactions between the resonating charmonium system and the $B \to X_s$ transition cannot be accounted for in a systematic way at present.

For values of q^2 above the charm threshold, the invariant mass of the hadronic final state is small, and the decay rate is dominated by a few exclusive states. To trust the OPE result for the inclusive spectrum, one has to smear the experimental spectrum over a "sufficiently" large q^2 range and rely on the (semi-local) duality approximation. For the description of the exclusive channels in that region, one has to rely on an expansion in terms of $4m_c^2/q^2$ within HQET [480]. In summary, to avoid contamination from charmonium or light vector resonances, one should consider the range $1 \leq q^2 \leq 6$ GeV^2.

Finally, one has to mention that light-quark loops need a similar investigation in order to assess the role of light vector resonances at small values of q^2. We also should stress that while analysing the $c\bar{c}$ background in inclusive $B \to X_s l^+l^-$ transitions, special care should be taken of the chain of $B \to J/\psi X_s$, $J/\psi \to l^+l^- X$ decays, mimicking $b \to s l^+l^-$ with $q^2 < m_{J/\psi}^2$.

3.2.3 Experimental studies of electroweak penguin decays

3.2.3.1 Measurements (prospects) at (super-)B factories The B-factory experiments BaBar and Belle have succeeded in measuring the $b \to s\ell^+\ell^-$ process in B decays, both exclusively [499–501] and inclusively [124, 125]. Measured observables include: total branching fractions, direct CP asymmetries, partial branching fractions vs. the dilepton q^2 and the hadronic X_s mass, and—for $B \to K^*\ell^+\ell^-$—the dilepton angular asymmetry A_{FB} vs. the dilepton q^2, the K^* longitudinal polarization vs. the dilepton q^2, and fits of the $d^2\Gamma/d\cos\theta\,dq^2$ distribution to extract experimentally A_9/A_7 and A_{10}/A_7. Upon accumulation of more data in current B factories or the proposed super B factories, it should be possible to extract most of the observables described in Sect. 3.2.2, in increasingly finer binning and precision. The expected experimental sensitivity of 50 ab^{-1} of $B \to K^*\ell^+\ell^-$ data at a super B factory is comparable to 3.3 fb^{-1} of $B^0 \to K^{*0}\mu^+\mu^-$ data at LHCb, as described below.

The optimal measurement technique is to completely reconstruct the signal B decay: selection of events with an

electron or muon pair, selection of all hadrons of the appropriate X_s system (K or K^* mesons for the exclusive case and a K plus 1, 2, 3 or 4 pions for the inclusive case) and then application of the standard kinematic requirements in mass and energy for the resulting B candidate. Partial or full reconstruction requirements for the recoil B are in general suboptimal. Triggering signal events is fully efficient and particle identification is both efficient (typically (80–90)% per particle) and pure (negligible fake rates for electrons, percent level fake rates for muons and kaons) down to low particle lab momenta (0.3 GeV/c for electrons and 0.7 GeV/c for muons). Charmonium background can be efficiently vetoed by the lepton-pair mass and does not significantly contaminate the q^2 regions dominated by the short-distance physics of interest. The remaining combinatorial background, mostly from semileptonic B and D decays, is significant, but it can be reliably separated from signal by extrapolation from distributions in kinematic sidebands, typically via an unbinned maximum likelihood fit. Branching fraction results are shown in Table 16. The effective signal to background ratio for these results varies from 1:2 (inclusive) up to 2:1 (Belle $K^*\ell\ell$). Comparable sensitivity is attained for both electron and muon decay channels.

Assuming HFAG branching fractions and the efficiencies and backgrounds observed in the Belle results, the expected signal yields (and their statistical precision) per 1 ab^{-1} are 229 ± 16 (7%), 215 ± 16 (7%) and 486 ± 24 (5%) for $K\ell\ell$, $K^*\ell\ell$ and $X_s\ell\ell$, respectively. The experimental uncertainty for total branching fractions should therefore be less than or comparable to current SM theoretical uncertainties, using B-factory data alone. Direct CP violation will be bounded at the level of 5–7% with 1 ab^{-1}, and thus a Super B factory would obtain a high precision test ($\sim$1%) of the null result expected in the SM. Similar precision is expected for measuring differences in branching fractions between electron and muon channels, which is also an interesting null test of the SM [435, 503]. A possible complicating factor

for the inclusive $X_s\ell\ell$ (partial) branching fractions is the necessity of an aggressive requirement on the mass M_{X_s} to be less than 1.8 GeV/c^2. Such a tight cut may introduce significant shape function effects into the interpretation of the results in the same manner as a photon energy cut does for $B \to X_s\gamma$ [504, 505]. A looser M_{X_s} requirement will have poorer precision, and thus Super B factory samples may be required to compare with the most precise predictions.

The B factories have also succeeded in accumulating large enough $B \to K^*\ell\ell$ samples to perform angular analyses as a function of dilepton mass. The angles analysed thus far include the angle, θ_ℓ, between the positive (negative) lepton and the B ($\bar{B}$) momentum in the dilepton rest frame and the angle, θ_K, of the K meson relative to the B momentum in the K^* rest frame. The integrated longitudinal K^* polarization F_L and the forward–backward asymmetry A_{FB} are related to the decay products' angular distribution via (91), which upon integration of one of the angular variables reduces to

$$\frac{d^2\Gamma}{dq^2\, d\cos\theta_K} = \left\{ \frac{3}{2}F_L \cos^2\theta_K + \frac{3}{4}(1-F_L)\sin^2\theta_K \right\} \frac{d\Gamma}{dq^2},$$
(93)

$$\frac{d^2\Gamma}{dq^2\, d\cos\theta_\ell} = \left\{ \frac{3}{4}F_L \sin^2\theta_\ell + \frac{3}{8}(1-F_L)\bigl(1+\cos^2\theta_\ell\bigr) \right.$$
$$\left. + A_{FB}\cos\theta_\ell \right\} \frac{d\Gamma}{dq^2}.$$
(94)

From the singly- or doubly-differential angular distributions (in a given q^2-bin) it is then possible to infer $A_{FB}(q^2)$ and $F_L(q^2)$ simultaneously. There is also the remaining angle, ϕ, between the decay planes of the lepton pair and K^* meson, which has yet to be analysed, see (92).

BaBar has measured A_{FB} and F_L in two bins of q^2 (above and below 8.4 GeV/c^2) via unbinned maximum likelihood fits to the singly-differential distributions of $\cos\theta_\ell$

Table 16 Branching fraction measurements at B factories for $b \to s\ell^+\ell^-$ decays, including integrated luminosity, signal yield, detection efficiency and the measured branching fraction over the full q^2 range. The HFAG averages are also included

Result	$\int \mathcal{L}$ (fb^{-1})	Yield	Efficiency (%)	$\mathcal{B}$ (10^{-6})
BaBar $B \to K\ell\ell$ [501]	208	46 ± 10	15 ± 1	$0.34 \pm 0.07 \pm 0.02$
Belle $B \to K\ell\ell$ [499]	253	79 ± 11	13 ± 1	$0.55 \pm 0.08 \pm 0.03$
HFAG $B \to K\ell\ell$ [502]				0.44 ± 0.05
BaBar $B \to K^*\ell\ell$ [501]	208	57 ± 14	7.9 ± 0.4	$0.78 \pm 0.19 \pm 0.11$
Belle $B \to K^*\ell\ell$ [499]	253	82 ± 11	4.6 ± 0.2	$1.65 \pm 0.23 \pm 0.11$
HFAG $B \to K^*\ell\ell$ [502]				1.17 ± 0.16
BaBar $B \to X_s\ell\ell$ [124]	82	40 ± 10	2.0 ± 0.4	$5.6 \pm 1.5 \pm 1.3$
Belle $B \to X_s\ell\ell$ [125]	140	68 ± 14	2.7 ± 0.5	$4.1 \pm 0.8 \pm 0.9$
HFAG $B \to X_s\ell\ell$ [502]				4.5 ± 1.0

356

Eur. Phys. J. C (2008) 57: 309–492

Table 17 Expected statistical precision of a Super B factory, in percent, for the angular observables A_{FB} and F_L versus the integrated luminosity, integrated over various ranges of q^2

$\int \mathcal{L}$ (ab^{-1})		1	5	10	50
$K^*\ell\ell$: A_{FB}	q^2 in (1–6) GeV^2/c^4	18	8.2	5.8	2.6
	$q^2 > 10$ GeV^2/c^4	11	4.7	3.3	1.5
	All	7.9	3.5	2.5	1.1
$K^*\ell\ell$: F_L	q^2 in (1–6) GeV^2/c^4	12	5.3	3.7	1.7
	$q^2 > 10$ GeV^2/c^4	9.4	4.2	3.0	1.3
	All	7.2	3.2	2.3	1.0
$K^+\ell\ell$: A_{FB}	All	8.4	3.7	2.6	1.2

and $\cos\theta_K$, which take into account signal efficiency as a function of angle as well as background angular distributions (which are in general nonuniform and forward–backward asymmetric) [501]. Table 17 shows the expected precision for these observables extrapolated to super B luminosities, assuming HFAG branching fractions and SM predictions for $d\Gamma/dq^2$. The ultimate 50 ab^{-1} precision of the A_{FB} of $B \to K^*\ell\ell$, integrated over the theoretically preferred range of (1–6) GeV^2/c^4, is 2.6%. If this region is extended more aggressively to the original BaBar choice of (0.1–8.4) GeV^2/c^4, the signal statistics are doubled, and the precision improves to 1.8%. Similar precision is expected for F_L. Measuring integrated angular observables of these types has the advantages of model independence in their interpretation; the underlying relation between these measurements, the Wilson coefficients and the form factors can change without necessitating revision of the measurement. The averaging of multiple experimental results is also very straightforward.

Alternatively, Belle has analysed the doubly-differential distribution $d^2\Gamma/d\cos\theta_\ell\, dq^2$ and then performed a maximum likelihood fit to extract the Wilson coefficient ratios A_9/A_7 and A_{10}/A_7 from the data [500]. Using the theoretical approximation in Ref. [434] and assuming the form factor model of Ref. [482], they find

$$A_9/A_7 \simeq -15.3^{+3.4}_{-4.8} \pm 1.1,$$
$$A_{10}/A_7 \simeq 10.3^{+5.2}_{-3.5} \pm 1.8, \tag{95}$$

where the A_i are the leading-order Wilson coefficients. This is in agreement with the LO Standard Model predictions of -12.3 and 12.8, respectively. The dominant systematic uncertainty is from theoretical model dependence, particularly the form factor model and parametric uncertainty from m_b. This method has been studied for super B-factory luminosities, as discussed in Ref. [506]. Figure 8 shows a projection of dA_{FB}/dq^2 from a likelihood fit to the Wilson coefficients, for a simulated sample of 5 ab^{-1}, compared to A_{FB} integrated over various bins in q^2 measured from the same sample. Employing the entire range of q^2, the expected statistical precision is shown in Table 18. With (5–10) ab^{-1},
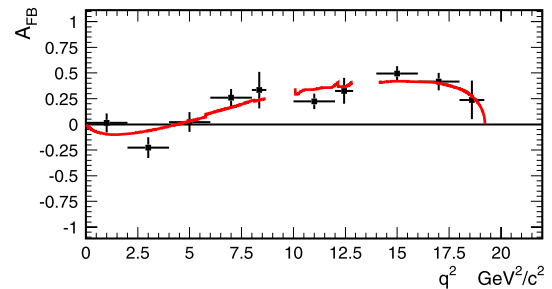
Fig. 8 Expected measurement of dA_{FB}/dq^2 for $B \to K^*\ell^+\ell^-$ (*points*) with 5 ab^{-1} of data from a super B factory; the best fit of that data for Wilson coefficients A_9 and A_{10} is superimposed (*solid line*) [506]

Table 18 Expected statistical precision for a super B factory, in percent, for Wilson coefficients A_9 and A_{10} versus the integrated luminosity, integrated over the entire range of q^2

$\int \mathcal{L}$ (ab^{-1})	1	5	10	50
A_9	25	11	7.8	3.5
A_{10}	29	13	9.2	4.1

the expected statistical uncertainty will be less than the current systematic uncertainty. The expected ultimate statistical sensitivity for 50 ab^{-1} is about 4% for each coefficient. These fits extract essentially the same information as that obtained from measuring the zero q_0^2 of dA_{FB}/dq^2 (a theoretically clean estimator of A_9/A_7), except that the distribution is analysed globally and not just in the vicinity of q_0^2; equivalent uncertainties for q_0^2 are identical to those of A_9. In order to control theoretical uncertainties, it may be necessary to restrict the fit to (1–6) GeV^2/c^4. For that measurement, the price in experimental statistics is roughly a factor of 0.6, with an even larger sacrifice in sensitivity for A_{10}, which is most relevant at high q^2.

With more data, it could also be possible to bound other Wilson coefficients which are negligible in the SM, such as those corresponding to scalar operator products or products with flipped chirality. Fitting triply- or quadruply-differential distributions with the additional decay angles

$\cos\theta_K$ and ϕ, as is currently done for large samples of $B \to VV$ decays, will also be possible.

Measuring the angular distribution of inclusive $B \to X_s\ell\ell$ decays has not yet been attempted, however with thousands of events expected at a super B factory, there will be sufficient statistics for a precise measurement of A_{FB} [507]. This is an attractive measurement, as observables such as q_0^2 are predicted more precisely than for the exclusive case ($\sim 5\%$). Scaling from the expected yield per ab^{-1} of 486 ± 24 and assuming the same sensitivity to A_9/A_7 per event as for the $B \to K^*\ell\ell$ Wilson coefficient fits, a 5% statistical precision for A_9/A_7 (and hence q_0^2) could be achieved with roughly 10 ab^{-1}, although again a critical issue for the precision is how wide a range of q^2 is appropriate for such fits. Understanding systematic uncertainties from a sum-of-exclusive-modes analysis will be challenging, in particular the effect of imprecise X_s fragmentation modeling on the multiply-differential efficiency.

3.2.3.2 $B_d \to K^{*0}\mu^+\mu^-$ at LHCb The exclusive $B_d \to K^{*0}\mu^+\mu^-$ decay can be triggered and reconstructed in LHCb with high efficiency due to the clear di-muon signature and K/π separation provided by the RICH detector [508].

The selection criteria including the trigger have an efficiency of 1.1% for signal. The trigger accepts 89% of the Monte Carlo signal events, which are reconstructed offline. In 2 fb^{-1} of integrated luminosity, this selection gives an estimated signal of 7200 events with a total background of 3500 events in a ± 50 MeV/c^2 mass window around the B mass and ± 100 MeV/c^2 window around the K^{*0} mass. The branching ratio for $B_d \to K^{*0}\mu^+\mu^-$ was assumed to be 1.22×10^{-6}. The irreducible nonresonant $B_d \to K^+\pi^-\mu^+\mu^-$ background was estimated at 1730 events; the branching ratio used for this was set using a 90%

upper limit estimate found from the sidebands of the K^{*0} mass in [501]. Other large components of the background are 1690 from events with two semileptonic B decays, 640 of which are from semileptonic decays of both the b and the c quarks within the same decay chain. Exclusive backgrounds from other $b \to s\mu^+\mu^-$ decays were considered and contribute at a very low level of 20 events.

The selection efficiency as a function of q^2 is flat in the region $4m_\mu^2$ to 9 GeV^2/c^4 due to the high boost of the B_d. For high q^2 values, the selection efficiency as a function of θ_l is flat, while for low q^2, the efficiency is highest around $\theta_l = \pi/2$ [509].

In addition to the well-known FB asymmetry, A_{FB}, LHCb will be able to extract information about the differential decay rate $d\Gamma/ds$ and the transversity amplitudes A_0, $A_\parallel$ and $A_\perp$ through the asymmetry $A_T^{(2)}$ and the K^{*0} longitudinal polarization F_L, see (91) and (92).

For measuring the zero point in A_{FB}, a linear fit is performed to the measured A_{FB} in the region (2–6) GeV^2/c^4 as illustrated in Fig. 9. For the resolution in the zero point of A_{FB} [509], we estimate 0.50(0.27) GeV^2/c^4 with 2(10) fb^{-1} of integrated luminosity. If the background is ignored, the resolution is 0.43(0.25) GeV^2/c^4.

The statistical errors for A_{FB}, $A_T^{(2)}$ and F_L have been estimated by performing simultaneous fits to the θ_l, θ_K and ϕ projections of the full angular distribution in 3 bins of q^2 below the ψ resonances [510]. In the theoretically favored region of $1 < q^2 < 6$ GeV^2/c^4, the resolution in $A_T^{(2)}$ is 0.42(0.16) with 2(10) fb^{-1} of integrated luminosity. See Table 19 for estimated statistical errors on all the parameters. In particular the resolution on $A_T^{(2)}$ would improve if the theoretically comfortable region could be expanded upwards from 6 GeV^2/c^4.

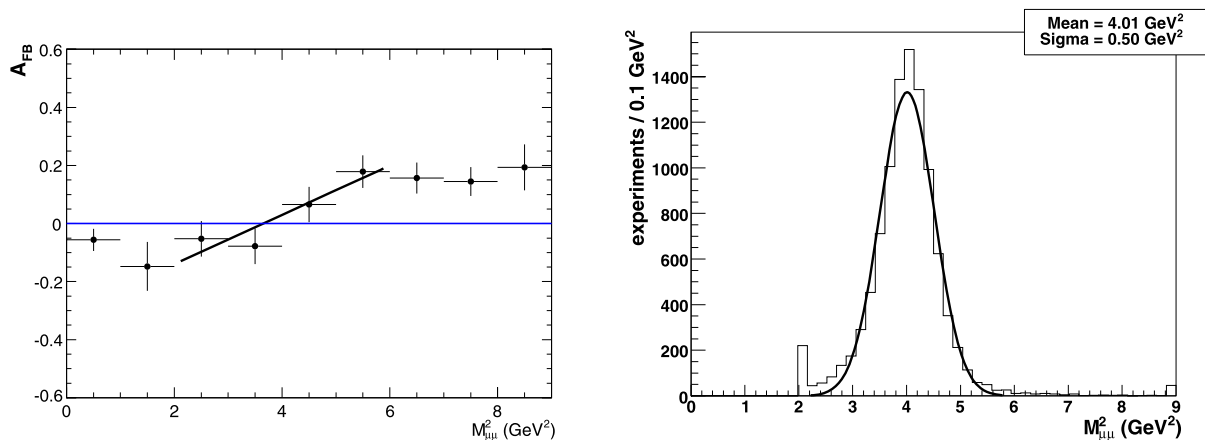**Fig. 9** The FB asymmetry in $B_d \to K^{*0}\mu^+\mu^-$ with 2 fb^{-1} of integrated luminosity at LHCb. To the *left* the FB asymmetry as a function of q^2 in a single toy Monte Carlo experiment, and to the *right* the fitted zero point location for an ensemble of Monte Carlo experiments. The peaks at 2 and 9 correspond to fits where the zero point was outside this region

358

Eur. Phys. J. C (2008) 57: 309–492

Table 19 The expected resolution for measurements of the parameters A_{FB}, $A_T^{(2)}$ and F_L for the $B_d \to K^{*0}\mu^+\mu^-$ decay at LHCb in regions of the squared di-muon mass q^2 with 2 and 10 fb^{-1} of integrated luminosity

q^2 region (GeV^2/c^4)	A_{FB} 2 fb^{-1}	10 fb^{-1}	$A_T^{(2)}$ 2 fb^{-1}	10 fb^{-1}	F_L 2 fb^{-1}	10 fb^{-1}
0.05–1.00	0.034	0.017	0.14	0.07	0.027	0.011
1.00–6.00	0.020	0.008	0.42	0.16	0.016	0.007
6.00–8.95	0.022	0.010	0.28	0.13	0.017	0.008

3.2.3.3 R_K at LHCb Reconstructing $B^+ \to K^+ e^+ e^-$ as well as $B^+ \to K^+ \mu^+ \mu^-$ allows us to extract the ratio R_K of the two branching fractions integrated over a given di-lepton mass range. The same reconstruction requirements are applied to $B^+ \to K^+ \mu^+ \mu^-$ and $B^+ \to K^+ e^+ e^-$ decay. A proper bremsstrahlung correction is essential in the latter channel. The correction for the lower reconstruction and trigger efficiency in the electron mode is extracted from $B^+ \to J/\psi K^+$ decays. The di-lepton mass range is chosen to be $4m_\mu^2 < q^2 < 6$ GeV^2/c^4 in order to avoid $c\bar{c}$ resonances (especially in the $e^+ e^-$ mode) and threshold effects due to the higher μ mass. The event yields are extracted from a fit to the $K\ell^+\ell^-$ mass distributions. Peaking backgrounds from $B^+ \to J/\psi K^+$ and $B_d \to K^*\ell^+\ell^-$ are measured using control samples and included in the fit.

The expected B candidate mass distributions are shown in Fig. 10 for five years (10 fb^{-1}) of data taking. The yields returned by the fit are given in Table 20. They are compatible with the number of true MC events. The B/S ratios are given for the full signal box within ±600 MeV around the B_u mass (shown in Fig. 10). The errors on the yields are the statistical error returned by the fit. Using these errors, one gets an error on R_K of 4.3% for 10 fb^{-1}.

3.2.3.4 Semileptonic rare B decays at ATLAS With the ATLAS experiment, NP effects in $b \to s l^+ l^-$ transitions will be searched for in the branching ratio and the FB asymmetry $A_{FB}(q^2)$ between b-hadron and l^+ momenta. With baryonic decays ($\Lambda_b \to \Lambda^0 \mu^+ \mu^-$), NP effects can also be extracted from Λ^0 polarization and asymmetry parameters (Figs. 2, 3, 4 from [489]), but influence of possible initial Λ_b polarization has to be accounted for [495]. Note that the measurement of the di-lepton mass spectrum is more sensitive to the ATLAS detector efficiency than to new physics.

The main part of B-physics studies will be performed in the initial LHC low-luminosity stage (3 years at $L = 10^{33}$ cm^{-2} s^{-1}). It is expected that the luminosity will vary by a factor of ~2 during beam-coast and there will be 2–3 interactions per collision. The production rate of $b\bar{b}$ pairs at ATLAS is ~500 kHz, which implies having 5×10^{12} $b\bar{b}$ pairs per year (10^7 seconds).

Experimental feasibility studies for rare decays of B_d^0, B_s^0, B^+ and Λ_b at ATLAS have been performed using the full detector simulation chain [511]. The decay kinematics was defined via matrix elements included into the b-physics

Table 20 Expected yields returned by the fit as described in the text

	Yield	B/S	$\sigma(m_{B_u})$
$B^+ \to K^+ \mu^+ \mu^-$	18774 ± 230	~29	14 MeV/c^2
$B^+ \to K^+ e^+ e^-$	9240 ± 380	~30	68 MeV/c^2

Pythia interface [512] (B_d^0, B_s^0) or using the EvtGen decay tool [513, 514] (B^+, Λ_b) with matrix elements taken from theoretical publications in [295, 434, 486, 488, 515]. The pp interactions were generated using Pythia6 [516] tuned for correct b-quark production [512]. Events were filtered at generator level to emulate the di-muonic LVL1 trigger cuts (see below), and charged tracks from the B-decays were required to fit in ATLAS tracking system capabilities ($p_T \gtrsim 0.5$ GeV, $|\eta| < 2.5$ [517]). These cuts influence the q^2 spectrum and A_{FB} shape. Study of the sample of $\Lambda_b \to \Lambda^0 \mu^+ \mu^-$ events have shown that higher di-muon mass values are preferred (fraction of events with q^2 below J/ψ mass decreased from 67 to 58%) and A_{FB} is affected in the $q^2/M_b^2 < 0.1$ region (suppression by 40% of $|A_{FB}|$ was found).

The trigger system at ATLAS consists of three levels: Level 1 trigger (LVL1), Level 2 trigger (LVL2) and Event Filter (EF) [518]. LVL1 stage is based on the detection of two high-p_T muons by the fast muon trigger chambers ($p_{T\mu_1} > 6$ GeV, $p_{T\mu_2} > 4$ GeV and $|\eta_{\mu_{1,2}}| < 2.5$ driven by detector acceptance). A preliminary study of the di-muonic LVL1 performance was shown in [519]. The LVL1 rate is dominated by real di-muons giving a rate of ~150 Hz but also by events with a single muon, doubly counted due to overlap of trigger chambers. In order to suppress the fake di-muon triggers, a system of overlap flags was introduced. The study indicated that signal rejection due to this overlap-removal algorithm is less than 0.5%. Efficiency suppression due to small di-muonic opening angles was also studied, finding the effect below 1%. Overall (75–80)% single muon and ~60% di-muon trigger efficiency was found for the sample of $\Lambda_b \to \Lambda^0 \mu^+ \mu^-$ events. At the second level, the muon p_T measurement will be confirmed in the Muon Precision Chambers, Tile Calorimeter and extrapolated to the Inner Detector in order to reject muons from K/π decays. The di-muon specific detailed LVL2 and EF strategies have not yet been set up. The purpose of LVL2 is to select preliminary candidates for the B-hadrons rare decay, based

Eur. Phys. J. C (2008) 57: 309–492

359
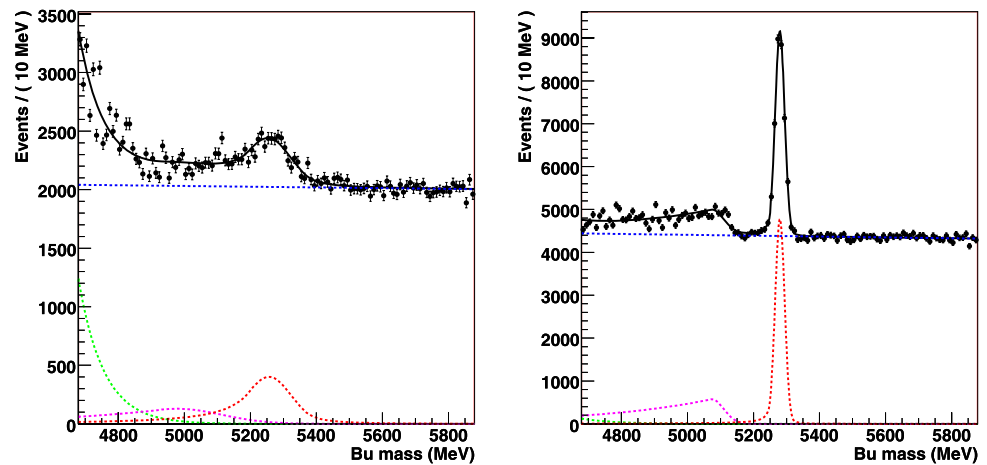
on track parameters and fast calculations. A secondary fast vertex fit can optionally be used at LVL2 level to achieve a satisfactory background rejection. At the EF level, offline-like selection cuts will be applied.

The key signature of rare decays is the presence of the opposite-charge muon pair. The di-muon pair is likely to form a secondary vertex which is detached from the primary vertex. The identification of this vertex, if particularly close to the interaction point, requires well-reconstructed leptons. The event selection is done in the following order: muon and di-muon identification; secondary hadron selection; B-hadron selection. The analysis has to rely on topological variables as vertex quality, vertex separation ($c\tau_B \geq 0.5$ ps) and pointing to primary vertex constraint on the B-hadron momentum. The vertexing algorithm used is the one adopted from the CDF Collaboration [520]. Simple vertex fits are used to select secondary hadrons and di-muon candidates, while for the B-hadron, the whole cascade decay topology is fitted at once.

Due to low signal BRs, great background suppression has to be achieved. The main background source comes from beauty decays producing a muon pair in the final state. The present study based on a sample of $b\bar{b} \to X \mu_{p_T > 6(4)}$ GeV $\mu_{p_T > 4}$ GeV events, provides upper limits for fake events as sketched in Table 21.

In Table 22, the reconstructed A_{FB} is presented for $B_d^0 \to K^{0*} \mu^+ \mu^-$ decay. We divide the q^2/M_B^2-region into three

Table 21 Expected number of events for signal and background upper limit after 30 fb^{-1} measurement

Decay	Signal	Background
$B_d^0 \to K^{0*} \mu^+ \mu^-$	2500	12000
$B_s^0 \to \phi \mu^+ \mu^-$	900	10000
$B^+ \to K^{*+} \mu^+ \mu^-$	2300	12000
$B^+ \to K^+ \mu^+ \mu^-$	4000	12000
$\Lambda_b \to \Lambda^0 \mu^+ \mu^-$	800	4000

Table 22 Averaged A_{FB} of $B_d^0 \to K^{0*} \mu^+ \mu^-$ from ATLAS simulations (not corrected for detector effects and background) at $L_{int} = 30$ fb^{-1}, its statistical precision and comparison to SM prediction

Interval of q^2/M_B^2	$-0.00 \atop 0.14$	$-0.14 \atop 0.33$	$-0.55 \atop 0.71$
Number of events	570	540	990
A_{FB}	11.8%	−6.1%	−13.7%
Statistical error	4.2%	4.3%	3.2%
SM prediction	10%	−14%	−29%

intervals: the first interval from $(2m_\mu/M_B)^2$ to the so-called "zero-point" [481], the second interval from the "zero-point" to the lower boundaries of the J/ψ and ψ' resonances and the last interval from the resonance area to $(M_B - M_{K^*})^2/M_B^2$. Data collected in 3 years of LHC operations, corresponding to 30 fb^{-1} of integrated luminosity, will be enough to confirm the Standard Model or to set strong limits on SM extensions.

An attempt to estimate the statistical errors of the branching ratio measurements has been made for $B^+ \to K^+ \mu^+ \mu^-$ and $B^+ \to K^{*+} \mu^+ \mu^-$ decays [521]. They were $\sim3.5\%$ and $\sim6.5\%$, respectively for $B^+ \to K^+ \mu^+ \mu^-$ and $B^+ \to K^{*+} \mu^+ \mu^-$ decays. These errors on the branching ratio measurements are much smaller than the current experimental and theoretical ones.

3.2.4 Phenomenological implications and new physics constraints

3.2.4.1 New Physics in exclusive $b \to s\ell^+\ell^-$ induced decays The potential of SM tests and NP searches with $b \to s\ell^+\ell^-$ transitions has been stressed and explored in several works, e.g., [507, 522] and references therein. Of particular interest for the LHC are the exclusive decays (i) $B_s \to \ell^+\ell^-$, (ii) $B \to K^{(*)}\ell^+\ell^-$, $B_s \to \phi\ell^+\ell^-$, $B_s \to \eta^{(')}\ell^+\ell^-$ and (iii) $\Lambda_b \to \Lambda\ell^+\ell^-$, where $\ell = e, \mu, (\tau)$. Decays involving additional photons, such as $B_s \to \ell^+\ell^-\gamma$ [523] are more

360

Eur. Phys. J. C (2008) 57: 309–492

sensitive to the hadronic QCD dynamics than the modes (i)–(iii). They are briefly considered in Sect. 3.4. Lepton flavor violating (LFV) decays such as $b \to s e^\pm \mu^\mp$ are discussed e.g. in [524, 525] and will not be considered further here. We stress that FCNCs with final state τ-leptons are poorly constrained experimentally to date, and it would be highly desirable to fill this gap since they test third generation couplings. The latter feature is also shared by the di-neutrino final states discussed, e.g., in [526] and in Sect. 3.3.

The presence of NP can lead to modified values for the short-distance coefficients C_i, including new CP-violating phases, and the generation of new operators in the weak effective Hamiltonian. These could include chirality flipped versions of the SM operators $\mathcal{O}_i'$ (down by m_s/m_b within the SM) from right-handed currents or scalar operators from Higgs exchanges $\mathcal{O}_{S,P}$ (down by $m_\ell m_b/m_W^2$ within the SM), or tensor currents. Scenarios with *light* NP particles require additional operators, build out of the latter, see [527] for the MSSM with light sbottom and gluino. Model-independent information on $C_{7,8,9,10}^{(\mathrm{eff})}$ has been previously extracted from combined analysis of $b \to s \ell^+\ell^-$ and radiative $b \to s\gamma, sg$ data [434, 482, 500], also including (pseudo)-scalar contributions $C_{S,P}$ [435, 528]. In this program, the study of correlations between decays and observables is an important ingredient, which enables identification of a possible SM breakdown and its sources.

The leptonic decay $\bar{B}_q^0 \to \ell^+\ell^-$ is a smoking gun for neutral Higgs effects in SUSY models with large $\tan\beta$ and is discussed in detail in Sect. 3.4. A clean test of minimal flavor violation (MFV, see Sect. 1.2.3) is the B_d–B_s-ratio $R_{\ell\ell} \equiv \mathcal{B}(\bar{B}_d^0 \to \ell^+\ell^-)/\mathcal{B}(\bar{B}_s^0 \to \ell^+\ell^-)$. In the SM and within MFV models, $0.02 \lesssim R_{\ell\ell|\mathrm{SM}} \lesssim 0.05$, whereas in non-MFV scenarios, $R_{\ell\ell}$ can be $\mathcal{O}(1)$ [529]. Phases in $C_{S,P}$ are probed with time-dependent and integrated CP-asymmetries requiring lepton-polarization measurements [530–532].

Besides the measurement of branching ratios, the $\bar{B} \to K\ell^+\ell^-$ and $\bar{B} \to K^*\ell^+\ell^-$ decays offer a number of orthogonal observables. For instance, the latest experimental results from Belle and BaBar for these modes [500, 501, 533] already include first investigations of angular distributions. The dilepton mass (q^2) spectra of $\bar{B} \to K^{(*)}\ell^+\ell^-$ are sensitive to the sign of $\mathrm{Re}(C_7^{\mathrm{eff}*}C_9^{\mathrm{eff}})$ and to NP contributions in $C_{9,10}$ and flipped $C_{9,10}'$ [534]—however, with rather large hadronic uncertainties from form factors and nonfactorizable long-distance effects (see Sect. 3.2.2). Using constraints on $|C_{S,P}|$ from $B_s \to \mu^+\mu^-$ [528] shows that $\bar{B} \to K^{(*)}\ell^+\ell^-$ spectra are rather insensitive to NP effects in C_S and C_P. A dedicated study of $B \to K\ell^+\ell^-$ angular distributions in the SM and beyond has been presented recently in [535].

The FB asymmetry for decays into light pseudoscalars, $A_{FB}(\bar{B} \to K\ell^+\ell^-)$, vanishes in the SM. Beyond the SM, it

is proportional to the lepton mass and the matrix elements of the new scalar and pseudoscalar penguin operators. The BaBar measurement of the angular distribution [501] is consistent with a zero FB asymmetry. Using model-independent constraints on $|C_{S,P}|$ from $B_s \to \mu^+\mu^-$ [528], one expects $A_{FB}(B \to K\mu^+\mu^-) < 4\%$. Moreover, in the MSSM with large $\tan\beta$, one has $C_S \simeq -C_P$, and the FB asymmetry comes out even smaller, $A_{FB}(B \to K\ell^+\ell^-) \lesssim 1(30)\%$ for $\ell = \mu(\tau)$ [503, 536, 537]. In contrast, for decays into light vector mesons, $A_{FB}(\bar{B} \to K^*\ell^+\ell^-)$ is nonzero in the SM and exhibits a characteristic zero q_0^2, whose position is relatively free of hadronic uncertainties, see Sect. 3.2.2. In a general model-independent NP analysis [534, 538], the position of the zero, the magnitude and shape of $A_{FB}(\bar{B} \to K^*\ell^+\ell^-)$ are found to depend on the modulus and phases of all Wilson coefficients. Note that also $\Lambda_b \to \Lambda\ell^+\ell^-$ decays share the universal SM A_{FB}-zero in lowest order of the $1/m_b$ and α_s expansion [485]. In off-resonance $B \to K\pi\ell^+\ell^-$ decays, the analogous A_{FB} zero is also sensitive to NP effects [484]. The CP-asymmetry for the FB asymmetry in $\bar{B} \to K^*\ell^+\ell^-$ is a quasi-null test of the SM [526], with $A_{FB}^{\mathrm{CP}}|_{\mathrm{SM}} < 10^{-3}$. Sizable values can arise beyond the SM, for instance from nonstandard CP-violating Z-penguins contributing to $\arg(C_{10})$.

The (CP-averaged) isospin asymmetry in $\bar{B} \to K^*\ell^+\ell^-$ is defined from the difference between charged and neutral B decays [539]. It vanishes in naive factorization (assuming isospin-symmetric form factors). A nonzero value arises from nonfactorizable interactions where the photon couples to the spectator quark. For small values of q^2, the isospin asymmetry can be analysed in QCDF [539]. The largest contributions are induced by the strong penguin operators $\mathcal{O}_{3-6}$, and the sign of the asymmetry depends on the sign of C_7^{eff}. Within the SM and minimal-flavor violating MSSM scenarios, the isospin asymmetry is found to be small. Sizable deviations of $A_I(\bar{B} \to K^*\ell^+\ell^-)$ from zero would thus signal NP beyond MFV.

Following Refs. [476, 477], one can construct further observables from an angular analysis of the decay $\bar{B}^0 \to K^{*0}(\to K^-\pi^+)\ell^+\ell^-$, see (90), (92). The SM predictions are consistent with the existing experimental data for the (integrated) value of the longitudinal K^* polarization F_L [501]. A model-independent analysis with flipped $\mathcal{O}_7'$ shows some sensitivity of the angular observables to right-handed currents [476, 477], see also [534]. The shapes of the transverse asymmetries $A_T(q^2)$ depend strongly on C_7 and C_7', whereas NP effects in $C_{9,10}$ are rather small taking into account constraints from other B-physics data. Moreover, the zeros of $A_T^{(1,2)}(q^2)$ are sensitive to C_7'. NP can give large contributions to the polarization parameter $\alpha_{K^*}(q^2)$ and $F_{L,T}(q^2)$ in extreme scenarios, however the influence of C_9 and C_{10} is stronger, and theoretical errors are larger than in $A_T^{(1,2)}$.

Eur. Phys. J. C (2008) 57: 309–492

361

The muon-to-electron ratios

$$R_H \equiv \int_{q_1}^{q_2} dq^2 \frac{d\Gamma(B \to H\mu^+\mu^-)}{dq^2}$$

$$\bigg/ \int_{q_1}^{q_2} dq^2 \frac{d\Gamma(B \to He^+e^-)}{dq^2},$$

$$H = \{K, K^*\}, \tag{96}$$

are probing for nonuniversal lepton couplings, for instance from Higgs exchange or R-parity violating interactions in SUSY models. Kinematic lepton-mass effects are tiny, $\mathcal{O}(m_\mu^2/m_b^2)$. Taking the same integration boundaries for muon and electrons, the SM predictions are rather free of hadronic uncertainties [435]

$$R_H^{SM} = 1 + \mathcal{O}(m_\mu^2/m_b^2), \quad \text{with}$$
$$R_K^{SM} = 1 \pm 0.0001, \qquad R_{K^*}^{SM} = 0.991 \pm 0.002, \tag{97}$$

and agree with the measurements $R_K = 1.06 \pm 0.48 \pm 0.08$ and $R_{K^*} = 0.91 \pm 0.45 \pm 0.06$ [501].

Studying correlations between different observables, one may be able to discriminate between different NP models. For instance, nontrivial correlation effects appear between R_K and $\mathcal{B}(B_s \to \mu^+\mu^-)$, since $\bar{B} \to K\ell^+\ell^-$ depends on $C_{S,P} + C'_{S,P}$, whereas $\mathcal{B}(\bar{B}_q^0 \to \ell^+\ell^-)$ on $C_{S,P} - C'_{S,P}$ [435]. Also, $\mathcal{B}(B_s \to \mu^+\mu^-)$ and Δm_s are strongly correlated in the minimal flavor-violating MSSM at large $\tan\beta$ [30], whereas no such correlation occurs in models with an additional gauge singlet, like the NMSSM studied in [540]. A summary of all observables with central results is given in Table 23.

3.2.4.2 $B \to K^*\ell\ell$ and universal extra dimensions FCNC B decays are sensitive to NP scenarios involving extra dimensions. As an example, we discuss here the possibility to constrain the model proposed in [180] (ACD model), which is an extension of the SM by a fifth (universal) extra dimension. The extra dimension is compactified to the orbifold S^1/Z_2, and all the SM fields are allowed to propagate in all dimensions. This model only requires a single additional parameter with respect to the SM, namely the radius R of the compactified extra dimension. The SM is recovered in the limit $1/R \to \infty$ where the predicted extra Kaluza–Klein particles decouple from the low-energy theory.

The effective Hamiltonian inducing $b \to s\ell^+\ell^-$, $b \to s\nu\bar{\nu}$ and $b \to s\gamma$ transitions in ACD has been computed in [17, 181]. In the case of the exclusive modes $B \to K^{(*)}\ell^+\ell^-$, $B \to K^{(*)}\nu\bar{\nu}$ and $B \to K^*\gamma$, there are several observables sensitive to $1/R$ that can be used to probe this scenario [182, 183]. At present, the most stringent experimental bound on $1/R$ comes from $B \to K^*\gamma$, leading to $1/R \geq 300$–400 GeV, depending on the assumed hadronic uncertainties.

For values of $1/R$ of the order of a few hundred GeV, one expects an enhancement of $B(B \to K^{(*)}\ell^+\ell^-)$ and $B(B \to K^{(*)}\nu\bar{\nu})$ with respect to the SM (of the order of 20% for $1/R = 300$ GeV) and a suppression of $B(B \to K^*\gamma)$ (at the same level for $1/R = 300$ GeV). In general, the sensitivity to $1/R$ is masked by the uncertainty of the hadronic $B \to K^{(*)}$ matrix elements. A useful observable with smaller hadronic uncertainties is the position of the FB asymmetry zero in $B \to K^*\ell^+\ell^-$, which in ACD is shifted to smaller values as $1/R$ decreases, as shown in Fig. 11 (left). Another interesting quantity, which however has a more pronounced dependence on hadronic uncertainties is the position $(q^2)_{max}$ of the maximum of the longitudinal helicity fraction of K^* in the same process; its sensitivity to $1/R$ is also shown in Fig. 11 (right).

In the case of $B \to K^{(*)}\tau^+\tau^-$ decays, τ-polarization asymmetries can be considered, in which the hadronic form factor dependence drops out for large K^* recoil energies. The transverse asymmetry decreases as $1/R$ is decreased, whereas the branching fraction increases. The combined observation of this pattern of deviations from SM results would represent a signature of the ACD scenario.

3.3 Neutrino modes[14]

Here we discuss the so-called neutrino modes. In particular, we talk about the rare SM modes $B \to X_s\nu\bar{\nu}$ and $B \to \tau\nu$. Experimentally, these modes are similar since both are associated with large missing energy. In $B \to X_s\nu\bar{\nu}$, there are the two neutrinos, in $B \to \tau\nu$, the τ decays very fast, yielding a final state with two neutrinos as well. Theoretically these two modes are different. $B \to X_s\nu\bar{\nu}$ is an FCNC process and thus occurs at one loop in the SM. $B \to \tau\nu$, on the other hand, occurs at tree level, but it is strongly suppressed for several reasons: helicity, a small CKM factor and the decay mechanism by weak annihilation $\sim 1/m_B$.

3.3.1 Neutrino modes: theory

3.3.1.1 Inclusive $b \to s\nu\bar{\nu}$ decays Here we follow [542] with necessary updates. The FCNC decay $B \to X_s\nu\bar{\nu}$ is very sensitive to extensions of the SM and provides a unique source of constraints on some NP scenarios which predict a large enhancement of this decay mode. In particular, the $B \to X_s\nu_\tau\bar{\nu}_\tau$ mode is very sensitive to the relatively unexplored couplings of third generation fermions.

From the theoretical point of view, the decay $B \to X_s\nu\bar{\nu}$ is a very clean process. Both the perturbative α_s and the nonperturbative $1/m_b^2$ corrections are known to be small. Furthermore, in contrast to the decay $B \to X_s\ell^+\ell^-$, which suffers from (theoretical and experimental) background

---

[14]Section coordinators: Y. Grossman, T. Iijima.

362

Eur. Phys. J. C (2008) 57: 309–492

Table 23 Summary of observables in $\bar{B} \to K\ell^+\ell^-$, $\bar{B} \to K^*\ell^+\ell^-$ and $\bar{B}_q^0 \to \ell^+\ell^-$ decays

Observable	Comments
$d\Gamma(\bar{B} \to K^{(*)}\ell^+\ell^-)/dq^2$	Hadronic uncertainties (form factors, nonfactorizable effects, $c\bar{c}$)
	SM: depends on $|C_{7,9,10}^{\mathrm{eff}}|$ and $\mathrm{Re}(C_7^{\mathrm{eff}*}C_9^{\mathrm{eff}})$
	NP: sensitive to Z-penguins, $C'_{9,10}$, $\mathrm{sgn}(C_7^{\mathrm{eff}})$, but not to $C_{S,P}^{(')}$
$A_{FB}(\bar{B} \to K\ell^+\ell^-)$	SM: $\simeq 0$ (quasi null test)
	NP: sensitive to $C_S + C'_S$
	using $B_s \to \mu^+\mu^-$ constraint: $<$(few % for $\mu^+\mu^-$)
$dA_{FB}(\bar{B} \to K^*\ell^+\ell^-)/dq^2$	Hadronic uncertainties
(shape and magnitude)	NP: sensitive to $\mathrm{sgn}(C_7^{\mathrm{eff}})$, $\mathrm{sgn}(C_{10}^{\mathrm{eff}})$, Z-penguins
FB asymmetry zero	Smaller uncertainties (test of the SM)
A_{FB}^{CP}	SM: $<10^{-3}$ (quasi null test)
	NP: CP-phase in C_{10} (+ dynamic strong phase)
$dA_I(\bar{B} \to K^*\ell^+\ell^-)/dq^2$	Hadronic uncertainties
	SM: $\mathcal{O}(+10\%)$ for $q^2 \leq 2$ GeV^2; depends on $C_{5,6}$ (cf. $A_I(\bar{B} \to K^*\gamma)$)
	$\mathcal{O}(-1\%)$ for $2 \leq q^2 \leq 7$ GeV^2; depends on $C_{3,4}$
	NP: sensitive to strong penguin operators; $\mathrm{sgn}(C_7^{\mathrm{eff}})$
$A_T^{(1,2)}$, α_{K^*}, $F_{L,T}$	Smaller uncertainties (test of SM)
	NP: right-handed currents, e.g., C'_7
$R_{K^{(*)}}$	Tiny uncertainties: $< \pm 1\%$
	SM: $1 + \mathcal{O}(m_\mu^2/m_b^2)$ (common cuts)
	NP: nonuniversal lepton couplings; $C_{S,P}^{(')}$, neutral Higgs exchange
$\mathcal{B}(\bar{B}_q^0 \to \ell^+\ell^-)$	Uncertainties: f_{B_q}
	SM: depends on $|C_{10}V_{tq}|$
	NP: lepton-mass effects; $C_{S,P}^{(')}$, neutral Higgs exchange
$R_{\ell\ell}$	Uncertainties: f_{B_d}/f_{B_s}
	SM: $\sim |V_{td}|^2/|V_{ts}|^2 f_{B_d}^2/f_{B_s}^2$
	NP: test of MFV

Fig. 11 Position of the zero, $s_0 \equiv q_0^2$, of A_{FB} (*left*) and of the maximum of the longitudinal K^* helicity fraction (*right*) in $B \to K^*\ell^+\ell^-$ as a function of $1/R$ in the ACD extra dimension scenario. R is the radius of the compactified extra dimension. The uncertainties only include the $B \to K^*$ form-factor dependence; nonfactorizable corrections have not been taken into account
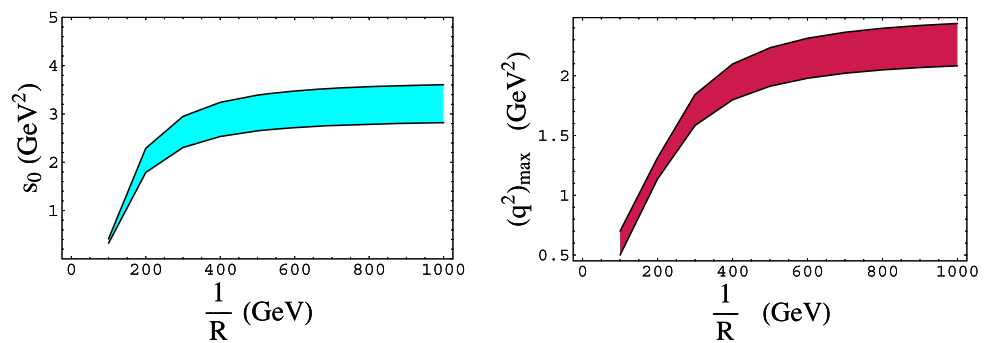
such as $B \to X_s J/\psi \to X_s \ell^+\ell^-$, there are no important long-distance QCD contributions. Therefore, the decay $B \to X_s \nu\bar{\nu}$ is well suited to search for and constrain NP effects.

Another advantage of the $B \to X_s \nu\bar{\nu}$ mode is that the missing energy spectrum can be calculated essentially in a model-independent way. Thus, one can directly compare experimental data with the theoretical expressions as derived in specific models. Under the only assumption of two-component left-handed neutrinos, the most general form of the four-fermion interaction responsible for $B \to X_q \nu_i \bar{\nu}_j$ reads

$$\mathcal{L} = C_L O_L + C_R O_R, \tag{98}$$

where

$$O_L = [\bar{q}_L \gamma_\mu b_L][\bar{v}_L^i \gamma^\mu v_L^j],$$
$$O_R = [\bar{q}_R \gamma_\mu b_R][\bar{v}_L^i \gamma^\mu v_L^j].$$
(99)

Here L and R denote left- and right-handed components, $q = d, s$, and $i, j = e, \mu, \tau$. As the flavors of the decay products are not detected, in certain models more than one final state can contribute to the observed decay rate. Then, in principle, both C_L and C_R carry three indices q, i, j, which label the quark and neutrino flavors in the final state.

In the SM, $B \to X_s \nu \bar{\nu}$ proceeds via W-box and Z-penguin diagrams, and only O_L is present. The corresponding coefficient reads

$$C_L^{\rm SM} \simeq \frac{\sqrt{2} G_F \alpha}{\pi \sin^2 \theta_W} V_{tb}^* V_{ts} X_0(x_t),$$
$$X_0(x) = \frac{x}{8}\left[\frac{2+x}{x-1} + \frac{3x-6}{(x-1)^2}\ln x\right],$$
(100)

where $x_t = m_t^2/m_W^2$. The leading $1/m_b^2$ and α_s corrections to the SM result are known. Thus, the theoretical uncertainties in the SM rate are rather small, less than $O(5\%)$. They come mainly from the uncertainties in m_t, $|V_{ts}|$ and unknown higher-order corrections. At lowest order, the missing energy spectrum in the B rest-frame is given by [541]

$$\frac{d\Gamma(B \to X_q \nu_i \bar{\nu}_j)}{dx} = \frac{m_b^5}{96\pi^3}\left(|C_L|^2 + |C_R|^2\right)\mathcal{S}(r, x). \quad (101)$$

Here we have not yet summed over the neutrino flavors. The function $\mathcal{S}(r, x)$ describes the shape of the missing energy spectrum

$$\mathcal{S}(r, x) = \sqrt{(1-x)^2 - r}\left[(1-x)(4x-1) + r(1-3x)\right.$$
$$\left. - 6\eta\sqrt{r}(1-2x-r)\right].$$
(102)

The dimensionless variable $x = E_{\rm miss}/m_b$ can range between $(1-r)/2 \leq x \leq 1 - \sqrt{r}$, and $r = m_s^2/m_b^2$. The parameter $\eta = -{\rm Re}(C_L C_R^*)/(|C_L|^2 + |C_R|^2)$ ranges between $-\frac{1}{2} \leq \eta \leq \frac{1}{2}$. Since r is very small, in practice the spectrum is independent of the relative size of C_L and C_R and therefore immune to the presence of NP.

It is convenient to define two "effective" coefficients $\tilde{C}_L$ and $\tilde{C}_R$, which can be computed in terms of the parameters of any model and are directly related to the experimental measurement. To remove the large uncertainty in the total decay rate associated with the m_b^5 factor, it is convenient to normalize $B(B \to X_s \nu \bar{\nu})$ to the semileptonic rate $B(B \to X_c e \bar{\nu})$. The contribution from $B \to X_u e \bar{\nu}$, as well as possible NP effects on the semileptonic decay rate are negligible. In constraining NP, we can also set $m_s = 0$ and neglect both order α_s and $1/m_b^2$ corrections. This is justified, since when averaged over the spectrum these effects are very

small, and would affect the numerical bounds on the NP parameters only in a negligible way. For the total $B \to X_q \nu_i \bar{\nu}_j$ decay rate into all possible $q = d, s$ and $i, j = e, \mu, \tau$ final state flavors, we then obtain

$$\frac{B(B \to X \nu \bar{\nu})}{B(B \to X_c e \bar{\nu})} = \frac{\tilde{C}_L^2 + \tilde{C}_R^2}{|V_{cb}|^2 f(m_c^2/m_b^2)},$$
(103)

where $f(x) = 1 - 8x + 8x^3 - x^4 - 12x^2 \ln x$ is the usual phase-space factor, and we defined

$$\tilde{C}_L^2 = \frac{1}{8G_F^2}\sum_{q,i,j}|C_L^{qij}|^2, \qquad \tilde{C}_R^2 = \frac{1}{8G_F^2}\sum_{q,i,j}|C_R^{qij}|^2.$$
(104)

Note that channels with a different lepton flavor in the final state do not interfere. Thus, the sum among different channels is in the rate and not in the amplitude. The SM prediction, including NLO QCD corrections [214, 557, 558], is $B^{\rm SM}(B \to X_s \nu \bar{\nu}) = 4 \times 10^{-5}$.

New physics can generate new contributions to C_L and/or to C_R. Many NP models were studied in [542]. In general, there are bounds from other processes, in particular, $b \to s\ell^+\ell^-$. In all models where these two processes are related, the NP contribution to the neutrino modes is bounded to be below the SM expectation. In that case, one needs to measure the neutrino mode at high precision in order to be able to probe these models of new physics.

The other case may be more interesting. In some models, there is an enhancement of the couplings to the third generation. Then $B \to X_s \nu \bar{\nu}$ is related only to $b \to s\tau^+\tau^-$. This mode is very hard to measure, and thus there is no tight bound on these models. In that cases, NP could enhance the rate much above the SM rate. That is, if we find that the rate of $B \to X_s \nu \bar{\nu}$ is much above the SM rate, it will be an indication for models where the third generation is different.

3.3.1.2 Exclusive $b \to s\nu\bar{\nu}$ decays In principle, the theoretically cleanest observables are provided by inclusive decays, on the other hand, the exclusive variants will be more readily accessible in experiment. Despite the sizable theoretical uncertainties in the exclusive hadronic form factors, these processes could therefore give interesting first clues on deviations from what is expected in the SM [526]. This is particularly true if those happen to be large or if they show striking patterns. In the following, we discuss integrated observables and distributions in the invariant mass of the dilepton system, q^2, for the three-body decays $B \to M\nu\bar{\nu}$ with $M = K, K^*$. The kinematical range of q^2 is given by $0 \leq q^2 \leq (m_B - m_M)^2$. In the $B \to M\nu\bar{\nu}$ decays, q^2 is not directly measurable but it is related to the kaon energy in the B-meson rest frame, E_M, by the relation $q^2 = m_B^2 + m_M^2 - 2m_B E_M$, where $m_M \leq E_M \leq (m_B^2 + m_M^2)/(2m_B)$.

364

Eur. Phys. J. C (2008) 57: 309–492

$B \to K \nu \bar{\nu}$ The dilepton spectrum of this mode is particularly simple and it is sensitive only to the combination $|C_L^\nu + C_R^\nu|^2$ [545, 546]. This is in contrast to the inclusive case where only the combination $|C_L^\nu|^2 + |C_R^\nu|^2$ entered the decay rate. In the inclusive case, all the interference terms average to zero when we sum over all the possible hadronic final states. In this way, exclusive processes are natural grounds where to perform tests of right-handed NP currents, given their interference with the purely left-handed SM current. Finally, the dilepton spectrum is [545, 546]

$$\frac{d\Gamma(B \to K \nu \bar{\nu})}{ds} = \frac{G_F^2 \alpha^2 m_B^5}{256\pi^5} |V_{ts}^* V_{tb}|^2 \lambda_K^{3/2}(s) f_+^2(s) |C_L^\nu + C_R^\nu|^2, \quad (105)$$

where we have defined the dimensionless variables $s = q^2/m_B^2$ and $r_M = m_M^2/m_B^2$ and the function

$$\lambda_M(s) = 1 + r_M^2 + s^2 - 2s - 2r_M - 2r_M s. \quad (106)$$

In the case of $M = K$, the hadronic matrix elements needed for our analysis are given by (53) with $P = K$. Up to small isospin breaking effects, which we shall neglect, the same set of form factors describes both charged ($B^- \to K^-$) and neutral ($\bar{B}^0 \to \bar{K}^0$) transitions. Thus, in the isospin limit, we get

$$\Gamma(B \to K \nu \bar{\nu}) \equiv \Gamma(B^+ \to K^+ \nu \bar{\nu}) = 2\Gamma(B^0 \to K_{L,S} \nu \bar{\nu}). \quad (107)$$

The absence of absorptive final-state interactions in this process also leads to $\Gamma(B \to K \nu \bar{\nu}) = \Gamma(\bar{B} \to \bar{K} \nu \bar{\nu})$, preventing the observation of any direct CP-violating effect. Integrating (105) over the full range of s leads to

$$\mathcal{B}(B \to K \nu \bar{\nu}) = \left(3.8^{+1.2}_{-0.6}\right) \times 10^{-6} \left|\frac{C_L^\nu + C_R^\nu}{C_L|_{\mathrm{SM}}^\nu}\right|^2, \quad (108)$$

where the error is due to the uncertainty in the form factors.

If the experimental sensitivity on $B(B \to K \nu \bar{\nu})$ reached the 10^{-6} level, then the uncertainty due the form factors would prevent a precise extraction of $|C_L^\nu + C_R^\nu|$ from (108). This problem can be substantially reduced by relating the differential distribution of $B \to K \nu \bar{\nu}$ to the one of $B \to \pi e \nu_e$ [547, 548]:

$$\frac{d\Gamma(B \to K \nu \bar{\nu})/ds}{d\Gamma(B^0 \to \pi^- e^+ \nu_e)/ds} = \frac{3\alpha^2}{4\pi^2} \left|\frac{V_{ts}^* V_{tb}}{V_{ub}}\right|^2 \left(\frac{\lambda_K(s)}{\lambda_\pi(s)}\right)^{3/2} \left|\frac{f_+^K(s)}{f_+^\pi(s)}\right|^2 |C_L^\nu + C_R^\nu|^2. \quad (109)$$

Indeed $f_+^K(s)$ and $f_+^\pi(s)$ coincide up to $SU(3)$-breaking effects, which are expected to be small, especially far from the endpoint region. An additional uncertainty in (109) is induced by the CKM ratio $|V_{ts}^* V_{tb}|^2/|V_{ub}|^2$, which, however, can independently be determined from other processes.

$B \to K^* \nu \bar{\nu}$ A great deal of information can be obtained from the channel $B \to K^* \nu \bar{\nu}$ investigating, together with the lepton invariant mass distribution, also the FB asymmetry in the dilepton angular distribution. This may reveal effects beyond the SM that could not be observed in the analysis of the decay rate. The dilepton invariant mass spectrum of $B \to K^* \nu \bar{\nu}$ decays is sensitive to both combinations $|C_L^\nu - C_R^\nu|$ and $|C_L^\nu + C_R^\nu|$ [545, 546, 549]:

$$\frac{d\Gamma(B \to K^* \nu \bar{\nu})}{ds}$$
$$= \frac{G_F^2 \alpha^2 m_B^5}{1024\pi^5} |V_{ts}^* V_{tb}|^2 \lambda_{K^*}^{1/2}(s)$$
$$\times \left\{ \frac{8s\lambda_{K^*}(s)V^2(s)}{(1+\sqrt{r_{K^*}})^2} |C_L^\nu + C_R^\nu|^2 \right.$$
$$+ \frac{1}{r_{K^*}} \left[(1+\sqrt{r_{K^*}})^2 (\lambda_{K^*}(s) + 12r_{K^*}s) A_1^2(s) \right.$$
$$+ \frac{\lambda_{K^*}^2(s) A_2^2(s)}{(1+\sqrt{r_{K^*}})^2}$$
$$\left. \left. - 2\lambda_{K^*}(s)(1 - r_{K^*} - s) A_1(s) A_2(s) \right] |C_L^\nu - C_R^\nu|^2 \right\}, \quad (110)$$

where the form factors $A_1(s)$, $A_2(s)$ and $V(s)$ are defined in (54). Integrating (110) over the full range of s leads to

$$B(B \to K^* \nu \bar{\nu}) = \left(2.4^{+1.0}_{-0.5}\right) \times 10^{-6} \left|\frac{C_L^\nu + C_R^\nu}{C_L|_{\mathrm{SM}}^\nu}\right|^2$$
$$+ \left(1.1^{+0.3}_{-0.2}\right) \times 10^{-5} \left|\frac{C_L^\nu - C_R^\nu}{C_L|_{\mathrm{SM}}^\nu}\right|^2, \quad (111)$$

$$B(B \to K^* \nu \bar{\nu})\big|_{\mathrm{SM}} = \left(1.3^{+0.4}_{-0.3}\right) \times 10^{-5}. \quad (112)$$

A reduction of the error induced by the poor knowledge of the form factors can be obtained by normalizing the dilepton distributions of $B \to K^* \nu \bar{\nu}$ to the one of $B \to \rho e \nu_e$ [548, 550]. This is particularly effective in the limit $s \to 0$, where the contribution proportional to $|C_L^\nu + C_R^\nu|$ (vector current) drops out.

3.3.1.3 $B \to \ell \nu$ Recently, the Belle [326] and BaBar [543] Collaborations have observed the purely leptonic decays $B^- \to \tau^- \bar{\nu}$, (120) and (121). Even if both measurements are still affected by large uncertainties, the observation of the $B^- \to \tau^- \bar{\nu}$ transition represents a fundamental

step forward towards a deeper understanding of both flavor and electroweak dynamics. The precise measurement of its decay rate could provide clear evidence of NP, such as a nonstandard Higgs sector with large $\tan\beta$ [31].

Due to the $V - A$ structure of the weak interactions, the SM contributions to $B \to \ell \nu$ are helicity suppressed. Hence, these processes are very sensitive to non-SM effects (such as multi-Higgs effects) which might induce an effective pseudoscalar hadronic weak current [31]. In particular, charged Higgs bosons ($H^{\pm}$) appearing in any model with two Higgs doublets (including the SUSY case) can contribute at tree level to the above processes. The relevant four-Fermi interaction for the decay of charged mesons induced by $W^{\pm}$ and $H^{\pm}$ has the following form:

$$
\frac{4G_F}{\sqrt{2}} V_{ub} \left[(\bar{u}\gamma_\mu P_L b)(\bar{\ell}\gamma^\mu P_L \nu) \right.
$$
$$
\left. - \tan^2\beta \left(\frac{m_b m_\ell}{m_{H^\pm}^2} \right) (\bar{u} P_R b)(\bar{\ell} P_L \nu) \right],
\tag{113}
$$

where $P_{R,L} = (1 \pm \gamma_5)/2$. Here we keep only the $\tan\beta$-enhanced part of the $H^{\pm}ub$ coupling, namely the $m_b \tan\beta$ term. The decays $B \to \ell \nu$ proceed via the axial-vector part of the $W^{\pm}$ coupling and via the pseudoscalar part of the $H^{\pm}$ coupling. The amplitude then reads

$$
\mathcal{A}_{B\to\ell\nu} = \frac{G_F}{\sqrt{2}} V_{ub} f_B \left[m_\ell - m_\ell \tan^2\beta \frac{m_B^2}{m_{H^\pm}^2} \right] \bar{l}(1 - \gamma_5)\nu.
\tag{114}
$$

We observe that the SM term is proportional to m_ℓ because of the helicity suppression, while the charged Higgs term is proportional to m_ℓ because of the Yukawa coupling.

The SM expectation for the $B^- \to \tau^- \bar{\nu}$ branching fraction is

$$
\mathcal{B}(B^- \to \tau^- \bar{\nu})^{\text{SM}} = \frac{G_F^2 m_B m_\tau^2}{8\pi} \left(1 - \frac{m_\tau^2}{m_B^2} \right)^2 f_B^2 |V_{ub}|^2 \tau_B
$$
$$
= (1.59 \pm 0.40) \times 10^{-4},
\tag{115}
$$

where we used $|V_{ub}| = (4.39 \pm 0.33) \times 10^{-3}$ from inclusive $b \to u$ semileptonic decays [389], $\tau_B = (1.643 \pm 0.010)$ ps and the recent unquenched lattice result $f_B = (0.216 \pm 0.022)$ GeV [321].

The inclusion of scalar charged currents leads to the following expression [31]:

$$
R_{B\tau\nu} = \frac{\mathcal{B}(B^- \to \tau^- \bar{\nu})}{\mathcal{B}(B^- \to \tau^- \bar{\nu})^{\text{SM}}} = r_H = \left[1 - \tan^2\beta \frac{m_B^2}{m_{H^\pm}^2} \right]^2.
\tag{116}
$$

Interestingly, in models where the two Higgs doublets are coupled separately to up- and down-type quarks, the interference between $W^{\pm}$ and $H^{\pm}$ amplitudes is necessarily *destructive*. For a natural choice of the parameters ($30 \lesssim \tan\beta \lesssim 50$, $0.5 \lesssim M_{H^\pm}/\text{TeV} \lesssim 1$), (116) implies a (5–30)% suppression with respect to the SM. The corresponding expressions for the $K \to \ell\nu$ channels are obtained with the replacement $m_B \to m_K$, while for the $D \to \ell\nu$ case, $m_B^2 \to (m_s/m_c)m_D^2$. It is then easy to check that a 30% suppression of $B(B \to \tau\nu)$ should be accompanied by a 0.3% suppression (relative to the SM) in $B(D \to \ell\nu)$ and $B(K \to \ell\nu)$. At present, the theoretical uncertainty on the corresponding decay constants does not allow one to observe such effects.

Apart from the experimental error, one of the difficulties in obtaining a clear evidence of a possible deviation of $R_{B\tau\nu}$ from unity is the large parametric uncertainty induced by $|f_B|$ and $|V_{ub}|$. An interesting way to partially circumvent this problem is obtained by normalizing $B(B^- \to \tau^- \bar{\nu})$ to the B_d^0–$\bar{B}_d^0$ mass difference (ΔM_{B_d}) [32]. Neglecting the tiny isospin-breaking differences in masses, life-times and decay constants between B_d and B^- mesons, we can write [32]

$$
\left. \frac{B(B^- \to \tau^- \bar{\nu})}{\tau_B \Delta M_{B_d}} \right|^{\text{SM}}
$$
$$
= \frac{3\pi}{4\eta_B S_0(m_t^2/M_W^2)\hat{B}_{B_d}} \frac{m_\tau^2}{M_W^2} \left(1 - \frac{m_\tau^2}{m_B^2} \right)^2 \left| \frac{V_{ub}}{V_{td}} \right|^2
\tag{117}
$$
$$
= 1.77 \times 10^{-4} \left(\frac{|V_{ub}/V_{td}|}{0.464} \right)^2 \left(\frac{0.836}{\hat{B}_{B_d}} \right).
\tag{118}
$$

Following standard notation, we have denoted by $S_0(m_t^2/M_W^2)$, η_B and B_{B_d} the Wilson coefficient, the QCD correction factor and the bag parameter of the $\Delta B = 2$ operator within the SM (see e.g. Ref. [29]), using the unquenched lattice result $\hat{B}_{B_d} = 0.836 \pm 0.068$ [320] and $|V_{ub}/V_{td}| = 0.464 \pm 0.024$ from the UTfit Collaboration [210].

The ratio $R'_{B\tau\nu} = B(B^- \to \tau^- \bar{\nu})/\tau_B \Delta M_{B_d}$ could become a more stringent test of the SM in the near future, with higher statistics on the $B^- \to \tau^- \bar{\nu}$ channel. In generic extensions of the SM, the NP impact on $R_{B\tau\nu}$ and $R'_{B\tau\nu}$ is not necessarily the same. However, it should coincide if the non-SM contribution to ΔM_{B_d} is negligible, which is an excellent approximation in the class of models considered in [32].

For consistency, the $|V_{ub}/V_{td}|$ combination entering in $R'_{B\tau\nu} = B(B^- \to \tau^- \bar{\nu})/\tau_B \Delta M_{B_d}$ should be determined without using the information on ΔM_{B_d} and $B^- \to \tau^- \bar{\nu}$ (a condition that is already almost fulfilled). In the near future, one could determine this ratio with negligible hadronic uncertainties using the relation $|V_{ub}/V_{td}| = |\sin\beta_{\text{CKM}}/\sin\gamma_{\text{CKM}}|$.

366

Eur. Phys. J. C (2008) 57: 309–492

From (116) it is evident that such tree level NP contributions, namely the r_H factor, do not introduce any lepton flavor-dependent correction, and thus departures from the SM lepton universality are not introduced. However, as pointed out in Ref. [544], this is no longer true in realistic supersymmetric frameworks if the model contains sizable sources of flavor violation in the lepton sector (a possibility that is well motivated by the large mixing angles in the neutrino sector). In the last case, we can expect observable deviations from the SM in the ratios

$$R_P^{\ell_1/\ell_2} = \frac{B(P \to \ell_1 \nu)}{B(P \to \ell_2 \nu)} \qquad (119)$$

with $P = \pi, K, B$ and $\ell_{1,2} = e, \mu, \tau$. The lepton-flavor violating (LFV) effects can be quite large in e or μ modes, while in first approximation they are negligible in the τ channels. In the most favorable scenarios, taking into account the constraints from LFV τ decays [165, 166], spectacular order-of-magnitude enhancements for $R_B^{e/\tau}$ and $\mathcal{O}(100\%)$ deviations from the SM in $R_B^{\mu/\tau}$ are allowed [32]. The key ingredients that allow visible non-SM contributions in $R_P^{\mu/e}$ within the MSSM are large values of $\tan\beta$ and sizable mixing angles in the right-slepton sector such that the $P \to \ell_i \nu_j$ rate (with $i \neq j$) becomes nonnegligible.

3.3.2 Neutrino modes: experiment

Experimental prospects for neutrino modes, such as $b \to s\nu\bar{\nu}$, $B \to \tau\nu$ and $b \to c\tau\nu$, are discussed. Because of the missing multiple neutrinos in the final state, these decays lack kinematic constraints, which could be used to suppress background processes. The e^+e^- B-factories, where background is relatively low and can be reduced by reconstructing the accompanying B meson, would be the ideal place to measure these decays. We also discuss the prospect for $B \to \mu\nu$, which can be used to test the lepton universality in comparison to $B \to \tau\nu$.

Belle and BaBar have used hadronic decays to reconstruct the accompanying B (hadronic tags), for which the tagging efficiency is about 0.3(0.1)% for the charged (neutral) B meson. BaBar has used also semileptonic decays

$B \to D^{(*)}\ell\nu$ (semileptonic tags) to increase the efficiency at the expense of the signal-to-noise ratio.

The present e^+e^- B-factory experiments are starting to measure some of these decays, as demonstrated by the first evidence of $B \to \tau\bar{\nu}$, which was recently reported by Belle. However, precision measurements and detection of very difficult modes, such as $b \to s\nu\bar{\nu}$, require at least a couple of tens ab^{-1} data, which can be reached only at the proposed super B-factories.

3.3.2.1 $b \to s\nu\bar{\nu}$ Presently, experimental limits on exclusive $b \to s\nu\bar{\nu}$ modes are available from Belle and BaBar. Belle has reported the result of a search for $B^- \to K^-\nu\bar{\nu}$ using a 253 fb^{-1} data sample [551]. The analysis utilizes the hadronic tags and requires that the event has neither remaining charged tracks nor neutral clusters other than the K^- candidate. Figure 12(a) shows the distribution of remaining neutral cluster energy recorded in the electromagnetic calorimeter (E_{ECL}) after all the selection cuts are applied. The signal detection efficiency is estimated to be 43% for the tagged events. In the signal region defined as $E_{\text{ECL}} < 0.3$ GeV, the expected number of signals is 0.70, assuming the SM branching fraction of $\mathcal{B}(B \to K\nu\bar{\nu}) = 4 \times 10^{-6}$, while the number of background estimated from the sideband data is 2.6 ± 1.6. The deduced upper limit (90% C.L.) on the branching fraction is $\mathcal{B}(B^- \to K^-\nu\bar{\nu}) < 3.6 \times 10^{-5}$. More recently, Belle has reported an upper limit of $\mathcal{B}(B^0 \to K^{*0}\nu\bar{\nu}) < 3.4 \times 10^{-4}$ from a similar analysis on a 492 fb^{-1} data sample [552].

BaBar has reported $\mathcal{B}(B^- \to K^-\nu\bar{\nu}) < 5.2 \times 10^{-5}$ by combining the hadronic and semileptonic tag events from a 82 fb^{-1} data sample [553]. The right panel of Fig. 12 shows the distribution of the remaining energy (E_{extra} in BaBar's notation) for the semileptonic tag sample. Because of the large $B^- \to D^{(*)}\ell\bar{\nu}$ branching fractions, the semileptonic tag method has a factor 2 to 3 higher efficiency than the hadronic tag method.

Based on a simple-minded extrapolation from the Belle analysis with the hadronic tags, the required integrated luminosity for observing the $B^- \to K^-\nu\bar{\nu}$ decay with $3(5)\sigma$ statistical significance is 12(33) ab^{-1}. The statistical precision for the branching fraction measurement will reach 18%

Fig. 12 Distribution of remaining energy for $B^- \to K^-\nu\bar{\nu}$ candidates: from Belle's analysis using the hadronic tag on a 253 fb^{-1} data sample (*left*) and from BaBar's analysis using the semileptonic tag on a 82 fb^{-1} data sample (*right*)
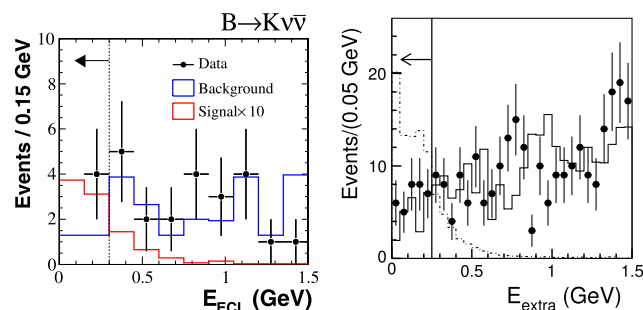
at 50 ab^{-1}. Addition of the semileptonic tag sample may improve the sensitivity (this is under investigation).

It is extremely difficult to perform an inclusive search for $b \to s\nu\bar{\nu}$. No serious studies have been made yet.

3.3.2.2 $B \to \tau\nu$ Detection of $B^- \to \tau^-\bar{\nu}$ is very similar to that of $B \to K^{(*)}\nu\bar{\nu}$, and it requires that the event has no extra charged tracks nor neutral clusters other than those from the τ decay and the accompanying B decay.

Recently Belle has reported the first evidence for $B^- \to \tau^-\bar{\nu}$ by applying the hadronic tag on a 414 fb^{-1} data sample [326]. The reconstructed τ decay modes are $\tau^- \to e^-\bar{\nu}_e\nu_\tau$, $\mu^-\bar{\nu}_\mu\nu_\tau$, $\pi^-\nu_\tau$, $\pi^-\pi^0\nu_\tau$, $\pi^-\pi^+\pi^-\nu_\tau$. The left panel of Fig. 13 presents the E_{ECL} distribution combined for all the τ decay modes, which shows an excess of events near $E_{ECL} = 0$. The number of signal (N_s) and background events (N_b) in the signal region are determined to be $N_s = 17.2^{+5.3}_{-4.7}$ and $N_b = 32.0 \pm 0.7$ by an unbinned maximum likelihood fit. The significance of the excess is 3.5σ including both statistical and systematic uncertainties. The obtained branching fraction is [326]

$$\mathcal{B}(B^- \to \tau^-\bar{\nu}) = \left[1.79^{+0.56}_{-0.49}(\text{sta})^{+0.46}_{-0.51}(\text{sys})\right] \times 10^{-4}. \quad (120)$$

BaBar has reported results of a $B^- \to \tau^-\bar{\nu}$ search using the semileptonic tag on a 288 fb^{-1} data sample [543]. The tag reconstruction efficiency is about 0.7%, depending slightly on run periods. When all the analysed τ decay modes are combined, 213 events are observed, while the background is estimated to be 191.7 ± 11.7. Since the excess is not significant, they provide an upper limit of $\mathcal{B}(B^- \to \tau^-\bar{\nu}) < 1.8 \times 10^{-4}$ (90% C.L.) and also quote the value [543]

$$\mathcal{B}(B^- \to \tau^-\bar{\nu}) = \left[0.88^{+0.68}_{-0.67}(\text{sta}) \pm 0.11(\text{sys})\right] \times 10^{-4}. \quad (121)$$

The semileptonic tag gives roughly two times higher efficiency than the hadronic tag but introduces more backgrounds.

Within the context of the SM, the product of the B meson decay constant and the magnitude of the CKM matrix element $|V_{ub}|$ is determined to be $f_B|V_{ub}| = (10.1^{+1.6}_{-1.4}(\text{sta})^{+1.3}_{-1.4}(\text{sys})) \times 10^{-4}$ GeV from the Belle result. Using the value of $|V_{ub}| = (4.39 \pm 0.33) \times 10^{-3}$ from inclusive charmless semileptonic B decay data [389], we obtain $f_B = 0.229^{+0.036}_{-0.031}(\text{sta})^{+0.034}_{-0.037}(\text{sys})$ GeV.

The charged Higgs can be constrained by comparing the measured branching fraction ($\mathcal{B}^{\text{exp}}$) to the SM value of $\mathcal{B}^{\text{SM}} = (1.59 \pm 0.40) \times 10^{-4}$, which is deduced from the above $|V_{ub}|$ value and $f_B = (0.216 \pm 0.022)$ GeV obtained from lattice QCD calculations [321]. Using the Belle result, the ratio (116) is $r_H = 1.13 \pm 0.53$, which then constrains the charged Higgs in the ($M_{H^+}, \tan\beta$) plane, as shown in Fig. 14 (top). The hatched area indicates the region excluded at a confidence level of 95.5%.

Further accumulation of data helps to improve on both the statistical and systematic uncertainties of the branching fraction. Some of the major systematic errors, such as ambiguities in the reconstruction efficiency and the signal and background shapes, come from the limited statistics of a control sample. On the other hand, the error in the ratio r_H depends on the errors in the determination of $|V_{ub}|$ and f_B. Figure 14 (bottom) shows the expected constraint at 5 ab^{-1}, assuming the scaling of the experimental error by $1/\sqrt{L}$ (L is the luminosity) and 5% relative error for both $|V_{ub}|$ and f_B. Figure 15 presents the M_{H^+} reach at $\tan\beta = 30$ as a function of the integrated luminosity. Here the M_{H^+} reach is defined as the upper limit of the 95.5% excluded region at a given $\tan\beta$. The figure shows the expectation for three cases, $(\Delta|V_{ub}|/|V_{ub}|, \Delta f_B/f_B) = (0\%, 0\%)$, $(2.5\%, 2.5\%)$ and $(5\%, 5\%)$. Precise determination of $|V_{ub}|$ and f_B is desired to maximize the physics reach.

Fig. 13 Distribution of the remaining energy for $B^- \to \tau^-\bar{\nu}$ candidates: from Belle's analysis using the hadronic tag on a 414 fb^{-1} data sample (*left*) and from BaBar's analysis using the semileptonic tag on a 288 fb^{-1} data sample (*right*)
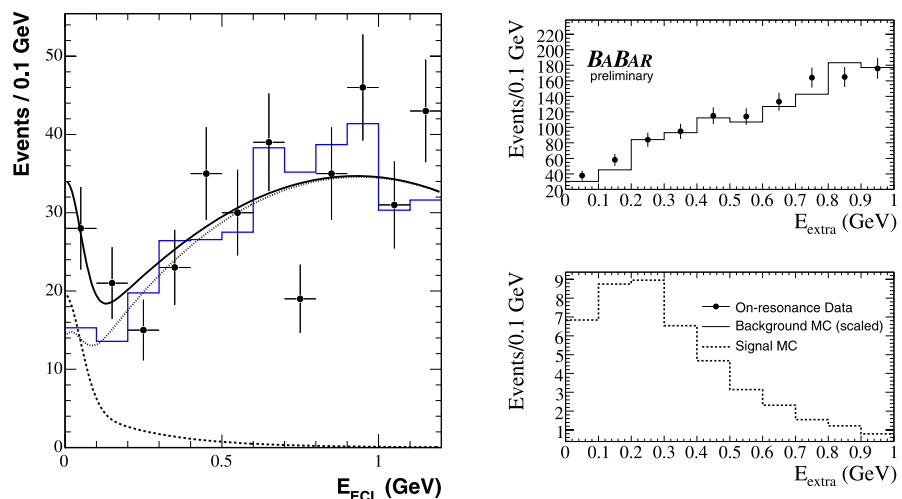
368

Eur. Phys. J. C (2008) 57: 309–492

Fig. 14 The constraint on the charged Higgs; $\pm 1\sigma$ boundary in the ratio r_H (*left*) and the 95.5% C.L. exclusion boundaries in the $(M_{H^+}, \tan\beta)$ plane (*right*). The *top figures* show the constraint from the present Belle result. The *bottom figures* show the expected constraints at 5 ab^{-1}
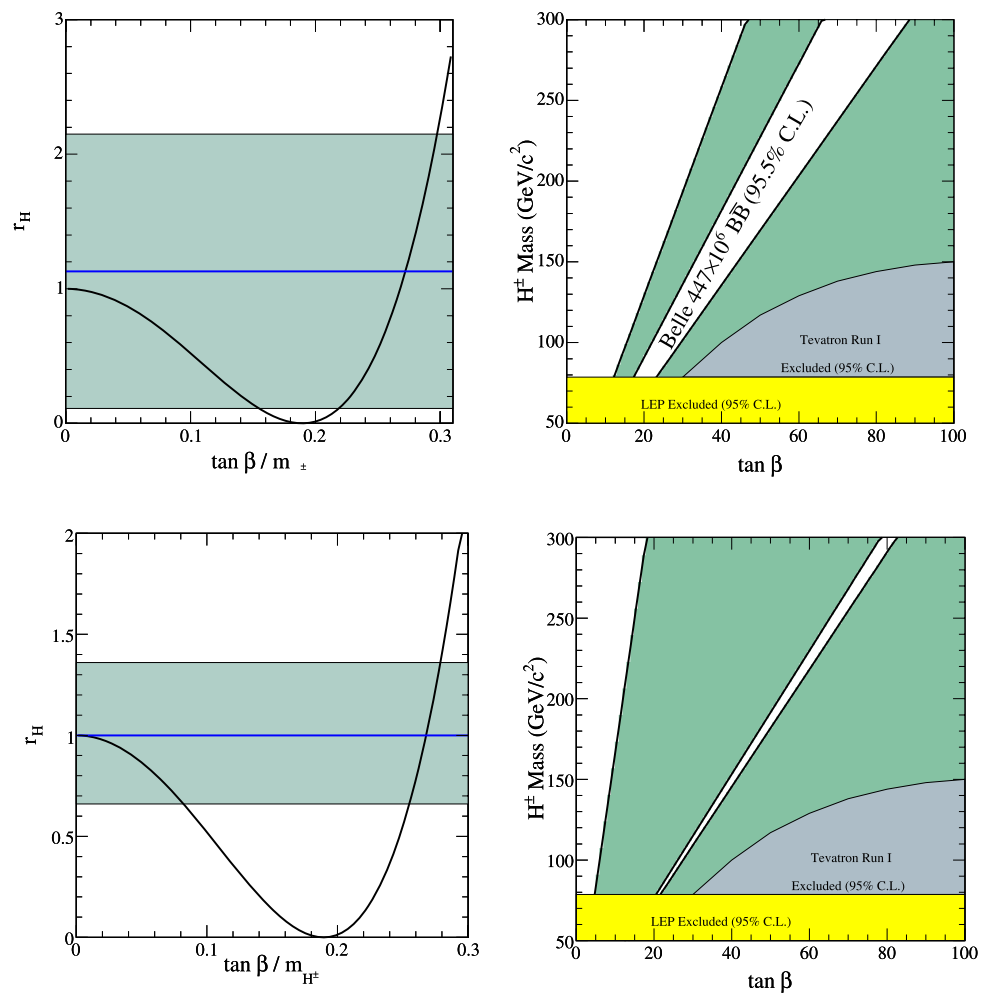
Fig. 15 Expected M_{H^+} reach at $\tan\beta = 30$ as a function of the integrated luminosity. The *three curves* correspond to $(\Delta|V_{ub}|/|V_{ub}|, \Delta f_B/f_B) =$ *upper*: (0%, 0%), *middle*: (2.5%, 2.5%) and *lower*: (5%, 5%)
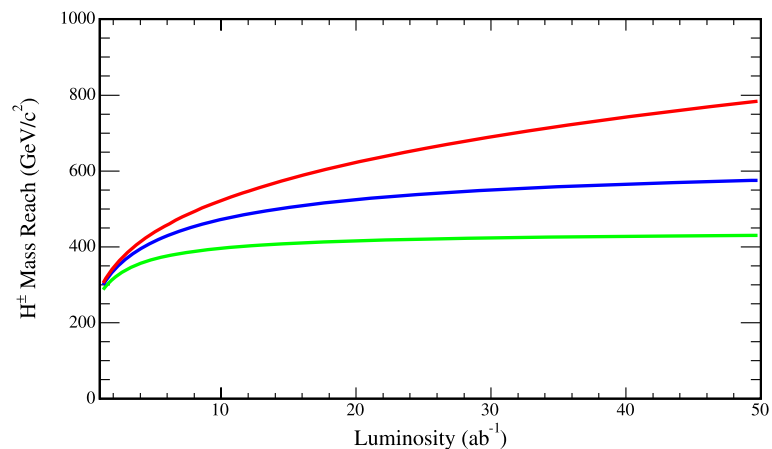
3.3.2.3 $B \to D^{(*)}\tau\nu$ The semileptonic B decay into τ final state, $B \to D^{(*)}\tau\bar\nu$, is also a sensitive probe for the charged Higgs. In the SM, the branching fractions are expected to be about 8×10^{-3} for $B \to D\tau\bar\nu$ and 1.6×10^{-2} for $B \to D^*\tau\bar\nu$, respectively. Because of the presence of at least two neutrinos in the final state, the reconstruction of

these modes requires the reconstruction of the other B meson in the event and hence requires a larger data sample with respect to that used to measure $B \to D^{(*)}\ell\bar\nu$, where $\ell = \mu, e$. Figure 16 presents the expected future constraint in the $(M_{H^+}, \tan\beta)$ plane for a super B factory with a 5 and 50 ab^{-1} data sample.

3.3.2.4 B → μν Contrary to the $B^- → τ\bar{ν}$ case, the $B^- → μ^-\bar{ν}$ decay has more kinematic constraint, because it has only one neutrino in the final state and the charged lepton at a fixed energy in the *B* rest frame. Therefore, present analyses by Belle and BaBar take a conventional approach,

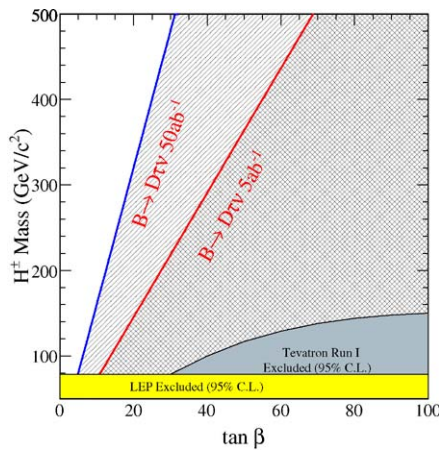where one looks for a single high momentum lepton and then inclusively reconstructs the accompanying *B* via a 4-vector sum of everything else in the event. The lepton momentum is smeared in the center-of-mass frame due to *B* momentum to give a couple of hundred MeV/*c* width.

The left panel of Fig. 17 shows the muon momentum distribution from the Belle analysis to search for the $B^- → μ^-\bar{ν}$ decay using the conventional approach on a 253 fb^{-1} data sample. The signal detection efficiency is 2.2%. The expected number of signals based on the SM branching fraction $7.1 × 10^{-7}$ is 4.2, while the estimated background is 7.4. The reported upper limit is $\mathcal{B}(B^- → μ^-\bar{ν}) ≤ 1.7 × 10^{-6}$ (90% C.L.) [554].

Recently BaBar has reported a result of the $B → μν$ search using the hadronic tags on a 208.7 fb^{-1} data sample. In this case, as the *B* momentum is determined by the full reconstruction, there is no smearing in the lepton momentum. The right panel of Fig. 17 is the muon momentum distribution after all the selection cuts are applied. The signal detection efficiency is about 0.15%, an order of magnitude lower than for the conventional analysis. The reported upper limit is $\mathcal{B}(B^- → μ^-\bar{ν}) ≤ 7.9 × 10^{-6}$ (90% C.L.) [555].

Fig. 16 Expected constraint on the charged Higgs parameters from measurements of the $B → Dτ\bar{ν}$ branching fraction at 5 and 50 ab^{-1}
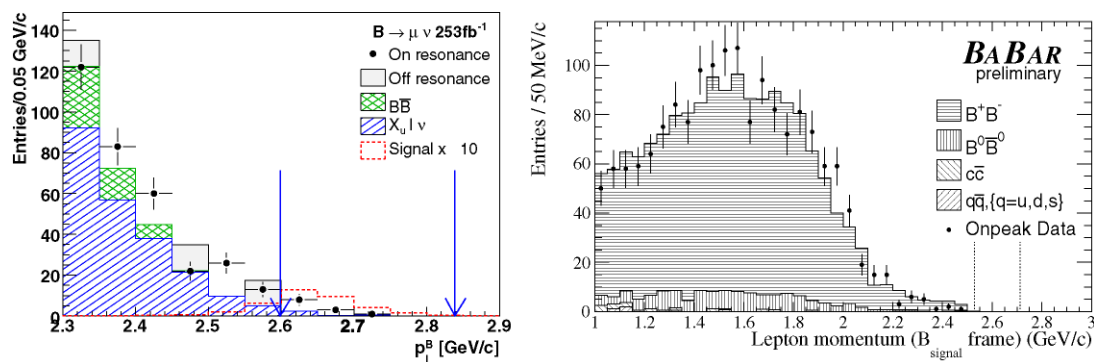

Fig. 17 Muon momentum distribution from the Belle analysis using an inclusive reconstruction of the accompanying *B* for a 253 fb^{-1} data sample (*left*); the same distribution from the BaBar analysis using the hadronic tags on a 208.7 fb^{-1} data sample (*right*)

Fig. 18 Expected sensitivity for $B^- → μ^-\bar{ν}$ as a function of the integrated luminosity
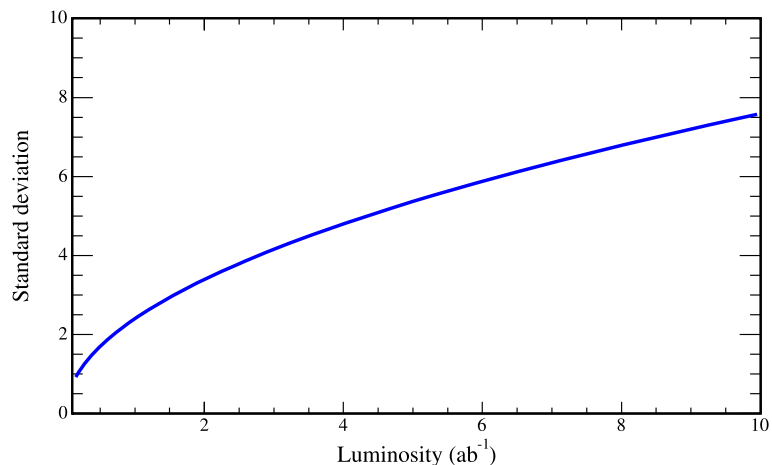
370

Eur. Phys. J. C (2008) 57: 309–492

Figure 18 shows the expected statistical significance as a function of the integrated luminosity, based on a simple extrapolation from the present Belle result. Accumulation of 1.6(4.3) ab^{-1} data will allow us to detect the $B^- \to \mu^- \bar\nu$ signal with 3(5) statistical significance. The 50 ab^{-1} data at super B-factories will allow us to detect about 800 signal events and measure the branching fraction with about 6% statistical precision.

There are some points which need to be further studied.

– Optimization of the tagging; there may be some improvement by using the semileptonic tag in addition to the hadronic tag, especially for $B^- \to K^- \nu \bar\nu$, for which the impact of additional neutrinos seems to be relatively small.
– Effects of backgrounds in a high luminosity environment; future prospects are discussed so far by extrapolation from the present results, which may be too simple. In particular, the impact of higher backgrounds to the tagging efficiency and the missing energy resolution have to be more carefully examined.

3.4 Very rare decays[15]

3.4.1 Theory of $B_q \to \ell^+ \ell^-$ and related decays

A particularly important class of very rare decays are the leptonic FCNC decays of a B_d or B_s meson. In addition to the electroweak loop suppression, the corresponding decay rates are helicity suppressed in the SM by a factor of m_ℓ^2 / m_B^2, where m_ℓ and M_B are the masses of lepton and B meson, respectively. The effective $|\Delta B| = |\Delta S| = 1$ Hamiltonian, which describes $b \to s$ decays, already contains 17 different operators in the SM; in a generic model-independent analysis of NP, this number will exceed 100. One virtue of purely leptonic B_s decays is their dependence on a small number of operators, so that they are accessible to model-independent studies of NP. These statements, of course, equally apply to $b \to d$ transitions and leptonic B_d decays. While in the SM all six $B_q \to \ell^+ \ell^-$ decays (with $q = d$ or s and $\ell = e, \mu$ or τ) are related to one another in a simple way, this is not necessarily so in models of NP. Therefore all six decay modes should be studied.

Other very rare decays, such as $B_q \to \ell^+ \ell^- \ell'^+ \ell'^-$, $\ell^+ \ell^- \gamma$, $e^+ \mu^-$, are briefly considered in Sect. 3.4.1.3 below.

3.4.1.1 $B_q \to \ell^+ \ell^-$ in the Standard Model
Photonic penguins do not contribute to $B_q \to \ell^+ \ell^-$ because a lepton–anti-lepton pair with zero angular momentum has charge conjugation quantum number $C = 1$, while the photon has $C = -1$. The dominant contribution stems from the Z-penguin diagram and is shown in Fig. 19.

Fig. 19 Z-penguin contribution to $B_s \to \ell^+ \ell^-$
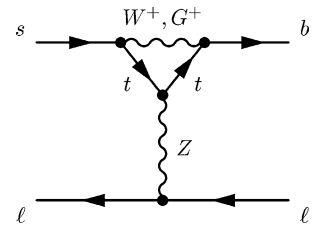
There is also a box diagram with two W bosons, which is suppressed by a factor of M_W^2 / m_t^2 with respect to the Z-penguin diagram. These diagrams determine the Wilson coefficient C_A of the operator

$$Q_A = \bar{b}_L \gamma^\mu q_L \bar{\ell} \gamma_\mu \gamma_5 \ell. \tag{122}$$

We will further need operators with scalar and pseudoscalar couplings to the leptons:

$$Q_S = m_b \bar{b}_R q_L \bar{\ell} \ell, \qquad Q_P = m_b \bar{b}_R q_L \bar{\ell} \gamma_5 \ell. \tag{123}$$

Their coefficients C_S and C_P are determined from penguin diagrams involving the Higgs or the neutral Goldstone boson, respectively. While C_S and C_P are tiny and can be safely neglected in the SM, the situation changes dramatically in popular models of NP discussed below. The effective Hamiltonian reads

$$H_{\text{eff}} = \frac{G_F}{\sqrt{2}} \frac{\alpha}{\pi \sin^2 \theta_W} V_{tb}^* V_{tq} [C_S Q_S + C_P Q_P + C_A Q_A] + \text{h.c.} \tag{124}$$

The operators Q'_S, Q'_P and Q'_A, where the chiralities of the quarks in the $\bar{b}q$ currents are flipped with respect to those in (122) and (123), may also become relevant in general extensions of the SM.

C_A has been determined in the next-to-leading order (NLO) of QCD [556–558]. The NLO corrections are in the percent range, and higher-order corrections play no role. C_A is commonly expressed in terms of the $\overline{\text{MS}}$ mass of the top quark, $\bar{m}_t$. A pole mass (usually quoted in the context of direct measurements and electroweak fits) of $m_t^{\text{pole}} = (171.4 \pm 2.1)$ GeV corresponds to $\bar{m}_t = (163.8 \pm 2.0)$ GeV. An excellent approximation to the NLO result for C_A, which holds with an accuracy of 5×10^{-4} for $149 < \bar{m}_t < 179$ GeV, is

$$C_A(\bar{m}_t) = 0.9636 \left[\frac{80.4 \text{ GeV}}{M_W} \frac{\bar{m}_t}{164 \text{ GeV}} \right]^{1.52}. \tag{125}$$

In the literature, $C_A(\bar{m}_t)$ is often called $Y(\bar{m}_t^2 / M_W^2)$. The exact expression can be found e.g. in (16)–(18) of [558]. The branching fraction can be compactly expressed in terms

of the Wilson coefficients C_A, C_S and C_P:

$$B(B_q \to \ell^+\ell^-)$$

$$= \frac{G_F^2 \alpha^2}{64\pi^3 \sin^4\theta_W} |V_{tb}^* V_{tq}|^2 \tau_{B_q} M_{B_q}^3 f_{B_q}^2 \sqrt{1 - \frac{4m_\ell^2}{M_{B_q}^2}}$$

$$\times \left[\left(1 - \frac{4m_\ell^2}{M_{B_q}^2}\right) M_{B_q}^2 C_S^2 + \left(M_{B_q} C_P - \frac{2m_\ell}{M_{B_q}} C_A\right)^2 \right]. \tag{126}$$

Here f_{B_q} and τ_{B_q} are the decay constant and the lifetime of the B_q meson, respectively, and θ_W is the Weinberg angle. Since $B_q \to \ell^+\ell^-$ is a short-distance process, the appropriate value of the fine-structure constant is $\alpha = \alpha(M_Z) = 1/128$. With (125) and $C_S = C_P = 0$, (126) gives the following SM predictions:

$$B(B_s \to \tau^+\tau^-)$$

$$= (8.20 \pm 0.31) \times 10^{-7}$$

$$\times \frac{\tau_{B_s}}{1.527 \text{ ps}} \left[\frac{|V_{ts}|}{0.0408}\right]^2 \left[\frac{f_{B_s}}{240 \text{ MeV}}\right]^2, \tag{127}$$

$$B(B_s \to \mu^+\mu^-)$$

$$= (3.86 \pm 0.15) \times 10^{-9}$$

$$\times \frac{\tau_{B_s}}{1.527 \text{ ps}} \left[\frac{|V_{ts}|}{0.0408}\right]^2 \left[\frac{f_{B_s}}{240 \text{ MeV}}\right]^2, \tag{128}$$

$$B(B_s \to e^+e^-)$$

$$= (9.05 \pm 0.34) \times 10^{-14}$$

$$\times \frac{\tau_{B_s}}{1.527 \text{ ps}} \left[\frac{|V_{ts}|}{0.0408}\right]^2 \left[\frac{f_{B_s}}{240 \text{ MeV}}\right]^2, \tag{129}$$

$$B(B_d \to \tau^+\tau^-)$$

$$= (2.23 \pm 0.08) \times 10^{-8}$$

$$\times \frac{\tau_{B_d}}{1.527 \text{ ps}} \left[\frac{|V_{td}|}{0.0082}\right]^2 \left[\frac{f_{B_d}}{200 \text{ MeV}}\right]^2, \tag{130}$$

$$B(B_d \to \mu^+\mu^-)$$

$$= (1.06 \pm 0.04) \times 10^{-10}$$

$$\times \frac{\tau_{B_d}}{1.527 \text{ ps}} \left[\frac{|V_{td}|}{0.0082}\right]^2 \left[\frac{f_{B_d}}{200 \text{ MeV}}\right]^2, \tag{131}$$

$$B(B_d \to e^+e^-)$$

$$= (2.49 \pm 0.09) \times 10^{-15}$$

$$\times \frac{\tau_{B_d}}{1.527 \text{ ps}} \left[\frac{|V_{td}|}{0.0082}\right]^2 \left[\frac{f_{B_d}}{200 \text{ MeV}}\right]^2. \tag{132}$$

The dependencies on the decay constants, which have sizable theoretical uncertainties, and on the relevant CKM factors have been factored out. While $|V_{ts}|$ is well determined through the precisely measured $|V_{cb}|$, the determination of $|V_{td}|$ involves the global fit to the unitarity triangle and suffers from larger uncertainties. The residual uncertainty in (127)–(132) stems from the 2 GeV error in $\bar{m}_t$.

Alternatively, within the standard model, the CKM dependence as well as the bulk of the hadronic uncertainty may be eliminated by normalizing to the well-measured meson mass differences ΔM_{B_q}, thus trading $f_{B_q}^2$ for a (less uncertain) bag parameter $\hat{B}_q$ [559]:

$$B(B_q \to \ell^+\ell^-) = C \frac{\tau_{B_q}}{\hat{B}_q} \frac{Y^2(\bar{m}_t^2/M_W^2)}{S(\bar{m}_t^2/M_W^2)} \Delta M_q, \tag{133}$$

where S is a perturbative short-distance function, $C = 4.36 \times 10^{-10}$ includes a normalization and NLO QCD corrections, and $\ell = e, \mu$. This reduces the *total* uncertainty within the SM below the 15 percent level. (A similar formula may be written for $\ell = \tau$.)

3.4.1.2 $B_q \to \ell^+\ell^-$ and new physics
• Additional Higgs bosons

The helicity suppression factor of m_ℓ/M_{B_q} in front of C_A in (126) makes $B(B_q \to \ell^+\ell^-)$ sensitive to physics with new scalar or pseudoscalar interactions, which contribute to C_S and C_P. This feature renders $B_q \to \ell^+\ell^-$ highly interesting to probe models with an extended Higgs sector. Practically all weakly coupled extensions of the SM contain extra Higgs multiplets, which puts $B(B_q \to \ell^+\ell^-)$ on the center stage of indirect NP searches. Higgs bosons couple to fermions with Yukawa couplings y_f. In the SM, $y_b \propto m_b/M_W$ and $y_\ell \propto m_\ell/M_W$ are so small that Higgs penguin diagrams, in which the Z-boson of Fig. 19 is replaced by a Higgs boson, play no role. In extended Higgs sectors, the situation can be dramatically different. Models with two or more Higgs multiplets can not only accommodate Yukawa couplings of order one, they also generically contain tree-level FCNC couplings of neutral Higgs bosons. In simple two-Higgs-doublet models, these unwanted FCNC couplings are usually switched off in an ad-hoc way by imposing a discrete symmetry on the Higgs and fermion fields, which leads to the celebrated two-Higgs-doublet models of type I and type II. Here we only discuss the latter model, in which one Higgs doublet H_u only couples to up-type fermions, while the other one, H_d, solely couples to down-type fermions [560]. The parameter controlling the size of the down-type Yukawa coupling is $\tan\beta = v_u/v_d$, the ratio of the vacuum expectation values acquired by H_u and H_d. The Yukawa coupling y_f of H_d to the fermion f satisfies $y_f \sin\beta = m_f \tan\beta/v$ with $v = \sqrt{v_u^2 + v_d^2} = 174$ GeV. Hence $y_b \approx 1$ for $\tan\beta \approx 50$. The dominant contributions to C_S and C_P for large $\tan\beta$ involve charged and neutral Higgs

372

Eur. Phys. J. C (2008) 57: 309–492

bosons, but the final result can be solely expressed in terms of $\tan \beta$ and the charged Higgs boson mass M_{H^+} [561]:

$$C_S = C_P = \frac{m_\ell}{4M_W^2} \tan^2 \beta \frac{\ln r}{r-1} \quad \text{with } r = \frac{M_{H^+}^2}{\bar{m}_t^2}, \qquad (134)$$

while C_A remains the same as in the SM. Although for very large values of $\tan \beta / M_{H^+}$ the branching fraction can be enhanced, the contributions in (134) typically reduce $B(B_q \to \ell^+ \ell^-)$ with respect to the SM value. The decoupling for $M_{H^+} \to \infty$ is slow, e.g., for $\tan \beta = 60$ and $M_{H^+} = 500$ GeV, the new Higgs contributions reduce $B(B_q \to \ell^+ \ell^-)$ by 50%!

• *Supersymmetry*

The generic Minimal Supersymmetric Standard Model (MSSM) contains many new sources of flavor violation in addition to the Yukawa couplings. These new flavor violating parameters stem from the supersymmetry-breaking terms, and their effects could easily exceed those of the CKM mechanism. In view of the success of the CKM description of flavor-changing transitions, one may supplement the MSSM with the hypothesis of MFV, which can be formulated systematically using symmetry arguments [10]. In the MFV–MSSM, the only sources of flavor violation are the Yukawa couplings, just as in the SM. In this section, the MSSM is always understood to be supplemented with the assumption of MFV. While in MFV scenarios the contributions from virtual supersymmetric particles to FCNC processes are normally smaller than the SM contribution, the situation is very different for $B_q \to \ell^+ \ell^-$.

The MSSM has two Higgs doublets. At tree-level the couplings are as in the two-Higgs-doublet model of type II, because the holomorphy of the superpotential forbids the coupling of H_u to down-type fermions and that of H_d to up-type fermions. At the one-loop level, however, the situation is different, and both doublets couple to all fermions. The loop-induced couplings are proportional to the product of a supersymmetry-breaking term and the μ parameter. If $\tan \beta$ is large, the loop-induced coupling of H_u^* and the tree-level coupling of H_d give similar contributions to the masses of the down-type fermions, because the loop suppression is compensated by a factor of $\tan \beta$ [20]. In this scenario, the Higgs sector is that of a *general* two-Higgs-doublet model, which involves FCNC Yukawa couplings of the heavy neutral Higgs bosons A^0 and H^0 [25]. The Wilson coefficients C_S and C_P differ from those in (134) in two important aspects: they involve three rather than two powers of $\tan \beta$ and they depend on the mass $M_{A^0} \sim M_{H^0}$ instead of the charged Higgs boson mass. The branching ratios scale as

$$B(B_q \to \ell^+ \ell^-)_{\text{SUSY}} \propto \frac{m_b^2 m_\ell^2 \tan^6 \beta}{M_{A^0}^4}$$

and could, in principle, exceed the SM results in (127)–(132) by a factor of 10^3 [27]. Thus the experimental upper limit on $B(B_s \to \mu^+ \mu^-)$ from the Tevatron, which is larger than $B(B_s \to \mu^+ \mu^-)_{\text{SM}}$ in (128) by a factor of 25, already severely cuts into the parameter space of the MSSM. $B(B_s \to \mu^+ \mu^-)$ in MSSM scenarios with large $\tan \beta$ has been studied extensively [27–30, 528, 562–564].

Very popular special cases of the MSSM are the minimal Supergravity Model (mSUGRA) [565–570] and the Constrained Minimal Supersymmetric Standard Mode (CMSSM). While the MSSM contains more than 100 parameters, mSUGRA involves only 5 additional parameters and is therefore much more predictive. In particular correlations between $B(B_s \to \mu^+ \mu^-)$ and other observables emerge, for example with the anomalous magnetic moment of the muon and the mass of the lightest neutral Higgs boson [564]. Other well-motivated variants of the MSSM incorporate the parameter constraints from grand unified theories (GUTs). $B(B_s \to \mu^+ \mu^-)$ is especially interesting in GUTs based on the symmetry group $SO(10)$ [564, 573, 574]. In the minimal $SO(10)$ GUT, the top and bottom Yukawa couplings y_b and y_t unify at a high scale implying that $\tan \beta$ is of order 50. While realistic $SO(10)$ models contain a nonminimal Higgs sector, any experimental information on the deviation of y_b/y_t from 1 is very desirable, as it probes the Higgs sectors of GUT theories. In conjunction with other observables like the mass difference in the $B_s^0 - \bar{B}_s^0$ system [30] or $B(B^+ \to \tau^+ \nu_\tau)$ [31, 32, 575], which depend in different ways on $\tan \beta$ and the masses of the non-Standard Higgs bosons and the supersymmetric particles, the measurement of $B(B_s \to \mu^+ \mu^-)$ at the LHC will, within the MSSM, answer the question whether the top and bottom Yukawa couplings unify at high energies.

3.4.1.3 Other very rare decays The decays $B_q \to \ell^+ \ell^- \gamma$ and $B_q \to \ell^+ \ell^- \ell'^+ \ell'^-$ are of little interest from a theoretical point of view. First, they are difficult to calculate, since they involve photon couplings to quarks and are thereby sensitive to soft hadron dynamics. Second, they are not helicity-suppressed, because the (real or virtual) photon can recoil against a lepton pair in a $J = 1$ state. This implies that they probe operators of the effective Hamiltonian which can more easily be studied from $B_q \to X\gamma$ and $B \to X\ell^- \ell^-$ decays. However, the absence of a helicity suppression makes $B_q \to \ell^+ \ell^- \gamma$ a possible threat to $B_q \to \ell^+ \ell^-$, as will be discussed in the experimental sections. A naive estimate gives $B(B_s \to \mu^+ \mu^- \gamma) \sim (m_B^2/m_\mu^2)\alpha/(4\pi) B(B_s \to \mu^+ \mu^-) \sim B(B_s \to \mu^+ \mu^-)$, while a more detailed analysis even finds $B(B_s \to \mu^+ \mu^- \gamma) > B(B_s \to \mu^+ \mu^-)$ [299].

Lepton-flavor violating (LFV) decays like $B_q \to \ell^\pm \mu^\mp$ and $\ell = e, \tau$ are negligibly small in the SM. They are suppressed by two powers of m_ν/M_W, where m_ν denotes the largest neutrino mass. However, this suppression factor

Eur. Phys. J. C (2008) 57: 309–492

373

is absent in certain models of new physics. In supersymmetric theories with R parity (such as the MSSM), their branching ratios are smaller than those of the corresponding lepton-flavor conserving decay, e.g. $B_q \to \mu^+\mu^-$. Large effects, however, are possible in models that contain LFV tree-level couplings or leptoquarks. Here supersymmetric theories without R parity and the Pati–Salam model should be mentioned. Supersymmetry without R parity involves a plethora of new couplings, which are different for all combinations of quark and lepton flavor involved, so that no other experimental constraints prevent large effects in $B_q \to \ell^{\pm}\mu^{\mp}$. Flavor physics in the Pati–Salam model has been studied in [576].

3.4.2 Present experimental status of $B_q \to \ell^+\ell^-$ decays

The experimental searches for $B_q \to \ell^+\ell^-$ have focused on $B_s \to \mu^+\mu^-$ and $B_d \to \mu^+\mu^-$. For the e^+e^- final states, the branching fractions are suppressed with respect to $B(B \to \mu^+\mu^-)$ by $m_e^2/m_\mu^2 = 2.3 \times 10^{-5}$. The best limit that has been set is $B(B \to e^+e^-) < 61 \times 10^{-9}$ (90% C.L.) [577]. Though the branching fraction of the $\tau^+\tau^-$ mode is enhanced by a factor of 212 with respect to that of the $\mu^+\mu^-$ mode, the only experimental upper limit from BaBar is $B(B_d \to \tau^+\tau^-) < 4.1 \times 10^{-3}$ (90% C.L.) [578]. This is

less sensitive than the decay $B \to \mu^+\mu^-$. Due to at least two missing neutrinos in the decays of the two τs, the reconstruction of this mode is rather difficult, since no kinematic constraint can be employed to eliminate backgrounds. At an e^+e^- super B factory, the $B_d \to \tau^+\tau^-$ mode may be observable by fully reconstructing one B meson in a hadronic mode and then searching for $B_d \to \tau^+\tau^-$ in the recoil system.

Thus, $B_{d,s} \to \mu^+\mu^-$ are the most promising modes to test the SM. Table 24 summarizes the searches for $B_s \to \mu^+\mu^-$ by different experiments in the past two decades. The 90% C.L. upper limits are shown in Fig. 20 in comparison to the SM prediction. The lowest limit of $B(B_s \to \mu^+\mu^-) < 93 \times 10^{-9}$ (95% C.L.) is obtained by the D0 experiment using about 2 fb^{-1} of $p\bar{p}$ data [579]. Using 780 pb^{-1} of $p\bar{p}$ data, CDF achieved a branching fraction upper limit of $B(B_s \to \mu^+\mu^-) < 100 \times 10^{-9}$ (95% C.L.) [580, 581]. The corresponding searches for $B_d \to \mu^+\mu^-$ are summarized in Table 25. Here, the lowest limit of $B(B_d \to \mu^+\mu^-) < 30 \times 10^{-9}$ (95% C.L.) is obtained by the CDF experiment using 780 pb^{-1} of $p\bar{p}$ data [580, 581]. The 90% C.L. upper limits are also shown in Fig. 20 in comparison with the SM prediction.

In the present CDF $B_s \to \mu^+\mu^-$ analysis, the background level is at about one event, while the branching fraction upper limit at 90% C.L. lies about a factor of 20 above

Table 24 Branching fraction upper limits (90% C.L.) for $B_s \to \mu^+\mu^-$ from different experiments

Experiment	Year	Limit $[10^{-9}]$	Process	Reference
D0	2007	75	$p\bar{p}$ at 1.96 TeV	[579]
CDF	2006	80	$p\bar{p}$ at 1.96 TeV	[580, 581]
CDF	2005	150	$p\bar{p}$ at 1.96 TeV	[582]
D0	2005	410	$p\bar{p}$ at 1.96 TeV	[583]
CDF	2004	580	$p\bar{p}$ at 1.96 TeV	[584]
CDF	1998	2,000	$p\bar{p}$ at 1.8 TeV	[585]
L3	1997	38,000	$e^+e^- \to Z$	[586]

Fig. 20 Compilation of the 90% C.L. upper limits for $B(B_s \to \mu^+\mu^-)$ (*left*) and $B(B_d \to \mu^+\mu^-)$ (*right*) from different experiments in comparison to the SM prediction
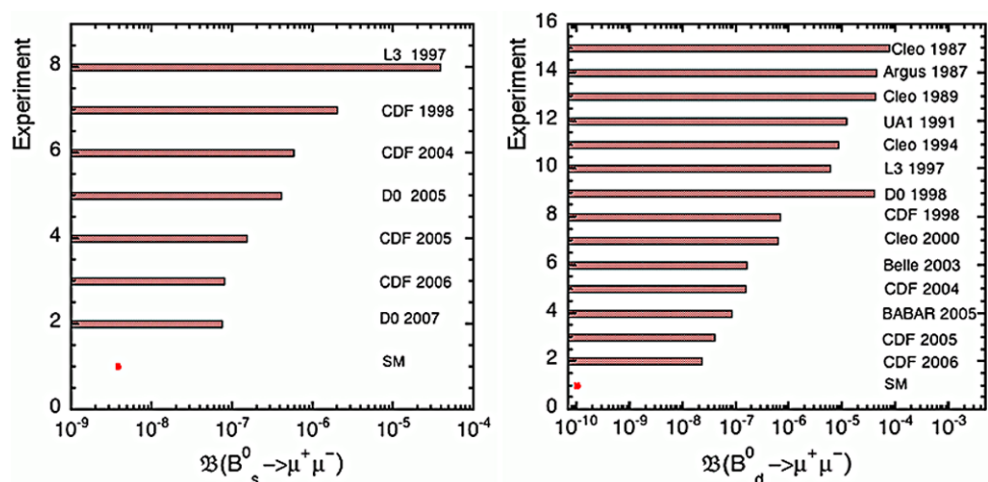
374

Eur. Phys. J. C (2008) 57: 309–492

Table 25 Branching fraction upper limits (90% C.L.) for $B_d \to \mu^+\mu^-$ from different experiments

Experiment	Year	Limit $[10^{-9}]$	Process	Reference
CDF	2006	23	$p\bar{p}$ at 1.96 TeV	[580, 581]
CDF	2005	39	$p\bar{p}$ at 1.96 TeV	[582]
BaBar	2005	83	$e^+e^- \to \Upsilon(4S)$	[577]
CDF	2004	150	$p\bar{p}$ at 1.96 TeV	[584]
Belle	2003	160	$e^+e^- \to \Upsilon(4S)$	[587]
CLEO	2000	610	$e^+e^- \to \Upsilon(4S)$	[588]
D0	1998	40,000	$p\bar{p}$ at 1.8 TeV	[589]
CDF	1998	680	$p\bar{p}$ at 1.8 TeV	[585]
L3	1997	10,000	$e^+e^- \to Z$	[586]
UA1	1991	8,300	$p\bar{p}$ at 630 GeV	[590]
ARGUS	1987	45,000	$e^+e^- \to \Upsilon(4S)$	[591]
CLEO	1987	77,000	$e^+e^- \to \Upsilon(4S)$	[592]

the SM value. Thus, any analysis attempting to reach a sensitivity at the level of the SM prediction needs a significant improvement in background rejection. Scaling the present CDF result to a luminosity of 10 fb^{-1} yields branching fraction upper limits at 90% C.L. of 6.2×10^{-9} for $B_s \to \mu^+\mu^-$ and 1.8×10^{-9} for $B_d \to \mu^+\mu^-$. A simple scaling of the BaBar result to 1 ab^{-1} yields $B(B_d \to \mu^+\mu^-) < 9 \times 10^{-9}$ (90% C.L.).

3.4.3 LHC preparations for measurements of the very rare B decays

Three LHC experiments, LHCb, ATLAS and CMS, are aiming for the measurement of very rare B decays. Differences in the detector layouts lead to different strategies in data-taking, triggers and the offline selections to maximize the gain of signal events.

3.4.3.1 Luminosity conditions and triggers Whilst the nominal LHCb luminosity will be $(2–5) \times 10^{32}$ cm^{-2} s^{-1}, the forward muon stations can identify muons with low values of transverse momenta, allowing the first level trigger (L0) to collect events with one or two muons with p_T values as low as 1.1 GeV/c [593]. Because the beauty cross section grows rapidly at small transverse momenta, the lower LHCb luminosity is compensated by higher b-production. ATLAS and CMS will start to collect the exclusive di-muon B decays at a luminosity of few times 10^{33} cm^{-2} s^{-1} and will later continue at the nominal LHC luminosity of 10^{34} cm^{-2} s^{-1}. Thus rare B-decays will be recorded at all LHC luminosities. However the central detector geometries will allow muons to be recorded only above $p_T \sim$ (3–6) GeV/c at the first trigger level (L1) [594, 595].

First level triggers for the exclusive di-muon B decays in LHCb, ATLAS and CMS are summarized in Table 26. In LHCb, the strategy relies on both the single muon trigger with $p_T \geq 1.1$ GeV/c and di-muon trigger streams with

Table 26 L1(0) trigger p_T thresholds. The output trigger rates are given for a luminosity of 2×10^{32} cm^{-2} s^{-1} (LHCb) and 2×10^{33} cm^{-2} s^{-1} (ATLAS/CMS)

Experiment	L1(0) momentum cut	L1(0) rate
ATLAS 2μ	p_T (μ) ≥ 6.0 GeV/c	0.7 kHz
CMS 2μ	p_T (μ) ≥ 3.0 GeV/c	3.8 kHz
LHCb 1μ	p_T (μ) ≥ 1.1 GeV/c	110 kHz
LHCb 2μ	Σp_T ($\mu\mu$) ≥ 1.3 GeV/c	145 kHz

Σp_T ($\mu\mu$) ≥ 1.3 GeV/c. ATLAS and CMS will collect the majority of their signal events at 2×10^{33} cm^{-2} s^{-1} through the di-muon trigger with the muon transverse momentum thresholds 6 and 3 GeV/c, respectively. Such triggers will result in output rates of about 700 Hz and 3500 Hz for ATLAS and CMS, respectively, and about 200 kHz for LHCb.

The high level trigger (HLT) strategy is similar for all three experiments. First, one confirms the presence of trigger muon(s) by reconstructing tracks within the so called region of interest (RoI) around a muon candidate and by matching reconstructed tracks in the inner detector with tracks from the muon system. Further, cuts are applied to the muons requiring the p_T values to be above 3 GeV/c for LHCb and above 4 and 6 GeV/c for CMS and ATLAS, respectively. Then, primary and secondary vertices are reconstructed. Cuts on vertex quality $\chi^2 \leq 20$ and on the flight path of B_s candidates $L_{xy} \geq 200$ μm (ATLAS) and $L_{3D} \geq 150$ μm (CMS) are applied. LHCb (single muon stream) uses an impact parameter cut $IP(\mu) \geq 3\sigma_{IP}$ and, for the di-muon stream, the secondary vertex quality cut $\chi^2 \leq 20$. Finally, a cut on the invariant mass of the two muons is applied, $4 \leq M_{\mu\mu} \leq 6$ GeV/c^2 (ATLAS), $M_{\mu\mu} \geq 2.5$ GeV/c^2 (LHCb di-muon stream), or a mass window around the nominal B_s mass of ± 150 MeV/c^2 (CMS). The HLT rate is less than 1.7 Hz for CMS and about 660 Hz for LHCb.

A detailed description of trigger algorithms can be found in [593–595].

3.4.3.2 Offline performance and signal selection After the trigger the offline analysis faces the challenge of selecting a signal from backgrounds of similar topology. The most important offline performance parameters for the di-muon events in the kinematic ranges accepted by triggers are given in Table 27. The differences lead consequently to different selection strategies.

In ATLAS, the reconstructed di-muon invariant mass $M_{\mu\mu}$ is required to be within an interval of $(-70 \text{ MeV}/c^2, +140 \text{ MeV}/c^2)$ around the B_s mass. The isolation cut in the ATLAS experiment requires no charged tracks with $p_T \geq 0.8 \text{ GeV}/c$ in an angular cone $\theta \leq 15°$ around the B_s candidate. For the reconstructed vertices, the significance of the reconstructed flight path in the transverse plane defined as L_{xy}/σ_L is required to be larger than 11 and the vertex reconstruction quality parameter $\chi^2 \leq 15$. The space separation between two muon candidates is $\Delta R = \sqrt{\Delta\phi^2 + \Delta\eta^2} \leq 0.9$. Details of the study can be found in [596].

In CMS, the isolation is defined as

$$I = \frac{p_T(B_s^0)}{p_T(B_s^0) + \Sigma_{\text{trk}}|p_T|} \geq 0.85. \qquad (135)$$

A value of $\Sigma_{\text{trk}}|p_T|$ is calculated for all charged tracks in a cone with $\Delta R = 1$ around the B_s candidate. For the muon separation, the value of ΔR should be in the range $(0.3, 1.2)$. The vertex cuts are the following: $L_{xy}/\sigma_L \geq 18$ and $\chi^2 \leq 1$. The momentum of the B_s candidate should point to the primary vertex: $\cos\alpha \geq 0.995$, where α is the angle between the momentum of the B_s candidate and the vector connecting the primary and secondary vertices $\vec{V}_{\text{sec}} - \vec{V}_{\text{prim}}$. A tight mass cut is applied: $|M_{\mu\mu} - M_{B_s}| \leq 100 \text{ MeV}/c^2$. Details of the study are given in [597].

In LHCb, the selection is divided into several steps [598]. First the following soft selection cuts are applied: $|M_{\mu\mu} - M_{B_s}| \leq 600 \text{ MeV}/c^2$, vertex quality cut $\chi^2 \leq 14$, $IP/\sigma_{IP} \leq 6$ for the B_s candidate, secondary and primary vertex separation $|Z_{\text{sec}} - Z_{\text{prim}}|/\sigma_V \geq 0$, pointing angle $\alpha < 0.1$ rad, soft muon identification for both candidates ($\epsilon_\mu = 95\%$ and $\epsilon_\pi = 1\%$). Further on three categories of discriminant variables are introduced: Geometry (G; lifetime, B_s and μ impact parameter, distance of closest approach (DOCA) and isolation), PID (particle identification) and IM (invariant mass). These variables are used to compute the S/B ratio event by event, while no further cuts are applied. Each event is weighted with its S/B ratio in the signal sensitivity calculation. Using this method, it is expected to reconstruct about 70 signal events per 2 fb^{-1} [598]. If the previous method is combined with the requirement $G > 0.7$, with no background events left, this leads to an estimate of 20 signal events to be reconstructed in the same period as above.

In Table 28, the number of signal events is shown for each experiment for different integrated luminosities. For ATLAS/CMS, the number for 2 fb^{-1} is simply scaled from the one for 10 fb^{-1}. In the same way, the LHCb number for 10 fb^{-1} is obtained by scaling the number for 2 fb^{-1}. The CMS and ATLAS studies for 100 fb^{-1} were published in [599] and [600], respectively. In the CMS study, harder selection criteria have been applied for high luminosity, hence the reconstruction efficiency for signal events is lower with respect to lower luminosity.

3.4.3.3 Background studies The search for $B_s \rightarrow \mu^+\mu^-$ has to deal with the problem of an enormous level of background.

The largest contribution is expected to come from combinatorial background. These events consist predominantly of beauty decays, where the di-muon candidates originate either from semileptonic decays of b and $\bar{b}$ quarks or from cascade decays of one of the $b\bar{b}$ quarks. To determine the contribution of this background, LHCb simulated a sample of inclusive $b\bar{b}$ events, requiring that both b-quarks have $|\theta| < 400$ mrad, to match, on the safe side, the LHCb acceptance of 300 mrad. Nevertheless, the sample of 34 million events corresponds to only 0.16 pb^{-1}. The study of this sample, however, showed that in the sensitive region of phase space, the relevant background contains two real muons from b-decays. Hence, a specific sample of 8 million

Table 27 LHC detector performance parameters for $B \rightarrow \mu^+\mu^-$ events in the kinematic ranges of trigger acceptances. σ_{Im} is the muon track impact parameter resolution, $\sigma_{M_{\mu\mu}}$ is the $B_s \rightarrow \mu^+\mu^-$ mass resolution

Experiment	LHCb	ATLAS	CMS
p_T^μ, GeV/c	>3	>6	>4
σ_{Im}, μm	14–26	25–70	30–50
$\sigma_{M_{\mu\mu}}$, MeV/c^2	18	84	36

Table 28 Number of signal events as a function of integrated luminosity. The time after which the corresponding luminosity will be delivered is indicated in parentheses

Experiment	2 fb^{-1}	10 fb^{-1}	30 fb^{-1}	100 fb^{-1}	130 fb^{-1}
ATLAS	1.4	7.0	21.0	92	113 (4 years)
CMS	1.2	6.1	18.3	26	44 (4 years)
LHCb	20	100 (5 years)	–	–	

376

Eur. Phys. J. C (2008) 57: 309–492

events was generated, corresponding to an effective luminosity of 30 pb^{-1}, where for both b-hadron decays a muon is required among the decay products. LHCb uses this sample to evaluate the background and extrapolates the result to a given integrated luminosity, for instance, 2 fb^{-1}. In the sensitive region ($G > 0.7$) [598], no background event was selected, hence an upper limit of 125 events is estimated at 90% C.L.. ATLAS simulated $b\bar{b}$ events with two muons, requiring to have transverse momenta $p_T > 6\,(4)$ GeV/c for the first (second) muon. In CMS, the cut for both muons was $p_T > 3$ GeV/c. The pseudorapidity of each of the muons was required to be in the range $|\eta| < 2.4$ in agreement with the trigger acceptances. Additionally the di-muon mass was required to be in the interval $M_{\mu\mu} < 8$ GeV/c^2 and $5 < M_{\mu\mu} < 6$ GeV/c^2 in ATLAS and CMS, respectively. The number of background events generated with these cuts corresponds to 10 (8) pb^{-1} for ATLAS (CMS). Both experiments evaluated the background using these samples and extrapolated the results to a given integrated luminosity. At 10 fb^{-1}, ATLAS expects 20 ± 12 events [601] and CMS 14^{+22}_{-14} events [597].

Due to the high sensitivity of the LHC experiments, the background composition may be changed relative to the situation at the Tevatron. In addition to combinatorial background, contributions from topologically similar rare exclusive decays as well as misidentification effects may become important. We give a classification of the different types of these potential backgrounds and several estimates of their contribution.

First, let us consider the very rare decays $B^{0\pm} \to (\pi^{0\pm}, \gamma)\mu^+\mu^-$ with branching ratios expected to be $\sim 2 \times 10^{-8}$ [299]. A background contribution may arise when the π/γ is soft and escapes detection. The di-muon invariant mass distribution has been modeled in ATLAS and CMS for cases where a $\pi^\pm$ is not reconstructed in the inner tracker, or a $\pi^0(\gamma)$ with $E_T \leq (2\text{–}4)$ GeV escapes detection in the electromagnetic calorimeter. Based on a full detector simulation, CMS concluded that neither of the processes $B^0 \to \gamma\mu^+\mu^-$, $B^\pm \to \pi^\pm\mu^+\mu^-$ or $B^0 \to \pi^0\mu^+\mu^-$ will contribute significantly in the signal region. ATLAS reached similar conclusions for the first two processes, while they plan to do a detailed study for the third decay. These very rare decay channels are worth studying in their own right, since some properties (for example the di-muon invariant mass spectrum) are also sensitive to NP contributions [299].

Decays into four leptons, such as $B^+_{(c)} \to \mu^+\mu^-\ell^+\nu_\ell$, are another possible background source to $B_s \to \mu^+\mu^-$. If the p_T of one of the leptons is below the detector reconstruction capabilities, then there are only two tracks observed from the B-meson vertex and the invariant mass of the di-lepton pair can be close to the $B_{d,s}$ mass. The expected branching fractions of these decays are 5×10^{-6} and 8×10^{-5} for B^+ and B^+_c, respectively [602]. Using the fast simulation tool (ATLFAST), ATLAS showed that the number of

background events from $B^+ \to \mu^+\mu^-\mu^+\nu$ can be as high as 50% of the accepted signal events from $B_s \to \mu^+\mu^-$ with a SM rate. In CMS, the analysis showed that the contribution from this source is negligible. The difference is due to different mass resolutions of ATLAS and CMS. LHCb simulated a resonant mode of the four-lepton channel $B^+_{(c)} \to (J/\psi \to \mu^+\mu^-)\mu\nu$ in which two muons are coming from J/ψ. The study led to the conclusion that the background from this channel in the mass region ± 60 MeV/c^2 around the B_s mass is less than 10% of a $B_s \to \mu^+\mu^-$ signal within the SM.

The last category considered are backgrounds from B-decay channels where secondary hadrons are misidentified as muons. The simplest backgrounds come from the two-body hadronic decays $B_{d,s} \to K^\pm\pi^\mp$, $B_{d,s} \to K^\pm K^\mp$ and $B_{d,s} \to \pi^\pm\pi^\mp$. The background contribution can be estimated by assigning to each of the final-state hadrons a probability that it would be registered as a muon. This probability was obtained from full detector simulations of large samples of beauty events. Such a study has been performed at LHCb, resulting in ~ 2 events per 2 fb^{-1} (in a $\pm 2\sigma$ mass window). CMS concluded that these backgrounds are negligible. ATLAS studies are in progress. Fake signal events can also be generated by semileptonic B decays such as $B^0 \to \pi^-\mu^+\nu_\mu$, which have a branching ratio $\sim 10^{-4}$. As in the previous case, background can arise from $\pi - \mu$ misidentification and a soft neutrino escaping an indirect identification. Similar channels to be accounted for are $B_s \to K^-\mu^+\nu_\mu$ and $B^+ \to K^+\mu^+\mu^-$.

3.4.3.4 LHC reach for $B_s \to \mu^+\mu^-$ The results of the signal and background studies described in the previous sections were finally used to estimate upper limits on the branching ratio of $B_s \to \mu^+\mu^-$, which are shown in Figs. 21 and 22. ATLAS and CMS used the algorithms of [164], while LHCb developed the new approach published in [598]. In all cases, the results were given at 90% confidence level as a function of integrated luminosity. The theory prediction for $B(B_s \to \mu^+\mu^-)$ shown in Figs. 21 and 22 uses the value of $f_{B_s} = (230 \pm 9)$ MeV extracted from the CDF measurement of $\Delta M_{B_s} = (17.8 \pm 0.1)$ ps^{-1}. The prediction therefore assumes that NP neither affects $B_s \to \mu^+\mu^-$ nor ΔM_{B_s}. Note that the above value for f_{B_s} is also consistent with direct QCD lattice calculations (see Sect. 2.4).

After one year of data taking at the LHC the expected results from LHCb will allow us to exclude or discover NP in $B_s \to \mu^+\mu^-$. ATLAS and CMS will reach this sensitivity after three years. After LHC achieves its nominal luminosity, the ATLAS and CMS statistics will increase substantially. After five years all three experiments will be in a position to provide a measurement of the branching ratio of $B_s \to \mu^+\mu^-$.
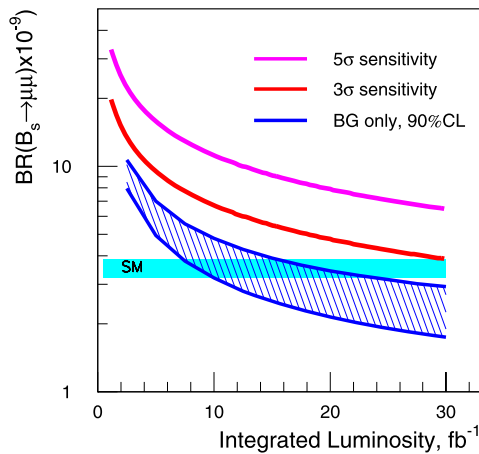
Fig. 21 Branching ratio of $B_s \to \mu^+\mu^-$ observed (3σ) or discovered (5σ) as a function of integrated luminosity for ATLAS/CMS
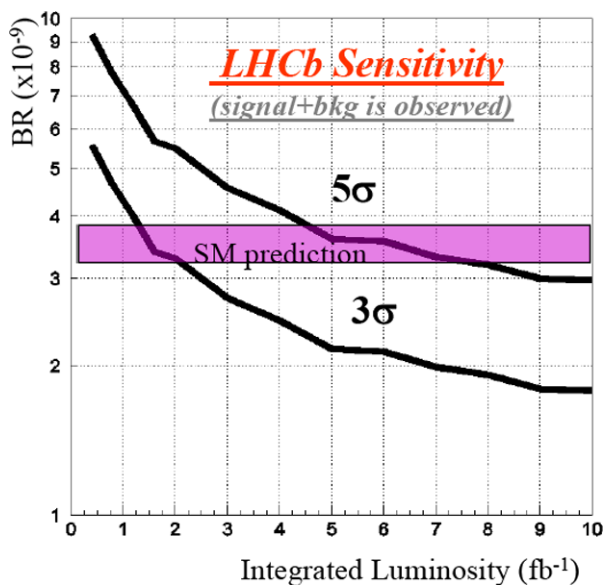

Fig. 22 Branching ratio of $B_s \to \mu^+\mu^-$ observed (3σ) or discovered (5σ) as a function of integrated luminosity for LHCb

3.4.4 Conclusions

The very rare decays $B_q \to \mu^+\mu^-$ are special in many respects. Their branching ratios are small in the SM but can be enhanced significantly in the widely studied MSSM. Leptonic meson decays belong to the physics topics that can be experimentally studied by three of the four major LHC experiments, namely LHCb, ATLAS and CMS. The LHC experiments will probe the branching fraction of $B_s \to \mu^+\mu^-$ down to the SM value and possibly reveal a smoking-gun signal of NP well ahead of the direct searches using high-p_T physics. Irrespectively of whether $B(B_s \to \mu^+\mu^-)$ is found in agreement with the SM prediction or not, the measurement will severely constrain the Higgs sector of the MSSM and will provide valuable input for LHC Higgs

physics: any sizable enhancement of $B(B_s \to \mu^+\mu^-)$ implies a large value of $\tan\beta$, so that the nonstandard Higgs bosons couple strongly to b-quarks and τ-leptons. Then these Higgs bosons will be dominantly produced in association with b-jets and will decay dominantly into b-hadrons and τ-leptons.

3.5 UT angles from tree decays[16]

3.5.1 Introduction

It is very fortunate that the B system allows an almost pristine determination of all the three angles from "tree" decays. $\beta(\phi_1)$ from $J/\psi K_S$-like modes and $\gamma(\phi_3)$ from DK-type modes are genuine tree decays and are theoretically very clean. The irreducible theory error (ITE) for β is expected to be less than 1% and may be even considerably less than that [603].[17] On γ, the ITE is estimated at O(0.1%). For $\alpha(\phi_2)$, the situation with regard to theory error is a bit more complicated. Isospin analysis allows, in principle, extraction of $\alpha(\phi_2)$ from $\pi\pi$, $\rho\pi$, or $\rho\rho$, but electroweak penguin contributions (EWP) do not respect isospin. So, in each of the three channels, the EWP contributions and other isospin violations are difficult to ascertain rigorously. But given that there are three channels, it seems reasonable that the theory error even for α will be small, O(few%) (see, e.g., [605]). Given that we now have theoretical methods that will allow us to quite precisely determine all the three angles, which are fundamental parameters of the SM, it is clearly important to determine them with accuracy roughly commensurate with what the theoretical methods promise. In this section, we will summarize the current status as to our attempts to extract these three angles directly from data collected primarily through the spectacular successes of the two asymmetric B factories, followed by our guess estimates for the potential of a super B factory (SBF) with regard to this goal. Of course, LHCb will soon begin operation, and our expectations for the precisions on tree-level angle determinations from LHCb are also presented.

3.5.2 Angles from B factories of today & of tomorrow

3.5.2.1 $\beta(\phi_1)$
Measurements of CP asymmetries in the proper-time distribution of neutral B decays to CP eigenstates mediated by $b \to c\bar{c}s$ transition provide a direct measurement of $\sin 2\beta$ ($= \sin 2\phi_1$). The time-dependent decay-rate asymmetry for decays to CP eigenstates containing a charmonium and a K_S^0 meson is given by

$$A_{\text{CP}}(t) = S_{b \to c\bar{c}s} \sin(\Delta m_d t) - C_{b \to c\bar{c}s} \cos(\Delta m_d t), \quad (136)$$

---

[16]Section coordinators: M. Bona, A. Soni, K. Trabelsi, G. Wilkinson.

[17]For a more conservative (but data driven) estimate see, e.g., Ref. [604].

378

Eur. Phys. J. C (2008) 57: 309–492

where Δm_d is the mass difference between the two B^0 mass eigenstates. Since these decays are dominated by a single (tree level) amplitude,[18] one expects to a very good approximation $S_{b \to c\bar{c}s} = -\eta_{CP} \sin 2\beta$ and $C_{b \to c\bar{c}s} = 0$, where η_{CP} is the CP eigenvalue of the final state.

In 2001, both BaBar and Belle Collaborations established CP violation in the B system through the $\sin 2\beta$ measurements in $b \to c\bar{c}s$ decays [606, 607].

In the latest results, the BaBar Collaboration [608], using a 348 million $B\bar{B}$ events, includes the CP-odd ($\eta_{CP} = -1$) final states $J/\psi K_S^0$, $\psi(2S) K_S^0$, $\chi_{c1} K_S^0$ and $\eta_c K_S^0$ as well as the CP-even ($\eta_{CP} = +1$) $J/\psi K_L^0$ final state. In addition, the vector–vector final state $J/\psi K^*$ with $K^* \to K_S^0 \pi^0$, which is found from an angular analysis to have η_{CP} close to $+1$ [610], is used. The Belle Collaboration [609] uses a sample of 535 million $B\bar{B}$ events where only $J/\psi K_S^0$ and $J/\psi K_L^0$ (*golden* modes) are analysed. The results for $-\eta_{CP} S_{b \to c\bar{c}s}$ and $C_{b \to c\bar{c}s}$ are given in Table 29 and in Fig. 23 and are at the 5% level for each collaboration.

The world average computed by the Heavy Flavor Averaging Group (HFAG) [502] includes also the results obtained by the ALEPH, OPAL and CDF experiments and is

$$\sin 2\beta = 0.675 \pm 0.026, \tag{137}$$

where most of the systematic uncertainties have been treated as uncorrelated. This result suggests that on the time scale of 2008, when an integrated luminosity of order of 2 fb^{-1} is expected from the B factories, the total uncertainty on $\sin 2\beta$ will be around 0.02.

The actual $\sin 2\beta$ result gives a precise constraint on the $(\bar{\rho}, \bar{\eta})$ plane, as shown in Fig. 23, and can be compared with the expected value obtained with other constraints from CP conserving quantities, and with CP violation in the kaon system, in the form of the parameter ε_K. Such comparisons have been performed by phenomenological groups: for example, the result from the global UT fit without the measurement of $\sin 2\beta$ is obtained by CKMfitter [8] to be $0.823^{+0.018}_{-0.085}$ or by UTfit [209] to be 0.759 ± 0.037. It is clear that the increased precision in the $\sin 2\beta$ measurement is now revealing some tension with the rest of the fit. This is mainly due to the actual V_{ub} value and in particular to the inclusive one, strikingly in countertendency with respect to the relatively *low* value of $\sin 2\beta$ [120].

With $\sin 2\beta$ being now a precision measurement, other analyses are being performed in order to remove the twofold ambiguity unavoidable with a sine determination.

Considering the B meson decays to the vector–vector final state $J\psi K^{*0}$ in the case of a final state not flavor-specific ($K^{*0} \to K_S^0 \pi^0$), a time-dependent transversity analysis

can be performed allowing sensitivity to both $\sin 2\beta$ and $\cos 2\beta$ [611]. Such analyses have been performed by both B factory experiments: from Table 30 we can remark that at present the results are dominated by large and non-Gaussian statistical errors, but nevertheless it can be said that $\cos 2\beta > 0$ is preferred by the experimental data in $J\psi K^*$.

Finally, decays of B mesons to final states such as $D\pi^0$ are governed by $b \to c\bar{u}d$ transitions. If the final state is a CP eigenstate, i.e. $D_{CP}\pi^0$, the usual time-dependence formulae are recovered, with the sine coefficient sensitive to $\sin 2\beta$. Since there is no penguin contribution to these decays, there is even less associated theoretical uncertainty than for $b \to c\bar{c}s$ decays like $B \to J/\psi K_S^0$. When multi-body D decays, such as $D \to K_S^0 \pi^+ \pi^-$, are used, a time-dependent analysis of the Dalitz plot of the neutral D decay allows a direct determination of the weak phase: 2β [612]. Such analyses have been performed by both B-factory experiments. The decays $B \to D\pi^0$, $B \to D\eta$, $B \to D\omega$, $B \to D^*\pi^0$ and $B \to D^*\eta$ are used. The daughter decays are $D^* \to D\pi^0$ and $D \to K_S^0 \pi^+ \pi^-$. The results are shown in Table 30. Again, it is clear that the data prefer $\cos 2\beta > 0$. Taken in conjunction with the $J/\psi K^*$ results, $\cos 2\beta < 0$ can be considered to be ruled out at approximately 2.3σ [209]. Time-dependent analysis of the decay $B \to D^{*+}D^{*-}K_S^0$ also prefers $\cos 2\beta > 0$.

3.5.2.2 $\alpha(\phi_2)$ The CKM unitarity angle $\alpha(= \phi_2)$, defined as $\alpha = \arg(-V_{td}V_{tb}^*/(V_{ud}V_{ub}^*))$, is a measure of the relative phase of the CKM elements V_{ub} and V_{td} in the usual parameterization of the CKM unitarity matrix. Most of the experimental information on α is extracted from measurements of the charmless decays $B \to \pi\pi$, $B \to \rho\pi$ and $B \to \rho\rho$, which can arise from the tree-level transition $b \to u(\bar{u}d)$, carrying the CKM element V_{ub} (left diagram in Fig. 24). In a simple world, where a decay mode such as $B \to \pi^+\pi^-$ is dominated by a single tree diagram, one needs only to measure the time-dependent CP asymmetry $S_{\pi\pi} = \sin 2\alpha$. However, a complication to this picture arises from the presence of loop (penguin) processes (right diagram in Fig. 24), involving different CKM matrix elements but leading to the same final states. The interference of the two diagrams then obscures the connection between the CP observables and the angle α, requiring a "tree and penguin disentanglement" strategy in the experimental program. This involves a larger set of experimental observables for the determination of the angle α that includes the time-dependent CP asymmetries S_f and C_f in B^0 decays and the branching fractions and direct CP asymmetries in both neutral and charged B decays. The net effect of the penguin amplitude is to introduce the possibility of direct CP violation ($C_f \neq 0$) and a nonzero value of $\Delta\alpha^f = \alpha_{\text{eff}}^f - \alpha$, where α_{eff}^f is determined from the relation $S_f = \sqrt{1 - C_f^2} \sin 2\alpha_{\text{eff}}^f$.

---

[18]The same processes can be described by a penguin diagram which brings corrections at order $\sim \lambda^4$.

Eur. Phys. J. C (2008) 57: 309–492

379

Table 29 Results for the CP-violating parameters in the $b \to c\bar{c}s$ decays: $S_{b \to c\bar{c}s}$ and $C_{b \to c\bar{c}s}$. The B-factory averages are given after ICHEP 2006 as calculated by HFAG [502]. The final world averages include also the results from ALEPH, OPAL and CDF, which use only the $J/\psi K_S^0$ final state

Experiment		$-\eta_{CP} S_{b \to c\bar{c}s}$	$C_{b \to c\bar{c}s}$
BaBar	[608]	$0.710 \pm 0.034 \pm 0.019$	$0.070 \pm 0.028 \pm 0.018$
Belle	[609]	$0.642 \pm 0.031 \pm 0.017$	$-0.018 \pm 0.021 \pm 0.014$
B factory average		0.674 ± 0.026	0.012 ± 0.022
Confidence level		0.18	0.02
Average		0.675 ± 0.026	0.012 ± 0.022
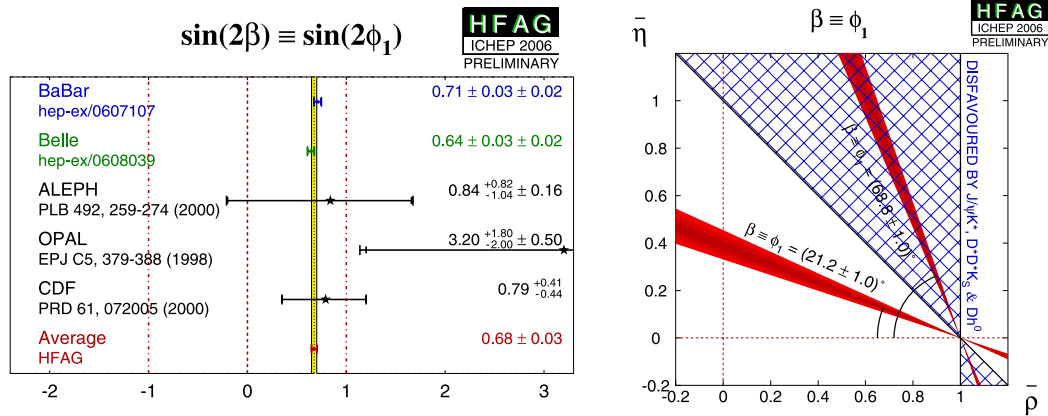
Fig. 23 World average of measurements of $S_{b \to c\bar{c}s}$ as calculated by HFAG [502] (*left*) and constraints on the $(\bar{\rho}, \bar{\eta})$ plane obtained from the average of $-\eta_{CP} S_{b \to c\bar{c}s}$ and (137) (*right*)

Table 30 Results from the B factories together with the HFAG averages [502] from the $B^0 \to J/\psi K^{*0}$ and the $B^0 \to D^{(*)}h^0$ analyses

$B^0 \to J/\psi K^{*0}$		$\sin 2\beta$	$\cos 2\beta$
BaBar	[613]	$-0.10 \pm 0.57 \pm 0.14$	$3.32^{+0.76}_{-0.96} \pm 0.27$
Belle	[614]	$-0.24 \pm 0.31 \pm 0.05$	$0.56 \pm 0.79 \pm 0.11$
Average		0.16 ± 0.28	1.64 ± 0.62
$B^0 \to D^{(*)}h^0$		$\sin 2\beta$	$\cos 2\beta$
BaBar	[615]	$0.45 \pm 0.36 \pm 0.05 \pm 0.07$	$0.54 \pm 0.54 \pm 0.08 \pm 0.18$
Belle	[616]	$0.78 \pm 0.44 \pm 0.22$	$1.87^{+0.40+0.22}_{-0.53-0.32}$
Average		0.57 ± 0.30	1.16 ± 0.42

Fig. 24 The tree (*left*) and penguin (*right*) diagrams contributing to "charmless" B decays such as $B \to \pi\pi$, $B \to \rho\rho$ and $B \to \rho\pi$
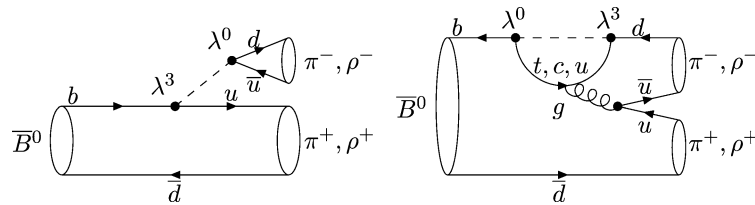
For the $B \to \pi\pi$ decays, the penguin correction $\Delta\alpha^{\pi\pi}$ can be determined from an isospin analysis [246] of the decay amplitudes of the $B \to \pi\pi$ and $\bar{B} \to \pi\pi$ decays, see Fig. 25. A key element of this analysis is the branching fraction for the decay $B \to \pi^0\pi^0$, which is an indicator of the size of the penguin effects and consequently of the penguin correction $\Delta\alpha^{\pi\pi}$, which is bounded [617] by $\sin^2 \Delta\alpha^{\pi\pi} < \bar{B}(B^0 \to \pi^0\pi^0)/B(B^\pm \to \pi^\pm\pi^0)$. Ref. [211] proposes to add information on the hadronic amplitudes to the isospin analysis, for example by using the branching ratio of $B_s \to K^+K^-$ to constraint the penguin contribution (even allowing $SU(3)$ breaking effects as large as 100%).

380

Eur. Phys. J. C (2008) 57: 309–492

Fig. 25 Isospin triangles for the $B \to \pi\pi$ system

This would help constraining the value of α, in particular eliminating the solutions at $\alpha \sim 0$.

A system analogous to that of the $B \to \pi\pi$ decays is the family of the $B \to \rho\rho$ decays ($B^0 \to \rho^+\rho^-$, $B^+ \to \rho^+\rho^0$, $B^0 \to \rho^0\rho^0$). While in general the $B^0 \to \rho\rho$ decays can be a mixture of CP-even and CP-odd components, the angular analysis of the decay $B^0 \to \rho^+\rho^-$ (and also $B^+ \to \rho^+\rho^0$) has shown that the CP-even component (longitudinal polarization) is dominant, hence significantly simplifying the time-dependent CP analysis of the process [618, 619]. As in the case of $B \to \pi\pi$, time-dependent CP asymmetries $S_{\rho\rho}^L$ and $C_{\rho\rho}^L$ are used to determine $\alpha_{\mathrm{eff}}^{\rho\rho}$. The branching ratio for $B^0 \to \rho^0\rho^0$ relative to $B \to \rho^+\rho^-$ and $B \to \rho^+\rho^0$ sets the scale of the penguin correction $\Delta\alpha^{\rho\rho} = \alpha_{\mathrm{eff}}^{\rho\rho} - \alpha$, which can be determined from an isospin analysis of the decay amplitudes.

In Table 31, we present the current status of measurements used in the determination of α in the $B \to \pi\pi$ and $B \to \rho\rho$ systems [502]. Nearly all components of the isospin analysis in the $B \to \pi\pi$ system are now measured, albeit with varying degrees of precision. Also the current measurements allow for the isospin triangles to close in both systems.[19]

The fact that the branching fraction for the decay $B \to \pi^0\pi^0$ is of the same order as the branching fractions for $B^+ \to \pi^+\pi^0$ and $B^0 \to \pi^+\pi^-$ is indicative of significant contributions from penguin amplitudes in this channel. Currently the $B \to \rho^0\rho^0$ search is giving the first evidence of a signal (BaBar reporting a 3σ effect [622]) and thus a very preliminary measurement of the rate. Still, the major advantage of the $B \to \rho\rho$ system over the $\pi\pi$ one is clearly evident from the suppression of $B \to \rho^0\rho^0$ relative to $B \to \rho^+\rho^-$ and $B \to \rho^+\rho^0$ decays, implying a much smaller $\Delta\alpha$ correction and smaller related uncertainties from this source. The current $\Delta\alpha$ correction upper limits are $\Delta\alpha_{\pi\pi} < 41°$ (90% C.L.) from BaBar and $\Delta\alpha_{\rho\rho} < 21°$ (90% C.L.) from BaBar.

One other advantage of the $\rho\rho$ system is that, in contrast to $\pi^0\pi^0$, a time-dependent CP-asymmetry analysis of the $\rho^0\rho^0$ final state will be possible as soon as enough statistics are available. This feature will allow both S^{00} and C^{00} to be accessed. From a feasibility study we can foresee for the $2\,\mathrm{ab}^{-1}$ scenario an error of 0.3 on S^{00} and 0.25 on C^{00}. This information will greatly help in reducing the ambiguities in the α extraction from this system.

The $B \to \rho\pi$ system presents a special case with the possibility of additional handles: the final states $\rho^+\pi^-$ and $\rho^-\pi^+$, which can be reached by both B^0 and $\bar{B}^0$, have substantial overlap in the Dalitz plot; thus their amplitudes interfere and generate additional dependence on α and the strong phases of the final states. Quinn and Snyder [623] have shown that the interference effect can be exploited to extract the angle α even in the presence of penguins. This involves the amplitude analysis of the 3π Dalitz distribution.

The $\rho^\pm\pi^\mp$ final states are not CP eigenstates, and four flavor-charge configurations ($B^0(\bar{B}^0) \to \rho^\pm\pi^\mp$) must be considered. Both experiments assume that the amplitudes corresponding to these final states are dominated by the three resonances ρ^+, ρ^- and ρ^0. The ρ resonances are assumed to be the sum of the ground state $\rho(770)$ and the radial excitations $\rho(1450)$ and $\rho(1700)$. Possible contributions to the $B^0 \to \pi^+\pi^-\pi^0$ decay other than the ρ's are studied as part of the systematic uncertainties. The time-dependent analyses use a general parameterization[20] that allows one to describe the differential decay width as a linear combination of independent functions, whose coefficients are the 26 free parameters of the fit.

From the bilinear coefficients both experiments extract the quasi-two-body (Q2B) parameters. Considering only the charged bands in the Dalitz plot, the Q2B analysis involves 5 different parameters $S_{\rho\pi}$, $C_{\rho\pi}$, $\Delta S_{\rho\pi}$, $\Delta C_{\rho\pi}$ and $\mathcal{A}_{\mathrm{CP}}^{\rho\pi}$. The first two parameterize mixing-induced CP violation related to the angle α and flavor-dependent direct CP violation, respectively. The second two are insensitive to CP violation: $\Delta S_{\rho\pi}$ is related to the strong phase difference between the amplitudes contributing to $B^0 \to \rho\pi$ decays, and $\Delta C_{\rho\pi}$ describes the asymmetry between the rates $\Gamma(B^0 \to \rho^+\pi^-) + \Gamma(\bar{B}^0 \to \rho^-\pi^+)$ and $\Gamma(B^0 \to \rho^-\pi^+) + \Gamma(\bar{B}^0 \to \rho^+\pi^-)$. Finally, $\mathcal{A}_{\mathrm{CP}}^{\rho\pi}$ is the time-independent charge asymmetry. CP symmetry is violated if either one of the following conditions is true: $\mathcal{A}_{\mathrm{CP}}^{\rho\pi} \neq 0$, $C_{\rho\pi} \neq 0$ or $S_{\rho\pi} \neq 0$. The first two correspond to CP violation in the decay, while the last condition is CP violation in the interference of decay amplitudes with and without B^0 mixing. In Table 32, we report the HFAG averages of the Q2B parameters provided by the experiments, which should be equivalent to determining average values directly from the averaged bilinear coefficients.

---

[19]This was not the case for the $B \to \rho\rho$ system with the pre-2006 measurements.

[20]See for details Refs. [502, 624, 625].

Table 31 Summary of measured decay properties of the $B \to \pi\pi$ and $B \to \rho\rho$ decays that are relevant to the determination of the CKM unitarity angle α. We quote here the averages updated after ICHEP 2006 as given by HFAG [502] with a total of 882 million $B\bar{B}$ pairs from BaBar (347 million events [620]) and Belle (535 million events [621]) experiments

Decay mode	BR($\times 10^6$)	S_f	C_f (or A_{CP} for B^+)
$B^0 \to \pi^+\pi^-$	5.2 ± 0.2	-0.59 ± 0.09	-0.39 ± 0.07
$B^+ \to \pi^+\pi^0$	5.7 ± 0.4	–	0.04 ± 0.05
$B^0 \to \pi^0\pi^0$	1.3 ± 0.2	–	$0.36^{+0.33}_{-0.31}$
$B^0 \to \rho^+\rho^-$	$23.1^{+3.2}_{-3.3}$		
	$[f_L = 0.968 \pm 0.023]$	-0.13 ± 0.19	-0.06 ± 0.14
$B^+ \to \rho^+\rho^0$	18.2 ± 3.0		
	$[f_L = 0.912^{+0.044}_{-0.045}]$	–	-0.08 ± 0.10
$B^0 \to \rho^0\rho^0$	1.16 ± 0.46		
	$[f_L = 0.86^{+0.12}_{-0.14}]$	–	–

Table 32 Summary of measured CP-asymmetry parameters of the $\rho\pi$ system following the convention used in [626]. We quote here the averages updated after ICHEP 2006 as given by the HFAG [502] with a total of 796 million $B\bar{B}$ pairs from BaBar (347 million events [624]) and Belle (449 million events [625]) experiments

$\rho^\pm\pi^\mp$ Q2B/Dalitz plot analysis

$S_{\rho\pi}$	$C_{\rho\pi}$	$\Delta S_{\rho\pi}$	$\Delta C_{\rho\pi}$	$\mathcal{A}^{\rho\pi}_{CP}$
0.03 ± 0.09	0.03 ± 0.07	-0.02 ± 0.10	0.36 ± 0.07	-0.13 ± 0.03
	$\mathcal{A}^{+-}_{\rho\pi}$		$\mathcal{A}^{-+}_{\rho\pi}$	
	0.11 ± 0.06		-0.19 ± 0.13	

One can transform the experimentally motivated CP parameters $\mathcal{A}^{\rho\pi}_{CP}$ and $C_{\rho\pi}$ into the direct CP violation parameters $\mathcal{A}^{+-}_{\rho\pi}$ and $\mathcal{A}^{-+}_{\rho\pi}$ defined in [626]. $\mathcal{A}^{-+}_{\rho\pi}$ ($\mathcal{A}^{+-}_{\rho\pi}$) describes CP violation in B^0 decays where the ρ is emitted (not emitted) by the spectator interaction. Both experiments obtain values for $\mathcal{A}^{-+}_{\rho\pi}$ and $\mathcal{A}^{+-}_{\rho\pi}$ which are averaged in Table 32. In addition to the $B^0 \to \rho^\pm\pi^\mp$ Q2B contributions to the $\pi^+\pi^-\pi^0$ final state, there can also be a $B^0 \to \rho^0\pi^0$ component. Belle and BaBar have extracted the Q2B parameters associated with this intermediate state which average to $S_{\rho^0\pi^0} = 0.30 \pm 0.38$ and $C_{\rho^0\pi^0} = 0.12 \pm 38$ (HFAG Summer 2007).

In Fig. 26, the plots of the averages and the separate results on the various CP-violating parameters are shown: it can be seen that the two collaborations, BaBar and Belle, are still discrepant at the level of 2σ (1.5σ) in the $B \to \pi^+\pi^-$ ($B \to \rho^\pm\pi^\pm$) system. In the $\rho\rho$ system, though, some updates to the entire currently available statistics are still missing.

We can get an estimate of the current experimental value of α putting together all the analyses in all the modes. The results on the SM solution from the two fitting groups are $(92 \pm 7)°$ for the Bayesian approach [209] and $(93^{+11}_{-9})°$ for the frequentest approach [8]. From the same analyses we can also extract the SM α values using the UT fit constraints and without using the α information: $(93 \pm 6)°$ for the Bayesian approach and $(98^{+5}_{-19})°$ for the frequentest one. We can remark how the current values are in very good agreement with the expected SM values.

3.5.2.3 $\gamma(\phi_3)$

● *Measurement of γ from B decays to open charm*

The possibility of observing direct CP violation in $B \to DK$ decays was first discussed by Bigi, Carter and Sanda [627, 628]. Since then, various methods to measure the weak angle γ ($=\phi_3$) using $B \to DK$ decays have been proposed. All these methods are based on two key observations: neutral D^0 and $\bar{D}^0$ mesons can decay to a common final state, and the decay $B^+ \to DK^+$ can produce neutral D mesons of both flavors via $\bar{b} \to \bar{c}u\bar{s}$ and $\bar{b} \to \bar{u}c\bar{s}$ transitions (Fig. 27) with a relative phase θ_+ between interfering amplitudes that is the sum, $\delta_B + \gamma$, of strong and weak interaction phases. For the decay, $B^- \to DK^-$, the relative phase is $\theta_- = \delta_B - \gamma$, so both δ_B and γ can be extracted from measurements of such charge conjugate B decay modes. The feasibility of the γ measurement crucially depends on the size of r_B, the ratio of the B decay amplitudes involved ($r_B = |A(B^+ \to DK^+)|/|A(B^+ \to \bar{D}K^+)|$). The value of r_B is given by the ratio of the CKM matrix elements $|V^*_{ub}V_{cs}|/|V^*_{cb}V_{us}|$ and the colour-suppression factor and is estimated to be in the range 0.1–0.2 [629]. These methods are theoretically clean because the main contributions come from tree-level diagrams (Fig. 27).[21] Various methods have been proposed to exploit this strategy using different

---

[21] $D^0-\bar{D}^0$ mixing is neglected in the current analyses. This effect can be included though [630] and is shown to be very small within the SM [631].
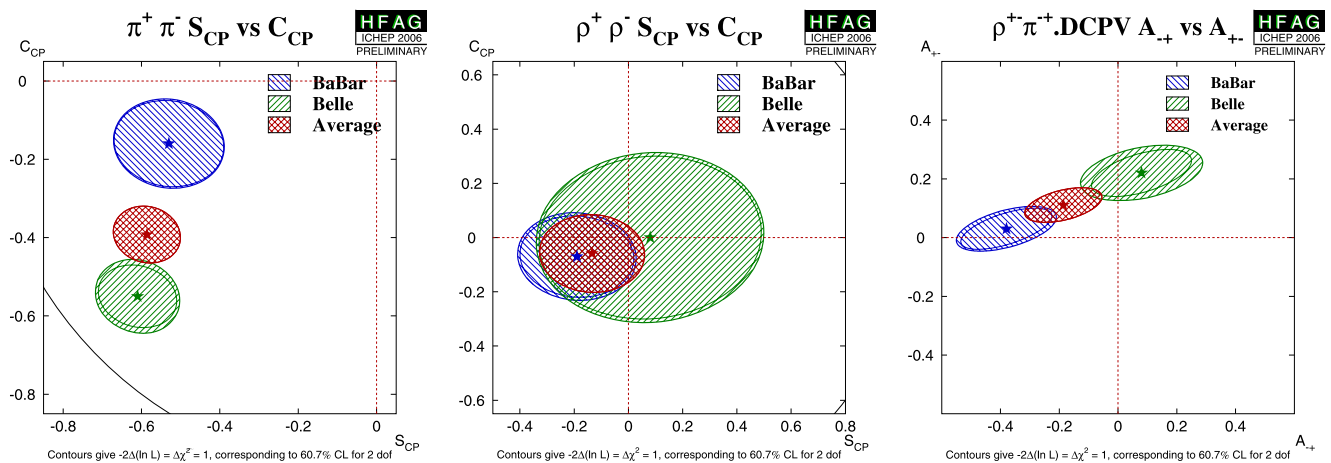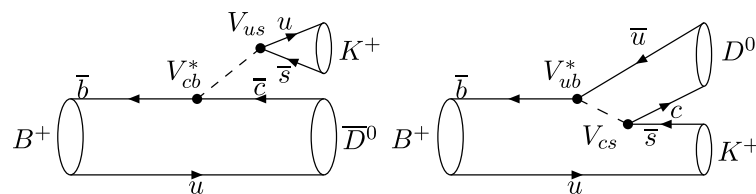
382

Eur. Phys. J. C (2008) 57: 309–492

Fig. 26 The experimental results on the CP asymmetry parameters in the $\pi\pi$ (*left*), $\rho\rho$ (*center*) and $\rho\pi$ (*right*) systems, as summarized by HFAG [502]

Fig. 27 Feynman diagram of the $B^+ \rightarrow \bar{D}^0 K^+$ and $B^+ \rightarrow D^0 K^+$ decays

combinations of final states. These approaches include using the branching ratios of decays to CP eigenstates (GLW method [632–634]) or using doubly Cabibbo-suppressed D modes (ADS method [635]). A Dalitz plot analysis of a three-body final state of the D meson allows one to obtain all the information required for the determination of γ in a single decay mode [636–638]. Three-body final states such as $K^0_S\pi^+\pi^-$ [637, 638] have been suggested as promising modes and give today the best estimate of the angle γ.

In the GLW method, the D is reconstructed through its decay to CP eigenstates. The experimental observables are the ratio of charge averaged partial rates, $R_{\text{CP}\pm}$, and the charge asymmetry, $A_{\text{CP}\pm}$, which are related to the model parameters through the relations $R_{\text{CP}\pm} = 1 + r_B^2 \pm 2r_B \cos\delta_B \cos\gamma$ and $A_{\text{CP}\pm} = \pm 2r_B \sin\delta_B \sin\gamma / R_{\text{CP}\pm}$. CP$_+$ refers to the CP-even final states, $\pi^+\pi^-$ and K^+K^-, and CP$_-$ refers to the CP-odd final states, $K^0_S\pi^0$, $K^0_S\phi$, $K^0_S\omega, \ldots$. Results are available from both BaBar and Belle in the decay modes $B^\pm \rightarrow DK^\pm$, $B^\pm \rightarrow D^*K^\pm$ and $B^\pm \rightarrow DK^{*\pm}$ (Fig. 28). The errors for $R_{\text{CP}\pm}$ and $A_{\text{CP}\pm}$ are typically 10% for the most promising mode, $B^\pm \rightarrow DK^\pm$. A 3σ significance for the charge asymmetry of the $B \rightarrow DK$ mode seems to be within reach in the near future, when 1 ab^{-1} of data will be collected by each experiment. For the ADS method, using a suppressed $D \rightarrow f$ decay ($D^0 \rightarrow K^+\pi^-$, $K^+\rho^-$, $K^*\pi^-$, …), the measured quantities are the partial rate asymmetry, A_{ADS}, and the charge averaged rate, $R_{\text{ADS}} = \Gamma(B^- \rightarrow [f]_D K^-)/\Gamma(B^- \rightarrow [\bar{f}]_D K^-)$. R_{ADS}

is related to the physical parameters by the expression $r_B^2 + r_D^2 + 2r_B r_D \cos(\delta_B + \delta_D)\cos\gamma$. The overall effective branching ratio is expected to be small ($\sim 10^{-7}$), but the two interfering diagrams are of the same order of magnitude, and large asymmetries are therefore expected. The method has four unknowns: γ, r_B, $\delta_B + \delta_D$ and the amplitude ratio r_D. However, the value of r_D can be measured using decays of D mesons of known flavor. If one wants to use the ADS method alone, two modes need to be used. Of course, one can also combine one ADS mode (as an example) with one GLW CP eigenstate. No significant signal has been yet observed for the ADS modes at the B factories, so only R_{ADS} has been measured so far for the $D^{(*)}K^{(*)}$ modes (Fig. 29). These measurements will bring soon valuable constraints on r_B.

In the Dalitz method, D^0 and $\bar{D}^0$ mesons decay into the same final state $K^0_S\pi^+\pi^-$ [637, 638] (or $K^+\pi^-\pi^0$ [636]). Assuming no CP asymmetry in neutral D decays, the amplitude of decay as a function of Dalitz plot variables $m^2_+ = m^2_{K^0_S\pi^+}$ and $m^2_- = m^2_{K^0_S\pi^-}$ is $M_\pm = f(m^2_\pm, m^2_\mp) + r_B e^{\pm i\gamma + i\delta_B} f(m^2_\mp, m^2_\pm)$, where $f(m^2_+, m^2_-)$ is the amplitude of the $\bar{D}^0 \rightarrow K^0_S\pi^+\pi^-$ decay. The method has a second ambiguous solution ($\gamma + 180°$, $\delta_B + 180°$), since this transformation does not change the sum or difference of phases that are actually measured.

Results from the two B factories Belle and BaBar are available. The Belle Collaboration uses a data sample of $386 \times 10^6 B\bar{B}$ pairs [639] where the reconstructed states
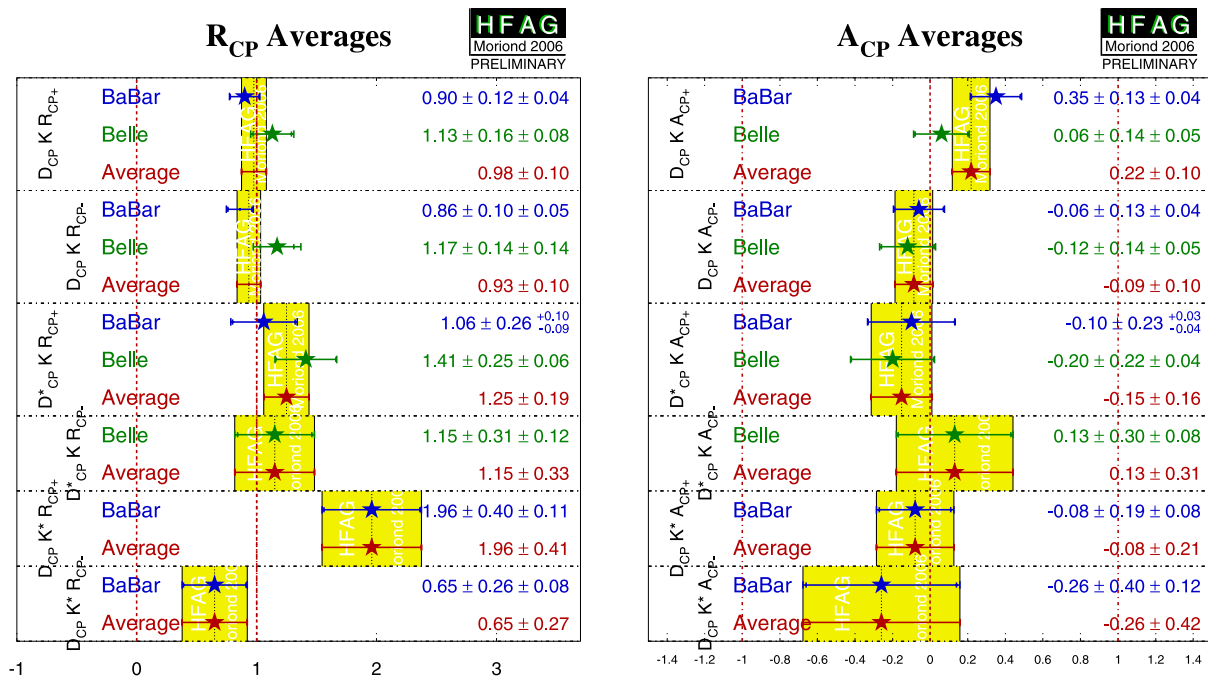
Eur. Phys. J. C (2008) 57: 309–492

383

Fig. 28 $R_{CP_\pm}$ and $A_{CP_\pm}$ averages obtained by the B factories [389]

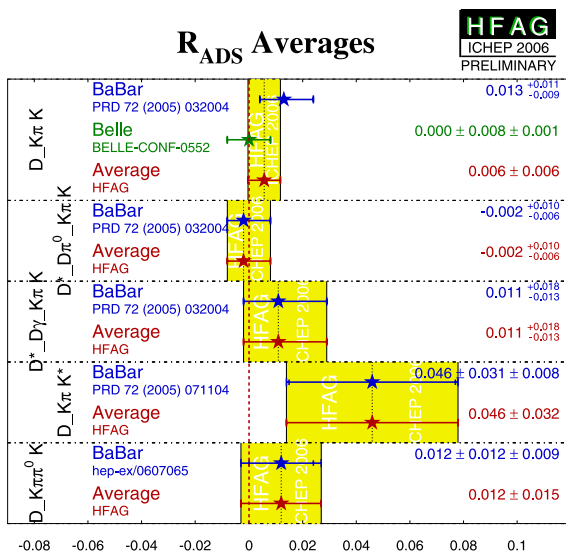**Fig. 29** R_{ADS} averages obtained by the B factories [389]

are $B^+ \to DK^+$, $B^+ \to D^*K^+$ with $D^* \to D\pi^0$ and $B^+ \to DK^{*+}$ with $K^{*+} \to K_S^0 \pi^+$. Analysis by the BaBar Collaboration [640] is based on $347 \times 10^6 B\bar{B}$ pairs using $B^+ \to DK^+$ and $B^+ \to D^*K^+$ with two D^* channels: $D^* \to D\pi^0$ and $D^* \to D\gamma$ (the previous BaBar [641] publication includes also the $B^+ \to DK^{*+}$ channel, but this mode is not included in the recent update). The number of reconstructed signal events in the Belle's data are 331 ± 23, 81 ± 11 and 54 ± 8 for the $B^+ \to DK^+$, $B^+ \to D^*K^+$ and

$B^+ \to DK^{*+}$ channels, respectively. BaBar finds 398 ± 23, 97 ± 13 and 93 ± 12 signal events in the $B^+ \to DK^+$, $B^+ \to D^*[D\pi^0]K^+$ and $B^+ \to D^*[D\gamma]K^+$ channels, respectively. The amplitude f is parametrized as a coherent sum of two-body decay amplitudes (16 for BaBar, 18 for Belle) plus a nonresonant decay amplitude and is determined directly in data from a large and clean sample of flavor-tagged decays produced in continuum e^+e^- annihilation. For example, Belle includes five Cabibbo-allowed amplitudes: $K^*(892)^+\pi^-$, $K^*(1410)^+\pi^-$, $K_0^*(1430)^+\pi^-$, $K_2^*(1430)^+\pi^-$ and $K^*(1680)^+\pi^-$, their doubly Cabibbo-suppressed partners, and eight channels with a K_S^0 and a $\pi\pi$ resonance: ρ, ω, $f_0(980)$, $f_2(1270)$, $f_0(1370)$, $\rho(1450)$, σ_1 and σ_2. The parameters of the σ resonances obtained in the fit are $M_{\sigma_1} = 519 \pm 6$ MeV/c^2, $\Gamma_{\sigma_1} = 454 \pm 12$ MeV/c^2, $M_{\sigma_2} = 1050 \pm 8$ MeV/c^2 and $\Gamma_{\sigma_2} = 101 \pm 7$ MeV/c^2 (the errors are statistical only), while the parameters of the other resonances are taken to be the same as in the CLEO analysis [642]. The agreement between the data and the fit result is satisfactory for the purpose of measuring γ, and the discrepancy is taken into account in the model uncertainty.

Once f is determined, a fit to $B^\pm$ data is performed to obtain the Cartesian parameters, $x_\pm = r_\pm \cos(\pm\gamma + \delta_B)$ and $y_\pm = r_\pm \sin(\pm\gamma + \delta_B)$, which have the advantage to be Gaussian-distributed, uncorrelated and unbiased (r_B is positive definite and hence exhibits a fit bias toward larger values when its central value is in a vicinity of zero) and simplify the averaging of the various measurements. Figure 30 shows the results of the separate B^+ and B^- data fits for $B \to DK$,
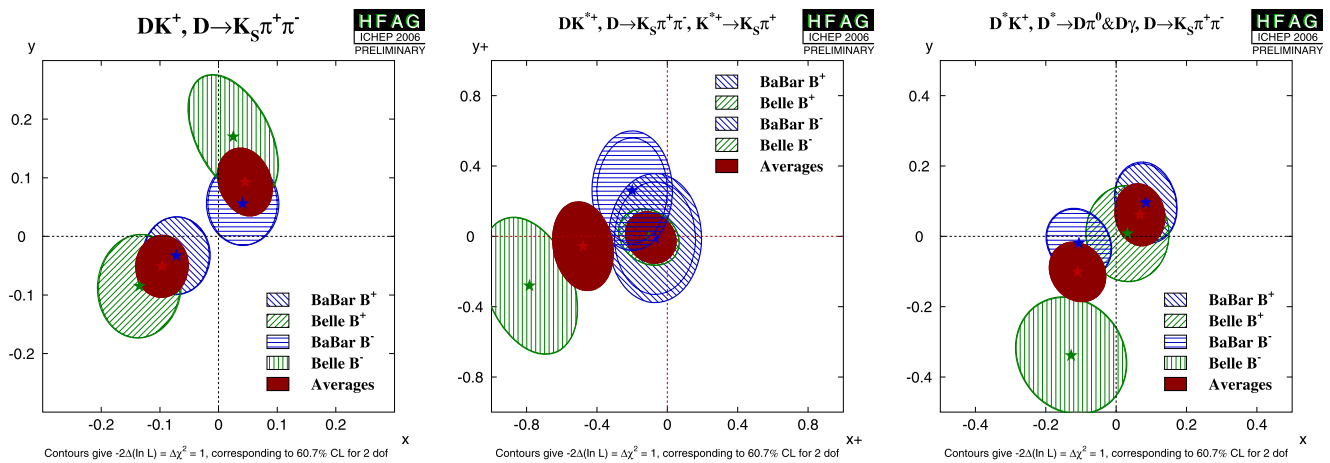
384

Eur. Phys. J. C (2008) 57: 309–492

Fig. 30 Results of signal fits with free parameters $x_{\pm} = r\cos\theta_{\pm}$ and $y_{\pm} = r\sin\theta_{\pm}$ for $B^{\pm} \to DK^{\pm}$, $D^*K^{\pm}$ and $DK^{*\pm}$ modes from the BaBar and Belle latest publications [639, 640]. The *contours* indicate one standard deviation

D^*K and DK^* modes in the x–y plane for the BaBar and Belle Collaborations. Confidence intervals were then calculated by each experiment using a frequentest technique (the so-called Neyman ordering in the BaBar case, the Feldman and Cousins ordering [643] in the Belle case). The central values for the parameters γ, r_B and δ_B from the combined fit (using the $(x_{\pm}, y_{\pm})$ obtained for all modes) with their one standard deviation intervals are presented in Table 33. Note that there are large correlations between the fit parameters γ and r_B. With the available data, the statistical error on γ increases with decreasing r_B and thus it depends strongly on the central value of r_B as determined by the fit. The uncertainties in the model used to parametrize the $\bar{D}^0 \to K_S^0 \pi^+ \pi^-$ decay amplitude lead to an associated systematic error in the fit result. These uncertainties arise from the fact that there is no unique choice for the set of quasi-2-body channels in the decay, as well as the various possible parameterizations of certain components, such as the nonresonant amplitude. To evaluate this uncertainty, several alternative models have been used to fit the data.

Despite similar statistical errors being obtained for $(x_{\pm}, y_{\pm})$ in both experiments, the resulting γ error is much

smaller in Belle's analysis. Since the uncertainty on γ scales roughly as $1/r_B$, the difference is explained by noticing that the BaBar $(x_{\pm}, y_{\pm})$ measurements favor values of r_B smaller than the Belle results.

All methods (GLW, ADS and Dalitz) are sensitive to the same parameters of the B decays, and can therefore be treated in a combined fit to extract γ. Such comparisons have been performed by various phenomenological groups, such as CKMfitter [8] and UTfit [209]. The CKMfitter group using a frequentest statistical framework obtains $(77 \pm 31)°$, whereas the UTfit group with a Bayesian approach obtains $(82 \pm 19)°$. This is in agreement with the prediction from the global CKM fit (where the direct γ measurement has been excluded from the fit). As mentioned earlier, the size of the r_B parameters play a crucial role in the γ determination, and they are found to be $r_B(DK) < 0.13$, $r_B(D^*K) < 0.13$ and $r_B(DK^*) < 0.27$ at 90% C.L. by Ref. [8] and $r_B(DK) < 0.10$, $r_B(D^*K) < 0.12$ and $r_B(DK^*) < 0.26$ at 90% C.L. by Ref. [209]. All values are in agreement with the naive expectation from CKM and colour suppression.

Clearly, the precision on γ will improve with more data. However, the dependence of the sensitivity on the value

Table 33 Results of the combination of $B^+ \to DK^+$, $B^+ \to D^*K^+$, and $B^+ \to DK^{*+}$ modes for BaBar and Belle analyses. The first error is statistical, the second is systematic, and the third one is the model error. In the case of BaBar, one standard deviation constraint is given for the r_B values

Parameter	BaBar	Belle
γ	$(92 \pm 41 \pm 11 \pm 12)°$	$(53^{+15}_{-18} \pm 3 \pm 9)°$
$r_B(DK)$	< 0.140	$0.159^{+0.054}_{-0.050} \pm 0.012 \pm 0.049$
$\delta_B(DK)$	$(118 \pm 63 \pm 19 \pm 36)°$	$(146^{+19}_{-20} \pm 3 \pm 23)°$
$r_B(D^*K)$	0.017–0.203	$0.175^{+0.108}_{-0.099} \pm 0.013 \pm 0.049$
$\delta_B(D^*K)$	$(-62 \pm 59 \pm 18 \pm 10)°$	$(302^{+34}_{-35} \pm 6 \pm 23)°$
$r_B(DK^*)$		$0.564^{+0.216}_{-0.155} \pm 0.041 \pm 0.084$
$\delta_B(DK^*)$		$(243^{+20}_{-23} \pm 3 \pm 49)°$

of r_B means that we should be careful when extrapolating the present results to a higher statistics scenario. Assuming a value of r_B in the range of 0.1–0.15, the statistical error obtained by the end of the B factories (2 ab^{-1}) will be (10–15)°. The way to improve the γ sensitivity in the near future is to include more D^0 (and use of D^{*0}) modes, with combined strategies [630], use of differential spectra [644], many body modes, charm factory inputs [645, 646], along with the use of B^0 modes [644, 647]. Although at present (and until the end of B factories era) the γ accuracy in the $K_S^0 \pi^+ \pi^-$ analysis is dominated by the statistical uncertainty, the model error will eventually dominate in the context of a super B factory. Model-independent ways to extract γ have been proposed [636, 637, 648]. One way to implement this is to notice that in addition to flavor tagged $\bar{D}^0 \to K_S^0 \pi^+ \pi^-$ decays, one can use CP tagged decays to $K_S^0 \pi^+ \pi^-$ from the $\psi(3770) \to D\bar{D}$ process. Combining the two data sets, the amplitude and phase could be measured for each point on the Dalitz plot in a model-independent way. Study with MC simulations (assuming $r = 0.2$) indicates that with 50 ab^{-1} of data γ can be measured with a total accuracy of few degrees [648]. Combining all the methods with the statistics anticipated at a super B factory (50 ab^{-1}), it is expected that an error of about two degrees is obtainable (Chapter 4).

3.5.2.4 Measurement of $\sin 2\beta + \gamma$ *from B decays to open charm* Interference between decays with and without mixing can occur in the non-CP eigenstates $B^0 \to D^{(*)\pm} \pi^{\mp}(\rho^{\mp})$. The Cabibbo-favored $\bar{b} \to \bar{c}$ decay amplitude interferes with the Cabibbo-suppressed $b \to u$ decay amplitude with a relative weak phase shift γ. These modes have the advantage of a relatively large branching fraction but a small ratio r of suppressed to favored amplitudes. Time-dependent asymmetries in these modes can be used to constraint $\sin(2\beta + \gamma)$ [653]: the coefficient of the $\sin(\Delta m \Delta t)$ term can be written, to a very good approximation, as $S^{\pm} = 2r \sin(2\beta + \gamma \pm \delta)$, where δ is the strong

phase shift due to final-state interaction between the decaying mesons.

Potential competing CP-violating effects can arise from $b \to u$ transitions on the tag side if a kaon is used to tag the flavor on the other B in the event, resulting in an additional sin term $S'^{\pm} = 2r' \sin(2\beta + \gamma \pm \delta')$ [649]. Here, r' (δ') is the effective amplitude (phase) used to parameterize the tag side interference. To account for this term, one can rewrite $S^{\pm}$ as $S^{\pm} = (a \pm c) + b$, where $a = 2r \sin(2\beta + \gamma) \cos \delta$, $c = \cos(2\beta + \gamma)[2r \sin \delta + 2r' \sin \delta']$ and $b = 2r' \sin(2\beta + \gamma) \cos \delta'$. The results from B factories [650–652] are shown for $D\pi$ and $D^*\pi$ modes in terms of a and c in Fig. 31. CP violation would appear as $a \neq 0$. External information is however needed to determine r or δ. Naively, one can estimate $r \sim |V_{cd}^* V_{ub} / V_{ud} V_{cb}^*| \simeq 0.02$. One popular choice is the use of $SU(3)$ symmetry to obtain r by relating decay mode to B decays involving D_s mesons [653].

3.5.3 Expectations from LHCb

3.5.3.1 Introduction This section summarizes the outlook for measurements of CKM angles through tree-level processes at LHCb. All estimates are given for 2 fb^{-1} of integrated luminosity, which is a canonical year of LHCb operation. (In the summary section, extrapolations are also made to 10 fb^{-1}, which represents five years of operation.) Background estimates have been made using 34 million simulated generic $b\bar{b}$ events and, where appropriate, with specific samples of known dangerous topologies. Full details may be found in the cited LHCb notes and other references.

3.5.3.2 Measuring β *with* $B^0 \to J/\psi K_S^0$ The channel $B^0 \to J/\psi K_S^0$, with the J/ψ decaying to $\mu^+ \mu^-$, is relatively easy to trigger on and reconstruct at LHCb. In order to minimize systematic effects, selection cuts have been developed which impose the least possible bias on the lifetime distribution of the decaying B^0.

Fig. 31 Results of the a and c measurements for the $D\pi$ (*left*) and $D^*\pi$ (*right*) modes
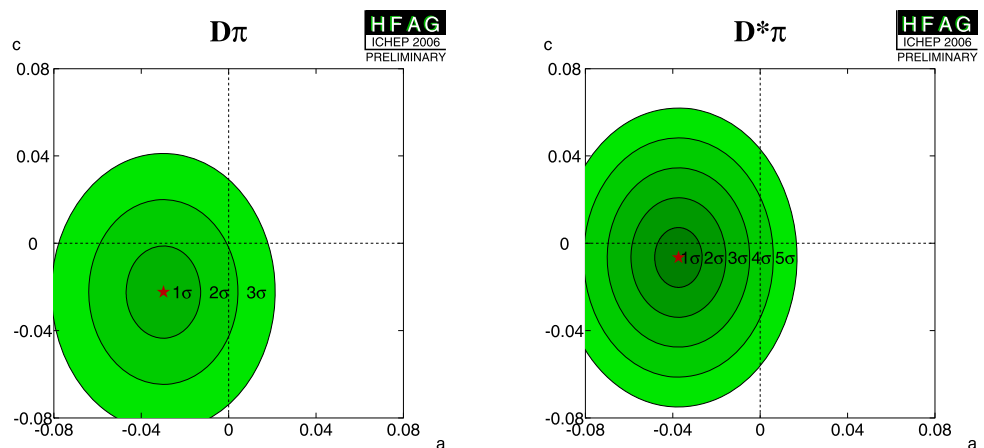
It is estimated that 333k untagged triggered events will be collected per 2 fb^{-1} of integrated luminosity. Background studies have been performed using a large sample of generic $b\bar{b}$ events and a dedicated sample of prompt J/ψ events. The results indicate that the expected B/S ratio from the two sources is 1.1 and 7.3, respectively. The high background from prompt J/ψ's has little consequence for the $\sin 2\beta$ sensitivity, as the events are restricted to low proper times. The performance of the flavor tag is determined from the similar topology $B^0 \to J/\psi K^{*0}$ control channel. The statistical precision on $\sin 2\beta$ with 2 fb^{-1} is estimated to be 0.015. More information may be found in [666].

3.5.3.3 Measuring α with $B^0 \to \rho\pi$ and $B^0 \to \rho\rho$ at LHCb
The potential of LHCb in the decay $B^0 \to \rho\pi \to \pi^+\pi^-\pi^0$ has been studied extensively [654]. The hard spectrum of the π^0, together with the vertex constrains on the $\pi^+\pi^-$ pair, means that the decay can be well isolated from background, even in the high multiplicity environment of the LHC. A! multivariate variable is built up to exploit all available discriminating variables. It is estimated that 1.4×10^4 events will be accumulated per 2 fb^{-1} of integrated luminosity. The acceptance for these events is fairly uniform over Dalitz space, apart from in the region of low $(m^2_{\pi^+\pi^0},$ $m^2_{\pi^-\pi^0})$, which is depopulated due to the minimum energy requirement on the π^0.

The background has been studied with large simulated samples of generic $b\bar{b}$ events and with specific charmless decay channels. It is concluded that the B/S ratio should not exceed one, a value which has been assumed for the subsequent sensitivity studies.

The expected precision on the angle α has been estimated using a toy Monte Carlo, taking the resolutions and acceptances from the full simulation and modeling the background as a combination of nonresonant and resonant contributions. Repeated toy experiments are performed, each of which has 10000 signal events. Various scenarios have been considered for the relative values of the penguin and tree amplitudes contributing to the final state. The results shown here assume the 'strong penguin' case [655]. An unbinned log likelihood fit is used to extract the physics parameters of interest, in particular α. The achievable precision on α varies between amplitude scenarios and fluctuates from experiment to experiment. The statistical error is below 10° for about 90% of experiments. The mean value is around 8°. On about 15% of occasions, the fit converges to a pseudo-mirror solution, but these effects diminish with larger data sets. Figure 32 shows the variation in χ^2 for fits to many toy experiments as a function of α, and the average of these curves with a clear minimum seen at the input value of $\alpha = 97°$. Studies of potential systematic uncertainties indicate that it will be important to have good understanding of the ρ lineshape.

The performance of LHCb has also been investigated in the modes $B^0 \to \rho^\pm\rho^\mp$ and $B^\pm \to \rho^\pm\rho^0$. It is concluded that although significant numbers of events can be accumulated, the total event samples are similar in size to those that will come from the B factories. More promising is the decay $B^0 \to \rho^0\rho^0$, which can be used in an isospin analysis to constrain the bias on α arising from penguin contamination in the channel $B^0 \to \rho^\pm\rho^\mp$. 1200 events will be obtained per 2 fb^{-1}, assuming a branching ratio of 1.2×10^{-6}. More details on this analysis and estimates of its impact on the α extraction within possible scenarios can be found in [654].

3.5.3.4 Measuring γ with $B \to DK$ strategies at LHCb
In principle all $B \to DK$ channels, where the D decays hadronically, carry information on the angle γ. LHCb has investigated several modes, with the emphasis on those where the decays involve charged tracks only. The presence of one or more kaons in the final state makes these decays particularly suited to LHCb, on account of its RICH system. The estimated event yields for the modes so far considered are summarized in Table 34. Background studies have been carried out using large simulation samples of generic $b\bar{b}$ events, as well as specific channels which are potential sources of contamination, for example $B \to D\pi$. In all cases, it is concluded that the background levels can be reduced to an acceptable level. More information can be found in the referenced notes. Many of the strategies that have been investigated are common to those pioneered at the B factories and discussed in Sect. 3.5.2.3.

The simplest topologies are $B \to DK$ decays where the $D^0(\bar{D}^0)$ decays to a CP-eigenstate such as K^+K^- or

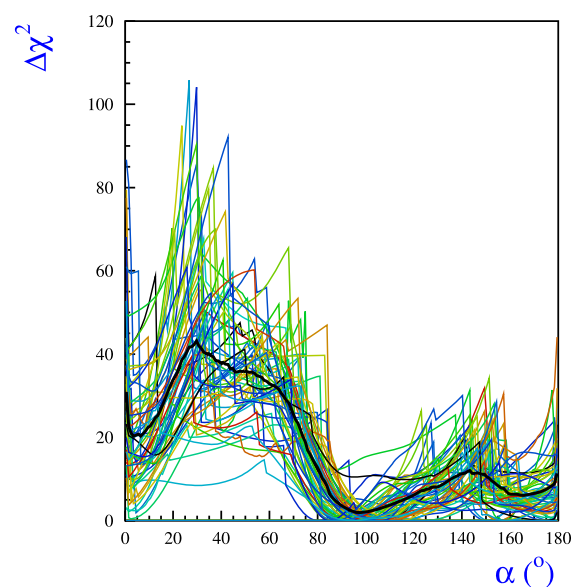**Fig. 32** Change in χ^2 with α for a fit to simulated experiments assuming the LHCb performance with 1000 signal events and a B/S ratio of 1. Each *curve* corresponds to a different experiment. Superimposed in *black* is the average of all experiments. The input value of α is 97°

Table 34 Expected event yields and estimated background for 2 fb^{-1} in $B \rightarrow DK$ decay modes so far considered at LHCb. In the rows where two signal yields are listed, the background corresponds to that expected in either channel. All numbers come from typical scenarios presented in the references quoted in the text. The background in the $D(K_S^0 K^+ K^-)K^\pm$ final state has not yet been studied, but it is expected to be significantly smaller than that in the $D(K_S^0 \pi^+ \pi^-)K^\pm$ mode

Decay mode	Signal	Background
$B^\pm \rightarrow D(K^+K^-)K^\pm$	2600, 3200	3700 ± 1000
$B^\pm \rightarrow D(\pi^+\pi^-)K^\pm$	900, 1100	3600 ± 1500
$B^\pm \rightarrow D(K^\pm\pi^\mp)K^\pm$	28000, 28300	17500 ± 1000
$B^\pm \rightarrow D(K^\mp\pi^\pm)K^\pm$	10, 400	800 ± 500
$B^\pm \rightarrow D(K^\pm\pi^\mp\pi^+\pi^-)K^\pm$	30400, 30700	20200 ± 2500
$B^\pm \rightarrow D(K^\mp\pi^\pm\pi^+\pi^-)K^\pm$	20, 410	1200 ± 360
$B^\pm \rightarrow D(K_S^0\pi^+\pi^-)K^\pm$	5000	1000–5000 (90% C.L.)
$B^\pm \rightarrow D(K_S^0 K^+K^-)K^\pm$	1000	/
$B^\pm \rightarrow D(K^+K^-\pi^+\pi^-)K^\pm$	1700	1500 ± 600
$B^\pm \rightarrow (D\pi^0)(K^\pm\pi^\mp)K^\pm$	16800, 16600	34300 ± 11500
$B^\pm \rightarrow (D\pi^0)(K^\mp\pi^\pm)K^\pm$	350, 100	4800 ± 3800
$B^\pm \rightarrow (D\gamma)(K^\pm\pi^\mp)K^\pm$	9400, 9300	34300 ± 11500
$B^\pm \rightarrow (D\gamma)(K^\mp\pi^\pm)K^\pm$	10, 140	4800 ± 3800
$B^0, \bar{B}^0 \rightarrow D(K^+K^-)K^{*0}, \bar{K}^{*0}$	240, 450	<1000 (90% C.L.)
$B^0, \bar{B}^0 \rightarrow D(\pi^+\pi^-)K^{*0}$	70, 140	<1000 (90% C.L.)
$B^0, \bar{B}^0 \rightarrow D(K^\pm\pi^\mp)K^{*0}, \bar{K}^{*0}$	1750, 1670	<1700 (90% C.L.)
$B^0, \bar{B}^0 \rightarrow D(K^\mp\pi^\pm)K^{*0}, \bar{K}^{*0}$	350, 260	<1700 (90% C.L.)

$\pi^+\pi^-$, or to $K^\pm\pi^\mp$. Of particular interest is the subset of highly suppressed 'ADS' decays $B^\pm \rightarrow D(K^\mp\pi^\pm)K^\pm$ where the interference effects are highest. The exact number of expected events in this mode depends on the assumption for r_B, the ratio of the interfering B decay amplitudes. Assuming a value of $r_B = 0.08$ leads to the expectation of around 400 events, integrated over B^+ and B^- channels, with a variation dependent on the value of the strong phase difference between the diagrams involved in both the B and D decays [656].

The 3-body Dalitz analysis of $K_S^0\pi^+\pi^-$ in $B \rightarrow DK$ decays has been successfully pioneered at the B factories. Here LHCb also expects to make a significant contribution with 5000 triggered and reconstructed decays per 2 fb^{-1} [658]. A technical challenge in selecting these events is presented by those K_S^0's which decay downstream of the VELO region; these decays account for around two thirds of the total sample. Although such events can be successfully reconstructed offline, this procedure is challenging to perform in the high-level trigger, where the existing track-search algorithm for K_S^0 daughters does not fit within the allocated CPU budget. It is hoped that this difficulty will be overcome. The problem is not so critical for the sister 3-body mode $D \rightarrow K_S^0 K^+K^-$, where the two kaons offer the possibility of devising an inclusive high-level trigger selection not dependent on the finding of the K_S^0.

The 4-body modes $D \rightarrow K^\pm\pi^\mp\pi^+\pi^-$ and $D \rightarrow K^+K^-\pi^+\pi^-$ are particularly attractive to LHCb as all the decay products are prompt charged tracks. Dependent on the charge of the decaying B and the charges of the particles in the D decay, the $K\pi\pi$ channel accesses four possible final states, of which the rarest two, $B^\pm \rightarrow D(K^\mp\pi^\pm\pi^+\pi^-)K^\pm$, possess large interference effects through the ADS mechanism. The expected sample size integrated over these two channels is about 400 events [659]. Provided that the sub-resonant decay structure can be fitted in a four-body amplitude analysis, these suppressed channels will provide high sensitivity to γ, either in isolation or in conjunction with the other ADS modes. An analysis of the 4-body Dalitz space of $K^+K^-\pi^+\pi^-$ accesses γ in a similar way to the 3-body self-conjugate mode $K_S^0\pi^+\pi^-$. Here 1700 events are expected [659].

Extensions of the standard $B \rightarrow DK$ strategies have also been considered at LHCb. Detailed studies have been performed of $B^0 \rightarrow DK^{*0}$, where the charge of the kaon in the $K^{*0} \rightarrow K^\pm\pi^\mp$ decay chain tags the flavor of the decaying B^0 [660]. Here both the interfering B^0 decay diagrams are colour suppressed, and hence the interference effects are higher than in the $B^\pm$ case, although the branching ratios are lower. Another method under study is $B^\pm \rightarrow D^*K^\pm$, where the D^* decays either through $D^0\pi^0$ or $D^0\gamma$. As there is a CP-conserving phase difference of π between these two paths, separation of the respective modes gives powerful additional constraints in the analysis. At LHCb, the energy of the neutral particles is too low to permit efficient selection. However, sufficient constraints exist in the decay topology to allow a full reconstruction using the charged tracks alone. Preliminary results indicate a promising performance, although there are at present insufficient Monte Carlo statistics to make a meaningful background estimate [657].

Assuming the 2 fb^{-1} event yields listed in Table 34 and the background estimates coming out of the Monte Carlo

studies, full sensitivity studies have been performed for several of the analyses. The precision on γ depends on the parameters assumed. Taking $r_B = 0.08$, the statistical uncertainty is found to be $(6–10)°$ for a combined $B^{\pm} \to DK^{\pm}$ analysis involving the two-body D decay modes, and $D \to K\pi\pi$, where the resonant substructure of the latter decay is so-far neglected [656]. A similar sensitivity is found for the $B^0 \to DK^{*0}$ study involving two body modes only, where the ratio of the interfering diagrams is taken to be 0.4 [660]. Estimates have also been made of the γ sensitivity in $K_S^0\pi^+\pi^-$ [658]. Including acceptance effects and background gives a typical sensitivity of $15°$, again taking $r_B = 0.08$. At present the only available studies of $K^+K^-\pi^+\pi^-$ [661] are for signal events only. A background free analysis with the LHCb annual signal yield would have a statistical uncertainty of $14°$, also with $r_B = 0.08$. Systematic effects have not yet been considered, but it is already known from the B factories that work is needed to improve the confidence in the $D \to K_S^0\pi^+\pi^-$ decay model, an issue which is likely to be important for all the 3- and 4-body D decays.

Other decay modes remain to be investigated, for example $B^{\pm} \to DK^{*\pm}$, $K^{*\pm} \to K_S^0\pi^{\pm}$. The full power of the $B \to DK$ sensitivity will only come with a combined analysis of all accessible decay modes. The preliminary indications suggest that $B \to DK$ decays will provide LHCb's most precise value of γ, with a few degrees uncertainty being achievable with 2 fb^{-1} of data. There is no reason to expect that the experimental systematics will significantly limit this sensitivity, although more detailed studies are required. It is clear, however, that residual uncertainties associated with the understanding of the D decay in the 3- and 4-body modes could be important. A possible scenario is presented in the Summary section based on arbitrary assumptions concerning this source of uncertainty.

3.5.3.5 Measuring γ with B_s, $\bar{B}_s \to D_s^{\pm}K^{\mp}$ and B^0, $\bar{B}^0 \to D^{\pm}\pi^{\mp}$ The isolation of $B_s \to D_s^{\pm}K^{\mp}$ decays is experimentally very challenging because of the low branching ratio and the order-of-magnitude more prolific $B_s \to D_s\pi$ decay mode. The LHCb trigger system gives good performance for fully hadronic modes and selects $B_s \to D_s^{\pm}K^{\mp}$ events with an efficiency of 29%. The π–K discrimination of the RICH system reduces the $B_s \to D_s\pi$ contamination to $\sim$10%. It is estimated that the experiment will accumulate 6.2k events per 2 fb^{-1} of integrated luminosity, with a combinatoric background to signal level of <0.6 [662]. The excellent $\sim$30 fs proper time precision provided by the silicon Vertex Locator will ensure that the B_s oscillations will be well resolved and hence allow the CP asymmetries to be measured. It is estimated that the statistical precision on γ from this channel alone will be $10°$ for 2 fb^{-1}, assuming $\Delta m_s = 17.5$ ps^{-1}, $|\Delta\Gamma_s|/\Gamma_s = 0.10$ [662]. Note that this

extraction requires knowledge of the weak mixing phase in the B_s system, which is imported from parallel LHCb studies performed with $B^0 \to J/\psi\phi$ decays.

A potential difficulty with the $B_s \to D_s^{\pm}K^{\mp}$ γ extraction arises from ambiguities. In the limit that $\Delta\Gamma_s$ is very small, the analysis returns an 8-fold ambiguity. A nonzero value of $\Delta\Gamma_s$ in principle ameliorates the problem, reducing the number of true ambiguities to four only, but even in this case, the eliminated solutions may in practice remain as false minima, on account of the limited experimental resolution. An attractive way to circumvent this difficulty is to make a combined analysis of the observables in the B_s decay and those in the U-spin symmetric $B^0 \to D^{\pm}\pi^{\mp}$ channel [663]. This approach has the added bonus of exploiting $B^0 \to D^{\pm}\pi^{\mp}$ decays in a manner which does not require knowledge of the ratio between the interfering tree diagrams, which in the B^0 system is known to be very small and hence hard to determine experimentally. LHCb will accumulate 1730k events per 2 fb^{-1} in this channel [664]. The combined analysis has the potential to reach a statistical precision of $5°$, depending on the values of the parameters involved. Any bias associated with the U-spin symmetry assumption also has a varying impact on the measurement, depending on the position in parameter space. In many scenarios, the effect is expected to be below the statistical uncertainty [665].

3.5.4 Summary

Table 35 presents a summary of the current status and the outlook for future direct measurements of the angles of the unitarity triangle from tree-dominated B decays. The last column of this table is an estimate of the ITE, which is the intrinsic error coming purely from theoretical limitations of the methods being used. It seems that for $\sin 2\beta$, at the end of the B factory era with an estimated $\approx$2 ab^{-1} of data, the experimental determination will be close to the expected theory error. In fact the theory error ($\lesssim$1%) is somewhat smaller, but apparently our current understanding is that experimental systematics are difficult to reduce below about (2–3)%. Measurement of $\sin 2\beta$ at LHCb also looks very promising so far as the statistical error goes.

For α, although each of the three methods, $\pi\pi$, $\rho\pi$, and $\rho\rho$ will have a residual theory error due to isospin violation by EWP and/or from other sources, it is quite likely that once the experimental information with high statistics on all the three modes becomes available, the remaining intrinsic theory error will be small, O(few%). The current B factories and LHCb are expected to be able to determine α to an accuracy around (5–8)$°$, i.e. considerably worse than the ITE. A super B factory should be able to attain the level of accuracy O(2%) $\approx$ ITE.

Unfortunately a precise determination of the angle γ is likely to remain a challenge for a long time to come. Admittedly we have been somewhat cautious in our projections for

Table 35 Unitarity Triangle from trees decays: Current status and future prospects. ITE means irreducible theory error; see text especially regarding the LHCb projections

$\int \mathcal{L}\,dt$	BF (Now) $\sim 1\ \text{ab}^{-1}$	BF(End '08) $2\ \text{ab}^{-1}$	LHCb $2\ \text{fb}^{-1}$	LHCb $10\ \text{fb}^{-1}$	SBF $50\ \text{ab}^{-1}$	ITE
$\sigma(\alpha)$	10° (11%)	7° (8%)	8.1° (9%)	4.6° (5%)	1.5° (1.6%)	O(few %)
$\sigma(\sin 2\beta)$	0.026 (4%)	0.023 (3.3%)	0.015 (2.1%)	0.007 (1%)	0.013 (2%)	$\lesssim 1\%$
$\sigma(\gamma)$	30° (46%)	15° (23%)	4.5° (7%)	2.4° (4%)	2° (3%)	$O(0.1\%)$

the B factories, and there is some chance that we will gain more from combined strategies, compared to projections in this table, as additional data becomes available in the next year or two. Indeed LHCb should however be able to do at least five times better than this (i.e. an accuracy of about 2.6 degrees), with a final uncertainty dependent on the errors associated with the knowledge of the D decay structure in the modes exploited in the $B \to DK$ channels. It is interesting to note that with a SBF, and the very high statistics associated with an LHCb upgrade, the experimental error on γ could approach 1 degree, but would still be larger than that of the associated ITE.

Lastly, we must caution the reader that the LHCb numbers in Table 35 are merely illustrative values, extrapolated from present simulation studies, together with certain (in some cases) arbitrary assumptions about systematic errors. The estimated precisions for $\sin 2\beta$ contain statistical uncertainties only, as the experimental systematics are impossible to estimate properly in advance of first data. The values for α are dominated by the input from the $B^0 \to \rho\pi$ analysis, with the conservative assumption of a limiting systematic of 6°, associated with issues in the Dalitz analysis and the understanding of the ρ lineshape. The γ estimates includes inputs from the $B_s \to D_s K^{\pm}$, $B^{\pm} \to D^{(*)}(hh, hhhh)K^{\pm}$, $B^{\pm} \to D(K_S^0 \pi\pi)K^{\pm}$ and $B^0 \to D(hh)K^*(K^+\pi^-)$ analyses. Here it is assumed that progress with the understanding of the D decay structure will result in systematics of 3° for the $D \to K_S^0 \pi\pi$ mode, and twice this for the 4-body decays. An arbitrary 5° error is assigned to the B^0 channel to account for the possibility of other amplitudes contributing the $D(hh)K^+\pi^-$ final state. The $B^{\pm} \to DK^{\pm}$ inputs assume an r_B value of 0.08. Assumed quantities for other parameters are given elsewhere in Sect. 3.5.3.4.

3.6 B-meson mixing[22]

3.6.1 Introduction

During this workshop, there has been a breakthrough in the experimental study of $B_s - \bar{B}_s$ mixing with the measurement of the following quantities: the oscillation frequency Δm_s

---

[22]Section coordinators: V. Lubicz, J. van Hunen.

by the CDF Collaboration [126], the time-integrated untagged charge asymmetry in semileptonic B_s decays $A_{SL}^{s,\text{unt}}$ and the dimuon asymmetry A_{SL} by DØ [667, 668], the B_s lifetime from flavor-specific final states [502, 669–673], $\Delta\Gamma_s/\Gamma_s$ from the time-integrated angular analysis of $B_s \to J/\psi\phi$ decays [674] by CDF [675], supplemented by the three-dimensional constraint on Γ_s, $\Delta\Gamma_s$, and the $B_s - \bar{B}_s$ mixing phase from the time-dependent angular analysis of $B_s \to J/\psi\phi$ decays by DØ [676]. These measurements can be compared with the SM predictions and used to constrain NP contributions to the $B_s - \bar{B}_s$ mixing amplitude.

In this section, we first discuss the theoretical predictions within the SM and their uncertainties. We then present the results of a model-independent analysis of NP in $B_s - \bar{B}_s$ mixing. We discuss the implications of the experimental data for SUSY models by either allowing new sources of flavor and CP violation in the B_s sector or by considering a constrained Minimal Flavor Violation SUSY scenario. The remainder of the section is devoted to the experimental aspects of the measurements listed above and gives an outlook for the LHC.

3.6.2 Standard Model predictions

The neutral B_d and B_s mesons mix with their antiparticles leading to oscillations between the mass eigenstates. The time evolution of the neutral $B - \bar{B}$ meson pair is described, in analogy to $K^0 - \bar{K}^0$ mixing, by a Schrödinger equation with the effective 2×2 Hamiltonian

$$i\frac{d}{dt}\begin{pmatrix} B_q \\ \bar{B}_q \end{pmatrix} = \left[\begin{pmatrix} M_{11}^q & M_{12}^q \\ M_{12}^{q\,*} & M_{11}^q \end{pmatrix} - \frac{i}{2}\begin{pmatrix} \Gamma_{11}^q & \Gamma_{12}^q \\ \Gamma_{12}^{q\,*} & \Gamma_{11}^q \end{pmatrix} \right] \begin{pmatrix} B_q \\ \bar{B}_q \end{pmatrix}$$

(138)

with $q = d, s$. The mass difference Δm_q and the width difference $\Delta\Gamma_q$ are defined as

$$\Delta m_q = m_H^q - m_L^q, \qquad \Delta\Gamma_q = \Gamma_L^q - \Gamma_H^q,$$

(139)

where H and L denote the Hamiltonian eigenstates with the heavier and lighter mass eigenvalue, respectively. These

states can be written as

$$\left|B_q^{H,L}\right\rangle = \frac{1}{\sqrt{1 + |(q/p)_q|^2}}\left(|B_q\rangle \pm (q/p)_q|\bar{B}_q\rangle\right). \qquad (140)$$

Theoretically, the experimental observables Δm_q, $\Delta \Gamma_q$ and $|(q/p)_q|$ are related to M_{12}^q and Γ_{12}^q. In the $B_d - \bar{B}_d$ and $B_s - \bar{B}_s$ systems, the ratio Γ_{12}^q/M_{12}^q is of $\mathcal{O}(m_b^2/m_t^2) \simeq 10^{-3}$ and, neglecting terms of $\mathcal{O}(m_b^4/m_t^4)$, one has

$$\Delta m_q = 2\left|M_{12}^q\right|, \qquad \frac{\Delta\Gamma_q}{\Delta m_q} = -\mathrm{Re}\left(\frac{\Gamma_{12}^q}{M_{12}^q}\right),$$
$$1 - \left|\left(\frac{q}{p}\right)_q\right| = \frac{1}{2}\mathrm{Im}\left(\frac{\Gamma_{12}^q}{M_{12}^q}\right). \qquad (141)$$

The matrix elements M_{12}^q and Γ_{12}^q are related to the dispersive and the absorptive parts of the $\Delta B = 2$ transitions, respectively. Short-distance QCD corrections to these matrix elements have been computed at the NLO for both M_{12}^q [701] and Γ_{12}^q [702–704]. The long distance effects are contained in the matrix elements of four-fermion operators which have been computed with lattice QCD using various approaches to treat the b quark (HQET, NRQCD, QCD) [352, 705–710]. The corresponding bag parameters B are found to be essentially insensitive to the effect of the quenched approximation (see Sect. 2.4).

The quantity $\mathrm{Im}(\Gamma_{12}^q/M_{12}^q)$ can be measured through the CP asymmetry in B_q decays to flavor-specific final states. An important example is the semileptonic asymmetry

$$A_{SL}^s = \mathrm{Im}\left(\frac{\Gamma_{12}^q}{M_{12}^q}\right) = \frac{N(\bar{B}_s \to l^+ X) - N(B_s \to l^- X)}{N(\bar{B}_s \to l^+ X) + N(B_s \to l^- X)}. \qquad (142)$$

Two updated theoretical predictions for $\Delta\Gamma_s/\Gamma_s$ and for the semileptonic asymmetry A_{SL}^s, obtained by including NLO QCD and $\mathcal{O}(1/m_b)$ [711] corrections, are

$$\Delta\Gamma_s/\Gamma_s = (7 \pm 3) \times 10^{-2},$$
$$A_{SL}^s = (2.56 \pm 0.54) \times 10^{-5} \quad [704],$$
$$\Delta\Gamma_s/\Gamma_s = (13 \pm 2) \times 10^{-2},$$
$$A_{SL}^s = (2.06 \pm 0.57) \times 10^{-5} \quad [712]. \qquad (143)$$

The difference in the central values of $\Delta\Gamma_s/\Gamma_s$ is mainly due to a different choice of the operator basis [712] and is related to unknown $\mathcal{O}(\alpha_s^2)$ and $\mathcal{O}(\alpha_s/m_b)$ corrections. Although the basis chosen in [712] leads to smaller theoretical uncertainties, the shift observed in the central values may signal that the effect of higher-order corrections on $\Delta\Gamma_s/\Gamma_s$ is larger than what could have been previously estimated. We take

into account this uncertainty by quoting, as final theoretical predictions in the SM, the more conservative estimate [713]

$$\Delta\Gamma_s/\Gamma_s = (11 \pm 4) \times 10^{-2},$$
$$A_{SL}^s = (2.3 \pm 0.5) \times 10^{-5}. \qquad (144)$$

Concerning Δm_s, the SM predictions obtained by the UTfit and CKMfitter Collaborations are

$$\Delta m_s = (18.4 \pm 2.4) \text{ ps}^{-1} \quad [120],$$
$$\Delta m_s = \left(18.9^{+5.7}_{-2.8}\right) \text{ ps}^{-1} \quad [8]. \qquad (145)$$

3.6.3 $B_s - \bar{B}_s$ mixing beyond the SM

We now discuss the analysis of $B_s - \bar{B}_s$ mixing in the presence of NP contributions to the $\Delta B = 2$ effective Hamiltonian. These can be incorporated in the analysis in a model independent way, parameterizing the shift induced in the mixing frequency and phase with two parameters, C_{B_s} and $\phi_s \equiv 2\phi_{B_s}$, having in the SM expectation values of 1 and 0, respectively [2–6]:

$$C_{B_s} e^{i\phi_s} \equiv C_{B_s} e^{2i\phi_{B_s}} = \frac{(M_{12}^s)^{\mathrm{SM+NP}}}{(M_{12}^s)^{\mathrm{SM}}}. \qquad (146)$$

As for the absorptive part of the $B_s - \bar{B}_s$ mixing amplitude, which is derived from the double insertion of the $\Delta B = 1$ effective Hamiltonian, it could be affected by NP effects in $\Delta B = 1$ transitions through penguin contributions. Such NP contributions were considered in [7, 210]. We shall neglect them in the present discussion. In this approximation, which is followed by most authors, NP enters $B_s - \bar{B}_s$ mixing only through the two parameters defined in (146).

Since the SM phase of Γ_{12}^s/M_{12}^s is small in comparison with the current experimental sensitivity, we shall assume in the following that CP violation in B_s mixing is dominated by the NP mixing phase ϕ_s. We then have

$$A_{SL}^s = \frac{\Delta\Gamma_s}{\Delta M_s}\tan\phi_s, \qquad (147)$$

and the same NP phase ϕ_s will also govern mixing-induced CP violation in the exclusive channel $B_s \to J/\psi\phi$. Note that the phases in $A_{SL}^s = \mathrm{Im}(\Gamma_{12}^s/M_{12}^s)$ and in the $B_s \to J/\psi\phi$ asymmetry are different from each other in the SM, where $\arg(-\Gamma_{12}^s/M_{12}^s) \approx -0.004$, while the phase measured in $B_s \to J/\psi\phi$ decay is $-2\beta_s \approx -2\lambda^2\eta \approx -0.04$ (see e.g. [674, 712]).

Making use of the experimental information described in Sect. 3.6.6, it is possible to constrain C_{B_s} and ϕ_{B_s} [7, 9, 210, 678, 712, 714, 715]. We report here the results obtained in [9].

The use of $\Delta\Gamma_s/\Gamma_s$ from the time-integrated angular analysis of $B_s \to J/\psi\phi$ decays is described for instance in

[7]. Here we use only the CDF measurement [675] as input, since the DØ analysis is now superseded by the new time-dependent study [676]. The latter provides the first direct constraint on the B_s–$\bar{B}_s$ mixing phase and also a simultaneous bound on $\Delta\Gamma_s$ and Γ_s. The time-dependent analysis determines the B_s–$\bar{B}_s$ mixing phase with a four-fold ambiguity. First of all, being untagged, it is not directly sensitive to $\sin\phi_s$, resulting in the ambiguity $(\phi_s, \cos\delta_{1,2}) \leftrightarrow (-\phi_s, -\cos\delta_{1,2})$, where $\delta_{1,2}$ represent the strong phase differences between the transverse polarization and the other ones. Second, at fixed sign of $\cos\delta_{1,2}$, there is the ambiguity $(\phi_s, \Delta\Gamma_s) \leftrightarrow (\phi_s + \pi, -\Delta\Gamma_s)$. One could be tempted to use factorization [712] or $B_d \to J/\psi K^*$ with $SU(3)$ [716] to fix the sign of $\cos\delta_{1,2}$. Unfortunately, neither factorization nor $SU(3)$ are accurate enough to draw firm conclusions on these strong phases. This is confirmed by the fact that the two approaches lead to opposite results. Waiting for future, more sophisticated experimental analyses, which could resolve this ambiguity with a technique similar to the one used by BaBar in $B_d \to J/\psi K^*$ [613], we prefer to be conservative and keep the four-fold ambiguity.

Compared to previous analyses, the additional experimental input discussed below improves considerably the determination of the phase of the B_s–$\bar{B}_s$ mixing amplitude. The fourfold ambiguity inherent in the untagged analysis of [676] is somewhat reduced by the measurements of A_{SL}^s and A_{SL} (see (150)), which slightly prefer negative values of ϕ_{B_s}. The results for C_{B_s} and ϕ_{B_s}, obtained from the general analysis allowing for NP in all sectors, are

$$C_{B_s} = 1.03 \pm 0.29,$$
$$\phi_{B_s} = (-75 \pm 14)^\circ \cup (-19 \pm 11)^\circ \cup (9 \pm 10)^\circ \qquad (148)$$
$$\cup (102 \pm 16)^\circ.$$

Thus, the deviation from zero in ϕ_{B_s} is below the 1σ level, although clearly there is still ample room for values of ϕ_{B_s} very far from zero. The corresponding p.d.f. in the C_{B_s}–ϕ_{B_s} plane is shown in Fig. 33.

3.6.4 B_s–$\bar{B}_s$ mixing in SUSY with nonminimal flavor violation

The results on C_{B_s} and ϕ_{B_s} obtained above can be used to constrain any NP model. As an interesting example, we discuss here the case of SUSY with new sources of flavor and CP violation, following [118].

To fulfill our task in a model-independent way, we use the mass-insertion approximation to evaluate the gluino mediated contribution to $b \to s$ transitions. Treating off-diagonal sfermion mass terms as interactions, we perform a perturbative expansion of FCNC amplitudes in terms of mass insertions. The lowest nonvanishing order of this expansion gives an excellent approximation to the full result, given the
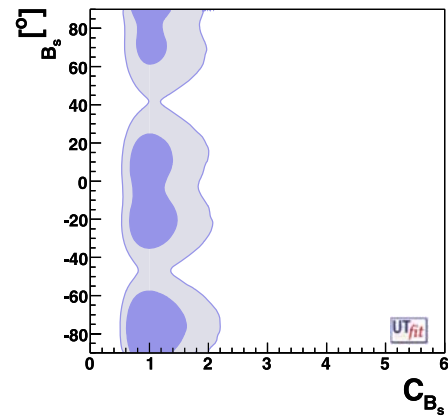

Fig. 33 Constraints on ϕ_{B_s} vs. C_{B_s} from the NP generalized analysis of Ref. [9]

tight experimental constraints on flavor-changing mass insertions. It is most convenient to work in the super-CKM basis, in which all gauge interactions carry the same flavor dependence as in the SM. In this basis, we define the mass insertions $(\delta_{ij}^d)_{AB}$ as the off-diagonal mass terms connecting down-type squarks of flavor i and j and helicity A and B, divided by the average squark mass (see Sect. 1.3).

The constraints on $(\delta_{23}^d)_{AB}$ have been studied in detail in [116] using as experimental input the branching ratios and CP asymmetries of $b \to s\gamma$ and $b \to s\ell^+\ell^-$ decays and the first measurement of B_s–$\bar{B}_s$ mixing. We perform the same analysis using the full information encoded in C_{B_s} and ϕ_{B_s} and the recently computed NLO corrections to the $\Delta B = 2$ SUSY effective Hamiltonian [118]. We refer the reader to [118] for all the details of this analysis.

For definiteness, we present here the results obtained by choosing an average squark mass of 350 GeV, a gluino mass of 350 GeV, $\mu = -350$ GeV and $\tan\beta = 3$. The dependence on μ and on $\tan\beta$ is induced by the presence of a chirality flipping, flavor conserving mass insertion proportional to $\mu\tan\beta$. In Fig. 34, we show the allowed ranges in the $\mathrm{Re}(\delta_{23}^d)_{AB}$–$\mathrm{Im}(\delta_{23}^d)_{AB}$ planes. The corresponding upper bounds at 95% probability are presented in Table 36.

One finds that the constraints on $(\delta_{23}^d)_{LL}$ and $(\delta_{23}^d)_{LL} = (\delta_{23}^d)_{RR}$ come from the interplay of B_s–$\bar{B}_s$ mixing with $b \to s$ decays. $(\delta_{23}^d)_{RR}$ is dominated by the information on B_s–$\bar{B}_s$ mixing, while $(\delta_{23}^d)_{LR}$ and $(\delta_{23}^d)_{RL}$ are dominated by $\Delta B = 1$ processes.

3.6.5 B_s–$\bar{B}_s$ mixing in SUSY with minimal flavor violation

As a second model-specific case for meson mixing, we mention that of SUSY with MFV. The MFV scenario is defined, in general, within the effective field theory approach of [10]. In the specific case of SUSY, the soft squark mass terms, parametrized in the previous section in terms of mass
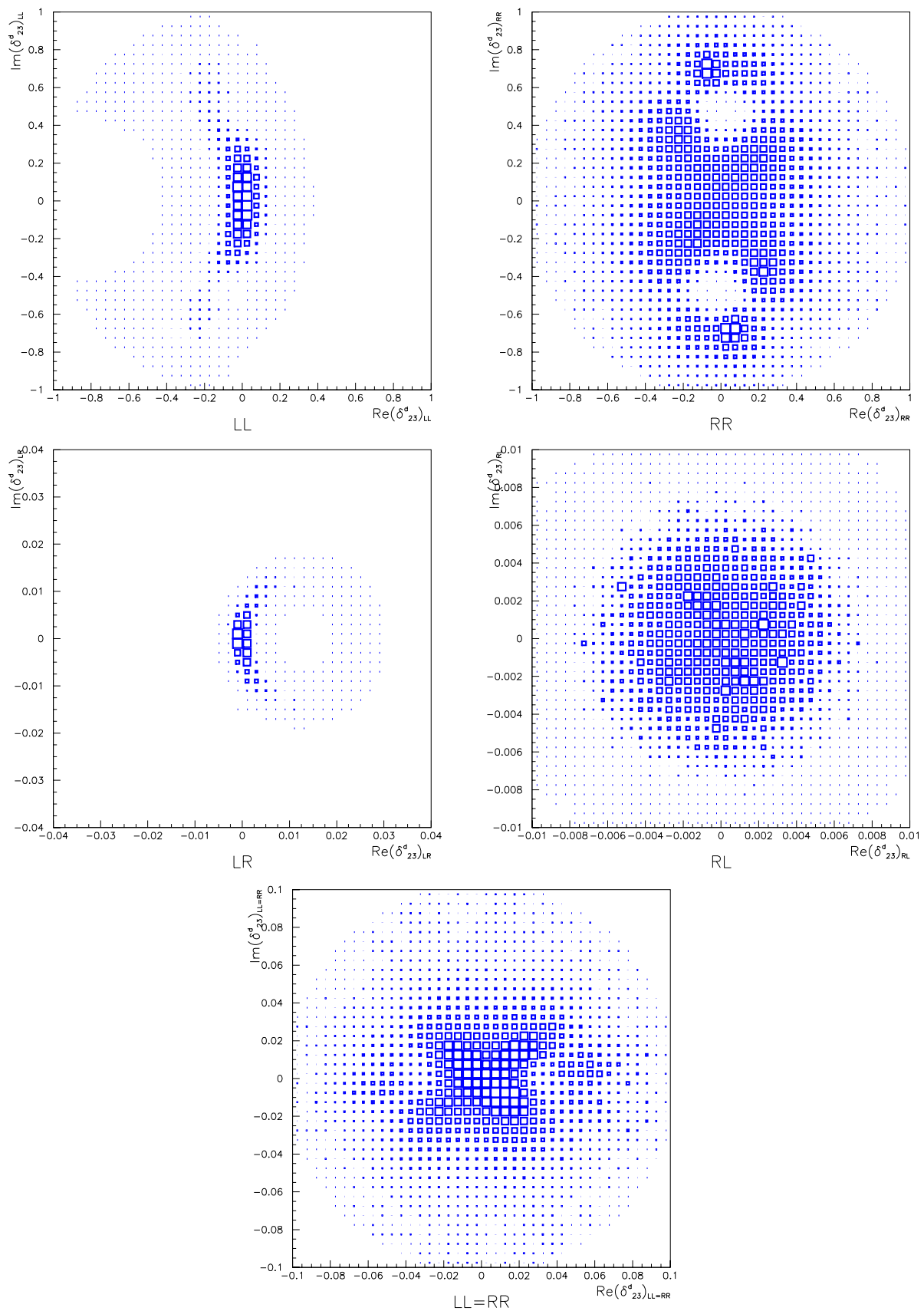
392

Eur. Phys. J. C (2008) 57: 309–492

Fig. 34 Allowed range in the $\text{Re}(\delta^d_{23})_{AB}$–$\text{Im}(\delta^d_{23})_{AB}$ plane, with $AB = LL$ (*top left*), $AB = RR$ (*top right*), $AB = LR$ (*middle left*), $AB = RL$ (*middle right*) and $AB = LL$ with $(\delta^d_{23})_{LL} = (\delta^d_{23})_{RR}$ (*bottom*)

Eur. Phys. J. C (2008) 57: 309–492

393

Table 36 Upper bounds (95% C.L.) on the mass insertion parameters $|(\delta_{23}^d)_{AB}|$, see the text for details

$|(\delta_{23}^d)_{LL}|$	$|(\delta_{23}^d)_{RR}|$	$|(\delta_{23}^d)_{LL=RR}|$	$|(\delta_{23}^d)_{LR,RL}|$
2×10^{-1}	7×10^{-1}	5×10^{-2}	5×10^{-3}

insertions, are expanded in terms of the SM Yukawa couplings [10, 38], and the relevant parameters become the expansion coefficients. A detailed meson mixing study within this approach has been performed in [42] and for low $\tan \beta$ shows that: (i) NP contributions are *naturally* small for ΔM_s of the order of 1/ps; (ii) such contributions are always positive; (iii) if μ is not small, gluino contributions enhance (even for low $\tan \beta$) scalar operators, which then spoil the phenomenological picture of $(V - A) \times (V - A)$ dominated MFV [12]. In particular item (i) emphasizes the importance of precision determinations for lattice parameters like ξ if NP is of minimal flavor violating nature.

3.6.6 Present experimental situation

New information concerning the B_s–$\bar{B}_s$ mixing parameters became available during this workshop. The highlight was the measurement of Δm_s by DØ and CDF. The DØ experiment used the semileptonic $B_s \to D_s \mu \nu X$ decays with $D_s \to \phi \pi$, and determined a 90% confidence range for Δm_s: $17 < \Delta m_s < 21$ ps^{-1}. The initial CDF result yielded a 3σ observation of B_s–$\bar{B}_s$ mixing by making use of semileptonic and hadronic decay modes [677]. Shortly after CDF published an improved analysis [126]. In this analysis, the signal yield was increased by improving the particle identification and by using a neural network for the event selection, which allows the use of additional decay modes. Moreover the flavor tagging was improved by adding an opposite-side flavor tag based on the charge of the kaons and by the use of a neural network for the combination of the kaon, lepton and jet-charge tags. The result for Δm_s equals

$$\Delta m_s = (17.77 \pm 0.010 \pm 0.07) \text{ ps}^{-1}. \tag{149}$$

The probability that a statistical fluctuation would produce this signal is 8×10^{-8} ($> 5\sigma$ evidence). This value for Δm_s is consistent with the SM expectation, see (145). The ratio $|V_{td}/V_{ts}|$ was determined by CDF as well [126] and equals $0.2060 \pm 0.0007(\Delta m_s)^{+0.0081}_{-0.0060}(\Delta m_d + \text{theory})$.

Also information on the B_s mixing phase became available [676]. The DØ experiment performed two independent measurements of A_{SL}^s, defined in (142), using the same sign dimuon pairs [668] and time-integrated semileptonic decays $B_s \to \mu \nu D_s$ with $D_s \to \phi \pi$ [667].

The same sign dimuon asymmetry in B decays at Tevatron can be expressed as [678]

$$A_{SL} = \frac{N(b\bar{b} \to \mu^+ \mu^+ X) - N(b\bar{b} \to \mu^- \mu^- X)}{N(b\bar{b} \to \mu^+ \mu^+ X) + N(b\bar{b} \to \mu^- \mu^- X)}$$
$$= \frac{f_d Z_d A_{SL}^d + f_s Z_s A_{SL}^s}{f_d Z_d + f_s Z_s}, \tag{150}$$
$$Z_q = \frac{1}{1 - y_q^2} - \frac{1}{1 + x_q^2},$$
$$x_q = \Delta M_q / \Gamma_q, \qquad y_q = \Delta \Gamma_q / (2\Gamma_q).$$

Here $f_d = 0.398 \pm 0.012$ and $f_s = 0.103 \pm 0.014$ are the B_d and B_s fragmentation fractions. The measured asymmetry A_{SL} was presented by DØ in Ref. [668]:

$$A_{SL}(\text{DØ}) = A_{SL}^d + \frac{f_s Z_s}{f_d Z_d} A_{SL}^s$$
$$= -0.0092 \pm 0.0044(\text{stat.}) \pm 0.0032(\text{syst.}). \tag{151}$$

Measurements of A_{SL}^d were performed by the b factories. The average value of A_{SL}^d is [678]

$$A_{SL}^d = +0.0011 \pm 0.0055. \tag{152}$$

This leads to the value of A_{SL}^s from the same sign dimuon asymmetry:

$$A_{SL}^s = -0.0064 \pm 0.0101. \tag{153}$$

Recently DØ has also presented a time-integrated direct measurement of A_{SL}^s using semileptonic $B_s \to D^{\pm} \mu^{\mp} \nu_{\mu}$ decays [667]. They measure:

$$A_{SL}^s = +0.0245 \pm 0.0193(\text{stat.}) \pm 0.0035(\text{syst.}). \tag{154}$$

These two measurements of A_{SL}^s are independent, and their combination gives the charge asymmetry in semileptonic B_s decays: $A_{SL}^s = 0.0001 \pm 0.0090$ [679]. The analysis of the time-dependent angular distributions in $B_s \to J/\psi \phi$ decays [674] yields both the decay width difference $\Delta \Gamma_s$ and CP violating phase ϕ_s [676]:

$$\Delta \Gamma_s = 0.17 \pm 0.09 \pm 0.03 \text{ ps}^{-1},$$
$$\phi_s = -0.79 \pm 0.56 \pm 0.01. \tag{155}$$

Combining the results for A_{SL}^s, $\Delta \Gamma_s$, ϕ_s and using the CDF result on the mass difference Δm_s [126] gives an improved

394

Eur. Phys. J. C (2008) 57: 309–492

estimate for ϕ_s and $\Delta\Gamma_s$ [679]:

$$\Delta\Gamma_s = 0.13 \pm 0.09 \text{ ps}^{-1},$$

$$\phi_s = -0.70^{+0.47}_{-0.39}. \tag{156}$$

Also new results have been released recently concerning the B_s lifetime and $\Delta\Gamma_s$. At DØ, the B_s lifetime for $B_s \to D_s\mu\nu X$ was measured to be

$$1.398 \pm 0.044(\text{stat.})^{+0.028}_{-0.025}(\text{syst.}) \text{ ps}^{-1}$$

[673]. The average B_s lifetime equals 1.466 ± 0.059 ps^{-1} [119]. CDF published the measurement of

$$\Delta\Gamma_s = \left(0.47^{+0.19}_{-0.24}(\text{stat.}) \pm 0.01(\text{syst.})\right) \text{ ps}^{-1}$$

[675].

In the near future, the LHC experiments LHCb, ATLAS and CMS will start to provide information on B_s–$\bar{B}_s$ mixing. In the following sections, the sensitivity of LHCb to the B_s mixing parameters Δm_s, $\Delta\Gamma_s$, ϕ_s and A_{SL} and the prospects for CMS will be discussed.

3.6.7 LHCb

The LHCb experiment is designed as a single-arm forward spectrometer to study b decays and CP violation. Its main characteristics are precise vertexing, efficient tracking and good particle identification. The high-precision measurements at LHCb will enable further tests of the CKM picture and probe physics beyond the SM. This is in particular true for the measurement of B_s–$\bar{B}_s$ mixing parameters such as Δm_s, $\Delta\Gamma_s$, ϕ_s and A_{SL}.

LHCb will run at a nominal luminosity of $\mathcal{L} = 2 \times 10^{32}$ cm^{-2} s^{-1}. Assuming a $b\bar{b}$ production cross-section of $\sigma_{b\bar{b}} = 500$ μb, this will correspond to an integrated luminosity of 2 fb^{-1} per nominal year of 10^7 s of data taking. All event yields quoted below are for 2 fb^{-1}. They have been obtained from a full Monte Carlo (MC) simulation of the experiment, which included the following: pileup generation, particle tracking through the detector material, detailed detector response (including timing effects such as spillover), full trigger simulation, offline reconstruction with full pattern recognition, and selection cuts. High-statistics samples of signal events have been produced for a detailed study of resolutions and efficiencies. Combinatorial background has been studied using a sample of $\sim$27M inclusive $b\bar{b}$ events corresponding to about 10 minutes of data taking, while identified physics background sources have been studied with large specific background samples.

3.6.7.1 Sensitivity to Δm_s from $B_s \to D_s\pi$ The mass difference Δm_s between the mass eigenstates of the B_s–$\bar{B}_s$ system is best measured as the frequency of the oscillatory behavior of the proper time distribution of flavor-tagged B_s mesons decaying to a flavor-specific final state. The best channel for this at LHCb is $B_s \to D_s\pi$, with the subsequent D_s^+ decay to $K^+K^-\pi^+$, because of its easy topology with four charged tracks and its relatively large branching fraction of $B(B_s \to D_s\pi) \times B(D_s^+ \to K^+K^-\pi^+) = (1.77 \pm 0.48) \times 10^{-4}$ [680]. Such decays can be detected, triggered, reconstructed and selected with a final mass resolution of $\sim$14 MeV/c^2 (see Fig. 35 left) and a total efficiency of about 0.4%, leading to a yield of (140k $\pm$ 40k) events in 2 fb^{-1}. After the trigger and selection, the combinatorial background is expected to be dominated by $b\bar{b}$ events and has been estimated to be less than 5% of the signal at 90% C.L., in a $\pm$50 MeV/c^2 mass window around
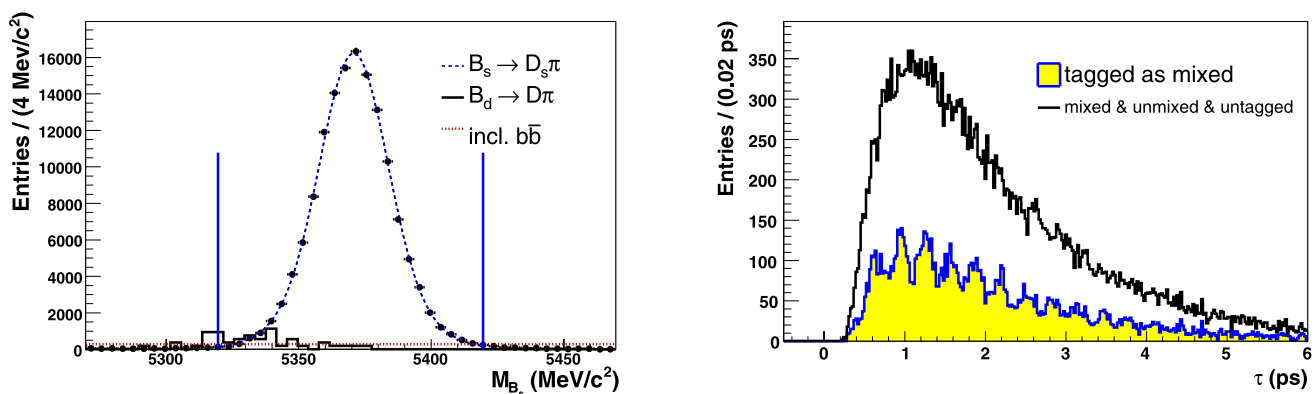

Fig. 35 *Left*: Reconstructed $B_s \to D_s\pi$ mass distribution from full MC simulation, after trigger and all selection cuts [680]. The *points with error bars* represent the signal (on an arbitrary vertical scale). The *histogram* represents the $B \to D^-\pi^+$ background and the *dotted flat line* represents the upper limit of the combinatorial background from $b\bar{b}$ events, normalized to the signal. *Right*: Reconstructed $B_s \to D_s\pi$ proper time distribution from full MC simulation of the signal, corresponding to an integrated luminosity of 0.5 fb^{-1} [680]. The *lower histogram* represents the events tagged as mixed. The background is not shown

the signal. Using the same sample of simulated $b\bar{b}$ events, the background from partially reconstructed b-hadron decays in the same mass window has been estimated to be less than 40% at 90% C.L.. This includes partially reconstructed Λ_b and B_d decays. A dedicated study showed that the background from $B \to D^-\pi^+$ decays (where one of the charged pions from the D decay could be misidentified as a kaon) is approximately 5% of the signal.

The proper time resolution, obtained on an event-by-event basis from the estimated tracking errors, typically varies between 15 and 80 fs with an average value of $\sim$40 fs (dedicated studies are being done at LHCb to model the proper time resolution [681] and to verify the estimated tracking errors [682, 683] with data). A flavor tagging power of ϵD^2 of at least 9% is achieved on the MC signal, combining several tags in a neural network: a muon or electron from the $b \to \ell$ decay of the other b-hadron, a charged kaon from the $b \to c \to s$ decay of the other b-hadron, the vertex charge of the other b-hadron, and a charged kaon accompanying the signal B_s in the fragmentation chain [684].

The statistical uncertainty on the measurement of Δm_s using an integrated luminosity of 2 fb^{-1} is expected to be ± 0.007 ps^{-1} [662]. It will be dominated by systematic uncertainties related to the determination of the proper time scale. Figure 35 (right) shows the proper time distribution from which such a measurement could be extracted.

The $B_s \to D_s\pi$ sample will play a crucial role as a control sample in all time-dependent B_s analyses; indeed it can be used to measure directly the dilution (due to flavor tagging and proper time resolution) on the $\sin(\Delta m_s t)$ and $\cos(\Delta m_s t)$ terms in time-dependent CP asymmetries. It will also be used as a normalization channel for many measurements of B_s branching fractions. More details on the selection of $B_s \to D_s\pi$ events can be found in [680].

3.6.7.2 Sensitivity to ϕ_s and $\Delta\Gamma_s$ from exclusive $\bar{b} \to \bar{c}c\bar{s}$ decays

The B_s–$\bar{B}_s$ mixing phase ϕ_s can be measured from the flavor-tagged B_s decays to CP eigenstates involving the $\bar{b} \to \bar{c}c\bar{s}$ quark-level transition. The best mode for this at LHCb is $B_s \to J/\psi\phi$. However, in this case, the vector nature of the two particles in the final state causes their relative angular momentum to take more than one value, resulting in a mixture of CP-even and CP-odd contributions. An angular analysis is therefore required to separate them on a statistical basis. This can be achieved with a simultaneous fit to the measured proper time and so-called transversity angle of the reconstructed decays. Such a fit is sensitive also to $\Delta\Gamma_s$ because of the presence of the two CP components.

The sensitivity to ϕ_s has been studied so far with the following modes:

- $B_s \to J/\psi(\mu^+\mu^-)\phi(K^+K^-)$ [685, 686];
- $B_s \to \eta_c(\pi^+\pi^-\pi^+\pi^-, \pi^+\pi^-K^+K^-, K^+K^-K^+K^-) \times \phi(K^+K^-)$ [685, 686];
- $B_s \to J/\psi(\mu^+\mu^-)\eta(\gamma\gamma, \pi^+\pi^-\pi^0)$ [685, 686];
- $B_s \to J/\psi(\mu^+\mu^-)\eta'(\eta(\gamma\gamma)\pi^+\pi^-, \rho(\pi^+\pi^-)\gamma)$ [687, 688];
- $B_s \to D_s^+(K^+K^-\pi^+)D_s^-(K^+K^-\pi^-)$ [685, 686].

The results are summarized in Table 37. For each signal event in the full simulation, the proper time and its error are estimated using a least-squares fit. The distributions of the proper time errors (scaled with the sigma of their pull distribution) are shown in Fig. 36. Most channels have a proper time resolution below 40 fs. A good proper time resolution is important for resolving the fast B_s–$\bar{B}_s$ oscillations.
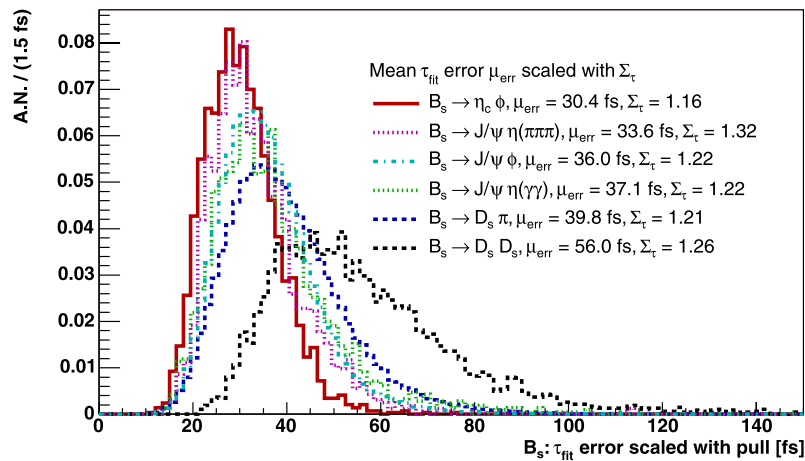
The sensitivities to the B_s–$\bar{B}_s$ mixing parameters are determined by means of fast parameterized simulations, with the results of Table 37 as inputs. A large number of experiments are generated assuming the following set of parameters: $\Delta m_s = 17.5$ ps^{-1}, $\phi_s = -0.04$ rad, $\Delta\Gamma_s/\Gamma_s = 0.15$,

Table 37 Characteristics of different exclusive $\bar{b} \to \bar{c}c\bar{s}$ modes for the measurement of ϕ_s. The first 6 columns of numbers are obtained from the full MC simulation. They represent the expected number of triggered, reconstructed and selected signal events with an integrated luminosity of 2 fb^{-1} (before tagging), the background-over-signal ratio determined mainly from inclusive $b\bar{b}$ events, the B_s mass resolution, the average value of the estimated event-by-event B_s proper time error scaled by the width of its pull distribution, the flavor tagging efficiency, and the mistag probability. These parameters have been used as input to a fast MC simulation to obtain the sensitivity on ϕ_s given in the last column. The last line describes the control channel (see text)

Channel	2 fb^{-1} yield	B/S	σ_{mass} [MeV/c^2]	σ_{time} [fs]	ϵ_{tag} [%]	ω_{tag} [%]	$\sigma(\phi_s)$ [rad]
$B_s \to J/\psi\phi$	131k	0.12	14	36	57	33	0.023
$B_s \to \eta_c\phi$	3k	0.6	12	30	66	31	0.108
$B_s \to J/\psi\eta(\gamma\gamma)$	8.5k	2.0	34	37	63	35	0.109
$B_s \to J/\psi\eta(\pi^+\pi^-\pi^0)$	3k	3.0	20	34	62	30	0.142
$B_s \to J/\psi\eta'(\eta\pi^+\pi^-)$	2.2k	1.0	19	34	64	31	0.154
$B_s \to J/\psi\eta'(\rho\gamma)$	4.2k	0.4	14	29	64	31	0.080
$B_s \to D_sD_s$	4k	0.3	6	56	57	34	0.133
$B_s \to D_s\pi$	140k	0.4	14	40	63	31	–

396

Eur. Phys. J. C (2008) 57: 309–492

$1/\Gamma_s = 1.45$ ps, and a fraction of CP-odd component of $R_T = 0.2$ (for $B_s \rightarrow J/\psi\phi$). The different parameters are extracted by performing a likelihood fit to the mass, proper time, and transversity angle (for $B_s \rightarrow J/\psi\phi$) distributions, including a background contribution. The $\bar{b} \rightarrow \bar{c}c\bar{s}$ likelihood is simultaneously maximized with a similar likelihood for the $B_s \rightarrow D_s\pi$ control sample such as to constrain Δm_s and the mistag fraction from the data. The background properties are determined from the B_s mass sidebands. The physics parameters, extracted in the signal region with all other parameters fixed, are ϕ_s, Δm_s, $\Delta\Gamma_s/\Gamma_s$, $1/\Gamma_s$, ω_{tag}, and R_T (for $B_s \rightarrow J/\psi\phi$).

The sensitivities to ϕ_s for the different channels, obtained as the rms of the distribution of the fit results, are given in the last column of Table 37. They gently decrease with increasing $|\phi_s|$ and do not depend much on $\Delta\Gamma_s/\Gamma_s$. For instance, the statistical uncertainty on ϕ_s for $\phi_s = -0.2$ rad is ± 0.026 rad from $B_s \rightarrow J/\psi\phi$ alone, with 2 fb^{-1} [685]. The best performance is achieved with the $B_s \rightarrow J/\psi\phi$ sample, which also yields a statistical precision of ± 0.0092 on $\Delta\Gamma_s/\Gamma_s$ (2 fb^{-1}). The ϕ_s sensitivities obtained from the other modes (which are pure CP-eigenstates) are not as good but still interesting. Combining all modes, a statistical uncertainty $\sigma(\phi_s) = \pm 0.0092$ rad is expected after 10 fb^{-1}.

LHCb has the potential to perform the first significant measurement of ϕ_s, test the consistency with the SM expectations, and possibly uncover NP that may be hiding in B_s–$\bar{B}_s$ mixing.

3.6.7.3 Sensitivity to A_{SL}^s from $B_s \rightarrow D_s\mu\nu X$ and $B_s \rightarrow D_s\pi$ The CP-violating charge asymmetry A_{SL}^s is an important parameter to constrain NP contributions in B_s mixing, see Sect. 3.6.3. A_{SL}^s is accessible by measuring the charge asymmetry of the time-integrated rates of untagged B_s decays to flavor-specific final states such as $D_s^-\mu^+\nu X$ or $D_s^-\pi^+$ [689]. In LHCb, the asymmetry A_{SL}^s is measured by fitting the time-dependent decay rates. This method allows

a determination of A_{SL}^s also for a nonzero production asymmetry of B_s and $\bar{B}_s$ mesons which, at the LHC, is expected to be of $\mathcal{O}(1\%)$. Based on a large sample of fully simulated inclusive $b\bar{b}$ events and a dedicated signal sample, LHCb estimates a signal yield of 1M $B_s \rightarrow D_s\mu\nu X$ events in 2 fb^{-1} of data, with a B/S ratio of about 0.36 [690]. This leads to a statistical precision of ± 0.002 on A_{SL}^s [691]. A similar analysis based on 140k $B_s \rightarrow D_s\pi$ events is expected to reach a precision of ± 0.005 with the same integrated luminosity of 2 fb^{-1} [691]. Systematic uncertainties are expected to be dominated by the detector charge asymmetry, which needs to be determined separately. A method is proposed to control the detector charge asymmetry by measuring the difference $A_{SL}^s - A_{SL}^d$ using B_s and B_d decays to the same final state, e.g. $B_s \rightarrow D_s^-\mu^+\nu X$ and $B_d \rightarrow D^-\mu^+\nu X$, where $D_s^- \rightarrow K^+K^-\pi^-$ and $D^- \rightarrow K^+K^-\pi^-$.

3.6.7.4 Correcting for trigger biases in lifetime fitting at LHCb Lifetime measurements at LHCb will help for the detector calibration and provide tests of theoretical predictions based on the heavy-quark expansion. In order to exploit the full range of decays available at LHCb, it is important to have a method for fitting lifetimes in hadronic channels, which are biased by the impact parameter cuts in the trigger. We have investigated a Monte-Carlo independent method to take into account the trigger effects. The method is based on calculating event-by-event acceptance functions from the decay geometry and does not require any external input. Current results with the method are given in [692]. The method for the case of two-body decays is described in [693].

The decay $B_d \rightarrow D^-\pi^+$ has an expected yield of 1.34M events per 2 fb^{-1}. The S/B ratio is expected to be around 5 [664]. Fitting the B_d lifetime with 60k toy Monte Carlo signal events achieves a statistical precision of 0.007 ps, while fitting to 60k signal and 15k background events achieves a precision of 0.009 ps (the current world average is 1.530 ± 0.009 ps [119]). A similar result is seen in

data generated with the full LHCb detector simulation [692]. Therefore, although the systematic errors associated with this method are unknown at the moment, we can expect a very good measurement of the B_d lifetime using the decay $B_d \rightarrow D^- \pi^+$.

3.6.8 CMS

3.6.8.1 Sensitivity to $\Delta \Gamma_s$ Also at CMS the decay $B_s \rightarrow J/\psi \phi \rightarrow \mu^+ \mu^- K^+ K^-$ is being studied [694]. Several important background processes have been identified. The prompt J/ψ production is the main source of background at trigger level, since it represents a dominant contribution to the Level-1 dimuon trigger rate. For the offline selection, the main background is the inclusive decay $b \rightarrow J/\psi X$. The decay $B_d \rightarrow J/\psi K^{*0} \rightarrow \mu^+ \mu^- K^+ \pi^-$ is of particular concern, since the pion can be mistaken to be a kaon, and hence the decay be misidentified as $B_s \rightarrow J/\psi \phi$. Furthermore, the final state of this B_d decay also displays a time-dependent angular distribution similar to that of the B_s decay under study, with different physical parameters. The B_s decay chain is selected at Level-1 by the dimuon trigger. The latter demands two muons with a transverse momentum above 3 GeV/c, and the additional requirement that these muons have opposite charge can be used.

In the HLT [695], b candidates are identified by doing a partial reconstruction of the decay products in the tracker in restricted tracking regions and imposing invariant mass and vertex requirements [696].

The HLT selection of the decay $B_s \rightarrow J/\psi \phi$ has been separated in two steps. In the first, called Level 2, J/ψ candidates with a displaced vertex are identified. Tracks are then reconstructed in the tracking regions defined by the Level 1 muon candidates, and all track pairs of opposite charge for which the invariant mass is within 150 MeV/c^2 of the world-average J/ψ mass are retained. To remove the prompt J/ψ background, the two muon candidates are then fitted to a common decay vertex, and the significance of the transverse decay length is required to be above 3. With this selection, the accepted rate is reduced to approximately 15 Hz, with 80% of the J/ψ originating in the decay of b hadrons.

Next, at Level 3, a further reduction is achieved by doing a full reconstruction of the B_s decay. To reconstruct the kaons, the tracking region is chosen around the direction of each J/ψ candidate. Assigning the kaon mass to the reconstructed tracks, all oppositely charged track pairs for which the invariant mass is within 20 MeV/c^2 of the world-average mass of the ϕ meson are retained for a resolution in the invariant mass of the ϕ meson of 4.5 MeV/c^2. With the two muon candidates, the four-track invariant mass is required to be within 200 MeV/c^2 of the world-average mass of the B_s meson. The resolution in the invariant mass of the B_s meson

is found to be 65 MeV/c^2. Here as well, a vertex fit of the four tracks is performed, imposing a similar requirement as above. The total rate for this selection is well below 0.1 Hz, and a yield of approximately 456000 signal events can be expected within 30 fb^{-1} of data.

In the offline selection, candidates are reconstructed by combining two muons of opposite charge with two further tracks of opposite charge. As CMS does not possess a particle identification system suitable for this measurement, all measured tracks have to be considered as possible kaon candidates, which adds a substantial combinatorial background. A kinematic fit is made, where the four tracks are constrained to come from a common vertex and the invariant mass of the two muons is constrained to be equal to the mass of the J/ψ. With this fit, a resolution on the invariant mass of the B_s meson of 14 MeV/c^2 is found. The invariant mass of the two kaons is required to be within 8 MeV/c^2 of the world-average mass of the ϕ meson.

With this selection, a yield of approximately 327000 signal events can be expected within 30 fb^{-1} of data, with a background of 39000 events. These do not include a requirement on the four-track invariant mass of the candidates, since the sidebands could be used later in the analysis. However, only a small fraction of these events are directly under the B_s peak, and even a simple cut will reduce the number of background events by a significant factor.

The measurement of the width difference $\Delta \Gamma_s$ can now be done on this sample of untagged B_s candidates. As mentioned earlier, the $J/\psi \phi$ final state is an admixture of CP-even and CP-odd states, and an angular analysis is required [674, 697]. As the CP-even and CP-odd components have different angular dependences and different time evolutions, the different parameters can be measured by performing an unbinned maximum likelihood fit on the observed time evolution of the angular distribution. In the absence of background and without distortion, the p.d.f. describing the data would be the original differential decay rate. The distortion of this distribution by the detector acceptance, trigger efficiency and the different selection criteria must be taken into account by an efficiency function modeling the effect of the decay length requirements and the distortion of the angular distribution.

A sample corresponding to an integrated luminosity of 1.3 fb^{-1} was considered, which allows us to have a realistic ratio of misidentified $B_d \rightarrow J/\psi K^*$ and signal events. With the low number of background events that remain after all selection requirements, an accurate modeling of the background is not possible, neither of its angular distribution nor of its time-dependent efficiency. Therefore the background events are simply added to the data set, and their expected distribution is not included in the p.d.f. used in the fit. The p.d.f. then simply describes the B_s distribution. With such a fit, in which the invariant mass of the candidates is not

398

Eur. Phys. J. C (2008) 57: 309–492

Table 38 Results of the maximum likelihood fit for an integrated luminosity of 1.3 fb^{-1} (signal and background)

Parameter	Input value	Result	Stat. error	Sys. error	Total error	Rel. error
$|A_0(0)|^2$	0.57	0.5823	0.0061	0.0152	0.0163	2.8%
$|A_{||}(0)|^2$	0.217	0.2130	0.0077	0.0063	0.0099	4.6%
$|A_\perp(0)|^2$	0.213	0.2047	0.0065	0.0099	0.0118	5.8%
$\bar{\Gamma}_s$	0.712 ps^{-1}	0.7060 ps^{-1}	0.0080 ps^{-1}	0.0227 ps^{-1}	0.0240 ps^{-1}	3.4%
$\Delta\Gamma_s$	0.142 ps^{-1}	0.1437 ps^{-1}	0.0255 ps^{-1}	0.0113 ps^{-1}	0.0279 ps^{-1}	19%
$\Delta\Gamma_s/\Gamma_s$	0.2	0.2036	0.0374	0.0173	0.0412	20%

taken into account, a restriction on the invariant mass of the candidates should obviously be made. Choosing a window of ± 36 MeV/c^2 around the world-average B_s mass reduces the number of B_d background events by another 59%, while reducing the number of signal candidates by only 2.9%. The result of the fit is given in Table 38, where both the statistical and expected systematic uncertainties are quoted. A first measurement of the width difference of the weak eigenstates could thus be made with an uncertainty of 20%. On a larger sample corresponding to an integrated luminosity of 10 fb^{-1}, it is foreseen that the statistical uncertainty would be reduced to 0.011.

3.6.8.2 Missing particles in the reconstruction   The best way to study the B_s–$\bar{B}_s$ oscillations is to have a fully reconstructed final state of the B_s decay. The disadvantage of such decay channels is the limited statistics. Many more signal events can be collected in semileptonic decays as $B_s \to D_s^- \ell^+ \nu$. Due to the missing neutrino in this decay, the B_s momentum, and hence the proper-time resolution for the B_s, is less precise than in the fully reconstructed case, even if a correction (k-factor) is applied. However, recently a new method (ν-reco) has been proposed [698], which allows us to calculate the neutrino momentum with the help of vertex information.

In order to verify the ν-reco method, an MC simulation has been developed to study B_s–$\bar{B}_s$ mixing in the semileptonic decay mode. Kinematical cuts, track parameters and vertex positions (primary and secondary) have been simulated according to typical hadron collider detector conditions [670, 673, 699, 700]. The proper time resolution obtained is $\sigma = 132$ fs with the k-factor method and $\sigma = 91$ fs with the ν-reco method.

3.7 Hadronic $b \to s$ and $b \to d$ transition[23]

FCNC processes can occur only at the loop level in the SM and therefore are potentially sensitive to new virtual particles. In particular, hadronic FCNC B decays are sensitive to NP contributions to penguin operators. Among these decays, the penguin-dominated $b \to s\bar{q}q$ transitions are the

most promising [717–721]. However, an accurate evaluation of the SM amplitudes is required in order to disentangle NP contributions. Unfortunately hadronic uncertainties hinder a pristine calculation of the decay amplitudes. In this chapter, various theoretical approaches to the calculation of the hadronic uncertainties are discussed. In addition, the present experimental status is presented together with prospects at B-factories and LHCb.

3.7.1 Theoretical estimates of ΔS with factorization

In the following, we quantify $\Delta S_f \equiv -\eta_f S_f - \sin(2\beta)$, where S_f is the sin-term of the time-dependent CP asymmetry, based on QCD factorization [215, 216] calculations of the $B \to f$ decay amplitudes. We may write the decay amplitude as

$$A(\bar{B} \to f) = V_{cb}V_{cs}^* a_f^c + V_{ub}V_{us}^* a_f^u \propto 1 + e^{-i\gamma} d_f, \quad (157)$$

where $d_f = \epsilon_{\mathrm{KM}} a_f^u / a_f^c \equiv \epsilon_{\mathrm{KM}} \hat{d}_f$ and $\epsilon_{\mathrm{KM}} = |V_{ub}V_{us}^* / (V_{cb}V_{cs}^*)| \sim 0.025$. The expectation that ΔS_f is small derives from the CKM suppression ϵ_{KM} and the expectation that the ratio of hadronic amplitudes, $\hat{d}_f$, is not much larger than 1. Then

$$\Delta S_f = 2\epsilon_{\mathrm{KM}} \mathrm{Re}(\hat{d}_f) \cos(2\beta) \sin\gamma + O(d_f^2). \quad (158)$$

QCD factorization calculations of ΔS_f for various final states have been performed at leading order [722] and next-to-leading order [240, 723, 724]. Other factorization-inspired calculations can be found in [241, 725]. The results are generally in good agreement with one another. The following is primarily an update of [723]. Ref. [724] also discusses an estimate of long-distance rescattering effects. Since the significance of the model underlying this estimate is unclear, these (small) effects will not be included here.

The hadronic amplitudes a_f^p are sums of "topological" amplitudes, referring to colour-allowed tree (T), colour-suppressed tree (C), QCD penguin (P^p), singlet penguin (S^p), electroweak penguin ($P_{\mathrm{EW}}^p, P_{\mathrm{EW},C}^p$) and annihilation contributions. The numerical analysis below takes into account all flavor amplitudes following [240], but it suffices to focus on a few dominant terms to understand the qualitative

---

[23]Section coordinators: M. Ciuchini, F. Muheim.

features of the result. Then, for the various final states, the relevant hadronic amplitude ratio is given by

$$\pi^0 K_S: \quad \hat{d}_f \sim \frac{[-P^u] + [C]}{[-P^c]},$$

$$\rho^0 K_S: \quad \hat{d}_f \sim \frac{[P^u] - [C]}{[P^c]},$$

$$\eta' K_S: \quad \hat{d}_f \sim \frac{[-P^u] - [C]}{[-P^c]},$$

$$\phi K_S: \quad \hat{d}_f \sim \frac{[-P^u]}{[-P^c]},$$

$$\eta K_S: \quad \hat{d}_f \sim \frac{[P^u] + [C]}{[P^c]},$$

$$\omega K_S: \quad \hat{d}_f \sim \frac{[P^u] + [C]}{[P^c]}.$$

(159)

The convention here is that the quantities in square brackets have positive real parts. (Recall from (158) that ΔS_f mainly requires the real part of $\hat{d}_f$.) In factorization, $\mathrm{Re}[P^u/P^c]$ is near unity, roughly independent of the particular final state, hence ΔS_f receives a nearly universal, small and *positive* contribution of about $2\epsilon_{\mathrm{KM}} \cos(2\beta) \sin\gamma \approx 0.03$. On the contrary, the magnitudes and signs of the penguin amplitudes' real parts can be very different. Hence the influence of the colour-suppressed tree amplitude C determines the difference in ΔS_f between the different modes. For $(\pi^0, \eta, \omega) K_S$, the effect of C is constructive, but for $(\rho, \eta') K_S$, it is destructive. However, the magnitude of $\mathrm{Re}[P_c]$ is much larger for $\eta' K_S$ than for ρK_S, hence $\mathrm{Re}(\hat{d}_f)$ remains small and positive for $\eta' K_S$ but becomes negative for ρK_S.

The result of the calculation of ΔS_f is shown in Table 39. The columns labeled "ΔS_f (Theory)" use the input parameters (CKM parameters, strong coupling, quark masses, form factors, decay constants, moments of light-cone distribution amplitudes) summarized in Table 1 of [240]. The uncertainty estimate is computed by adding in quadrature the individual parameter uncertainties. The result displays the anticipated pattern. The variation of the central value from the nearly universal contribution of approximately ϵ_{KM} is

due to $\mathrm{Re}[C/P^c]$, and the error comes primarily from this quantity. It is therefore dominated by the uncertainty in the hard-spectator scattering contribution to C and the penguin annihilation contribution to P^c. In general one expects the prediction of the asymmetry S_f in factorization to be more accurate than the prediction of the direct CP asymmetry C_f, since S_f is determined by $\mathrm{Re}(a_f^u/a_f^c)$ which is large and calculated at next-to-leading order. The resultant error on ΔS_f is roughly of the size of ΔS_f itself. Quadratic addition of theoretical errors may not always lead to a conservative error estimate. Therefore we also perform a random scan of the allowed theory parameter space, taking the minimal and maximal value of an observable attained in this scan to define its predicted range. In doing so, we discard all theoretical parameter sets which give CP-averaged branching fractions not compatible within 3 sigma with the experimental data, that is we require $8.1 < 10^6\ Br(\pi^0 K^0) < 11.8$, $2.5 < 10^6\ Br(\rho^0 K^0) < 8.2$, $5.3 < 10^6\ Br(\phi K^0) < 11.9$, $2.9 < 10^6\ Br(\omega K^0) < 7.5$, $0.2 < 10^6\ Br(\eta K^0) < 2.4$. Note that we do not require the theoretical parameters to reproduce the $\eta' K^0$ branching fraction for reasons explained in [723]. The resulting ranges for ΔS_f from a scan of 200000 theoretical parameter sets are shown in the columns labeled "ΔS_f [Range]" in Table 39. It is seen that the ranges are not much different from those obtained by adding parameter uncertainties in quadrature—except for the ηK_S final state. For ηK_S, large negative values of ΔS_f originate from small regions of the parameter space, where by cancellations the leading penguin amplitude P_c becomes very small. This leads to large amplifications of C/P^c and hence of ΔS_f. Except for the case of ηK_S, these parameter space regions are excluded by the lower limits on the branching fractions.

Factorization-based calculations of two-body final states with scalar mesons and three-body final states are on a less solid footing than the final states discussed above. The following estimates have been obtained for the three-kaon modes [726]:

$$\Delta S_{K^+ K^- K_S} = 0.06^{+0.08}_{-0.02}, \qquad \Delta S_{K_S K_S K_S} = 0.06^{+0.00}_{-0.00}.$$

(160)

The quoted error should be regarded with due caution.

Table 39 Comparison of theoretical and experimental results for ΔS_f

Mode	ΔS_f (Theory)	ΔS_f [Range]	Mode	ΔS_f (Theory)	ΔS_f [Range]
$\pi^0 K_S$	$0.07^{+0.05}_{-0.04}$	$[+0.03, 0.13]$	$\rho^0 K_S$	$-0.08^{+0.08}_{-0.12}$	$[-0.29, 0.01]$
$\eta' K_S$	$0.01^{+0.01}_{-0.01}$	$[+0.00, 0.03]$	ϕK_S	$0.02^{+0.01}_{-0.01}$	$[+0.01, 0.05]$
ηK_S	$0.10^{+0.11}_{-0.07}$	$[-0.76, 0.27]$	ωK_S	$0.13^{+0.08}_{-0.08}$	$[+0.02, 0.21]$

400

Eur. Phys. J. C (2008) 57: 309–492

In conclusion, QCD calculations of the time-dependent CP asymmetry in hadronic $b \to s$ transitions yield only small corrections to the expectation $-\eta_f S_f \approx \sin(2\beta)$. With the exception of the $\rho^0 K_S$ final state, the correction ΔS_f is positive. The effect and theoretical uncertainty is particularly small for the two final states ϕK_S and $\eta' K_S$ [240]. The final-state dependence of ΔS_f is ascribed to the colour-suppressed tree amplitude. It appears difficult to constrain ΔS_f theory-independently by other observables. In particular, the direct CP asymmetries or the charged decays corresponding to $f = M K_S$ probe hadronic quantities other than those relevant to ΔS_f if these observables take values in the expected range. Here M stands for a charged light meson. Large deviations from expectations such as large direct CP asymmetries would clearly indicate a defect in our understanding of hadronic physics, but even then the quantitative implications for S_f would be unclear. A hadronic interpretation of large ΔS_f would probably involve an unknown long-distance effect that discriminates strongly between the up- and charm-penguin amplitude resulting in an enhancement of the up-penguin amplitude. No model is known that could plausibly produce such an effect.

3.7.2 Theoretical estimates of ΔS from three-body decays

While a possibility of constraining the CKM weak phase from three-body $\Delta S = 1$ B decays has been raised a long time ago [727], a discussion of three-body final states as probes of CKM phase has gained more momentum only recently with the experimental advances. The present experimental situation that includes measurements of time-dependent CP asymmetries in $B^0 \to K_S K_S K_S$, $B^0 \to \pi^0 \pi^0 K_S$ and $B^0 \to K^+ K^- K_{S,L}$ is summarized in Table 40. The quoted CP asymmetries are phase space $(dp\,s)$ integrated quantities with

$$S_f^{\text{3-body}} \equiv (1 - 2f_+) \sin 2\beta^{\text{eff}}$$
$$= \frac{2\,\text{Im} \int dp\,s(e^{-2i\beta} A_f \bar{A}_f^*)}{\int dp\,s|A_f|^2 + \int dp\,s|\bar{A}_f|^2}. \qquad (161)$$

Here f_+ is the CP-even component fraction, while A_f and $\bar{A}_f$ denote the $A(B^0 \to f)$ and $A(\bar{B}^0 \to f)$ amplitudes respectively. While $B^0 \to K_S K_S K_S$ and $B^0 \to \pi^0 \pi^0 K_S$ are decays into completely CP even final states [728], the decay $B^0 \to K^+ K^- K_S$ has both components but is still

mostly CP-even with $f_+ \sim 0.9$. This is obtained either from isospin analysis from $B^+ \to K_S K_S K_S$ decay assuming penguin dominance [729–733] or directly from angular analysis [734], in agreement with each other.

A $\Delta S = 1$ B decay amplitude can be in general decomposed in terms of "tree" $(\sim V_{ub}^* V_{us})$ and "penguin" $(\sim V_{cb}^* V_{cs})$ contributions as shown in (157) for the case of two-body $\bar{B}$ decays. An expression analogous to (158) holds for ΔS_f, here given by

$$\Delta S_f = \sin 2\beta^{\text{eff}} - \sin 2\beta = 2 \cos 2\beta \sin \gamma \, \text{Re}(\xi_f), \qquad (162)$$

where $\sin 2\beta^{\text{eff}}$ is defined in (161), and the ratio

$$\xi_f \equiv \frac{V_{ub}^* V_{us}}{V_{cb}^* V_{cs}} \frac{\int dp\,s\,T_f^* P_f}{\int dp\,s\,P_f^* P_f}, \qquad (163)$$

suitably averaged over the final phase space, replaces the ratio d_f defined in the previous section for two-body decays. In addition, the direct CP asymmetries are given by

$$C_f = -2 \sin \gamma \, \text{Im}(\xi_f). \qquad (164)$$

The difference ΔS_f was analysed using $SU(3)$ flavor symmetries [729, 736, 737] and was calculated in a model-dependent way in Ref. [726]. The approach is based on flavor $SU(3)$ and exploits the fact that the related $\Delta S = 0$ final states, f', are more sensitive to the "tree" amplitudes which are CKM enhanced when compared to the $\Delta S = 1$ amplitudes (because $V_{us} < V_{ud}$). However, "penguin" amplitudes are CKM suppressed (because $V_{cs} \to V_{cd}$). This then leads to a bound on ξ_f of the form

$$\xi_f < \lambda \sum_{f'} a_{f'} \sqrt{\frac{Br(f')}{Br(f)}}, \qquad (165)$$

where $\lambda = 0.22$, $a_{f'}$ are the coefficients arising from $SU(3)$ Clebsch–Gordan coefficients, and the sum is over $\Delta S = 0$ final states f'. The bounds are better if less modes enter the sum, which can be achieved through a dynamical assumption of small annihilation-like amplitudes. This then gives

$$\xi_{K^+ K^- K^0} < 1.02 \quad [736], \qquad \xi_{K_S K_S K_S} < 0.31 \quad [737], \qquad (166)$$

with bounds for a number of other modes listed in [736]. These are only very conservative upper bounds not at all

Table 40 Measured CP asymmetries in $B^0 \to 3P$ decays [502]

Mode	$\sin(2\beta^{\text{eff}})$	C_f
$K_S K_S K_S$ [609, 735]	0.51 ± 0.21	-0.23 ± 0.15
$\pi^0 \pi^0 K_S$ [829]	$-0.84 \pm 0.71 \pm 0.08$	$0.27 \pm 0.52 \pm 0.13$
$K^+ K^- K_{S,L}$ [732, 734]	$0.58 \pm 0.13^{+0.12}_{-0.09}$	0.15 ± 0.09

indicative of the expected size $\xi_f \sim \lambda^2 T_f/P_f$. One also expects $\xi_{K^+K^-K^0} < \xi_{K_S K_S K_S}$, since in the latter case, all the tree operator contributions are OZI suppressed as the final state does not contain valence u-quarks. This expectation was confirmed by a model-dependent calculation that combined QCD factorization with heavy-meson chiral perturbation theory [726]. This approach is valid only in a region of phase space where one of the light mesons is slow and the other two are very energetic, while for the remaining phase space, a model for the form factors was used. Ref. [726] then obtains

$$\Delta S_{K_S K_S K_S} = 0.02, \qquad \Delta S_{K^+K^-K_S} \lesssim O(0.1). \qquad (167)$$

An argument exists that the latter could be smaller [738], but one should also keep in mind the comment at the end of the previous section.

A different use of three-body final states is provided by the time-dependent Dalitz plot analysis with a fit to quasi-two body resonant modes. Interferences between resonances then fix relative strong phases giving additional experimental information. In this way, BaBar was able to resolve the $\beta \to \pi/2 - \beta$ discrete ambiguity using a $B^0 \to K^+K^-K_{S,L}$ Dalitz plot analysis [739]. The interference of CP-even and CP-odd contributions leads to a $\cos 2\beta^{\text{eff}}$ term (with $\beta^{\text{eff}} \to \beta$ in the limit of no tree pollution). Another example is measuring phases of $\Delta I = 1$ amplitudes of $B \to (K^*\pi)_{I=1/2,3/2}$, $B_s \to (K^*\bar{K})_{I=1}$ and $B_s \to (\bar{K}^*K)_{I=1}$ from resonance interferences in $B \to K\pi\pi$ and $B_s \to K\bar{K}\pi$. This then gives information on CKM parameters complementary to other methods [740–742]. Using $SU(3)$ hadronic uncertainties due to electroweak penguin operators O_9 and O_{10} were shown to be very small in $B \to K\pi\pi$ and $B_s \to K\pi\pi$ and somewhat larger in $B_s \to K\bar{K}\pi$ [742]. The first processes imply a precise linear relation between $\bar{\rho}$ and $\bar{\eta}$, with a measurable slope and an intercept at $\bar{\eta} = 0$ involving a theoretical error of 0.03. The decays $B_s \to K\pi\pi$ permit a measurement of γ involving a theoretical error below a degree. Furthermore, while time-dependence is required when studying B^0 decays at the $\Upsilon(4S)$, it may not be needed when studying B_s decays at hadronic colliders.

3.7.3 Flavor symmetries and estimates of $b \to s$ transitions

Decomposing the $B \to MM$ amplitudes in terms of flavor $SU(3)$ or isospin reduced matrix elements leads to relations between different amplitudes, since the effective weak Hamiltonian usually transform only under a subset of all possible representations [743]. The group-theoretical approach based on reduced matrix elements [245, 744, 745] is equivalent to a diagrammatic approach of topological amplitudes [746–750]. In the latter, it is easier to introduce dynamical assumptions such as neglecting annihilation-like

amplitudes. These were shown to be $1/m_b$ suppressed for decays into nonisosinglets [751], while not all of them are $1/m_b$ suppressed if η, η' occur in the final state (see Appendix C of [241]).

The $SU(3)$ approach has been used in global fits to the experimentally measured $B \to PP$ and $B \to PV$ decays [752–761] in which both the values of hadronic parameters as well as the value of weak phase γ are determined. However, in order to obtain a stable fit, a number of dynamical assumptions are needed. In the most recent fit to $B \to PP$ [756], t-quark dominance in penguin amplitudes and negligible annihilation-like topologies (also for isosinglets) were assumed. Both β and γ were determined with central values slightly above the CKMfitter and UTfit determinations. Allowing for a new weak phase in P_{EW} for $\Delta S = 1$ modes leads to statistically significant reduction of χ^2, while choosing this phase to be zero does give the size of $|P_{\text{EW}}|$ in excellent agreement with the Neubert–Rosner relation [762–765]. A large strong phase difference $\arg(C/T) \sim -60°$ was found, while expected to be $1/m_b$ suppressed from QCD factorization and SCET [221, 240, 766]. As stressed in Ref. [767], the direct CP asymmetries $A_{\text{CP}}(B^0 \to K^+\pi^-)$ and $A_{\text{CP}}(B^+ \to K^+\pi^0)$ would be of the same sign for $\arg(C/T)$ small, which is excluded at 4.7σ at present.

Assumption of negligible annihilation topologies used in $SU(3)$ fits can be tested by comparing $B^0 \to K^0\bar{K}^0$, $B^+ \to K^+\bar{K}^0$, where annihilation is CKM enhanced, with $B^+ \to K^0\pi^+$ [768, 769]. $SU(3)$ breaking has been addressed in [756, 770] showing a small effect on the values of extracted parameters. Further tests of $SU(3)$ breaking or searches of NP will be possible using B_s decays [771–776], with the first CDF measurement of $Br(B_s \to K^+K^-)$ leading the way [777]. Errors due to the dynamical assumptions can be reduced if fits are made to only a subset of modes, e.g. to $\pi\pi$, πK [756, 760, 770, 778–781]. Furthermore, dynamical assumptions can be avoided entirely if only a set of modes related through U-spin is used [771, 782, 783]. This leads to stable fits, while giving γ with a theoretical error of a few degrees. Further studies of $SU(3)$ breaking effects are called for, though.

Because of the different CKM hierarchy of tree and penguin amplitudes in $\Delta S = 1$ and $\Delta S = 0$ decays, tree pollution in $\Delta S = 1$ decays can be bounded using $SU(3)$ related $\Delta S = 0$ modes [729]. Correlated bounds on ΔS_f and C_f for $\eta' K_S$ and $\pi^0 K_S$ final states have been presented in [784–787]. Such a model-independent bound on $\Delta S_{\phi K_S}$ is not available at present, since many more $\Delta S = 0$ modes enter, some of which have not been measured yet [788].

Very precise relations between $\Delta S = 1$ $B \to \pi K$ CP asymmetries or decay rates can be obtained using isospin decompositions. The sum rule between decay widths $\Gamma(K^0\pi^+) + \Gamma(K^+\pi^-) = 2\Gamma(K^+\pi^0) + 2\Gamma(K^0\pi^0)$ [789,

402

Eur. Phys. J. C (2008) 57: 309–492

790] (equivalent to $R_n = R_c$ [791]) is violated by CKM doubly suppressed terms calculable in $1/m_b$ expansion [221, 240, 241, 766], while harder to calculate isospin-breaking corrections cancel to first order [792]. The sum rule $\Delta(K^+\pi^-) + \Delta(K^0\pi^+) - 2\Delta(K^+\pi^0) - 2\Delta(K^0\pi^0) = 0$ for the rate differences $\Delta(f) = \Gamma(\bar{B} \to \bar{f}) - \Gamma(B \to f)$ is valid in the isospin limit and is thus violated by EWP. However, these corrections vanish in the $SU(3)$, $m_b \to \infty$ limit making the sum rule very precise [793].

3.7.4 Applications of U-spin symmetry to B_d and B_s decays

The current data in B physics suggests that B_d decays agree well with SM predictions, while B_s decays remain poorly known and might be affected by NP. Within the SM, the CKM mechanism correlates the electroweak part of these transitions, but quantitative predictions are difficult due to hadronic effects. The latter can be estimated relying on the approximate $SU(3)$-flavor symmetry of QCD: information on hadronic effects, extracted from data in one channel, can be exploited in other channels related by flavor symmetry, leading to more accurate predictions within the SM.

In addition to isospin symmetry, an interesting theoretical tool is provided by U-spin symmetry, which relates d- and s-quarks [771]. Indeed, this symmetry holds for long- and short-distances and does not suffer from electroweak corrections, making it a valuable instrument to analyse processes with significant penguins and thus a potential sensitivity to NP. However, due to the significant difference $m_s - m_d$, U-spin breaking corrections of order 30% may occur, depending on the processes.

As a first application of U-spin, relations were obtained between $B_d \to \pi^+\pi^-$ and $B_s \to K^+K^-$. This led to correlations among the observables in the two decays such as branching ratios and CP asymmetries [771–774] and to a prediction for $BR(B_s \to K^+K^-) = (35^{+73}_{-20}) \times 10^{-6}$ [780]. These results helped to investigate the potential of such decays to discover NP [775, 794]. Unfortunately, the accuracy of the method is limited not only by the persistent discrepancy between BaBar and Belle on $B_d \to \pi^+\pi^-$ CP asymmetries but also by poorly known U-spin corrections. In these analyses, the ratio of tree contributions $R_c = |T^s_{K\pm}/T^d_{\pi\pm}|$ was taken from QCD sum rules as 1.76 ± 0.17 [250] (updated to $1.52^{+0.18}_{-0.14}$ [272]). In addition, the ratio of penguin-to-tree ratios $\xi = |(P^s_{K\pm}/T^s_{K\pm})/(P^d_{\pi\pm}/T^d_{\pi\pm})|$ was assumed equal to 1 [780] or 1 ± 0.2 [775, 794] in agreement with rough estimates within QCD factorization (QCDF) [795].

Indeed QCDF may complement flavor symmetries by a more accurate study of short-distance effects. However, QCDF cannot predict some significant $1/m_B$-suppressed long-distance effects, which have to be estimated through models. Recently, it was proposed to combine QCDF and U-spin in the decays mediated by penguin operators $B_d \to K^0\bar{K}^0$ and $B_s \to K^0\bar{K}^0$ [796] and in their vector–vector analogues [797].

First, tree (T^{d0}) and penguin (P^{d0}) contributions to $B_d \to K^0\bar{K}^0$ can be determined by combining the currently available data with $|T^{d0} - P^{d0}|$, which can be accurately computed in QCDF because long-distance effects, seen as infrared divergences, cancel in this difference. U-spin suggests accurate relations between these hadronic parameters in $B_d \to K^0\bar{K}^0$ and those in $B_s \to K^0\bar{K}^0$. Actually, we expect similar long-distance effects since the $K^0\bar{K}^0$ final state is invariant under the d–s exchange. Short distances are also related since the two processes are mediated by penguin operators through diagrams with the same topologies. U-spin breaking arises only in a few places: factorizable corrections encoded in $f = [M^2_{B_s} F^{B_s \to K}(0)]/[M^2_{B_d} F^{B_d \to K}(0)]$ and non-factorizable corrections from weak annihilation and spectator scattering. Because of these expected tight relations, QCDF can be relied upon to assess U-spin breaking between the two decays. Indeed, up to the factorizable factor f, penguin (as well as tree) contributions to both decays are numerically very close. Penguins in $B_d \to K^0\bar{K}^0$ and $B_s \to K^+K^-$ should have very close values as well, whereas no such relation exists for the (CKM-suppressed) tree contribution to the latter, to be estimated in QCDF.

These relations among hadronic parameters, inspired by U-spin considerations and quantified within QCD factorization, can be exploited to determine the tree and penguin contributions to $B_s \to KK$ decays and the corresponding observables. In particular, one gets $BR(B_s \to K^0\bar{K}^0) = (18 \pm 7 \pm 4 \pm 2) \times 10^{-6}$ and $BR(B_s \to K^+K^-) = (20 \pm 8 \pm 4 \pm 2) \times 10^{-6}$, in very good agreement with the latest CDF measurement. The same method provides significantly improved determinations of the U-spin breaking ratios $\xi = 0.83 \pm 0.36$ and $R_c = 2.2 \pm 0.7$. These results have been exploited to determine the impact of supersymmetric models on these decays [798].

New results on $B \to K$ form factors and on the $B_d \to K^0\bar{K}^0$ branching ratio and direct CP-asymmetry should lead to a significant improvement of the predictions in the B_s sector. The potential of other pairs of nonleptonic B_d and B_s decays remains to be investigated.

3.7.5 Applications of the RGI parametrization to $b \to s$ transitions

Few general parameterizations of the $\Delta B = 1$ hadronic amplitudes exist in the literature. Here we use the parametrization proposed in [799] which decomposes decay amplitudes in terms of Renormalization-Group-Invariant (RGI) parameters. For our purpose, we just need to recall a few basic facts about the classification of RGI's. First of all,

we have six nonpenguin parameters, containing only non-penguin contractions of the current–current operators $Q_{1,2}$: emission parameters $E_{1,2}$, annihilation parameters $A_{1,2}$ and Zweig-suppressed emission–annihilation parameters $EA_{1,2}$. Then, we have four parameters containing only penguin contractions of the current–current operators $Q_{1,2}$ in the GIM-suppressed combination $Q_{1,2}^c - Q_{1,2}^u$: P_1^{GIM} and Zweig suppressed P_{2-4}^{GIM}. Finally, we have four parameters containing penguin contractions of current–current operators $Q_{1,2}^c$ (the so-called charming penguins [800]) and all possible contractions of penguin operators Q_{3-12}: $P_{1,2}$ and the Zweig-suppressed $P_{3,4}$. In the following, Zweig-suppressed parameters are neglected. We refer the reader to the original reference for details. We can then write schematically the $b \to s$ decay amplitude as

$$\mathcal{A}(B \to F) = -V_{ub}^* V_{us} \sum \left(T_i + P_i^{\text{GIM}}\right) - V_{tb}^* V_{ts} \sum P_i,$$
(168)

where $T_i = \{E_i, A_i, EA_i\}$ are not present in pure-penguin decays.

The idea developed in [801] is to write down the RGI parameters as the sum of their expression in the infinite mass limit, for example using QCD factorization, plus an arbitrary contribution corresponding to subleading terms in the power expansion. These additional contributions are then determined by a fit to the experimental data. In $b \to s$ penguins, the dominant power-suppressed correction is given by

charming penguins, and the corresponding parameter can be determined with high precision from data and is found to be compatible with a Λ/m_b correction to factorization [801]. However, nondominant corrections, for example GIM penguin parameters in $b \to s$ decays, can be extracted from data only in a few cases (for example in $B \to K\pi$ decays). Yet predictions for ΔS_f depend crucially on these corrections, so that one needs external input to constrain them. One interesting avenue is to extract the support of GIM penguins from $SU(3)$-related channels ($b \to d$ penguins), in which they are not Cabibbo-suppressed, and to use this support, including a possible large $SU(3)$ breaking of 100%, in the fit of $b \to s$ penguin decays. Alternatively, one can omit the calculation in factorization and fit directly the RGI parameters from the experimental data, instead of fitting the power-suppressed corrections [604, 802].

Compared to factorization approaches, general parameterizations have less predictive power but are more general. In particular, they tend to overestimate the theoretical uncertainty and are thus best suited to search for NP in a conservative way. In addition, these methods have the advantage that for several channels, the predicted ΔS decreases with the experimental uncertainty in BR's and CP asymmetries of $b \to s$ and $SU(3)$-related $b \to d$ penguins.

In the analysis reported here [88, 803], we vary the absolute values of the subdominant amplitudes in the range $[0, UL]$ (while the phases are unconstrained) and study the dependence of the predictions on the upper limit UL. For example, we show in Fig. 37 the effect of changing the up-
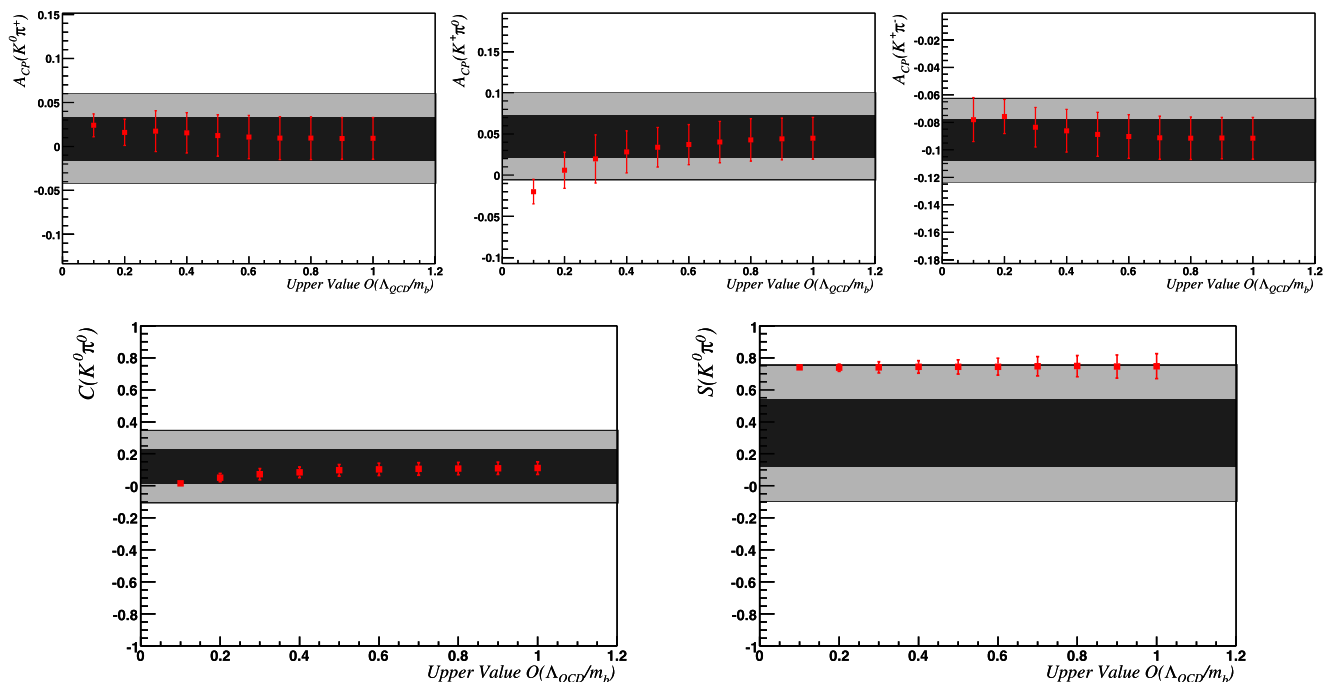

Fig. 37 CP asymmetries for $B \to K\pi$ decays, obtained varying subdominant contributions in the range [0, UV], with the upper value UV scanned between zero and one (in units of E_1). For comparison, the experimental 68% (95%) probability range is given by the *dark* (*light*) band

404

Eur. Phys. J. C (2008) 57: 309–492

per limit of the range in which subdominant terms are varied on the prediction of some observables in $B \to K\pi$ decays. It can be seen that reasonable subdominant terms make any $K\pi$ puzzle disappear. Furthermore, the prediction of $S_{\pi^0 K_S}$ has small theoretical error and is quite stable against the effect of subdominant terms.

In Table 41, we collect predictions for ΔS_f obtained using the method sketched above for $UL = 0.5$ (in units of the leading amplitude), as suggested by the $SU(3)$-related modes $B \to KK$. Notice that the theoretical uncertainty is smaller for $B \to \pi^0 K_S$, because the number of observables in the $B \to K\pi$ system is sufficient to constrain efficiently the hadronic parameters. This means that the theoretical error can be kept under control by improving the experimental data in these channels. On the other hand, the information on $B \to \phi K_S$ is not sufficient to bound the subleading terms, and this results in a relatively large theoretical uncertainty that cannot be decreased without additional input on hadronic parameters. Furthermore, using $SU(3)$ to constrain $\Delta S_{\phi K_S}$ is difficult, because the number of amplitudes involved is very large [245, 736, 737, 788].

The ideal situation would be represented by a pure penguin decay for which the information on P_i^{GIM} is available with minimal theoretical input. Such a situation is realized by the pure penguin decays $B_s \to K^{0(*)}\bar{K}^{0(*)}$. An upper bound for the P_i^{GIM} entering this amplitude can be obtained from the $SU(3)$-related channels $B_d \to K^{0(*)}\bar{K}^{0(*)}$. Then, even adding a generous 100% $SU(3)$ breaking and an arbitrary strong phase, it is possible to have full control over the theoretical error in ΔS [802].

3.7.6 $b \to s$ transitions in the MSSM

In this section, we discuss phenomenological effects of the new sources of flavor and CP violation in $b \to s$ processes that arise in the squark sector [104, 108, 109, 804–823] of the MSSM. In general, in the MSSM, squark masses are neither flavor-universal nor aligned to quark masses, so that they are not flavor diagonal in the super-CKM basis, in which quark masses are diagonal and all neutral current vertices are flavor diagonal. The ratios of off-diagonal squark mass terms to the average squark mass define four new sources of flavor violation in the $b \to s$ sector: the mass insertions $(\delta_{23}^d)_{AB}$ with $A, B = L, R$ referring to the helicity of the corresponding quarks. These δ's are in general complex, so that they also violate CP. One can think of them as additional CKM-type mixings arising from the SUSY sector. Assuming that the dominant SUSY contribution comes

from the strong interaction sector, i.e. from gluino exchange, all FCNC processes can be computed in terms of the SM parameters plus the four δ's plus the relevant SUSY parameters: the gluino mass $m_{\tilde{g}}$, the average squark mass $m_{\tilde{q}}$, $\tan\beta$ and the μ parameter. The impact of additional SUSY contributions such as chargino exchange has been discussed in detail in Ref. [816]. We consider only the case of small or moderate $\tan\beta$, since for large $\tan\beta$, the constraints from $B_s \to \mu^+\mu^-$ and Δm_s preclude the possibility of having large effects in $b \to s$ hadronic penguin decays [28, 29, 32, 34, 114, 115, 813].

Barring accidental cancellations, one can consider one single δ parameter, fix the SUSY masses and study the phenomenology. The constraints on δ's come at present from $B \to X_s\gamma$, $B \to X_s l^+l^-$ and from the $B_s - \bar{B}_s$ mixing amplitude. We refer the reader to Refs. [88, 107, 116, 824] for all the details and results of this analysis.

Fixing as an example $m_{\tilde{g}} = m_{\tilde{q}} = |\mu| = 350$ GeV and $\tan\beta = 3$, one obtains the following constraints on δ's:

$$\begin{aligned} \left|(\delta_{23}^d)_{LL}\right| &< 2 \times 10^{-1}, & \left|(\delta_{23}^d)_{RR}\right| &< 7 \times 10^{-1}, \\ \left|(\delta_{23}^d)_{RL,LR}\right| &< 5 \times 10^{-3}. \end{aligned} \quad (169)$$

Notice that all constraints scale approximately linearly with the squark and gluino masses.

Having the present experimental bounds on the δ's, we can turn to the evaluation of the time-dependent CP asymmetries. The uncertainty in the calculation of SUSY effects is larger than the SM one. Following [107], we use QCDF enlarging the range for power-suppressed contributions to annihilation chosen in [240] as suggested in [825]. We warn the reader about the large theoretical uncertainties that affect this evaluation.

In Fig. 38, we present the results for $S_{\phi K_s}$, $S_{\pi^0 K_s}$, $S_{\eta' K_s}$ and $S_{\omega K_s}$. They do not show a sizable dependence on the sign of μ or on $\tan\beta$ for the chosen range of SUSY parameters. We see that:

– deviations from the SM expectations are possible in all channels, and the present experimental central values can be reproduced;
– deviations are more easily generated by LR and RL insertions, due to the enhancement mechanism discussed above;
– as noticed in [826, 827], the correlation between S_{PP} and S_{PV} depends on the chirality of the NP contributions. For example, we show in Fig. 39 the correlation between $S_{K_S\phi}$ and $S_{K_S\pi^0}$ for the four possible choices for mass insertions. We see that the $S_{K_S\phi}$ and $S_{K_S\pi^0}$ are correlated for LL and LR mass insertions and anticorrelated for RL and RR mass insertions.

Table 41 Predictions for ΔS_f using the RGI parametrization

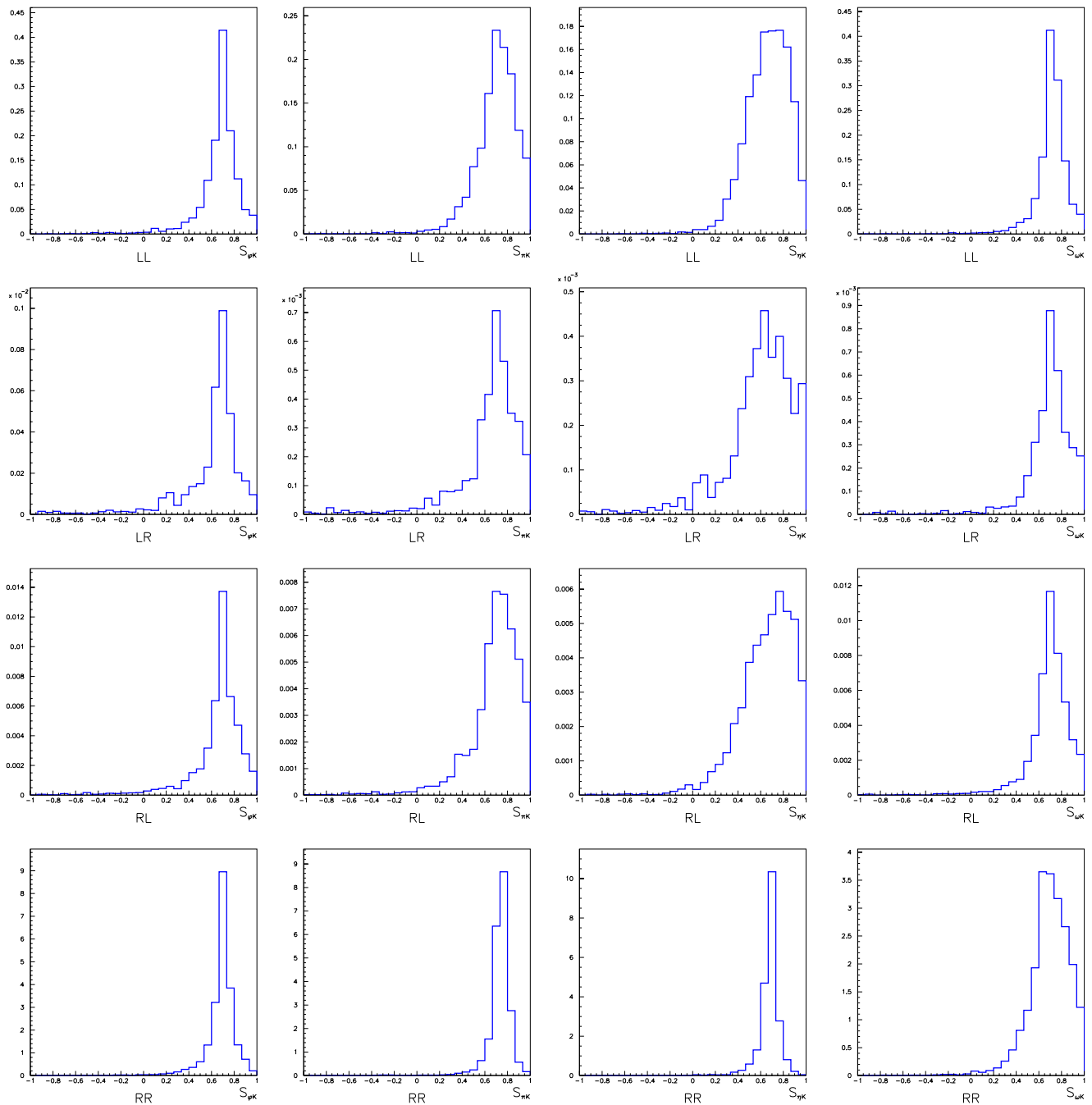|			
$\Delta S_{\pi^0 K_S}$	$(2.4 \pm 5.9) \times 10^{-2}$	$\Delta S_{\eta' K_S}$	$(-0.7 \pm 5.4) \times 10^{-2}$
$\Delta S_{\phi K_S}$	$(0.4 \pm 9.2) \times 10^{-2}$	$\Delta S_{\rho^0 K_S}$	$(-6.2 \pm 8.4) \times 10^{-2}$
$\Delta S_{\omega K_S}$	$(5.6 \pm 10.7) \times 10^{-2}$		

Fig. 38 Probability density functions for $S_{\phi K_s}$, $S_{\pi^0 K_s}$, $S_{\eta' K_s}$ and $S_{\omega K_s}$ induced by $(\delta_{23}^d)_{AB}$ with $A, B = \{L, R\}$

An interesting issue is the scaling of SUSY effects in S_f with squark and gluino masses. Similarly to the constraints from other processes, the dominant SUSY contribution to S_f scales linearly with SUSY masses as long as $m_{\tilde{g}} \sim m_{\tilde{q}} \sim \mu$. This means that there is no decoupling of SUSY contributions to S_f as long as the constraints from other processes can be satisfied with $\delta < 1$. The bounds on LL and RR mass insertions quickly reach the physical boundary at $\delta = 1$. On the other hand, LR and RL are well

below that bound. Chirality flipping LR and RL mass insertions cannot become too large in order to avoid charge and colour breaking minima and unbounded from below directions in the scalar potential [828]. Nevertheless, it is easy to check that the flavor bounds used above are stronger for SUSY masses above the TeV scale. We conclude that LR and RL mass insertions can give observable effects to S_f for SUSY masses within the reach of LHC and even above.

406

Eur. Phys. J. C (2008) 57: 309–492
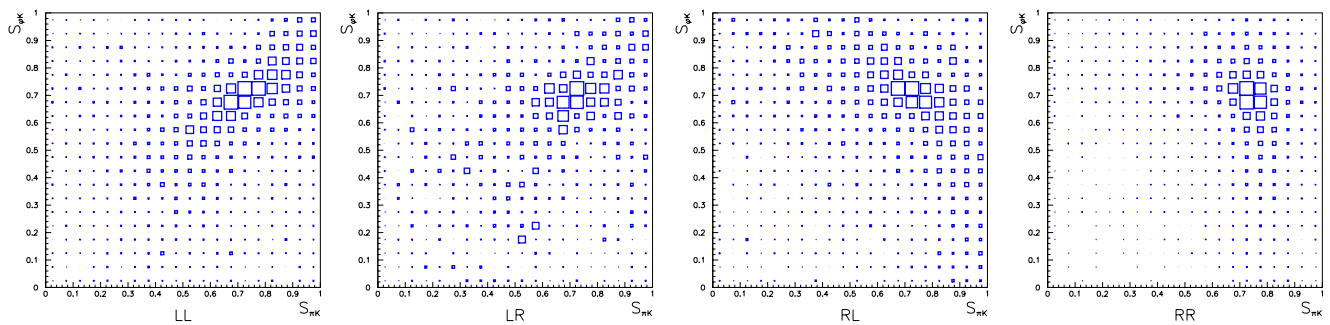
Fig. 39 Correlation between $S_{\phi K_s}$ and $S_{\pi^0 K_s}$ for LL, LR, RL and RR mass insertions

3.7.7 Experimental status and future prospects for time-dependent CP violation in hadronic $b \to s(d)$ transitions

CP asymmetries in B^0 and B_s decays that are governed by the $b \to s$ transition are very sensitive to new CP-violating phases beyond the Standard Model (SM). There are a few golden modes that are practically free from hadronic uncertainties; examples include $B^0 \to \phi K_S^0$, $\eta' K_S^0$, $K_S^0 K_S^0 K_S^0$ and $B_s^0 \to \phi\phi$, see Fig. 40. Precise measurements for these decays have been among the most important topics of quark flavor physics in the last few years and will also remain crucially important in the future.

At the B factories, the decay chain $\Upsilon(4S) \to B^0 \bar{B}^0 \to f_{\rm CP} f_{\rm tag}$ is used to measure time-dependent CP asymmetries, where one of the B mesons decays at time $t_{\rm CP}$ to a final state $f_{\rm CP}$ and the other decays at time $t_{\rm tag}$ to a final state $f_{\rm tag}$ that distinguishes between B^0 and $\bar{B}^0$. The rate of this decay chain has a time dependence [627, 628] given by

$$\mathcal{P}(\Delta t) = e^{-|\Delta t|/\tau_{B^0}} 4\tau_{B^0}$$
$$\times \left\{ 1 + q \cdot \left[\mathcal{S} \sin(\Delta m_d \Delta t) + \mathcal{A} \cos(\Delta m_d \Delta t) \right] \right\}. \tag{170}$$

Here $\mathcal{S}$ and $\mathcal{A}$ are CP-violation parameters, τ_{B^0} is the B^0 lifetime, Δm_d is the mass difference between the two B^0 mass eigenstates, $\Delta t = t_{\rm CP} - t_{\rm tag}$, and the b-flavor charge $q = +1 (-1)$ when the tagging B meson is a B^0 ($\bar{B}^0$). To a good approximation, the SM predicts $\mathcal{S} = -\xi_f - -\sin 2\phi_1$ and $\mathcal{A} = 0$ for both tree transitions (e.g. $b \to c\bar{c}s$) and penguin transitions (e.g. $b \to s\bar{s}s$) unless V_{ub} or V_{td} is involved in the decay amplitude. Here $\xi_f = +1(-1)$ corresponds to CP-even (-odd) final states.

BaBar and Belle have accumulated more than 10^9 $B\bar{B}$ pairs with both experiments combined and have measured time-dependent CP asymmetries in various B^0 decays that are dominated by the $b \to s$ transition. Details of the measurements are described elsewhere [609, 732, 735, 739, 829–832]; here we briefly explain the essence of the measurements. Branching fractions for these charmless decay modes are typically around 10^{-5} ignoring daughter branching fractions. Efficient continuum suppression using sophisticated techniques such as Fisher discriminants, likelihood ratios and neural network has been performed to keep a reasonable signal-to-noise ratio. The flavor of the accompanying B meson is identified from inclusive properties of remaining particles; information from primary and secondary leptons, charged kaons, Λ baryons, slow and fast pions is combined by using a neural network (BaBar) or a lookup-table (Belle). A typical effective efficiency for flavor tagging is 30% in both cases. Good understanding of the vertex resolution function is obtained by using large-statistics control samples such as $B \to D^{(*)}\pi$, $D^*\ell\nu$ etc. Lifetime and mixing measurements with a precision of $\mathcal{O}(1)\%$ are obtained as byproducts.

The present status of the measurements is summarized in Fig. 41. Although the result for each individual mode does not significantly differ from the SM expectation (i.e. $\mathcal{S}_{J/\psi K^0}$), most of the $\mathcal{S}$ values are smaller than the SM expectation. When all the $b \to s$ modes are combined, the result differs from the SM expectation by 1.1σ.[24] Combining the results of all the $b \to s$ modes is naive as the theoretical uncertainties vary considerably amongst the modes. Much more data are needed to firmly establish a new CP-violating phase beyond the SM for each golden mode.

Measurements of the $\mathcal{A}$ terms yield values consistent with zero, i.e. consistent with the SM at the moment. Nonzero $\mathcal{A}$ requires a strong phase difference between the SM amplitude and the NP amplitude. Therefore it is possible to observe significant deviations from the SM for $\mathcal{S}$ while $\mathcal{A}$ is consistent with zero. Also, since $\mathcal{A}$ is not calculable precisely, in general it is hard to obtain quantitative information from the measurements of $\mathcal{A}$ terms. An exception is the $B^0 \to K^0\pi^0$ decay. Thanks to a precise sum rule based on the isospin symmetry [793], the value for $\mathcal{A}_{K^0\pi^0}$ can be

---

[24]Due to the highly non-Gaussian errors of the result from $B^0 \to f_0 K_S^0$ with $f_0 \to \pi^+\pi^-$ and the fact that this result has a significant effect on the χ^2 of the naive $b \to s$ penguin average, this outlying point is excluded.

Fig. 40 The penguin diagrams for the hadronic B^0 and B_s^0 decays such as $B^0 \to \phi K_S^0$, $B^0 \to \eta' K_S^0$ (left) and $B_s^0 \to \phi\phi$ (right)
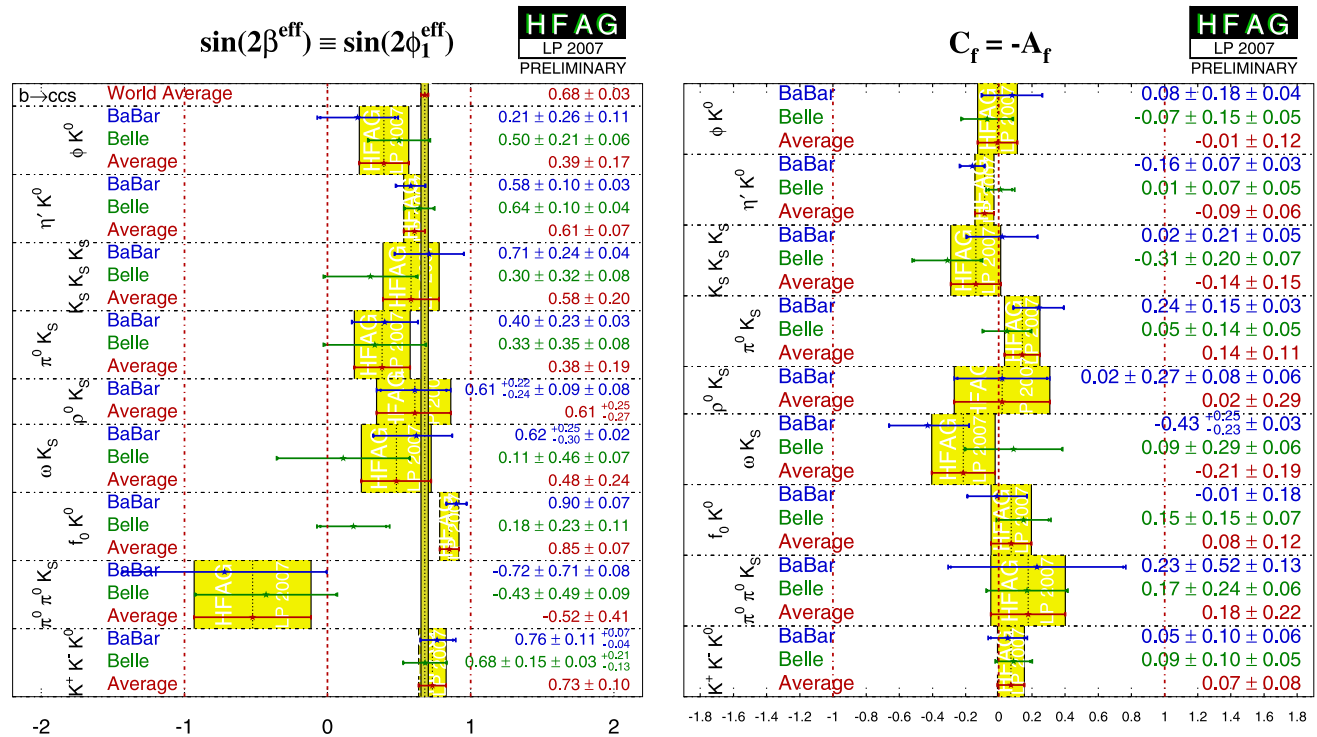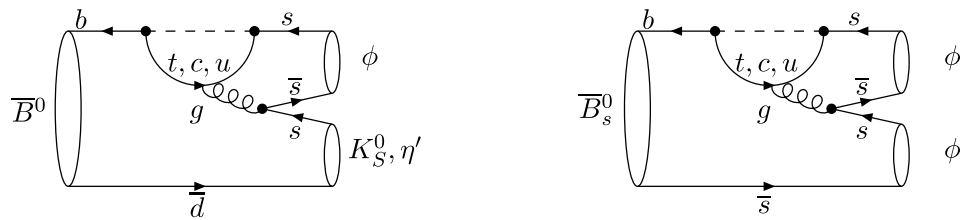

Fig. 41 Summary of the experimental results for time-dependent CP asymmetries from BaBar and Belle as of August 2007

predicted within the SM from measurements of branching fractions and CP asymmetries of the other $B \to K\pi$ decays; $\mathcal{A}_{K^0\pi^0} = -0.16 \pm 0.04$ is predicted, while measurements yield $\mathcal{A}_{K^0\pi^0} = -0.12 \pm 0.11$.

Due to further CKM-suppression, CP asymmetry measurements for modes dominated by the $b \to d$ transition require even higher statistics than those required for the studies of the $b \to s$ transition. The only measurement available at the moment is $\mathcal{S}_{B^0 \to K_S^0 K_S^0} = -1.28^{+0.80+0.11}_{-0.73-0.16}$ [833], where the first error is statistic and the second error is systematic.

In the near future, the LHCb experiment will probe new CP violating phases beyond the SM in $b \to s$ transitions. With the copious production of B_s^0 mesons, LHCb will be able to study $b \to s$ transitions using the decay $B_s^0 \to \phi\phi$, see Fig. 40. In the SM, the CP-violating phase $\mathcal{S}_{\phi\phi}$ for $B_s^0 \to \phi\phi$ is expected to be very close to zero as there is a cancellation of the B_s^0 mixing and decay phases [834].

In the LHCb experiment, the reconstruction efficiency for $B_s^0 \to \phi\phi$ is expected to be larger than for $B^0 \to \phi K_S^0$ which

compensates for the four times smaller fraction of b-quarks to hadronize into a B_s^0 meson. In addition, flavor tagging is also favorable for B_s^0 decays where the same-side kaon tagging contributes significantly to the effective flavor tagging efficiency. From a full simulation LHCb expects a yield of 3100 reconstructed $B_s^0 \to \phi\phi$ events in a 2 fb^{-1} data sample with a background to signal ratio $B/S < 0.8$ at 90% C.L. [835]. The $\mathcal{S}_{\phi\phi}$ sensitivity has been studied using a toy Monte Carlo, taking the resolutions and acceptances from the full simulation. A unbinned likelihood fit is performed on 500 toy data sets. This is used to extract $\mathcal{S}_{\phi\phi}$ and all other physical parameters which cannot be determined from elsewhere. In a 2 fb^{-1} data set, $\mathcal{S}_{\phi\phi}$ can be measured with a precision of $\sigma(\mathcal{S}_{\phi\phi}) = 0.11$ (statistical error only). After about 5 years of data taking, LHCb is expected to accumulate a data sample of 10 fb^{-1}, which will give a statistical uncertainty of $\sigma(\mathcal{S}_{\phi\phi}) = 0.05$ [835].

In a similar study, LHCb investigated the decay $B^0 \to \phi K_S^0$. A yield of 920 events is expected in 2 fb^{-1} of integrated luminosity with a background to signal ratio $0.3 <$

408

Eur. Phys. J. C (2008) 57: 309–492

$B/S < 1.1$ at 90% C.L. The sensitivity for the CP violating asymmetry $\sin 2\beta^{\mathrm{eff}}$ is 0.23 (0.10) in a 2 (10) fb^{-1} data sample [836].

Table 42 lists the expected CP reach at LHCb and a super-B factory for the theoretically cleanest $b \to s$ decay modes. We expect that the precision will be better by an order of magnitude than now. Such measurements will thus allow us to detect effects from physics beyond the SM even if the mass scale of NP is $\mathcal{O}(1)$ TeV.

3.7.8 Two-body hadronic B decay results from the B-factories

This class of B decays manifests a wide range of interesting phenomena, from direct CP violation and broken $SU(3)$ symmetry constraints on the SM uncertainties in measurements of the unitarity triangle angles to the amplitude hierarchy found in decays to final states containing two spin-one particles (vector or axial-vector mesons, V and A, respectively).

The only direct CP violation signal observed by the B-factories is in the $B_d^0 \to K^\pm \pi^\mp$ channel. In contrast to the small effect observed in kaon decay, the direct CP asymmetry in $B_d^0 \to K^\pm \pi^\mp$ is large: -0.093 ± 0.015 [620, 838]. The quest for additional signals of direct CP violation in B meson decays is ongoing in a plethora of different channels [502]. The next goals of the B-factories are to observe direct CP violation in the decay of $B_u^\pm$ mesons and other B_d^0 channels.

The B-factories have recently observed CPV in $B_d^0 \to \eta' K^0$ decays [609, 832]. These $b \to s$ penguin processes are probes of NP and have the most precisely measured time-dependent CP asymmetry parameters of all of the penguin modes. Any deviation ΔS of the measured asymmetry parameter $S_{\eta' K^0}$ from $\sin 2\beta$ is an indication of NP (For example, see [507, 839]). In addition to relying on theoretical calculations of the SM pollution to these decays [241, 723, 726], it is possible to experimentally constrain the SM pollution using $SU(3)$ symmetry [784]. This requires precision knowledge of the branching fractions of the B_d^0 meson decays to

the following pseudo-scalar pseudo-scalar (PP) final states: $\pi^0 \pi^0, \pi^0 \eta, \pi^0 \eta', \eta\eta, \eta' \eta, \eta' \eta'$ final states [840, 841]. The related decays $B_{u,d} \to \eta' \rho$ and $B_{u,d} \to \eta' K^*$ [842, 843] can also be used to understand the standard model contributions to $B_d^0 \to \eta' K^0$ decays and the hierarchy of ηK^0 to $\eta' K^0$ decays.

The angular analysis of $B \to VV$ decays provides eleven observables (six amplitudes and five relative phases) that can be used to test theoretical calculations [611]. The hierarchy of A_0, A_+ and A_- amplitudes obtained from a helicity (or A_0, $A_\parallel$ and $A_\perp$ in the transversity basis) analysis of such decays allows one to search for possible right-handed currents in any NP contribution to the total amplitude. For low statistics studies, a simplified angular analysis is performed, where one measures the fraction of longitudinally polarized events defined as $f_L = |A_0|^2 / \sum |A_i|^2$. Tree dominated decays such as $B_d^0 \to \rho^+ \rho^-$ have $f_L \sim 1.0$ [844, 845]. Current data for penguin dominated processes ($\phi K^*(892)$ [846, 847], $K^*(892)\rho$ [848, 849]) that are observed to have non-trivial values of f_L can be accommodated in the SM. In addition to this, one can search for T-odd CP violating asymmetries in triple products constructed from the angular distributions [850]. It has also been suggested that nonstandard model effects could be manifest in a number of other observables [851]. The measured rates of electroweak penguin dominated B decays to final states involving a ϕ meson are also probes of NP [852]. The study of $B \to AV$ decays also provides this rich set of observables to study, however current results only yield an upper limit on $B_d^0 \to a_1^\pm \rho^\mp$ decays [853]. BaBar have recently studied the angular distribution for the vector-tensor decay $B_d^0 \to \phi K^*(1430)$ [846].

3.7.9 $B \to h^+ h'^-$ decays at LHCb

The charmless decays of B mesons to two-body modes have been extensively studied at the B-factories. Even if the current knowledge in the B_d and B_u sectors starts to be quite constrained, the B_s sector still remains an open field. At present, by using a displaced vertex trigger CDF has already collected an interesting sample of $B \to h^+ h'^-$ decays

Table 42 CP reach at LHCb [1048] and at a super-B factory for the $b \to s$ decay modes that are theoretically cleanest. The estimated accuracy from the B factories (2 ab^{-1}) is given for comparison. We assume an integrated luminosity of 10 fb^{-1} for LHCb and 50 ab^{-1} for a super B factory, which are the goals of the experiments. Errors for LHCb are statistical only. Projections for the super B factory are from Ref. [837] and include both statistical and systematic uncertainties and $\Delta \sin 2\phi_1 \equiv \sin 2\phi_1^{\mathrm{eff}} - \sin 2\phi_1$

Mode	Observable	B factories 2 ab^{-1}	LHCb 10 fb^{-1}	Super B factory 50 ab^{-1}
$B^0 \to \phi K^0$	$\Delta \sin 2\phi_1$	0.13	0.10	0.029
$B^0 \to \eta' K^0$	$\Delta \sin 2\phi_1$	0.05	–	0.020
$B^0 \to K_S^0 K_S^0 K_S^0$	$\Delta \sin 2\phi_1$	0.15	–	0.037
$B_s^0 \to \phi\phi$	$\mathcal{S}_{\phi\phi}$	–	0.05	–

[854], providing a first observation of the two-body mode $B_s \to K^+K^-$. However it will most likely not be able to perform precision measurements of the time-dependent CP asymmetry of the $B_s \to K^+K^-$ decay.

The LHCb experiment, thanks to the large beauty production cross section at the LHC and to its excellent vertexing and triggering capabilities, will be able to collect huge samples of $B \to h^+h'^-$ decays [855]. Furthermore, its particle identification system, composed in particular by two RICH detectors, will allow one to disentangle various $B \to h^+h'^-$ modes with a purity exceeding 90% as well as high efficiency. The PID capabilities of LHCb are clearly visible in Fig. 42, which shows the distribution of the $\pi^+\pi^-$ invariant mass from Monte Carlo samples of $B \to h^+h'^-$ modes, before and after the employment of the PID information.

In order to calibrate the PID response, LHCb will make use of a dedicated trigger line—not making use of PID information in order not to introduce biases—intended to collect very large samples of D^* decay chains to charged kaons and pions. In order to reject combinatorial background, the event selection is based on a series of cuts, optimized by means of a multivariate technique, which include the transverse momenta and the impact parameter significances of the charged legs with respect to the primary vertex, the χ^2 of the common vertex fit, the transverse momentum, the im-

pact parameter significance and the distance of flight significance of the candidate b-hadron and the invariant mass (the resolution for the $B \to h^+h'^-$ modes is expected to be about 18 MeV/c^2). The event yields and background-to-signal ratios estimated using a full GEANT4 based simulation are reported in Table 43.

In order to measure CP violation from the time-dependent CP asymmetries, other key ingredients are the tagging capability and the propertime resolution, the latter being particularly relevant to resolve the fast B_s oscillations. The effective tagging power for a B_d decay at LHCb, according to full simulations, is expected to be about 5%, while for a B_s decay, it is significantly larger, due to the larger efficiency of the same side kaon tagging, and is about 9%. The calibration of the tagging power for $B \to h^+h'^-$ modes will be performed by using the flavor-specific modes $B_d \to K^+\pi^-$ and $B_s \to \pi^+K^-$. As far as the propertime resolution is concerned, it is predicted by the full simulation to be about 40 fs, and it will be calibrated on data by using large samples of $J/\psi \to \mu^+\mu^-$ decays collected through a dedicated di-muon trigger line thought not to introduce biases in the J/ψ propertime.

The direct CP asymmetries of the flavor specific $B \to h^+h'^-$ modes can be measured without a time-dependent fit and without the need of tagging the B meson. The sta-
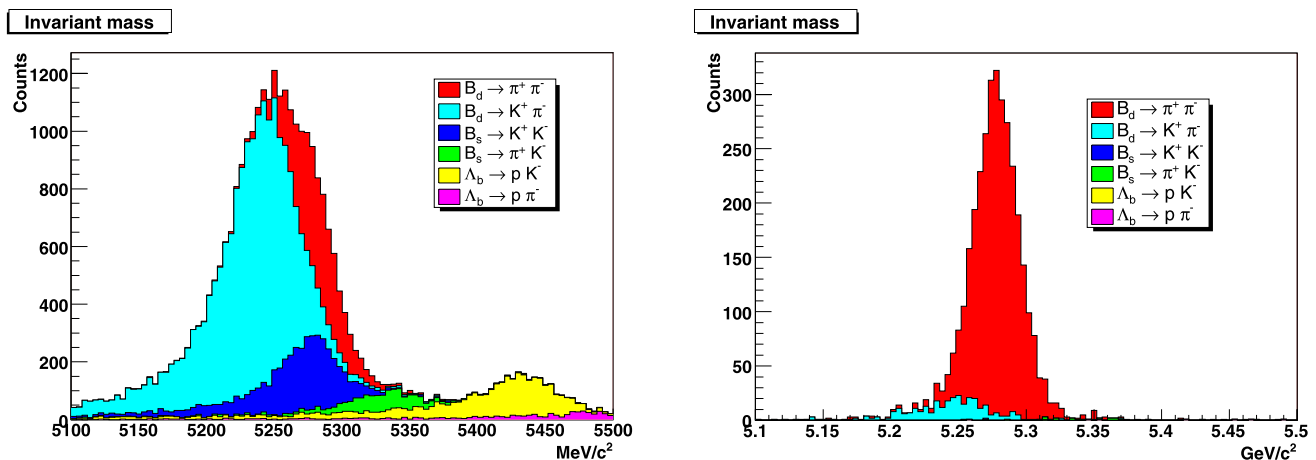

Fig. 42 *Left*: $\pi^+\pi^-$ invariant mass distribution for $B \to h^+h'^-$ decays expected at LHCb, obtained without using PID information. *Right*: same plot after PID cuts are applied

Table 43 Annual yields and background-to-signal ratios for $B \to h^+h'^-$ decays at LHCb [855]

Channel	Assumed *BR*	Annual yield	B/S (combinatorial)	B/S (two-body)
$B_d^0 \to \pi^+\pi^-$	4.8	36000	0.46	0.08
$B_d^0 \to K^+\pi^-$	18.5	138000	0.14	0.02
$B_s^0 \to \pi^+K^-$	4.8	10000	1.92	0.54
$B_s^0 \to K^+K^-$	18.5	36000	<0.06	0.08
$\Lambda_b \to p\pi^-$	4.8	9000	1.66	0.11
$\Lambda_b \to pK^-$	18.5	32000	<0.08	0.02

410

Eur. Phys. J. C (2008) 57: 309–492

tistical sensitivity on the charge asymmetry corresponding to a running time of 10^7 s at the nominal LHCb luminosity 2×10^{32} cm^{-2} s^{-1} ("one nominal LHCb year" in the following) is 0.003 for the $B_d \to K^+\pi^-$ decay and 0.02 for the $B_s \to \pi^+K^-$ decay. In order to extract the direct (C) and mixing-induced (S) CP violation terms from the time-dependent decay rates of the $B_d \to \pi^+\pi^-$ and $B_s \to K^+K^-$ and estimate the statistical sensitivity, we performed unbinned maximum likelihood fits on fast Monte Carlo data sets which parametrize the decay rates according to the outcomes of the full simulation. The expected sensitivity for C and S, corresponding to one nominal LHCb year, both for the $B_d \to \pi^+\pi^-$ and $B_s \to K^+K^-$ channels, is about 0.04.

According to the method proposed in [771], the employment of the U-spin symmetry allows us to combine the measurements of C and S for the $B_d \to \pi^+\pi^-$ and $B_s \to K^+K^-$ modes in order to extract the γ angle. Assuming a perfect U-spin symmetry, we predict a sensitivity on γ for a nominal LHCb year around 5°. If a 20% U-spin breaking is taken into account, the sensitivity deteriorates up to about 10°, still not spoiling the method of its predictive capabilities on γ. Being these modes characterized by the presence of loops inside the penguins, they could reveal NP effects, pointing to a value of γ in contrast with the one determined from pure tree-level decays, such as $B \to DK$ modes.

In Table 43, LHCb also reports expected yields for Λ_b baryon decays. An additional application of the Λ_b baryon that has been considered is testing CP and T symmetries using the decay modes $\Lambda_b \to \Lambda V$, where $V = J/\psi, \rho^0, \omega$. This is discussed in [856].

3.8 Kaon decays[25]

3.8.1 Introduction

The rare decays $K^+ \to \pi^+\nu\bar{\nu}$ and $K_L \to \pi^0\nu\bar{\nu}$ play an important role in the search for the underlying mechanism of flavor mixing and CP violation [857–860]. As such, they are excellent probes of physics beyond the Standard Model (SM). Among the many rare K- and B-decays, the $K^+ \to \pi^+\nu\bar{\nu}$ and $K_L \to \pi^0\nu\bar{\nu}$ modes are unique, since their SM branching ratios can be computed to an exceptionally high degree of precision, not matched by any other FCNC process involving quarks.

The main reason for the exceptional theoretical cleanness of the $K^+ \to \pi^+\nu\bar{\nu}$ and $K_L \to \pi^0\nu\bar{\nu}$ decays is the fact that, within the SM, these processes are mediated by electroweak amplitudes of $\mathcal{O}(G_F^2)$, described by Z^0-penguins and box diagrams which exhibit a power-like GIM mechanism. This

property implies a severe suppression of nonperturbative effects, which is generally not the case for meson decays receiving contributions of $\mathcal{O}(G_F\alpha_s)$ (gluon penguins) and/or $\mathcal{O}(G_F\alpha_{\text{em}})$ (photon penguins), which therefore have only a logarithmic GIM mechanism. A related important virtue, following from this peculiar electroweak structure, is the fact that $K \to \pi\nu\bar{\nu}$ amplitudes can be described in terms of a single effective operator, namely

$$Q_{sd}^{\nu\bar{\nu}} = (\bar{s}_L\gamma^\mu d_L)(\bar{\nu}_L\gamma_\mu \nu_L). \tag{171}$$

The hadronic matrix elements of $Q_{sd}^{\nu\bar{\nu}}$ relevant for $K \to \pi\nu\bar{\nu}$ amplitudes can be extracted directly from the well-measured $K^+ \to \pi^0 e^+\nu$ decay, including the leading isospin breaking (IB) corrections [861]. The estimation of the matrix elements is improved and extended [862] beyond the leading order analysis.

In the case of $K_L \to \pi^0\nu\bar{\nu}$, which is CP-violating and dominated by the dimension-six top quark contribution, the SM Short-Distance (SD) dynamics is then encoded in a perturbatively calculable real function X that multiplies the CKM factor $\lambda_t = V_{ts}^* V_{td}$. In the case of $K^+ \to \pi^+\nu\bar{\nu}$, also a charm-quark contribution proportional to $\lambda_c = V_{cs}^* V_{cd}$ has to be taken into account, but the recent NNLO QCD calculation of the dimension-six charm quark corrections [863, 864] and the progress in the evaluation of dimension-eight charm and long-distance (LD) up quark effects [865] elevated the theoretical cleanness of $K^+ \to \pi^+\nu\bar{\nu}$ almost to the level of $K_L \to \pi^0\nu\bar{\nu}$. More details will be given in Sect. 3.8.2.

The important virtue of $K \to \pi\nu\bar{\nu}$ decays is that their clean theoretical character remains valid in essentially all extensions of the SM and that $Q_{sd}^{\nu\bar{\nu}}$, due to the special properties of the neutrinos, remains the only relevant operator. Consequently, in most SM extensions, the NP contributions to $K^+ \to \pi^+\nu\bar{\nu}$ and $K_L \to \pi^0\nu\bar{\nu}$ can be parametrized by just two parameters, the magnitude and the phase of the function, in a model-independent manner [866]

$$X = |X|e^{i\theta_X} \tag{172}$$

that multiplies λ_t in the relevant effective Hamiltonian. In the SM, $|X| = X_{\text{SM}}$ and $\theta_X = 0$.

The parameters $|X|$ and θ_X can be extracted from $\mathcal{B}(K_L \to \pi^0\nu\bar{\nu})$ and $\mathcal{B}(K^+ \to \pi^+\nu\bar{\nu})$ without hadronic uncertainties, while the function X can be calculated in any extension of the SM within perturbation theory. Of particular interest is the ratio

$$\frac{\mathcal{B}(K_L \to \pi^0\nu\bar{\nu})}{\mathcal{B}(K_L \to \pi^0\nu\bar{\nu})_{\text{SM}}} = \left|\frac{X}{X_{\text{SM}}}\right|^2 \left[\frac{\sin(\beta - \theta_X)}{\sin\beta}\right]^2. \tag{173}$$

Bearing in mind that $\beta \approx 21.4°$, (173) shows that $K_L \to \pi^0\nu\bar{\nu}$ is a very sensitive function of the new phase θ_X. The
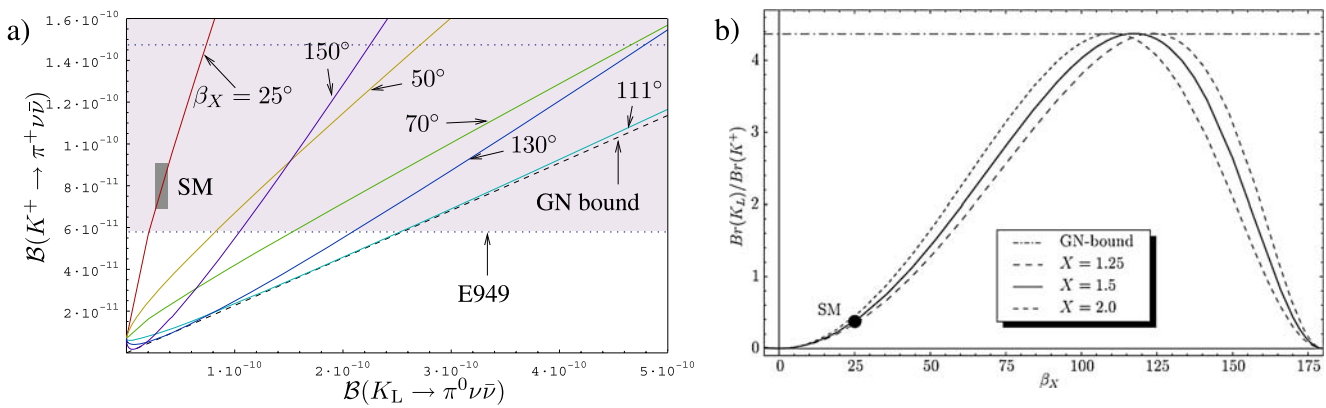
---

[25]Section coordinators: A.J. Buras, T.K. Komatsubara.

Fig. 43 (**a**) $\mathcal{B}(K^+ \to \pi^+ \nu\bar{\nu})$ vs. $\mathcal{B}(K_L \to \pi^0 \nu\bar{\nu})$ for various values of $\beta_X = \beta - \theta_X$ (including E949 data) [780]. The *dotted horizontal lines* indicate the lower part of the experimental range [867–869] and the *grey area* the SM prediction. We also show the Grossman–Nir (GN)

bound [870]. (**b**) The ratio of the $K \to \pi \nu\bar{\nu}$ branching ratios as a function of β_X for $|X| = 1.25,\ 1.5,\ 2.0$. The *horizontal line* is again the GN bound

pattern of the two $K \to \pi\nu\bar{\nu}$ branching ratios as a function of θ_X is illustrated in Fig. 43a. We note that the ratio of the two modes shown in Fig. 43b depends very mildly on $|X|$ and therefore provides an excellent tool to extract the non-standard CP-violating phase θ_X.

An interesting and complementary window to $|\Delta S| = 1$ SD transitions is provided by the $K_L \to \pi^0 \ell^+ \ell^-$ system ($\ell = \mu, e$). While the latter is theoretically not as clean as the $K \to \pi\nu\bar{\nu}$ system, it is sensitive to different types of SD operators. The $K_L \to \pi^0 \ell^+ \ell^-$ decay amplitudes have three main ingredients: (i) a clean direct-CP-violating (CPV) component determined by SD dynamics; (ii) an indirect-CPV term due to K^0–$\bar{K}^0$ mixing; (iii) an LD CP-conserving (CPC) component due to two-photon intermediate states. Although generated by very different dynamics, these three components are of comparable size and can be computed (or indirectly determined) to good accuracy within the SM [871, 872]. In the presence of nonvanishing NP contributions, the combined measurements of $K \to \pi\nu\bar{\nu}$ and $K_L \to \pi^0 \ell^+ \ell^-$ decays provide a unique tool to distinguish among different NP models.

The following discussion concentrates on the $K \to \pi\nu\bar{\nu}$ and $K_L \to \pi^0 \ell^+ \ell^-$ decays in the SM (Sects. 3.8.2 and 3.8.3) and its most popular extensions (Sects. 3.8.4 and 3.8.5). In Sect. 3.8.6, we stress the complementarity of K- and B-physics as well as the interplay with the high-p_T physics at the LHC. Recent theoretical updates on kaon decays are found in [873–875]. Experimental programs at CERN and J-PARC are described in Sects. 3.8.7 and 3.8.8,

respectively. The current experimental status is summarized in Table 44.

3.8.2 $K^+ \to \pi^+ \nu\bar{\nu}$ and $K_L \to \pi^0 \nu\bar{\nu}$ in the SM

After summation over the three lepton families the SM branching ratios for the $K \to \pi\nu\bar{\nu}$ decays can be written as

$$\mathcal{B}\big(K^+ \to \pi^+ \nu\bar{\nu}\big)_{\text{SM}}$$

$$= \kappa_+ \left[\left(\frac{\text{Im}\,\lambda_t}{\lambda^5} X_{\text{SM}} \right)^2 \right.$$

$$\left. + \left(\frac{\text{Re}\,\lambda_t}{\lambda^5} X_{\text{SM}} + \frac{\text{Re}\,\lambda_c}{\lambda}(P_c + \delta P_{c,u}) \right)^2 \right], \quad (174)$$

$$\mathcal{B}\big(K_L \to \pi^0 \nu\bar{\nu}\big)_{\text{SM}} = \kappa_L \left(\frac{\text{Im}\,\lambda_t}{\lambda^5} X_{\text{SM}} \right)^2, \quad (175)$$

where $\lambda = |V_{us}|$, while $\kappa_+ = (5.26 \pm 0.06) \times 10^{-11} (\lambda/0.225)^8$ and $\kappa_L = (2.29 \pm 0.03) \times 10^{-10} (\lambda/0.225)^8$ [879] include the leading IB corrections in relating $K \to \pi\nu\bar{\nu}$ to $K^+ \to \pi^0 e^+ \nu$ [861]. The dimension-six top-quark contribution $X_{\text{SM}} = 1.464 \pm 0.041$ [863, 864] accounts for around 63% and almost 100% of the total rates. It is known to NLO [557, 558], with a scale uncertainty of about 1%. In $K^+ \to \pi^+ \nu\bar{\nu}$, dimension-six charm quark corrections and subleading dimension-eight charm and LD up quark effects, characterized by $P_c = 0.38 \pm 0.04$ [863, 864] and

Table 44 Current experimental results or limits for rare K decay branching fractions	$B(K^+ \to \pi^+ \nu\bar{\nu})$	$B(K_L \to \pi^0 \nu\bar{\nu})$	$B(K_L \to \pi^0 e^+ e^-)$	$B(K_L \to \pi^0 \mu^+ \mu^-)$
	$(1.47^{+1.30}_{-0.89}) \times 10^{-10}$	$< 6.7 \times 10^{-8}$	$< 2.8 \times 10^{-10}$	$< 3.8 \times 10^{-10}$
	[867–869]	[876]	[877]	[878]

412

Eur. Phys. J. C (2008) 57: 309–492

$\delta P_{c,u} = 0.04 \pm 0.02$ [865], amount to a moderate 33% and a mere 4%. Light quark contributions are negligible in the case of the $K_L \to \pi^0 \nu\bar{\nu}$ decay [880].

Taking into account all the indirect constraints from the latest global UT fit, the SM predictions for the two $K \to \pi \nu\bar{\nu}$ rates read

$$\begin{aligned} \mathcal{B}(K^+ \to \pi^+ \nu\bar{\nu})_{\mathrm{SM}} &= (8.4 \pm 1.0) \times 10^{-11}, \\ \mathcal{B}(K_L \to \pi^0 \nu\bar{\nu})_{\mathrm{SM}} &= (2.7 \pm 0.4) \times 10^{-11}. \end{aligned} \tag{176}$$

The quoted central value of $K^+ \to \pi^+ \nu\bar{\nu}$ corresponds to $m_c = 1.3\,\mathrm{GeV}$, and the given error breaks down as follows: residual scale uncertainties (13%), m_c (22%), CKM, α_s, and m_t (37%), and matrix-elements from $K^+ \to \pi^0 e^+ \nu$ and light quark contributions (28%). The main source of uncertainty in $K_L \to \pi^0 \nu\bar{\nu}$ is parametric (74%), while the impact of scales (11%) and IB (15%) is subdominant. SM predictions for $K \to \pi \nu\bar{\nu}$ with total uncertainties at the level of 5% or below are thus possible through a better knowledge of m_c, of the IB in the $K \to \pi$ form factors, and/or by a lattice study [881] of higher-dimensional and LD contributions.

While the determination of $|V_{td}|$, $\sin 2\beta$, and γ from the $K \to \pi \nu\bar{\nu}$ system is without doubt still of interest, with the slow progress in measuring the relevant branching ratios and much faster progress in the extraction of the angle γ from the $B_s \to DK$ system to be expected at the LHC, the role of the $K \to \pi \nu\bar{\nu}$ system will shift towards the search for NP rather than the determination of the CKM parameters.

In fact, determining the UT from tree-level dominated K- and B-decays and thus independently of NP will allow us to find the "true" values of the CKM parameters. Inserting these, hopefully accurate, values in (174) and (175) will allow us to obtain very precise SM predictions for the rates of both rare K-decays. A comparison with future data on $K \to \pi \nu\bar{\nu}$ may then give a clear signal of potential NP contributions in a theoretically clean environment. Even deviations by 20% from the SM expectations could be considered as signals of NP, while such a conclusion cannot be drawn in most other decays, in which the theoretical errors are at least 10%.

3.8.3 $K_L \to \pi^0 \ell^+ \ell^-$ in the SM

As mentioned in the introduction, the $K_L \to \pi^0 \ell^+ \ell^-$ amplitudes have three main components. The interesting direct-CPV component, proportional to $\mathrm{Im}\lambda_t$, is generated by Z^0-, γ-penguins and box diagrams and is SD dominated. It is encoded by local dimension-six vector $Q_{7V} = (\bar{s}d)_V (\bar{\ell}\ell)_V$

and axial-vector $Q_{7A} = (\bar{s}d)_V (\bar{\ell}\ell)_A$ operators, whose Wilson coefficients $y_{7V,7A}$ are known to NLO [882]. The former produces the $\ell^+\ell^-$ pair in a 1^{--} state, the latter both in 1^{++} and 0^{-+} states. As in the $K \to \pi\nu\bar{\nu}$ case, the corresponding hadronic matrix elements are obtained precisely from $K_{\ell 3}$ decays [861].

The other two components are of electromagnetic origin and are dominated by LD dynamics. These contributions cannot be computed from first principles. However, they can be related to measurable quantities within Chiral Perturbation Theory (CHPT). The indirect CPV amplitude, $\mathcal{A}(K_L \approx \varepsilon K_1 \to \pi^0 \gamma^* \to \pi^0 \ell^+ \ell^-)$, is determined [883]— up to a sign ambiguity—by the measurements of $\mathcal{B}(K_S \to \pi^0 \ell^+ \ell^-)$. In this case, the $\ell^+\ell^-$ pair is produced in a 1^{--} state and interferes with the SD contribution of Q_{7V}. As discussed in [871, 884], various theoretical arguments point toward a constructive interference. Finally, the CPC contribution ($K_L \to \pi^0 \gamma^* \gamma^* \to \pi^0 \ell^+ \ell^-$) produces the $\ell^+\ell^-$ pair either in a helicity-suppressed 0^{++} state or in a phase-space suppressed 2^{++} state. Within CHPT, only the 0^{++} state is produced at LO through the finite two-loop process $K_L \to \pi^0 P^+ P^- \to \pi^0 \gamma\gamma \to \pi^0 \ell^+ \ell^-$ ($P = \pi, K$). Higher-order corrections are estimated using $K_L \to \pi^0 \gamma\gamma$ experimental data for both the 0^{++} and 2^{++} contributions [871, 872].

Altogether, the branching ratios can be expressed as [871, 872]

$$\begin{aligned} &\mathcal{B}(K_L \to \pi^0 \ell^+ \ell^-) \\ &= \left(C_{\mathrm{dir}}^\ell \pm C_{\mathrm{int}}^\ell |a_S| + C_{\mathrm{mix}}^\ell |a_S|^2 + C_{\gamma\gamma}^\ell \right) \times 10^{-12}, \end{aligned} \tag{177}$$

where the C_i are reported in Table 45, $w_{7A,7V} = \mathrm{Im}(\lambda_t y_{7A,7V})/\mathrm{Im}\lambda_t$, and $|a_S| = 1.2 \pm 0.2$ is fixed from $\mathcal{B}^{\mathrm{exp}}(K_S \to \pi^0 \ell^+ \ell^-)$ [885, 886]. Using the SM values of $y_{7A,7V}$ [882], the predicted rates are

$$\begin{aligned} \mathcal{B}_{\mathrm{SM}}^{e^+e^-} &= 3.54^{+0.98}_{-0.85}(1.56^{+0.62}_{-0.49}) \times 10^{-11}, \\ \mathcal{B}_{\mathrm{SM}}^{\mu^+\mu^-} &= 1.41^{+0.28}_{-0.26}(0.95^{+0.22}_{-0.21}) \times 10^{-11} \end{aligned} \tag{178}$$

for constructive (destructive) interference. Currently, the theory error (see Fig. 46a) is dominated by the uncertainty on $|a_S|$. Better measurements of $\mathcal{B}(K_S \to \pi^0 \ell^+ \ell^-)$ would thus be very welcome. Also, better measurements of $K_L \to \pi^0 \gamma\gamma$ would help in reducing the error on the 0^{++} and 2^{++} contributions. Alternatively, they can be partially cut away through energy cuts or Dalitz plot analyses [871, 872, 887]. As shown in Fig. 46a, the irreducible theoretical errors on

Table 45 Numerical coefficients for the evaluation of $\mathcal{B}(K_L \to \pi^0 \ell^+ \ell^-)$ as given in (177)

	C_{dir}^ℓ	C_{int}^ℓ	C_{mix}^ℓ	$C_{\gamma\gamma}^\ell$
$\ell = e$	$(4.62 \pm 0.24)(w_{7V}^2 + w_{7A}^2)$	$(11.3 \pm 0.3)w_{7V}$	$14.5 \pm 0.5,$	≈ 0
$\ell = \mu$	$(1.09 \pm 0.05)(w_{7V}^2 + 2.32w_{7A}^2)$	$(2.63 \pm 0.06)w_{7V}$	3.36 ± 0.20	5.2 ± 1.6

these modes can be pushed below the 10% level, allowing very significant tests of flavor physics.

The integrated forward–backward (or lepton-energy) asymmetry (see references in [887]) generated by the interference between CPC and CPV amplitudes cannot be reliably estimated at present for $\ell = e$ because of the poor theoretical control on the 2^{++} contribution. In the case of A_{FB}^{μ}, the situation is better, since the 2^{++} part is negligible. One has $A_{FB}^{\mu} \approx 20\%$ (-12%) for constructive (destructive) interference. Interestingly, though the error is large, A_{FB}^{μ} can be used to fix the sign of a_S.

Let us close with a short comment on $K_L \to \mu^+\mu^-$. Here the SD part is CPC and has recently been evaluated at NNLO [888]. The much larger LD contribution proceeds via two photons. While its absorptive part is fixed from $K_L \to \gamma\gamma$, its dispersive part is difficult to estimate, requiring unknown counterterms in CHPT [889]. Moreover, in this case, the two-photon LD amplitude interferes with the SD one (they both produce a lepton pair in a 0^{-+} state). This interference, which depends on the sign of $\mathcal{A}(K_L \to \gamma\gamma)$, is presumably constructive [890], and better measurements of $K_S \to \pi^0\gamma\gamma$ or $K^+ \to \pi^+\gamma\gamma$ could settle this sign. However, even with the help of this information it is difficult to reduce the theoretical error below $\sim 50\%$ of the SD contribution.

3.8.4 $K^+ \to \pi^+\nu\bar{\nu}$ and $K_L \to \pi^0\nu\bar{\nu}$ beyond the SM

Minimal flavor violation In models with Minimal Flavor Violation (MFV) [10, 12], both decays are, like in the SM, governed by a single real function X that can take a different value than in the SM due to new particle exchange in the relevant Z^0-penguin and box diagrams (see Fig. 43a). Restricting first our discussion to the so-called constrained MFV (CMFV) (see [891]), in which strong correlations between K- and B-decays exist, one finds that the branching ratios for $K^+ \to \pi^+\nu\bar{\nu}$ and $K_L \to \pi^0\nu\bar{\nu}$ cannot be much larger than their SM values given in (176). The 95% probability bounds read [190]

$$\mathcal{B}(K^+ \to \pi^+\nu\bar{\nu})_{\mathrm{CMFV}} \leq 11.9 \times 10^{-11},$$
$$\mathcal{B}(K_L \to \pi^0\nu\bar{\nu})_{\mathrm{CMFV}} \leq 4.6 \times 10^{-11}. \tag{179}$$

Explicit calculations in a model with one Universal Extra Dimension (UED) [181] and in the Littlest Higgs model without T-parity [142] give explicit examples of this scenario with the branching ratios within 20% of the SM expectations. The latest detailed analysis of $K \to \pi\nu\bar{\nu}$ in the MSSM with MFV can be found in [879].

Probably the most interesting property of this class of models is a theoretically clean determination of the angle β of the standard UT, which utilizes both branching ratios and is independent of the value of X [892, 893]. Consequently,

this determination is universal within the class of MFV models, and any departure of the resulting value of β from the corresponding one measured in B-decays would signal non-MFV interactions.

Littlest Higgs model with T-parity The structure of $K \to \pi\nu\bar{\nu}$ decays in the Littlest Higgs model with T-parity (LHT) differs notably from the one found in MFV models due to the presence of mirror quarks and leptons that interact with the light fermions through the exchange of heavy charged ($W_H^{\pm}$) and neutral (Z_H^0, A_H^0) gauge bosons. The mixing matrix V_{Hd} that governs these interactions can differ from V_{CKM}, which implies the presence of non-MFV interactions. Instead of a single real function X that is universal within the K-, B_d- and B_s-systems in MFV models, one now has three functions

$$X_K = |X_K|e^{i\theta_K}, \qquad X_d = |X_d|e^{i\theta_d}, \qquad X_s = |X_s|e^{i\theta_s} \tag{180}$$

that due to the presence of mirror fermions can have different phases and magnitudes.

Moreover, it is important to note that mirror fermion contributions are enhanced by a CKM factor $1/\lambda_t^{(i)}$ with $i = K, d, s$ for the K-, B_d- and B_s-systems, respectively. As $\lambda_t^{(K)} \simeq 4 \times 10^{-4}$, whereas $\lambda_t^{(d)} \simeq 1 \times 10^{-2}$ and $\lambda_t^{(s)} \simeq 4 \times 10^{-2}$, the deviation from the SM prediction in the K-system is found to be by more than an order of magnitude larger than in the B_d-system and even by two orders of magnitude larger than in the B_s-system. This possibility can have a major impact on the $K \to \pi\nu\bar{\nu}$ system, since the correlations between K- and B-decays are partially lost and the presence of a large phase θ_K can change the pattern of these decays from the one observed in MFV. A detailed analysis [158] shows that both branching ratios can depart significantly from their SM values and can be as high as 5.0×10^{-10}. As shown in Fig. 44a, there are two branches of allowed values with strong correlations between both branching ratios within a given branch. In the lower branch, only $\mathcal{B}(K^+ \to \pi^+\nu\bar{\nu})$ can differ substantially from the SM expectations reaching values well above the present central experimental value. In the second branch, $\mathcal{B}(K_L \to \pi^0\nu\bar{\nu})$ and $\mathcal{B}(K^+ \to \pi^+\nu\bar{\nu})$ can be as high as 5.0×10^{-10} and 2.3×10^{-10}, respectively. Moreover, $\mathcal{B}(K_L \to \pi^0\nu\bar{\nu})$ can be larger than $\mathcal{B}(K^+ \to \pi^+\nu\bar{\nu})$, which is excluded within MFV models. Other features distinguishing this model from MFV are thoroughly discussed in [158].

Supersymmetry Within the MSSM with R-parity conservation, sizable nonstandard contributions to $K \to \pi\nu\bar{\nu}$ decays can be generated if the soft-breaking terms have a non-MFV structure. The leading amplitudes giving rise to large effects are induced by: (i) chargino/up-squark loops [131,
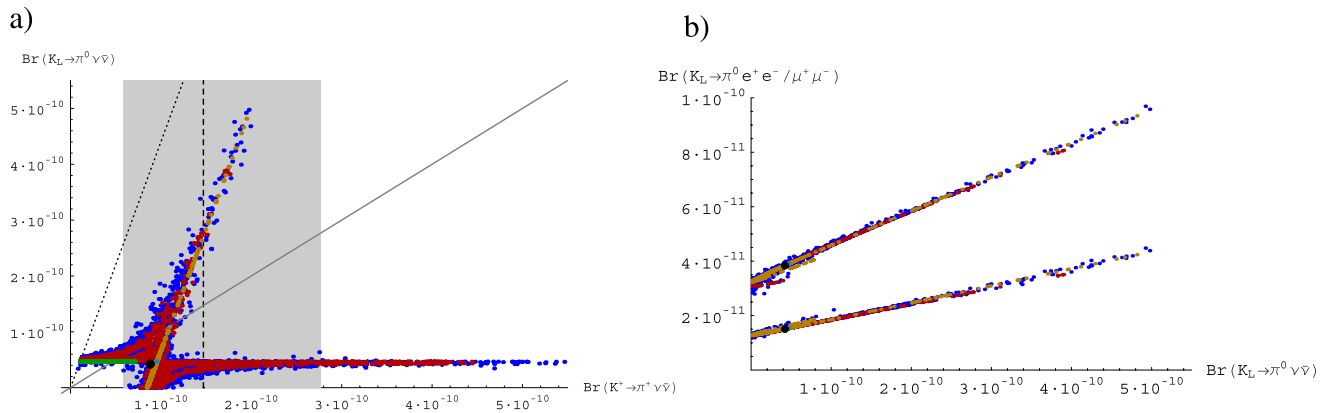
414

Eur. Phys. J. C (2008) 57: 309–492

a)

b)

Fig. 44 (**a**) $\mathcal{B}(K_L \to \pi^0 \nu\bar{\nu})$ vs. $\mathcal{B}(K^+ \to \pi^+ \nu\bar{\nu})$ in the LHT model [158]. The *shaded area* represents the experimental 1σ-range for $\mathcal{B}(K^+ \to \pi^+ \nu\bar{\nu})$. The GN bound is displayed by the *dotted line*, while the *solid line* separates the two areas where $\mathcal{B}(K_L \to \pi^0 \nu\bar{\nu})$ is larger or smaller than $\mathcal{B}(K^+ \to \pi^+ \nu\bar{\nu})$. (**b**) $\mathcal{B}(K_L \to \pi^0 e^+ e^-)$ (*upper curve*) and $\mathcal{B}(K_L \to \pi^0 \mu^+ \mu^-)$ (*lower curve*) as functions of $\mathcal{B}(K_L \to \pi^0 \nu\bar{\nu})$ in the LHT model [158]

866, 894, 895]; (ii) charged Higgs/top quark loops [896]. In the first case, large effects are generated if the left–right mixing (*A* term) of the up-squarks has a non-MFV structure [10]. In the second case, deviations from the SM are induced by non-MFV terms in the right–right down sector, provided that the ratio of the two Higgs vacuum expectation values ($\tan\beta = v_u/v_d$) is large ($\tan\beta \sim 30$–50).

The effective Hamiltonian encoding SD contributions in the general MSSM has the following structure:

$$\mathcal{H}_{\text{eff}}^{\text{(SD)}} \propto \sum_{l=e,\mu,\tau} V_{ts}^* V_{td} \big[X_L (\bar{s}_L \gamma^\mu d_L)(\bar{\nu}_{lL} \gamma_\mu \nu_{lL}) $$
$$+ X_R (\bar{s}_R \gamma^\mu d_R)(\bar{\nu}_{lL} \gamma_\mu \nu_{lL}) \big], \qquad (181)$$

where the SM case is recovered for $X_R = 0$ and $X_L = X_{\text{SM}}$. In general, both X_R and X_L are nonvanishing, and the misalignment between quark and squark flavor structures implies that they are both complex quantities. Since the $K \to \pi$ matrix elements of $(\bar{s}_L \gamma^\mu d_L)$ and $(\bar{s}_R \gamma^\mu d_R)$ are equal, the combination $X_L + X_R$ allows us to describe all the SD contributions to $K \to \pi\nu\bar{\nu}$ decays. More precisely, we can simply use the SM expressions for the branching ratios in (174) to (175) with the replacement

$$X_{\text{SM}} \to X_{\text{SM}} + X_L^{\text{SUSY}} + X_R^{\text{SUSY}}. \qquad (182)$$

In the limit of almost degenerate superpartners, the leading chargino/up-squarks contribution is [895]

$$X_L^{\chi^\pm} \approx \frac{1}{96} \left[\frac{(\delta_{LR}^u)_{23}(\delta_{RL}^u)_{31}}{\lambda_t} \right] = \frac{1}{96\lambda_t} \frac{(\tilde{M}_u^2)_{2L3R}(\tilde{M}_u^2)_{3R1L}}{(\tilde{M}_u^2)_{LL}(\tilde{M}_u^2)_{RR}}. \qquad (183)$$

As pointed out in [895], a remarkable feature of the above result is that no extra $\mathcal{O}(M_W/M_{\text{SUSY}})$ suppression and no explicit CKM suppression is present (as it happens in the chargino/up-squark contributions to other processes). Furthermore, the (δ_{LR}^u)-type mass insertions are not strongly constrained by other *B*- and *K*-observables. This implies that large departures from the SM expectations in $K \to \pi\nu\bar{\nu}$ decays are allowed, as confirmed by the complete analyses in [192, 879]. As illustrated in Fig. 45a, $K \to \pi\nu\bar{\nu}$ are the best observables to determine/constrain from experimental data the size of the off-diagonal (δ_{LR}^u) mass insertions or, equivalently, the up-type trilinear terms A_{i3} [$(\tilde{M}_u^2)_{iL3R} \approx m_t A_{i3}$]. Their measurement is therefore extremely interesting also in the LHC era.

In the large $\tan\beta$ limit, the charged Higgs/top quark exchange leads to [896]

$$X_R^{H^\pm} \approx \left[\left(\frac{m_s m_d t_\beta^2}{2M_W^2} \right) \right.$$
$$+ \frac{(\delta_{RR}^d)_{31}(\delta_{RR}^d)_{32}}{\lambda_t} \left(\frac{m_b^2 t_\beta^2}{2M_W^2} \right) \frac{\epsilon_{RR}^2 t_\beta^2}{(1+\epsilon_i t_\beta)^4} \right]$$
$$\times f_H(y_{tH}), \qquad (184)$$

where $y_{tH} = m_t^2/M_H^2$, $f_H(x) = x/4(1-x) + x \log x/4(x-1)^2$ and $\epsilon_{i,RR} t_\beta = \mathcal{O}(1)$ for $t_\beta = \tan\beta \sim 50$. The first term of (184) arises from MFV effects, and its potential $\tan\beta$ enhancement is more than compensated by the smallness of $m_{d,s}$. The second term on the r.h.s. of (184), which would appear only at the three-loop level in a standard loop expansion, can be largely enhanced by the $\tan^4\beta$ factor and does not contain any suppression due to light quark masses. Similarly to the double mass-insertion mechanism of (183), also in this case the potentially leading effect is the one generated when two off-diagonal squark mixing terms replace the two CKM factors V_{ts} and V_{td}.
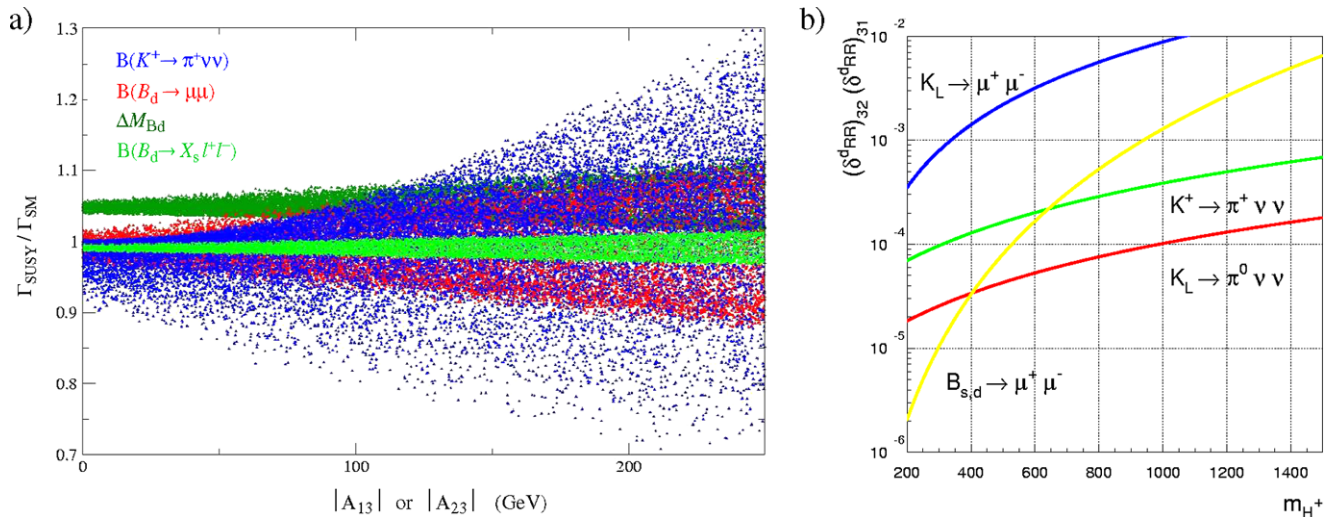
Fig. 45 Supersymmetric contributions to $K \to \pi \nu \bar{\nu}$. (**a**) Dependence of various FCNC observables (normalized to their SM value) on the up-type trilinear terms A_{13} and A_{23} for $A_{ij} \leq \lambda A_0$ and $\tan \beta = 2$–4 (other key parameters in GeV: $\mu = 500 \pm 10$, $M_2 = 300 \pm 10$, $M_{\tilde{u}_R} = 600 \pm 20$, $M_{\tilde{q}_L} = 800 \pm 20$, $A_0 = 1000$) [879]. (**b**) Sensitivity to $(\delta^d_{RR})_{23}(\delta^d_{RR})_{31}$ of various rare K- and B-decays as a function of M_{H^+}, setting $\tan \beta = 50$, $\mu < 0$ and assuming almost degenerate superpartners (the bounds from the two $K \to \pi \nu \bar{\nu}$ modes are obtained assuming a 10% measurement of their branching ratios, while the $B_{s,d} \to \mu^+ \mu^-$ bounds refer to the present experimental limits [896])

The coupling of the $(\bar{s}_R \gamma^\mu d_R)(\bar{\nu}_L \gamma_\mu \nu_L)$ effective FCNC operator generated by charged-Higgs/top quark loops is phenomenologically relevant only at large $\tan \beta$ and with non-MFV right–right soft-breaking terms: a specific but well-motivated scenario within grand-unified theories (see e.g. [897, 898]). These nonstandard effects do not vanish in the limit of heavy squarks and gauginos and have a slow decoupling with respect to the charged-Higgs boson mass. As shown in [896], the B-physics constraints still allow a large room of nonstandard effects in $K \to \pi \nu \bar{\nu}$ even for flavor-mixing terms of CKM size (see Fig. 45b).

3.8.5 $K_L \to \pi^0 \ell^+ \ell^-$ beyond the SM

Within the SM, $K_L \to \pi^0 e^+ e^-$ and $K_L \to \pi^0 \mu^+ \mu^-$ decays have a very similar dynamics but for the different lepton masses. This makes them an ideal probe of NP effects when taken in combination [872, 887]. Moreover, $K_L \to \pi^0 \mu^+ \mu^-$ is sensitive to Higgs-induced helicity-suppressed operators, to which $K \to \pi \nu \bar{\nu}$ (and $K_L \to \pi^0 e^+ e^-$) are blind.

NP with SM operators In many scenarios, such as enhanced electroweak penguins (EEWP) [780], the MSSM at moderate $\tan \beta$ [899], Little Higgs models (LHT) [158], UED [181] and leptoquark models [900], NP only modifies the strength of the SM operators, without introducing new structures. In general, these models induce larger effects for $K_L \to \pi^0 \nu \bar{\nu}$ than for $K_L \to \pi^0 \ell^+ \ell^-$. Still, the latter modes should not be disregarded as they offer the possibility to disentangle effects in the vector and axial-vector

currents. Indeed, Q_{7A} produces the final lepton pair also in a helicity-suppressed 0^{-+} state, hence contributes differently to $K_L \to \pi^0 e^+ e^-$ and $K_L \to \pi^0 \mu^+ \mu^-$, while the Q_{7V} contributions are identical for both modes (up to phase-space corrections, and assuming lepton flavor universality) [872].

As a consequence, the area spanned in the $\mathcal{B}(K_L \to \pi^0 e^+ e^-) - \mathcal{B}(K_L \to \pi^0 \mu^+ \mu^-)$ plane for arbitrary $w_{7A,7V}$ is nontrivial, see Fig. 46b. Taking all errors into account, this translates into the bounds $0.1 + 0.24 \mathcal{B}^{ee} \leq \mathcal{B}^{\mu\mu} \leq 0.6 + 0.58 \mathcal{B}^{ee}$ with $\mathcal{B}^{\ell\ell} = \mathcal{B}(K_L \to \pi^0 \ell^+ \ell^-) \times 10^{11}$ [887].

Usually, in specific models, there are correlations between the effects of NP on Q_{7V} and Q_{7A} operators. In the MSSM at moderate $\tan \beta$, the dominant effect is due to chargino contributions to Z^0- and γ-penguins [131, 866, 894, 895] sensitive to the double up-squark mass insertions. Since Z^0- and γ-penguins are correlated, so are Q_{7V} and Q_{7A}, and only a subregion of the red area can be reached. This is true whether or not there are new CP-phases. Interestingly, in the LHT model [158], the contributions to w_{7V} cancel each other to a large extent, leading to a quasi one-to-one correspondence, see Fig. 44b. This constitutes a powerful test of the model. In the case of MFV, the overall effect is found to be always smaller than for $K_L \to \pi^0 \nu \bar{\nu}$, with a maximum enhancement w.r.t. the SM of about 10% [879]. Finally, the contribution of the dipole operator $(\bar{s} \sigma^{\mu\nu} d) F_{\mu\nu}$ can be absorbed into w_{7V} [131], and NP contributions of this type cannot be singled out.

NP with new operators NP could of course also induce new operators. A systematic analysis of the impact of all possible dimension-six semileptonic operators on

416

Eur. Phys. J. C (2008) 57: 309–492

$K_L \to \pi^0 \ell^+ \ell^-$ can be found in [887]. Here we concentrate on the most interesting case of (pseudo-)scalar operators $Q_S = (\bar{s}d)(\bar{\ell}\ell)$ and $Q_P = (\bar{s}d)(\bar{\ell}\gamma_5\ell)$ inducing a CPC (CPV) contribution. These operators are enhanced in the MSSM at large $\tan\beta$ where they originate from neutral Higgs exchanges and are sensitive to down-squark mass insertions [563]. Being helicity-suppressed, they affect only the muon mode and can lead to a clear signal outside the red region in Fig. 46b. Of course, in the MSSM, the $(\bar{s}\gamma_5 d)(\bar{\ell}\ell)$ and $(\bar{s}\gamma_5 d)(\bar{\ell}\gamma_5\ell)$ operators contributing to $K_L \to \ell^+\ell^-$ are also generated. Interestingly, the current $\mathcal{B}(K_L \to \mu^+\mu^-)^{\mathrm{exp}}$ still leaves open the large yellow region in Fig. 46b, when combined with general $Q_{7V,7A}$ operators.

Finally, note that tree-level leptoquark exchange [900] or sneutrino exchange in SUSY without R-parity [901–904] can also induce (pseudo-)scalar operators but without helicity-suppression. However, to evade the strong constraint from $\mathcal{B}(K_L \to e^+e^-)^{\mathrm{exp}} = (9^{+6}_{-4}) \times 10^{-12}$, one would need to invoke a large breaking of lepton-flavor universality to have a visible effect in $K_L \to \pi^0\mu^+\mu^-$.

3.8.6 Conclusions on the theoretical prospects

Rare K-decays are excellent probes of NP. Firstly, their exceptional cleanness allows one to access very high energy scales. As stressed recently in [35, 158, 860, 879], NP could be seen in rare K-decays without significant signals in $B_{d,s}$-decays and, in specific scenarios, even without new particles within the LHC reach. Secondly, if LHC finds NP, its energy scale will be fixed. Then, the combined measurements of the four rare K-modes would help in discriminating among NP models. For instance, we have seen that specific corre-

lations exist in MFV or LHT, which can be used as powerful tests (see Fig. 44). Further, in all cases, the information extracted from the four modes is essential to establish the NP flavor structure in the $s \to d$ sector, as illustrated in the MSSM at both moderate (see Fig. 45a) and large $\tan\beta$ (see Figs. 45b and 46b). Rare K-decays are thus an integral part, along with B-physics and collider observables, of the grand project of reconstructing the NP model from data. Experimentally, together with these very rare modes, improving bounds on forbidden decays (e.g. $K \to \pi e\mu$) can be interesting. Also, rare K-decays would benefit from experimental progress in (less rare) radiative K-decays like $K_S \to \pi^0 \ell^+\ell^-$ (see Fig. 46a). For all these reasons, it is very important to pursue ambitious K-physics programs in the era of the LHC.

3.8.7 Program at CERN

The proposed experiment NA62 (formerly NA48/3) at CERN-SPS [905] aims to collect about 80 $K^+ \to \pi^+\nu\bar{\nu}$ events with an excellent signal over background ratio in two years of running, allowing for a 10% measurement of the branching ratio of the $K^+ \to \pi^+\nu\bar{\nu}$ decay. The data taking should start in 2010. NA62 will replace the NA48 apparatus at CERN and will make use of the existing beam line. The layout of the experiment is sketched in Fig. 47.

The experiment proposes to exploit a kaon decay in flight technique to achieve 10% of signal acceptance. An intense 400 GeV/c proton beam, extracted from the SPS, produces a secondary charged beam by impinging on a Be target. A 100 m long beam line selects a 75 GeV/c momentum beam with a 1% RMS momentum band. This beam covers
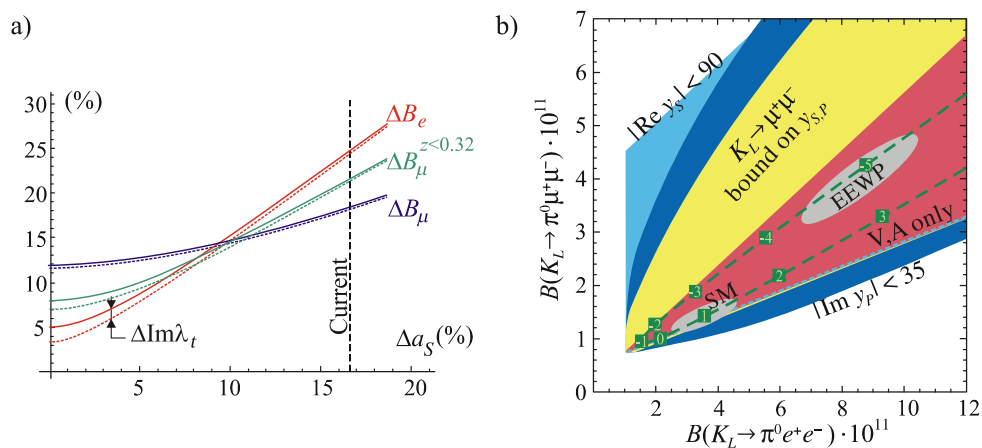

Fig. 46 (Color online) (**a**) Theory error as a function of the error on $|a_S|$. (**b**) $\mathcal{B}(K_L \to \pi^0\mu^+\mu^-)$ against $\mathcal{B}(K_L \to \pi^0 e^+e^-)$ for various NP scenarios [887]. The *red sector* is allowed for the Wilson coefficients y_{7A} and y_{7V}, exclusively, to take arbitrary values; the *green broken line* with squares corresponds to a common rescaling of the two coefficients. The LHT result of [158] lies between EEWP and

V, *A* only. *Light blue* (*dark blue*) corresponds to arbitrary $y_{7A,7V}$ together with $|\operatorname{Re} y_S| < 90$ ($|\operatorname{Im} y_P| < 35$), respectively, while the *yellow region* corresponds to $y_{7A,7V,S,P}$ arbitrary but compatible with the $\mathcal{B}(K_L \to \mu^+\mu^-)$ measurement, where y_S and y_S are the coefficients for scalar and pseudoscalar operators

Fig. 47 Layout of the NA62 (NA48/3) experiment

a 16 cm^2 area, has an average rate of about 800 MHz and is composed by 6% of K^+ and 94% of π^+, e^+ and protons. A differential Cerenkov counter (CEDAR) placed along the beam line ensures a positive kaon identification. The beam enters in a 80 m long decay region evacuated at a level of 10^{-6} mbar, enough to avoid sizable background from the interaction of the particles with the residual gas. The kaon decay rate in the decay region is about 6 MHz: it provides about 10^{13} K^+ decays in two years of data taking, assuming 100 days as running time at 60% of efficiency, which is a very realistic estimate based on the decennial NA48 experience at the SPS.

The experimental signature of a $K^+ \to \pi^+ \nu \bar{\nu}$ is one reconstructed positive track in the downstream detector. The squared missing mass allows a kinematical separation between the signal and about 90% of the total background (see Fig. 48). The precise kinematical reconstruction of the event requires a performing tracking system for the beam particles and the charged decay products of the kaons.

The beam tracker consists of three Si pixels stations (SPIBES) having a surface of 36×48 mm^2. The charged

particle rate on each station is about 60 MHz cm^{-2} on average. The stations are made up by 300×300 μm^2 pixels, 300 μm thick and containing the sensor and the chip bump-bonded on it. At least 200 ps time resolution per station is required to provide a suitable tag of the kaon track. A mistagging of the kaon, in fact, may be a source of background, because it spoils the resolution of the reconstructed squared missing mass.

Six straw chambers, 0.5% radiation length thick, placed in the same vacuum of the decay region form the downstream spectrometer. Two magnets provide a redundant measurement of the particle momentum, useful to keep the non-Gaussian tails of the reconstruction under control. The central hole of each station, which lets the undecayed beam pass through, must be displaced in the bending plane of the magnets according to the path of the 75 GeV/c positive beam. This configuration allows the tracker to be used as a veto for negative particles up to 60 GeV/c, needed for the rejection of backgrounds like $K^+ \to \pi^+ \pi^- e^+ \nu$. A reduced size prototype will be built and tested in 2007.

Fig. 48 Squared missing mass for kaon decays. The squared missing mass is defined as the square of the difference between the 4-momentum of the kaon and of the decayed track in the hypothesis that it is a pion

418

Eur. Phys. J. C (2008) 57: 309–492

A system of γ vetoes, a μ veto and a RICH complement the tracking system to guarantee a 10^{13} level of background rejection.

A 18 m long RICH located after the spectrometer and filled with Ne at atmospheric pressure is the core of the $e^+/\pi/\mu$ separation. A 11 cm radius beam pipe crosses the RICH, and two tilted mirrors at the end reflect the Cerenkov light toward an array of about 2000 phototubes placed in the focal plane. Simulations showed that enough photoelectrons can be collected per track to achieve a better than 3σ π/μ separation between 15 and 35 GeV/c. The RICH provides also the timing of the downstream track with a 100 ps time resolution. The construction and test of a full length prototype is planned for 2007.

A combination of calorimeters covering up to 50 mrad serves to identify the photons. Ring-shaped calorimeters, most of them laying in the high vacuum of the decay region, cover the angular region between 10 and 50 mrad. Tests on prototypes built using lead scintillator tiles and scintillating fibers are scheduled for 2007 at a tagged γ facility at LNF. The existing NA48 liquid krypton calorimeter (LKr) [906] is intended to be used as a veto for γ down to 1 mrad. Data taken by NA48/2 in 2004 and a test run performed in 2006 using a tagged γ beam at CERN show that the LKr matches our requests in terms of efficiency. A program of consolidation and update of the readout electronics of the LKr is under way. Small calorimeters around the beam pipe and behind the muon veto cover the low angle region.

Six meters of alternated plates of iron and extruded scintillators form a hadronic sampling calorimeter (MAMUD) able to provide a 10^5 μ rejection. An aperture in the center lets the beam pass through, and a magnetic field inside deflects the beam out of the acceptance of the last γ veto.

Simulations of the whole apparatus based on GEANT3 and GEANT4 showed that 10% signal acceptance are safely achievable. The use of the RICH constrains the accepted pion track within the (15, 35) GeV/c momentum range. The higher cut is an important loss of signal acceptance but assures that events like $K^+ \to \pi^+\pi^0$ deposit at least 40 GeV of electromagnetic energy, making their rejection easier. The simulations indicate that a 10% background level is nearly achievable.

The overall experimental design requires a sophisticated technology for which an intense R&D program is started. Actually we propose an experiment able to reach a sensitivity of 10^{-12} per event, employing existing infrastructure and detectors at CERN.

3.8.8 Program at J-PARC

The Japan Proton Accelerator Research Complex (J-PARC) [907] is a new facility being constructed in the Tokai area of Japan as a joint project of High Energy Accelerator Research Organization (KEK) and Japan Atomic Energy Agency. Slow-extracted proton beam, which is of 30 GeV and whose intensity is 2×10^{14} protons per 0.7-s spill every 3.3 s at the Phase-1, is transported to the experimental area called NP Hall (Fig. 49). The proton beam hits the target and produces a variety of secondary particles, including low-energy K^+'s and K_L's.

The first PAC meeting for Nuclear and Particle Physics Experiments at J-PARC was held in the early summer of 2006 [908]. Concerning kaon physics, two proposals, "Measurement of T-violating Transverse Muon Polarization in $K^+ \to \pi^0\mu^+\nu$ Decays" and "Proposal for $K_L \to \pi^0\nu\bar{\nu}$ Experiment at J-Parc" received scientific approval. The latter proposal on the $K_L \to \pi^0\nu\bar{\nu}$ decay is discussed in this section; the former one is discussed in Chapter *Flavor physics of leptons and dipole moments* of this volume.

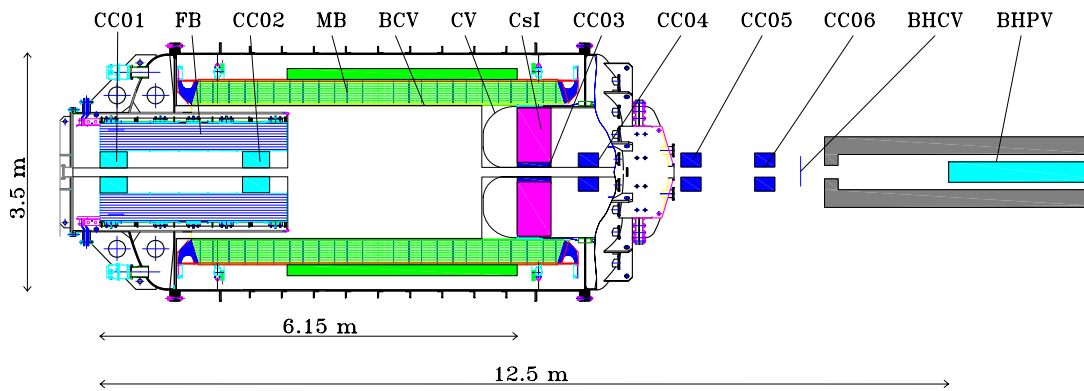**Fig. 49** A plan for the layout of NP Hall at J-PARC
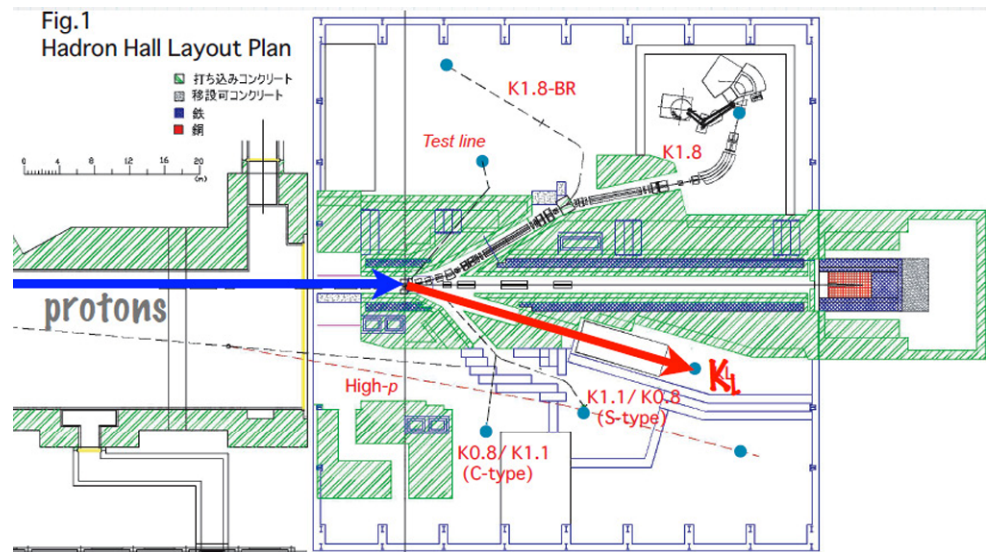
Fig. 50 Schematic view of the detector setup for the E14 experiment at J-PARC

The branching ratio for $K_L \rightarrow \pi^0 \nu\bar{\nu}$ is predicted to be $(2.7 \pm 0.4) \times 10^{-11}$ in the Standard Model, while the experimental upper limit, 6.7×10^{-8} at the 90% confidence level, is currently set by the E391a Collaboration at the KEK 12-GeV PS using the data collected during the second period of data taking [876]. E391a was the first dedicated experiment for $K_L \rightarrow \pi^0 \nu\bar{\nu}$ and aimed to be a pilot experiment. The new proposal at J-PARC [909] is to measure the branching ratio with an uncertainty less than 10% and takes a step-by-step approach to achieve this goal.

The common T1 target on the A-line and the beamline with a 16-degree extraction angle, as shown in Fig. 49, will be used in the first stage of the experiment (E14). Survey of a new neutral beamline in the first year of J-PARC commissioning and operation is essential to understand the beam-related issues at J-PARC. The E14 experiment will be performed by the date of "5 years of LHC" ($\sim$2012/2013); the goal is to make the first observation of the decay. In the current simulation, 3.5 SM events with 1.8×10^{21} protons on target in total are expected with the S/N ratio of 1.4. The beamline elements and the detector of E391a will be re-used by imposing necessary modifications. A schematic view of the detector setup is shown in Fig. 50. In particular, the undoped CsI crystals in the calorimeter for measuring the two photons from π^0 in $K_L \rightarrow \pi^0 \nu\bar{\nu}$ will be replaced with the smaller-size and longer crystals used in the Fermilab KTeV experiment (Fig. 51); discussions on the loan of the crystals are in progress. The technique of waveform digitization will be used on the outputs of the counters in the detector to distinguish pile-up signals from legitimate two-photon signals under the expected high-rate conditions. A new extra photon detection system to reduce the $K_L \rightarrow \pi^0 \pi^0$ background will cover the regions in or around the neutral beam.

After the E14 experiment establishes the experimental techniques to achieve the physics goal, the beamline and the detector will be upgraded for the next stage. More than 100 SM events (equivalent to a single event sensitivity of less
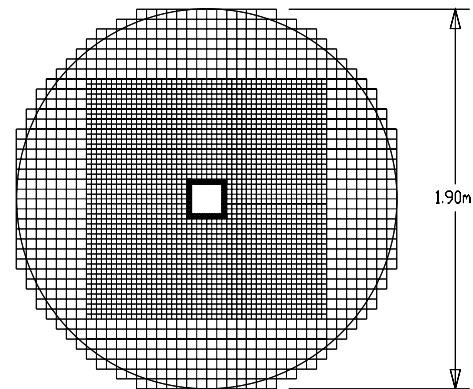
Fig. 51 Layout of the calorimeter for the J-PARC K_L experiment with the KTeV CsI crystals

than 3×10^{-13}) with an S/N ratio of 4.8 will be accumulated by the era of a "super B-factory" ($\sim$2020).

3.9 Charm physics[26]

3.9.1 Case for continuing charm studies in a nutshell

While nobody can doubt the seminal role that charm studies played for the evolution and acceptance of the SM, conventional wisdom is less enthused about their future. Yet on closer examination a strong case emerges in two respects, both of which are based on the weak phenomenology predicted by the SM for charm:

– to gain new insights into and make progress in establishing theoretical control over QCD's nonperturbative dynamics, which will also calibrate our theoretical tools for B studies;
– to use charm transitions as a novel window into NP.

Lessons from the first item will have an obvious impact on the tasks listed under the second one. They might actually

---

[26]Section coordinators: D.M. Asner, S. Fajfer.

420

Eur. Phys. J. C (2008) 57: 309–492

be of great value even beyond QCD if the NP anticipated for the TeV scale is of strongly interacting variety.

Detailed analyses of leptonic and semileptonic decays of charm hadrons provide a challenging testbed for validating lattice QCD, which is the only known framework with the promise for a truly quantitative treatment of charm hadrons that can be improved *systematically*.

While significant 'profit' can be 'guaranteed' for the first item, the situation is less clear concerning the second one, the search for NP. While it had to be expected that no sign of NP would show up at the present level of experimental sensitivity, no clear-cut benchmark has been set at which level NP could emerge with even odds. In that sense, one is dealing with hypothesis-generating rather than probing research. It will be essential to harness the statistical power of the LHC for high-quality charm studies.

Yet the situation is much more promising than it seems at first glance. NP scenarios in general induce FCNCs that a priori have little reason to be as much suppressed as in the SM. More specifically, they could be substantially stronger for up-type than for down-type quarks; this can happen in particular in models which have to reduce strangeness changing neutral currents below phenomenologically acceptable levels by some alignment mechanism.

In such scenarios, charm plays a unique role among the up-type quarks u, c and t; for only charm allows the full range of probes for NP in general and flavor-changing neutral currents in particular: (i) Since top quarks do not hadronize [910], there can be no T^0–$\bar{T}^0$ oscillations. More generally, hadronization, while hard to bring under theoretical control, enhances the observability of CP violation. (ii) As far as u quarks are concerned, π^0, η and η' decay electromagnetically, not weakly. They are their own antiparticles and thus cannot oscillate. CP asymmetries are mostly ruled out by CPT invariance.

Our basic contention can then be formulated as follows: *Charm transitions provide a unique portal for a novel access to flavor dynamics with the experimental situation being a priori quite favorable (apart from the absence of Cabibbo suppression). Yet even that handicap can be overcome by statistics.*

The truly committed reader can find more nourishment for her/his curiosity in several recent reviews [911–913].

These points alluded to above will be addressed in somewhat more detail in the following sections.

3.9.2 Charm mixing

Prior observations of mixing in all down-type quark mixing systems puts charm physics in a unique position in the modern investigations of flavor physics as the system where the first evidence for the phenomena has emerged only recently (just before the publication of this document). Results of

these studies are addressed after a short phenomenological introduction.

The SM contributions to charm mixing are suppressed to $\tan^2 \theta_c \approx 5\%$, because D^0 decays are Cabibbo favored. The GIM cancellation could further suppress mixing through off-shell intermediate states to 10^{-2}–10^{-6}. SM predictions for charm mixing rates span several orders of magnitude [913–917]. Fortunately, CP violation in mixing is $\mathcal{O}(10^{-6})$ in the SM, so CP violation involving D^0–$\bar{D}^0$ oscillations is a reliable probe of NP.

Charm physics studies are complementary to the corresponding programs in bottom or strange systems due to the fact that D^0–$\bar{D}^0$ mixing is influenced by the dynamical effects of *down-type particles*.

Effective $\Delta C = 2$ interactions generate contributions to the effective operators that change a D^0 state into a $\bar{D}^0$ state, leading to the mass eigenstates

$$|D_{\frac{1}{2}}\rangle = p|D^0\rangle \pm q|\bar{D}^0\rangle, \qquad R_m^2 = \left|\frac{q}{p}\right|^2, \qquad (185)$$

where the complex parameters p and q are obtained from diagonalizing the D^0–$\bar{D}^0$ mass matrix with $|p|^2 + |q|^2 = 1$. If CP-violation in mixing is neglected, p becomes equal to q, so $|D_{\frac{1}{2}}\rangle$ become CP eigenstates, $\text{CP}|D_\pm\rangle = \pm|D_\pm\rangle$.

The time evolution of a D^0 or $\bar{D}^0$ is conventionally described by an effective Hamiltonian which is non-Hermitian and allows the mesons to decay. We write

$$i\frac{\partial}{\partial t}\begin{bmatrix}|D^0(t)\rangle \\ |\bar{D}^0(t)\rangle\end{bmatrix} = \left(\boldsymbol{M} - \frac{i}{2}\boldsymbol{\Gamma}\right)\begin{bmatrix}|D^0(t)\rangle \\ |\bar{D}^0(t)\rangle\end{bmatrix},$$

where $\boldsymbol{M}$ and $\boldsymbol{\Gamma}$ are 2×2 matrices. We invoke CPT invariance so that $M_{11} = M_{22} \equiv M$ and $\Gamma_{11} = \Gamma_{22} \equiv \Gamma$. The eigenvalues of this Hamiltonian are

$$\lambda_{1,2} = M_{1,2} - \frac{i}{2}\Gamma_{1,2} \equiv \left(M - \frac{i}{2}\Gamma\right) \pm \frac{q}{p}\left(M_{12} - \frac{i}{2}\Gamma_{12}\right),$$

where $M_{1,2}$ are the masses of the $D_{1,2}$ and $\Gamma_{1,2}$ are their decay widths, and

$$\frac{q}{p} = \sqrt{\frac{M_{12}^* - \frac{i}{2}\Gamma_{12}^*}{M_{12} - \frac{i}{2}\Gamma_{12}}}.$$

The mass and width splittings between these eigenstates are given by

$$x \equiv \frac{m_1 - m_2}{\Gamma}, \qquad y \equiv \frac{\Gamma_1 - \Gamma_2}{2\Gamma}, \qquad R_M = \frac{x^2 + y^2}{2}. \tag{186}$$

These parameters are experimentally observable and can be studied using a variety of methods to be discussed below.

SM and all reasonable models of NP predict $x, y \ll 1$ [913–917], which influences the available strategies for those measurements.

3.9.3 Semileptonic decays

The most natural way to search for charm mixing is to employ semileptonic decays. It is also not the most sensitive way, as it is only sensitive to R_M, a quadratic function of x and y. The use of the D^0 semileptonic decays for the mixing search involves the measurement of the time-dependent or time-integrated rate for the wrong-sign (WS) decays of D, where $c \to \bar{c} \to \bar{s}\ell^-\bar{\nu}$, relative to the right-sign (RS) decay rate, $c \to s\ell^+\nu$. Decays $D^0 \to K^{(*)-}\ell^+\bar{\nu}$ have been experimentally searched for [918–922]. Although the time-integrated rate is measured, several experiments use the time dependence of D^0 decays to increase the sensitivity. Currently the best sensitivity is reached by the Belle experiment, $R_M = (0.20 \pm 0.47 \pm 0.14) \times 10^{-3}$, using 253 fb^{-1} of data in $e^\pm$ mode only. Projecting to a possible 2 ab^{-1}, one can hope for a sensitivity of about $\pm 0.2 \times 10^{-3}$, including also systematic uncertainty.

3.9.4 Nonleptonic decays to non-CP eigenstates

A decay mode providing one of the best sensitivities to the mixing parameters is $D^0 \to K^+\pi^-$. Time-dependent studies allow separation of the direct doubly-Cabibbo suppressed (DCS) $D^0 \to K^+\pi^-$ amplitude from the mixing contribution $D^0 \to \bar{D}^0 \to K^+\pi^-$ [923, 924],

$$\Gamma[D^0 \to K^+\pi^-]$$
$$= e^{-\Gamma t}|A_{K^-\pi^+}|^2 \big[R_D + \sqrt{R_D}\, R_m (y'\cos\phi - x'\sin\phi)\Gamma t$$
$$+ R_m^2 R_M^2 (\Gamma t)^2 \big], \tag{187}$$

where R_D is the ratio of DCS and Cabibbo-favored (CF) decay rates. Since x and y are small, the best constraint comes from the linear terms in t that are also *linear* in x and y. A direct extraction of x and y from (187) is not possible due to the unknown relative strong phase $\delta_{K\pi}$ of DCS and CF amplitudes, as $x' = x\cos\delta_{K\pi} + y\sin\delta_{K\pi}$, $y' = y\cos\delta_{K\pi} - x\sin\delta_{K\pi}$. This phase can be measured independently (see CLEO-c result in Sect. 3.9.8). The corresponding formula can also be written [925] for $\bar{D}^0$ decay with $x' \to -x'$ and $R_m \to R_m^{-1}$.

Experimentally, this method of D^0 mixing search requires a good understanding of the detector decay time resolution to model correctly the measured distribution. Several experiments performed fits to disentangle the individual contributions in (187) [926–932]. The most recent study by BaBar Collaboration [933] finds an evidence for nonzero values of the mixing parameters. The preliminary 95% C.L. contours of the measured values are shown in Fig. 52. In terms of single parameter errors to be used for projections the most accurate is the measurement by Belle, using 400 fb^{-1} of data. Several fits to decay time distributions are performed; assuming that the CP violation is negligible, the result is $x'^2 = (0.18 \pm^{0.21}_{0.23}) \times 10^{-3}$, $y' = (0.6 \pm^{4.0}_{3.9}) \times 10^{-3}$ and $R_D = (3.64 \pm 0.17) \times 10^{-3}$, where the errors are statistical only. Projections of the 95% C.L. (x'^2, y') contour to the axes yield confidence intervals of $x'^2 < 0.72 \times 10^{-3}$ and $y' \in [-9.9, 6.8] \times 10^{-3}$. With a 2 ab^{-1} data sample, a statistical accuracy of 0.1×10^{-3} and 2×10^{-3} can be expected for x'^2 and y', respectively, similar to the current systematic uncertainties; a large contribution to the latter is due to the background modeling, the understanding of which might improve with a larger data sample as well.

CDF has demonstrated the potential of experiments at hadron colliders to make mixing-related measurements using hadronic decays through the recent study of WS $D^0 \to$

Fig. 52 Allowed regions in the x' vs y' plane (*left*) and x vs y for the measurements described in the text. We assume $\delta_{K\pi} = 0$ to place the y results in x' vs y'. A nonzero $\delta_{K\pi}$ would rotate the $D^0 \to$ CP eigenstates (y results) confidence region clockwise about the origin by δ

422

Eur. Phys. J. C (2008) 57: 309–492
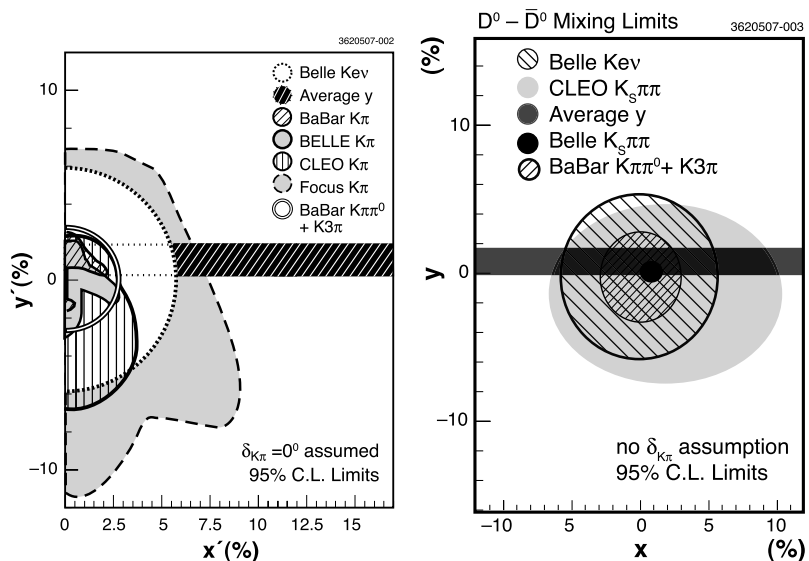
$K^+\pi^-$ events [934]. Using the distinctive $D^* \to D^0\pi$ signature and an integrated luminosity of $0.35\,\text{fb}^{-1}$, a sample of around 2000 WS decays have been accumulated with a background to signal level of order 1. The ratio of WS to RS decays is found to be $[4.05 \pm 0.21(\text{stat}) \pm 0.11(\text{syst})] \times 10^{-3}$. This ratio is equivalent to R_D in the limit that x' and y' are zero, and CP violation is negligible. Provided that the systematic uncertainties can continue to be kept under control, the full Tevatron dataset of several fb^{-1} will give a more precise result for R_D than the B-factories, under the stated assumption. More interesting results are to be expected should it prove possible to perform a time-dependent measurement.

LHCb expects to collect very high statistics in all charged two-body D^0 decays through the inclusion of a dedicated $D^* \to D^0(hh')\pi$ filter in the experiment's high-level trigger [935]. In one year of operation at nominal luminosity $(2\,\text{fb}^{-1})$, 0.2 million WS and 50 million RS $K\pi$ events will be written to tape, where the triggered D^* has originated from a B decay. A similar number of decays are expected where the D^* is produced in the primary event vertex.

In a mixing analysis, it is necessary to measure the proper lifetime of the decaying D^0. LHCb's good vertexing allows the decay point of the D^0 to be well determined, and also the production point in the case of D^*'s produced in the primary vertex. For that sample where the D^* arises from a B decay, it is necessary to vertex the D^0 direction with other B decay products in order to find the production point, a procedure which entails a loss in efficiency. Additional cuts are needed to enhance the purity of the WS signal and combat the most significant background source, where the wrong 'slow pion' is associated with a genuine D^0. This contamination is dangerous for the reason that is the charge of the slow pion which tags the initial flavor of the D^0 meson. After this selection, 46,500 WS decays are expected from B events per $2\,\text{fb}^{-1}$, with a background to signal ratio of around 2.5.

These performance figures have been used as input to a 'toy Monte Carlo' study to determine LHCb's sensitivity to the mixing parameters, including both the effects of background and the estimated proper time resolution and acceptance. The study was performed for event yields corresponding to 10 fb^{-1} of integrated luminosity, that is 5 years of operation at nominal operation. It was found that with such a sample, LHCb will have a statistical sensitivity on x'^2 and y' of 0.6×10^{-4} and 0.9×10^{-3}, respectively. Further work is needed to identify and combat the possible sources of systematic uncertainty.

3.9.5 Multi-body hadronic D^0 decays

In multi-body hadronic D^0 decays, possible differences in the resonant structure between the CF and DCS decays

must be taken into account and, as discussed below, be exploited. The time integrated relative rates $R_{WS} = \Gamma(D^0 \to K^+\pi^-(n\pi))/\Gamma(D^0 \to K^-\pi^+(n\pi))$, which assuming negligible CP violation equal to $R_D + \sqrt{R_D}y' + (x'^2 + y'^2)/2$, have been measured for $n\pi = \pi^0, \pi^+\pi^-$ [937, 942, 946, 947]. For the latter mode, Belle measures $R_{WS}(K\pi\pi\pi) = (0.320 \pm 0.018 \pm 0.013)\%$. Assuming a particular value of x' in combination with the previous equation gives an allowed band in the (R_D, y') plane; however, one should note that the value of x' is decay mode dependent. Studies with $D^0 \to K^\mp\pi^\pm\pi^-\pi^+$ events will also be possible at LHCb, where plans are under consideration to extend the $D^* \to D^0(h^+h'^-)\pi$ high-level trigger stream to include charged 4-body D^0 decays. The foreseen event yields would be similar to those anticipated for the $D^0 \to K^\mp\pi^\pm$ case.

The BaBar Collaboration studied the time-dependence of the above multi-body decay modes [948]. Since the possible mixing contribution followed by CF decay needs to be distinguished from the DCS decays, the sensitivity of the measurement is increased by selecting regions of phase space where the ratio of the two is the largest. The preliminary value of R_M, which is not affected by this selection, is found to be $R_M = (0.023 \pm^{0.018}_{0.014} \pm 0.004)\%$ ($R_M < 0.054\%$ at 95% C.L. using a Bayesian approach) in the $D^0 \to K^+\pi^-\pi^0$ mode, and without selecting a region of phase-space $R_{WS}(K\pi\pi^0) = (0.214 \pm 0.008 \pm 0.008)\%$ is obtained. By combining the obtained $\delta\log\mathcal{L}(R_M)$ curve with the one from the study of the $D^0 \to K^+\pi - \pi^+\pi^-$ channel $R_M = (0.020 \pm^{0.011}_{0.010})\%$ ($R_M < 0.042\%$ at 95% C.L. using a Bayesian approach) is obtained (stat. uncertainty only). The combined data are compatible with the no-mixing hypothesis at the 2.1% C.L.

3.9.6 Time-dependent Dalitz-plot analysis

Due to the strong variation of the interference effects over the $D^0 \to K^+\pi^-(n\pi)$ phase-space, a Dalitz analysis of these modes can give further insight into the D^0 mixing. Such an analysis has been performed for $D^0 \to K_S\pi^-\pi^+$ channel by CLEO Collaboration [949], and recently results from Belle Collaboration became available [950]. Different intermediate states contributing to $K_S\pi^-\pi^+$ (CP even or odd, like $K_S f_0$ or $K_S\rho^0$, or flavor eigenstates, like $K^*(892)^+\pi^-$), that can be determined by inspection of the Dalitz plane, contribute differently to the decay time distribution of $D^0 \to K_S\pi^-\pi^+$. A simultaneous fit of the Dalitz and decay time distributions is used to determine the mixing parameters $x = (0.80 \pm 0.29 \pm 0.17)\%$ and $y = (0.33 \pm 0.24 \pm 0.15)\%$. Important systematic error arises due to the uncertainty of the model used for the description of the Dalitz structure (around $\pm 0.15\%$ and $\pm 0.10\%$ on x and y, respectively). Projecting the amount of data used in the analysis ($540\,\text{fb}^{-1}$) to the amount possibly available to the B-factories in the future ($2\,\text{ab}^{-1}$), the statistical

Eur. Phys. J. C (2008) 57: 309–492

423

precision on each parameter could be improved to ∼0.15%. Hence the systematic error, receiving contributions from the uncertainty of the t distribution modeling (similar as for the case of $D^0 \rightarrow K^+\pi^-$ decays) as well as from the Dalitz model, will need to be studied carefully.

3.9.7 Nonleptonic decays to CP eigenstates

D^0 mixing can be measured by comparing the lifetimes extracted from the analysis of D decays into the CP-even and CP-odd final states. In practice, the lifetime measured in D decays into CP-even final state f_{CP}, such as $K^+K^-, \pi^+\pi^-, \phi K_S$, etc., is compared to the one obtained from a measurement of decays to a non-CP eigenstate, such as $K^-\pi^+$. This analysis is also sensitive to a *linear* function of y via

$$y_{CP} = \frac{\tau(D \rightarrow K^-\pi^+)}{\tau(D \rightarrow K^+K^-)} - 1 = y\cos\phi - x\sin\phi\left[\frac{R_m^2 - 1}{2}\right],$$

(188)

where ϕ is a CP-violating phase. In the limit of vanishing CP violation, $y_{CP} = y$. This measurement requires precise determination of lifetimes. It profits from some cancellation of the systematic uncertainties in the ratio $\tau(K^-\pi^+)/\tau(f_{CP})$. To date CP = +1 final states K^+K^- and $\pi^+\pi^-$ have been used [951–957].

In the course of preparation of this document, the Belle Collaboration obtained a new result on y_{CP} using 540 fb^{-1} of data [957]. It represents evidence for the D^0–$\bar{D}^0$ mixing with $y_{CP} = 1.31 \pm 0.32 \pm 0.25\%$ differing from zero by 3.2 standard deviations.

With the currently available statistical samples at the B-factories, the statistical uncertainty of the measurements using the D^{*+} tag is comparable to the systematic one. The latter arises mainly from an imperfect modeling of the t distribution of the background (although the overall background level is small, and the systematic uncertainty due to this source might decrease with increased data sample) and from a possible noncancellation of systematic errors on individual lifetime measurements. With the final B-factories' data set, one can hope for a total uncertainty on y_{CP} of around $\pm0.25\%$. To this, systematic error contributes $\pm0.10\%$ if the sources expected to scale with the luminosity are taken into account.

LHCb intends to make an important contribution to the measurements of a nonzero value of y_{CP} through the high statistics available from the D^* trigger and the excellent particle identification capabilities of its RICH system. A sample of 1.6×10^6 $D^0 \rightarrow K^+K^-$ events is expected from B decays alone after all selection cuts. The expected sensitivity to y_{CP} from this source with 5 years of data is 0.5×10^{-3}.

3.9.8 Quantum-correlated final states

The construction of tau-charm factories introduces new *time-independent* methods that are sensitive to a linear function of y. One can use the fact that heavy meson pairs produced in the decays of heavy quarkonium resonances have the useful property that the two mesons are in the CP-correlated states [958, 959]. For instance, by tagging one of the mesons as a CP eigenstate, a lifetime difference may be determined by measuring the leptonic branching ratio of the other meson. The final states reachable by neutral charmed mesons are determined by a set of selection rules according to the initial virtual photon quantum numbers $J^{PC} = 1^{--}$ [959, 960]. Currently, the decay rates of several singly-tagged (only a single meson is fully reconstructed) and doubly-tagged (both mesons reconstructed) final states of the $D^0\bar{D}^0$ pairs are measured at CLEO-c [961], where the individual fractions depend on the mixing parameters y and R_M, D^0 branching fractions and phases between DCS and CF decays. Types of decays considered include semi-leptonic decays and decays to flavor and CP eigenstates. The above parameters are determined from a fit to the efficiency-corrected yields using 281 pb^{-1} of data, with the preliminary results most relevant to the D^0 mixing $y = -0.058 \pm 0.066$, $R_M = (1.7 \pm 1.5) \times 10^{-3}$ and $\cos\delta_{K\pi} = 1.09 \pm 0.66$. The systematic uncertainties, expected to be of smaller size, are being evaluated. At CLEO-c, the precision of results is expected to be reduced by increasing the data sample by a factor of three, increasing the number of CP eigenstate modes and using constraints from other measurements of D^0 branching fractions. The same method will be exploited by BES III with an expected data sample of 20 fb^{-1}. Statistical uncertainty could be reduced to $\sigma(y) \sim 0.002$, $\sigma(R_M) \sim 0.2 \times 10^{-3}$ and $\sigma(\cos\delta_{K\pi}) \sim 0.02$.

3.9.9 Summary of experimental D mixing results

The constraints in x' vs. y' and x vs y are shown in Fig. 52. Approximate uncertainties of the measured quantities, as expected from the data samples assumed above, are shown in Table 46. The errors shown include scaled statistical errors from the most precise existing measurements and estimates of possible systematic uncertainties.

As a simple illustration of the projected results, a χ^2 minimization in terms of the mixing parameters x and y and of $\cos\delta_{K\pi}$ can be performed. For the unknown true values $x = 5 \times 10^{-3}$, $y = 1 \times 10^{-2}$ and $\delta_{K\pi} = 0°$, one finds the central 68% C.L. intervals of $x \in [3, 7] \times 10^{-3}$, $y \in [0.85, 1.15] \times 10^{-2}$ and $\delta_{K\pi} \in [-12°, 12°]$. In some cases, the p.d.f.'s for the estimated parameters are significantly non-Gaussian.

The HFAG charm decays subgroup [389] is preparing world averages of all the charm measurements. For charm
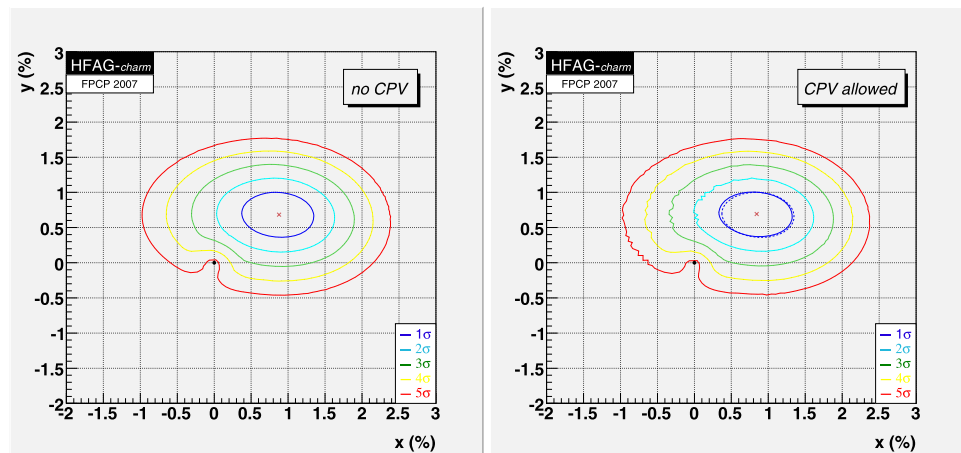
424

Eur. Phys. J. C (2008) 57: 309–492

Table 46 Approximate expected precision (σ) on the measured quantities using methods described in the text for the integrated luminosity of 10 fb^{-1} at LHCb, 2 ab^{-1} at the B-factories at 10 GeV and 20 fb^{-1} at BESIII running at charm threshold. The LHCb numbers do not include the effect of systematic errors but neglect the contribution of events from prompt charm production. Entries marked '/' in the LHCb column are where expected performance numbers are not yet available

Mode	Observable	LHCb (10 fb^{-1})	B-factories (2 ab^{-1})	$\psi(3770)$ (20 fb^{-1})
$D^0 \to K^{(*)-}\ell^+\bar{\nu}$	R_M	/	0.2×10^{-3}	
$D^0 \to K^+\pi^-$	x'^2	0.6×10^{-4}	1.5×10^{-4}	
	y'	0.9×10^{-3}	2.5×10^{-3}	
$D^0 \to K^+K^-$	y_{CP}	0.5×10^{-3}	3×10^{-3}	
$D^0 \to K_S^0\pi^+\pi^-$	x	/	2×10^{-3}	
	y	/	2×10^{-3}	
$\psi(3770) \to D^0\bar{D}^0$	x^2			3×10^{-4}
	y			4×10^{-3}
	$\cos\delta$			0.05

mixing, the averages not only take into account correlations between measurements but combine the multidimensional likelihood functions associated with each measurement. A very preliminary average is available [389] giving $x = (8.7^{+3.0}_{-3.4}) \times 10^{-3}$ and $y = (6.6^{+2.1}_{-2.0}) \times 10^{-3}$. Allowing for CP violation, the very preliminary average is $x = (8.4^{+3.2}_{-3.4}) \times 10^{-3}$ and $y = (6.9 \pm 2.1) \times 10^{-3}$.

The constraints in the x vs y plane are shown in Fig. 53. The significance of the oscillation effect exceeds 5σ.

The interpretation of the new results in terms of NP is inconclusive. It is not yet clear whether the effect is caused by $x = 0$ or $y = 0$ or both, although the latter is favored, as shown in Table 47. Both an upgraded LHCb and a high luminosity super B-factory will be able to observe both life-

Fig. 53 All charm mixing measurements are combined by HFAG [389] to provide constraints in the x vs. y plane. Contours (1 through 5σ) of the allowed region are shown. The significance of the oscillation effect exceeds 5σ

Table 47 Approximate expected precision (σ) on the measured quantities using methods described in the text for the integrated luminosity of 100 fb^{-1} at an upgraded LHCb, 75 ab^{-1} at a super B-factory at 10 GeV and 200 fb^{-1} at a super B-factory running at charm threshold. The upgraded LHCb numbers are merely the results from Table 46 scaled to the new integrated luminosity

Mode	Observable	LHCb (100 fb^{-1})	Super B (75 ab^{-1})	$\psi(3770)$ (200 fb^{-1})
$D^0 \to K^+\pi^-$	x'^2	2.0×10^{-5}	3×10^{-5}	
	y'	2.8×10^{-4}	7×10^{-4}	
$D^0 \to K^+K^-$	y_{CP}	1.5×10^{-4}	5×10^{-4}	
$D^0 \to K_S^0\pi^+\pi^-$	x	/	5×10^{-4}	
	y	/	5×10^{-4}	
$\psi(3770) \to D^0\bar{D}^0$	x^2			$<0.2 \times 10^{-4}$
	y			$(1\text{–}2) \times 10^{-3}$
	$\cos\delta$			<0.05

time and mass differences in the D^0 system if they lie in the range of SM predictions.

A serious limitation in the interpretation of charm oscillations in terms of NP is the theoretical uncertainty on the SM prediction. Nonetheless, if oscillations occur at the level suggested by the recent results, this will open the window to searches for CP asymmetries that do provide unequivocal NP signals.

3.9.10 New Physics contributions to D mixing

As one can see from the previous discussion, mixing in the charm system is very small. As it turns out, theoretical predictions of x and y in the SM are very uncertain, from a percent to orders of magnitude smaller [914–917, 962–964]. Thus, NP contributions are difficult to distinguish in the absence of large CP violation in mixing.

In order to see how NP might affect the mixing amplitude, it is instructive to consider off-diagonal terms in the neutral D mass matrix,

$$\left(M - \frac{i}{2}\Gamma\right)_{12}$$
$$= \frac{1}{2M_D}\langle \bar{D}^0|\mathcal{H}_w^{\Delta C=-2}|D^0\rangle$$
$$+ \frac{1}{2M_D}\sum_n \frac{\langle \bar{D}^0|\mathcal{H}_w^{\Delta C=-1}|n\rangle\langle n|\mathcal{H}_w^{\Delta C=-1}|D^0\rangle}{M_D - E_n + i\epsilon}, \quad (189)$$

where $\mathcal{H}_w^{\Delta C=-1}$ is the effective $|\Delta C| = 1$ Hamiltonian. Since all new physics particles are much heavier than the SM ones, the most natural place for NP to affect mixing amplitudes is in the $|\Delta C| = 2$ contribution, which corresponds to a local interaction at the charm quark mass scale.

As can be seen from Fig. 54, predictions for x vary by orders of magnitude for different models. It is interesting to note that some models *require* large signals in the charm system if mixing and FCNCs in the strange and beauty systems are to be small (e.g. the SUSY alignment model).

New Physics mixing predictions
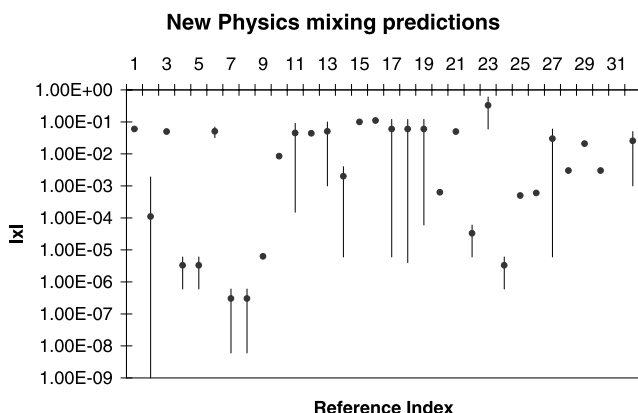
Fig. 54 NP predictions for $|x|$. Horizontal line references are tabulated in Table 5 of Refs. [914–917]

The local $|\Delta C| = 2$ interaction cannot, however, affect $\Delta\Gamma_D$, because it does not have an absorptive part. Thus, naively, NP cannot affect the lifetime difference y. This is, however, not quite correct. Consider a D^0 decay amplitude which includes a small NP contribution, $A[D^0 \to n] = A_n^{(SM)} + A_n^{(NP)}$. Here, $A_n^{(NP)}$ is assumed to be smaller than the current experimental uncertainties on those decay rates. Then it is a good approximation to write y as

$$y \simeq \sum_n \frac{\rho_n}{\Gamma_D} A_n^{(SM)} \bar{A}_n^{(SM)} + 2\sum_n \frac{\rho_n}{\Gamma_D} A_n^{(NP)} \bar{A}_n^{(SM)}. \quad (190)$$

The SM contribution to y is known to vanish in the limit of exact flavor $SU(3)$. Moreover, the first-order correction is also absent, so the SM contribution arises only as a *second-*order effect. Thus, those NP contributions which do not vanish in the flavor $SU(3)$ limit must determine the lifetime difference there, even if their contributions are tiny in the individual decay amplitudes [965]. A simple calculation reveals that NP contribution to y can be as large as several percent in R-parity-violating SUSY models or as small as $\sim 10^{-10}$ in the models with interactions mediated by charged Higgs particles [965]. Assuming that the projected precisions on x, y and $\cos(\delta_{K\pi})$ discussed below are achieved, a range of NP models can be ruled out. On the other hand, the uncertainty of SM predictions for the mixing parameters can in some scenarios (positive measurement, $y > x$) make the identification of NP contribution difficult. It is important to make a precise determination of individual parameters, using all the experimental methods mentioned (and possibly new ones) in order to pin down possible cracks in the SM.

3.9.11 D mixing impact on the CKM angle γ/ϕ_3

Beside the importance of the mixing in the charm sector per-se discussed above, the results of mentioned measurements can also have an impact on the determination of the UT angle γ/ϕ_3. Several proposed methods for measuring γ/ϕ_3 use the interference between $B^- \to D^0K^-$ and $B^- \to \bar{D}^0K^-$ which occurs when both D^0 and $\bar{D}^0$ decay to the same final state [627, 632, 633, 636, 645, 646].

The quantity sensitive to the angle γ/ϕ_3 is the asymmetry $A_{DK} = [Br(B^- \to f_D K^-) - Br(B^+ \to \bar{f}_D K^+)]/[Br(B^- \to f_D K^-) + Br(B^+ \to \bar{f}_D K^+)]$, where f_D denotes the common final state of D^0 and $\bar{D}^0$. A_{DK} can be expressed as

$$A_{DK} = \frac{2r_B r_D e^{-\epsilon}\sin(\delta_B + \delta_D)\sin\gamma/\phi_3}{r_B^2 + r_D^2 + 2r_B r_D e^{-\epsilon}\cos(\delta_B + \delta_D)\cos\gamma/\phi_3}, \quad (191)$$

where δ_B is the difference of the strong phases in decays $B^- \to D^0K^-$ and $B^- \to \bar{D}^0K^-$, δ_D is the difference of the

strong phases for $D^0 \to f_D$ and $\bar{D}^0 \to f_D$, r_B is the ratio of amplitudes $|\mathcal{A}(B^- \to \bar{D}^0 K^-)|/|\mathcal{A}(B^- \to D^0 K^-)|$, and r_D is the ratio $|\mathcal{A}(D^0 \to f_D)|/|\mathcal{A}(\bar{D}^0 \to f_D)|$. The dilution factor $e^{-\epsilon}$ arises if $x, y \neq 0$.

In case of nonnegligible D^0 mixing, the time integrated interference term between $\mathcal{A}(D^0 \to f_D)$ and $\mathcal{A}(\bar{D}^0 \to f_D)$ depends on x and y, resulting in [631]

$$\epsilon = \frac{1}{8}(x^2 + y^2)\left(\frac{1}{r_D^2} + r_D^2\right) - \frac{1}{4}(x^2 \cos 2\delta_D + y^2 \sin 2\delta_D).$$
(192)

Using f_D which is a CP eigenstate [632, 633] (the case where $f_D = K_S^0 \pi^+ \pi^-$ is discussed in Sect. 3.9.27.1) and neglecting CP violation in D^0 decays, the above expressions simplify due to $r_D = 1$, $\delta_D = 0$, and thus $\epsilon = y^2/4$. For $f = K^+ K^-, \pi^+ \pi^-$, the asymmetry A_{DK} is measured to be $0.06 \pm 0.14 \pm 0.05$ using an integrated luminosity of 250 fb^{-1} [966]. Projecting the result to 2 ab^{-1}, the expected statistical accuracy is ± 0.05. An uncertainty on y of 2%, on the other hand, reflects in an error of $\sigma(A_{DK}) \approx 5 \times 10^{-5}$ using the above equations (conservatively assuming that $r_B = 0.25$ and $\sin \delta_B = \sin \phi_3 = 1$). It is thus save to conclude that neglecting the effect of D^0 mixing in this method of γ/ϕ_3 determination is appropriate.

Besides f_D being a CP eigenstate, the final state can be chosen to arise from DCS decays [636, 645, 646]. In this case, the strong phase δ_D enters the expressions. To illustrate the effect of δ_D on extraction of the angle γ/ϕ_3, one can envisage usage of two distinct final states, for example the above mentioned $f = K^+ K^-, \pi^+ \pi^-$ and $K^+ \pi^-$, which can also be reached from either D^0 or $\bar{D}^0$. For the former, the same asymmetry A_{DK} can be measured, while for the latter, the ratio $R_{DK} = Br(B^- \to D_{\text{sup}} K^-)/Br(B^- \to D_{\text{fav}} K^-)$ is also sensitive to γ/ϕ_3. Here, D_{sup} denotes DCS decays $D^0 \to K^+ \pi^-$, and D_{fav} stands for $D^0 \to K^- \pi^+$. R_{DK} depends on the unknown angles:

$$R_{DK} = r_B^2 + r_D^2 + 2 r_B r_D \cos(\delta_B + \delta_D) \cos \gamma/\phi_3 \quad (193)$$

with $r_D = (6.2 \pm 0.1) \times 10^{-2}$ [119]. Assuming that r_B is known, measuring A_{DK} and R_{DK} constrains possible ranges for δ_B and γ/ϕ_3. Knowledge of δ_D clearly helps in limiting the $(\gamma/\phi_3, \delta_B)$ allowed region. We can use the projected result $A_{DK} = 0.06 \pm 0.05$ and the ratio $R_{DK} = (2.3 \pm 1.5 \pm 0.1) \times 10^{-2}$ as obtained using 250 fb^{-1} of data [967]. Hence one can expect $R_{DK} = (2.3 \pm 0.6) \times 10^{-2}$ with the final B-factories data set. The approximate two-dimensional 68% C.L. contour obtained by plotting the corresponding χ^2 of the two projected measurements as a function of γ/ϕ_3 and δ_B is shown in Fig. 55. The left plot shows the allowed region for the current value of $\delta_D = (0 \pm 1.15)$ rad [961]. To show the effect of an improved knowledge of the D-meson decays strong phase, the value $\delta_D = (0 \pm 0.45)$ rad (see Table 46) is used in the right plot. The allowed region of the unknown angles is significantly reduced, although it should be noted that the actual region strongly depends on the central values of δ_D as well as r_B (for the latter, the value 0.12 was used in the plots).
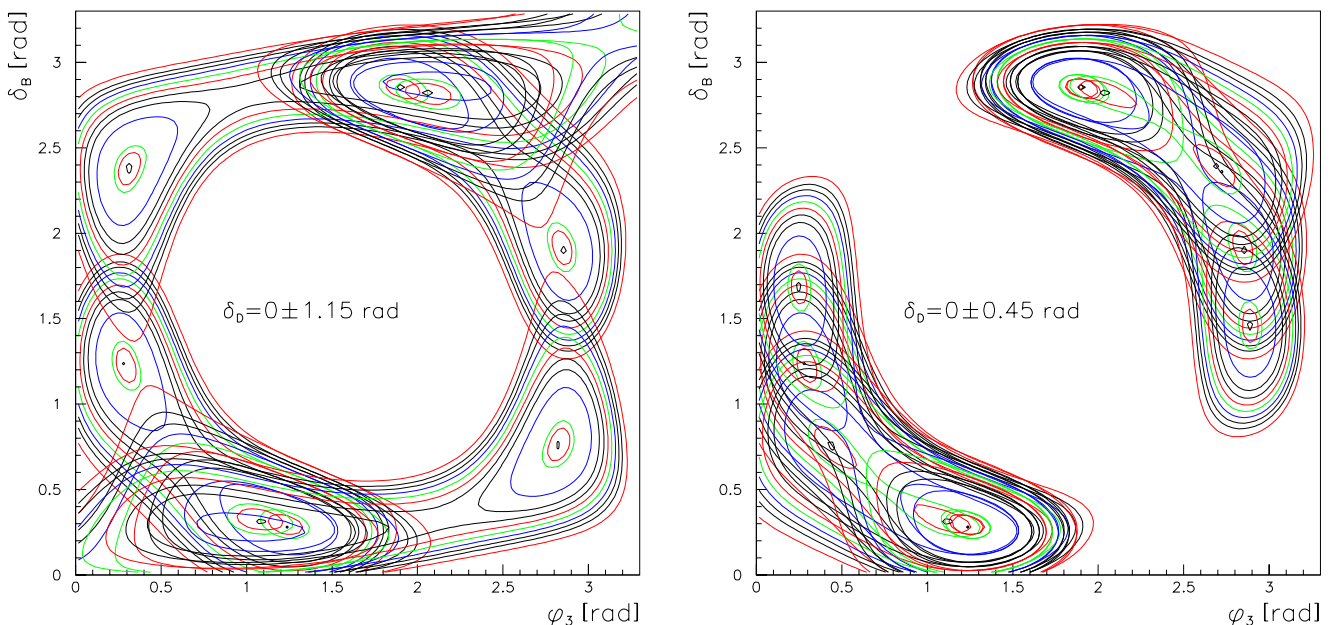

Fig. 55 The 68% C.L. contour for γ/ϕ_3 and δ_B using the projected results of measurements described in the text. The strong phase difference δ_D between $D^0 \to K^+ \pi^-/K^- \pi^+$ decays is assumed to have the values marked in the plots

3.9.12 CP violation with and without oscillations

3.9.13 Theoretical overview

Most factors favor or even call for dedicated searches for CP violation in charm transitions:

⊕ Since baryogenesis implies the existence of NP in CP-violating dynamics, it would be unwise not to undertake dedicated searches for CP asymmetries in charm decays, where the 'background' from known physics is between absent and small: for within the SM, the effective weak phase is highly diluted, namely $\sim \mathcal{O}(\lambda^4)$, and it can arise only in *singly-Cabibbo-suppressed* transitions, where one expects asymmetries to reach the $\mathcal{O}(0.1\%)$ level; significantly larger values would signal NP. *Any asymmetry in Cabibbo-allowed or doubly-suppressed* channels requires the intervention of NP—except for $D^\pm \to K_S \pi^\pm$ [912], where the CP impurity in K_S induces an asymmetry of 3.3×10^{-3}. One should keep in mind that in going from Cabibbo-allowed to Cabibbo singly- and doubly-suppressed channels, the SM rate is *suppressed* by factors of about twenty and four hundred, respectively:

$$\Gamma_{\rm SM}\big(H_c \to [S = -1]\big) : \Gamma_{\rm SM}\big(H_c \to [S = 0]\big)$$
$$: \Gamma_{\rm SM}\big(H_c \to [S = +1]\big)$$
$$\simeq 1 : 1/20 : 1/400. \tag{194}$$

One would expect that this suppression will enhance the visibility of NP.

⊕ Strong phase shifts required for *direct* CP violation to emerge in partial widths are in general large as are the branching ratios into relevant modes; while large final-state interactions complicate the interpretation of an observed signal in terms of the microscopic parameters of the underlying dynamics, they enhance its observability.

⊕ Since the SM provides many amplitudes for charm decays, CP asymmetries can be linear in NP amplitudes, thus increasing sensitivity to the latter.

⊕ Decays to final states of *more than* two pseudoscalar or one pseudoscalar and one vector meson contain more dynamical information than given by their widths; their distributions, as described by Dalitz plots or T odd moments, can exhibit CP asymmetries that might be considerably larger than those for the width. This will be explained in a bit more detail later on.

⊕ The distinctive channel $D^{\pm*} \to D\pi^\pm$ provides a powerful tag on the flavor identity of the neutral D meson.

⊖ The 'fly in the ointment' is that D^0–$\bar{D}^0$ oscillations are on the slow side.

⊕ Nevertheless one should take on this challenge. For CP violation involving D^0–$\bar{D}^0$ oscillations is a reliable

probe of NP: the asymmetry is controlled by $\sin \Delta m_D t \cdot \mathrm{Im}(q/p)\bar{\rho}(D \to f)$. Within the SM, both factors are small, namely $\sim \mathcal{O}(10^{-3})$, making such an asymmetry unobservably tiny—unless there is NP; for a recent NP model, see [433]. One should note that this observable is *linear* in x_D rather than quadratic as for CP insensitive quantities like $D^0(t) \to l^- X$. D^0–$\bar{D}^0$ oscillations, CP violation and NP might thus be discovered simultaneously in a transition. We will return to this point below.

⊖ Honesty compels us to concede there is no attractive, let alone compelling scenario of NP for charm transitions whose footprints should not be seen also in B decays.

⊕ It is all too often overlooked that CPT invariance can provide nontrivial constraints on CP asymmetries. For it imposes equality not only on the masses and total widths of particles and antiparticles but also on the widths for 'disjoint' *sub*sets of channels. 'Disjoint' subsets are the decays to final states that can*not* rescatter into each other. Examples are semileptonic vs. nonleptonic modes with the latter subdivided further into those with strangeness $S = -1, 0, +1$. Observing a CP asymmetry in one channel one can then infer in which other channels the 'compensating' asymmetries have to arise [912].

3.9.14 Direct CP violation in partial rates

CP violation in $\Delta C = 1$ dynamics can be searched for by comparing partial widths for CP-conjugate channels. For an observable effect, two conditions have to be satisfied simultaneously: a transition must receive contributions from two coherent amplitudes with (a) different weak and (b) different strong phases as well. While condition (a) is just the requirement of CP violation in the underlying dynamics, condition (b) is needed to make the relative weak phase observable. Since the decays of charm hadrons proceed in the nearby presence of many hadronic resonances inducing virulent final state interactions (FSI), requirement (b) is in general easily met; thus it provides no drawback for the *observability* of a CP asymmetry—albeit it does for its *interpretation*.

As already mentioned, CKM dynamics does not support any CP violation in Cabibbo-allowed and doubly suppressed channels due to the absence of a second weak amplitude; the only exception are modes containing a K_S (or K_L) like $D^+ \to K_S \pi^+$ vs. $D^- \to K_S \pi^-$ which have to exhibit an asymmetry of 0.0032 reflecting the CP impurity in the K_S (or K_L) wave function. In once-Cabibbo-suppressed transitions one expects CP asymmetries, albeit highly diluted ones of order $\lambda^4 \sim 10^{-3}$.

While we have good information on the size of the weak phase, we do not know how to predict the size of the relevant matrix elements and strong phases in a reliable way. Even if a direct CP asymmetry larger than about 10^{-3} were

428

Eur. Phys. J. C (2008) 57: 309–492

observed in a Cabibbo-suppressed mode, say even as large as 10^{-2}, at present, we could not claim such a signal to establish the intervention of NP. A judicious exercise in 'theoretical engineering' could, however, solve our conundrum.

3.9.15 Theoretical engineering

CP asymmetries in integrated partial widths depend on hadronic matrix elements and (strong) phase shifts, neither of which can be predicted accurately. However the craft of theoretical engineering can be practiced with profit here. One makes an ansatz for the general form of the matrix elements and phase shifts that are included in the description of $D \to PP$, PV, VV etc. channels, where P and V denote pseudoscalar and vector mesons, and fits them to the measured branching ratios on the Cabibbo-allowed, once and twice forbidden level. If one has sufficiently accurate and comprehensive data, one can use these fitted values of the hadronic parameters to predict CP asymmetries. Such analyses have been undertaken in the past [968], but the data base was not as broad and precise as one would like. *CLEO-c and BESIII measurements will certainly lift such studies to a new level of reliability.*

3.9.16 CP violation in final-state distributions

Once the final state in $D \to f$ is more complex than a pair of pseudoscalar mesons or a pseudoscalar plus a vector meson, it contains more dynamical information than given by the modulus of its amplitude, since its kinematics are no longer trivial. CP asymmetries in final-state distributions can be substantially larger than in integrated partial widths.

The simplest such case is given by decays into three pseudoscalar mesons, for which Dalitz plots analyses represent a very sensitive tool with the phase information they yield. They require large statistics; yet once those have been obtained, the return is very substantial. For the constraints, one has on a Dalitz plot population provide us with powerful weapons to control systematic uncertainties.

Such phenomenological advantages of having more complex final states apply also for four-body etc. final states. Measuring T odd moments with

$$O_T \stackrel{T}{\Longrightarrow} -O_T \qquad (195)$$

is an efficient way to make use of data with limited statistics. A simple example for a final state with four mesons a, b, c and d is given by $O_T = \langle \vec{p}_c \cdot (\vec{p}_a \times \vec{p}_b) \rangle$.

While FSI are not necessary for the emergence of such effects—unlike the situation for partial width asymmetries—, they can fake a signal of T violation with T being an *anti*linear operator; yet that can be disentangled by comparing T odd moments for CP conjugate modes [969]:

$$O_T(D \to f) \neq -O_T(\bar{D} \to \bar{f}) \implies \text{ CP violation.}$$
$$(196)$$

A dramatic example for CP violation manifesting itself in a final-state distribution much more dramatically than in a partial width has been found in K_L decays. Consider the rare mode $K_L \to \pi^+ \pi^- e^+ e^-$ and define by ϕ the angle between the $\pi^+ \pi^-$ and $e^+ e^-$ planes. The differential width has the general form

$$\frac{d\Gamma}{d\phi}(K_L \to \pi^+ \pi^- e^+ e^-)$$
$$= \Gamma_1 \cos^2 \phi + \Gamma_2 \sin^2 \phi + \Gamma_3 \cos \phi \sin \phi. \qquad (197)$$

Upon integrating over ϕ the Γ_3 term drops out from the total width, which thus is given in terms of $\Gamma_{1,2}$ with Γ_3 representing a forward–backward asymmetry:

$$\langle A \rangle \equiv \frac{\int_0^{\pi/2} \frac{d\Gamma}{d\phi} - \int_{\pi/2}^\pi \frac{d\Gamma}{d\phi}}{\int_0^\pi \frac{d\Gamma}{d\phi}} = \frac{2\Gamma_3}{\pi(\Gamma_1 + \Gamma_2)}. \qquad (198)$$

Under P and T, one has $\cos \phi \sin \phi \to -\cos \phi \sin \phi$. Accordingly $\langle A \rangle$ and Γ_3 constitute a T odd correlation, while $\Gamma_{1,2}$ are T even. Γ_3 is driven by the CP impurity ϵ_K in the kaon wave function. $\langle A \rangle$ has been measured to be large in full agreement with theoretical predictions [970]:

$$\langle A \rangle = 0.138 \pm 0.022. \qquad (199)$$

One should note that this observable is driven by $|\epsilon_K| \simeq 0.0023$.

D decays can be treated in an analogous way. Consider the Cabibbo-suppressed channel[27]

$$\overset{(-)}{D} \to K\bar{K}\pi^+\pi^- \qquad (200)$$

and define ϕ to be the angle between the $K\bar{K}$ and $\pi^+\pi^-$ planes. Then one has

$$\frac{d\Gamma}{d\phi}(D \to K\bar{K}\pi^+\pi^-)$$
$$= \Gamma_1 \cos^2 \phi + \Gamma_2 \sin^2 \phi + \Gamma_3 \cos \phi \sin \phi, \qquad (201)$$
$$\frac{d\Gamma}{d\phi}(\bar{D} \to K\bar{K}\pi^+\pi^-)$$
$$= \bar{\Gamma}_1 \cos^2 \phi + \bar{\Gamma}_2 \sin^2 \phi + \bar{\Gamma}_3 \cos \phi \sin \phi. \qquad (202)$$

As before, the partial width for $D[\bar{D}] \to K\bar{K}\pi^+\pi^-$ is given by $\Gamma_{1,2}[\bar{\Gamma}_{1,2}]$; $\Gamma_1 \neq \bar{\Gamma}_1$ or $\Gamma_2 \neq \bar{\Gamma}_2$ represents direct CP violation in the partial width. Γ_3 & $\bar{\Gamma}_3$ constitute T odd correlations. By themselves they do not necessarily indicate CP vi-

---

[27]This mode can exhibit direct CP violation even within the SM.

olation, since they can be induced by strong final-state interactions. However

$$\Gamma_3 \neq \bar{\Gamma}_3 \implies \text{CP violation!} \tag{203}$$

It is quite possible or even likely that a difference in Γ_3 vs. $\bar{\Gamma}_3$ is significantly larger than in Γ_1 vs. $\bar{\Gamma}_1$ or Γ_2 vs. $\bar{\Gamma}_2$. Furthermore one can expect that differences in detection efficiencies can be handled by comparing Γ_3 with $\Gamma_{1,2}$ and $\bar{\Gamma}_3$ with $\bar{\Gamma}_{1,2}$.

3.9.17 CP asymmetries involving oscillations

For final states that are common to D^0 and $\bar{D}^0$ decays, one can search for CP violation manifesting itself with the help of D^0–$\bar{D}^0$ oscillations in qualitative—though certainly not quantitative—analogy to $B_d \to J/\psi K_S$. Such common states can be CP eigenstates—like $D^0 \to K^+K^-/\pi^+\pi^-/K_S\eta^{(\prime)}$—but do not have to be: two very promising candidates are $D^0 \to K_S\pi^+\pi^-$, where one can bring the full Dalitz plot machinery to bear, and $D^0 \to K^+\pi^-$ vs. $\bar{D}^0 \to K^-\pi^+$, since its SM amplitude is doubly-Cabibbo-suppressed. Undertaking *time-dependent* Dalitz plot studies requires a higher initial overhead, yet in the long run this should pay handsome dividends exactly, since Dalitz analyses can invoke many internal correlations that in turn serve to control systematic uncertainties.

Searching for such effects with the required sensitivity (see below) will be quite challenging. Nevertheless one should take on this challenge. For CP violation involving D^0–$\bar{D}^0$ oscillations is a reliable probe of NP: the asymmetry is controlled by $\sin \Delta m_D t \cdot \text{Im}(q/p)\bar{\rho}(D \to f)$. Within the SM, both factors are small, namely $\sim \mathcal{O}(10^{-3})$, making such an asymmetry unobservably tiny—unless there is NP; for a recent NP model, see [433]. One should note that this observable is *linear* in x_D rather than quadratic as for CP-insensitive quantities like $D^0(t) \to l^-X$. D^0–$\bar{D}^0$ oscillations, CP violation and NP might thus be discovered simultaneously in a transition.

3.9.18 Experimental searches for CP violation

Let the amplitude for D^0 to decay to a final state f be written as

$$A_f \equiv \langle f | \mathcal{H}_{\text{int}} | D^0 \rangle,$$

where $\mathcal{H}_{\text{int}}$ is the interaction Hamiltonian responsible for $D^0 \to f$. If CP is conserved, that is if $[\mathcal{H}_{\text{int}}, CP] = 0$, then we can clearly write

$$
\begin{aligned}
A_f &= \langle f | (\text{CP})^\dagger (\text{CP}) \mathcal{H}_{\text{int}} | D^0 \rangle \\
&= \langle f | (\text{CP})^\dagger \mathcal{H}_{\text{int}} (\text{CP}) | D^0 \rangle \\
&= -\langle \bar{f} | \mathcal{H}_{\text{int}} | \bar{D}^0 \rangle \equiv -\bar{A}_{\bar{f}},
\end{aligned} \tag{204}
$$

where $\bar{f}$ is the conjugate final state to f. Consequently, a measurement that shows $\Gamma(D^0 \to f) \neq \Gamma(\bar{D}^0 \to \bar{f})$ is a demonstration that CP is violated in this decay.

Most CP violation results are from the FNAL fixed target experiments E791 and FOCUS and from the CLEO experiment and search for direct CP violation. The CP violation asymmetry is defined as

$$A_{\text{CP}} \equiv \frac{\Gamma(D \to f) - \Gamma(\bar{D} \to \bar{f})}{\Gamma(D \to f) + \Gamma(\bar{D} \to \bar{f})}. \tag{205}$$

A few results from CLEO, BaBar and Belle experiments consider CP violation in mixing. Typically, precisions of a few percent are obtained [119]. No evidence for CP violation is observed consistent with SM expectations.

Certainly very large samples will be available from hadron colliders. From an existing CDF measurement [971] it is possible to anticipate yields of over 0.5–1 million $D^0 \to K^+K^-$ events being available with the likely final Tevatron integrated luminosity of 5–10 fb^{-1}. This sample will have an intrinsic statistical precision of $\leq 0.2\%$. With the higher production cross-section and its dedicated D^* trigger, LHCb will accumulate samples of up to 10 million tagged events in each year of nominal operation [935]. The RICH system will ensure a low background, and these decays will be complemented by those selected in the $D^0 \to \pi^+\pi^-$ mode. In order to exploit these enormous statistics, it will be necessary to pay great attention to systematics biases. Initial state asymmetries and detector asymmetries will be the main concerns.

3.9.18.1 Three-body decays
Direct CP violation searches in analyses of charm decays to three-body final states are more complicated than two-body decays. Three methods have been used to search for CP asymmetries: (1) integrate over phase space and construct A_{CP} as in two-body decays; (2) examine CP asymmetry in the quasi-two-body resonances; (3) perform a full Dalitz-plot analysis for D and $\bar{D}$ separately. The Dalitz-plot analysis procedure [936] allows increased sensitivity to CP violation by probing decay amplitudes rather than the decay rate. E791 [937], FOCUS [938] and BaBar [939] have analysed $D^+ \to K^+K^-\pi^+$ using method (1). E791 and BaBar have also analysed $D^+ \to K^-K^+\pi^+$ using method (2). FOCUS has a Dalitz-plot analysis in progress [940]. The $D^+ \to K^+K^-\pi^+$ Dalitz plot is well described by eight quasi-two-body decay channels. A signature of CP violation in charm Dalitz-plot analyses is different amplitudes and phases for D and $\bar{D}$ samples. No evidence for CP violation is observed.

The decay $D^{*+} \to D^0\pi^+$ enables the discrimination between D^0 and $\bar{D}^0$. The CLEO Collaboration has searched for CP violation integrated across the Dalitz plot in $D^0 \to K^\mp\pi^\pm\pi^0$ [941, 942], $K_S^0\pi^+\pi^-$ [943] and $\pi^+\pi^-\pi^0$ [944] decays. No evidence of CP violation has been observed.

430

Eur. Phys. J. C (2008) 57: 309–492

CLEO has considered CP violation more generally in a simultaneous fit to the $D^0 \to K_S^0 \pi^+ \pi^-$ and $\bar{D}^0 \to K_S^0 \pi^+ \pi^-$ Dalitz plots. The possibility of interference between CP-conserving and CP-violating amplitudes provides a more sensitive probe of CP violation. The constraints on the square of the CP-violating amplitude obtained in the resonant submodes of $D^0 \to K_S^0 \pi^+ \pi^-$ range from 3.5×10^{-4} to 28.4×10^{-4} (95% C.L.) [943].

3.9.18.2 Four-body decays FOCUS has searched for T-violation using the four-body decay modes $D^0 \to K^+ K^- \pi^+ \pi^-$ [969]. As described in Sect. 3.9.16, a T-odd correlation can be formed with the momenta, $C_T \equiv (\vec{p}_{K^+} \cdot (\vec{p}_{\pi^+} \times \vec{p}_{\pi^-}))$. Under time-reversal, $C_T \to -C_T$, however $C_T \neq 0$ does not establish T-violation. Since time reversal is implemented by an anti-unitary operator, $C_T \neq 0$, it can be induced by FSI [945]. This ambiguity can be resolved by measuring $\bar{C}_T \equiv (\vec{p}_{K^+} \cdot (\vec{p}_{\pi^+} \times \vec{p}_{\pi^-}))$ in $\bar{D}^0 \to K^+ K^- \pi^+ \pi^-$; $C_T \neq \bar{C}_T$ establishes T violation. FOCUS reports a preliminary asymmetry $A_T = 0.075 \pm 0.064$ from a sample of ~ 400 decays. More restrictive constraints are anticipated from CLEO-c, where in 281 pb^{-1} a sample of 2300 $D^\pm \to K_S^0 K^\pm \pi^+ \pi^-$ have been accumulated.

3.9.19 Experiments exploiting quantum correlations

Most high-statistics measurements of D^0 decay employ "flavor tagging", through the sign of the slow pion in $D^* \to \pi_{\text{slow}} D$. That is, if combined with a slow π^+ to make a D^{*^+}, the neutral D meson is a D^0. Conversely, a slow π^- implies a $\bar{D}^0$.

An entirely different way to tag flavor and CP is to exploit quantum correlations in $D^0 \bar{D}^0$ production in $e^+ e^-$ annihilation [958–960].

The production process $e^+ e^- \to \psi(3770) \to D^0 \bar{D}^0$ produces an eigenstate of $CP+$ in the first step, since the $\psi(3770)$ has J^{PC} equal to 1^{--}. Now consider the case where both the D^0 and $\bar{D}^0$ decay into CP eigenstates. Then the decays $\psi(3770) \to f_+^i f_+^j$ or $f_-^i f_-^j$ are forbidden, where f_+ denotes a CP$+$ eigenstate, and f_- denotes a CP$-$ eigenstate. This is because $\text{CP}(f_\pm^i f_\pm^j) = (-1)^\ell = -1$ for $\ell = 1$ $\psi(3770)$. Hence, if a final state such as $(K^+ K^-)(\pi^+ \pi^-)$ is observed, one immediately has evidence of CP violation. Moreover, all CP$+$ and CP$-$ eigenstates can be summed over for this measurement. The expected sensitivity to direct CP violation is $\sim 1\%$. This measurement can also be performed at higher energies, where the final state $D^{*0} \bar{D}^{*0}$ is produced. When either D^* decays into a π^0 and a D^0, the situation is the same as above. When the decay is $D^{*0} \to \gamma D^0$, the CP parity is changed by a multiplicative factor of -1 and all decays $f_+^i f_-^j$ violate CP [945]. Additionally, CP asymmetries in CP even initial states depend linearly on x allowing sensitivity to CP violation in mixing of $\sim 3\%$.

For $e^+ e^-$ machines running at the $\psi(3770)$, the D mesons are produced with very little momentum in the laboratory. Hence, their flight distance is virtually impossible to determine, and we instead measure time-integrated decay rates. From Ref. [960] we have

$$\Gamma(j, k) = Q_M |A(j, k)|^2 + R_M |B(j, k)|^2, \qquad (206)$$

where

$$A(j, k) \equiv A_j \bar{A}_k - \bar{A}_j A_k$$

is the "unmixed" contribution to the decay rate, and

$$B(j, k) \equiv \frac{p}{q} A_j A_k - \frac{q}{p} \bar{A}_j \bar{A}_k$$

is the contribution from D^0–$\bar{D}^0$ mixing. The integrations also yield the factors

$$Q_M = \frac{1}{2} \left[\frac{1}{1 - y^2} + \frac{1}{1 + x^2} \right] \approx 1 - \frac{x^2 - y^2}{2},$$

$$R_M = \frac{1}{2} \left[\frac{1}{1 - y^2} - \frac{1}{1 + x^2} \right] \approx \frac{x^2 + y^2}{2}.$$

Mixing does not occur if the eigenstates of the decay Hamiltonian have the same mass and width, i.e. $x = y = 0$. In any case, we expect $R_M \ll Q_M \approx 1$. Nevertheless, mixing would result in the second term of (206), and it is here that one obtains sensitivity to CP violation through $q \neq p$. This will be exploited at CLEO-c and eventually to a greater extent at BES III.

3.9.20 Benchmarks for future searches

Since the primary goal is to establish the intervention of NP, one 'merely' needs a sensitivity level above the reach of the SM; 'merely' does not mean that it can easily be achieved. As far as *direct* CP violation is concerned—in partial widths as well as in final-state distributions—this means asymmetries down to the 10^{-3} or even 10^{-4} level in Cabibbo-allowed channels and 1% level or better in twice Cabibbo-suppressed modes; in Cabibbo-once-suppressed decays one wants to reach the 10^{-3} range, although CKM dynamics can produce effects of that order, because future advances might sharpen the SM predictions—and one will get them along with the other channels. For *time-dependent* asymmetries in $D^0 \to K_S \pi^+ \pi^-$, $K^+ K^-$, $\pi^+ \pi^-$ etc. and in $D^0 \to K^+ \pi^-$, one should strive for the $\mathcal{O}(10^{-4})$ and $\mathcal{O}(10^{-3})$ levels, respectively.

Statisticswise these are not utopian goals considering the very large event samples foreseen at LHCb.

When probing asymmetries below the $\sim 1\%$ level, one has to struggle against systematic uncertainties, in particular since detectors are made from matter. There are three powerful weapons in this struggle: (i) Resolving the time

evolution of asymmetries that are controlled by x_D and y_D, which requires excellent microvertex detectors; (ii) Dalitz plot consistency checks; (iii) quantum statistics constraints on distributions, T odd moments etc. [958, 960].

3.9.21 Rare decays

Searches for rare-decay processes have played an important role in the development of the SM. FCNC processes have been studied extensively for K and B mesons in both K^0–$\bar{K}^0$ and B^0–$\bar{B}^0$ mixing and in rare FCNC decays. The corresponding processes in the charm sector has received less attention, and the experimental upper limits are currently above SM predictions. Short-distance FCNC processes in charm decays are much more highly suppressed by the GIM mechanism than the corresponding down-type quark decays because of the large top quark mass.

Observation of D^+ FCNC decays $D^+, D_s^+ \to \pi^+ l^+ l^-$ and $K^+ l^+ l^-$ could therefore provide an indication of NP or of unexpectedly large rates for long-distance SM processes like $D^+ \to \pi^+ V$, $V \to l^+ l^-$, with a real or virtual vector meson V. Detailed description on rare charm decays can be found in Refs. [911, 913]. The charm meson radiative decays are also very important to understand final state interaction which may enhance the decay rates. In Refs. [911, 913], the decay rates of $D \to V\gamma$ (V can be ϕ, ω, ρ and K^*) had been estimated to be 10^{-5}–10^{-6}, which can be reached at BES-III and the B-factories.

3.9.22 Inclusive $c \to u$ transitions

The $s \to d$ and $b \to s$ transitions offer the possibility to investigate effects of NP in the down-type quark sector. The $c \to u$ transition, however, gives a chance to study effects of NP in the up-type quark sector. In the SM, the contribution coming from the penguin diagrams in $c \to u\gamma$ transition is strongly GIM suppressed giving a branching ratio of order 10^{-18} [972]. The QCD-corrected effective Lagrangian gives $BR(c \to u\gamma) \simeq 3 \times 10^{-8}$ [973, 974]. A variety of models beyond the standard model were investigated, and it was found that the gluino exchange diagrams [975] within general minimal supersymmetric SM (MSSM) might lead to the enhancement

$$\frac{BR(c \to u\gamma)_{\text{MSSM}}}{BR(c \to u\gamma)_{\text{SM}}} \simeq 10^2. \tag{207}$$

Within SM, the $c \to u l^+ l^-$ amplitude is given by the γ and Z penguin diagrams and W box diagram at one-loop electroweak order in the SM. It is dominated by the light quark contributions in the loop. The leading order rate for the inclusive $c \to u l^+ l^-$ calculated within SM [976] was found to be suppressed by QCD corrections in [911]. The inclusion of the renormalization group equations for the Wilson coefficients gave an additional significant suppression [977] leading to the rates $\Gamma(c \to u e^+ e^-)/\Gamma_{D^0} = 2.4 \times 10^{-10}$ and

$\Gamma(c \to u\mu^+\mu^-)/\Gamma_{D^0} = 0.5 \times 10^{-10}$. These transitions are largely driven by virtual photon at low dilepton mass m_{ll}.

The leading contribution to $c \to u l^+ l^-$ in general MSSM with the conserved R parity comes from one-loop diagrams with gluino and squarks in the loop [911, 975, 976]. It proceeds via virtual photon and significantly enhances the $c \to u l^+ l^-$ spectrum at small dilepton mass m_{ll}. The authors of [911] have investigated a SUSY extension of the SM with R parity breaking and they found that it can modify the rate. Using the most recent CLEO [978] results for the $D^+ \to \pi^+ e^+ e^-$, one can set the bound for the product of the relevant parameters entering the R-parity violating $\tilde{\lambda}'_{22k}\tilde{\lambda}'_{21k} \simeq 0.001$ (assuming that the mass of squark $M_{\tilde{D}_k} \simeq 100$ GeV). This bound give the rates $BR_R(c \to u e^+ e^-) \simeq 1.6 \times 10^{-8}$ and $BR_R(c \to u\mu^+\mu^-) \simeq 1.8 \times 10^{-8}$.

Recently, the effects of Littlest Higgs models were investigated in rare D decays [145], and it was found that there is a new tree level coupling which gives a $c \to uZ$ transition. However, that effect is insignificant due to the parameters constrained by the present electroweak data (see Ref. [25] in [145]). A number of models of NP contain an extra up-type heavy quark [980] causing the appearance of the FCNCs at tree level for the up-quark sector. The Lagrangian which describes this FCNC interaction is given by

$$\mathcal{L}_{\text{NC}} = \frac{g}{\cos\theta_W} Z_\mu \left(J^\mu_{W^3} - \sin^2\theta_W J^\mu_{EM} \right), \tag{208}$$

where J^μ_{EM} is the same electromagnetic current as in the SM, while $J^\mu_{W^3}$ is given by

$$J^\mu_{W^3} = \frac{1}{2} \bar{U}^m_L \gamma^\mu \Omega U^m_L - \frac{1}{2} \bar{D}^m_L \gamma^\mu D^m_L \tag{209}$$

with $L = \frac{1}{2}(1 - \gamma_5)$ and mass eigenstates $U^m_L = (u_L, c_L, t_L, T_L)^T$, $D^m_L = (d_L, s_L, b_L)^T$. The neutral current for the down-type quarks is the same as in the SM, while the up sector has additional currents (see Ref. [145]). The unitarity conditions of the CKM matrix might constrain this coupling. However, the present bound on Δm in D^0–$\bar{D}^0$ mixing limits the parameter describing the cuZ vertex to be $\Omega_{uc} \simeq 0.004$, giving the more strict limit on that parameter. The invariant dilepton mass distribution of the $c \to u l^+ l^-$ distribution is only moderately enhanced.

3.9.23 Exclusive rare D decays

The study of exclusive D meson rare decay modes is very difficult due to the dominance of the long-distance effects [145, 911–913, 972–984]. The $D \to V\gamma$ decay rates were calculated in [913, 972, 981, 983]. The long-distance contribution is induced by the effective nonleptonic $|\Delta c| = 1$ weak Lagrangian. In calculations of [983], the long-distance effects were determined using a heavy meson chiral Lagrangian. The factorization approximation has been used

432

Eur. Phys. J. C (2008) 57: 309–492

for the calculation of weak transition elements. The results of [972] obtained within a different framework are in very good agreement with the results of [983]. In Table 48, the branching ratios of $D \to V\gamma$ decays [983] are given. The uncertainty is due to relative unknown phases of various contributions. Although the branching ratios are dominated by the long-distance contributions, the size of the short-distance contribution can be extracted from the difference of the decay widths $\Gamma(D^0 \to \rho^0\gamma)$ and $\Gamma(D^0 \to \omega\gamma)$ [982]. Namely, the long-distance mechanism $c\bar{u} \to d\bar{d}\gamma$ screens the $c\bar{u} \to u\bar{u}\gamma$ transition in $D^0 \to \rho^0\gamma$ and $D^0 \to \omega\gamma$, the ρ^0 and ω mesons being mixtures of $u\bar{u}$ and $d\bar{d}$. Fortunately, the LD contributions are mostly canceled in the ratio

$$R = \frac{BR(D^0 \to \rho^0\gamma) - BR(D^0 \to \omega\gamma)}{BR(D^0 \to \omega\gamma)}$$

$$\propto \mathrm{Re}\,\frac{A(D^0 \to u\bar{u}\gamma)}{A(D^0 \to d\bar{d}\gamma)}, \tag{210}$$

which is proportional to the SD amplitude $A(D^0 \to u\bar{u}\gamma)$ driven by $c \to u\gamma$. This ratio is $R_{\mathrm{SM}} = (6 \pm 15)\%$ in Ref. [982] and can be enhanced up to $\mathcal{O}(1)$ in the MSSM. In addition to the $c \to u\gamma$ searches in the charm meson decays, in Ref. [976], it was suggested to search for this transition in the decay $B_c \to B_u^*\gamma$, where the long-distance contribution is much smaller.

The inclusive $c \to ul^+l^-$ process can be tested in the rare decays $D \to \mu^+\mu^-$, $D \to P(V)l^+l^-$ [911, 913, 976, 977]. The branching ratio for the rare decay $D \to \mu^+\mu^-$ is very small in the SM. The detailed treatment of this decay rate [911] gives $Br(D \to \mu^+\mu^-) \simeq 3 \times 10^{-13}$ [911]. This decay rate can be enhanced within a study which considers SUSY with R-parity breaking effects [911, 912]. Using the bound $\tilde{\lambda}'_{22k}\tilde{\lambda}'_{21k} \simeq 0.001$, one obtains the limit $Br(D \to \mu^+\mu^-)_R \simeq 4 \times 10^{-7}$, a value which would be accessible at LHCb [935]. The $D \to P(V)l^+l^-$ decays offer another possibility to study the $c \to ul^+l^-$ transition in charm sector. The $D^+ \to \pi^+l^+l^-$ and $D^0 \to \rho^0e^+e^-$ decay modes are simplest to be accessed by experiment [145]. The effects

of SUSY with R parity violation were studied in [911]. The recent experimental results of [978] restrict the R parity violating parameters found in [911] more than one order of magnitude.

The most appropriate decay modes for the experimental searches of the NP coming from the FCNC tree level current are $D^+ \to \pi^+l^+l^-$ and $D^0 \to \rho^0e^+e^-$. The total rate for $D \to Xl^+l^-$ is dominated by the long-distance resonant contributions at dilepton mass $m_{ll} = m_\rho$, m_ω, m_ϕ, and even the largest contributions from NP are not expected to affect the total rate significantly [911, 976]. NP could only modify the SM differential spectrum at low m_{ll} below ρ or the spectrum at high m_{ll} above ϕ. In the case of $D \to \pi l^+l^-$ differential decay distribution, there is a broad region at high m_{ll} (see Fig. 56), which presents a unique possibility to study the $c \to ul^+l^-$ transition [145, 976]. In Table 49, we present the branching ratios for $D^+ \to \pi^+e^+e^-$ and $D^0 \to \rho^0l^+l^-$, giving the SM short-distance, long-distance contributions, as well as the effects of NP arising from the existence of one extra up-type quark. The total rates in the SM and NP scenarios are completely dominated by the resonant long-distance contribution $D \to XV_0 \to Xl^+l^-$ [145, 911]. The SM short-distance contribution for $D^0 \to \rho^0l^+l^-$ (see Fig. 56) is not shown, since it is completely negligible in comparison to the long-distance contribution. The forward–backward asymmetry for $D^0 \to \rho^0l^+l^-$ vanishes in SM, while it is reaching 0.05 in an NP model with extra up-type quark, as given in Fig. 57. Such an asymmetry is still small and will be difficult to observe in present or planned experiments given that the rate itself is already small.

3.9.24 Experimental results

There are a large number of FCNC charm decays including radiative, fully leptonic decays, lepton flavor violating (LFV) and lepton number violating (LNV) that have been measured experimentally.

Belle has reported the observation of the decay $D^0 \to \phi\gamma$. This is the first observation of a flavor-changing radiative decay of a charmed meson. The Cabibbo- and colour-suppressed decays $D^0 \to \phi\pi^0$, $\phi\eta$ are also observed for the first time. The branching fractions are $\mathcal{B}(D^0 \to \phi\gamma) = [2.60^{+0.70+0.15}_{-0.61-0.17}] \times 10^{-5}$ (somewhat higher than predicted in Table 48), $\mathcal{B}(D^0 \to \phi\pi^0) = [8.01 \pm 0.26 \pm 0.47] \times 10^{-4}$ and $\mathcal{B}(D^0 \to \phi\eta) = [1.48 \pm 0.47 \pm 0.09] \times 10^{-4}$.

Recently, CLEO-c reported the branching fraction of the resonant decay $\mathcal{BR}(D^+ \to \pi^+\phi \to \pi^+e^+e^-) = (2.8 \pm 1.9 \pm 0.2) \times 10^{-6}$ [978]. The LNV or LFV decays $D^+ \to \pi^-l^+l^+$, $K^-l^+l^+$ and $\pi^+\mu^+e^-$ are forbidden in the SM. Past searches have set upper limits for the dielectron and dimuon decay modes [119].

The BaBar Collaboration has recently reported on FCNC decays of the form $D^+/D_s^+/\Lambda_c^+ \to \pi^+/K^+/p^+\ell^+\ell'^-$, where the two leptons, ℓ^+ and ℓ'^-, can each be either an

Table 48 Predicted branching ratios for $D \to V\gamma$ decays

$D \to V\gamma$	BR
$D^0 \to \bar{K}^{*0}\gamma$	$[6\text{–}36] \times 10^{-5}$
$D_s^+ \to \rho^+\gamma$	$[20\text{–}80] \times 10^{-5}$
$D^0 \to \rho^0\gamma$	$[0.1\text{–}1] \times 10^{-5}$
$D^0 \to \omega\gamma$	$[0.1\text{–}0.9] \times 10^{-5}$
$D^0 \to \phi\gamma$	$[0.4\text{–}1.9] \times 10^{-5}$
$D^+ \to \rho^+\gamma$	$[0.4\text{–}6.3] \times 10^{-5}$
$D_s^+ \to K^{*+}\gamma$	$[1.2\text{–}5.1] \times 10^{-5}$
$D^+ \to K^{*+}\gamma$	$[0.3\text{–}4.4] \times 10^{-6}$
$D^0 \to K^{*0}\gamma$	$[0.3\text{–}2.0] \times 10^{-6}$

Table 49 Branching ratios for the decays probing the $c \rightarrow u l^+ l^-$ transition

Br	Short-distance contribution only		Total rate $\simeq$ long-distance contr.	Experiment
	SM	SM + NP		
$D^+ \rightarrow \pi^+ e^+ e^-$	6×10^{-12}	8×10^{-9}	1.9×10^{-6}	$< 7.4 \times 10^{-6}$
$D^+ \rightarrow \pi^+ \mu^+ \mu^-$	6×10^{-12}	8×10^{-9}	1.9×10^{-6}	$< 8.8 \times 10^{-6}$
$D^0 \rightarrow \rho^0 e^+ e^-$	negligible	5×10^{-10}	1.6×10^{-7}	$< 1.0 \times 10^{-4}$
$D^0 \rightarrow \rho^0 \mu^+ \mu^-$	negligible	5×10^{-10}	1.5×10^{-7}	$< 2.2 \times 10^{-5}$

Fig. 56 The dilepton mass distribution dBr/dm_{ee}^2 for the decay $D^+ \rightarrow \pi^+ e^+ e^-$ as a function of the dilepton mass square $m_{ee}^2 = (p_+ + p_-)^2$ (*left*) and the dilepton mass distribution for $D^0 \rightarrow \rho^0 e^+ e^-$ (*right*)
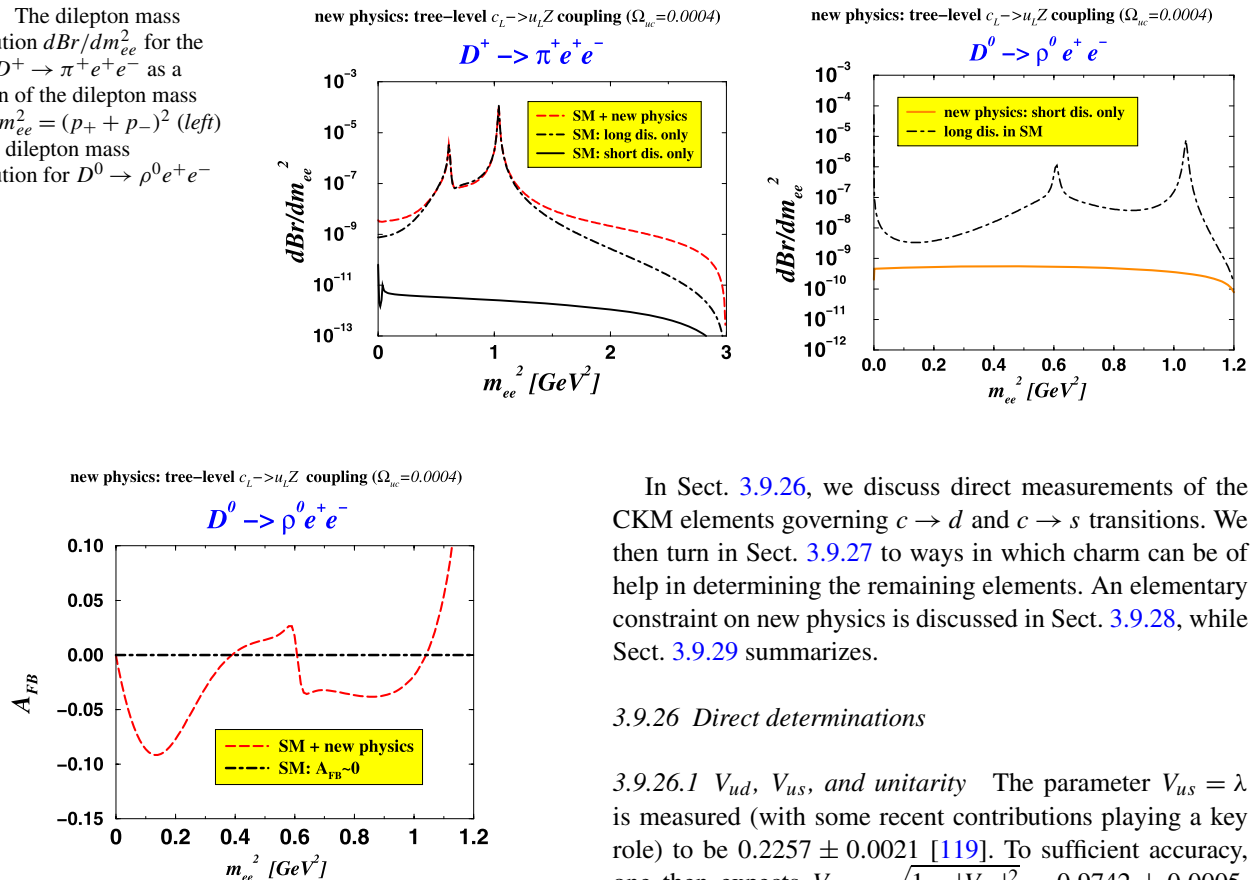
Fig. 57 The figure shows the forward–backward asymmetry for $D^0 \rightarrow \rho^0 e^+ e^-$

electron or a muon. Upper limits are set at the 90% C.L. between 4×10^{-6} and 40×10^{-6} on the SM and LFV processes [979].

In Table 50, the current limits and expected sensitivities at BES-III are summarized for D^+ and D^0, respectively.

3.9.25 Precision CKM physics

Precision measurements of the CKM matrix continue to be of great interest, despite impressive strides in determining its parameters [7–9, 120, 209–211]. We first give an overview of ways in which studies of charm can help this effort. More details on some aspects are given in subsequent subsections.

In Sect. 3.9.26, we discuss direct measurements of the CKM elements governing $c \rightarrow d$ and $c \rightarrow s$ transitions. We then turn in Sect. 3.9.27 to ways in which charm can be of help in determining the remaining elements. An elementary constraint on new physics is discussed in Sect. 3.9.28, while Sect. 3.9.29 summarizes.

3.9.26 Direct determinations

3.9.26.1 V_{ud}, V_{us}, and unitarity The parameter $V_{us} = \lambda$ is measured (with some recent contributions playing a key role) to be 0.2257 ± 0.0021 [119]. To sufficient accuracy, one then expects $V_{ud} = \sqrt{1 - |V_{us}|^2} = 0.9742 \pm 0.0005$, since $|V_{ub}| \simeq 0.004$ and hence its square can be neglected in the unitarity relation $|V_{ud}|^2 + |V_{us}|^2 + |V_{ub}|^2 = 1$. The experimental value for V_{ud}, based primarily upon comparing beta-decays of certain nuclei to muon decays, is $V_{ud} = 0.97377 \pm 0.00027$, so unitarity is adequately satisfied for the first row.

3.9.26.2 V_{cd} For the first column, one expects $|V_{ud}|^2 + |V_{cd}|^2 + |V_{td}|^2 = 1$. With the value of V_{ud} quoted above and $|V_{td}| \simeq 0.008$, one then expects $|V_{cd}| = 0.227 \pm 0.001$. This is to be compared with the value 0.230 ± 0.011 obtained from neutrino interactions [119] and $0.213 \pm 0.008 \pm 0.021$ from charm semileptonic decays [992]. The first error is experimental, and the second one is associated with uncertainty in the form factor. Measurements of the branching fractions for $D \rightarrow \pi \ell \nu$ decay are improving somewhat

434

Eur. Phys. J. C (2008) 57: 309–492

Table 50 Current and projected 90% C.L. upper limits on rare D^+ and D^0 decay modes at BES-III with 20 fb^{-1} data at $\psi(3770)$ peak

Mode	Reference experiment	Best upper limits (10^{-6})	BES-III ($\times 10^{-6}$)	Mode	Reference experiment	Best upper limits (10^{-6})	BES-III ($\times 10^{-6}$)
D^+				D^0			
$\pi^+e^+e^-$	CLEO-c [978]	7.4	0.03	$\gamma\gamma$	CLEO [985]	28	0.05
$\pi^+\mu^+\mu^-$	FOCUS [986]	8.8	0.03	$\mu^+\mu^-$	D0 [987]	2.4	0.03
$\pi^+\mu^\pm e^\mp$	BaBar [979]	5.9/10.8	0.03	μ^+e^-	E791 [988]	8.1	0.03
$\pi^-e^+e^+$	CLEO-c [978]	3.6	0.03	e^+e^-	E791 [988]	6.2	0.03
$\pi^-\mu^+\mu^+$	FOCUS [986]	4.8	0.03	$\pi^0\mu^+\mu^-$	E653 [989]	180	0.05
$\pi^-\mu^+e^+$	E791 [988]	50	0.03	$\pi^0\mu^+e^+$	CLEO [990]	86	0.05
$K^+e^+e^-$	CLEO-c [978]	6.2	0.03	$\pi^0e^+e^-$	CLEO [990]	45	0.05
$K^+\mu^+\mu^-$	FOCUS [986]	9.2	0.03	$K_S\mu^+\mu^-$	E653 [989]	260	0.1
$K^+\mu^\pm e^\mp$	BaBar [979]	5.9/5.7	0.03	$K_S\mu^+e^-$	CLEO [990]	100	0.1
$K^-e^+e^+$	CLEO-c [978]	4.5	0.03	$K_Se^+e^-$	CLEO [990]	110	0.1
$K^-\mu^+\mu^+$	FOCUS [986]	13	0.03	$\eta\mu^+\mu^-$	CLEO [990]	530	0.1
$K^-\mu^+e^+$	E687 [991]	130	0.03	$\eta\mu^+e^-$	CLEO [990]	100	0.1
				ηe^+e^-	CLEO [990]	110	0.1

(Sect. 3.9.29.2), so the precision of $|V_{cd}|$ from this source will improve. However, from the current uncertainties in $\mathcal{B}(D\to\pi\ell\nu)$ it is clear that one will not be able to match the precision of the unitarity test for the first row of the CKM matrix anytime soon. *Given* CKM unitarity, which says to sufficient accuracy that we should expect the value of $|V_{cd}|$ mentioned above, one can use it to constrain form factors in semileptonic charm decays and compare them with lattice QCD calculations.

3.9.26.3 V_{cs} A similar philosophy applies to the CKM element V_{cs}. Unitarity applied to the second column of the CKM matrix implies $|V_{cs}| = \sqrt{1 - |V_{us}|^2 - |V_{ts}|^2}$. Taking the experimental value of V_{us} mentioned above and the unitarity-based estimate $V_{ts} \simeq -V_{cb}$, we estimate $|V_{cs}| = 0.9733 \pm 0.0006$. This precision will not be matched by experiment soon. The best measurements come from semileptonic charm decays and yield $|V_{cs}| = 0.957 \pm 0.017 \pm 0.093$, with the second error coming from uncertainty in the form factor. Again, assuming unitarity, one will be able to subject lattice gauge theory predictions to important tests.

3.9.27 Indirect tests

3.9.27.1 V_{ub} The primary difficulty in measuring the matrix element V_{ub} is that it must be extracted from b semileptonic decays which proceed to charm all but 2% of the time. Inclusive methods must rely on kinematic separation techniques, the oldest of which is the study of leptons with energies beyond the endpoint for $b\to c\ell\nu$. Exclusive decays such as $B\to\pi\ell\nu$ and $B\to\rho\ell\nu$ do not share this problem, but one must understand the corresponding form factors.

Tests of form factors in *charm* decays predicted by lattice gauge theories can help validate predictions for B decays.

The phase of V_{ub}^* (γ or ϕ_3 in the standard parameterizations) can be measured in several ways with the help of information from charm decays. These help, for example, in using decays such as $B\to D_{CP}K$ decays to learn γ. For D modes such as $K_S\pi^+\pi^-$, $\pi^+\pi^-\pi^0$, $K^+K^-\pi^0$, and $K_SK^\pm\pi^\mp$, Dalitz plots yield information on CP-eigenstate and flavor-eigenstate modes and their relative phases [993].

The interference of $b\to c\bar{u}s$ (real) and $b\to u\bar{c}s$ ($\sim e^{-i\gamma}$) subprocesses in $B^-\to D^0K^-$ and $B^-\to \bar{D}^0K^-$, respectively, is sensitive to the weak phase γ. This interference may be probed by studying common decay products of D^0 and $\bar{D}^0$ into neutral D CP eigenstates or into doubly-Cabibbo-suppressed modes [627, 632, 633, 636, 645, 646].

As one example, the decays $B^\pm\to K^\pm(K^{*+}K^-)_D$ and $B^\pm\to K^\pm(K^{*-}K^+)_D$ provide information on γ if the relative (strong) phase between $D^0\to K^{*+}K^-$ and $D^0\to K^{*-}K^+$ is known [994]. One can learn this relative phase from the study of $D^0\to K^+K^-\pi^0$, since both final states occur and interfere with one another where K^{*+} and K^{*-} bands cross on the Dalitz plot [995]. This method was used recently by the CLEO Collaboration [996] to show that this interference was predominantly destructive in the overlap region.

As another example, one can determine γ using $B^\pm\to DK^\pm$ followed by $D\to K_S\pi^+\pi^-$, $K_SK^+K^-$, $K_S\pi^+\pi^-\pi^0$ [637, 997]. Recent high-statistics studies have been performed by BaBar [641] and Belle [639]. The precision of these measurements will eventually be limited by the understanding of the $D\to K_S^0\pi^+\pi^-$ Dalitz plot. K-matrix descriptions of the $\pi\pi$ S-wave may yield improved models

of charm Dalitz plots, and these models will be tested using the CP tagged sample of charm decays at CLEO-c and later at BES-III. The model uncertainty, which is currently $\pm 10°$, may be reduced to a few degrees.

Model independent methods [648, 998] use CP tagged $K_S^0 \pi^+ \pi^-$ and $D\bar{D} \to (K_S^0 \pi^+ \pi^-)^2$ to control the Dalitz plot model uncertainty. Analyses underway at CLEO-c are expected to control this systematic uncertainty on γ/ϕ_3 to a few degrees.

3.9.27.2 V_{cb} The semileptonic decays of B mesons to D or D^* mesons are one source of information about the element V_{cb}, but one must understand form factors satisfactorily. Lattice gauge theories make predictions for such form factors; the validation of lattice form factor predictions in charm decays again is a key ingredient in establishing credibility of the $B \to D^{(*)}$ form factor predictions. Moreover, under some circumstances, it is helpful to have precise information about D branching ratios to specific final states, which detailed charm studies can provide.

3.9.27.3 V_{td} and $|V_{td}/V_{ts}|$ The mixing of B^0 and $\bar{B}^0$ is governed primarily by the CKM product $|V_{tb}^* V_{td}|$. If unitarity is assumed, $|V_{tb}|$ is very close to 1, so the dominant CKM source of uncertainty is $|V_{td}|$. However, the matrix element of the short-distance operator inducing the $b\bar{d} \to d\bar{b}$ transition contains an unknown factor $f_B^2 B_B$, where f_B is the B meson decay constant, while $B_B = \mathcal{O}(1)$ is known as the "bag constant" or "vacuum saturation factor" and expresses the degree to which the vacuum intermediate state dominates the transition. The corresponding mixing of strange B's and their antiparticles is governed by $|V_{tb}^* V_{ts}|$ and $f_{B_s}^2 B_{B_s}$.

Lattice gauge theories predict not only f_B and f_{B_s} (as well as the constants B_B and B_{B_s}) but also the decay constants f_D and f_{D_s} for charmed mesons. Thus, the study of charmed meson decay constants (Sect. 3.9.29.1) and their ratios and comparison with lattice predictions can shed indirect light on quantities of interest in determining the CKM matrix elements V_{td} and V_{ts}.

To give one example of the role charm measurements can play, it is expected on rather general grounds [999] that f_{B_s}/f_B and f_{D_s}/f_D are equal to within a few percent. Now, the ratio f_{B_s}/f_B is a key ingredient in the extraction of $|V_{td}/V_{ts}|$ from measurements of B^0–$\bar{B}^0$ and B_s^0–$\bar{B}_s^0$ mixing. The determination of Ref. [677] utilized the estimate $(f_{B_s}\sqrt{B_{B_s}}/f_B\sqrt{B_B}) = 1.21^{+0.047}_{-0.035}$ from the lattice [301]. With a sufficiently good measurement of f_{D_s}/f_D and the theoretical input (again, from the lattice) that $B_{B_s}/B_B \simeq 1$, one could check the lattice prediction or simply substitute an experimental measurement for it.

3.9.28 New physics constraint

To see how great an impact even modest improvements in testing CKM unitarity in the charm sector would have, we consider a model in which a fourth family (t', b') of quarks is added to the usual three, with neutrinos heavy enough to evade the constraint $N_\nu = 3$ due to invisible Z decays. Unitarity relations involving the first two rows and columns of the expanded 4×4 CKM matrix allow us to calculate the following 90% C.L. upper limits using the best-measured quantities mentioned above:

$$|V_{ub'}| = \sqrt{1 - |V_{ud}|^2 - |V_{us}|^2 - |V_{ub}|^2} \le 0.05, \qquad (211)$$

$$|V_{cb'}| = \sqrt{1 - |V_{cd}|^2 - |V_{cs}|^2 - |V_{cb}|^2} \le 0.5, \qquad (212)$$

$$|V_{t'd}| = \sqrt{1 - |V_{ud}|^2 - |V_{cd}|^2 - |V_{td}|^2} \le 0.07, \qquad (213)$$

$$|V_{t's}| = \sqrt{1 - |V_{us}|^2 - |V_{cs}|^2 - |V_{ts}|^2} \le 0.5. \qquad (214)$$

The poor quality of the bounds on $|V_{cb'}|$ and $|V_{t's}|$ is largely due to the 10% error on $|V_{cs}|$, which translates to errors of 0.18 on $|V_{cb}|^2$ and $|V_{td}|^2$ and 90% C.L. upper limits on them of about 1/4. Thus improved measurements of V_{cs} could have a great impact on closing a rather gaping window for new physics or even revealing it.

3.9.29 Summary of overview

The above examples show that charmed particle studies have a large role to play in precision CKM physics, affecting nearly all the elements of the CKM matrix. In turn, precision CKM physics is important as a clue to the very origin of quark masses, since the CKM matrix arises from the same physics which generates those masses.

3.9.29.1 Leptonic decays Purely leptonic decays of charm mesons are of prime importance for checks of theoretical QCD calculations and searches for NP. Extraction of precise CKM information from neutral B mixing requires precision knowledge of the ratio of decay constants for B_s and B^0 [214]. While QCD calculations provide this estimate, the uncertainties are large, and the methods need to checked by seeing if they can reproduce charm measurements. Leptonic decays proceed in the SM by annihilation of the charm quark and spectator antiquark into a virtual W^+ that transforms to a lepton-antineutrino pair, as shown for the D^+ meson in Fig. 58.

In the SM, the decay width is given by [1000]

$$\Gamma\left(D^+ \to \ell^+ \nu\right) = \frac{G_F^2}{8\pi} f_{D^+}^2 m_\ell^2 M_{D^+} \left(1 - \frac{m_\ell^2}{M_{D^+}^2}\right)^2 |V_{cd}|^2,$$
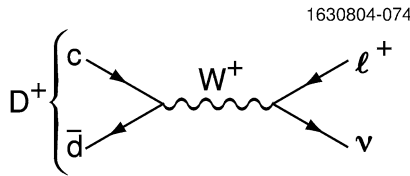
$$(215)$$

Fig. 58 The decay diagram for $D^+ \rightarrow \ell^+ \nu$

where M_{D^+} is the D^+ mass, m_ℓ is the mass of the final-state lepton, $|V_{cd}|$ is a CKM matrix element assumed to be equal to $|V_{us}|$, and G_F is the Fermi coupling constant. (The same formula applies to $D_s^+ \rightarrow \ell^+ \nu$ decays with the replacement of D_s^+ mass and $|V_{cs}|$.)

NP can affect the expected widths; any undiscovered charged bosons would interfere with the SM W^+. These effects may be difficult to ascertain, since they would simply change the values of the f_i's. The ratio $f_{D_s^+}/f_{D^+}$ is much better predicted in the SM than the values individually, so deviations seen here could point to beyond the SM charged bosons. For example, Akeroyd [1001] predicts that the presence of a charged Higgs boson would suppress this ratio significantly.

We can also measure the ratio of decay rates to different leptons, and the predictions then are fixed only by well-known masses. For example, for $\tau^+ \nu$ to $\mu^+ \nu$:

$$R \equiv \frac{\Gamma(D^+ \rightarrow \tau^+ \nu)}{\Gamma(D^+ \rightarrow \mu^+ \nu)} = \frac{m_{\tau^+}^2 (1 - \frac{m_{\tau^+}^2}{M_{D^+}^2})^2}{m_{\mu^+}^2 (1 - \frac{m_{\mu^+}^2}{M_{D^+}^2})^2}. \tag{216}$$

Any deviation from this formula would be a manifestation of physics beyond the SM. This could occur if any other charged intermediate boson existed that coupled to leptons differently than mass-squared. Then the couplings would be different for muons and τ's. This would be a manifest violation of lepton universality, which has identical couplings of the muon, the tau, and the electron to the gauge bosons (γ, Z^0 and $W^\pm$) [1002]. (We note that in some models of supersymmetry, the charged Higgs boson couples as mass-squared to the leptons and therefore its presence would not cause a deviation from (216) [31].)
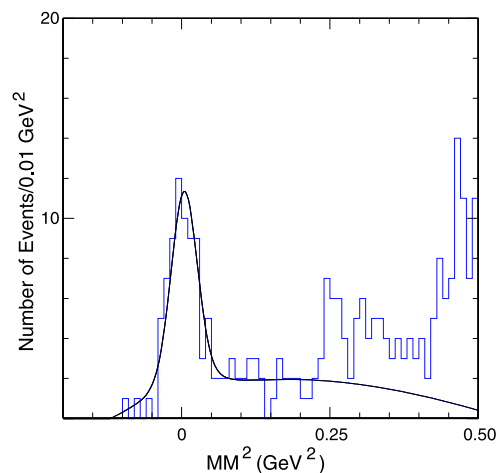
The CLEO-c Collaboration has published a result for f_{D^+} [323, 1003]. Several results have been obtained for $f_{D_s^+}$, the most precise being a preliminary result from CLEO-c. To measure f_{D^+}, CLEO-c uses a "double-tag" method, possible because at an e^+e^- centre-of-mass energy of 3770 GeV, the location of the ψ'' resonance, D^+D^- final states are produced without any extra particles. Here one D^- is fully reconstructed, and then there are enough kinematic constraints (energy and momentum) to search for $D^+ \rightarrow \mu^+ \nu$ by constructing the missing mass-squared (MM^2) opposite the D^- and the muon, which should peak at the essentially zero neutrino mass-squared. Explicitly,

$$\text{MM}^2 = (E_{\text{beam}} - E_{\mu^+})^2 - (-\boldsymbol{p}_{D^-} - \boldsymbol{p}_{\mu^+})^2, \tag{217}$$

where $\boldsymbol{p}_{D^-}$ is the three-momentum of the fully reconstructed D^-. The CLEO-c MM^2 distribution is shown in Fig. 59. The peak near zero contains 50 signal events of which 2.8 are estimated background.

The resulting rate is

$$\mathcal{B}(D^+ \rightarrow \mu^+ \nu) = (4.40 \pm 0.66^{+0.09}_{-0.12}) \times 10^{-4}. \tag{218}$$

Fig. 59 CLEO-c missing mass-squared distributions. (*Left*) Using D^- tags and one additional opposite sign charged track depositing <300 MeV (consistent with a muon) in the calorimeter and no extra energetic clusters. The *inset* shows the signal region for $D^+ \rightarrow \mu^+ \nu$ enlarged; the defined signal region is shown between the two arrows.

(*Right*) Using D_s^- tags but allowing any energy deposit in the calorimeter (consistent with muon or pion). The *curve* is the predicted shape for the sum $D_s^+ \rightarrow \mu^+ \nu + D_s^+ \rightarrow \tau^+ \nu$, $\tau^+ \rightarrow \pi^+ \nu$ normalized to the data for MM^2 < 0.2 GeV^2

The decay constant f_{D^+} is then obtained from (215) using 1.040 ± 0.007 ps as the D^+ lifetime [119] and $|V_{cd}| = 0.2238 \pm 0.0029$, giving

$$f_{D^+} = \left(222.6 \pm 16.7^{+2.8}_{-3.4}\right) \text{ MeV}. \tag{219}$$

CLEO-c also sets limits on $\mathcal{B}(D^+ \to e^+ \nu_e) < 2.4 \times 10^{-5}$ [323, 1003] and $\mathcal{B}(D^+ \to \tau^+ \nu)$ branching ratio to $< 2.1 \times 10^{-3}$ (90% C.L.) [1004]. These limits are consistent with SM expectations.

Before turning to theoretical prediction of f_{D^+}, we discuss the current status of $D_s^+ \to \mu^+ \nu$. Results here have been obtained by several experiments [119]. However, these results have been subject to sizable systematic errors, the largest of which usually is the uncertainty on $\mathcal{B}(D_s^+ \to \phi \pi^+)$ that is important because the measurements are usually normalized by taking the ratio of the observed number of $\ell^+ \nu$ events to $\phi \pi^+$ events.

CLEO-c eliminates this uncertainty by making absolute measurements directly. Data are obtained near 4.170 GeV. Here the cross-section for $D_s^{*\pm} D_s^{\mp}$ is ~ 1 nb. Both $\mu^+ \nu$ and $\tau^+ \nu$ decays are examined with two different decay modes of the τ^+ used, $\pi^+ \bar{\nu}$ and $e^+ \nu \bar{\nu}$. The MM^2 distribution for the sum of $D_s^+ \to \mu^+ \nu + D_s^+ \to \tau^+ \nu$, $\tau^+ \to \pi^+ \nu$ is shown on the right side of Fig. 59. Analysing these samples separately, they find the ratio R from (216) is consistent with the SM expectation of 9.72. Combining both gives a measurement using (215) of $f_{D_s} = 282 \pm 16 \pm 7$ MeV. CLEO-c also uses the $D_s^+ \to \tau^+ \nu$, $\tau \to e^+ \nu \bar{\nu}$ to find $f_{D_s} = 278 \pm 17 \pm 12$ MeV. Combining the two results gives

$$f_{D_s} = 280.1 \pm 11.6 \pm 6.0 \text{ MeV}. \tag{220}$$

Using only the $D_s^+ \to \tau^+ \nu$, $\tau \to e^+ \nu \bar{\nu}$ and the $D_s^+ \to \mu^+ \nu$, CLEO-c finds

$$R = \frac{\Gamma(D_s^+ \to \tau^+ \nu)}{\Gamma(D_s^+ \to \mu^+ \nu)} = 9.9 \pm 1.7 \pm 0.7, \tag{221}$$

again consistent with the SM expectation. Furthermore CLEO-c also sets limits on $\mathcal{B}(D_s^+ \to e^+ \nu_e) < 3.1 \times 10^{-4}$.

The branching fractions, modes and derived values of $f_{D_s^+}$ from all measurements are listed in Table 51. Most measurements of $D_s^+ \to \ell^+ \nu$ are normalized with respect to $\mathcal{B}(D_s^+ \to \phi \pi^+)$. These measurements are difficult to average because of the uncertainty in this scale, and we do not attempt this here. We can extract a value for ratio using the CLEO-c measurements only, since the scale error is absent:

$$f_{D_s^+} / f_{D^+} = 1.26 \pm 0.11 \pm 0.03. \tag{222}$$

Theoretical calculations of $f_{D_s^+}$, f_{D^+} and the ratio $\frac{f_{D_s^+}}{f_{D^+}}$ are listed in Table 52. While the CLEO-c decay constant results are slightly higher than most theoretical expectations, the ratio is quite consistent with lattice gauge theory and most other models. Furthermore, no deviations from SM expectations are found in the ratio of decay rates for various lepton species.

3.9.29.2 Semileptonic decays The study of semileptonic charm decays has several important ramifications. Figure 60 shows the Feynman diagram describing these decays. It shows that the matrix element describing these decays can be expressed as the product of a leptonic current, unaffected by strong interactions, and a hadronic current, where the nonperturbative QCD effects are generally modeled with form factors. Theoretical predictions for these form factors have been derived in the framework of quark models, QCD sum rules and lattice QCD. Thus the study of inclusive and exclusive semileptonic decay branching fractions and form factors provides the experimental constraints needed to assess whether theoretical calculations are reliable and feature well-understood errors.

On the other hand, once computational techniques developed to predict relevant form factors demonstrate that

Table 51 Measurements of $f_{D_s^+}$. Results have been updated for new values of the D_s lifetime. ALEPH uses both measurements to derive a value for the decay constant

Exp.	Mode	$\mathcal{B}$	$\mathcal{B}_{\phi\pi}$ (%)	$f_{D_s^+}$ (MeV)
CLEO-c	$\mu^+\nu$	$(6.57 \pm 0.90 \pm 0.34) \times 10^{-3}$		$281 \pm 19 \pm 7$
CLEO-c	$\tau^+\nu, \tau \to \pi\nu$	$(7.1 \pm 1.4 \pm 0.3) \times 10^{-2}$		$296 \pm 29 \pm 7$
CLEO-c	$\tau^+\nu, \tau \to e\nu\nu$	$(6.29 \pm 0.78 \pm 0.52) \times 10^{-2}$		$278 \pm 17 \pm 12$
CLEO-c	combined	–		$280.1 \pm 11.6 \pm 6.0$
CLEO [1005]	$\mu^+\nu$	$(6.2 \pm 0.8 \pm 1.3 \pm 1.6) \times 10^{-3}$	3.6 ± 0.9	$273 \pm 19 \pm 27 \pm 33$
BEATRICE [1006]	$\mu^+\nu$	$(8.3 \pm 2.3 \pm 0.6 \pm 2.1) \times 10^{-3}$	3.6 ± 0.9	$315 \pm 43 \pm 12 \pm 39$
ALEPH [1007]	$\mu^+\nu$	$(6.8 \pm 1.1 \pm 1.8) \times 10^{-3}$	3.6 ± 0.9	$285 \pm 19 \pm 40$
ALEPH [1007]	$\tau^+\nu$	$(5.8 \pm 0.8 \pm 1.8) \times 10^{-2}$		
OPAL [1008]	$\tau^+\nu$	$(7.0 \pm 2.1 \pm 2.0) \times 10^{-3}$		$286 \pm 44 \pm 41$
L3 [1009]	$\tau^+\nu$	$(7.4 \pm 2.8 \pm 1.6 \pm 1.8) \times 10^{-3}$		$302 \pm 57 \pm 32 \pm 37$
BaBar [325]	$\mu^+\nu$	$(6.7 \pm 0.8 \pm 0.3 \pm 0.7) \times 10^{-3}$	4.7 ± 0.5	$283 \pm 17 \pm 7 \pm 14$

438

Eur. Phys. J. C (2008) 57: 309–492

Table 52 Theoretical predictions of f_{D^+} and $f_{D_s^+}/f_{D^+}$. QL indicates quenched lattice calculations

Model	$f_{D_s^+}$ (MeV)	f_{D^+} (MeV)	$f_{D_s^+}/f_{D^+}$
Lattice ($n_f = 2 + 1$) [313]	$249 \pm 3 \pm 16$	$201 \pm 3 \pm 17$	$1.24 \pm 0.01 \pm 0.07$
QL (Taiwan) [1010]	$266 \pm 10 \pm 18$	$235 \pm 8 \pm 14$	$1.13 \pm 0.03 \pm 0.05$
QL (UKQCD) [709]	$236 \pm 8^{+17}_{-14}$	$210 \pm 10^{+17}_{-16}$	$1.13 \pm 0.02^{+0.04}_{-0.02}$
QL [1011]	$231 \pm 12^{+6}_{-1}$	$211 \pm 14^{+2}_{-12}$	1.10 ± 0.02
QCD Sum Rules [1012]	205 ± 22	177 ± 21	$1.16 \pm 0.01 \pm 0.03$
QCD Sum Rules [1013]	235 ± 24	203 ± 20	1.15 ± 0.04
Quark Model [1014]	268	234	1.15
Quark Model [1015]	248 ± 27	230 ± 25	1.08 ± 0.01
Potential Model [1016, 1017]	241	238	1.01
Isospin Splittings [1018]		262 ± 29	
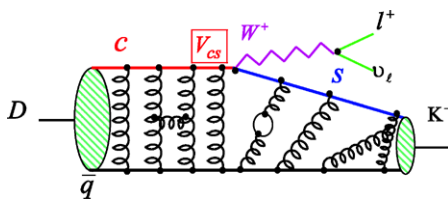
Fig. 60 Feynman diagram for the semileptonic decay of charmed mesons. The QCD nonperturbative effects are described by q^2-dependent form factors

they can achieve reliable results with well understood errors, these data allow precise determinations of the CKM matrix elements V_{cs} and V_{cd}. Moreover a combination of charm and beauty semileptonic decay studies can be used to determine V_{ub}.

3.9.30 Branching fractions

We are now progressing towards a complete precision determination of the absolute inclusive and exclusive charm semileptonic branching fractions. Inclusive semileptonic widths can provide some information on weak annihilation diagrams [912]. Finally, better knowledge of the inclusive positron spectra can be used to improved modeling of the "cascade" decays $b \to c \to se^+\nu_e$ and thus it affects the precision of several measurements of b decays.

CLEO-c uses the two tagging modes with lowest background ($\bar{D}^0 \to K^+\pi^-$ and $D^- \to K^+\pi^-\pi^-$) to measure the inclusive D^0 and D^+ semileptonic branching fractions [1019]. The kinematic constraints available through the use of D tagged samples from data taken at the $\psi(3770)$ provide a unique tool to select a pure sample of electrons/positrons coming from D semileptonic decays. They obtain $\mathcal{B}(D^0 \to X\ell\nu_e) = (6.46 \pm 0.17 \pm 0.13)\%$ and $\mathcal{B}(D^+ \to X\ell\nu_e) = (16.13 \pm 0.20 \pm 0.33)\%$. The inclusive branching fractions can be translated into inclusive semileptonic widths Γ_{D^+} and Γ_{D^0}, using the well-known D lifetimes [119]. These

widths are expected to be equal, modulo isospin violations, and indeed the measured ratio $\Gamma^{\text{sl}}_{D^+}/\Gamma^{\text{sl}}_{D^0} = 0.985 \pm 0.028 \pm 0.015$: thus isospin violations are limited to be below $\sim 3\%$.

BES-II [340, 1020] and CLEO-c [1021, 1022] have recently published data on exclusive semileptonic branching fractions. BES-II results are based on 33 pb^{-1}; the CLEO-c published data are based on the first 57 pb^{-1}, preliminary results included in this report are based on 281 pb^{-1}.

The variable $U \equiv E_{\text{miss}} - |c\vec{p}_{\text{miss}}|$, where E_{miss} and $\vec{p}_{\text{miss}}$ represent the missing energy and momentum of the D meson decaying semileptonically, is used to select signal events. This variable is a non-Lorentz invariant version of MM^2. Table 53 summarizes the recent data, as well as the averages reported in the PDG 2006 [119].

A comparison between the inclusive branching fractions of the D^+ and D^0 mesons with the sum of the measured exclusive branching fractions determines whether there are unobserved semileptonic decay modes. The corresponding sums of exclusive branching fractions are: $\sum_i \mathcal{B}(D^0 \to X_i\ell\nu_e) = 6.1 \pm 0.2 \pm 0.2$ and $\sum_i \mathcal{B}(D^+ \to X_i\ell\nu_e) = 15.1 \pm 0.50 \pm 0.50$; the measured exclusive modes are consistent with saturating the inclusive widths, although there is some room left for higher multiplicity modes. In particular, CLEO-c also provides the first evidence for $D^0 \to K^-\pi^+\pi^-e^+\nu_e$ [1023]. They study the MM^2 inferred from the missing energy and momentum in the event, and they obtain the preliminary branching fractions:

$$\mathcal{B}(D^0 \to K^-\pi^+\pi^-e^+\nu_e) = \left(2.9^{+1.5}_{-1.1} \pm 0.5\right) \times 10^{-4}, \quad (223)$$

$$\mathcal{B}(D^0 \to K_1(1270)e^+\nu_e) \times \mathcal{B}(K_1(1270) \to K^-\pi^+\pi^-)$$
$$= \left(2.2^{+1.4}_{-1.0} \pm 0.2\right) \times 10^{-4}. \quad (224)$$

This branching fraction is about at the level predicted by Isgur and Scora [292] and is consistent with the expectation that charm semileptonic decays are dominated by the pseudoscalar and vector lowest mass resonances.

Eur. Phys. J. C (2008) 57: 309–492

439

Table 53 CLEO-c branching fractions and new world averages

D^+ mode	Recent data $\mathcal{B}$ (%)	PDG 2006	D^0 mode	Recent data $\mathcal{B}$ (%)	PDG 2006
$\bar{K}^0 e^+ \nu_e$	$8.86 \pm 0.17 \pm 0.20$	8.7 ± 0.5	$K^- e^+ \nu_e$	$3.58 \pm 0.05 \pm 0.05$	3.47 ± 0.13
$\pi^0 e^+ \nu_e$	$0.397 \pm 0.027 \pm 0.028$	0.44 ± 0.06	$\pi^- e^+ \nu_e$	$0.309 \pm 0.012 \pm 0.006$	0.262 ± 0.026
$\eta e^+ \nu_e$	$0.129 \pm 0.019 \pm 0.07$		$K^{*-} e^+ \nu_e$	$2.16 \pm 0.15 \pm 0.08$	2.16 ± 0.16
$\bar{K}^{*0} e^+ \nu_e$	$5.56 \pm 0.27 \pm 0.23$	5.61 ± 0.31	$\rho^- e^+ \nu_e$	$0.156 \pm 0.016 \pm 0.009$	0.194 ± 0.41
$\rho^0 e^+ \nu_e$	$0.232 \pm 0.020 \pm 0.012$	0.22 ± 0.04			
$\omega e^+ \nu_e$	$0.149 \pm 0.027 \pm 0.005$	$0.16^{+0.07}_{-0.06}$			

Finally, D semileptonic decays are a tool to explore light quark spectroscopy. For example, a few years ago, the FOCUS Collaboration reported some evidence for an s-wave interference effect in the decay amplitude of $D^+ \to K^{\star 0} \mu^+ \nu_\mu$ [1024]. This observation can shed some light on our understanding of the elusive scalar meson κ. This observation has been recently confirmed by CLEO-c in the channel $D^+ \to K^{\star 0} e^+ \nu_e$ [1025]. This study will acquire soon a broader scope when CLEO-c will pursue similar analyses in the D_s system.

3.9.31 Form factors for $D \to K(\pi)\ell\nu$ and $D \to K^*(\rho)\ell\nu$

Recently, nonquenched lattice QCD calculations for $D \to K\ell\bar{\nu}$ and $D \to \pi\ell\nu$ have been reported [332]. The chiral extrapolation is performed at fixed $E = \vec{v} \cdot \vec{p}_P$, where E is the energy of the light meson in the centre-of-mass D frame, $\vec{v}$ is the unit 4-velocity of the D meson, and $\vec{p}_P$ is the 4-momentum of the light hadron P (K or π). The results are presented in terms of the parametrization originally proposed by Becirevic and Kaidalov (BK) [280]:

$$f_+\left(q^2\right) = \frac{F}{(1 - \tilde{q}^2)(1 - \alpha\tilde{q}^2)},$$
$$f_0\left(q^2\right) = \frac{F}{1 - \tilde{q}^2/\beta},$$
(225)

where q^2 is the 4-momentum of the electron-ν pair, $\tilde{q}^2 = q^2/m_{D_x^*}^2$, $F = f_+(0)$, and α and β are fit parameters. This formalism models the effects of higher mass resonances other than the dominant spectroscopic pole ($D_S^{\star +}$ for the $K\ell\nu$ final state and $D^{\star +}$ for $\pi\ell\nu$ [1026]).

Table 54 shows the fit results obtained from FOCUS [341], CLEO III [1027], Belle [1028] and BaBar [1029] compared to the lattice QCD predictions [332]. In addition, all these experiments perform a single pole fit, traditionally used because of the conventional ansatz of several quark models [1030], and the BK parametrization discussed before. In Table 55, we include preliminary results of fits obtained with the simple pole model by CLEO-c. All of these experiments obtain very good fits also with simple pole form

Table 54 Measured shape parameter α compared to lattice QCD predictions

	$\alpha(D^0 \to K\ell\nu)$	$\alpha(D^0 \to \pi\ell\nu)$
Lattice QCD [332]	$0.5 \pm 0.04 \pm 0.07$	$0.44 \pm 0.04 \pm 0.07$
FOCUS [341]	$0.28 \pm 0.08 \pm 0.07$	
CLEOIII [1027]	$0.36 \pm 0.10^{+0.03}_{-0.07}$	$0.37^{+0.20}_{-0.31} \pm 0.15$
Belle [1028]	$0.40 \pm 0.12 \pm 0.09$	$0.03 \pm 0.27 \pm 0.13$
BaBar [1029]	$0.43 \pm 0.03 \pm 0.04$	

Table 55 Measured values of M_{pole}

	$M_{\text{pole}}(D^0 \to K\ell\nu)$ (GeV)	$M_{\text{pole}}(D^0 \to \pi\ell\nu)$ (GeV)
FOCUS [341]	$1.93 \pm 0.05 \pm 0.03$	$1.91^{+0.30}_{-0.15} \pm 0.07$
CLEOIII [1027]	$1.89 \pm 0.05^{+0.04}_{-0.03}$	$1.86^{+0.10+0.07}_{-0.06-0.03}$
Belle [1028]	$1.88 \pm 0.06 \pm 0.03$	$2.01 \pm 0.13 \pm 0.04$
BaBar [1029]	$1.854 \pm 0.016 \pm 0.020$	
CLEO-c [1023]	$1.96 \pm 0.03 \pm 0.01$	$1.95 \pm 0.04 \pm 0.02$

factors; however the simple pole fit does not yield the expected spectroscopic mass. This may hint that other higher-order resonances are contributing to the form factors [1026]. It has been argued [1031] that even the BK parametrization is too simple and that a three parameter form factor is more appropriate. This issue can be resolved by larger data samples, with better sensitivity to the curvature of the form factor near the high recoil region.

In experimental studies of $D \to K^*(\rho)\ell\nu$, usually a single pole parametrization of form factors was used. Following the Becirevic–Kaidalov approach [1032, 1033], a new parametrization of the relevant form factors was given by

$$A_1\left(q^2\right) = \frac{A_1(0)}{1 - b'x}, \qquad A_2\left(q^2\right) = \frac{A_2(0)}{(1 - b'x)(1 - b''x)},$$
$$A_0\left(q^2\right) = \frac{A_0(0)}{(1 - y)(1 - a'y)},$$
$$V\left(q^2\right) = \frac{A_1(0)}{\xi(1 - x)(1 - ax)}.$$

440

Eur. Phys. J. C (2008) 57: 309–492

This parametrization takes into account all known scaling properties of the decay to light vector semileptonic transition. The study of nonparametric determination of helicity amplitudes in the semileptonic $D \to K^*(\rho)\ell\nu$ decays will shed more light on the corresponding decays in B physics.

3.9.32 Lattice QCD checks

By combining the information of the measured leptonic and semileptonic widths, the ratio

$$R_{\rm sl} = \sqrt{\frac{\Gamma(D^+ \to \mu^+ \nu_\mu)}{\Gamma(D \to \pi e \nu_e)}}, \tag{226}$$

independent of $|V_{cd}|$, can be evaluated, which is a pure check of the theory. We assume isospin symmetry, and thus $\Gamma(D \to \pi e^+ \nu_e) = \Gamma(D^0 \to \pi^- e^+ \nu_e) = 2\Gamma(D^+ \to \pi^0 e^+ \nu_e)$. For the theoretical inputs, we use the recent unquenched lattice QCD calculations in three flavors [313], as they reflect the state of the art of the theory and have been evaluated in a consistent manner. The theory ratio is

$$R_{\rm sl}^{\rm th} = \sqrt{\frac{\Gamma^{\rm th}(D^+ \to \mu^+ \nu_\mu)}{\Gamma^{\rm th}(D \to \pi e \nu_e)}} = 0.212 \pm 0.028. \tag{227}$$

The quoted error is evaluated through a careful study of the theory statistical and systematic uncertainties, assuming Gaussian errors. The corresponding experimental $R_{\rm sl}^{\rm exp}$ is calculated using the CLEO-c f_D and isospin averaged $\Gamma(D \to \pi e^+ \nu_e)$:

$$R_{\rm sl}^{\rm exp} = \sqrt{\frac{\Gamma^{\rm exp}(D^+ \to \mu^+ \nu)}{\Gamma^{\rm exp}(D \to \pi e \nu_e)}} = 0.237 \pm 0.019. \tag{228}$$

The theory and data are in good agreement, though the errors need to be reduced both in theory and experiment to validate the theory at the needed level of precision ($\sim$1–3%).

3.9.32.1 Hadronic decays

While the dynamical issues are considerably more complex in nonleptonic than in semileptonic decays—both a blessing and a curse—, the available theoretical tools are more limited. For inclusive rates like lifetimes, one can turn to expansions in powers of $1/m_c$ to obtain at least a semi-quantitative description. For exclusive modes, we have 'Old Faithful,' namely quark models, but also QCD sum rules and chiral dynamics with the latter two (in contrast to the first one) firmly rooted in QCD. Lattice QCD, usually perceived as panacea, faces much more daunting challenges in dealing with nonleptonic charm transitions than for semileptonic modes due to the central role played by strong final-state interactions. Yet comprehensive measurements can teach us valuable lessons that can enlighten us about light flavor spectroscopy and also serve as cross checks on B studies. Below we list some core examples for such lessons.

3.9.32.2 Lifetime ratios

Heavy quark theory (HQT) allows us to describe inclusive decays of charm hadrons through an expansion in powers of $1/m_c$ implemented by the OPE. With the charm quark mass m_c exceeding ordinary hadronic scales merely by a moderate amount, the expansion parameter is not much smaller than unity. In the description of fully integrated widths like lifetimes, the leading nonperturbative contributions arise in order $1/m_c^2$ rather than $1/m_c$, which might be their saving grace. Indeed the resulting theoretical description of the lifetime ratios for the seven weakly decaying $C = 1$ charm hadrons has been remarkably successful [912]. Note that these seven charm lifetimes vary by a factor of 15, while the four singly-beautiful hadrons differ by less than 30%. The B_c meson is shorter lived by a factor of three than the other four beauty hadrons—not surprisingly, since it represents a glorified charm decay.

The same framework allows us to predict also the lifetimes of the $C = 2$ double-heavy baryons Ξ_{cc}, Ω_{cc} and even the $C = 3$ Ω_{ccc} [912]:

$$\begin{aligned} \tau(\Xi_{cc}^{++}) &\sim 0.35 \text{ ps}, & \tau(\Xi_{cc}^+) &\sim 0.07 \text{ ps}, \\ \tau(\Omega_{cc}^+) &\sim 0.1 \text{ ps}, & \tau(\Omega_{ccc}^{++}) &\sim 0.14 \text{ ps}. \end{aligned} \tag{229}$$

The SELEX Collaboration has found tantalizing evidence for $\Xi_{cc}^{+,++}$ baryons all decaying with ultrashort lifetimes below 0.03 ps. This feature cannot be accommodated in HQT. *If* confirmed, one would have to view the apparent successes of the HQT description of the $C = 1$ lifetimes as mere coincidences.

3.9.32.3 Absolute branching ratios

Precision absolute branching fraction measurements are difficult due to normalization and systematic effects. Only one *golden mode* is needed to anchor the rest for each state. A desire to use all-charged final states necessitates use of some three-body modes where proper modeling of the Dalitz structure is needed to ensure an accurate efficiency simulation. These results serve not only to normalize charm physics but also much B physics due to dominance of $b \to c$ decays. For example, charm branching fractions affect $B \to D^*\ell\nu$, used to extract V_{cb}.

Near-threshold $D\bar{D}$ pairs from $\psi(3770)$ decays and $D_s^{*\pm}D_s^{\mp}$ produced at 4170 MeV from CLEO-c now provide the best precision. Systematics are controlled, and normalization provided with tagging: studying one D vs. a fully-reconstructed *tag* $\bar{D}$. Precision on the golden modes $D^0 \to K^-\pi^+$ and $D^+ \to K^-\pi^+\pi^+$ results are limited by uncertainties of about 1% per track [1034] from tracking-finding and particle-identification efficiencies. Further studies [1035] are reducing these to less than 0.5% per track. Current statistical precision for $D_s^+ \to K^+K^-\pi^+$ decays [1035] is 5%; final CLEO-c accuracy should be about 3%, limited by statistics. Producing a useful new result for the

popular $D_s^+ \to \phi\pi^+$ mode is complicated by several factors: a nonresonant contribution under the ϕ, Breit–Wigner tails of the ϕ, treatment of nearby resonances like the $f(980)$ and lack of detail in existing publications. The merit of such studies goes beyond determining the branching ratio for $D_s^+ \to \phi\pi^+$ and learning about hadronic resonances (see below). Their greatest impact might come in precision analyses of $B_d \to \phi K_S$ and its CP asymmetries.

3.9.32.4 Dalitz plot studies & light flavor spectroscopy
Dalitz plot studies represent powerful analysis tools that are deservedly experiencing a renaissance in heavy flavor decays. Constructing a satisfactory description of the Dalitz plot populations allows one to extract the maximal amount of information from the data in a self-consistent way. One has to keep in mind, though, that a priori different parameterizations can be chosen; one has to make a judicious choice based on theoretical considerations. Along with better theoretical descriptions of the decay rate, improved treatments of background and efficiency may also be needed.

One important application concerns the spectroscopy of light flavor hadrons, i.e. those made up from u, d and s quarks. Modes like $D_{(s)} \to 3\pi, 3K, K\pi\pi, K\bar{K}\pi$ offer more than a treasure trove of additional data: since the final state evolves from a well-defined initial one, we know some quantum numbers of the overall system. Finding evidence for, say, a $\pi\pi$ resonance like the σ in Cabibbo-favored D and Cabibbo-suppressed D_s modes with parameters consistent with what is inferred from low-energy $\pi\pi$ scattering would constitute a powerful validation for the σ being a bona fide resonance.

Such lessons possess considerable intrinsic value. The latter is greatly amplified, since these insights will turn out to be of great help in understanding B decays into the analogous final states when searching for CP asymmetries there.

3.9.32.5 QCD sum rules More than twenty years ago a pioneering analysis of D and D_s decays into two-body final states of the PP and PV type was performed by Blok and Shifman through a novel application of QCD sum rules. Those are—unlike quark models—genuinely based on the QCD. Their drawback, as for most applications of QCD sum rules, is that one has to allow for an irreducible theoretical uncertainty of about 20%; furthermore they are very labor intensive. The authors of Ref. [1036] assumed $SU(3)_{fl}$ symmetry to make their analysis manageable—clearly a source of significant theoretical uncertainty. It would be marvelous if some courageous minds would take up the challenge of updating and extending this study.

3.9.32.6 On theoretical engineering Even without reliable predictions for exclusive nonleptonic widths, it makes a lot of sense to measure as many as precisely as possible on the Cabibbo-allowed, once and twice suppressed levels. It can provide vital input into searches for direct CP violation in charm decays.

CP asymmetries in integrated partial widths depend on hadronic matrix elements and (strong) phase shifts, neither of which can be predicted accurately. However the craft of theoretical engineering can be practiced with profit here. One makes an ansatz for the general form of the matrix elements and phase shifts that are included in the description of $D \to PP$, PV, VV etc. channels, where P and V denote pseudoscalar and vector mesons, and fits them to the measured branching ratios on the Cabibbo-allowed, once and twice forbidden level. If one has sufficiently accurate and comprehensive data, one can use these fitted values of the hadronic parameters to predict CP asymmetries. Such analyses have been undertaken in the past [968] and more recently by [1037–1042], but the data base was not as broad and precise as one would like. CLEO-c and BESIII measurements will certainly lift such studies to a new level of reliability.

Similar information can be obtained in a more subtle and model independent way using quantum entanglement in [958]

$$e^+ e^- \to \psi(3770) \to D^0 \bar{D}^0 \qquad (230)$$

and observing the subsequent decay of the neutral D mesons into final states like $f(D) = K^-\pi^+, K^+\pi^-, K^+K^-, \pi^+\pi^-$. Since the $D^0\bar{D}^0$ pair forms a coherent system, one can extract the strong phases reliably. This procedure is described in detail in Sect. 3.9.2.

3.9.32.7 Time dependent Dalitz studies Tracking three-body channels like $D^0 \to K\bar{K}\pi, K_S^0\pi\pi$ through time-dependent Dalitz plot studies is a very powerful way to look for NP through CP asymmetries involving D^0–$\bar{D}^0$ oscillations, as described in more detail in Sects. 3.9.2 and 3.9.12.

3.9.33 Summary on ongoing and future charm studies

Even accepting for the moment that the SM can provide a complete description of all charm transitions, detailed and comprehensive measurements of the latter will continue to teach us important and quite possible even novel lessons on QCD. Those lessons are of considerable intellectual value and would also prepare us if the anticipated NP driving the electroweak phase transition were of the strongly interacting variety.

Yet most definitely those lessons will sharpen both our experimental and theoretical tools for studying B decays and thus will be essential in saturating the discovery potential for NP there. Analyses of (semi)leptonic charm decays will yield powerful validation challenges to LQCD that, if passed successfully, will be of great benefit to extractions of $|V_{ub}|$ in particular. Careful studies of three-body final states

442

Eur. Phys. J. C (2008) 57: 309–492

in charm decays will yield useful constraints in analyses of the corresponding *B* modes and their CP asymmetries. The relevant measurements can be made at the tau-charm, the *B* and super-flavor factories. Yet there is one area in *this* context where hadronic experiments and in particular LHCb can make important contributions, namely in the search for and observation of doubly-heavy charm baryons of the [*ccq*] type and their lifetimes.

The study of charm dynamics was crucial in establishing the SM paradigm. Even so it is conceivable that another revolution might originate there in particular by observing non-SM type CP violation with and without oscillations. For on one hand the SM predicts practically zero results (except for direct CP violation in Cabibbo-suppressed channels), and on the other hand FCNCs might well be considerably less suppressed for up- than for down-type quarks. Charm is the only up-type quark that allows the full range of searches for CP violation. Modes like $D^0 \to K^+ K^-$, $K^+ \pi^-$ have the potential to exhibit (time-dependent) CP asymmetries that— if observed—would establish the presence of NP. Likewise for asymmetries in final-state distributions like Dalitz plots or for T odd moments. Again especially LHCb appears well positioned to bring the statistical muscle of the LHC to bear on analysing these transitions.

3.10 Impact of the LHC experiments[28]

3.10.1 Overview

The LHC will start operating in 2008. This will allow the LHC experiments—ATLAS, CMS and LHCb—to make substantial progress in heavy flavor physics and possibly to open a window to new physics beyond the Standard Model. LHCb is a heavy flavor physics experiment designed to make precision measurements of CP violation and of rare decays of *B* hadrons. The general purpose experiments AT-LAS and CMS also have a *B* physics programme, which will be carried out mainly during the first years of LHC operation with lower luminosity. The large cross section of 500 μb for $b\bar{b}$-quark production in *pp* collisions at 14 TeV centre-of-mass energy will allow the LHC experiments to collect much larger data samples of *B* hadrons than previously available.

Many of the expected LHC results have been reported in Sect. 3 of this report. Here we summarize a few of the anticipated highlights and provide the interested reader with a guide to more detailed discussions in Sects. 3.1 to 3.9. We also present the LHCb detector and illustrate how the different sub-detectors are crucial to achieve the expected performance on selected decays.

[28]Section coordinator: F. Muheim.

3.10.2 The LHCb experiment

LHCb is a dedicated heavy flavor experiment at the LHC. The LHCb detector is a single arm forward spectrometer which exploits the fact that a large fraction of the $b\bar{b}$ cross section is in the forward region. The LHCb experiment will operate at a luminosity of 2 to 5×10^{32} cm^{-2} s^{-1} and expects to accumulate a data sample of ~10 fb^{-1} over the next five years.

The LHCb detector layout is shown in Fig. 61. A silicon vertex detector (VELO) will be used to determine very precisely the decay length of *B* mesons. A typical proper time resolution of about 40 fs will be achieved for fully reconstructed decays. Charged tracks are momentum analysed by a dipole magnet, and their trajectories are recorded in four tracking stations. LHCb also features excellent particle identification: two Ring Imaging Cherenkov (RICH) detectors are employed to distinguish pions from kaons over a large momentum range; an electromagnetic calorimeter (ECAL) will measure electrons and photons; and muons are cleanly identified in the muon stations. A challenging task is to discriminate the interesting events from the much more copious minimum bias events at a hadron collider. A first-level hardware trigger (L0) operating at the interaction rate of 40 MHz is triggering on collisions containing muons with large transverse momenta, $p_T > 1$ GeV/c, hadrons which deposit a transverse energy $E_T > 3.5$ GeV in the hadron calorimeter (HCAL) and electrons or photons above an ECAL threshold of $E_T > 2.5$ GeV. The L0 trigger reduces the rate of interactions to below 1.1 MHz, at which all LHCb data will be read out. Events will then be examined by the High Level Trigger (HLT) running on a large computer farm. The HLT will reduce the output rate to 2 kHz which will be written to storage.

3.10.3 Expected highlights from LHC results

In the SM, flavor changing neutral current (FCNC) transitions are suppressed as these only occur through loop diagrams. These processes are thus sensitive to contributions from new heavy particles to the virtual loops and pose excellent probes to new physics (NP) beyond the SM. The LHC experiments will collect very large data samples of *B* and charm hadrons. These will allow them to probe NP at much increased sensitivities and to make precision tests of CP violation which, in the SM, arises solely through the CKM mechanism.

FCNC $b \to s$ transitions are an exciting NP probe and have been studied extensively. The very rare decay $B_s \to \mu^+ \mu^-$ has a well-predicted SM rate which could be enhanced considerably in many NP models. As shown for LHCb in Fig. 61, the three LHC experiments all have excellent muon identification systems to identify the final-state

Fig. 61 Schematic of the LHCb detector layout, showing the Vertex Locator (VELO), the dipole magnet, the two RICH detectors, the four tracking stations TT and T1–T3, the Scintillating Pad Detector (SPD), Preshower (PS), Electromagnetic (ECAL) and Hadronic (HCAL) calorimeters and the five muon stations M1–M5
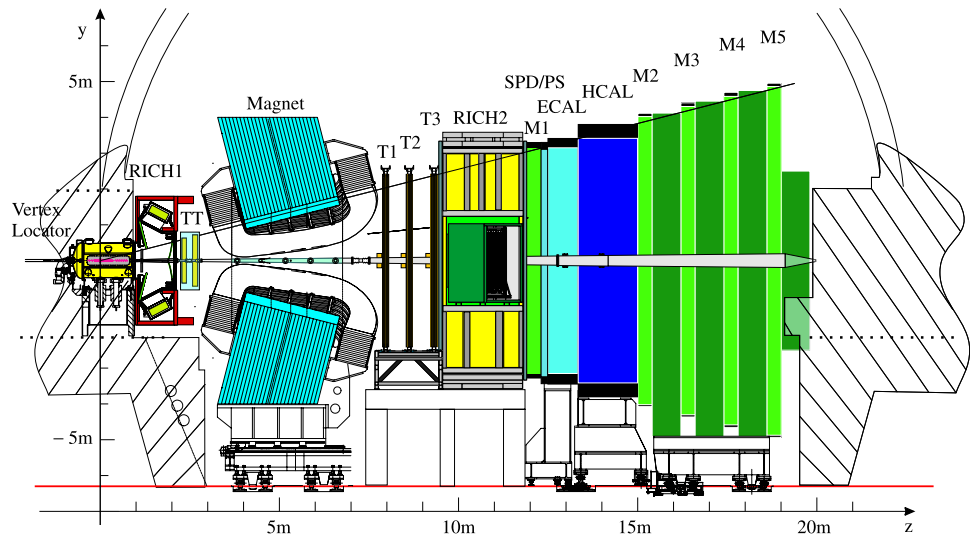
particles of this powerful NP probe. The ATLAS, CMS and LHCb trigger and selection efficiencies as well as sensitivities for $B_s \to \mu^+ \mu^-$ are described in detail in Sect. 3.4.3. The muon detectors will also enable the LHC experiments to investigate electroweak penguin transitions in the decays $B_d \to K^{*0} \mu^+ \mu^-$ and $\Lambda_b \to \Lambda^0 \mu^+ \mu^-$. The sensitivity to the forward–backward asymmetry A_{FB}, the transversity asymmetry $A_T^{(2)}$ and the K^{*0} longitudinal polarization F_L as well as the Λ^0 polarization from LHCb and ATLAS are presented in Sect. 3.2.3. LHCb is equipped with an electromagnetic calorimeter, which will be employed to trigger and reconstruct the photon of the radiative penguin decays $B^0 \to K^{*0} \gamma$ and $B_s \to \phi \gamma$. This is discussed in detail in Sect. 3.1.4.2.

The LHCb experiment will be able to measure the CP violating weak phase ϕ_s in the interference of B_s mixing and $B_s \to J/\psi \phi$ decays down to the SM prediction. This will require the measurement of a time-dependent CP asymmetry, and the fast oscillations of the B_s meson need to be resolved. This ϕ_s determination will be made possible with the excellent vertex resolution of the VELO detector. In addition, the flavor of the B_s at production must be determined. Good flavor tagging is also required. This will be achieved with the RICH detectors which will cleanly identify charged kaons from the $b \to c \to s$ decays of the other B hadron or accompanying the signal B_s in the fragmentation chain. The sensitivity of measurements of ϕ_s, the B_s oscillation frequency Δm_s and the lifetime difference $\Delta \Gamma_s$ expected from LHCb and CMS are discussed in detail in Sects. 3.6.7 and 3.6.8.

LHCb will also perform precise measurements of the angles of the CKM unitarity triangle (α, β and γ). The expected sensitivities are presented in Sect. 3.5.3. The CKM angle γ can be measured using two interfering diagrams in neutral and charged $B \to DK$ decays as well as in $B_s \to$

$D_s^\mp K^\pm$ decays. The excellent kaon-pion separation from the RICH will greatly facilitate these analyses. A precision of a few degrees is expected, which is significantly better than current results. CP asymmetries in hadronic $b \to s$ transitions are sensitive to new physics in penguin loops. The best modes for LHCb are the decays $B_s \to \phi \phi$ and $B^0 \to \phi K_S^0$, as these are experimentally accessible and have small theoretical uncertainties. The expected sensitivities are discussed in Sect. 3.7.7. LHCb will also measure γ in loops with two-body hadronic decays $B \to hh'$, which is presented in Sect. 3.7.9.

In addition, the LHCb experiment will reconstruct large samples of charm mesons. This will substantially improve the precision of the D^0 mixing parameters, and a detailed discussion is given in Sects. 3.9.4 to 3.9.10.

4 Prospects for future facilities[29]

There are several new facilities for flavor physics discussed in the community among which the Super Flavor Factories (SFF) and the upgrade of the LHCb experiment are the most important ones for B physics. These are analysed in this chapter (for future kaon and charm physics facilities, see also Sects. 3.8 and 3.9).

The physics case of an SFF is worked out in Sect. 4.1. All opportunities of such a facility in B, charm and τ lepton physics are discussed. Then the two existing proposals for such a machine, namely Super$B$ and SuperKEKB, are presented in Sects. 4.2 and 4.3, respectively. Finally, the physics, detector and accelerator issues of a possible future upgrade of the LHCb experiment are discussed in Sect. 4.4.

---

[29]Section coordinator: T. Hurth.

444

Eur. Phys. J. C (2008) 57: 309–492

4.1 On the physics case of a super flavor factory

We summarize the physics case of a high-luminosity e^+e^- flavor factory collecting an integrated luminosity of (50–75) ab^{-1}. Many NP sensitive measurements involving B and D mesons and τ leptons, unique to a SFF, can be performed with excellent sensitivity to new particles with masses up to ~ 100 (or even ~ 1000) TeV. Flavor- and CP-violating couplings of new particles that may be discovered at the LHC can be measured in most scenarios, even in unfavorable cases assuming MFV. Together with the LHC, an SFF, following either the SuperKEKB or the Super$B$ proposal, could be soon starting the project of reconstructing the NP Lagrangian.

4.1.1 Introduction

In spite of the tremendous success of the SM, it is fair to say that the flavor sector of the SM is much less understood than its gauge sector. Masses and mixing of the quarks and leptons, which have a significant but unexplained hierarchy pattern, enter as free parameters to be determined experimentally. In fact, while symmetries shape the gauge sector, no principle governs the flavor structure of the SM Lagrangian. Yukawa interactions provide a phenomenological description of the flavor processes which, while successful so far, leaves most fundamental questions unanswered. Hence the need to go beyond the SM.

Indeed the search for evidence of physics beyond the SM is the main goal of particle physics in the next decades. The LHC at CERN will start soon looking for the Higgs boson, the last missing building block of the SM. At the same time, it will intensively search for NP, for which there are solid theoretical motivations related to the quantum stabilization of the Fermi scale to expect an appearance at energies around 1 TeV. However, pushing the high-energy frontier, i.e. increasing the available centre-of-mass energy in order to produce and observe new particles, is only one way to look for NP, the other being high-precision studies of rare processes. New particles could reveal themselves through their virtual effects in processes involving only standard particles as has been the case several times in the history of particle physics. Flavor physics is the best candidate as a tool for NP searches through quantum effects for several reasons. FCNCs, neutral meson–anti-meson mixing and CP violation occur at the loop level in the SM and therefore are potentially subject to $\mathcal{O}(1)$ NP virtual corrections. In addition, quark flavor violation in the SM is governed by the weak interaction and suppressed by the small quark mixing angles. Both these features are not necessarily shared by NP which, in such cases, could produce very large effects. Indeed, the inclusion in the SM of generic NP flavor-violating terms with natural $\mathcal{O}(1)$ couplings is known to violate present experimental constraints unless the NP scale is

pushed up to (10–100) TeV depending on the flavor sector. This difference between the NP scale emerging from flavor physics and the one suggested by Higgs physics could be a problem for model builders (the so-called flavor problem), but it clearly indicates that flavor physics has the potential to push the explored NP scale in the 100 TeV region. On the other hand, if the NP scale is indeed close to 1 TeV, the flavor structure of NP must be highly nontrivial, and the experimental determination of the flavor-violating couplings is particularly interesting. Any NP model established at the TeV scale to solve the gauge hierarchy problem includes new flavored particles and new flavor- and CP-violating parameters. Therefore, such a model must provide a solution also to the flavor and CP problems. This may be related to other interesting questions. For instance, in supersymmetry, the flavor problem is directly linked to the crucial issue of supersymmetry breaking. Similar problems also occur in models of extra-dimensions (flavor properties of Kaluza–Klein states), Technicolour models (flavor couplings of Techni-fermions), little-Higgs models (flavor couplings of new gauge bosons and fermions) and multi-Higgs models (CP-violating Higgs couplings). Once NP is found at the TeV scale, precision measurements of flavor- and CP-violating observables would shed light on the detailed structure of the underlying model.

In the light of the above considerations, an SFF, following the recent proposals for SuperKEKB (see Sect. 4.3 and Ref. [839]) and Super$B$ (see Sect. 4.2 and Ref. [1045]), has one mission: to search for NP in the flavor sector exploiting a huge leap in integrated luminosity and the wide range of observables that it can measure. However, this goal can be pursued in different ways depending on whether evidence of NP has been found at the time an SFF starts taking data, or not.

In both cases, an SFF can search for evidence of NP irrespective of the values of the new particle masses and of the unknown flavor-violating couplings. A first set is given by measurements of observables which are predicted by the SM with small uncertainty, including those which are vanishingly small (null tests). Among them, there are the flavor-violating τ decays, direct CP asymmetries in $B \to X_{s+d}\gamma$, in τ decays and in some nonleptonic D decays, CP violation in neutral charm meson mixing, the dilepton invariant mass at which the forward–backward asymmetry of $B \to X_s \ell^+\ell^-$ vanishes, and lepton universality violating B and τ decays. Any deviation, as small as an SFF could measure, from its SM value of any observable in this set could be ascribed to NP with essentially no uncertainty. A second set of NP-sensitive observables, including very interesting decays such as $b \to s$ penguin-dominated nonleptonic B decays, $B \to \tau\nu$, $B \to D^{(*)}\tau\nu$, $B \to K^*\gamma$, $B \to \rho\gamma$, and many others, require more accurate determinations of SM contributions and improved control of the hadronic uncertainties with respect to what we can do today in order to

match the experimental precision achievable at an SFF and to allow for an unambiguous identification of an NP signal. The error on the SM can be reduced using the improved determination of the CKM matrix provided by an SFF itself. This can be achieved using generalized CKM fits which allow for a 1% determination of the CKM parameters using tree-level and $\Delta F = 2$ processes even in the presence of generic NP contributions. As far as hadronic uncertainties are concerned, the extrapolation of our present knowledge and techniques shows that it is possible to reach the required accuracy by the time an SFF will be running using improved lattice QCD results obtained with next-generation computers [1045] and/or bounding the theoretical uncertainties with data-driven methods exploiting the huge SFF data sample.

Finally, it must be emphasized that while an SFF will perform detailed studies of beauty, charm and tau lepton physics, the results will be highly complementary to those on several important observables related to B_s meson oscillations, kaon and muon decays that will be measured elsewhere. Most benchmark charm measurements, in particular interesting NP-related measurements such as CP violation in charm mixing, will still be statistics-limited after the CLEOc, BESIII and B factory projects are completed and can only be pursued to their ultimate precision at an SFF. Operation at the $\Upsilon(5S)$ resonance provides the possibility of exploiting the clean e^+e^- environment to measure B_s^0 decays with neutral particles in the final state, thus of complementing the measurements at LHCb. An SFF has sensitivity for τ physics that is far superior to any other existing or proposed experiment, and the physics reach can be extended even further by the possibility to operate with polarized beams. It is particularly noteworthy that the combined information on μ and τ flavor violating decays that will be provided by MEG [1043] together with an SFF can shed light on the mechanism responsible for lepton flavor violation.

4.1.2 Experimental sensitivities

An SFF with integrated luminosity of (50–75) ab^{-1} can perform a wide range of important measurements and dramatically improve upon the results from the current generation of B factories. Many of these measurements cannot be made in a hadronic environment and are unique to an SFF. In Table 56, we give indicative estimates of the precision on some of the most important observables that can be achieved by an SFF with integrated luminosity of (50–75) ab^{-1}. Here we have not attempted to comment on the whole range of measurements that can be performed by such a machine but instead focus on channels with the greatest phenomenological impact. For more details, including a wide range of additional measurements, we guide the reader to the existing reports [1044–1047, 1059], where also all original references are given.

The most important measurements within the CKM metrology are the UT angles, the angle β (also known as ϕ_1) measured using mixing-induced CP violation in $B^0 \to J/\psi K^0$, the angle α (ϕ_2) measured using rates and asymmetries in $B \to \pi\pi$, $\rho\pi$ and $\rho\rho$, and the angle γ (ϕ_3) measured using rates and asymmetries in $B \to D^{(*)}K^{(*)}$ decays, using final states accessible to both D^0 and $\bar{D}^0$. Moreover, an SFF will improve our knowledge of the lengths of the UT sides. In particular, the CKM matrix element $|V_{ub}|$ will be precisely measured through both inclusive and exclusive semileptonic $b \to u$ decays.

Among the measurements sensitive for NP, there are the mixing-induced CP violation parameters in charmless hadronic B decays dominated by the $b \to s$ penguin transition, $S(\phi K^0)$, $S(\eta' K^0)$ and $S(K_S^0 K_S^0 K_S^0)$. Within the Standard Model, these give the same value of $\sin(2\beta)$ that is determined in $B^0 \to J/\psi K^0$ decays, up to a level of theoret-

Table 56 Expected sensitivity that can be achieved on some of the most important observables by an SFF with integrated luminosity of (50–75) ab^{-1}. The range of values given allow for possible variation in the total integrated luminosity, in the accelerator and detector design and in limiting systematic effects. For further details, refer to [1045, 1047]

Observable	SFF sensitivity
$\sin(2\beta)$ ($J/\psi K^0$)	0.005–0.012
γ ($B \to D^{(*)}K^{(*)}$)	(1–2)°
α ($B \to \pi\pi, \rho\rho, \rho\pi$)	(1–2)°
$|V_{ub}|$ (exclusive)	(3–5)%
$|V_{ub}|$ (inclusive)	(2–6)%
$\bar{\rho}$	(1.7–3.4)%
$\bar{\eta}$	(0.7–1.7)%
$S(\phi K^0)$	0.02–0.03
$S(\eta' K^0)$	0.01–0.02
$S(K_S^0 K_S^0 K_S^0)$	0.02–0.04
ϕ_D	(1–3)°
$\mathcal{B}(B \to \tau\nu)$	(3–4)%
$\mathcal{B}(B \to \mu\nu)$	(5–6)%
$\mathcal{B}(B \to D\tau\nu)$	(2–2.5)%
$\mathcal{B}(B \to \rho\gamma)/\mathcal{B}(B \to K^*\gamma)$	(3–4)%
$A_{CP}(b \to s\gamma)$	0.004–0.005
$A_{CP}(b \to (s+d)\gamma)$	0.01
$S(K_S^0 \pi^0 \gamma)$	0.02–0.03
$S(\rho^0 \gamma)$	0.08–0.12
$A^{FB}(B \to X_s \ell^+ \ell^-) s_0$	(4–6)%
$\mathcal{B}(B \to K\nu\bar{\nu})$	(16–20)%
$\mathcal{B}(\tau \to \mu\gamma)$	(2–8) × 10^{-9}
$\mathcal{B}(\tau \to \mu\mu\mu)$	(0.2–1) × 10^{-9}
$\mathcal{B}(\tau \to \mu\eta)$	(0.4–4) × 10^{-9}

446

Eur. Phys. J. C (2008) 57: 309–492

ical uncertainty that is estimated to be $\sim$(2–5)% within factorization. (The theoretical error in these and other modes, such as $B \to K_S \pi^0$, can be also bounded with data-driven methods [88, 778–781]. Presently these give larger uncertainties but will become more precise as more data is available.) Many extensions of the SM result in deviations from this prediction. Another distinctive probe of new sources of CP violation is ϕ_D, the CP violating phase in neutral D meson mixing, which is negligible in the SM and can be precisely measured using, for example, $D \to K_S^0 \pi^+ \pi^-$ decays. Furthermore, branching fractions for leptonic and semileptonic B decays are sensitive to charged Higgs exchange. In particular these modes are sensitive to new physics, even in the unfavorable MFV scenario, with a large ratio of the Higgs vacuum expectation values, $\tan \beta$. Measurements of rare radiative and electroweak penguin processes are well known to be particularly sensitive to NP: the ratio of branching fractions $\mathcal{B}(B \to \rho \gamma)/\mathcal{B}(B \to K^* \gamma)$ depends on the ratio of CKM matrix parameters $|V_{td}/V_{ts}|$, with additional input from lattice QCD. Within the SM, this result must be consistent with constraints from the UT fits. The inclusive CP asymmetries $A_{\mathrm{CP}}(b \to s \gamma)$ or $A_{\mathrm{CP}}(b \to (s+d)\gamma)$ are predicted in the SM to be small or exactly zero respectively with well-understood theoretical uncertainties. The mixing-induced CP asymmetry in radiative $b \to s$ transitions measured for example through $S(K_S^0 \pi^0 \gamma)$ is sensitive to the emitted photon polarization. Within the SM, the photon is strongly polarized, and the mixing-induced asymmetry small but new right-handed currents can break this prediction even without the introduction of any new CP violating phase. Similarly, $S(\rho^0 \gamma)$ probes radiative $b \to d$ transitions. The dilepton invariant mass squared s at which the forward–backward asymmetry in the distribution of $B \to X_s \ell^+ \ell^-$ decays is zero (denoted $A^{\mathrm{FB}}(B \to X_s \ell^+ \ell^-) s_0$), for which the theoretical uncertainty of the SM prediction is small, is sensitive to NP in electroweak penguin operators; finally, the branching fraction for the rare electroweak penguin decay $B \to K \nu \bar{\nu}$ is an important probe for NP even if this appears only well above the electroweak scale. An SFF also allows for the measurement of branching ratios of lepton flavor violating τ decays, such as $\tau \to \mu \gamma$, $\tau \to \mu \mu \mu$ and $\tau \to \mu \eta$. Within the SM, these are negligibly small, but many models of new physics create observable lepton flavor violation signatures.

The sensitivities of these measurements to NP effects may be shown by a few examples: In Fig. 62, we show a simulation of the time-dependent asymmetry in $B^0 \to \phi K^0$, compared to that for $B^0 \to J/\psi K^0$. The events are generated using the current central values of the measurements. With the precision of an SFF and the present central values, the difference between the two data sets is larger than the theoretical expectation, showing evidence of NP contributions.

In Fig. 63, we show how lepton flavor violation in the decay $\tau \to \mu \gamma$ may be discovered at an SFF. The simulation corresponds to a branching fraction of $\mathcal{B}(\tau \to \mu \gamma) = 10^{-8}$, which is within the range predicted by many new physics models. The signal is clearly observable, and well within the reach of an SFF. The simulation includes the effects of irreducible background from initial state radiation photons, though improvements in the detector and in the analysis may lead to better control of this limitation. Other lepton flavor violating decay modes, such as $\tau \to \mu \mu \mu$, do not suffer from this background and have correspondingly cleaner experimental signatures.
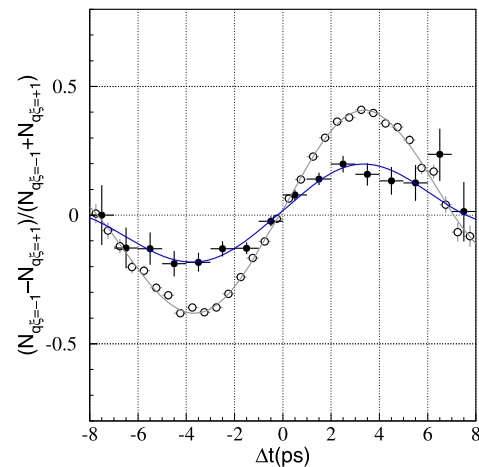

Fig. 62 Simulation of NP effects in $B^0 \to \phi K^0$, as could be observed by an SFF. The open circles show simulated $B^0 \to J/\psi K^0$ events, the *filled circles* show simulated $B^0 \to \phi K^0$ events. Both have *curves* showing fit results superimposed (from [1047])
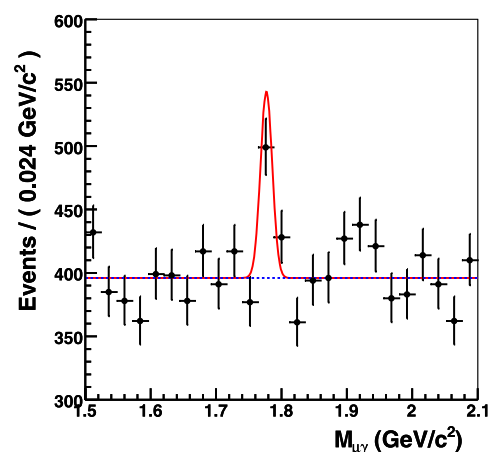

Fig. 63 Monte Carlo simulation of the appearance of $\tau \to \mu \gamma$ at an SFF. A clear peak in the $\mu \gamma$ invariant mass distribution is visible above the background. The branching fraction used in the simulation is $\mathcal{B}(\tau \to \mu \gamma) = 10^{-8}$, an order of magnitude below the current upper limit. With 75 ab^{-1} of data, the significance of such a decay is expected to exceed 5σ

The differences between the SFF physics programme and those of the current B factories are striking. At an SFF, measurements of known rare processes such as $b \to s\gamma$ or CP violation in hadronic $b \to s$ penguin transitions such as $B^0 \to \phi K_S^0$ will be advanced to unprecedented precision. Channels which are just being observed in the existing data, such as $B^0 \to \rho^0 \gamma$, $B^+ \to \tau^+ \nu_\tau$ and $B \to D^{(*)} \tau \nu$ will become precision measurements at an SFF. Furthermore, detailed studies of decay distributions and asymmetries that cannot be performed with the present statistics will enable the sensitivity to NP to be significantly improved. Another salient example lies in D^0–$\bar{D}^0$ oscillations: the current evidence for charm mixing, which cannot be interpreted in terms of NP, opens the door for precise measurements of the CP violating phase in charm mixing, which is known to be zero in the SM with negligible uncertainty.

In addition, these measurements will be accompanied by dramatic discoveries of new modes and processes. These will include decays such as $B \to K\nu\bar{\nu}$, which is the signature of the theoretically clean quark level process $b \to s\nu\bar{\nu}$. The high statistics and clean environment of an SFF allow for the accompanying B meson to be fully reconstructed in a hadronic decay mode, which then in turn allows a one-charged prong rare decay to be isolated. Another example is $B^+ \to \pi^+ \ell^+ \ell^-$, the most accessible $b \to d\ell^+\ell^-$ process. These decays are the next level beyond $b \to s\ell^+\ell^-$ decays, which were first observed in the B-factory era. Such significant advances will result in a strong phenomenological impact of the SFF physics programme.

Since an SFF will take data in the LHC era, it is reasonable to ask how the physics reach compares with the B physics potential of the LHC experiments, most notably LHCb. By 2014, the LHCb experiment is expected to have accumulated 10 fb^{-1} of data from pp collisions at a luminosity of $\sim 2 \times 10^{32}$ cm^{-2} s^{-1}. In the following, we assume the most recent estimates of LHCb sensitivity with that data set [1048]. Note that LHCb is planning an upgrade where they would run at 10 times the initial design luminosity and record a data sample of about 100 fb^{-1}, see Sect. 4.4 and [1049].

The most striking outcome of any comparison between SFF and LHCb is that the strengths of the two experiments are largely complementary. For example, the large boost of the B hadrons produced at LHCb allows studies of the oscillations and mixing-induced CP violation of B_s mesons, while many of the measurements that constitute the primary physics motivation for an SFF cannot be performed in the hadronic environment, including rare decay modes with missing energy such as $B^+ \to \ell^+ \nu_\ell$ and $B^+ \to K^+ \nu\bar{\nu}$. Measurements of the CKM matrix elements $|V_{ub}|$ and $|V_{cb}|$ and inclusive analyses of processes such as $b \to s\gamma$ also benefit greatly from the SFF environment. At LHCb, the reconstruction efficiencies are reduced for channels containing

several neutral particles and for studies where the B decay vertex must be determined from a K_S^0 meson. Consequently, an SFF has unique potential to measure the photon polarization via mixing-induced CP violation in $B^0 \to K_S^0 \pi^0 \gamma$. Similarly, an SFF is well placed to study possible NP effects in hadronic $b \to s$ penguin decays as it can measure precisely the CP asymmetries in many B_d^0 decay modes including ϕK^0, $\eta' K^0$, $K_S^0 K_S^0 K_S^0$ or $K_S^0 \pi^0$. While LHCb will have limited capability for these channels, it can achieve complementary measurements using decay modes such as $B_s^0 \to \phi\gamma$ and $B_s^0 \to \phi\phi$ for radiative and hadronic $b \to s$ transitions, respectively. Where there is overlap, the strength of the SFF programme in its ability to use multiple approaches to reach the objective becomes apparent. For example, LHCb will be able to measure α to about 5° precision using $B \to \rho\pi$ but would not be able to access the full information in the $\pi\pi$ and $\rho\rho$ channels, which is necessary to drive the uncertainty down to the (1–2)° level of an SFF. Similarly, LHCb can certainly measure $\sin(2\beta)$ through mixing-induced CP violation in $B^0 \to J/\psi K_S^0$ decay to high accuracy (about 0.01) but will have less sensitivity to make the complementary measurements (e.g., in $J/\psi \pi^0$ and Dh^0) that help to ensure that the theoretical uncertainty is under control. LHCb plans to measure the angle γ with a precision of (2–3)°. An SFF is likely to be able to improve this precision to about 1°. LHCb can make a precise measurement of the zero of the forward–backward asymmetry in $B^0 \to K^{*0} \mu^+ \mu^-$, but an SFF can also measure the inclusive channel $b \to s\ell^+\ell^-$, which is theoretically a significantly cleaner observable [463].

The broad program of an SFF thus provides a very comprehensive set of measurements, extending what will already have been achieved by LHCb at that time. This will be of great importance for the study of flavor physics in the LHC era and beyond.

4.1.3 Phenomenological impact

The power of an SFF to observe NP and to determine the CKM parameters precisely is manifold. In the following, we present a few highlights of the phenomenological impact (for more detailed analyses, see [1044–1047, 1059]).

The measurements described in the previous section can be used to select a region in the $\bar{\rho}$–$\bar{\eta}$ plane. The numerical results in Table 57 indicate that a precision of a fraction of a percent can be reached, significantly improving the current situation and providing a generic test of the presence of NP at that level of precision.

There is also an impressive impact of an SFF on the parameters of the MSSM with generic squark mass matrices parameterized using the mass insertion (MI) approximation [97]. The analysis presented here is based on results and techniques developed in Refs. [104, 105, 107]. Figure 64

shows a simulation of how well the mass insertions (MIs), related to the off-diagonal entries of the squark mass matrices, could be reconstructed at an SFF. Figure 64 displays the allowed region in the $\mathrm{Re}(\delta^d_{ij})_{AB}$–$\mathrm{Im}(\delta^d_{ij})_{AB}$ plane with a value of $(\delta^d_{ij})_{AB}$ allowed from the present upper bound, $m_{\tilde{g}} = 1$ TeV and using the SFF measurements as constraints. The relevant constraints come from $\mathcal{B}(b \to s\gamma)$, $A_{CP}(b \to s\gamma)$, $\mathcal{B}(b \to s\ell^+\ell^-)$, $A_{CP}(b \to s\ell^+\ell^-)$, Δm_{B_s} and A^s_{SL}. It is apparent the key role of $A_{CP}(b \to s\gamma)$ together with the branching ratios of $b \to s\gamma$ and $b \to s\ell^+\ell^-$. The zero of the forward–backward asymmetry in $b \to s\ell^+\ell^-$, missing in the present analysis, is expected to give an additional strong constraint, further improving the already excellent extraction of $(\delta^d_{23})_{LR}$ shown in Fig. 64.

The search for FCNC transitions of charged leptons is one of the most promising directions to search for physics beyond the SM. In the last few years, neutrino physics has provided unambiguous indications about the nonconservation of lepton flavor, we therefore expect this phenomenon to occur also in the charged lepton sector.

Rare FCNC decays of the τ lepton are particularly interesting since the LFV sources involving the third generation are naturally the largest. In Fig. 65, we show the prediction

for $\mathcal{B}(\tau \to \mu\gamma)$ within a SUSY $SO(10)$ framework for the accessible LHC SUSY parameter space $M_{1/2} \leq 1.5$ TeV, $m_0 \leq 5$ TeV and $\tan\beta = 40$ [1051]. Note that the measurement of $\mathcal{B}(\tau \to \mu\gamma)$ at an SFF can distinguish the scenario where LFV is governed by neutrino mixing matrix U_{PMNS} from the scenario where LFV is governed by the quark mixing matrix V_{CKM}.

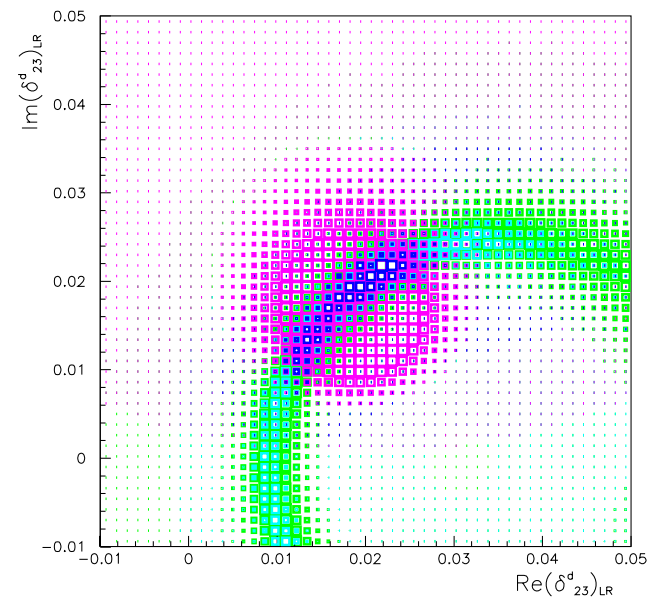In SUSY models, the squark and slepton mass matrices are determined by various SUSY-breaking parameters,

Fig. 64 (Color online) Density plot of the region in the $\mathrm{Re}(\delta^d_{23})_{LR}$–$\mathrm{Im}(\delta^d_{23})_{LR}$ plane for $m_{\tilde{q}} = m_{\tilde{g}} = 1$ TeV generated using SFF measurements. Different colours correspond to different constraints: $\mathcal{B}(B \to X_s\gamma)$ (*green*), $\mathcal{B}(B \to X_s\ell^+\ell^-)$ (*cyan*), $A_{\mathrm{CP}}(B \to X_s\gamma)$ (*magenta*), all together (*blue/black*). Central values of constraints corresponds to assuming $(\delta^d_{13})_{LL} = 0.028 e^{i\pi/4}$
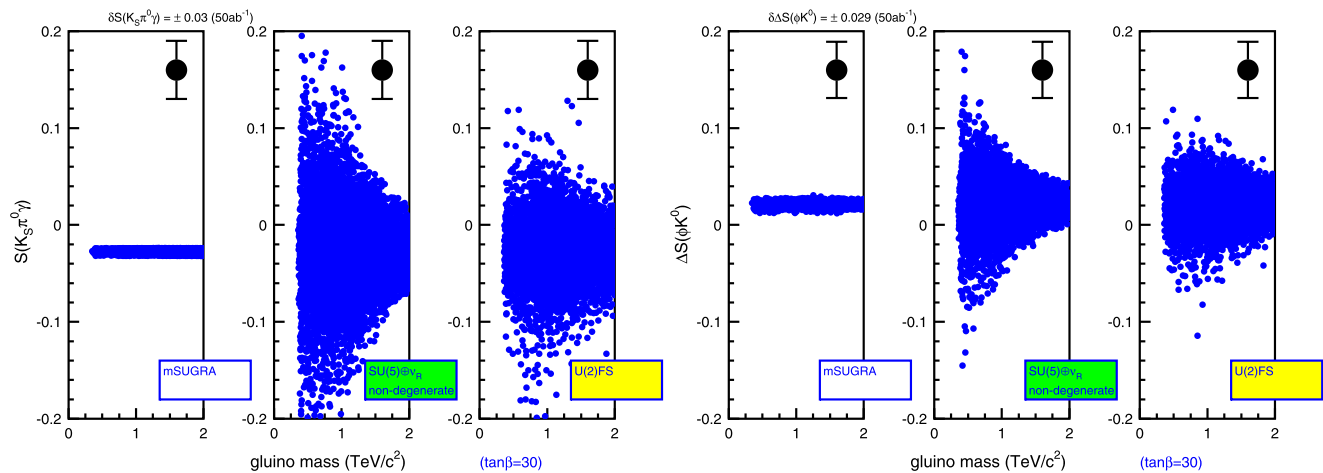
Table 57 Uncertainties of the CKM parameters obtained from the SM fit using the experimental and theoretical information available today (left) and at the time of an SFF (right)

Parameter	SM fit today	SM fit at an SFF
$\bar{\rho}$	0.163 ± 0.028	± 0.0028
$\bar{\eta}$	0.344 ± 0.016	± 0.0024
α (°)	92.7 ± 4.2	± 0.45
β (°)	22.2 ± 0.9	± 0.17
γ (°)	64.6 ± 4.2	± 0.38

Fig. 65 $\mathcal{B}(\tau \to \mu\gamma)$ in units of 10^{-7} vs. the high-energy universal gaugino mass ($M_{1/2}$) within an $SO(10)$ framework [1051]. The plot is obtained by scanning the LHC accessible parameter space $m_0 \leq 5$ TeV for $\tan\beta = 40$. *Green* or *light* (*red* or *dark*) *points* correspond to the scenario where LFV is governed by the PMNS (CKM) mixing matrix. The *thick horizontal line* denotes the present experimental sensitivity. The expected SFF sensitivity is 2×10^{-9}

Fig. 66 Time-dependent asymmetry of $B^0 \to K_S^0 \pi^0 \gamma$ and the difference between the time-dependent asymmetries of $B^0 \to \phi K_S^0$ and $B^0 \to J/\psi K_S^0$ modes for three SUSY breaking scenarios: mSUGRA (*left*), $SU(5)$ SUSY GUT with right-handed neutrinos in nondegenerate case (*middle*), and MSSM with $U(2)$ flavor symmetry (*right*). The expected SFF sensitivities are also shown

and hence an SFF has the potential to study SUSY breaking scenarios through quark and lepton flavor signals. This will be particularly important when SUSY particles are found at the LHC, because flavor off-diagonal terms in these mass matrices could carry information on the origin of SUSY breaking and interactions at high-energy scales such as the GUT and the seesaw neutrino scales. Combined with the SUSY mass spectrum obtained at energy frontier experiments, it may be possible to clarify the whole structure of SUSY breaking. In order to illustrate the potential of an SFF to explore the SUSY breaking sector, three SUSY models are considered, and various flavor signals are compared. These are (i) the minimal supergravity model (mSUGRA), (ii) an $SU(5)$ SUSY GUT model with right-handed neutrinos, (iii) the MSSM with $U(2)$ flavor symmetry [1052, 1053]. Flavor signals in the $b \to s$ sector are shown in Fig. 66 for these three SUSY breaking scenarios. Scatter plots of the time-dependent asymmetry of $B \to K_S^0 \pi^0 \gamma$ and the difference between the time-dependent asymmetries of $B \to \phi K_S^0$ and $B \to J/\psi K_S^0$ modes are presented as a function of the gluino mass. Sizable deviations can be seen for $SU(5)$ SUSY GUT and $U(2)$ flavor symmetry cases even if the gluino mass is 1 TeV. The deviation is large enough to be identified at SFF. On the other hand, the deviations are much smaller for the mSUGRA case.

The correlation between $\mathcal{B}(\tau \to \mu\gamma)$ and $\mathcal{B}(\mu \to e\gamma)$ is shown in Fig. 67 for the nondegenerate $SU(5)$ SUSY GUT case. In this case, both processes can reach current upper bounds. It is thus possible that improvements in the $\mu \to e\gamma$ search at the MEG experiment and in the $\tau \to \mu\gamma$ search at an SFF lead to discoveries of muon and tau LFV processes, respectively.
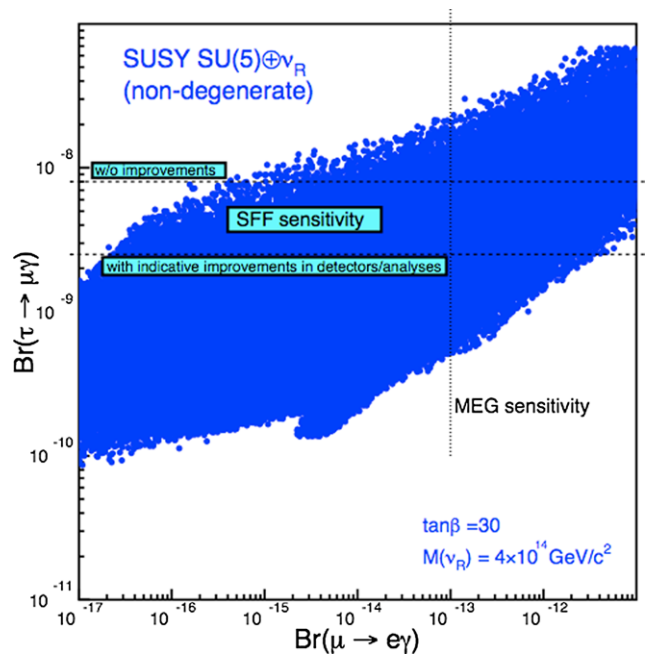

Fig. 67 Correlation between $\mathcal{B}(\tau \to \mu\gamma)$ and $\mathcal{B}(\mu \to e\gamma)$ for $SU(5)$ SUSY GUT with right-handed neutrinos in the nondegenerate case. Expected search limits at the SFF for $\mathcal{B}(\tau \to \mu\gamma)$ and for $\mathcal{B}(\mu \to e\gamma)$ from MEG are also shown

4.1.4 Summary

In conclusion, the physics case of an SFF collecting an integrated luminosity of (50–75) ab^{-1} is well established. Many NP sensitive measurements involving B and D mesons and τ leptons, unique to a SFF, can be performed with excellent sensitivity to new particles with masses up to ~100 (or even ~1000) TeV. The possibility to operate at the $\Upsilon(5S)$ resonance makes some measurements with B_s mesons also

450

Eur. Phys. J. C (2008) 57: 309–492

accessible, and options to run in the tau–charm threshold region and possibly with one or two polarized beams further broadens the physics reach. Flavor- and CP-violating couplings of new particles accessible at the LHC can be measured in most scenarios, even in the unfavorable cases assuming MFV. Together with the LHC, an SFF could be soon starting the project of reconstructing the NP Lagrangian. Admittedly, this daunting task would be difficult and take many years, but it provides an exciting objective for accelerator-based particle physics in the next decade and beyond.

4.2 Super B proposal

The two asymmetric B factories, PEP-II [1054, 1055] and KEKB [1056], and their companion detectors, BaBar [1057] and Belle [1058], have produced a wealth of flavor physics results, subjecting the quark and lepton sectors of the SM to a series of stringent tests, all of which have been passed. With the much larger data sample that can be produced at a super B factory, qualitatively new studies will be possible, including searches for FCNCs, lepton-flavor violating processes and new sources of CP violation at sensitivities that could reveal physics beyond the SM. These studies will provide a uniquely important source of information about the details of the NP uncovered at hadron colliders in the coming decade [1059].

In light of this strong physics motivation, there has been a great deal of activity over the past six years aimed at designing an e^+e^- B factory that can produce samples of b, c and τ decays 50 to 100 times larger than will exist when the current B factory programs end.

Upgrades of PEP-II [1060] and KEKB [1061] to super B factories that accomplish this goal have been considered

at SLAC and at KEK. These machines are extrapolations of the existing B factories with higher currents, more bunches and smaller β functions (1.5 to 3 mm). They also use a great deal of power (90 to 100 MW), and the high currents, approaching 10 A, pose significant challenges for detectors. To minimize the substantial wallplug power, the SuperPEP-II design doubled the current RF frequency to 958 MHz. In the case of SuperKEKB, a factor of two increase in luminosity is assumed for the use of crab crossing, which is currently being tested at KEKB, see Sect. 4.3.

SLAC has no current plans for an on-site accelerator-based high-energy physics program, so the SuperPEP-II proposal is moribund. The SuperKEKB proposal is considered as a future option of KEK. The problematic power consumption and background issues associated with the SLAC and KEK-based super B factory designs have now, however, motivated a new approach to super B factory design, using low emittance beams to produce a collider with a luminosity of 10^{36} but with reduced power consumption and lower backgrounds. This collider is called Super$B$. Design parameters of the existing colliders PEP-II and KEKB are compared with those of SuperPEP-II, SuperKEKB and Super$B$ in Table 58.

The Super B Conceptual Design Report [1045] describes a nascent international effort to construct a very high luminosity asymmetric e^+e^- flavor factory. The machine can use an existing tunnel or it could be built at a new site, such as the campus of the University of Rome "Tor Vergata", near the INFN National Laboratory of Frascati. The report was prepared by an international study group set up by the President of INFN at the end of 2005, with the charge of studying the physics motivation and the feasibility of constructing a SFF that would come into operation in the first

Table 58 Comparison of B factory and super B factory designs

	PEP-II	KEKB	SuperPEP-II	SuperKEKB	Super B
E_{LER} (GeV)	3.1	3.5	3.5	3.5	4
E_{HER} (GeV)	9	8	8	8	7
N_{part} ($\times 10^{10}$)	8	5.8	10	12	6
I_{LER} (A)	2.95	1.68	4.5	9.4	2.28
I_{HER} (A)	1.75	1.29	2.5	4.1	1.3
Wallplug power (MW)	22.5	45	~100	~90	17
Crossing angle (mrad)	0	±15	0	0	±17
Bunch length σ_z (mm)	11	6	1.7	3	7
σ_y^* (nm)	6900	2000	700	367	35
σ_x^* (µm)	160	110	58	42	5.7
β_y^* (mm)	11	6	1.5	3	0.3
Vertical beam–beam tune shift ξ_y	0.068	0.055	0.12	0.25	0.17
Luminosity (cm^{-2} s^{-1}) ($\times 10^{34}$)	1.1	1.6	70	80	100

Eur. Phys. J. C (2008) 57: 309–492

451

half of the next decade with a peak luminosity in excess of 10^{36} cm^{-2} s^{-1} at the $\Upsilon(4S)$ resonance.

The key idea in the Super B design is the use of low emittance beams produced in an accelerator lattice derived from the ILC Damping Ring Design, together with a new collision region, again with roots in the ILC final focus design, but with important new concepts developed in this design effort. Remarkably, Super B produces this very large improvement in luminosity with circulating currents and wallplug power similar to those of the current B factories. There is clear synergy with ILC R&D; design efforts have already influenced one another, and many aspects of the ILC Damping Rings and Final Focus would be operationally tested at SuperB in which the bending magnets bear a treater burden in producing the needed damping. A comparison of the SuperB HER and LER rings with the ILC damping rings is given in Table 59.

There is quite a lot of siting flexibility in the Super B CDR design. Since the required damping times are produced by wigglers in straight sections, the radius of the ring can be varied (within limits, of course) to accommodate other sites and/or to optimize cost. Smaller radius designs are also be-

ing explored, in which the bending magnets bear a greater burden in producing the needed damping.

Employing concepts developed for the ILC damping rings and final focus in the design of the SuperB collider, one can produce a two-order-of-magnitude increase in luminosity with beam currents that are comparable to those in the existing asymmetric B factories. Background rates and radiation levels associated with the circulating currents are comparable to current values; luminosity-related backgrounds such as those due to radiative Bhabhas increase substantially. With careful design of the interaction region, including appropriate local shielding, and straightforward revisions of detector components, upgraded detectors based on BaBar or Belle are a good match to the machine environment: in this discussion, we use BaBar as a specific example. Required detector upgrades include: reduction of the radius of the beam pipe, allowing a first measurement of track position closer to the vertex and improving the vertex resolution (this allows the energy asymmetry of the collider to be reduced to 7 on 4 GeV); replacement of the drift chamber, as the current chamber will have exceeded its design lifetime; replacement of the endcap calorimeter, with faster crystals

Table 59 Parameters of the Super B HER and LER rings compared with the ILC damping rings

	LER	HER	ILC DR
Energy (GeV)	4	7	5
Luminosity (cm^{-2} s^{-1})	1×10^{36}		–
C (m)	2249		6695
Crossing angle (mrad)	2×17		–
Longitudinal polarization (%)	0	80	80
Wiggler field Bw (T)	1.00	0.83	1.67
L_{bend} (m) (Arc/FF)	0.45/0.75/5.4	5.4/5.4	3/6/–
Number of Bends (Arc/FF)	120/120/16	120/16	126/–
U_0 (MeV/turn)	1.9	3.3	8.7
Wiggler length: L_{tot}(m)	100	50	200
Damping time τ_s, τ_x (ms)	16/32	16/32	12.9/25.7
σ_z (mm)	6	6	9
ϵ_x (nm-rad)	1.6	1.6	0.8
ϵ_y (pm-rad)	4	4	2
σ_E (%)	0.084	0.09	0.13
Momentum compaction	1.8×10^{-4}	3.1×10^{-4}	4.2×10^{-4}
Synchrotron tune ν_s	0.011	0.02	0.067
V_{RF} (MV), N_{cavities}	6, 8	18, 24	24, 18
N_{part} ($\times 10^{10}$)	6.16	3.52	2.0
I_{beam} (A)	2.3	1.3	0.4
P_{beam} (MW)	4.4	4.3	3.5
f_{rf} (MHz)	476		650
N_{bunches}	1733		2625

452

Eur. Phys. J. C (2008) 57: 309–492

having a smaller Molière radius, since there is a large increase in Bhabha electrons in this region.

Super *B* has two additional features: the capability of running at center-of-mass energies in the τ/charm threshold region and longitudinal polarization of the electron (high energy) beam. The luminosity in the 4 GeV region will be an order of magnitude below that in the $\Upsilon(4S)$ region, but even so, data-taking runs of only one month at each of the interesting energies ($\psi(3770)$, 4.03 GeV, τ threshold, etc.) would produce an order of magnitude more integrated luminosity than will exist at the conclusion of the BES-II program. The polarization scheme is discussed in some detail in the Super *B* CDR [1045]. The electron beam can be polarized at a level of 85%, making it possible to search for *T* violation in τ production due to the presence of an electric dipole moment or for CP violation in τ decay, which is not expected in the Standard Model.

The Super *B* design has been undertaken subject to two important constraints: (1) the lattice is closely related to the ILC Damping Ring lattice and (2) as many PEP-II components as possible have been incorporated into the design. A large number of PEP-II components can, in fact, be reused: The majority of the HER and LER magnets, the magnet power supplies, the RF system, the digital feedback system and many vacuum components. This will reduce the cost and engineering effort needed to bring the project to fruition.

The crabbed waist design employs a large "Piwinski angle" $\phi = \frac{\theta}{2}\frac{\sigma_z}{\sigma_x}$, where θ is the full geometric crossing angle of the beams at the interaction point. By producing the large Piwinski angle through the use of a large crossing angle and a very small horizontal beam size and having β_y comparable to the size of the beam overlap area, it is possible simultaneously to produce a very small beam spot, reduce the vertical tune shift and suppress vertical synchrobetatron resonances. However, new beam resonances then arise, which can be suppressed by using sextupoles in phase with the IP in the *x* plane and with a $\pi/2$ phase difference in the *y* plane. This is the crabbed waist transformation. These optical elements have an impact on the dynamic aperture of the lattice; studies carried out after the Super *B* CDR indicate that an adequate dynamic aperture can be achieved. The longer bunch length made possible by the new scheme has the further advantage of reducing the problems of higher-order mode heating, coherent synchrotron radiation and high power consumption. Beam sizes and particle densities are, however, in a regime where Touschek scattering is an important determinant of beam lifetime.

The Super *B* concept is a breakthrough in collider design. The invention of the "crabbed waist" final focus can, in fact, have impact even on the current generation of colliders. A test of the crabbed waist concept is planned to take place at Frascati in late 2007 or early 2008; a positive result of this test would be an important milestone as the Super *B* design progresses. The low emittance lattice, fundamental as well to the ILC damping ring design, allows high luminosity with modest power consumption and demands on the detector.

Since the circulating currents in Super *B* are comparable to those in the current *B* factories, an upgrade of one of the existing *B* factory detectors, BaBar or Belle is an excellent match to the Super *B* machine environment. As an example, we will describe the changes envisioned in an upgrade of BaBar, beginning with the components closest to the beamline.

Developments in silicon sensors and materials technology make it possible to improve the resolution of the silicon vertex tracker (SVT) and to reduce the diameter of the beam pipe. This allows reduction of the energy asymmetry of Super *B* to 7 on 4 GeV, saving on power costs and slightly improving solid angle coverage. The first layer of the SVT will initially be composed of striplets, with an upgrade to pixels in the highest luminosity regime. The main tracking chamber will still be a drift chamber, although with smaller cell size. The radiators of the DIRC particle identification system will be retained, but the readout system will be replaced with a version that occupies a smaller volume. The barrel CsI (Tl) electromagnetic calorimeter will also be retained, but the forward endcap will be replaced with LYSO (Ce) crystals, which are faster and more radiation-hard. A small backward region calorimeter will be added, mainly to serve as a veto in missing energy analyses. The superconducting coil and instrumented flux return (IFR) will be retained, with the flux return segmentation and thickness modified to improve muon identification efficiency. The instrumentation in the endcap regions of the IFR will be replaced with scintillator strips for higher rate capability. The basic architecture of the trigger and data acquisition system will be retained, but components must be upgraded to provide a much-increased bandwidth.

Super *B* [1062] is an extremely promising approach to producing the very high luminosity asymmetric *B* factory that is required to observe and explore the contributions of physics beyond the SM to heavy quark and τ decays. Its physics capabilities are complementary to those of an experiment such as LHC*b* at a hadron machine [1063].

INFN has formed an International Review Committee to critically examine the Super *B* Conceptual Design Report and give advice as to further steps, including submission of the CDR to the CERN Strategy Group, requests for funding to the Italian government and application for European Union funds.

Should the proposal process move forward, it is expected that the collider and detector projects will be realized as an international collaborative effort. Members of the Super *B* community will apply to their respective funding agencies for support, which will ultimately be recognized in Memoranda of Understanding. A cadre of accelerator experiments

must be assembled to detail the design of Super *B*, while an international detector/physics collaboration is formed. The prospect of the reuse of substantial portions of PEP-II and BaBar raises the prospect of a major in-kind contribution from the US DOE and/or other agencies that contributed to BaBar construction; support of the project with other appropriate in-kind contributions is also conceivable. It is anticipated that the bulk of the US DOE contribution would be in kind, in the form of PEP-II components made available with the termination of the SLAC heavy flavor program. These include the HER and LER magnets, the RF and digital feedback systems, power supplies and vacuum components and the BaBar detector as the basis for an upgraded Super *B* detector.

The BaBar model of international collaboration, based on experience gained at CERN and other major laboratories in building and managing international collaborations over the past several decades, is expected to serve as a model for the Super *B* effort [1062]. The funding agencies of the participating countries will have a role, together with the host agency and host laboratory, in the management of the enterprise, as well as a fiscal role through an International Finance Committee and various review committees.

4.3 Accelerator design of SuperKEKB

The design of SuperKEKB has been developed since 2002 [1064]. The baseline design extends the same scheme as the present KEKB, as described below. The recently developed nano-beam scheme will be further studied as an option of SuperKEKB, while maintaining the baseline design for the time being. The possibility of an intermediate solution between these two schemes is not excluded a priori.

4.3.1 Baseline design of SuperKEKB

SuperKEKB is a natural extension of present KEKB. The baseline parameters of SuperKEKB are listed in Table 60.

The luminosity goal, 8×10^{35} cm^{-2} s^{-1}, is about 50 times higher than present KEKB. The gains of the luminosity will be achieved by higher currents ($\times 3-\times 6$), smaller focus parameter β_y^* ($\times 2$) and higher beam–beam parameter ξ_y ($\times 4.5$).

A higher stored current requires more RF sources and accelerating cavities. The baseline design adopts the same RF frequency, 509 MHz, as the present KEKB. The number of klystrons will be doubled, and the number of cavities will be increased by 50%. The total wall-plug power will be doubled. An option to adopt 1 GHz RF system to reduce the power is under consideration. The cavities will be modified for high current operation. The normal conducting accelerator with resonantly-coupled energy storage (ARES) cavity will have higher stored energy ratio of the storage cavity to the accelerating cavity. The superconducting cavity will have a new higher-order mode (HOM) absorber to dissipate 5 times more HOM power, namely 50 kW per cavity. The design of the RF system and the cavities has been basically done and prototyping is going on [1065–1069].

To store the high current, it is necessary to replace all existing beam pipes in both rings. In the positron ring, beam pipes with antechamber and special surface treatment such as TiN coating are required to suppress the electron cloud. The antechambers are necessary to store such high currents to absorb the power of the synchrotron radiation in both rings. Also all vacuum components such as bellows and gate valves must be replaced with low-impedance and high-current capable version. The small β_y^* requires shorter bunch length, which raises another reason to replace the beam pipes, otherwise the HOM loss and associated heating of the components will be crucial. The design of the beam pipes, of the bellows and of the gate valves for SuperKEKB has been done, and some prototypes were tested at present KEKB. There still remain a few R&D issues in beam collimators and coherent synchrotron radiation [1070–1075].

SuperKEKB will switch the charges of the beams from present KEKB to store positrons and electrons in the HER

Table 60 Parameters of SuperKEKB and present KEKB for the low (LER) and high (HER) energy rings

	SuperKEKB LER/HER	KEKB LER/HER	
Flavor	e^+/e^-	e^-/e^+	
Beam energy	3.5/8	3.5/8	GeV
Beam current	9.4/4.1	1.7/1.4	A
β_y^*/β_x^*	3/200	6/600	mm
Beam-beam ξ_y	~0.25	0.055	
Number of bunches/beam	5000	1400	
Horizontal emittance ε_x	6–12	18–24	nm
Bunch length σ_z	3	6	mm
Peak luminosity $\mathcal{L}$	8	0.17	10^{35} cm^{-2} s^{-1}
Wall-plug power	~100	45	MW

454

Eur. Phys. J. C (2008) 57: 309–492

and the LER, respectively. The charge switch will relax the electron-cloud instability and reduce the amount of the positron production. For the charge switch, the injector linac will be upgraded with a C-band system, whose prototype has already been built and tested successfully. Also new ideas such as single-crystal target for the positron production have been already utilized to increase the intensity of the positrons [1076, 1077].

All existing magnets of KEKB will be reused in SuperKEKB, except the interaction region (IR), which must be renewed for smaller β^*. The final focusing superconducting quadrupole with compensation solenoid will be made stronger and their prototype has already been produced. Also the crossing angle will be increased from 22 to 30 mrad. A local chromaticity correction system, which is currently installed in the LER, will be added in the HER. Another issue with the smaller β^* is the aperture for the injected beam, especially for positrons. A new damping ring for positrons will be necessary in the injector linac to reduce the injection emittance and to increase the capture efficiency of the positrons [1078].

The boost in the beam–beam parameter ξ_y assumes the success of "crab crossing", which recovers an effective head-on collision under crossing angle by tilting each bunch by a half crossing angle. The crab cavities have been built and operated at KEKB since February 2007, basically showing the design performance in the voltage, Q-value, phase stability, etc. The associated tilt of the beam and the effective head-on collision have been confirmed in various observations including streak cameras. The resulting beam–beam parameter reached 0.086, which is higher than the geometrical gain by about 15%. Further studies are necessary to realize higher beam–beam parameters (>0.1) predicted by simulations for the present KEKB [1079–1084].

A number of beam instrumentations and controls will be upgraded at SuperKEKB, including beam position monitors, feedbacks, visible light and X-ray monitors, etc. Also utilities such as water cooling system will be reinforced [1085].

The current estimate of the total cost of the upgrade for SuperKEKB is about 300 M€ (1 € ∼ 150 Y), excluding the salaries for the KEK employees in the accelerator group (about 90 FTE/year). If the upgrade of the RF system is deferred, the initial cost will be reduced to 200 M€.

One of the options to reduce the cost of the construction and electricity is to change the energy asymmetry from $8 + 3.5$ GeV to $7 + 4$ GeV. An early study has been done for the option resulting in a reduction by about 30 M€ in the construction and 12 MW in the electricity. Such a possibility will be investigated further.

This machine should have a flexibility to run at the charm threshold. The damping time and the emittance can be controlled by adding wigglers in the HER for that purpose. A polarized beam for the collision needs an intensive study on the implementation of spin rotators.

4.3.2 Studies for nano-beam scheme at KEK

The crab waist scheme is one of the most innovative features of the nano-beam Super$B$ design (Sect. 4.2 and [1045]). Simulation by K. Ohmi has shown that the crab waist scheme can improve the luminosity of present KEKB as powerfully as crab crossing with crab cavities. Actually crab waist can be even better than crab crossing, as it only needs conventional sextupole magnets whose construction and operation will be much easier than the state-of-the-art crab cavities. Special efforts have been made at KEK to develop such a design of the lattice to involve sextupole magnets at present KEKB.

This study of the lattice has shown that the dynamic aperture of the ring is drastically reduced by tuning on the crab sextupole magnets. These sextupoles are paired via I or $-I$ transformation, and the IP is located within the pair. If the transformation between the pair is completely linear, the nonlinearity of the first sextupole is completely absorbed by the second. This kind of cancellation has been successfully shown in existing machines including KEKB. In the case of the crab waist, however, there is the IP in the middle of the pair, and the nonlinearities around the IP violate the cancellation of the nonlinear terms of the sextupoles. At least two kinds of nonlinearity, the fringe field of the final focusing quadrupoles and the kinematical terms in the drift space around the IP, has been known to be inevitable, and either one of them is enough to degrade the dynamic aperture by 50%. As the fringe field and the kinematical terms are quite fundamental for the elements around the IP, it is not possible to remove them. The hope is to put several nonlinear magnets around the IP to cancel the nonlinearity at the IP.

The degradation of the dynamic aperture by the crab waist sextupoles will be also a serious problem for the future Super$B$. The dynamic aperture for a Super$B$ lattice was studied. The stable horizontal amplitude with the crab-sextupoles were dropped by 70% for the on-momentum particles and even worse for the off-momentum, synchrotron-oscillating particles. Again it has been known that the fringe field and the kinematical terms at the IP are the reasons of the reduction of the dynamic aperture.

One of the questions on the nano-beam scheme is that no strong-strong simulation has been done. Because of the relatively long bunch length, such a simulation will need more than 100 times more computer power than what is needed for usual schemes. Some preliminary efforts are going on for intermediate bunch length or with simplified models.

The nano-beam scheme can be also attractive even without the crab waist, because it has the potential to achieve 10^{36} cm^{-2} s^{-1} with smaller beam current. Therefore the KEKB team has decided to study the nano-beam scheme as an option of SuperKEKB, to make a flexible lattice and an IP design which is compatible with the nano-beam and

also with the high-current scheme. Such a design study will identify fundamental and technical issues on the nano-beam scheme more specifically.

4.4 LHCb upgrade

4.4.1 Introduction

Flavor physics has played a major role in the formulation of the SM of particle physics. An example is the observation of CP violation which, in the SM, can be explained with three generations of quarks. However despite its success, the SM is seen as an effective low-energy theory because it cannot explain dark matter and the force hierarchy. The search for evidence of physics beyond the SM is the main goal of particle physics over the next decade.

The LHC at CERN will start operating in 2008 and will start to look for the Higgs boson and for NP particles which are expected in many models at the 1 TeV scale. However probing NP at the TeV scale is not restricted to direct searches at the high-energy frontier.

Flavor physics also has excellent potential to probe NP. In the SM, FCNCs are suppressed as these only occur through loop diagrams. Hence these decays are very sensitive to NP contributions which, in principle, could contribute with magnitude $\mathcal{O}(1)$ to these virtual quantum loops. The NP flavor sector could also exhibit CP violation and be very different from what is observed in the SM. In fact, the existing experimental limits from the flavor physics point to either a suppression of the couplings also for NP or an even higher NP mass scale.

LHCb is a dedicated heavy-flavor physics experiment designed to make precision measurements of CP violation and of rare decays of B hadrons at the LHC [1086]. LHCb will start taking data in 2008 and plans to record an integrated luminosity of ~ 0.5 fb^{-1} in the first physics run. During the following five years, LHCb expects to accumulate a data sample of ~ 10 fb^{-1}. This will put LHCb in an excellent position to probe physics beyond the SM. The expected performance is summarized in Sect. 4.4.2.

During this first phase of LHC operations, particle physics will reach a branch point. Either new physics beyond the SM will have been discovered at the general purpose detectors (ATLAS and CMS) and LHCb or new physics will be at a higher mass scale. In both scenarios, we will then almost certainly require a substantial increase in sensitivities to flavor observables, either to study the flavor structure of the newly discovered particles or to probe NP through loop processes at even higher mass scales.

The LHCb detector is optimized to operate at a luminosity of 2 to 5×10^{32} cm^{-2} s^{-1}, which is a factor of 20 to 50 below the LHC design luminosity. The LHC accelerator will reach its design luminosity of 10^{34} cm^{-2} s^{-1} after a few years of operation. The LHC machine optics allows LHCb to focus the beams in order to run at a luminosity of up to 50% of the LHC luminosity. To profit from the higher peak luminosities that are available at the LHC, the LHCb experiment is proposing an upgrade to extend its physics programme. The plan to operate the LHCb detector at ten times the design luminosity, i.e. at 2×10^{33} cm^{-2} s^{-1}, is described in Sect. 4.4.3. The LHCb upgrade would allow the LHCb experiment to probe NP in the flavor sector at unprecedented sensitivities.

Initial studies of the physics reach of the proposed LHCb upgrade are discussed in Sect. 4.4.4. To profit from these higher luminosities, the LHCb experiment requires an upgrade such that the detectors and triggers are able to cope with these larger luminosities. This is described in Sect. 4.4.5. A summary and conclusions are given in Sect. 4.4.6.

4.4.2 LHCb physics programme—the first five years

The large cross section of 500 μb for $b\bar{b}$-quark production in pp collisions at 14 TeV centre-of-mass energy will allow the LHCb experiment to collect much larger data samples of B mesons than previously available. The expected performance for measurements with LHCb has been determined by a full simulation [1048]. Many of these results have been described in detail in Sect. 3 of this report. We expect exciting results from the LHCb experiments over the next five years. Here we summarize some of the anticipated highlights.

In the SM, FCNC $b \to s$ transitions are suppressed as these only occur through loop diagrams. Of particular interest is the decay $B_s^0 \to \mu^+\mu^-$, which is very rare. The SM branching ratio $\mathcal{B}(B_s^0 \to \mu^+\mu^-)$ is calculated at $(3.86 \pm 0.15) \times 10^{-9}$ (see (128)) [27]. Physics beyond the SM can enhance this branching ratio considerably. For example, in the CMSSM [571], the branching ratio increases as $\tan^6 \beta$, where $\tan \beta$ is the ratio of the Higgs vacuum expectation values. The current limits from CDF and D0 are about a factor 20 above the SM prediction. Using their good invariant mass resolution $\sigma(M_{\mu\mu}) \approx 20$ MeV and low trigger threshold on the transverse momentum $p_T \geq 1$ GeV, LHCb will be able to probe the full CMSSM parameter space. With 10 fb^{-1} of data, LHCb expects to discover $B_s^0 \to \mu^+\mu^-$ with 5σ significance at the SM level [598].

Another major goal is to probe the weak phase ϕ_s of B_s^0 mixing. This is another excellent NP probe as the SM prediction for ϕ_s is very small: $\phi_s = -2\lambda^2\eta \approx -0.035$,

456

Eur. Phys. J. C (2008) 57: 309–492

where λ and η are Wolfenstein parameters of the CKM matrix [1087]. Currently there are no strong constraints on ϕ_s available, and large CP violation in B_s^0 mixing is allowed [676, 678, 712, 714, 715]. The LHCb experiment expects to collect 131k $B_s^0 \to J/\psi\phi$ decays with a 2 fb^{-1} data sample. The corresponding precision on ϕ_s is estimated to be $\sigma(\phi_s) \approx 0.023$ [686]. A value of ϕ_s of $\mathcal{O}(0.1)$ or larger could be observed by LHCb. This would be a clear signal for NMFV beyond the SM [10].

LHCb will perform measurements of the CKM angle γ using two interfering diagrams in neutral and charged $B \to DK$ decays as well as $B_s^0 \to D_s^\mp K^\pm$ decays. The interference arises due to decays which are common to D^0 and $\bar{D}^0$ mesons such as $D^0(\bar{D}^0) \to K_S^0\pi^+\pi^-$ (Dalitz decay [637]) and $D^0(\bar{D}^0) \to K^\mp\pi^\pm$, K^+K^- (ADS and GLW [629, 635]), or through B_s mixing. The expected γ sensitivities for 2 fb^{-1} of LHCb data are estimated at $\sigma(\gamma) \sim 7°–15°$. When combining these measurements LHCb expects to achieve a precision $\sigma(\gamma) \sim 2.5°$ in a 10 fb^{-1} data sample [1048]. This will improve substantially the γ measurements from the B factories, which currently have an uncertainty of about 30° [389].

In Table 61, we show expected LHCb signal yields, background to signal ratios and sensitivity to physics observables based on a 2 fbinv data sample.

4.4.3 LHCb luminosity upgrade

After the first five years of operation of the LHCb experiment, the LHC will hopefully provide answers to some of the open questions of particle physics and, very possible, produce a few new puzzles. To be able to make progress in determining the flavor structure of new physics beyond the SM or probing higher mass scales, it is very likely that the required precision for several flavor physics observables will need to be improved substantially. It is also expected that the precision of many LHCb physics results will remain limited by the statistical error of the collected data. The following questions arise: What is the scientific case for collecting even larger data samples? Is LHCb exploiting the full potential for B physics at hadron colliders? Note that LHCb is the only dedicated heavy flavor experiment approved to run after 2010. In the remainder of this report, we will try to answer these questions.

The LHCb experiment has commenced studying the feasibility of upgrading the detector such that it can operate at a luminosity $\mathcal{L} \sim 2 \times 10^{33}$ cm^{-2} s^{-1}, which is ten times larger than the design luminosity [1089]. This upgrade would allow LHCb to collect a data sample of about 100 fb^{-1} during five years of running. This increased luminosity is achievable by decreasing the amplitude function β^* at the LHCb interaction point. The LHCb upgrade does not require the

Table 61 Expected signal yields S, signal to background ratios B/S and sensitivities for 2 fb^{-1} of data. The parameter s_0 is the zero point in the forward–backward asymmetry A_{FB}, and A_{CP} is the asymmetry in direct CP violation

	Decay	Yield S	B/S	Precision
γ	$B_s^0 \to D_s^\mp K^\pm$	6.2k	<0.18	$\sigma(\gamma) \sim 10°$
	$B^0 \to \pi^+\pi^-$	36k	0.46	$\sigma(\gamma) \sim 5°$
	$B_s^0 \to K^+K^-$	36k	<0.06	
	$B^0 \to D^0(K^-\pi^+, K^+\pi^-)K^{*0}$	3.4k, 0.6k	<1.0, <2.8	$\sigma(\gamma) \sim 6°–10°$
	$B^0 \to D^0(K^+K^-, \pi^+\pi^-)K^{*0}$	0.7k, 0.2k	<1.4, <5	
	$B^- \to D^0(K^-\pi^+, K^+\pi^-)K^-$	56k, 410	0.6, 2.0	$\sigma(\gamma) \sim 6°–10°$
	$B^- \to D^0(K^+K^-/\pi^+\pi^-)K^-$	5.8k, 2.0k	1.0, 3.6	
	$B^- \to D^0(K_S^0\pi^+\pi^-)K^-$	5k	<0.2–1	$\sigma(\gamma) \sim 15°$
α	$B^0 \to \pi^+\pi^-\pi^0$	14k	<0.8	$\sigma(\alpha) \sim 8.5°$
	$B^{+,0} \to \rho^+\rho^0, \rho^+\rho^-, \rho^0\rho^0$	7k, 2k, 1.2k	1, <5, <5	
β	$B^0 \to J/\psi K_S^0$	333k	1.1	$\sigma(\sin 2\beta) \sim 0.015$
Δm_s	$B_s^0 \to D_s^-\pi^+$	140k	<0.4	$\sigma(\Delta m_s) \sim 0.007$ ps^{-1}
ϕ_s	$B_s^0 \to J/\psi\phi$	131k	0.12	$\sigma(\phi_s) \sim 0.023$ rad
	$B_s^0 \to \phi\phi$	3.1k	<0.8	$\sigma(\phi_s) \sim 0.11$ rad
Rare	$B_s^0 \to \mu^+\mu^-$	20	<6.2	
Decays	$B^0 \to K^{*0}\mu^+\mu^-$	7.2k	0.5	$\sigma(s_0) \sim 0.46$ GeV^2
	$B^0 \to K^{*0}\gamma$	68k	0.6	$\sigma(A_{\text{CP}}) \sim 0.01$
	$B_s^0 \to \phi\gamma$	11.5k	<0.55	

planned LHC luminosity upgrade (Super-LHC) as the LHC design luminosity is 10^{34} cm^{-2} s^{-1}, although it could operate at Super-LHC. Thus an upgrade of LHCb could be implemented as early as 2014.

As the number of interactions per beam crossing will increase to $n \sim 4$, this will require improvements to the LHCb sub-detectors and trigger. A major component of the LHCb upgrade will be the addition of a first-level detached vertex trigger, which will use information from the tracking detectors [1090, 1091]. This trigger has the potential of increasing the trigger efficiencies for decays into hadronic final states by at least a factor of two. The implementation of this detached vertex trigger will require large modifications to the detector read-out electronics which will be discussed in Sect. 4.4.5.

4.4.4 Physics with the LHCb upgrade

A 100 fb^{-1} data sample would allow one to improve the sensitivity of LHCb to unprecedented levels such that NP can be probed at the 1% level. Here we present estimates for a few selected channels. These are based on the following assumptions, which have yet to be demonstrated: maintaining trigger and reconstruction efficiencies at high luminosity running and making use of a detached vertex trigger to double the trigger efficiency for hadronic modes. Systematic errors are only treated in a very simplified way. Hence the quoted sensitivities have very large uncertainties and should be treated with caution. However, these estimates are extremely useful to motivate simulation studies for validating these assumptions. In addition, as soon as LHCb will start taking data, the simulations for low luminosity running can be verified with data.

NP can be probed by studying FCNCs in hadronic $b \rightarrow s$ transitions. One approach is to compare the time-dependent CP asymmetry in a hadronic penguin loop decay with a decay based on a tree diagram when both decays have the same weak phase. In hadronic FCNC transitions, unknown massive particles could make a sizable contribution to the $b \rightarrow s$ penguin loop, whereas tree decays are generally insensitive to NP. The B factories measure the CP asymmetry $\sin 2\beta^{\mathrm{eff}}$ in the penguin decay $B^0 \rightarrow \phi K_S^0$. A value for $\sin 2\beta^{\mathrm{eff}}$, which is different from $\sin 2\beta$ measured in $B^0 \rightarrow J/\psi K_S^0$, would signal physics beyond the SM. Within the current available precision, all $\sin 2\beta^{\mathrm{eff}}$ measurements are in reasonable agreement with the SM, but most central values are lower than expected. For example, we find for the decay $B^0 \rightarrow \phi K_S^0$ that $\Delta S(\phi K_S^0) = \sin 2\beta^{\mathrm{eff}} - \sin 2\beta = 0.29 \pm 0.17$ [1088].

This approach can also be applied to B_s^0 mesons which will be exploited by LHCb. Within the SM, the weak mixing phase ϕ_s is expected to be almost the same when comparing the time-dependent CP asymmetry of the hadronic penguin

decay $B_s^0 \rightarrow \phi\phi$ with the tree decay $B_s^0 \rightarrow J/\psi\phi$. Due to a cancellation of the B_s^0 mixing and decay phase, the SM prediction for the sine-term, $S(\phi\phi)$, in the time-dependent asymmetry of $B_s^0 \rightarrow \phi\phi$ is very close to zero [834]. Thus any measurement of $S(\phi\phi) \neq 0$ would be a clear signal for NP and definitively rule out MFV [10]. From a full simulation LHCb expects to collect 3100 $B_s^0 \rightarrow \phi\phi$ events in 2 fb^{-1} of data with a background to signal ratio $B/S < 0.8$ at 90% C.L. [835]. The $S(\phi\phi)$ sensitivity has been studied using a toy Monte Carlo, taking resolutions and acceptance from the full simulation. After about 5 years LHCb expects to have accumulated a data sample of 10 fb^{-1} and will measure $S(\phi\phi)$ with a precision of $\sigma(S(\phi\phi)) = 0.05$ [835]. This precision is expected to be statistically limited, since systematic errors are likely much lower.

The LHCb upgrade will substantially improve the measurement of $S(\phi\phi)$, since this is a hadronic decay mode which will benefit most from the first-level detached vertex trigger. Scaling the sensitivity up to a data sample of 100 fb^{-1}, we estimate a precision of $\sigma(S(\phi\phi)) \sim 0.01$ to 0.02 rad. This sensitivity presents an exciting NP probe at the percent level which will arguably be (one of) the most precise time-dependent CP study in $b \rightarrow s$ transitions.

In a similar study, LHCb investigated the $b \rightarrow s$ penguin decay $B_d^0 \rightarrow \phi K_S^0$. A yield of 920 events is expected in 2 fb^{-1} of integrated luminosity, and the background to signal ratio is $0.3 < B/S < 1.1$. The sensitivity for the time-dependent CP violating asymmetry $\sin 2\beta^{\mathrm{eff}}$ is estimated to be 0.10 in a 10 fb^{-1} data sample [836]. This is a hadronic decay which will also profit from a first-level detached vertex trigger. With 100 fb^{-1} of integrated luminosity, LHCb upgrade will allow to improve the $\sin 2\beta^{\mathrm{eff}}$ sensitivity for $B_d^0 \rightarrow \phi K_S^0$ to ~ 0.025 to 0.035.

Using the tree decay $B_s^0 \rightarrow J/\psi\phi$, LHCb will also probe NP in the CP violation of B_s^0 mixing. With a 10 fb^{-1} data sample, the weak phase ϕ_s will be determined with a precision of 0.01 [1048]. This corresponds to $\sim 3.5\sigma$ significance for the SM expectation of ϕ_s for which the theoretical uncertainty is very precise ($\mathcal{O}(0.1\%)$). This precision is expected to be still statistically limited. A significantly larger data-set would allow LHCb to search for NP in B meson mixing at an unprecedented level. An upgrade of LHCb has the potential to measure the SM value of ϕ_s with $\sim 10\sigma$ significance ($\sigma(\phi_s) \sim 0.003$) in $B_s^0 \rightarrow J/\psi\phi$ decays. To control systematic errors at this level will be very challenging.

In the SM, the angle γ can be determined very precisely with tree decays, which are theoretically very clean. When combining all γ measurements in $B \rightarrow DK$ and $B_s^0 \rightarrow D_s^\mp K^\pm$ (including systematics), LHCb will constrain the value of γ to about 2.5°. However, it will not be possible to push below the desired 1° precision. Therefore, a very precise determination of γ in tree decays is an important objective of the LHCb upgrade physics programme. The

458

Eur. Phys. J. C (2008) 57: 309–492

expected yields in 100 fb^{-1} of data are very large: Examples are 620k $B_s^0 \to D_s^{\mp} K^{\pm}$, 500k $B \to D(K_S^0 \pi^+ \pi^-)K$ and 5600k $B \to D(K\pi)K$ events, respectively. All these γ modes will benefit greatly from an improved first-level trigger strategy that does not rely solely on high transverse momentum hadrons. Simple statistical extrapolations show that several individual modes will give a potential statistical uncertainty close to 1°. Systematic uncertainties will be very important. However, these uncertainties are largely uncorrelated amongst the modes and, in many cases, can be measured in control samples. Therefore, a global determination to below 1° of the tree level unitarity triangle will be possible [1049]. This will act as a standard candle to be compared to all loop determinations of the unitarity triangle parameters.

The very rare decay $B_s^0 \to \mu^+ \mu^-$ is a key to many extensions beyond the SM. With a 100 fb^{-1} data sample, LHCb upgrade would be able to make a precision measurement of the branching ratio $\mathcal{B}(B_s^0 \to \mu^+ \mu^-)$ to about ~5% at the SM level. This will allow LHCb upgrade to either measure precisely the flavor properties of new SUSY particles discovered at the LHC or to put very stringent constraints on all SUSY models in the large $\tan \beta$ regime [571].

The LHCb upgrade should also aim to observe the even rarer decay $B_d^0 \to \mu^+ \mu^-$ which has an SM branching ratio of $(1.06 \pm 0.04) \times 10^{-10}$ (see (131)). The ratio $\mathcal{B}(B_d^0 \to \mu^+ \mu^-)/\mathcal{B}(B_s^0 \to \mu^+ \mu^-)$ is sensitive to new physics beyond the SM and will allow to distinguish between different models. This search will be extremely challenging as it requires an excellent understanding of the detector to reduce the muon fake rate due to backgrounds from hadronic two body modes to an acceptable level.

LHCb will exploit the semileptonic decay $B \to K^{*0} \mu^+ \mu^-$, which is sensitive to new physics in the small $\tan \beta$ range. Using a full simulation LHCb expects to collect 7200 $B \to K^{*0} \mu^+ \mu^-$ per 2 fb^{-1} [508]. In addition to the forward–backward asymmetry, A_{FB}, these large data samples will allow LHCb to measure the differential decay rates in the di-muon mass squared, q^2, and the angular distributions and to probe NP through the transversity amplitude $A_T^{(2)}$ and the K^{*0} longitudinal polarization [476]. In the theoretically favored region of $1 < q^2 < 6$ GeV$^2/c^4$, the resolution in $A_T^{(2)}$ is estimated at 0.16 with 10 fb^{-1} of integrated luminosity [510]. While this data sample might provide a hint of NP, a ten-fold increase in statistics will allow one to probe new physics at the few percent level and cover a large region of the MSSM parameter space. With a 100 fb^{-1} data sample, LHCb upgrade expects to collect 360k $B \to K^{*0} \mu^+ \mu^-$ events. The corresponding precision for $A_T^{(2)}$ is estimated to be 0.05 to 0.06.

There are several other channels which have a large potential for probing NP with a 100 fb^{-1} data sample. An excellent example is $B_s^0 \to \phi \gamma$, which is sensitive to the photon polarization and right-handed currents [407]. Using a full simulation, LHCb expects a yield of 11.5k $B_s^0 \to \phi \gamma$ events in 2 fb^{-1} of data with a background to signal ratio <0.55 at 90% C.L. [454]. The sensitivity of this decay to NP arising in right-handed currents is under study. LHCb upgrade would also be able to search for NP by studying the decays $B_s \to \phi \mu^+ \mu^-$ and $B \to \pi(\rho) \mu^+ \mu^-$.

The very large charm sample would allow LHCb upgrade to search for NP in D^0 mixing and CP violation in charm decays. The expected statistical sensitivity on the parameters x'^2, y' and y_{CP} are 2×10^{-5}, 2.8×10^{-4} and 1.5×10^{-4}, respectively (Table 47). An LHCb upgrade could also probe lepton flavor violation in the decay mode $\tau \to \mu^+ \mu^- \mu^+$ with an estimated sensitivity of 2.4×10^{-9} [1092].

The SM as well as SUSY or extra dimension models can be augmented by additional gauge sectors [1093–1095]. This is a very general consequence of string theories [1096–1098]. These gauge sectors can only be excited by high-energy collisions. An example is the "hidden valley" sector. The manifestations of many of these models could be new v-flavored particles with a long lifetime [1093]. These can decay to a pair of b and $\bar{b}$ quarks that produce jets in the detector. An example is the Higgs decay process $H \to \pi_v^0 \pi_v^0$ followed by $\pi_v^0 \to b\bar{b}$. LHCb is designed to detect b-flavored hadrons and thus in a good position to detect decays of long-lived new particles. The LHCb vertex detector (VELO) is ~1 m long making it possible to measure these decays. LHCb upgrade will increase the sensitivity to much lower production cross section for these processes.

In Table 62, we present a summary of the expected sensitivities for selected key measurements, discussed above and that could be performed with an upgrade of the LHCb experiment. These sensitivities will exceed the range for probing NP from LHCb and B factories considerably, and they will also improve upon the precision of SM parameters.

We now compare the physics potential of the LHCb upgrade collecting a 100 fb^{-1} data sample with that of an SFF

Table 62 Expected sensitivity for LHCb upgrade with an integrated luminosity of 100 fb^{-1}. A factor two of improvement for the L0 hadron trigger and systematic error estimates are shown as a range

Observable	LHCb upgrade sensitivity
$S(B_s \to \phi\phi)$	0.01–0.02
$S(B_d \to \phi K_S^0)$	0.025–0.035
ϕ_s ($J/\psi\phi$)	0.003
$\sin(2\beta)$ ($J/\psi K_S^0$)	0.003–0.010
γ ($B \to D^{(*)} K^{(*)}$)	<1°
γ ($B_s \to D_s K$)	(1–2)°
$\mathcal{B}(B_s \to \mu^+ \mu^-)$	(5–10)%
$\mathcal{B}(B_d \to \mu^+ \mu^-)$	3σ
$A_T^{(2)}(B \to K^{*0} \mu^+ \mu^-)$	0.05–0.06
$A_{\mathrm{FB}}(B \to K^{*0} \mu^+ \mu^-) \, s_0$	0.07 GeV^2

based on a 50 to 75 ab^{-1} data sample, which is discussed in Sect. 4.1.

The strengths of the two proposals are surprisingly complementary. For example, the cleaner environment of an e^+e^- collider allows the SFF to make inclusive measurements of $b \to s\gamma$, of the CKM matrix element V_{ub} and of rare decays with missing energy such as $B^+ \to \ell^+\nu$. However, LHCb upgrade is unique in its potential to exploit the physics of B_s^0 mesons, especially in B_s^0 oscillations. A key motivation for LHCb upgrade is the ability to probe new physics in hadronic $b \to s$ penguin transitions by measuring the time-dependent CP asymmetry in the decay $B_s^0 \to \phi\phi$ with a precision of 0.01 to 0.02. The SFF will make complementary measurements by studying the time-dependent CP asymmetries of $b \to s$ transitions in several B_d^0 decays.

The LHCb upgrade will be able to measure CP violation in the interference of mixing and decay in both B_s^0 and B_d^0 mesons. This will allow LHCb to probe NP simultaneously in FCNC with $B_d^0 \to J/\psi K_s^0$ and $B_s^0 \to J/\psi \phi$ (tree) and $B_d^0 \to \phi K_s^0$ and $B_s^0 \to \phi\phi$ (hadronic $b \to s$ penguin) to the unprecedented level of $\sim 1\%$.

The LHCb upgrade will probe NP contributions to right-handed currents by measuring the time-dependent CP asymmetry in the decay $B_s^0 \to \phi\gamma$. The SFF will make complementary measurements and exploit their better reconstruction efficiencies for decays with several neutral particles in the final state to measure the photon polarization of $B_d^0 \to K_S^0 \pi^0 \gamma$.

In channels where both approaches are possible, the sensitivities are often comparable. LHCb upgrade usually will have larger statistics, but systematic errors in the hadronic environment will be more difficult to control. Both LHCb upgrade and SFF propose to measure $\sin 2\beta$ to 0.01 and the UT angle γ with 1° precision.

A SFF can measure the zero of the forward–backward asymmetry in the inclusive channel $b \to s\ell^+\ell^-$, but the LHCb upgrade will collect a substantially larger sample of 360k $B_d^0 \to K^{*0}\mu^+\mu^-$ decays compared to 11k at an SFF. This will enable LHCb to measure the asymmetry $A_T^{(2)}$ to $\sim 5\%$. Only the LHCb upgrade will be able to measure the $B_s^0 \to \mu^+\mu^-$ branching ratio to $\sim 5\%$. This will either help to determine the flavor structure of new particles discovered at the LHC or will severely constrain the corresponding model parameters.

4.4.5 LHCb detector and trigger upgrade

We start out by presenting the limitations of the LHCb detector and trigger which prevent LHCb from operating the detectors at higher luminosity. At the design luminosity of 2×10^{32} cm^{-2} s^{-1}, the visible cross section is 63 mb which corresponds to about 10 MHz of bunch crossings with at least one visible interaction. Note that increasing the luminosity from 2 to 10×10^{32} cm^{-2} s^{-1} will only increase the

number of interactions by a factor of two, since the number of bunch crossings with visible interactions increases from 10 to 26 MHz.

The LHCb experiment has a two-level trigger system. The Level-0 trigger (L0) is implemented in hardware, and the Higher Level Trigger (HLT) is running on a large CPU farm. The L0 trigger operates at 40 MHz. The purpose of L0 is to reduce this rate to 1.1 MHz, which is the maximum at which all LHCb detectors can be read-out by the front-end electronics. The L0 trigger selects objects (hadron h, e, and γ) with high transverse energy, $E_T^{h,e,\gamma}$, in the electromagnetic and hadronic calorimeters and the two highest transverse momentum (p_T^μ) muons in the muon system. At the nominal luminosity of 2×10^{32} cm^{-2} s^{-1}, the typical trigger thresholds are $E_T^h \geq 3.5$ GeV, $E_T^{e,\gamma} \geq 2.5$ GeV and $p_T^\mu \geq 1$ GeV. Events with multiple interactions are vetoed.

Simulations show that the L0 muon trigger efficiency for reconstructible events at the design luminosity of 2×10^{32} cm^{-2} s^{-1} is around 90% and that the output rate raises almost linearly with luminosity up to 5×10^{32} cm^{-2} s^{-1}. For larger luminosities, the loss in efficiency is minor. At the design luminosity, the muon trigger uses about 15% of the L0 bandwith. However, the L0 hadron trigger has a lower performance. The efficiencies of this trigger for hadronic decays are only about 40% at the design luminosity, whereas the L0 hadron trigger uses about 70% of the L0 bandwith. At higher peak luminosity, the rate of visible pp interaction increases, which requires an increase in the threshold. The corresponding loss in efficiency results in an almost constant yield for the hadron trigger [1090].

This illustrates that the existing trigger does not scale with luminosity, in particular the hadronic trigger will not allow operating the LHCb experiment at ten times the design luminosity. The total trigger efficiency including the HLT for hadronic B decays is expected to be 25 to 30% [1048]. The goal of the LHCb upgrade should also be to improve the hadron trigger efficiency by at least a factor two.

We have commenced initial studies which investigate how to upgrade the LHCb detector and triggers such that the experiment can operate at luminosities $\mathcal{L} \sim 2 \times 10^{33}$ cm^{-2} s^{-1}. These show that the only way to achieve this is to measure both the momentum and the impact parameter of charged B decay products simultaneously. The present front-end architecture is not compatible with this requirement. The vertex and tracking detectors are read-out at a maximum rate of 1.1 MHz, thus this information is not available to the L0 trigger.

Hence the LHCb upgrade has opted for a front-end electronics which will read-out all LHCb sub-detectors at the full bunch crossing rate of 40 MHz of the LHC. Data will be transmitted over optical fibres to an off detector interface board which is read out by the DAQ. This has clear advantages as it would allow the implementation of a L0 displaced

460

Eur. Phys. J. C (2008) 57: 309–492

vertex trigger in a CPU farm. In fact all trigger decisions would be software-based which allows flexibility.

A initial study for the 40 MHz trigger uses $B_s^0 \to D_s^\mp K^\pm$ decays simulated at a luminosity of 6×10^{32} cm^{-2} s^{-1}. Events with large numbers of interactions are employed to simulate larger effective luminosities up to 2×10^{33} cm^{-2} s^{-1}. Assuming enough CPU power to process an event rate of 5 MHz, we obtain a trigger efficiency of 66% for this channel. The requirements are a transverse energy $E_T > 3$ GeV from the L0 hadron trigger which has an efficiency of 76% for signal combined with a matched track that has a transverse momentum $p_T > 2$ GeV/c and an impact parameter $\delta > 50\mu$m. In this combined trigger, the minimum bias rate does not depend strongly on the luminosity, and the triggered event yield scales linearly with the luminosity. In addition, the total trigger efficiency is 60% larger when compared with the existing baseline.

However, this approach requires a replacement of the front-end electronics for all sub-detectors, with the exception of the muon chambers which are already read out at 40 MHz. Replacing the front-end electronics will require new sensors for several sub-systems. Besides the VELO silicon sensors, the silicon sensors of the tracking stations will need to be replaced. The sensors close to the beam will suffer from a ten-fold increase in radiation, and hence more radiation hard sensors will be required. The RICH photon detectors have encapsulated front-end electronics and need to be replaced entirely.

The vertex detector (VELO) silicon sensors undergo radiation damage, and it is expected that these will need to be replaced when 6 to 8 fb^{-1} of luminosity has been collected [1099]. However the channel occupancy in the VELO is ∼1% at design luminosity. When increasing the luminosity by a factor of ten to 2×10^{33} cm^{-2} s^{-1}, the occupancy only increases to ∼3%, and the corresponding efficiency loss is small.

A preliminary study of the performance of the electromagnetic calorimeter (ECAL) at high luminosity shows only a small degradation for the selection efficiency of the decay $B_s^0 \to \phi\gamma$. It might be necessary to upgrade the inner section of ECAL to improve its granularity and energy resolution. The increased radiation level of irradiation leads to a degradation of the energy resolution and will require that half the inner ECAL section will need to be replaced after 3 years of operation at 2×10^{33} cm^{-2} s^{-1}.

R&D efforts have started on technologies for radiation-hard vertex detectors that will be able to operate in the LHC radiation environments at LHCb upgrade luminosities. The detector sensors will need to be able to operate at radiation doses of about 10^{15} 1 MeV equivalent neutrons/cm^2. Initial studies of Czochralski and n-on-p sensors irradiated up to 4.5×10^{14} 24 GeV protons/cm^2 are promising and show that the charge collection efficiencies saturate at acceptable

bias voltages [1099]. Pixel sensors are very radiation hard, and R&D on this technology has started.

Two different vertex-detector geometries are envisaged. One is to shorten the strips, the other is to use pixels. Removing the RF foil that separates the VELO sensors from the primary beam-pipe vacuum would reduce the radiation length before the first measurement by 3% and improve the proper time resolution of B-meson decays.

4.4.6 Summary and conclusions

The LHC will open a new window for discovering NP. The LHCb experiment will probe NP with precision studies of flavor observables, whereas the general purpose detectors ATLAS and CMS aim to directly observe new particles. Both approaches are required to study the mass hierarchy and the couplings of the NP. LHCb will collect an integrated luminosity of about 10 fb^{-1} during its first five years. Very likely the LHC results will show that a significantly better sensitivity will be required for both, the direct and indirect approaches. Here we present a proposal to upgrade the LHCb detectors to be able to operate at ten times the design luminosity, i.e. at 2×10^{33} cm^{-2} s^{-1}, and to collect a data sample of 100 fb^{-1} with an improved detector. Initial sensitivities for physics with LHCb upgrade are presented. These show that LHCb upgrade has the potential to probe new physics at unprecedented levels that is mainly complementary to the proposed SFF. The upgraded LHCb experiment will include a first-level detached vertex trigger for which a new front-end architecture must be designed. A more radiation hard vertex detector is required to cope with the increased radiation doses.

5 Assessments[30]

In Sect. 1, we briefly introduced several NP scenarios and discussed their impact on FCNC and CP-violating processes. Then, in Sect. 3, we considered several benchmark channels that are particularly sensitive to NP, discussing the present status and future developments. The aim of this section is to summarize the present status of NP flavor scenarios, to identify possible patterns of NP signals and to describe the first attempts that have been made during this workshop to connect constraints on NP (and possible NP signals) in flavor and high-energy physics. The first two items are discussed in Sect. 5.1, the last one is presented in Sect. 5.3.

---

[30]Section coordinators: S. Heinemeyer, F. Parodi, L. Silvestrini.

5.1 New-physics patterns and correlations

The past decade has witnessed enormous progress in the field of flavor physics: B factories have studied flavor and CP violation in $B_d - \bar{B}_d$ mixing and in an impressive number of B decays; the Tevatron has produced the first results on $B_s - \bar{B}_s$ mixing and has studied several BRs and CP asymmetries in B and B_s decays; very recently, B-factories have established the first evidence of $D - \bar{D}$ mixing. This flourishing of experimental results has been accompanied by several remarkable improvements on the theory side, both in perturbative and nonperturbative computations. Let us just mention the NNLO calculation of $BR(b \to s\gamma)$, the proof of factorization in nonleptonic B decays in the infinite mass limit and the first unquenched results on B physics from lattice QCD.

Thanks to these experimental and theoretical achievements, we now have a rather precise idea of the flavor structure of viable NP extensions of the SM. The general picture emerging from the generalized Unitarity Triangle analysis performed in [7, 9, 210] and from the very recent data on $D - \bar{D}$ mixing [933, 950, 957, 1100] is that no new sources of CP violation of $\mathcal{O}(1)$ are observed in B_d, K and D mixing amplitudes. However, the possibility of NP CP-violating effects in B_s mixing is still open. Concerning $\Delta F = 1$ processes, the situation is quite different. In particular, large NP contributions to $s \to dg$, $b \to dg$ and $b \to sg$ transitions are not at all excluded. Sizable NP effects in $s \to dZ$, $b \to dZ$ and $b \to sZ$ vertices are also possible, although the available experimental data excludes order-of-magnitude enhancements. Finally, FC Higgs interactions generated by NP can still give large enhancements of scalar vertices, although the upper bounds on $B_s \to \mu^+ \mu^-$ are getting tighter and tighter.

To summarize, we can say that, although the idea of MFV is phenomenologically appealing [10, 12, 82, 84, 190, 891, 1050], an equally possible alternative is that NP is contributing more to $\Delta F = 1$ transitions than to $\Delta F = 2$ ones. Within the class of $\Delta F = 1$ transitions, (chromo-)magnetic and scalar vertices are peculiar, since they require a chirality flip to take place, which leads to a down-type quark mass suppression within the SM. On the other hand, NP models can weaken this suppression if they contain additional heavy fermions and/or additional sources of chiral mixing. In this case, they can lead to spectacular enhancements for the coefficients of (chromo-)magnetic and scalar operators. Furthermore, if the relevant new particles are colored, they can naturally give a strong enhancement of chromomagnetic operators, while magnetic operators might be only marginally modified. The electric dipole moment of the neutron puts strong constraints on new sources of CP violation in chirality-flipping flavor-conserving operators involving light quarks, but this does not necessarily imply the suppression of flavor-violating operators, especially those involving b quarks. Therefore, assuming that NP is sizable in several $\Delta F = 1$ processes is perfectly legitimate given the present information available on flavor physics.

Thus, we can identify at least three classes of viable weakly-interacting NP extensions of the SM:[31]

1. Models with exact MFV.
2. Models with small ($\mathcal{O}(10\%)$) departures from MFV.
3. Models with enhanced scalar or chromomagnetic $\Delta F = 1$ vertices and a suitable suppression of NP contributions to $\Delta F = 2$ processes.

In models belonging to the third class, we expect sizable NP effects in B physics. From a theoretical point of view, a crucial observation is the strong breaking of the SM $SU(3)^5$ flavor symmetry by the top quark Yukawa coupling. This breaking necessarily propagates in the NP sector, so that in general it is very difficult to suppress NP contributions to CP violation in b decays, and these NP contributions could be naturally larger in $b \to s$ transitions than in $b \to d$ ones. This is indeed the case in several flavor models (see for example Ref. [1101]).

Another interesting argument is the connection between quark and lepton flavor violation in grand unified models [110, 1102–1104]. The idea is very simple: the large flavor mixing present in the neutrino sector, if mainly generated by Yukawa couplings, should be shared by right-handed down-type quarks that sit in the same $SU(5)$ multiplet with left-handed leptons. Once again, one expects in this case large NP contributions to $b \to s$ transitions.

5.2 Correlations between FCNC processes

On general grounds, it is difficult to establish correlations between FCNC processes without specifying not only the NP flavor structure but also the details of the NP model. However, there is a notable exception given by models of Constrained Minimal Flavor Violation (see Sect. 1 for the definition of this class of MFV models). While correlating $\Delta F = 1$ to $\Delta F = 2$ processes is not possible without specifying the details of the model, in the case of CMFV, there are several interesting correlations between FCNC processes. In CMFV, all NP effects can be reabsorbed in a redefinition of the top-mediated contribution to FCNC amplitudes. Thus, all processes that involve the same top-mediated amplitude are exactly correlated. This has interesting phenomenological consequences, allowing for stringent tests of CMFV by looking at correlated observables [10, 12, 190, 893, 1105].

It is enough to go from CMFV to MFV to destroy many of these correlations: for example, in MFV models with two

---

[31] Strongly-interacting NP most probably lies beyond the reach of direct searches at the LHC and so will not be discussed here [9].

462

Eur. Phys. J. C (2008) 57: 309–492

Higgs doublets at large $\tan\beta$, it is in general not possible to connect K, B and B_s decays in a model-independent way. However, interesting correlations remain present also at large $\tan\beta$. For example, the enhancement of $B_s \to \mu^+\mu^-$ corresponds in general to a depletion of Δm_s [30] (actually, both features might be phenomenologically acceptable [32]).

Of course, within a specific model, it is in general possible to correlate $\Delta F = 1$ and $\Delta F = 2$ processes and to fully exploit the constraining power of flavor physics. The most popular example is given by the minimal supergravity models, where one can combine not only all the information from flavor physics but also the available lower bounds on SUSY particles and the constraints from electroweak physics, dark matter and cosmology [1106–1122, 1151–1155]. Interesting correlations between FCNC processes are also present in the CMSSM if one considers more general SUSY spectra than minimal supergravity [86, 1050].

Even allowing for new sources of flavor and CP violation to be present, correlations remain present between the several flavor observables generically affected by the same NP flavor-violating parameter. An interesting example is given by SUSY models with enhanced chromomagnetic $b \to s$ vertices (see e.g. [107]).

Another general class of NP models in which interesting correlations between FCNC processes can be established is given by SUSY-GUTs. Grand unification implies the equality of soft SUSY breaking terms at the GUT scale. Thus, any new source of flavor and CP violation present in squark masses must also be present in slepton masses, leading to a correlation between squark and slepton FCNC processes [69]. An extensive discussion of these correlations has been carried out in [70]. As an example, we present in Fig. 68 (from [70]) the constraints on $(\delta^d_{13})_{RR}$ (defined in Sect. 1.3.5) from hadronic constraints only (upper left), leptonic constraints only (upper right), all constraints (lower left) and all constraints with improved leptonic bounds (lower right). In this interesting case, hadronic and leptonic bounds have comparable strengths. Exploiting the GUT correlation, it is possible to combine them to obtain a much tighter constraint on $(\delta^d_{13})_{RR}$.

5.3 Connection to high-energy physics

Recent low-energy data from flavor physics experiments showed relatively good agreement with the SM prediction (taking into account the theory uncertainties). This imposes strong constraints on any NP scenario. In view of the new results and the new bounds on physics beyond the SM, the demand for scenarios that could be used for studies at ATLAS or CMS (or more generally for setting up the infrastructure for future studies once ATLAS and CMS have collected their first data) was issued. These scenarios should be in agreement with all existing B and K physics data and possibly show interesting signatures at the LHC experiments.

Fig. 68 Allowed region in the $\mathrm{Re}(\delta^d_{13})_{RR}$–$\mathrm{Im}(\delta^d_{13})_{RR}$ plane using hadronic constraints only (*upper left*), leptonic constraints only (*upper right*), all constraints (*lower left*) and all constraints with improved leptonic bounds (*lower right*)
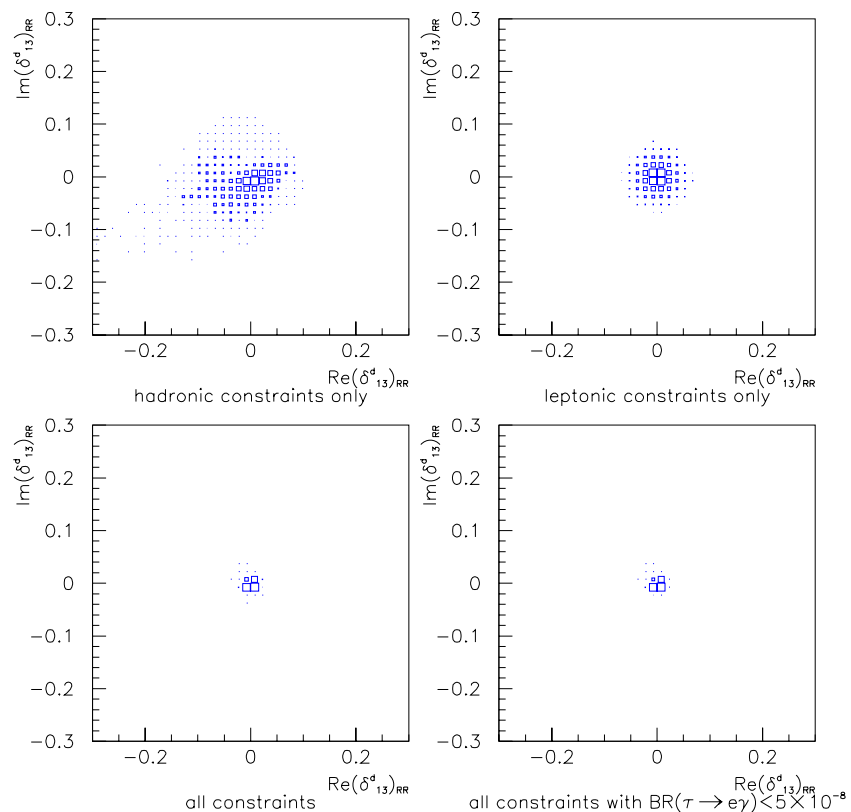
In this respect, the question which parameter choices are useful as a benchmark scenario depends on the purpose of the actual investigation. If one is interested, for instance, in setting exclusion limits on the SUSY parameter space from the nonobservation of SUSY signals at the experiments performed up to now, it is useful to use a benchmark scenario which gives rise to "conservative" exclusion bounds. An example for a benchmark scenario of this kind is the m_h^{max}-scenario [1123, 1124] used for the Higgs search at LEP [1125] and the Tevatron [1126, 1127]. Another purpose for using benchmark scenarios is to study "typical" experimental signatures of e.g. SUSY models and to investigate the experimental sensitivities and the achievable experimental precisions for these cases. For this application, it seems reasonable to choose "typical" parameters (a notion which is of course hard to define) of certain SUSY-breaking scenarios (see e.g. the "Snowmass Points and Slopes" [1129]). In this context, it can also be useful to consider "pathological" regions of parameter space or "worst-case" scenarios.

In the perspective of future improvements on B and K physics data, it is also worth to consider the possibility of a *positive* signal of NP selected by some low-energy observable. In this perspective, it is useful to consider benchmark scenarios with well-defined low-energy signatures, such as the MFV scenario with large $\tan \beta$ discussed in [32], or models with small flavor-breaking structures departing from the minimal structure of the constrained MSSM. These cases are particularly useful to explore the capability of future flavor-physics measurements in constraining a limited set of the SUSY parameter space, both separately and in conjunction with future ATLAS/CMS data.

A related issue concerning the definition of appropriate scenarios is whether a benchmark scenario chosen for investigating physics at ATLAS and CMS should be compatible with additional information from other experiments (beyond B and K physics). This refers in particular to constraints from cosmology or the measurement of the anomalous magnetic moment of the muon, $(g-2)_\mu$ [1128]. On the one hand, applying constraints of this kind gives rise to "more realistic" benchmark scenarios (see e.g. [1129]). On the other hand, one relies in this way on further assumptions (and has to take account of experimental and theoretical uncertainties related to these additional constraints), and it could eventually turn out that one has narrowed down the range of possibilities too much by applying these constraints. This applies in particular if slight modifications of the model under investigation have a minor impact on collider phenomenology but could significantly alter the bounds from cosmology and low-energy experiments. For instance, the presence of a small amount of R-parity violation in a SUSY model would strongly affect the constraints from dark matter relic abundance, while leaving the phenomenology at high-energy colliders essentially unchanged. Thus we restrict ourselves to scenarios which are compatible with flavor physics, with existing lower bounds on new particles (e.g. the bound on the lightest MSSM Higgs boson [1125, 1130]) and with other electroweak precision data, see Ref. [1131] and references therein.

The general procedure of setting up new scenarios follows the steps:

1. Identify the models of interest.
2. Identify within these models the regions of the parameter space that are compatible with the existing constraints from flavor physics, electroweak precision physics and direct bounds.
3. Identify specific sub-regions which could be selected by future improvements on flavor physics.
4. Study the most interesting points in view of their high-energy phenomenology that can be explored at ATLAS and CMS.
5. Set up the infrastructure for the analysis of (possible) data that will be collected at ATLAS and CMS to test the new high-energy results against existing low-energy data.

Concerning the first step, the model(s) which exhibited most interest during this workshop are the MSSM with (N)MFV. Consequently, in the following, we concentrate on this class of SUSY models.

Within the second and third step, it is desirable to connect different codes (e.g. working in the (N)MFV MSSM, see Sect. 1.5.1) to each other. Especially interesting is the combination of codes that provide the evaluation of (low-energy) flavor observables and others that deal with high-energy (high-p_T) calculations for the same set of parameters. This combination would allow one to test the ((N)MFV MSSM) parameter space with the results from flavor experiments as well as from high-energy experiments such as ATLAS or CMS.

A relatively simple approach for the combination of different codes is their implementation as sub-routines, called by a "master code" (see Sects. 5.3.3, 1.5.2). This master code takes care of the correct definition of the input parameters for the various subroutines. Concerning the last step, the application and use of the master code would change once experimental data showing a deviation from the SM predictions is available. This can come either from the ongoing flavor experiments or latest (hopefully) from ATLAS and CMS. If such a "signal" appears at the LHC, it has to be determined to which model and to which parameters within a model it can correspond. Instead of checking parameter points (to be investigated experimentally) for their agreement with experimental data, now a scan over a chosen model could be performed. Using the master code with its subroutines, each scan point can be tested against the "signal", and preferred parameter regions can be obtained using

a χ^2 evaluation. It is obvious that the number of evaluated observables has to be as large as possible, i.e. the number of subroutines (implemented codes) should be as big as possible.

5.3.1 The first approach: prediction of b-physics observables from SUSY measurements

The first approach was followed in collaboration with AT-LAS.

An LHC experiment will hopefully be able to measure a significant number of SUSY parameters based on the direct measurement of SUSY decays. The experimental potential in this field has been studied in detail for various benchmark points. Based on these studies, a possible approach is to focus on specific models for which many SUSY parameters can be measured at the LHC and to try to answer the following questions:

1. How precisely can b-physics variables be predicted using measured SUSY parameters?
2. Vice versa: can we use b-physics measurements to constrain badly measured SUSY parameters?
3. Is the precision of the measurements on the two sides adequate to rule out minimal flavor violation and/or to constrain flavor violation in the squark sector?

We will show in the following the application of this approach, especially of question (1), to a point of the MSSM space which was adopted as a benchmark point by the Supersymmetry Parameter Analysis (SPA) group [1132]. This model is defined in terms of the parameters of the mSUGRA model ($m_0 = 70$ GeV, $m_{1/2} = 250$ GeV, $A_0 = -300$ GeV, $\tan \beta = 10$, $\mu > 0$). This is a modification of the point SPS1a, essentially achieved by lowering m_0 from 100 to

70 GeV, originally defined in [1129] to take into account more recent results on dark matter density.

The values of the sparticle masses at tree level, computed with the program ISASUSY 7.71 [1133], are given in Table 63. Constraints on the sparticles masses can be obtained from measurements of the kinematics of the SUSY cascade decays [1134–1136]. This program has been carried out recently for the SPS1a model point [1137], assuming the performance of the ATLAS detector. The resulting constraints allow the measurement of the masses of $\tilde{\chi}_1^0$, $\tilde{\chi}_2^0$, $\tilde{\chi}_4^0$, $\tilde{g}$, $\tilde{q}_L$, $\tilde{q}_R$, $\tilde{b}_1$, $\tilde{b}_2$ $\tilde{\ell}_R$ $\tilde{\ell}_L$, $\tilde{\tau}_1$, where $\tilde{q}_L$ and $\tilde{q}_R$ are the average of the masses of the squarks of the first two generations. All these masses should be measurable with an uncertainties of a few percent for an integrated luminosity of 300 fb^{-1}. The estimated uncertainties will be used as an input to this study.

For the stop sector, a detailed study is available [1139], always performed in the framework of the ATLAS Collaboration. This analysis studies the tb invariant mass distribution in SUSY events. This distribution, shown in the left panel of Fig. 69, shows the characteristic kinematic edge which can be expressed as a function of the masses. Two

Table 63 Masses of the sparticles in the considered model as calculated at tree level with ISAJET 7.71 [1133]

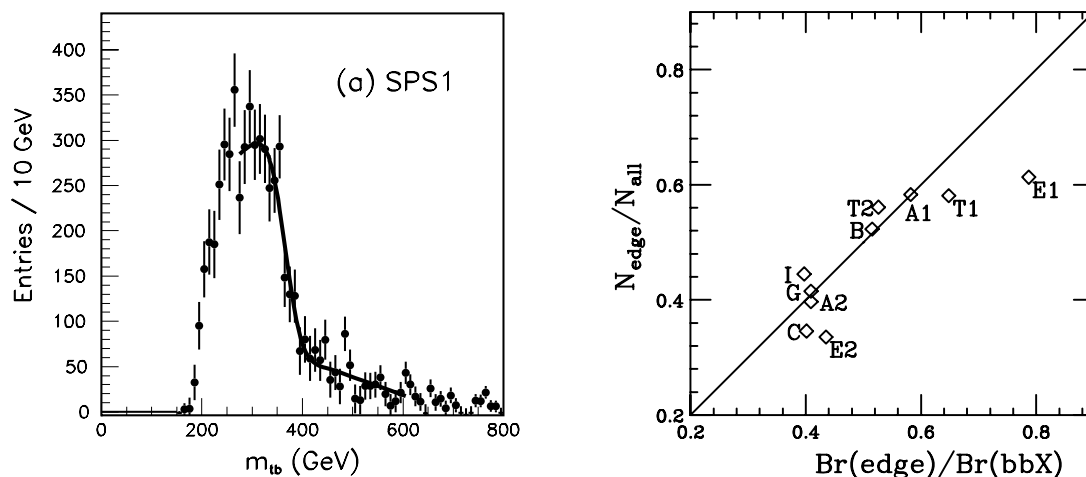| Sparticle	Mass [GeV]	Sparticle	Mass [GeV]
$\tilde{\chi}_1^0$	97.2	$\tilde{\chi}_2^0$	180.1
$\tilde{\chi}_3^0$	398.4	$\tilde{\chi}_4^0$	413.8
$\tilde{\ell}_L$	189.4	$\tilde{\ell}_R$	124.1
$\tilde{\tau}_1$	107.7	$\tilde{\tau}_2$	194.2
$\tilde{t}_1$	347.3	$\tilde{t}_2$	562.3
$\tilde{u}_L$	533.3	$\tilde{g}$	607.0
h	116.8	A	424.6

Fig. 69 *Left*: m_{tb} distribution for model point SPS1a. *Right*: relationship between N_{edge}/N_{all} and BR(edge)$/BR$(bbX) for different model points as described in [1139]. Both figures from [1139]

main SUSY decay chains yield a tb final state signature:

$$\tilde{g} \rightarrow \tilde{t}_1 t \rightarrow tb \tilde{\chi}_1^{\pm} \tag{231}$$

and

$$\tilde{g} \rightarrow \tilde{b}_1 b \rightarrow tb \tilde{\chi}_1^{\pm}. \tag{232}$$

Therefore the position of the end-point in the tb mass distribution (M_{tb}^{fit}) will measure the average of the edges for the two decays weighted by the relative BR, which yields a constraint on a number of MSSM parameters:

$$M_{tb}^{\text{fit}} = f(m_{\tilde{t}_1}, m_{\tilde{b}_1}, m_{\tilde{g}}, m_{\tilde{\chi}_1^{\pm}}, \theta_{\tilde{t}}, \theta_{\tilde{b}}).$$

From the height of the observed kinematic distribution one can also measure the ratio of events in the tb mass distribution to all SUSY events with a b pair in the final state, $N_{\text{edge}}/N_{\text{all}}$. This observable is well correlated, as shown in the right panel of Fig. 69, with the quantity $BR(\text{edge})/BR(\tilde{g} \rightarrow bbX)$, where $BR(\text{edge})$ is the sum of the BR's for the decays (231) and (232) above. Finally direct searches in the SUSY Higgs sector yield additional constraints on the MSSM soft parameters.

The next step is the extraction of the soft SUSY-breaking parameters from the measured sparticle masses and branching ratios. We use a Monte Carlo technique relying on the generation of simulated experiments sampling the probability density functions of the measured observables. We proceed in the following way:

1. An 'experiment' is defined as a set of measurements, each of which is generated by picking a value from a Gaussian distribution with mean given by the central value calculated from the input parameters of the considered model and width given by the estimated statistical + systematic uncertainty of each measurement.
2. For each experiment, we extract the constraints on the MSSM model as we will describe in the following.

As a result of this calculation, we obtain a set of MSSM models, each of which is the "best" estimate for a given Monte Carlo experiment of the model generating the observed measurement pattern. For each of these models, the b-physics observables can be calculated.

Three groups of soft SUSY-breaking parameters are relevant for the prediction of b-physics observables:

– the parameters of the neutralino mixing matrix, M_1, M_2, μ, $\tan\beta$;
– m_A, the mass of the pseudoscalar Higgs, defining (together with $\tan\beta$) the Higgs sector at tree level;
– the masses and mixing angles of third generation squarks $\tilde{t}$ and $\tilde{b}$.

For the first two, a detailed discussion is given in [1140], which we will briefly summarize here.

In the SPA point, only the mass of three neutralinos (1, 2 and 4) can be measured. The three masses give a strong constraint on M_1, M_2, μ but have little sensitivity to $\tan\beta$. Therefore we use a fixed input value for $\tan\beta$ and calculate the values of M_1, M_2, μ from numerical inversion of the neutralino mixing matrix. We will then study 'a posteriori' the dependence on $\tan\beta$. The resultant uncertainty on M_1, M_2, μ is $\sim$(5–6) GeV, corresponding to the uncertainty on neutralino masses. By varying $\tan\beta$ in the range $3 < \tan\beta < 30$, the calculated values vary by less than 5 GeV.

Information on $\tan\beta$ and m_A can in principle be extracted from the study of the Higgs sector. The ATLAS potential for discovery is shown in Fig. 70 from [1135]. The light Higgs boson h can be discovered over the whole parameter space, but the measurement of its mass only provides somewhat loose constraints depending on the knowledge of the parameters of the stop sector. Much stronger constraints would be provided by the measurement of the mass and production cross-section of one or more of the heavy Higgs bosons. For the model under consideration with $\tan\beta = 10$ and $m_A \sim 425$ GeV, heavy Higgs bosons cannot be discovered at the LHC in their SM decay modes. Moreover, the heavy Higgs bosons cannot be produced in chargino–neutralino cascade decays, because the decays are kinematically closed. The only possibility would be the detection of $A/H \rightarrow \tilde{\chi}_2^0 \tilde{\chi}_2^0 \rightarrow 4\ell\ell$. Unfortunately the rate is very small, $\sim$40 events/experiment for 300 fb^{-1} before experimental cuts. A very detailed background study would be needed to assess the detectability of this signal.

Fig. 70 Reach of the ATLAS experiment in the m_A–$\tan\beta$ plane for an integrated luminosity of 300 fb^{-1}. For each region in the plane, the detectable Higgs bosons are marked

466

Eur. Phys. J. C (2008) 57: 309–492

We can now turn to the extraction of parameters of the stop-sbottom sector. The sector is defined by 5 soft SUSY-breaking parameters: $m(Q_3)$, the mass of the left-handed third generation doublet; $m(t_R)$ and $m(b_R)$, the masses of the stop and sbottom right-handed singlets; A_t and A_b, the stop and sbottom trilinear couplings. More convenient mixing variables would be $\theta_{\tilde{b}}$ and $\theta_{\tilde{t}}$, the left–right sbottom and stop mixing angles. For the considered point, 5 measurements will be available at the LHC:

– $m_{\tilde{b}_1}, m_{\tilde{b}_2}, BR(\tilde{g} \to b\tilde{b}_2 \to bb\tilde{\chi}_2^0)/BR(\tilde{g} \to b\tilde{b}_1 \to bb\tilde{\chi}_2^0)$ $(BR(\tilde{b}))$ [1137];
– $M_{tb}^{\text{fit}}, BR(\text{edge})/BR(\tilde{g} \to bbX)$ $(BR(\tilde{t}))$ [1139].

The assumed experimental errors on these variables are given in Table 64.

It is therefore possible to solve the available constraints for $m_{\tilde{t}_1}, \theta_{\tilde{b}}, \theta_{\tilde{t}}$, as discussed in [1141]. In [1141], the parameters of the gaugino matrix were assumed to be measured with infinite precision at the ILC, and the errors on the parameters in the stop sector were estimated by mapping the region in the $\theta_{\tilde{t}}$–$m_{\tilde{t}_1}$ plane compatible within the estimated errors with the nominal values of the five observables.

We incorporate the LHC uncertainties on the measurement of M_1, M_2, μ, and we use the technique of building Monte Carlo experiments described above.

The strategy is to scan the three-dimensional space $m_{\tilde{t}_1}$, $\theta_{\tilde{b}}$, $\theta_{\tilde{t}}$ and to find the point in space which reproduces the measured values of M_{tb}, $BR(\tilde{t})$, $BR(\tilde{b})$. For fixed $m_{\tilde{t}_1}$, the measurement of the position in the $\theta_{\tilde{b}}$–$\theta_{\tilde{t}}$ plane is given by combining the crossing of the line corresponding to the measured value of $BR(\tilde{b})$ with the line corresponding to the measured values of $BR(\tilde{b})$. We show in Fig. 71 respectively the band constrained by $\pm 1\sigma$ around the input values of $BR(\tilde{b})$ and $BR(\tilde{t})$ when all the other MSSM parameters are kept fixed. Because of the rather loose constraints on $BR(\tilde{b})$ and the low statistics in the $\tilde{b}_2$ peak, the region where the two bands cross, which roughly represents the allowed region in the plane, extends from the region around the input value $(\theta_{\tilde{t}} = 0.933, \theta_{\tilde{b}} = 0.42)$ with a very low tail towards the region of high $\theta_{\tilde{b}}$ and low $\theta_{\tilde{t}}$.

Table 64 Assumed uncertainties for the LHC measurements in stop-bottom sector. The assumed statistics is 300 fb^{-1}. The only systematic error considered is the jet energy scale error on the mass/end point measurements

Variable	Value	Error
$m_{\tilde{g}} - m_{\tilde{b}_1}$	128.7 GeV	1.6 GeV
$m_{\tilde{g}} - m_{\tilde{b}_2}$	86.9 GeV	2.5 GeV
$BR(\tilde{b})$	0.70	0.05
$BR(\tilde{t})$	0.21	0.08
M_{tb}	411.3 GeV	5.4 GeV

The results of the scan are shown in Fig. 72. In the left plot, we show the distribution of the measured $m_{\tilde{t}_1}$ values for the considered ensemble of MC experiments. The RMS of the distribution is ~ 17 GeV, corresponding to a $\sim 5\%$ uncertainty on the light stop mass. The measured values in the $\theta_{\tilde{t}}$ versus $\theta_{\tilde{b}}$ plane are shown in the plot on the right of Fig. 72. As expected from the discussion above, a significant number of experiments yield a high value of $\theta_{\tilde{b}}$ and a low value of $\theta_{\tilde{t}}$.

The conclusions on the MSSM parameter measurement for the SPA model point under the assumption of no FCNC effects from sfermion mixing matrices are thus:

– neutralino/chargino mixing matrices fixed with $\sim 5\%$ if the value of $\tan\beta$ is known;
– slepton sector well constrained, including stau mixing angle;
– masses of first two generations squarks (L & R) and of gluino measured at $\sim (5\text{–}10)\%$ level;
– enough constraints to fix the 5 parameters of the stop/sbottom sector. For fixed $\tan\beta$, uncertainty of $\sim 5\%$ on stop mass, long tails in the measurement of $\theta_{\tilde{b}}$ and $\theta_{\tilde{t}}$;
– weak constraints on $\tan\beta$ and m_A.

We can now, based on the expected precision for the measurement of MSSM parameters, estimate how precisely observables in the b-sector can be predicted. We focus on two variables:

– $BR(B_s \to \mu\mu)$;
– $BR(B \to X_s\gamma)$.

Two public programs micrOMEGAs 1.3.6 [1142] and IS-ARED [1133] allow the evaluation of these two variables from an input set of MSSM parameters. Both programs work in the MFV framework and are based on the most recent NLO calculations. The results from micrOMEGAs 1.3.6 were used for the present exercise.
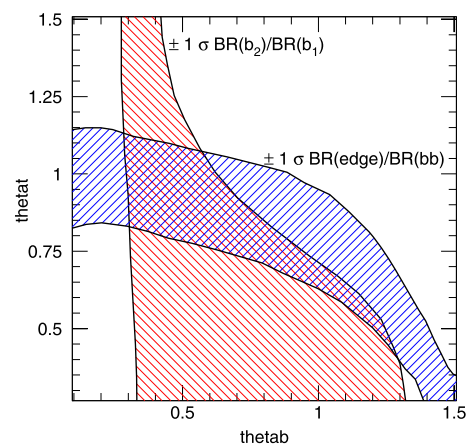
Fig. 71 Allowed 1σ bands on the $\theta_{\tilde{b}}$–$\theta_{\tilde{t}}$ plane respectively for the measurement of $BR(\tan\beta)$ (*downwards hatching*) and of $BR(\tilde{t})$ (*upwards hatching*)

Fig. 72 *Left*: distribution of the calculated $\tilde{t}_1$ mass for an ensemble of Monte Carlo experiments at the LHC. *Right*: distribution of the calculated $\theta_{\tilde{t}}$ versus $\theta_{\tilde{b}}$ for an ensemble of Monte Carlo experiments. The assumed statistics is 300 fb^{-1}
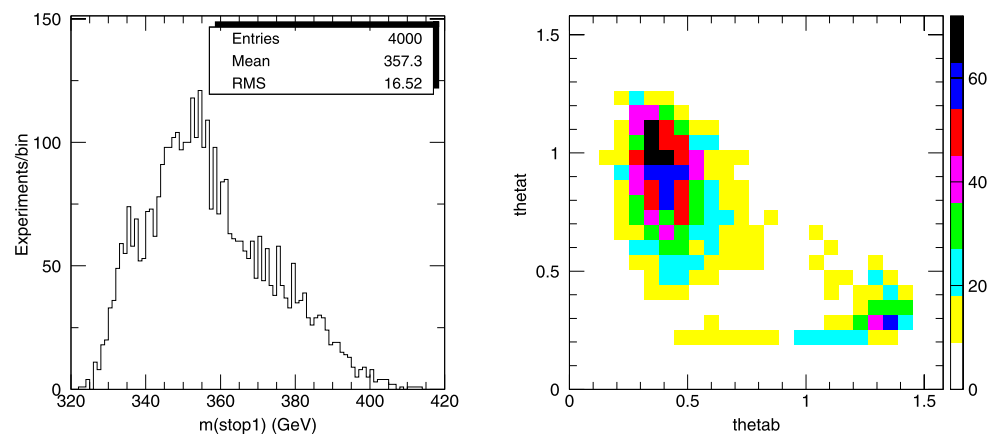
The study is done in different steps. We first perform scans in the parameter space to evaluate the sensitivity of the two observables to the key parameters. Thereafter, based on the method of Monte Carlo experiments described above, we evaluate the expected value of $BR(B_s \to \mu\mu)$ and $BR(B \to X_s\gamma)$ for each Monte Carlo experiment. The spread of the obtained distributions is taken as the experimental uncertainty of the observables. Since m_A and $\tan\beta$ are badly constrained by the LHC measurements, this is done keeping m_A and $\tan\beta$ fixed.

The dependence of $BR(B_s \to \mu\mu)$ on m_A, $\tan\beta$ is shown in the left panel of Fig. 73. Since $BR(B_s \to \mu\mu) \propto \tan^6\beta/m_A^4$, this measurement has a strong constraining power on $\tan\beta$ if $\tan\beta \gtrsim 15$. For lower values of $\tan\beta \sim$, the effect becomes too small, and SUSY is indistinguishable from the SM. The present limits from the Tevatron experiments only eliminate a small region of the parameter space with small m_A and large $\tan\beta$. The expected 90% bound from ATLAS, 6.6×10^{-9} for 30 fb^{-1} [1143], would allow us to exclude a region in the m_A–$\tan\beta$ plane similar to the one excluded by nondiscovery of $H/A \to \tau\tau$. For higher $\tan\beta$, the measurement of a deviation from the SM would provide a nice cross-check with $\tan\beta$ as measured from H/A production.

The value of $BR(B \to X_s\gamma)$ in the m_A–$\tan\beta$ plane is shown in the right panel of Fig. 73. The present world average for $BR(B \to X_s\gamma)$ [502], $(3.3 \pm 0.4) \times 10^{-4}$, would select a narrow band in the m_A–$\tan\beta$ plane, thus providing essentially no bound on m_A and a strong constraint on the allowed $\tan\beta$ range, in the MFV hypothesis.

We show in Fig. 74 the values of $BR(B_s \to \mu\mu)$ and $BR(B \to X_s\gamma)$ in the $m_{\tilde{t}_1}$–$\theta_{\tilde{t}}$ plane with the other parameters fixed (see Fig. 75 below for an analysis of the effect of their uncertainty). The variation of $BR(B_s \to \mu\mu)$ over the considered space is moderate. The present experimental error on the measurement of $BR(B \to X_s\gamma)$ already defines a very small slice in the $m_{\tilde{t}_1}$–$\theta_{\tilde{t}}$ plane. For fixed $\theta_{\tilde{t}}$, the dependence on $m_{\tilde{t}_1}$ is not very strong. We therefore conclude

that a precise measurement of $\theta_{\tilde{t}}$ is the key ingredient for the prediction of $BR(B \to X_s\gamma)$ from the LHC SUSY data.

As a next step, we verify that the experimental uncertainty on the two considered observables is indeed dominated by the measurement of m_A, $\tan\beta$, $m_{\tilde{t}_1}$ and $\theta_{\tilde{t}}$. To this effect, we calculate $BR(B_s \to \mu\mu)$ and $BR(B \to X_s\gamma)$ for all the Monte Carlo experiments, letting all of the MSSM parameters fluctuate according to the experimental error, except the four parameters mentioned above. The result is shown in Fig. 75. In these conditions, the uncertainty is small, 0.3% on the prediction of $BR(B_s \to \mu\mu)$ and 1% for the prediction of $BR(B \to X_s\gamma)$. These parametric uncertainties do not include the theoretical uncertainties in the calculation of the two observables.

Finally, we can evaluate how precisely we can predict the b-physics observables by varying all the MSSM parameters, according to the expected measurement precision at the LHC for the SPA point, except m_A and $\tan\beta$, which are kept fixed. The results are shown in Fig. 76. We observe a ~5% uncertainty on the prediction for $BR(B_s \to \mu\mu)$ and a ~15% uncertainty on the prediction for $BR(B \to X_s\gamma)$. For both observables, one can roughly observe two populations corresponding to the regions in the $\theta_{\tilde{b}}$–$\theta_{\tilde{t}}$ plane observed in Fig. 72. The experiments in the tail of mismeasured $\theta_{\tilde{t}}$ and $\theta_{\tilde{b}}$ contribute respectively to the region of high values of $BR(B_s \to \mu\mu)$, and to the bump for low values of $BR(B \to X_s\gamma)$.

We have thus shown that for the considered model, good enough measurements of MSSM parameters are possible at the LHC to provide predictions for $BR(B \to X_s\gamma)$, $BR(B_s \to \mu\mu)$ as a function of the two unconstrained variables, m_A and $\tan\beta$.

Once the LHC data are available, one can imagine different scenarios, e.g.:

– $A/H \to \tau\tau$ is observed, and $\tan\beta$ and m_A measured: at this point, a consistency check would be possible among the $\tan\beta$ constraints provided by the Higgs measurement and the one provided by the b-physics observ-

468

Eur. Phys. J. C (2008) 57: 309–492

Fig. 73 *Left*: curves of equal value for $BR(B_s \to \mu\mu)$ in the $m_A-\tan\beta$ plane. *Right*: curves of equal value for $BR(B \to X_s\gamma)$. The MSSM parameters are as defined for the SPA point, and the calculations are performed using MicrOMEGAs
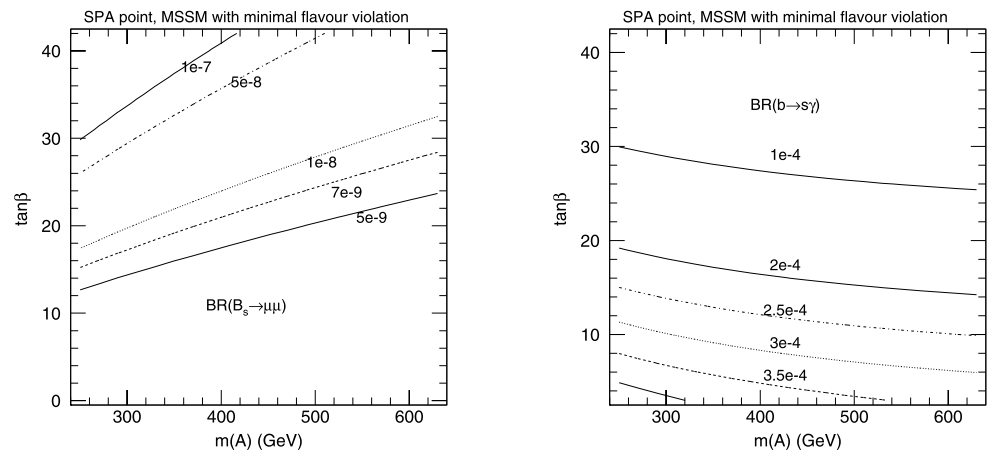
Fig. 74 *Left*: curves of equal value for $BR(B_s \to \mu\mu)$ in the $m_{\tilde{t}_1}-\theta_{\tilde{t}}$ plane. *Right*: curves of equal value for $BR(B \to X_s\gamma)$ in the $m_{\tilde{t}_1}-\theta_{\tilde{t}}$ plane. The MSSM parameters are as defined for the SPA point, and the calculations are performed using MicrOMEGAs
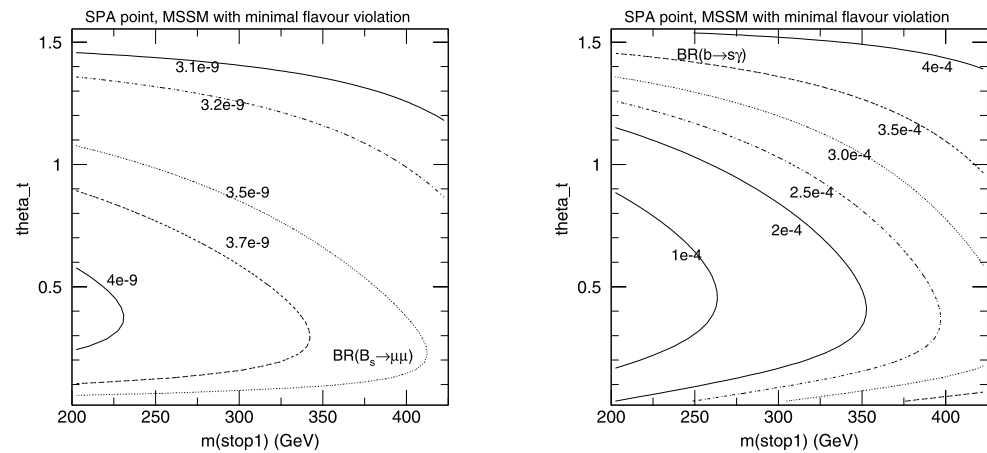
Fig. 75 Distribution of the predictions $BR(B_s \to \mu\mu)$ (*left*) and $BR(B \to X_s\gamma)$ (*right*) for an ensemble of LHC experiments when m_A, $\tan\beta$, $m_{\tilde{t}_1}$, $\theta_{\tilde{t}}$, $\theta_{\tilde{b}}$ are kept fixed at the nominal values, and all the remaining MSSM parameters are smeared according to the expected measurement uncertainty
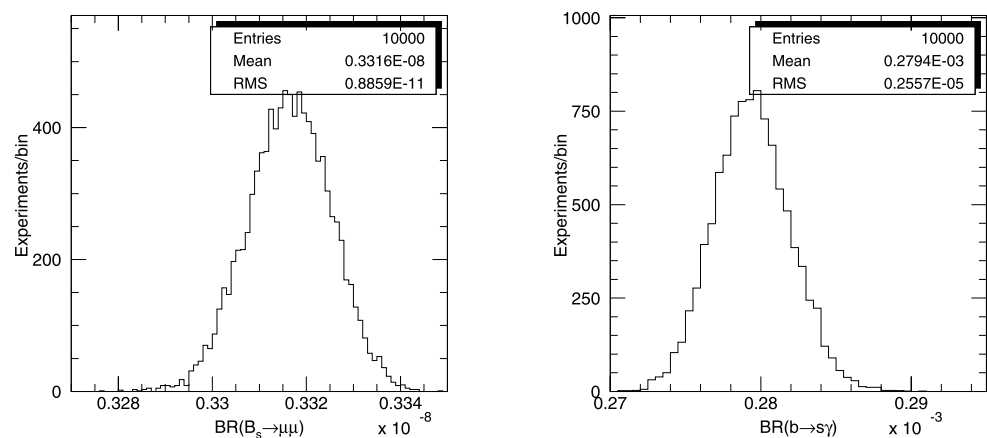
ables calculated in the MFV scheme. A significant disagreement, once all the experimental and statistical uncertainties are evaluated, would indicate the presence of flavor violation in the squark sector.

- $\tan\beta$ is not constrained by high-p_T searches:

  a signal for nonminimal flavor violation could still be provided by the inconsistency of the $\tan\beta$ regions constrained by respectively $m(h)$, $BR(B \to X_s\gamma)$, and

$BR(B_s \to \mu\mu)$. In case of consistency, the results could be taken as a measurement of the $\tan\beta$ parameter.

Relevant questions at this point are: what are the precisions required on the MSSM, on the b-physics measurements and on the theoretical calculations to be able to claim a signal for flavor-changing terms in the squark mass matrices?

In case the measurements are consistent with MFV, what additional constraints on the flavor violation sector can be

Fig. 76 Distribution of the predictions $BR(B_s \to \mu\mu)$ (*left*) and $BR(B \to X_s\gamma)$ (*right*) for an ensemble of LHC experiments when m_A, $\tan\beta$, are kept fixed at the nominal values, and all the remaining MSSM parameters, including the ones defining the stop sector, are smeared according to the expected measurement uncertainty
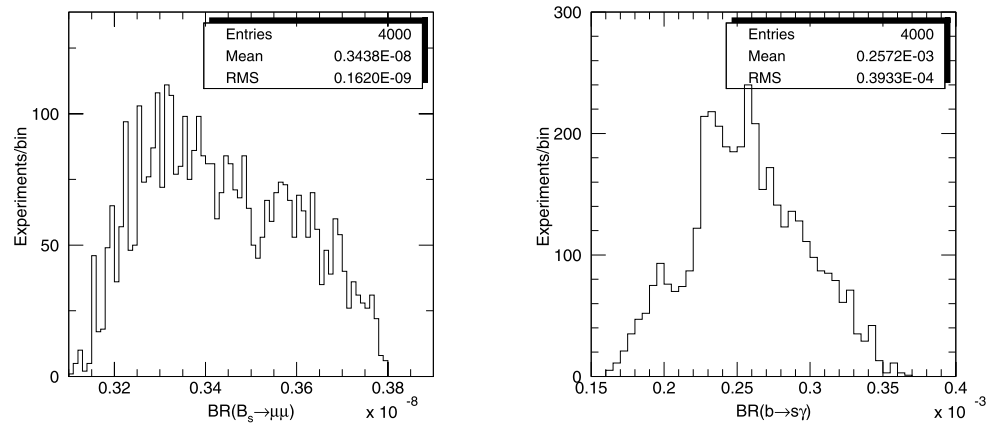
extracted by combining MSSM studies and *b*-physics measurements?

Various analyses are available in the literature [107, 113], based on assessing present allowed regions of nondiagonal elements in the super-CKM matrix, parametrized in terms of $(\delta^d_{23})_{AB}$, where AB can be RR, LL, RL, LR. Bounds on δ are normally given for some special choice of soft SUSY-breaking parameters, e.g., $m(\tilde{q}) = m_{\tilde{g}} = \mu = -A_u$ for different choices of $m(\tilde{q})$. Additional variables are also considered, such as ΔM_B, $BR(B \to X_s\ell^+\ell^-)$, $A_{CP}(B \to X_s\gamma)$.

Based on the study presented here, it would be interesting to repeat these analyses but for the parameters of a specific SUSY point, incorporating the expected experimental errors on the SUSY parameters. As a result of these studies, one could get guidance on which are the MSSM measurements crucial to discover flavor violation, thus pointing the way for the investigation of SUSY models in high-p_T physics.

5.3.2 The second approach: SUSY measurements in *b*-physics favored parameter spaces

A second, somewhat complementary, approach was followed in collaboration with CMS physicists.

5.3.2.1 B-physics favored parameter space　The model under investigation is the MSSM, in the first step with MFV, and possibly in a later stage also with NMFV. The compatibility with flavor physics was taken into account following [32], where the MSSM parameter space was analysed under the assumption of heavy scalar quarks and leptons and of large $\tan\beta$. The range of SUSY parameters has been restricted to the values listed in Table 65. Here $\tan\beta$ is the ratio of the two vacuum expectation values, M_A denotes the mass of the CP-odd Higgs boson, μ is the Higgs mixing parameter, $M_{\tilde{q},\tilde{l}}$ are the diagonal soft SUSY-breaking parameters in the scalar quark and scalar lepton sectors, respectively. All the trilinear couplings are set to be equal to A_t (the trilinear Higgs–stop coupling), while $m_{\tilde{g}}$, M_2 and M_1 are the gluino mass and the soft SUSY-breaking parameters in the

Table 65 Selected ranges and "best values" of the SUSY parameters for the "CMS analysis" in the MFV MSSM (following [32]): $\tan\beta$ is the ratio of the two vacuum expectation values, M_A denotes the mass of the CP-odd Higgs boson, μ is the Higgs mixing parameter, $M_{\tilde{q},\tilde{l}}$ are the diagonal soft SUSY-breaking parameters in the scalar quark and scalar lepton sectors, respectively; A_t is the trilinear Higgs–stop coupling, where all trilinear couplings are set equal; $m_{\tilde{g}}$, M_2 and M_1 are the gluino mass and the soft SUSY-breaking parameters in the gaugino sector. All parameters are assumed to be real

Parameter	Range	"Best" value(s)
$\tan\beta$	30–50	40
M_A [GeV]	300–1000	300, 500, 800, 1000
A_t [GeV]	−2000–(−1000)	−1000, −2000
μ [GeV]	500–1000	500, 1000
$M_{\tilde{q}}$ [GeV]	>1000	1000, 2000
$M_{\tilde{l}}$	1/2 $M_{\tilde{q}}$	
$M_{\tilde{g}}$	$M_{\tilde{q}}$	
M_2 [GeV]		300, 500
M_1	1/2 M_2	

chargino/neutralino sector. All parameters are assumed to be real. The upper part of Table 65 is the more relevant parameters, while the lower part has a smaller impact on the flavor physics phenomenology.

The ranges in [32] are generally compatible with the existing low-energy constrains. However, one expects to be able to select narrow sub-regions by more precise measurements of specific *B*-physics observables, such as $BR(B \to \tau\nu)$ or $BR(B_s \to \mu^+\mu^-)$. The "best" values denote specific points for which a more detailed investigation of the high-energy signatures at CMS has been performed.

5.3.2.2 Experimental analysis　The strategy followed by CMS physicists is to apply an already understood search analysis to the sample of MSSM points that are consistent with flavor constraints as described above. The starting point is [1144], in which CMS studied the production and decay of SUSY particles via inclusive final states including

470

Eur. Phys. J. C (2008) 57: 309–492

muons, high-p_T jets, and large missing transverse energy. In that work, a fully simulated and reconstructed low mass (LM1) Constrained MSSM (CMSSM) point was taken as the benchmark for selection optimization and study of systematic effects. Even though the study was performed within the context of CMSSM, the method is not specific to the CMSSM framework and should apply equally well in other contexts including, i.e. also in the general MSSM.

The response of the CMS detector to incident particles was simulated using a GEANT4-based framework [1145], known as the Object-oriented Simulation for CMS Analysis and Reconstruction (OSCAR) [1146]. The inclusion of pile-up and the reconstruction of analysis objects (muons, jets, etc) from hits in the detector was performed by a software framework known as the Object-oriented Reconstruction for CMS Analysis (ORCA) [1146]. In addition, a stand-alone fast simulation, known as the CMS FAst MOnte Carlo Simulation (FAMOS) framework [1146], was used to facilitate simulations involving CMSSM parameter scans. The fast simulation FAMOS has been shown to adequately represent the full CMS simulation [1144]. In both the full and fast simulations, hits from minimum bias events are superimposed on the main simulated event to reproduce the pile-up conditions expected for a luminosity of 2×10^{33} cm^{-2} s^{-1}.

Because the work presented in [1144] is an inclusive study of signatures involving at least one muon accompanied by multiple jets and large $E\!\!\!/_T$, several SM processes contribute as sources of background and had to be taken into account. Accordingly, the main backgrounds studied in [1144] correspond to QCD dijet (2.8 million events with $0 < \hat{p}_T < 4$ TeV/c), top ($t\bar{t}$) production (3.3 million events), electroweak single-boson production (4.4 million events with $0 < \hat{p}_T < 4.4$ TeV/c) and electroweak dibosons production (1.2 million events). All backgrounds used were fully simulated and reconstructed.

The method employed in [1144] is to search for an excess in the number of selected events, compared with the number of events predicted from the SM. A Genetic Algorithm (GARCON [1147]) was used for the optimization of cuts to select the LM1 CMSSM point and results in: $E_T^{\text{miss}} > 130$ GeV, $E_T^{j1} > 440$ GeV, $E_T^{j2} > 440$ GeV, $|\eta^{j1}| < 1.9$, $|\eta^{j2}| < 1.5$, $|\eta^{j3}| < 3$, $\cos[\Delta\phi(\text{j1, j2})] < 0.2$, $-0.95 < \cos[\Delta\phi(E\!\!\!/_T, \text{j1})] < 0.3$, $\cos[\Delta\phi(E\!\!\!/_T, \text{j2})] < 0.85$. Assuming 10 fb^{-1} of collected data, this set of cuts would expect to select a total of 2.5 background events from the SM and 311 signal events from the CMSSM LM1 benchmark signal point [1144].

In order to extend the work presented in [1144] to the context of the MSSM parameter space suggested by flavor considerations as described above, several points within the ranges of the MSSM parameters listed in Table 65 were sampled and simulated using the CMS fast simulation FAMOS. (The Pythia parameters used to generate each MSSM point

may be found in [1144].) In the CMS exercise, the same set of selection cuts presented above, is directly applied (i.e., not reoptimized) to each simulated MSSM point. Finally, the number of selected events from each simulated MSSM point is tallied and compared with the expected number of standard model background events ($N_B = 2.5$).

It has been shown that the analysis method also works for this "new" part of the MSSM parameter space. Clearly, an optimization could enhance the analysis power. More detailed results will be presented elsewhere.

5.3.3 The "master code": multi-parameter fit to electroweak and low-energy observables

A first attempt to develop a "master code" as described above (see also Sect. 1.5.2) has been started in the course of this workshop in collaboration with physicists from CMS [208].

Based on flavor physics computer code from [32] and the more high-energy observable oriented computer code `FeynHiggs` [199–201], a first version of a "master code" has been developed. This "master code" combines calculations from both low-energy and electroweak observables in one common code. Great care has been taken to ensure that both sets of calculations are steered with a consistent set of input parameters. The current version of the "master code" is restricted to applications in the MSSM parameter space assuming MFV. Table 66 shows the observables which are currently considered in the "master code".

However, in the future, it is foreseen to significantly extend the "master code" by including other calculations both for different NP models as well as additional observables (e.g. cosmology constraints), see [1122] for the latest updates and developments. With the help of the "master code", it will eventually be possible to test model points from the low-energy side (via flavor and electroweak observables) and from the high-energy side (via the measurements of ATLAS/CMS). Thus a model point can be tested with *all* existing data.

Using the "master code" as a foundation, an additional code layer containing a χ^2 fit [1150] has been added to determine the consistency of a given set of MSSM parameters with the constraints defined in Table 66. Other studies of this kind using today's data can been performed in [1151–1155]. Studies using the anticipated data from the LHC and the ILC are carried out and documented in [1156, 1157].

Using the "master code", we will present a few showcases for a global χ^2 fit using a *simplified* version of the MSSM. The fit considers the following parameters: M_A (the CP-odd Higgs boson mass), $\tan\beta$ (the ratio of the two vacuum expectation values), $M_{\tilde{q}, \tilde{l}}$ (a common diagonal soft SUSY-breaking parameter for squarks and sleptons, respectively), A (a common trilinear Higgs-sfermion coupling), μ

Table 66 List of available constraints in the "master code". The shown values and errors represent the current best understanding of these constraints. Smaller errors for M_W^{SUSY} and $\sin^2\theta_W^{\mathrm{SUSY}}$ are possible using a dedicated code [1148, 1149], which is, however, so far not included in the "master code" (see, however, [1122])

Observable	Source	Constraint	Theo. error
$R_{BR_{b\to s\gamma}} = BR_{b\to s\gamma}^{\mathrm{SUSY}}/BR_{b\to s\gamma}^{\mathrm{SM}}$	[32]	1.127 ± 0.12	0.1
$R_{\Delta M_s} = \Delta M_s^{\mathrm{SUSY}}/\Delta M_s^{\mathrm{SM}}$	[32]	0.8 ± 0.2	0.1
$BR_{b\to\mu\mu}$	[32]	$<8.0 \times 10^{-8}$	2×10^{-9}
$R_{BR_{b\to\tau\nu}} = BR_{b\to\tau\nu}^{\mathrm{SUSY}}/BR_{b\to\tau\nu}^{\mathrm{SM}}$	[32]	1.125 ± 0.52	0.1
$\Delta a_\mu = a_\mu^{\mathrm{SUSY}} - a_\mu^{\mathrm{SM}}$	FeynHiggs	$(27.6 \pm 8.4) \times 10^{-10}$	2.0×10^{-10}
M_W^{SUSY}	FeynHiggs	(80.398 ± 0.025) GeV	0.020 GeV
$\sin^2\theta_W^{\mathrm{SUSY}}$	FeynHiggs	0.23153 ± 0.00016	0.00016
$M_h^{\mathrm{light}}(\mathrm{SUSY})$	FeynHiggs	>114.4 GeV	3.0 GeV

(the Higgs mixing parameter), M_1 and M_2 (the soft SUSY-breaking parameters in the chargino/neutralino sector) and $m_{\tilde{g}} = M_3$ (the gluino mass). All parameters are assumed to be real. Some further simplifying restrictions are applied: For the parameter μ, we require $|\mu| > M_2$. This ad-hoc ansatz is fully sufficient for our illustrative studies, but in the future, it will be replaced with a more sophisticated treatment of the parameters and of the experimentally excluded phase space regions (e.g. sparticle mass limits, etc.). In addition, the ansatz assumes $M_{\tilde{l}} = a_{\tilde{q},\tilde{l}} \times M_{\tilde{q}}$ as well as fixed values for M_1, M_2 and M_3. The initially assumed values of $a_{\tilde{q},\tilde{l}} = 0.5$, $M_2 = 200$ GeV, $M_3 = 300$ GeV and $M_1 = M_2/2$ are later varied within reasonable ranges to evaluate the systematic impact of the assumption on the final results.

The χ^2 is defined as

$$\chi^2 = \sum_i^{N_{\mathrm{const.}}} \frac{(\mathrm{Const.}_i - \mathrm{Pred.}_i(\mathrm{MSSM}))^2}{\Delta\mathrm{Const.}^2 + \Delta\mathrm{Pred.}^2}, \tag{233}$$

where $\mathrm{Const.}_i$ represents the measured values (constraints), and $\mathrm{Pred.}_i$ defines the MSSM parameter-dependent predictions of a given constraint. These predictions are obtained from the "master code". They depend on SM parameters like m_t, m_b and α_s. Some of these parameters still exhibit significant uncertainties which need to be taken into account in the fit procedure. In a simple χ^2 approach, it is straightforward to include these parametric uncertainties as fit parameters with penalty constraints. For our study, the uncertainty of the top quark mass was found to be by far the dominating parametric uncertainty. The required minimization of the χ^2 is carried out by the well-known and very reliable fit package Minuit [1150].

In the following section, we present some illustrative showcases that utilize this global χ^2 fit to extract quantitative results. However, these studies are mainly meant to demonstrate the potential and usefulness of "external" constraints for the interpretation of forthcoming discoveries and for the corresponding model parameter extraction.

5.3.3.1 Scan in the lightest Higgs-boson mass M_h One of the most important predictions of the MSSM is the existence of a light neutral Higgs boson with $M_h \leq 135$ GeV [199, 200]. This upper limit, together with the lower limit obtained at LEP, $M_h^{\mathrm{direct}} \geq 114.4$ GeV [1125, 1130][32] represents a tight constraint on the remaining allowed parameter space of the MSSM. In the MSSM (with the simplifications explained above), M_h depends mainly on the average squark mass $M_{\tilde{q}}$, the Higgs mixing parameter μ, the trilinear Higgs-squark coupling A and $\tan\beta$. However, these parameters are also important for the predictions of low-energy and electroweak observables in the MSSM. Therefore, a global fit using the constraints listed in Table 66 not only allows a consistent extraction of the important MSSM parameters but will also provide a prediction for the most probable light Higgs boson mass M_h in the MSSM. A convenient way to illustrate the sensitivity of these parameters to M_h is a scan of the preferred parameter space as a function of this variable. For this procedure, the global χ^2 fit is performed repeatedly each time with a different value for the M_h constraint. Therefore, the extracted set of MSSM parameters for each individual fit corresponds to the preferred parameter space for a given value of M_h. While all M_h scan values below the lower limit of $M_h^{\mathrm{direct}} > 114.4$ GeV are already excluded by experiment, it is nevertheless interesting to see the results of the M_h scan over the entire parameter space (i.e. also for M_h values $\lesssim 115$ GeV). For that reason, the lower M_h limit from the direct search at LEP has not been included in the χ^2 fit.

5.3.3.2 M_h scan using today's (pre-LHC) constraint values and errors Figure 77 shows the results of the M_h scan using the constraint values listed in Table 66. Since these values represent today's best knowledge of these observables, this result provides a first estimate of how low-energy and electroweak measurements constrain the MSSM parameter space. In the following, we will refer to this scan result as *today's M_h scan*.

It is important to note that the $M_h \approx [110, 125]$ GeV region seems to be preferred by the χ^2 scan. On the one hand,

---

[32]It is possible that the current lower limit could be even further improved before the LHC will start data taking in 2008 by the currently running Tevatron experiments CDF and D0.
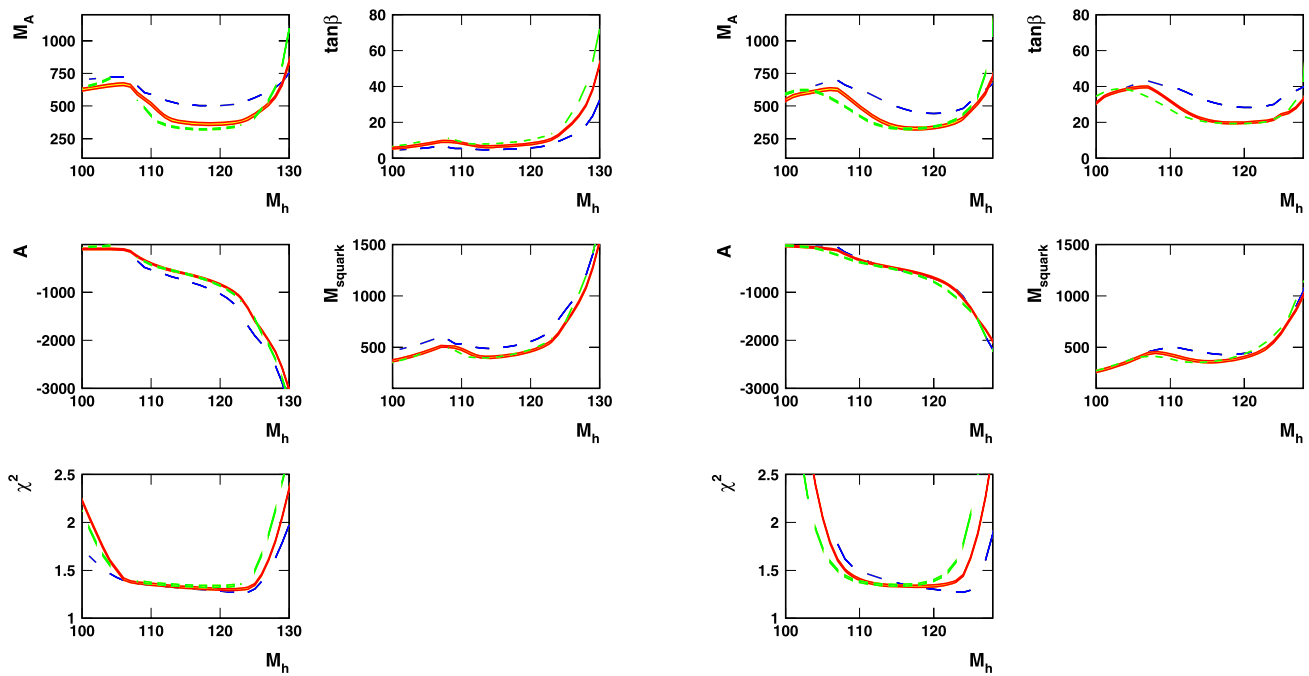
472

Eur. Phys. J. C (2008) 57: 309–492

Fig. 77 (Color online) This figure shows the result of the extracted MSSM fit parameters and the corresponding χ^2 distribution (*lower right plot* in each case) for the two scan scenarios: *today's M_h scan* (*left five plots*) and *2009-EW-LowE M_h scan* (*right five plots*). Each *plot* shows three scan results, where the *full-red curve* corresponds to the default assumptions of $M_2 = 200$ GeV, $M_3 = 300$ GeV and $a_{\tilde{q},\tilde{l}} = 0.5$. The *blue-dashed line* (*large dash*) changes $a_{\tilde{q},\tilde{l}} = 0.33$ with respect to the default setting, while the *green-dashed line* (*small dash*) modifies $M_2 = 300$ GeV, $M_3 = 500$ GeV with respect to the default setting

all M_h values in this distinguished region of minimal χ^2 are almost equally likely. On the other hand, values outside this window (i.e. <110 GeV or >125 GeV) are clearly disfavored by the low-energy and electroweak constraints. This is an interesting observation suggesting that today's low-energy and electroweak data prefer a light MSSM Higgs boson with a mass significantly higher than the most probable value for the SM Higgs boson. For comparison, the current preferred value from the general electroweak fit is $M_h^{\text{SM}} \approx 80$ GeV [1158–1160].

In order to qualitatively estimate the systematic impact of the assumed parameter values ($M_2 = 200$ GeV, $M_3 = 300$ GeV and $a_{\tilde{q},\tilde{l}} = 0.5$) on the scan results, a variation of the parameter values within reasonable ranges has been carried out. Figure 77 shows the results of two of these cross checks: the blue-dashed line corresponds to the parameter setting $M_2 = 200$ GeV, $M_3 = 300$ GeV and $a_{\tilde{q},\tilde{l}} = 0.33$, while the green-dashed line uses $M_2 = 300$ GeV, $M_3 = 500$ GeV and $a_{\tilde{q},\tilde{l}} = 0.5$. The observed variation is rather small indicating that the general conclusions are not strongly affected by the assumed parameter setting of these quantities. In particular the preferred minimal χ^2 region of M_h remains almost unchanged.

The overall χ^2 minimum of *today's M_h scan* is at $M_h \approx 123$ GeV, and the preferred values of the important MSSM parameters are $M_A \approx 400$ GeV, $\tan\beta \approx 10$,

$A \approx -1000$ GeV and $M_{\tilde{q}} \approx 500$ GeV. These values are qualitatively compatible with the range of "allowed" MSSM parameter space reported in Sect. 5.3.2. The fact that *today's M_h scan* prefers somewhat lower values for $\tan\beta$ and $M_{\tilde{q}}$ is mainly explained by the change in the experimental Belle result of $R_{BR_{b\to\tau\nu}}$ from 0.7 ± 0.3 to 1.125 ± 0.52 [326]. Using 0.7 ± 0.3 instead of the other more recent (corrected) value yields $\tan\beta \approx 30$, $M_{\tilde{q}} \approx 700$ GeV and $A \approx -1500$ GeV but does not change the general conclusion of the results (e.g. the preferred M_h range remains the same).

Figure 78 shows a comparison of the predicted constraint values and their corresponding measurements obtained from *today's M_h scan*. The measurements and their errors are also listed in Table 66. In general, good agreement between prediction and measurement is observed in the preferred minimal χ^2 region of $M_h \approx [110, 125]$ GeV. The fact that the χ^2 scan prefers a prediction of $R_{\Delta M_s}$ very close to unity is explained by (1) the already rather tight limit on $BR(B_s \to \mu^+\mu^-) < 8 \times 10^{-8}$ and (2) the large value of $R_{BR_{b\to\tau\nu}}$. Both constraints prefer low values of $\tan\beta$ and thus result in a prediction of $R_{\Delta M_s} \approx 1$. However, today's experimental value is still within one sigma compatible with this prediction.

Another interesting observation is the prediction of $BR(B_s \to \mu^+\mu^-)$. Although the constraint used for this quantity allows values up to $BR(B_s \to \mu^+\mu^-) < 8 \times 10^{-8}$, the scan predicts (in the interesting M_h region) an almost

Eur. Phys. J. C (2008) 57: 309–492

473
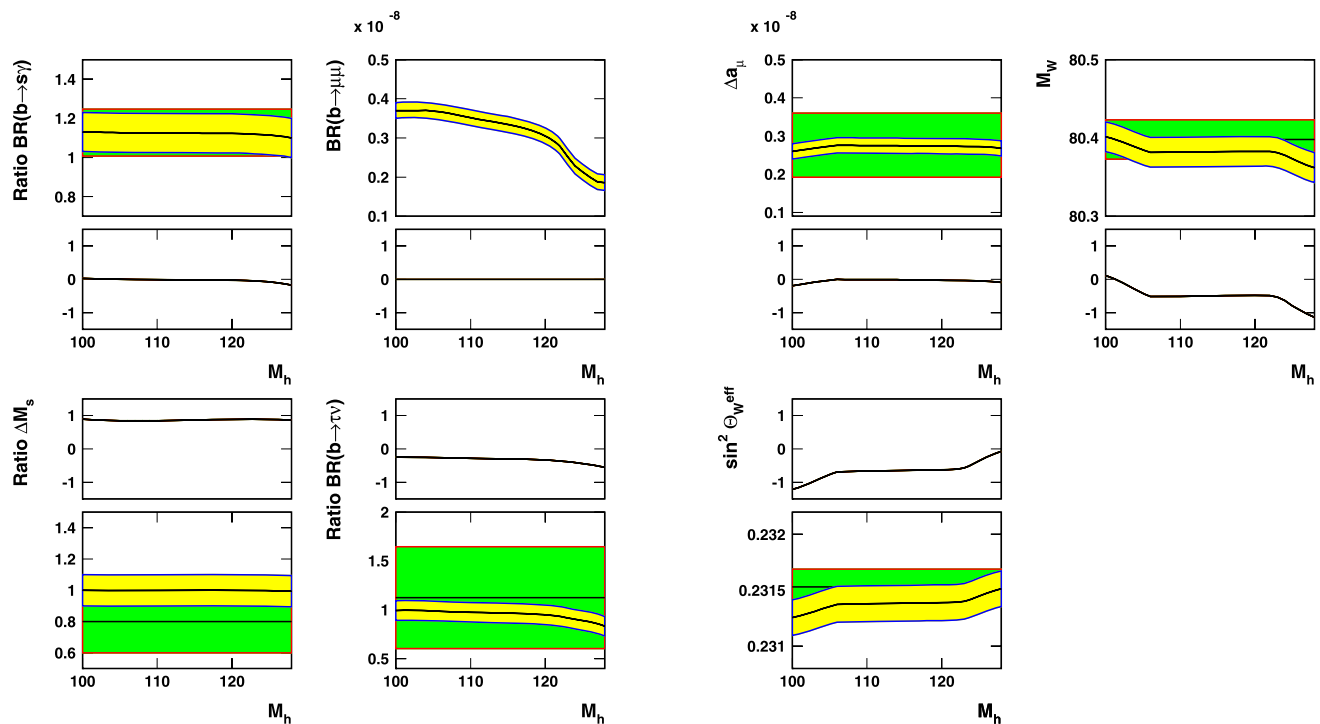
Fig. 78 This figure shows a comparison of the predicted constraint values (*yellow/light shaded band*) and their corresponding measurements (constant *green/dark shaded band*) obtained from *today's M_h scan*. All *plots* show a comparison of prediction versus measurement (*plots with bands*) as well as their corresponding pull contributions $\frac{\text{Const.}_i - \text{Pred.}_i(\text{MSSM})}{\sqrt{\Delta\text{Const.}^2 + \Delta\text{Pred.}^2}}$ to the overall χ^2

constant value of $BR(B_s \rightarrow \mu^+\mu^-) \approx (3.0$–$4.0) \times 10^{-9}$. This is an interesting observation, because this value coincides well with the SM prediction of $BR(B_s \rightarrow \mu^+\mu^-)^{\text{SM}} \approx 3.5 \times 10^{-9}$. This might suggest that the current low-energy and electroweak data prefer a value of $BR(B_s \rightarrow \mu^+\mu^-)$ close to its SM prediction. It will be interesting to see whether the soon forthcoming combined result of $R_{BR_{b \rightarrow \tau\nu}}$ from BaBar and Belle will confirm this trend. If this is the case, spectacular effects from new (MSSM) physics contributions seem rather unlikely for $B_s \rightarrow \mu^+\mu^-$.

5.3.3.3 Interpretation of potential LHC discoveries The LHC will start collecting physics data in 2008. For that reason, the first results are not expected before early 2009. In the meantime, however, it is likely that most of the considered low-energy and electroweak constraints will further improve. Therefore, in 2009, it will be possible to even more strongly restrict the allowed MSSM parameter space. Table 67 lists the assumed constraint values that might be achieved by this time period. The assumed values and errors are only chosen for illustrative purposes. The sole intention of this study is to demonstrate the potential of low-energy and electroweak data to constrain the parameter space of NP and to eventually provide guidance for the interpretation of potential NP discoveries at the LHC. Figure 77 (five

Table 67 Assumed constraint values and errors for the *2009-EW-LowE* scenario

Observable	Constraint	Theo. error
$R_{BR_{b \rightarrow s\gamma}}$	1.127 ± 0.1	0.1
$R_{\Delta M_s}$	0.8 ± 0.2	0.1
$BR_{b \rightarrow \mu\mu}$	$(3.5 \pm 0.35) \times 10^{-8}$	2×10^{-9}
$R_{BR_{b \rightarrow \tau\nu}}$	0.8 ± 0.2	0.1
Δa_μ	$(27.6 \pm 8.4) \times 10^{-10}$	2.0×10^{-10}
M_W^{SUSY}	(80.392 ± 0.020) GeV	0.020 GeV
$\sin^2\theta_W^{\text{SUSY}}$	0.23153 ± 0.00016	0.00016
$M_h^{\text{light}}(\text{SUSY})$	>114.4 GeV	3.0 GeV

plots on the right) shows the results of the χ^2 scan using the constraints listed in Table 67. In the following, we refer to these results as *2009-EW-LowE M_h scan*. Similar to the results from the *today's M_h scan*, the general results and conclusions of this study are largely unaffected by the variation of the assumed values for M_2, M_3 and $a_{\tilde{q},\tilde{l}}$. As shown in Fig. 77, the χ^2-preferred M_h region becomes even more pronounced. Hence, the allowed MSSM parameters space is further reduced. In particular this information will become very useful in the case of LHC discoveries and their corre-

474

Eur. Phys. J. C (2008) 57: 309–492

sponding interpretation. In order to illustrate this property, we define a few hypothetical scenarios:

– *2009-EW-LowE*:

This scenario includes only the observables listed in Table 67. The overall χ^2 minima for this scenario is achieved for $M_A \approx 350$ GeV, $\tan\beta \approx 22$, $\mu \approx 5$ GeV, $A \approx -450$ GeV and $M_{\tilde{q}} \approx 350$ GeV. The corresponding prediction of the light MSSM Higgs boson mass is $M_h \approx 115$ GeV.

– *LHC-$M_{\tilde{q}}$*:

This scenario includes *2009-EW-LowE* and additionally assumes that the relevant squark mass[33] $M_{\tilde{q}}$ is known at the level of 10%. To be consistent with *2009-EW-LowE*, we therefore define: $M_{\tilde{q}} = 350 \pm 35$ GeV.

– *LHC-$M_{\tilde{q}}$-M_A*:

This scenario includes *LHC-$M_{\tilde{q}}$* and additionally assumes that the mass of $M_{AH^\pm}$ is known to 10%. To be consistent with *2009-EW-LowE*, we therefore define: $M_A = 355 \pm 35$ GeV.

– *LHC-$M_{\tilde{q}}$-M_A-M_h*:

This scenario includes *LHC-$M_{\tilde{q}}$-M_A* and additionally assumes that the mass of M_h is measured with a 3 GeV error. To be consistent with *2009-EW-LowE*, we therefore define: $M_h = 115 \pm 3$ GeV.

Figure 79 shows the results of the M_h scan for the scenario *2009-EW-LowE* and the scenario *LHC-$M_{\tilde{q}}$-M_A*. As expected, the χ^2 allowed region of M_h is reduced to a small window by including the additional information of $M_A = 355 \pm 35$ GeV and $M_{\tilde{q}} = 350 \pm 35$ GeV. This information can, for example, be utilized to test the consistency of a discovered light Higgs boson candidate with:

(a) other discoveries of MSSM particle candidates (in our case squark and heavy Higgs candidates);

(b) low-energy and electroweak constraints.

Assuming that a light Higgs boson candidate has been observed and that its mass is measured with an error of $\Delta M_h = \pm 3$ GeV, Fig. 80 shows the $\Delta\chi^2$ distributions for the scenario *2009-EW-LowE* (green small-dashed line), *LHC-$M_{\tilde{q}}$* (blue large-dashed line) and *LHC-$M_{\tilde{q}}$-M_A* (red full line).

As defined above, all scenarios correspond to one MSSM parameter set that has a χ^2 minimum for $M_h \approx 115$ GeV, see Fig. 81. The $\Delta\chi^2$, and therefore also the exclusion limits, are defined with respect to this MSSM parameter set. For the most constraining scenario, all masses above ≈ 130 GeV are excluded at 95% C.L. Therefore, in this hypothetical case, M_h must be below 130 GeV in order to be compatible with the other observed LHC discoveries as

[33]For example, this could be achieved by a determination of the stop mass. In particular this mass is important for the determination of the lightest Higgs boson mass M_h in the MSSM.
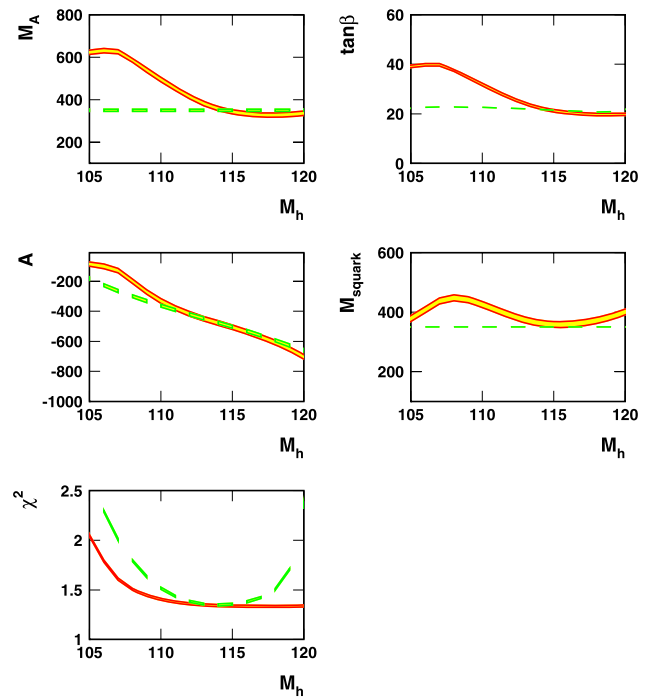
Fig. 79 This figure shows the result of the extracted MSSM fit parameter and the corresponding χ^2 distribution for the two scan scenarios: *2009-EW-LowE M_h scan* (*full-red curve*) and *LHC-$M_{\tilde{q}}$-M_A-M_h scan* (*green-dashed curve*)
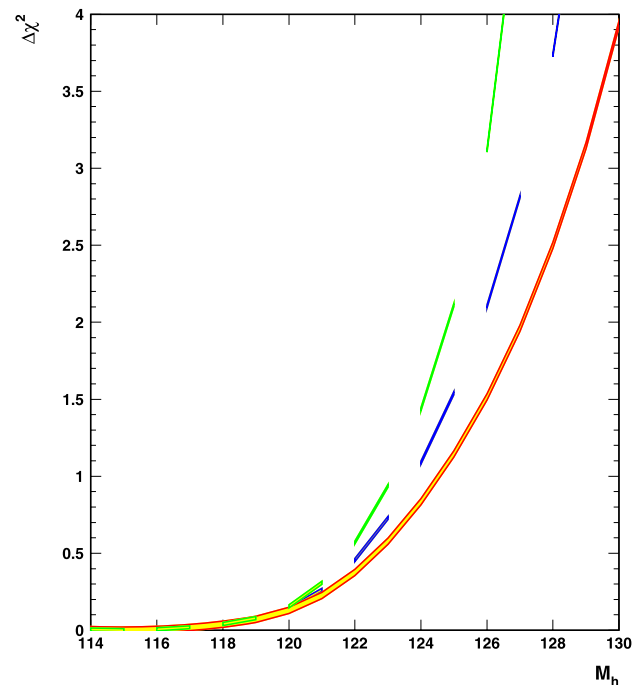
Fig. 80 $\Delta\chi^2$ distribution for scenario *LHC-$M_{\tilde{q}}$-M_A* testing the hypothesis that a discovered light Higgs boson candidate with a mass error of: $\Delta M_h = 3$ GeV (*red curve*), 2 GeV (*blue/dark dashed curve*) and 1 GeV (*green/light dashed curve*) is compatible with the MSSM

Fig. 81 χ^2 distribution as a function of M_h for the three scenarios: *2009-EW-LowE M_h scan (full-red curve)*, *today's M_h scan (green-small-dashed curve)* and *LHC-$M_{\tilde{q}}$-M_A-M_h scan (blue-large-dashed curve)*
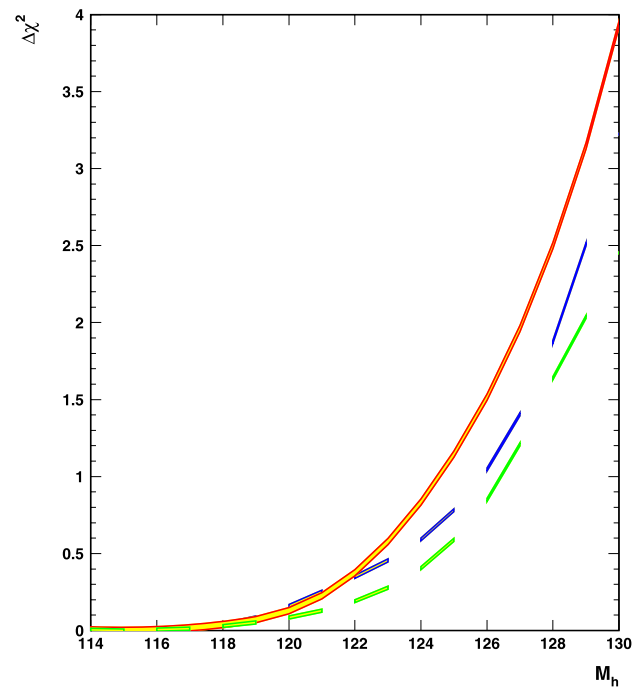

Fig. 82 $\Delta\chi^2$ distribution for scenario *LHC-$M_{\tilde{q}}$-M_A (red curve)*, *LHC-$M_{\tilde{q}}$ (blue/dark dashed curve)* and *2009-EW-LowE (green/light dashed curve)*. All curves are evaluated with an assumed error of $\Delta M_h = 3$ GeV
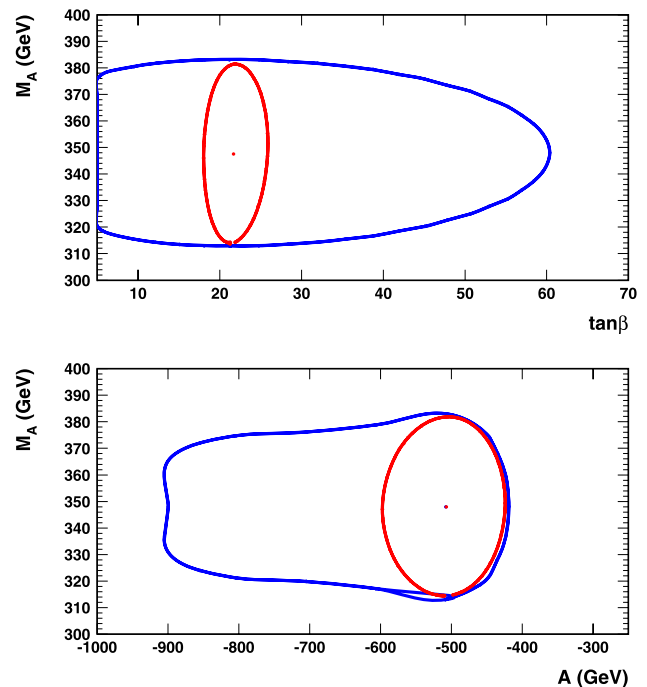
well as with the low-energy and electroweak constraints. A discovery of a lightest Higgs boson with a mass above 130 GeV would rule out the MSSM at 95% C.L. It is clear that the exclusion limit depends on the assumed error for M_h. For scenario *LHC-$M_{\tilde{q}}$-M_A*, Fig. 82 compares the results for $\Delta M_h = \pm 3$, $\Delta M_h = \pm 2$ and $\Delta M_h = \pm 1$. With an assumed error of 2 GeV, the 95% C.L. exclusion limit would be around $M_h \approx 128$ GeV, while for a 1 GeV error, it would be as stringent as $M_h \approx 126$ GeV.

Therefore, together with the discoveries of a stop candidate and a heavy Higgs candidate, the consistency of a measured light Higgs candidate within the MSSM hypothesis can be tested. It should be noted that without the use of low-energy and electroweak constraints, this consistency test would be much weaker. For example, the three LHC discoveries alone will not significantly constrain the important MSSM parameters $\tan\beta$ and A. This feature is clearly demonstrated in Fig. 83. Without the inclusion of the low-energy and electroweak constraints, the parameters $\tan\beta$ and A are much less determined. Thus, the overall sensitivity of the consistency test is significantly worse.

Another way to illustrate the potential of external constraints for the interpretation of NP discoveries and the eventual extraction of the model parameters is shown in Fig. 84, which displays the $\Delta\chi^2 = 1$ contours of the four different scenarios for various parameter combinations. Although

Fig. 83 The *red/lighter contour* corresponds to scenario *LHC-$M_{\tilde{q}}$-M_A-M_h* that includes the low-energy and electroweak constraints, while the *blue/darker contour* makes the same assumptions about the assumed LHC discoveries but does not include any external constraints
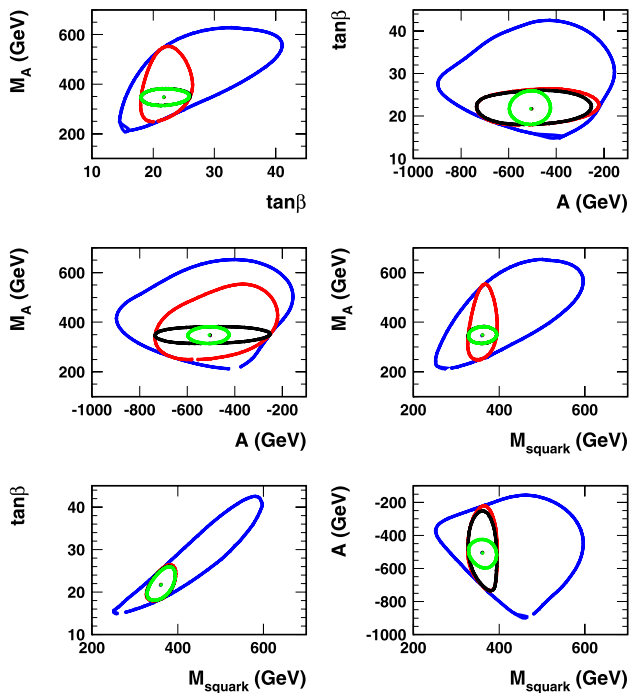
Fig. 84 This figure shows the $\Delta\chi^2 = 1$ contours of the four scenarios: *2009-EW-LowE* (*blue/outermost contour*), *LHC-$M_{\tilde{q}}$* (*red/lighter contour*), *LHC-$M_{\tilde{q}}$-M_A* (*black contour*) and *LHC-$M_{\tilde{q}}$-M_A-M_h* (*green/innermost contour*). Sometimes the inner contours partially (or even completely) overlap. In this case, the *green/innermost contour* covers the *black*, or the *black* covers the *red/lighter* one

2009-EW-LowE (blue contour) only utilizes indirect constraints (i.e. no direct measurement of NP quantities), the MSSM parameter space is already rather restricted. Adding $M_{\tilde{q}} = (350 \pm 35)$ GeV (red contour) in particular helps to further constrain $\tan\beta$ and to some extent also M_A, while measuring also the heavy (black contour) and also the light Higgs boson mass (green contour) will restrict the allowed range for A rather significantly. Also here the use of the external low-energy and electroweak constraints is essential to determine the important MSSM parameters $\tan\beta$ and A.

5.3.3.4 Outlook In order to fully exploit this interesting potential, it will be important to extend the "master code" by adding additional calculations such as extra low-energy observables, as well as, potentially, constraints from cosmology data (see [1122]). This will eventually yield an important tool for the comprehensive interpretation of future NP discoveries.

5.4 Discrimination between new physics scenarios

At present, the SM gives a fully consistent description of all experimental data in the flavor sector, apart from a few, not yet statistically significant deviations. This means that flavor physics can at present only rule out models that produce too large deviations from the SM; in practice, this means giving

an upper bound on new sources of flavor and CP violation for a fixed NP scale or giving a lower bound on the NP scale for fixed values of the NP flavor parameters. As discussed in Sect. 5.1, this gives us hints on the flavor structure of NP models with new particles up to the TeV range. However, to fully exploit the constraining power of flavor physics, additional (external) information on the spectrum of new particles must be provided. First examples of the combination of flavor and high-p_T information have been presented in Sect. 5.3, and there is increasing activity in this direction.

References

1. R. Fleischer, G. Isidori, J. Matias, J. High Energy Phys. **0305**, 053 (2003). arXiv:hep-ph/0302229
2. J.M. Soares, L. Wolfenstein, Phys. Rev. D **47**, 1021 (1993)
3. N.G. Deshpande, B. Dutta, S. Oh, Phys. Rev. Lett. **77**, 4499 (1996). arXiv:hep-ph/9608231
4. J.P. Silva, L. Wolfenstein, Phys. Rev. D **55**, 5331 (1997). arXiv:hep-ph/9610208
5. A.G. Cohen, D.B. Kaplan, F. Lepeintre, A.E. Nelson, Phys. Rev. Lett. **78**, 2300 (1997). arXiv:hep-ph/9610252
6. Y. Grossman, Y. Nir, M.P. Worah, Phys. Lett. B **407**, 307 (1997). arXiv:hep-ph/9704287
7. M. Bona et al. (UTfit Collaboration), Phys. Rev. Lett. **97**, 151803 (2006). arXiv:hep-ph/0605213
8. J. Charles et al. (CKMfitter Group), Eur. Phys. J. C **41**, 1 (2005). arXiv:hep-ph/0406184
9. M. Bona et al. (UTfit Collaboration), arXiv:0707.0636 [hep-ph]
10. G. D'Ambrosio, G.F. Giudice, G. Isidori, A. Strumia, Nucl. Phys. B **645**, 155 (2002). arXiv:hep-ph/0207036
11. R.S. Chivukula, H. Georgi, Phys. Lett. B **188**, 99 (1987)
12. A.J. Buras, P. Gambino, M. Gorbahn, S. Jager, L. Silvestrini, Phys. Lett. B **500**, 161 (2001). arXiv:hep-ph/0007085
13. A. Ali, D. London, Eur. Phys. J. C **9**, 687 (1999). arXiv:hep-ph/9903535
14. A. Bartl, T. Gajdosik, E. Lunghi, A. Masiero, W. Porod, H. Stremnitzer, O. Vives, Phys. Rev. D **64**, 076009 (2001). arXiv:hep-ph/0103324
15. S. Laplace, Z. Ligeti, Y. Nir, G. Perez, Phys. Rev. D **65**, 094040 (2002). arXiv:hep-ph/0202010
16. A.J. Buras, Acta Phys. Pol. B **34**, 5615 (2003). arXiv:hep-ph/0310208
17. A.J. Buras, A. Poschenrieder, M. Spranger, A. Weiler, Nucl. Phys. B **678**, 455 (2004). arXiv:hep-ph/0306158
18. K. Agashe, M. Papucci, G. Perez, D. Pirjol, arXiv:hep-ph/0509117
19. T. Feldmann, T. Mannel, J. High Energy Phys. **0702**, 067 (2007). arXiv:hep-ph/0611095

20. L.J. Hall, R. Rattazzi, U. Sarid, Phys. Rev. D **50**, 7048 (1994). arXiv:hep-ph/9306309
21. T. Blazek, S. Raby, S. Pokorski, Phys. Rev. D **52**, 4151 (1995). arXiv:hep-ph/9504364
22. M. Carena, D. Garcia, U. Nierste, C.E.M. Wagner, Nucl. Phys. B **577**, 88 (2000). arXiv:hep-ph/9912516
23. G. Degrassi, P. Gambino, G.F. Giudice, J. High Energy Phys. **0012**, 009 (2000). arXiv:hep-ph/0009337
24. M. Carena, D. Garcia, U. Nierste, C.E.M. Wagner, Phys. Lett. B **499**, 141 (2001). arXiv:hep-ph/0010003
25. C. Hamzaoui, M. Pospelov, M. Toharia, Phys. Rev. D **59**, 095005 (1999). arXiv:hep-ph/9807350
26. S.R. Choudhury, N. Gaur, Phys. Lett. B **451**, 86 (1999). arXiv:hep-ph/9810307
27. K.S. Babu, C.F. Kolda, Phys. Rev. Lett. **84**, 228 (2000). arXiv:hep-ph/9909476
28. G. Isidori, A. Retico, J. High Energy Phys. **0111**, 001 (2001). arXiv:hep-ph/0110121
29. A.J. Buras, P.H. Chankowski, J. Rosiek, L. Slawianowska, Nucl. Phys. B **659**, 3 (2003). arXiv:hep-ph/0210145
30. A.J. Buras, P.H. Chankowski, J. Rosiek, L. Slawianowska, Phys. Lett. B **546**, 96 (2002). arXiv:hep-ph/0207241
31. W.S. Hou, Phys. Rev. D **48**, 2342 (1993)
32. G. Isidori, P. Paradisi, Phys. Lett. B **639**, 499 (2006). arXiv:hep-ph/0605012
33. E. Lunghi, W. Porod, O. Vives, Phys. Rev. D **74**, 075003 (2006). arXiv:hep-ph/0605177
34. G. Isidori, F. Mescia, P. Paradisi, D. Temes, arXiv:hep-ph/0703035
35. B. Grinstein, V. Cirigliano, G. Isidori, M.B. Wise, Nucl. Phys. B **763**, 35 (2007). arXiv:hep-ph/0608123
36. V. Cirigliano, B. Grinstein, G. Isidori, M.B. Wise, Nucl. Phys. B **728**, 121 (2005). arXiv:hep-ph/0507001
37. M. Grassi (MEG Collaboration), Nucl. Phys. Proc. Suppl. **149**, 369 (2005)
38. L.J. Hall, L. Randall, Phys. Rev. Lett. **65**, 2939 (1990)
39. M. Dine, A.E. Nelson, Phys. Rev. D **48**, 1277 (1993). arXiv:hep-ph/9303230
40. M. Dine, A.E. Nelson, Y. Shirman, Phys. Rev. D **51**, 1362 (1995). arXiv:hep-ph/9408384
41. G.F. Giudice, R. Rattazzi, Phys. Rep. **322**, 419 (1999). arXiv:hep-ph/9801271
42. W. Altmannshofer, A.J. Buras, D. Guadagnoli, arXiv:hep-ph/0703200
43. J.R. Ellis, D.V. Nanopoulos, Phys. Lett. B **110**, 44 (1982)
44. R. Barbieri, R. Gatto, Phys. Lett. B **110**, 211 (1982)
45. M. Dine, W. Fischler, M. Srednicki, Nucl. Phys. B **189**, 575 (1981)
46. S. Dimopoulos, S. Raby, Nucl. Phys. B **192**, 353 (1981)
47. M. Dine, W. Fischler, Phys. Lett. B **110**, 227 (1982)
48. M. Dine, M. Srednicki, Nucl. Phys. B **202**, 238 (1982)
49. M. Dine, W. Fischler, Nucl. Phys. B **204**, 346 (1982)
50. L. Alvarez-Gaume, M. Claudson, M.B. Wise, Nucl. Phys. B **207**, 96 (1982)
51. C.R. Nappi, B.A. Ovrut, Phys. Lett. B **113**, 175 (1982)
52. S. Dimopoulos, S. Raby, Nucl. Phys. B **219**, 479 (1983)
53. M. Dine, A.E. Nelson, Y. Nir, Y. Shirman, Phys. Rev. D **53**, 2658 (1996). arXiv:hep-ph/9507378
54. E. Poppitz, S.P. Trivedi, Phys. Rev. D **55**, 5508 (1997). arXiv:hep-ph/9609529
55. N. Arkani-Hamed, J. March-Russell, H. Murayama, Nucl. Phys. B **509**, 3 (1998). arXiv:hep-ph/9701286
56. H. Murayama, Phys. Rev. Lett. **79**, 18 (1997). arXiv:hep-ph/9705271
57. S. Dimopoulos, G.R. Dvali, R. Rattazzi, G.F. Giudice, Nucl. Phys. B **510**, 12 (1998). arXiv:hep-ph/9705307
58. S. Dimopoulos, G.R. Dvali, R. Rattazzi, Phys. Lett. B **413**, 336 (1997). arXiv:hep-ph/9707537
59. M.A. Luty, Phys. Lett. B **414**, 71 (1997). arXiv:hep-ph/9706554
60. T. Hotta, K.I. Izawa, T. Yanagida, Phys. Rev. D **55**, 415 (1997). arXiv:hep-ph/9606203
61. L. Randall, Nucl. Phys. B **495**, 37 (1997). arXiv:hep-ph/9612426
62. Y. Shadmi, Phys. Lett. B **405**, 99 (1997). arXiv:hep-ph/9703312
63. N. Haba, N. Maru, T. Matsuoka, Phys. Rev. D **56**, 4207 (1997). arXiv:hep-ph/9703250
64. C. Csaki, L. Randall, W. Skiba, Phys. Rev. D **57**, 383 (1998). arXiv:hep-ph/9707386
65. Y. Shirman, Phys. Lett. B **417**, 281 (1998). arXiv:hep-ph/9709383
66. P. Langacker, N. Polonsky, J. Wang, Phys. Rev. D **60**, 115005 (1999). arXiv:hep-ph/9905252
67. K.S. Babu, Y. Mimura, arXiv:hep-ph/0101046
68. A. Delgado, G.F. Giudice, P. Slavich, arXiv:0706.3873 [hep-ph]
69. M. Ciuchini, A. Masiero, L. Silvestrini, S.K. Vempati, O. Vives, Phys. Rev. Lett. **92**, 071801 (2004). arXiv:hep-ph/0307191
70. M. Ciuchini, A. Masiero, P. Paradisi, L. Silvestrini, S.K. Vempati, O. Vives, arXiv:hep-ph/0702144
71. M. Albrecht, W. Altmannshofer, A.J. Buras, D. Guadagnoli, D.M. Straub, arXiv:0707.3954 [hep-ph]
72. S. Weinberg, Phys. Rev. D **26**, 287 (1982)
73. N. Sakai, T. Yanagida, Nucl. Phys. B **197**, 533 (1982)
74. A.Y. Smirnov, F. Vissani, Phys. Lett. B **380**, 317 (1996). arXiv:hep-ph/9601387
75. C.S. Aulakh, R.N. Mohapatra, Phys. Lett. B **119**, 136 (1982)
76. L.J. Hall, M. Suzuki, Nucl. Phys. B **231**, 419 (1984)
77. I.H. Lee, Nucl. Phys. B **246**, 120 (1984)
78. J.R. Ellis, G. Gelmini, C. Jarlskog, G.G. Ross, J.W.F. Valle, Phys. Lett. B **150**, 142 (1985)
79. L.E. Ibanez, G.G. Ross, Nucl. Phys. B **368**, 3 (1992)
80. V.D. Barger, G.F. Giudice, T. Han, Phys. Rev. D **40**, 2987 (1989)
81. K. Enqvist, A. Masiero, A. Riotto, Nucl. Phys. B **373**, 95 (1992)
82. M. Misiak, S. Pokorski, J. Rosiek, Adv. Ser. Direct. High Energy Phys. **15**, 795 (1998). arXiv:hep-ph/9703442
83. M. Ciuchini, G. Degrassi, P. Gambino, G.F. Giudice, Nucl. Phys. B **527**, 21 (1998). arXiv:hep-ph/9710335
84. M. Ciuchini, G. Degrassi, P. Gambino, G.F. Giudice, Nucl. Phys. B **534**, 3 (1998). arXiv:hep-ph/9806308
85. A. Freitas, E. Gasser, U. Haisch, arXiv:hep-ph/0702267
86. A.J. Buras, P. Gambino, M. Gorbahn, S. Jager, L. Silvestrini, Nucl. Phys. B **592**, 55 (2001). arXiv:hep-ph/0007313
87. R. Barbieri, L.J. Hall, A. Strumia, Nucl. Phys. B **449**, 437 (1995). arXiv:hep-ph/9504373
88. L. Silvestrini, arXiv:0705.1624 [hep-ph]
89. M. Dugan, B. Grinstein, L.J. Hall, Nucl. Phys. B **255**, 413 (1985)
90. S. Dimopoulos, S.D. Thomas, Nucl. Phys. B **465**, 23 (1996). arXiv:hep-ph/9510220
91. M.J. Duncan, J. Trampetic, Phys. Lett. B **134**, 439 (1984)
92. E. Franco, M.L. Mangano, Phys. Lett. B **135**, 445 (1984)
93. J.M. Gerard, W. Grimus, A. Raychaudhuri, G. Zoupanos, Phys. Lett. B **140**, 349 (1984)
94. J.M. Gerard, W. Grimus, A. Masiero, D.V. Nanopoulos, A. Raychaudhuri, Phys. Lett. B **141**, 79 (1984)
95. J.M. Gerard, W. Grimus, A. Masiero, D.V. Nanopoulos, A. Raychaudhuri, Nucl. Phys. B **253**, 93 (1985)
96. P. Langacker, B. Sathiapalan, Phys. Lett. B **144**, 401 (1984)
97. L.J. Hall, V.A. Kostelecky, S. Raby, Nucl. Phys. B **267**, 415 (1986)

478

Eur. Phys. J. C (2008) 57: 309–492

98. M.J. Duncan, Nucl. Phys. B **221**, 285 (1983)
99. J.F. Donoghue, H.P. Nilles, D. Wyler, Phys. Lett. B **128**, 55 (1983)
100. A. Bouquet, J. Kaplan, C.A. Savoy, Phys. Lett. B **148**, 69 (1984)
101. F. Gabbiani, A. Masiero, Nucl. Phys. B **322**, 235 (1989)
102. J.S. Hagelin, S. Kelley, T. Tanaka, Nucl. Phys. B **415**, 293 (1994)
103. E. Gabrielli, A. Masiero, L. Silvestrini, Phys. Lett. B **374**, 80 (1996). arXiv:hep-ph/9509379
104. F. Gabbiani, E. Gabrielli, A. Masiero, L. Silvestrini, Nucl. Phys. B **477**, 321 (1996). arXiv:hep-ph/9604387
105. D. Becirevic et al., Nucl. Phys. B **634**, 105 (2002). arXiv:hep-ph/0112303
106. M. Ciuchini et al., J. High Energy Phys. **9810**, 008 (1998). arXiv:hep-ph/9808328
107. M. Ciuchini, E. Franco, A. Masiero, L. Silvestrini, Phys. Rev. D **67**, 075016 (2003) [Erratum: Phys. Rev. D **68**, 079901 (2003)]. arXiv:hep-ph/0212397
108. T. Besmer, C. Greub, T. Hurth, Nucl. Phys. B **609**, 359 (2001). arXiv:hep-ph/0105292
109. G.L. Kane, P. Ko, H.b. Wang, C. Kolda, J.h. Park, L.T. Wang, Phys. Rev. D **70**, 035015 (2004). arXiv:hep-ph/0212092
110. R. Harnik, D.T. Larson, H. Murayama, A. Pierce, Phys. Rev. D **69**, 094024 (2004). arXiv:hep-ph/0212180
111. K.I. Okumura, L. Roszkowski, J. High Energy Phys. **0310**, 024 (2003). arXiv:hep-ph/0308102
112. J. Foster, K.I. Okumura, L. Roszkowski, Phys. Lett. B **609**, 102 (2005). arXiv:hep-ph/0410323
113. J. Foster, K.I. Okumura, L. Roszkowski, J. High Energy Phys. **0508**, 094 (2005). arXiv:hep-ph/0506146
114. J. Foster, K.I. Okumura, L. Roszkowski, J. High Energy Phys. **0603**, 044 (2006). arXiv:hep-ph/0510422
115. J. Foster, K. Okumura, L. Roszkowski, Phys. Lett. B **641**, 452 (2006). arXiv:hep-ph/0604121
116. M. Ciuchini, L. Silvestrini, Phys. Rev. Lett. **97**, 021803 (2006). arXiv:hep-ph/0603114
117. M. Ciuchini, E. Franco, V. Lubicz, G. Martinelli, I. Scimemi, L. Silvestrini, Nucl. Phys. B **523**, 501 (1998). arXiv:hep-ph/9711402
118. M. Ciuchini, E. Franco, D. Guadagnoli, V. Lubicz, V. Porretti, L. Silvestrini, J. High Energy Phys. **0609**, 013 (2006). arXiv:hep-ph/0606197
119. W.M. Yao et al. (Particle Data Group), J. Phys. G **33**, 1 (2006)
120. M. Bona et al. (UTfit Collaboration), J. High Energy Phys. **0610**, 081 (2006). arXiv:hep-ph/0606167
121. S. Chen et al. (CLEO Collaboration), Phys. Rev. Lett. **87**, 251807 (2001). arXiv:hep-ex/0108032
122. P. Koppenburg et al. (Belle Collaboration), Phys. Rev. Lett. **93**, 061803 (2004). arXiv:hep-ex/0403004
123. B. Aubert et al. (BaBar Collaboration), Phys. Rev. D **72**, 052004 (2005). arXiv:hep-ex/0508004
124. B. Aubert et al. (BaBar Collaboration), Phys. Rev. Lett. **93**, 081802 (2004). arXiv:hep-ex/0404006
125. M. Iwasaki et al. (Belle Collaboration), Phys. Rev. D **72**, 092005 (2005). arXiv:hep-ex/0503044
126. A. Abulencia et al. (CDF Collaboration), arXiv:hep-ex/0609040
127. D. Becirevic, V. Gimenez, G. Martinelli, M. Papinutto, J. Reyes, J. High Energy Phys. **0204**, 025 (2002). arXiv:hep-lat/0110091
128. C.R. Allton et al., Phys. Lett. B **453**, 30 (1999). arXiv:hep-lat/9806016
129. R. Babich, N. Garron, C. Hoelbling, J. Howard, L. Lellouch, C. Rebbi, Phys. Rev. D **74**, 073009 (2006). arXiv:hep-lat/0605016
130. Y. Nakamura et al. (CP-PACS Collaboration), arXiv:hep-lat/0610075
131. A.J. Buras, G. Colangelo, G. Isidori, A. Romanino, L. Silvestrini, Nucl. Phys. B **566**, 3 (2000). arXiv:hep-ph/9908371
132. M. Ciuchini et al., J. High Energy Phys. **0107**, 013 (2001). arXiv:hep-ph/0012308
133. N. Arkani-Hamed, A.G. Cohen, H. Georgi, Phys. Lett. B **513**, 232 (2001). arXiv:hep-ph/0105239
134. D.E. Kaplan, M. Schmaltz, J. High Energy Phys. **0310**, 039 (2003). arXiv:hep-ph/0302049
135. M. Schmaltz, J. High Energy Phys. **0408**, 056 (2004). arXiv:hep-ph/0407143
136. N. Arkani-Hamed, A.G. Cohen, E. Katz, A.E. Nelson, T. Gregoire, J.G. Wacker, J. High Energy Phys. **0208**, 021 (2002). arXiv:hep-ph/0206020
137. N. Arkani-Hamed, A.G. Cohen, E. Katz, A.E. Nelson, J. High Energy Phys. **0207**, 034 (2002). arXiv:hep-ph/0206021
138. T. Han, H.E. Logan, B. McElrath, L.T. Wang, Phys. Rev. D **67**, 095004 (2003). arXiv:hep-ph/0301040
139. C. Csaki, J. Hubisz, G.D. Kribs, P. Meade, J. Terning, Phys. Rev. D **67**, 115002 (2003). arXiv:hep-ph/0211124
140. A.J. Buras, A. Poschenrieder, S. Uhlig, Nucl. Phys. B **716**, 173 (2005). arXiv:hep-ph/0410309
141. A.J. Buras, A. Poschenrieder, S. Uhlig, arXiv:hep-ph/0501230
142. A.J. Buras, A. Poschenrieder, S. Uhlig, W.A. Bardeen, J. High Energy Phys. **0611**, 062 (2006). arXiv:hep-ph/0607189
143. S.R. Choudhury, N. Gaur, A. Goyal, N. Mahajan, Phys. Lett. B **601**, 164 (2004). arXiv:hep-ph/0407050
144. J.Y. Lee, J. High Energy Phys. **0412**, 065 (2004). arXiv:hep-ph/0408362
145. S. Fajfer, S. Prelovsek, Phys. Rev. D **73**, 054026 (2006). arXiv:hep-ph/0511048
146. W.J. Huo, S.H. Zhu, Phys. Rev. D **68**, 097301 (2003). arXiv:hep-ph/0306029
147. H.C. Cheng, I. Low, J. High Energy Phys. **0309**, 051 (2003). arXiv:hep-ph/0308199
148. H.C. Cheng, I. Low, J. High Energy Phys. **0408**, 061 (2004). arXiv:hep-ph/0405243
149. J. Hubisz, P. Meade, A. Noble, M. Perelstein, J. High Energy Phys. **0601**, 135 (2006). arXiv:hep-ph/0506042
150. I. Low, J. High Energy Phys. **0410**, 067 (2004). arXiv:hep-ph/0409025
151. N. Cabibbo, Phys. Rev. Lett. **10**, 531 (1963)
152. M. Kobayashi, T. Maskawa, Prog. Theor. Phys. **49**, 652 (1973)
153. J. Hubisz, S.J. Lee, G. Paz, J. High Energy Phys. **0606**, 041 (2006). arXiv:hep-ph/0512169
154. B. Pontecorvo, Sov. Phys. JETP **6**, 429 (1957) [Zh. Eksp. Teor. Fiz. **33**, 549 (1957)]
155. B. Pontecorvo, Sov. Phys. JETP **7**, 172 (1958) [Zh. Eksp. Teor. Fiz. **34**, 247 (1957)]
156. Z. Maki, M. Nakagawa, S. Sakata, Prog. Theor. Phys. **28**, 870 (1962)
157. M. Blanke, A.J. Buras, A. Poschenrieder, S. Recksiegel, C. Tarantino, S. Uhlig, A. Weiler, Phys. Lett. B **646**, 253 (2007). arXiv:hep-ph/0609284
158. M. Blanke, A.J. Buras, A. Poschenrieder, S. Recksiegel, C. Tarantino, S. Uhlig, A. Weiler, J. High Energy Phys. **0701**, 066 (2007). arXiv:hep-ph/0610298
159. M. Blanke, A.J. Buras, A. Poschenrieder, C. Tarantino, S. Uhlig, A. Weiler, J. High Energy Phys. **0612**, 003 (2006). arXiv:hep-ph/0605214
160. S.R. Choudhury, A.S. Cornell, A. Deandrea, N. Gaur, A. Goyal, arXiv:hep-ph/0612327
161. M. Blanke, A.J. Buras, B. Duling, A. Poschenrieder, C. Tarantino, arXiv:hep-ph/0702136
162. D. Lucchesi (CDF and D0 Collaborations), Nucl. Phys. Proc. Suppl. **163**, 165 (2007)
163. C. Promberger, S. Schatt, F. Schwab, arXiv:hep-ph/0702169

Eur. Phys. J. C (2008) 57: 309–492

479

164. S. Eidelman et al. (Particle Data Group), Phys. Lett. B **592**, 1 (2004)
165. P. Paradisi, J. High Energy Phys. **0510**, 006 (2005). arXiv:hep-ph/0505046
166. P. Paradisi, J. High Energy Phys. **0602**, 050 (2006). arXiv:hep-ph/0508054
167. P. Paradisi, J. High Energy Phys. **0608**, 047 (2006). arXiv:hep-ph/0601100
168. T. Kaluza, Sitzungsber. Preuss. Akad. Wiss. Berlin (Math. Phys.) **1921**, 966 (1921)
169. O. Klein, Z. Phys. **37**, 895 (1926) [Surv. High Energy Phys. **5**, 241 (1986)]
170. I. Antoniadis, Phys. Lett. B **246**, 377 (1990)
171. J.D. Lykken, Phys. Rev. D **54**, 3693 (1996). arXiv:hep-th/9603133
172. E. Witten, Nucl. Phys. B **471**, 135 (1996). arXiv:hep-th/9602070
173. P. Horava, E. Witten, Nucl. Phys. B **475**, 94 (1996). arXiv:hep-th/9603142
174. P. Horava, E. Witten, Nucl. Phys. B **460**, 506 (1996). arXiv:hep-th/9510209
175. E. Caceres, V.S. Kaplunovsky, I.M. Mandelberg, Nucl. Phys. B **493**, 73 (1997). arXiv:hep-th/9606036
176. N. Arkani-Hamed, S. Dimopoulos, G.R. Dvali, Phys. Lett. B **429**, 263 (1998). arXiv:hep-ph/9803315
177. I. Antoniadis, N. Arkani-Hamed, S. Dimopoulos, G.R. Dvali, Phys. Lett. B **436**, 257 (1998). arXiv:hep-ph/9804398
178. N. Arkani-Hamed, S. Dimopoulos, G.R. Dvali, Phys. Rev. D **59**, 086004 (1999). arXiv:hep-ph/9807344
179. L. Randall, R. Sundrum, Phys. Rev. Lett. **83**, 3370 (1999). arXiv:hep-ph/9905221
180. T. Appelquist, H.C. Cheng, B.A. Dobrescu, Phys. Rev. D **64**, 035002 (2001). arXiv:hep-ph/0012100
181. A.J. Buras, M. Spranger, A. Weiler, Nucl. Phys. B **660**, 225 (2003). arXiv:hep-ph/0212143
182. P. Colangelo, F. De Fazio, R. Ferrandes, T.N. Pham, Phys. Rev. D **73**, 115006 (2006). arXiv:hep-ph/0604029
183. P. Colangelo, F. De Fazio, R. Ferrandes, T.N. Pham, Phys. Rev. D **74**, 115006 (2006). arXiv:hep-ph/0610044
184. T. Inami, C.S. Lim, Prog. Theor. Phys. **65**, 297 (1981) [Erratum: Prog. Theor. Phys. **65**, 1772 (1981)]
185. P. Skands et al., J. High Energy Phys. **0407**, 036 (2004). arXiv:hep-ph/0311123
186. B.C. Allanach et al., arXiv:0801.0045 [hep-ph]
187. L. Silvestrini, Int. J. Mod. Phys. A **21**, 1738 (2006). arXiv:hep-ph/0510077
188. P. Gambino, U. Haisch, M. Misiak, Phys. Rev. Lett. **94**, 061803 (2005). arXiv:hep-ph/0410155
189. C. Bobeth, A.J. Buras, T. Ewerth, Nucl. Phys. B **713**, 522 (2005). arXiv:hep-ph/0409293
190. C. Bobeth, M. Bona, A.J. Buras, T. Ewerth, M. Pierini, L. Silvestrini, A. Weiler, Nucl. Phys. B **726**, 252 (2005). arXiv:hep-ph/0505110
191. G. Degrassi, P. Gambino, P. Slavich, arXiv:0712.3265 [hep-ph]
192. A.J. Buras, T. Ewerth, S. Jager, J. Rosiek, Nucl. Phys. B **714**, 103 (2005). arXiv:hep-ph/0408142
193. S. Bejar, J. Guasch, J. Sola, Nucl. Phys. B **600**, 21 (2001). arXiv:hep-ph/0011091
194. S. Bejar, J. Guasch, J. Sola, in *Proceedings of the 5th International Symposium on Radiative Corrections (RADCOR 2000)*, ed. by H.E. Haber. arXiv:hep-ph/0101294
195. S. Bejar, J. Guasch, J. Sola, Nucl. Phys. B **675**, 270 (2003). arXiv:hep-ph/0307144
196. S. Bejar, F. Dilme, J. Guasch, J. Sola, J. High Energy Phys. **0408**, 018 (2004). arXiv:hep-ph/0402188
197. S. Bejar, J. Guasch, J. Sola, J. High Energy Phys. **0510**, 113 (2005). arXiv:hep-ph/0508043
198. S. Bejar, J. Guasch, J. Sola, Nucl. Phys. Proc. Suppl. **157**, 147 (2006). arXiv:hep-ph/0601191
199. S. Heinemeyer, W. Hollik, G. Weiglein, Eur. Phys. J. C **9**, 343 (1999). arXiv:hep-ph/9812472
200. G. Degrassi, S. Heinemeyer, W. Hollik, P. Slavich, G. Weiglein, Eur. Phys. J. C **28**, 133 (2003). arXiv:hep-ph/0212020
201. S. Heinemeyer, W. Hollik, F. Merz, S. Penaranda, Eur. Phys. J. C **37**, 481 (2004). arXiv:hep-ph/0403228
202. T. Hahn, M. Perez-Victoria, Comput. Phys. Commun. **118**, 153 (1999). arXiv:hep-ph/9807565
203. T. Hahn, Comput. Phys. Commun. **140**, 418 (2001). arXiv:hep-ph/0012260
204. T. Hahn, W. Hollik, J.I. Illana, S. Penaranda, arXiv:hep-ph/0512315
205. T. Hahn, arXiv:hep-ph/0605049
206. B.C. Allanach, Comput. Phys. Commun. **143**, 305 (2002). arXiv:hep-ph/0104145
207. W. Porod, Comput. Phys. Commun. **153**, 275 (2003). arXiv:hep-ph/0301101
208. O. Buchmüller, private communication
209. M. Bona et al. (UTfit Collaboration), J. High Energy Phys. **0507**, 028 (2005). arXiv:hep-ph/0501199
210. M. Bona et al. (UTfit Collaboration), J. High Energy Phys. **0603**, 080 (2006). arXiv:hep-ph/0509219
211. M. Bona et al. (UTfit Collaboration), arXiv:hep-ph/0701204
212. R. Brun, F. Rademakers, Nucl. Instrum. Methods A **389**, 81 (1997)
213. ckmfitter.in2p3.fr
214. G. Buchalla, A.J. Buras, M.E. Lautenbacher, Rev. Mod. Phys. **68**, 1125 (1996). arXiv:hep-ph/9512380
215. M. Beneke, G. Buchalla, M. Neubert, C.T. Sachrajda, Phys. Rev. Lett. **83**, 1914 (1999). arXiv:hep-ph/9905312
216. M. Beneke, G. Buchalla, M. Neubert, C.T. Sachrajda, Nucl. Phys. B **591**, 313 (2000). arXiv:hep-ph/0006124
217. C.W. Bauer, S. Fleming, D. Pirjol, I.W. Stewart, Phys. Rev. D **63**, 114020 (2001). arXiv:hep-ph/0011336
218. C.W. Bauer, D. Pirjol, I.W. Stewart, Phys. Rev. D **65**, 054022 (2002). arXiv:hep-ph/0109045
219. J. Chay, C. Kim, Phys. Rev. D **68**, 071502 (2003). arXiv:hep-ph/0301055
220. J. Chay, C. Kim, Nucl. Phys. B **680**, 302 (2004). arXiv:hep-ph/0301262
221. C.W. Bauer, D. Pirjol, I.Z. Rothstein, I.W. Stewart, Phys. Rev. D **70**, 054015 (2004). arXiv:hep-ph/0401188
222. Y.Y. Keum, H.N. Li, A.I. Sanda, Phys. Rev. D **63**, 054008 (2001). arXiv:hep-ph/0004173
223. H.N. Li, S. Mishima, A.I. Sanda, Phys. Rev. D **72**, 114005 (2005). arXiv:hep-ph/0508041
224. M. Beneke, G. Buchalla, M. Neubert, C.T. Sachrajda, Nucl. Phys. B **606**, 245 (2001). arXiv:hep-ph/0104110
225. R.J. Hill, T. Becher, S.J. Lee, M. Neubert, J. High Energy Phys. **0407**, 081 (2004). arXiv:hep-ph/0404217
226. T. Becher, R.J. Hill, J. High Energy Phys. **0410**, 055 (2004). arXiv:hep-ph/0408344
227. G.G. Kirilin, arXiv:hep-ph/0508235
228. M. Beneke, D. Yang, Nucl. Phys. B **736**, 34 (2006). arXiv:hep-ph/0508250
229. M. Beneke, S. Jäger, Nucl. Phys. B **751**, 160 (2006). arXiv:hep-ph/0512351
230. P. Colangelo, A. Khodjamirian, arXiv:hep-ph/0010175
231. P. Ball, R. Zwicky, Phys. Rev. D **71**, 014015 (2005). arXiv:hep-ph/0406232
232. P. Ball, R. Zwicky, Phys. Rev. D **71**, 014029 (2005). arXiv:hep-ph/0412079
233. P. Ball, R. Zwicky, Phys. Lett. B **633**, 289 (2006). arXiv:hep-ph/0510338

234. F. De Fazio, T. Feldmann, T. Hurth, Nucl. Phys. B **733**, 1 (2006). arXiv:hep-ph/0504088
235. J. Chay, C. Kim, A.K. Leibovich, Phys. Lett. B **628**, 57 (2005). arXiv:hep-ph/0508157
236. A. Khodjamirian, T. Mannel, N. Offen, Phys. Lett. B **620**, 52 (2005). arXiv:hep-ph/0504091
237. S.J. Lee, M. Neubert, Phys. Rev. D **72**, 094028 (2005). arXiv:hep-ph/0509350
238. V.M. Braun, D.Y. Ivanov, G.P. Korchemsky, Phys. Rev. D **69**, 034014 (2004). arXiv:hep-ph/0309330
239. M. Beneke, M. Neubert, Nucl. Phys. B **651**, 225 (2003). arXiv:hep-ph/0210085
240. M. Beneke, M. Neubert, Nucl. Phys. B **675**, 333 (2003). arXiv:hep-ph/0308039
241. A.R. Williamson, J. Zupan, Phys. Rev. D **74**, 014003 (2006). arXiv:hep-ph/0601214
242. M. Beneke, G. Buchalla, M. Neubert, C.T. Sachrajda, Phys. Rev. D **72**, 098501 (2005). arXiv:hep-ph/0411171
243. A. Khodjamirian, T. Mannel, M. Melcher, B. Melic, Phys. Rev. D **72**, 094012 (2005). arXiv:hep-ph/0509049
244. A. Khodjamirian, arXiv:hep-ph/0607347
245. D. Zeppenfeld, Z. Phys. C **8**, 77 (1981)
246. M. Gronau, D. London, Phys. Rev. Lett. **65**, 3381 (1990)
247. Y. Nir, H.R. Quinn, Phys. Rev. Lett. **67**, 541 (1991)
248. J. Charles et al., arXiv:hep-ph/0607246
249. E. Baracchini, G. Isidori, Phys. Lett. B **633**, 309 (2006). arXiv:hep-ph/0508071
250. A. Khodjamirian, T. Mannel, M. Melcher, Phys. Rev. D **68**, 114007 (2003). arXiv:hep-ph/0308297
251. M. Beneke, T. Feldmann, Nucl. Phys. B **685**, 249 (2004). arXiv:hep-ph/0311335
252. N. Kivel, J. High Energy Phys. **0705**, 019 (2007). arXiv:hep-ph/0608291
253. V. Pilipp, Nucl. Phys. B **794**, 154 (2008). arXiv:0709.3214 [hep-ph]
254. V. Pilipp, arXiv:0709.0497 [hep-ph]
255. G. Bell, Nucl. Phys. B **795**, 1 (2008). arXiv:0705.3127 [hep-ph]
256. G. Bell, PhD thesis, LMU München, 2006. arXiv:0705.3133 [hep-ph]
257. M. Beneke, S. Jäger, Nucl. Phys. B **768**, 51 (2007). arXiv:hep-ph/0610322
258. B. Aubert et al. (BaBar Collaboration), arXiv:hep-ex/0608003
259. Y. Chao et al. (Belle Collaboration), PoS **HEP2005**, 256 (2006)
260. P. Golonka, Z. Was, Eur. Phys. J. C **45**, 97 (2006). arXiv:hep-ph/0506026
261. V.L. Chernyak, A.R. Zhitnitsky, Phys. Rep. **112**, 173 (1984)
262. V.M. Braun, arXiv:hep-ph/0608231
263. P. Ball, V.M. Braun, N. Kivel, Nucl. Phys. B **649**, 263 (2003). arXiv:hep-ph/0207307
264. A.G. Grozin, Int. J. Mod. Phys. A **20**, 7451 (2005). arXiv:hep-ph/0506226
265. P. Ball, R. Zwicky, arXiv:hep-ph/0609037
266. P. Ball, R. Zwicky, J. High Energy Phys. **0604**, 046 (2006). arXiv:hep-ph/0603232
267. V.M. Braun et al., Phys. Rev. D **68**, 054501 (2003). arXiv:hep-lat/0306006
268. D. Becirevic, V. Lubicz, F. Mescia, C. Tarantino, J. High Energy Phys. **0305**, 007 (2003). arXiv:hep-lat/0301020
269. P. Ball, V.M. Braun, Phys. Rev. D **54**, 2182 (1996). arXiv:hep-ph/9602323
270. P. Ball, G.W. Jones, R. Zwicky, Phys. Rev. D **75**, 054004 (2007). arXiv:hep-ph/0612081
271. P. Ball, M. Boglione, Phys. Rev. D **68**, 094006 (2003). arXiv:hep-ph/0307337
272. A. Khodjamirian, T. Mannel, M. Melcher, Phys. Rev. D **70**, 094002 (2004). arXiv:hep-ph/0407226
273. V.M. Braun, A. Lenz, Phys. Rev. D **70**, 074020 (2004). arXiv:hep-ph/0407282
274. P. Ball, R. Zwicky, J. High Energy Phys. **0602**, 034 (2006). arXiv:hep-ph/0601086
275. P.A. Boyle et al. (UKQCD Collaboration), Phys. Lett. B **641**, 67 (2006). arXiv:hep-lat/0607018
276. V.M. Braun et al., arXiv:hep-lat/0606012
277. P. Ball, V.M. Braun, A. Lenz, J. High Energy Phys. **0605**, 004 (2006). arXiv:hep-ph/0603063
278. P. Ball, G.W. Jones, arXiv:hep-ph/0702100
279. P. Ball, A.N. Talbot, J. High Energy Phys. **0506**, 063 (2005). arXiv:hep-ph/0502115
280. D. Becirevic, A.B. Kaidalov, Phys. Lett. B **478**, 417 (2000). arXiv:hep-ph/9904490
281. P. Ball, R. Zwicky, Phys. Lett. B **625**, 225 (2005). arXiv:hep-ph/0507076
282. S.W. Bosch, G. Buchalla, J. High Energy Phys. **0501**, 035 (2005). arXiv:hep-ph/0408231
283. M. Beneke, T. Feldmann, D. Seidel, Eur. Phys. J. C **41**, 173 (2005). arXiv:hep-ph/0412400
284. P. Ball, R. Zwicky, arXiv:hep-ph/0608009
285. R.N. Faustov, V.O. Galkin, Z. Phys. C **66**, 119 (1995)
286. D. Melikhov, Phys. Rev. D **56**, 7089 (1997). arXiv:hep-ph/9706417
287. W. Lucha, D. Melikhov, S. Simula, Phys. Rev. D **74**, 054004 (2006). arXiv:hep-ph/0606281
288. S. Godfrey, N. Isgur, Phys. Rev. D **32**, 189 (1985)
289. D. Ebert, V.O. Galkin, R.N. Faustov, Phys. Rev. D **57**, 5663 (1998). [Erratum: Phys. Rev. D **59**, 019902 (1999)]. arXiv:hep-ph/9712318
290. M. Wirbel, B. Stech, M. Bauer, Z. Phys. C **29**, 637 (1985)
291. N. Isgur, D. Scora, B. Grinstein, M.B. Wise, Phys. Rev. D **39**, 799 (1989)
292. D. Scora, N. Isgur, Phys. Rev. D **52**, 2783 (1995). arXiv:hep-ph/9503486
293. D. Melikhov, Phys. Rev. D **53**, 2460 (1996). arXiv:hep-ph/9509268
294. D. Melikhov, M. Beyer, Phys. Lett. B **452**, 121 (1999). arXiv:hep-ph/9901261
295. D. Melikhov, B. Stech, Phys. Rev. D **62**, 014006 (2000). arXiv:hep-ph/0001113
296. M. Beyer, D. Melikhov, Phys. Lett. B **436**, 344 (1998). arXiv:hep-ph/9807223
297. M. Beyer, D. Melikhov, N. Nikitin, B. Stech, Phys. Rev. D **64**, 094006 (2001). arXiv:hep-ph/0106203
298. F. Krüger, D. Melikhov, Phys. Rev. D **67**, 034002 (2003). arXiv:hep-ph/0208256
299. D. Melikhov, N. Nikitin, Phys. Rev. D **70**, 114028 (2004). arXiv:hep-ph/0410146
300. M.A. Ivanov, J.G. Körner, S.G. Kovalenko, C.D. Roberts, Phys. Rev. D **76**, 034018 (2007). arXiv:nucl-th/0703094
301. M. Okamoto, PoS **LAT2005**, 013 (2006). arXiv:hep-lat/0510113
302. T. Onogi, PoS **LAT2006**, 017 (2006). arXiv:hep-lat/0610115
303. M. Della Morte, PoS **LAT2007**, 008 (2007). arXiv:0711.3160
304. C. Dawson, PoS **LAT2005**, 007 (2006).
305. W. Lee, PoS **LAT2006**, 015 (2006). arXiv:hep-lat/0610058
306. A. Jüttner, PoS **LAT2007**, 014 (2007). arXiv:0711.1239
307. C. Allton et al. (RBC/UKQCD Collaboration), arXiv:hep-lat/0701013
308. S.R. Beane, P.F. Bedaque, K. Orginos, M.J. Savage, arXiv:hep-lat/0606023
309. C. Bernard et al. (MILC Collaboration), arXiv:hep-lat/0609053
310. E. Follana, C.T.H. Davies, G.P. Lepage, J. Shigemitsu, arXiv:0706.1726 [hep-lat]
311. A. Jüttner, J. Rolf (ALPHA Collaboration), Phys. Lett. B **560**, 59 (2003). arXiv:hep-lat/0302016

312. G.M. de Divitiis et al., Nucl. Phys. B **672**, 372 (2003). arXiv:hep-lat/0307005

313. C. Aubin et al., Phys. Rev. Lett. **95**, 122002 (2005). arXiv:hep-lat/0506030

314. H.W. Lin, S. Ohta, A. Soni, N. Yamada, Phys. Rev. D **74**, 114506 (2006). arXiv:hep-lat/0607035

315. M. Della Morte et al. (ALPHA Collaboration), Phys. Lett. B **581**, 93 (2004) [Erratum: Phys. Lett. B **612**, 313 (2005)]. arXiv:hep-lat/0307021

316. D. Guazzini, R. Sommer, N. Tantalo, arXiv:hep-lat/0609065

317. A. Ali Khan et al. (CP-PACS Collaboration), Phys. Rev. D **64**, 054504 (2001). arXiv:hep-lat/0103020

318. C. Bernard et al. (MILC Collaboration), Phys. Rev. D **66**, 094501 (2002). arXiv:hep-lat/0206016

319. M. Wingate et al., Phys. Rev. Lett. **92**, 162001 (2004). arXiv:hep-ph/0311130

320. S. Aoki et al. (JLQCD Collaboration), Phys. Rev. Lett. **91**, 212001 (2003). arXiv:hep-ph/0307039

321. A. Gray et al. (HPQCD Collaboration), Phys. Rev. Lett. **95**, 212001 (2005). arXiv:hep-lat/0507015

322. V. Gadiyak, O. Loktik, Phys. Rev. D **72**, 114504 (2005). arXiv:hep-lat/0509075

323. M. Artuso et al. (CLEO Collaboration), Phys. Rev. Lett. **95**, 251801 (2005). arXiv:hep-ex/0508057

324. M. Artuso et al. (CLEO Collaboration), arXiv:hep-ex/0607074

325. B. Aubert et al. (BaBar Collaboration), arXiv:hep-ex/0607094

326. K. Ikado et al., Phys. Rev. Lett. **97**, 251802 (2006). arXiv:hep-ex/0604018

327. D. Becirevic et al., Nucl. Phys. B **705**, 339 (2005). arXiv:hep-ph/0403217

328. N. Tsutsui et al. (JLQCD Collaboration), PoS **LAT2005**, 357 (2006). arXiv:hep-lat/0510068

329. C. Dawson et al., Phys. Rev. D **74**, 114502 (2006). arXiv:hep-ph/0607162

330. D.J. Antonio et al., arXiv:hep-lat/0610080

331. M. Okamoto (Fermilab Lattice Collaboration), arXiv:hep-lat/0412044

332. C. Aubin et al. (Fermilab Lattice Collaboration), Phys. Rev. Lett. **94**, 011601 (2005). arXiv:hep-ph/0408306

333. M. Okamoto et al., Nucl. Phys. Proc. Suppl. **140**, 461 (2005). arXiv:hep-lat/0409116

334. E. Dalgic et al., Phys. Rev. D **73**, 074502 (2006) [Erratum, to appear]. arXiv:hep-lat/0601021

335. G.M. de Divitiis, E. Molinaro, R. Petronzio, N. Tantalo, arXiv:0707.0582 [hep-lat]

336. K.C. Bowler et al. (UKQCD Collaboration), Phys. Lett. B **486**, 111 (2000). arXiv:hep-lat/9911011

337. A. Abada et al., Nucl. Phys. B **619**, 565 (2001). arXiv:hep-lat/0011065

338. A.X. El-Khadra et al., Phys. Rev. D **64**, 014502 (2001). arXiv:hep-ph/0101023

339. S. Aoki et al. (JLQCD Collaboration), Phys. Rev. D **64**, 114505 (2001). arXiv:hep-lat/0106024

340. M. Ablikim et al. (BES Collaboration), Phys. Lett. B **597**, 39 (2004). arXiv:hep-ex/0406028

341. J.M. Link et al. (FOCUS Collaboration), Phys. Lett. B **607**, 233 (2005). arXiv:hep-ex/0410037

342. A. Ali Khan et al. (CP-PACS Collaboration), Phys. Rev. D **64**, 114506 (2001). arXiv:hep-lat/0105020

343. T.A. DeGrand (MILC Collaboration), Phys. Rev. D **69**, 014504 (2004). arXiv:hep-lat/0309026

344. D. Becirevic et al., Eur. Phys. J. C **37**, 315 (2004). arXiv:hep-lat/0407004

345. Y. Aoki et al., Phys. Rev. D **73**, 094507 (2006). arXiv:hep-lat/0508011

346. P. Dimopoulos et al. (ALPHA Collaboration), Nucl. Phys. B **749**, 69 (2006). arXiv:hep-ph/0601002

347. J.M. Flynn, F. Mescia, A.S.B. Tariq (UKQCD Collaboration), J. High Energy Phys. **0411**, 049 (2004). arXiv:hep-lat/0406013

348. Y. Aoki et al., Phys. Rev. D **72**, 114505 (2005). arXiv:hep-lat/0411006

349. E. Gamiz et al. (HPQCD Collaboration), Phys. Rev. D **73**, 114502 (2006). arXiv:hep-lat/0603023

350. D.J. Antonio et al., arXiv:hep-ph/0702042

351. D. Becirevic et al., PoS **LAT2005**, 218 (2006). arXiv:hep-lat/0509165

352. E. Dalgic et al., arXiv:hep-lat/0610104

353. A. Donini et al., Phys. Lett. B **470**, 233 (1999). arXiv:hep-lat/9910017

354. D. Becirevic, G. Villadoro, Phys. Rev. D **70**, 094036 (2004). arXiv:hep-lat/0408029

355. D. Becirevic et al. (SPQcdR Collaboration), Phys. Lett. B **501**, 98 (2001). arXiv:hep-ph/0010349

356. H. Neuberger, Phys. Lett. B **417**, 141 (1998). arXiv:hep-lat/9707022

357. H. Neuberger, Phys. Lett. B **427**, 353 (1998). arXiv:hep-lat/9801031

358. P.H. Ginsparg, K.G. Wilson, Phys. Rev. D **25**, 2649 (1982)

359. M. Lüscher, Phys. Lett. B **428**, 342 (1998). arXiv:hep-lat/9802011

360. C. Gattringer et al. (BGR Collaboration), Nucl. Phys. B **677**, 3 (2004). arXiv:hep-lat/0307013

361. R. Sommer, Nucl. Phys. B **411**, 839 (1994). arXiv:hep-lat/9310022

362. J. Gasser, H. Leutwyler, Ann. Phys. **158**, 142 (1984)

363. J. Gasser, H. Leutwyler, Nucl. Phys. B **250**, 465 (1985)

364. C. Aubin, C. Bernard, Phys. Rev. D **68**, 034014 (2003). arXiv:hep-lat/0304014

365. C. Aubin, C. Bernard, Phys. Rev. D **68**, 074011 (2003). arXiv:hep-lat/0306026

366. C.W. Bernard, M.F.L. Golterman, Phys. Rev. D **49**, 486 (1994). arXiv:hep-lat/9306005

367. S.R. Sharpe, Phys. Rev. D **56**, 7052 (1997) [Erratum: Phys. Rev. D **62**, 099901 (2000)]. arXiv:hep-lat/9707018

368. S.R. Sharpe, N. Shoresh, Phys. Rev. D **62**, 094503 (2000). arXiv:hep-lat/0006017

369. S. Dürr, PoS **LAT2005**, 021 (2006). arXiv:hep-lat/0509026

370. S.R. Sharpe, PoS **LAT2006**, 022 (2006). arXiv:hep-lat/0610094

371. M. Creutz, PoS **LAT2007**, 007 (2007). arXiv:0708.1295

372. A.S. Kronfeld, PoS **LAT2007**, 016 (2007). arXiv:0711.0699

373. M.A. Clark, PoS **LAT2006**, 004 (2006). arXiv:hep-lat/0610048

374. J.M. Flynn, J. Nieves, Phys. Rev. D **75**, 013008 (2007). arXiv:hep-ph/0607258

375. S. Bertolini, F. Borzumati, A. Masiero, Phys. Rev. Lett. **59**, 180 (1987)

376. M. Misiak et al., Phys. Rev. Lett. **98**, 022002 (2007). arXiv:hep-ph/0609232

377. C. Bobeth, M. Misiak, J. Urban, Nucl. Phys. B **574**, 291 (2000). arXiv:hep-ph/9910220

378. M. Misiak, M. Steinhauser, Nucl. Phys. B **683**, 277 (2004). arXiv:hep-ph/0401041

379. M. Gorbahn, U. Haisch, Nucl. Phys. B **713**, 291 (2005). arXiv:hep-ph/0411071

380. M. Gorbahn, U. Haisch, M. Misiak, Phys. Rev. Lett. **95**, 102004 (2005). arXiv:hep-ph/0504194

381. M. Czakon, U. Haisch, M. Misiak, J. High Energy Phys. **0703**, 008 (2007). arXiv:hep-ph/0612329

382. K. Melnikov, A. Mitov, Phys. Lett. B **620**, 69 (2005). arXiv:hep-ph/0505097

383. I. Blokland et al., Phys. Rev. D **72**, 033014 (2005). arXiv:hep-ph/0506055

384. H.M. Asatrian et al., Nucl. Phys. B **749**, 325 (2006). arXiv:hep-ph/0605009

482

Eur. Phys. J. C (2008) 57: 309–492

385. H.M. Asatrian et al., Nucl. Phys. B **762**, 212 (2007). arXiv:hep-ph/0607316

386. H.M. Asatrian et al., arXiv:hep-ph/0611123

387. K. Bieri, C. Greub, M. Steinhauser, Phys. Rev. D **67**, 114019 (2003). arXiv:hep-ph/0302051

388. M. Misiak, M. Steinhauser, Nucl. Phys. B **764**, 62 (2007). arXiv:hep-ph/0609241

389. E. Barberio et al. (Heavy Flavor Averaging Group (HFAG) Collaboration), arXiv:0704.3575 [hep-ex]

390. A.F. Falk, M.E. Luke, M.J. Savage, Phys. Rev. D **49**, 3367 (1994). arXiv:hep-ph/9308288

391. I.I. Bigi et al., arXiv:hep-ph/9212227

392. G. Buchalla, G. Isidori, S.J. Rey, Nucl. Phys. B **511**, 594 (1998). arXiv:hep-ph/9705253

393. M.B. Voloshin, Phys. Lett. B **397**, 275 (1997). arXiv:hep-ph/9612483

394. A. Khodjamirian et al., Phys. Lett. B **402**, 167 (1997). arXiv:hep-ph/9702318

395. Z. Ligeti, L. Randall, M.B. Wise, Phys. Lett. B **402**, 178 (1997). arXiv:hep-ph/9702322

396. A.K. Grant et al., Phys. Rev. D **56**, 3151 (1997). arXiv:hep-ph/9702380

397. S.J. Lee, M. Neubert, G. Paz, arXiv:hep-ph/0609224

398. T. Becher, M. Neubert, Phys. Rev. Lett. **98**, 022003 (2007). arXiv:hep-ph/0610067

399. J.R. Andersen, E. Gardi, J. High Energy Phys. **0701**, 029 (2007). arXiv:hep-ph/0609250

400. I. Bigi, N. Uraltsev, Int. J. Mod. Phys. A **17**, 4709 (2002). arXiv:hep-ph/0202175

401. A. Kapustin, Z. Ligeti, H.D. Politzer, Phys. Lett. B **357**, 653 (1995). arXiv:hep-ph/9507248

402. Z. Ligeti et al., Phys. Rev. D **60**, 034019 (1999). arXiv:hep-ph/9903305

403. A. Ali, A.Y. Parkhomenko, Eur. Phys. J. C **23**, 89 (2002). arXiv:hep-ph/0105302

404. A. Ali, E. Lunghi, A.Y. Parkhomenko, Phys. Lett. B **595**, 323 (2004). arXiv:hep-ph/0405075

405. S.W. Bosch, G. Buchalla, Nucl. Phys. B **621**, 459 (2002). arXiv:hep-ph/0106081

406. T. Becher, R.J. Hill, M. Neubert, Phys. Rev. D **72**, 094017 (2005). arXiv:hep-ph/0503263

407. D. Atwood, M. Gronau, A. Soni, Phys. Rev. Lett. **79**, 185 (1997). arXiv:hep-ph/9704272

408. B. Grinstein, Y. Grossman, Z. Ligeti, D. Pirjol, Phys. Rev. D **71**, 011504 (2005). arXiv:hep-ph/0412019

409. B. Grinstein, D. Pirjol, Phys. Rev. D **73**, 014013 (2006). arXiv:hep-ph/0510104

410. A.L. Kagan, M. Neubert, Phys. Lett. B **539**, 227 (2002). arXiv:hep-ph/0110078

411. C. Sachrajda, T. Vladikas, private communication

412. R. Zwicky, in preparation

413. A. Khodjamirian, Nucl. Phys. B **605**, 558 (2001). arXiv:hep-ph/0012271

414. P. Ciafaloni, A. Romanino, A. Strumia, Nucl. Phys. B **524**, 361 (1998). arXiv:hep-ph/9710312

415. F.M. Borzumati, C. Greub, Phys. Rev. D **58**, 074004 (1998). arXiv:hep-ph/9802391

416. S. Bertolini, F. Borzumati, A. Masiero, G. Ridolfi, Nucl. Phys. B **353**, 591 (1991)

417. R. Barbieri, G.F. Giudice, Phys. Lett. B **309**, 86 (1993). arXiv:hep-ph/9303270

418. N. Oshimo, Nucl. Phys. B **404**, 20 (1993)

419. M.A. Diaz, Phys. Lett. B **304**, 278 (1993). arXiv:hep-ph/9303280

420. Y. Okada, Phys. Lett. B **315**, 119 (1993). arXiv:hep-ph/9307249

421. R. Garisto, J.N. Ng, Phys. Lett. B **315**, 372 (1993). arXiv:hep-ph/9307301

422. F. Borzumati, Z. Phys. C **63**, 291 (1994). arXiv:hep-ph/9310212

423. V.D. Barger et al., Phys. Rev. D **51**, 2438 (1995). arXiv:hep-ph/9407273

424. F. Borzumati, C. Greub, T. Hurth, D. Wyler, Phys. Rev. D **62**, 075005 (2000). arXiv:hep-ph/9911245

425. C. Bobeth, M. Misiak, J. Urban, Nucl. Phys. B **567**, 153 (2000). arXiv:hep-ph/9904413

426. F. Borzumati, C. Greub, Y. Yamada, Phys. Rev. D **69**, 055005 (2004). arXiv:hep-ph/0311151

427. G. Degrassi, P. Gambino, P. Slavich, Phys. Lett. B **635**, 335 (2006). arXiv:hep-ph/0601135

428. M.E. Gomez et al., Phys. Rev. D **74**, 015015 (2006). arXiv:hep-ph/0601163

429. K.i. Okumura, L. Roszkowski, Phys. Rev. Lett. **92**, 161801 (2004). arXiv:hep-ph/0208101

430. K. Agashe, N.G. Deshpande, G.H. Wu, Phys. Lett. B **514**, 309 (2001). arXiv:hep-ph/0105084

431. C.S. Kim, J.D. Kim, J.h. Song, Phys. Rev. D **67**, 015001 (2003). arXiv:hep-ph/0204002

432. K. Agashe, G. Perez, A. Soni, Phys. Rev. Lett. **93**, 201804 (2004). arXiv:hep-ph/0406101

433. K. Agashe, G. Perez, A. Soni, Phys. Rev. D **71**, 016002 (2005). arXiv:hep-ph/0408134

434. A. Ali, E. Lunghi, C. Greub, G. Hiller, Phys. Rev. D **66**, 034002 (2002). arXiv:hep-ph/0112300

435. G. Hiller, F. Kruger, Phys. Rev. D **69**, 074020 (2004). arXiv:hep-ph/0310219

436. G. Belanger, F. Boudjema, A. Pukhov, A. Semenov, Comput. Phys. Commun. **174**, 577 (2006). arXiv:hep-ph/0405253

437. A. Djouadi, J.L. Kneur, G. Moultaka, arXiv:hep-ph/0211331

438. S. Heinemeyer, W. Hollik, G. Weiglein, Comput. Phys. Commun. **124**, 76 (2000). arXiv:hep-ph/9812320

439. K. Abe et al. (Belle Collaboration), Phys. Lett. B **511**, 151 (2001). arXiv:hep-ex/0103042

440. M. Nakao et al. (Belle Collaboration), Phys. Rev. D **69**, 112001 (2004). arXiv:hep-ex/0402042

441. S. Nishida et al. (Belle Collaboration), Phys. Rev. Lett. **93**, 031803 (2004). arXiv:hep-ex/0308038

442. Y. Ushiroda et al. (Belle Collaboration), Phys. Rev. D **74**, 111104 (2006). arXiv:hep-ex/0608017

443. Y. Ushiroda et al., Phys. Rev. Lett. **94**, 231601 (2005). arXiv:hep-ex/0503008

444. B. Aubert et al. (BaBar Collaboration), Phys. Rev. D **72**, 052004 (2005). arXiv:hep-ex/0508004

445. B. Aubert et al. (BaBar Collaboration), Phys. Rev. Lett. **97**, 171803 (2006). arXiv:hep-ex/0607071

446. B. Aubert et al. (BaBar Collaboration), arXiv:0708.1652 [hep-ex]

447. B. Aubert et al. (BaBar Collaboration), Phys. Rev. Lett. **96**, 221801 (2006). arXiv:hep-ex/0601046

448. B. Aubert et al. (BaBar Collaboration), Phys. Rev. D **73**, 012006 (2006). arXiv:hep-ex/0509040

449. B. Aubert et al. (BaBar Collaboration), Phys. Rev. Lett. **93**, 021804 (2004). arXiv:hep-ex/0403035

450. B. Aubert et al. (BaBar Collaboration), Phys. Rev. D **70**, 112006 (2004). arXiv:hep-ex/0407003

451. B. Aubert et al. (BaBar Collaboration), Phys. Rev. D **75**, 051102 (2007). arXiv:hep-ex/0611037

452. B. Aubert et al. (BaBar Collaboration), Phys. Rev. D **72**, 051103 (2005). arXiv:hep-ex/0507038

453. I. Belyaev (LHCb Collaboration), Acta Phys. Pol. B **38**, 905 (2007), LHCb note LHCb-2005-001,2005

454. L. Shchutska, I. Belyaev, A. Golutvin, LHCb Public note LHCb-2007-030, 2007

455. S. Viret, F. Ohlsson-Malek, M. Smizanska ATLAS-PHYS-PUB-2005-006, 2004
456. F. Legger, LHCb Public note LHCb-2006-012, 2006
457. F. Legger, LHCb Public note LHCb-2006-013, 2006
458. G. Hiller et al., arXiv:hep-ph/0702191
459. H.H. Asatryan, H.M. Asatrian, C. Greub, M. Walker, Phys. Rev. D **65**, 074004 (2002). arXiv:hep-ph/0109140
460. H.H. Asatryan, H.M. Asatrian, C. Greub, M. Walker, Phys. Lett. B **507**, 162 (2001). arXiv:hep-ph/0103087
461. A. Ghinculov, T. Hurth, G. Isidori, Y.P. Yao, Nucl. Phys. B **648**, 254 (2003). arXiv:hep-ph/0208088
462. H.M. Asatrian, K. Bieri, C. Greub, A. Hovhannisyan, Phys. Rev. D **66**, 094013 (2002). arXiv:hep-ph/0209006
463. A. Ghinculov, T. Hurth, G. Isidori, Y.P. Yao, Nucl. Phys. B **685**, 351 (2004). arXiv:hep-ph/0312128
464. P. Gambino, M. Gorbahn, U. Haisch, Nucl. Phys. B **673**, 238 (2003). arXiv:hep-ph/0306079
465. C. Bobeth, P. Gambino, M. Gorbahn, U. Haisch, J. High Energy Phys. **0404**, 071 (2004). arXiv:hep-ph/0312090
466. G. Buchalla, G. Isidori, Nucl. Phys. B **525**, 333 (1998). arXiv:hep-ph/9801456
467. A. Ali, G. Hiller, L.T. Handoko, T. Morozumi, Phys. Rev. D **55**, 4105 (1997). arXiv:hep-ph/9609449
468. C.W. Bauer, C.N. Burrell, Phys. Lett. B **469**, 248 (1999). arXiv:hep-ph/9907517
469. C.W. Bauer, C.N. Burrell, Phys. Rev. D **62**, 114028 (2000). arXiv:hep-ph/9911404
470. Z. Ligeti, F.J. Tackmann, Phys. Lett. B **653**, 404 (2007). arXiv:0707.1694 [hep-ph]
471. H.H. Asatryan, H.M. Asatrian, C. Greub, M. Walker, Phys. Rev. D **66**, 034009 (2002). arXiv:hep-ph/0204341
472. H.M. Asatrian, H.H. Asatryan, A. Hovhannisyan, V. Poghosyan, Mod. Phys. Lett. A **19**, 603 (2004). arXiv:hep-ph/0311187
473. T. Huber, E. Lunghi, M. Misiak, D. Wyler, Nucl. Phys. B **740**, 105 (2006). arXiv:hep-ph/0512066
474. T. Huber, T. Hurth, E. Lunghi, arXiv:0712.3009 [hep-ph]
475. K.S.M. Lee, Z. Ligeti, I.W. Stewart, F.J. Tackmann, Phys. Rev. D **75**, 034016 (2007). arXiv:hep-ph/0612156
476. F. Krüger, J. Matias, Phys. Rev. D **71**, 094009 (2005). arXiv:hep-ph/0502060
477. E. Lunghi, J. Matias, J. High Energy Phys. **0704**, 058 (2007). arXiv:hep-ph/0612166
478. M. Beneke, T. Feldmann, D. Seidel, Nucl. Phys. B **612**, 25 (2001). arXiv:hep-ph/0106067
479. A. Ali, G. Kramer, G.h. Zhu, Eur. Phys. J. C **47**, 625 (2006). arXiv:hep-ph/0601034
480. B. Grinstein, D. Pirjol, Phys. Rev. D **70**, 114005 (2004). arXiv:hep-ph/0404250
481. G. Burdman, Phys. Rev. D **57**, 4254 (1998). arXiv:hep-ph/9710550
482. A. Ali, P. Ball, L.T. Handoko, G. Hiller, Phys. Rev. D **61**, 074024 (2000). arXiv:hep-ph/9910221
483. P. Ball, V.M. Braun, Phys. Rev. D **58**, 094016 (1998). arXiv:hep-ph/9805422
484. B. Grinstein, D. Pirjol, Phys. Rev. D **73**, 094027 (2006). arXiv:hep-ph/0505155
485. G. Hiller, A. Kagan, Phys. Rev. D **65**, 074038 (2002). arXiv:hep-ph/0108074
486. C.H. Chen, C.Q. Geng, Phys. Rev. D **64**, 074001 (2001). arXiv:hep-ph/0106193
487. T.M. Aliev, A. Ozpineci, M. Savci, Phys. Rev. D **67**, 035007 (2003). arXiv:hep-ph/0211447
488. T.M. Aliev, A. Ozpineci, M. Savci, Nucl. Phys. B **649**, 168 (2003). arXiv:hep-ph/0202120
489. A.K. Giri, R. Mohanta, J. Phys. G **31**, 1559 (2005)
490. G. Turan, J. Phys. G **31**, 525 (2005)
491. T.M. Aliev, M. Savci, J. Phys. G **26**, 997 (2000) arXiv:hep-ph/9906473
492. G. Turan, J. High Energy Phys. **0505**, 008 (2005)
493. A.K. Giri, R. Mohanta, Eur. Phys. J. C **45**, 151 (2006). arXiv:hep-ph/0510171
494. C.H. Chen, C.Q. Geng, J.N. Ng, Phys. Rev. D **65**, 091502 (2002). arXiv:hep-ph/0202103
495. T.M. Aliev, M. Savci, J. High Energy Phys. **0605**, 001 (2006). arXiv:hep-ph/0507324
496. M.B. Voloshin, Phys. Lett. B **397**, 275 (1997)
497. J.W. Chen, G. Rupak, M.J. Savage, Phys. Lett. B **410**, 285 (1997)
498. F. Krüger, L.M. Sehgal, Phys. Lett. B **380**, 199 (1996)
499. K. Abe et al. (Belle Collaboration), Belle-CONF-0415. arXiv:hep-ex/0410006
500. A. Ishikawa et al., Phys. Rev. Lett. **96**, 251801 (2006). arXiv:hep-ex/0603018
501. B. Aubert et al. (BaBar Collaboration), Phys. Rev. D **73**, 092001 (2006). arXiv:hep-ex/0604007
502. E. Barberio et al. (Heavy Flavor Averaging Group (HFAG)), arXiv:hep-ex/0603003
503. Q.S. Yan, C.S. Huang, W. Liao, S.H. Zhu, Phys. Rev. D **62**, 094023 (2000). arXiv:hep-ph/0004262
504. K.S.M. Lee, I.W. Stewart, Phys. Rev. D **74**, 014005 (2006). arXiv:hep-ph/0511334
505. K.S.M. Lee, Z. Ligeti, I.W. Stewart, F.J. Tackmann, Phys. Rev. D **74**, 011501 (2006). arXiv:hep-ph/0512191
506. A. Ishikawa, in *6th Workshop on a Higher Luminosity B Factory*, KEK, Tsukuba, Japan, 16–18 November 2004
507. J. Hewett et al., SLAC-R-709. arXiv:hep-ph/0503261
508. J. Dickens, V. Gibson, C. Lazzeroni, M. Patel, LHCb Public note, LHCb-2007-038
509. J. Dickens, V. Gibson, C. Lazzeroni, M. Patel, LHCb Public note, LHCb-2007-039
510. U. Egede, LHCb Public note, LHCb-2007-057
511. A. Rimoldi, A. Dell'Acqua, eConf **C0303241**, TUMT001 (2003). arXiv:physics/0306086
512. M. Smizanska, CERN ATLAS Communication Note, ATL-COM-PHYS-2003-038
513. D.J. Lange, Nucl. Instrum. Methods A **462**, 152 (2001)
514. M. Smizanska, J. Catmore, CERN ATLAS Communication Note, ATL-COM-PHYS-2004-041
515. D. Melikhov, N. Nikitin, S. Simula, Phys. Rev. D **57**, 6814 (1998). arXiv:hep-ph/9711362
516. T. Sjostrand, L. Lonnblad, S. Mrenna, P. Skands, arXiv:hep-ph/0308153
517. ATLAS Collaboration, CERN-LHCC-97-16
518. ATLAS Collaboration, CERN-LHCC-2003-022
519. T. Lagouri, N. Kanaya, A. Krasznahorkay, CERN ATLAS Communication Note, ATL-COM-PHYS-2006-007
520. J. Marriner, CDF Internal Note 2724, 1994
521. A. Policicchio, G. Crosetti, CERN ATLAS Communication Note, ATL-COM-PHYS-2007-005
522. G. Hiller, eConf **C030603**, MAR02 (2003). arXiv:hep-ph/0308180
523. Y. Dincer, L.M. Sehgal, Phys. Lett. B **521**, 7 (2001). arXiv:hep-ph/0108144
524. A. Dedes, J.R. Ellis, M. Raidal, Phys. Lett. B **549**, 159 (2002). arXiv:hep-ph/0209207
525. T. Fujihara, S.K. Kang, C.S. Kim, D. Kimura, T. Morozumi, Phys. Rev. D **73**, 074011 (2006). arXiv:hep-ph/0512010
526. G. Buchalla, G. Hiller, G. Isidori, Phys. Rev. D **63**, 014015 (2001). arXiv:hep-ph/0006136
527. T. Becher, S. Braig, M. Neubert, A.L. Kagan, Phys. Lett. B **540**, 278 (2002). arXiv:hep-ph/0205274

484

Eur. Phys. J. C (2008) 57: 309–492

528. C. Bobeth, T. Ewerth, F. Kruger, J. Urban, Phys. Rev. D **64**, 074014 (2001). arXiv:hep-ph/0104284

529. C. Bobeth, T. Ewerth, F. Kruger, J. Urban, Phys. Rev. D **66**, 074021 (2002). arXiv:hep-ph/0204225

530. C.S. Huang, W. Liao, Phys. Lett. B **525**, 107 (2002). arXiv:hep-ph/0011089

531. A. Dedes, A. Pilaftsis, Phys. Rev. D **67**, 015012 (2003). arXiv:hep-ph/0209306

532. P.H. Chankowski, J. Kalinowski, Z. Was, M. Worek, Nucl. Phys. B **713**, 555 (2005). arXiv:hep-ph/0412253

533. K. Abe et al. (Belle Collaboration), arXiv:hep-ex/0508009

534. T.M. Aliev, C.S. Kim, Y.G. Kim, Phys. Rev. D **62**, 014026 (2000). arXiv:hep-ph/9910501

535. C. Bobeth, G. Hiller, G. Piranishvili, J. High Energy Phys. **0712**, 040 (2007). arXiv:0709.4174 [hep-ph]

536. D.A. Demir, K.A. Olive, M.B. Voloshin, Phys. Rev. D **66**, 034015 (2002). arXiv:hep-ph/0204119

537. S.R. Choudhury, A.S. Cornell, N. Gaur, G.C. Joshi, Phys. Rev. D **69**, 054018 (2004). arXiv:hep-ph/0307276

538. A.S. Cornell, N. Gaur, S.K. Singh, arXiv:hep-ph/0505136

539. T. Feldmann, J. Matias, J. High Energy Phys. **0301**, 074 (2003). arXiv:hep-ph/0212158

540. G. Hiller, Phys. Rev. D **70**, 034018 (2004). arXiv:hep-ph/0404220

541. R.E. Marshak, Riazuddin, C.P. Ryan, *Theory of Weak Interactions in Particle Physics* (Wiley, New York, 1969)

542. Y. Grossman, Z. Ligeti, E. Nardi, Nucl. Phys. B **465**, 369 (1996). [Erratum: Nucl. Phys. B **480**, 756 (1996)]. arXiv:hep-ph/9510378

543. B. Aubert et al. (BaBar Collaboration), arXiv:hep-ex/0608019

544. A. Masiero, P. Paradisi, R. Petronzio, Phys. Rev. D **74**, 011701 (2006). arXiv:hep-ph/0511289

545. P. Colangelo, F. De Fazio, P. Santorelli, E. Scrimieri, Phys. Lett. B **395**, 339 (1997). arXiv:hep-ph/9610297

546. D. Melikhov, N. Nikitin, S. Simula, Phys. Lett. B **428**, 171 (1998). arXiv:hep-ph/9803269

547. A.F. Falk, B. Grinstein, Nucl. Phys. B **416**, 771 (1994). arXiv:hep-ph/9306310

548. T.M. Aliev, C.S. Kim, Phys. Rev. D **58**, 013003 (1998). arXiv:hep-ph/9710428

549. C.S. Kim, Y.G. Kim, T. Morozumi, Phys. Rev. D **60**, 094007 (1999). arXiv:hep-ph/9905528

550. Z. Ligeti, M.B. Wise, Phys. Rev. D **53**, 4937 (1996). arXiv:hep-ph/9512225

551. K. Abe et al. (Belle Collaboration), arXiv:hep-ex/0507034

552. K. Abe et al. (Belle Collaboration), arXiv:hep-ex/0608047

553. B. Aubert et al. (BaBar Collaboration), Phys. Rev. Lett. **94**, 101801 (2005). arXiv:hep-ex/0411061

554. N. Satoyama et al. (Belle Collaboration), arXiv:hep-ex/0611045

555. BaBar Collaboration, B. Aubert et al., arXiv:hep-ex/0607110

556. G. Buchalla, A.J. Buras, Nucl. Phys. B **400**, 225 (1993)

557. M. Misiak, J. Urban, Phys. Lett. B **451**, 161 (1999). arXiv:hep-ph/9901278

558. G. Buchalla, A.J. Buras, Nucl. Phys. B **548**, 309 (1999). arXiv:hep-ph/9901288

559. A.J. Buras, Phys. Lett. B **566**, 115 (2003). arXiv:hep-ph/0303060

560. J.F. Gunion, H.E. Haber, G.L. Kane, S. Dawson, arXiv:hep-ph/9302272

561. H.E. Logan, U. Nierste, Nucl. Phys. B **586**, 39 (2000). arXiv:hep-ph/0004139

562. P.H. Chankowski, L. Slawianowska, Phys. Rev. D **63**, 054012 (2001). arXiv:hep-ph/0008046

563. G. Isidori, A. Retico, J. High Energy Phys. **0209**, 063 (2002). arXiv:hep-ph/0208159

564. A. Dedes, H.K. Dreiner, U. Nierste, Phys. Rev. Lett. **87**, 251804 (2001). arXiv:hep-ph/0108037

565. H.P. Nilles, Phys. Lett. B **115**, 193 (1982)

566. H.P. Nilles, Nucl. Phys. B **217**, 366 (1983)

567. A. Chamseddine, R. Arnowitt, P. Nath, Phys. Rev. Lett. **49**, 970 (1982)

568. R. Barbieri, S. Ferrara, C. Savoy, Phys. Lett. B **119**, 343 (1982)

569. L. Hall, J. Lykken, S. Weinberg, Phys. Rev. D **27**, 2359 (1983)

570. S.K. Soni, H.A. Weldon, Phys. Lett. B **126**, 215 (1983)

571. J.R. Ellis, K.A. Olive, V.C. Spanos, Phys. Lett. B **624**, 47 (2005). arXiv:hep-ph/0504196

572. J.R. Ellis, K.A. Olive, Y. Santoso, V.C. Spanos, J. High Energy Phys. **0605**, 063 (2006). arXiv:hep-ph/0603136

573. R. Dermisek, S. Raby, L. Roszkowski, R. Ruiz De Austri, J. High Energy Phys. **0304**, 037 (2003). arXiv:hep-ph/0304101

574. R. Dermisek, S. Raby, L. Roszkowski, R. Ruiz de Austri, J. High Energy Phys. **0509**, 029 (2005). arXiv:hep-ph/0507233

575. A.G. Akeroyd, S. Recksiegel, J. Phys. G **29**, 2311 (2003). arXiv:hep-ph/0306037

576. G. Valencia, S. Willenbrock, Phys. Rev. D **50**, 6843 (1994). arXiv:hep-ph/9409201

577. B. Aubert et al. (BaBar Collaboration), Phys. Rev. Lett. **94**, 221803 (2005). arXiv:hep-ex/0408096

578. B. Aubert et al. (BaBar Collaboration), Phys. Rev. Lett. **96**, 241802 (2006). arXiv:hep-ex/0511015

579. D0 Collaboration, D0-NOTE-CONF-5344-2007

580. CDF-Run II Collaboration, CDF-PUBLIC-NOTE-8176

581. R.P. Bernhard, arXiv:hep-ex/0605065

582. A. Abulencia et al. (CDF Collaboration), Phys. Rev. Lett. **95**, 221805 (2005) [Erratum: Phys. Rev. Lett. **95**, 249905 (2005)]. arXiv:hep-ex/0508036

583. V.M. Abazov et al. (D0 Collaboration), Phys. Rev. Lett. **94**, 071802 (2005). arXiv:hep-ex/0410039

584. D. Acosta et al. (CDF Collaboration), Phys. Rev. Lett. **93**, 032001 (2004). arXiv:hep-ex/0403032

585. F. Abe et al. (CDF Collaboration), Phys. Rev. D **57**, 3811 (1998)

586. M. Acciarri et al. (L3 Collaboration), Phys. Lett. B **391**, 474 (1997)

587. M.C. Chang et al. (Belle Collaboration), Phys. Rev. D **68**, 111101 (2003). arXiv:hep-ex/0309069

588. T. Bergfeld et al. (CLEO Collaboration), Phys. Rev. D **62**, 091102 (2000). arXiv:hep-ex/0007042

589. B. Abbott et al. (D0 Collaboration), Phys. Lett. B **423**, 419 (1998). arXiv:hep-ex/9801027

590. C. Albajar et al. (UA1 Collaboration), Phys. Lett. B **262**, 163 (1991)

591. H. Albrecht et al. (ARGUS Collaboration), Phys. Lett. B **199**, 451 (1987)

592. P. Avery et al. (CLEO Collaboration), Phys. Lett. B **183**, 429 (1987)

593. R. Antunes-Nobrega et al. (LHCb Collaboration), CERN-LHCC-2003-031

594. N. Panikashvili (ATLAS Collaboration), Nucl. Phys. Proc. Suppl. **156**, 129 (2006)

595. CMS Collaboration, CERN-LHCC-2002-026

596. N. Nikitin et al., Nucl. Phys. Proc. Suppl. **156**, 119 (2006)

597. C. Eggel, U. Langenegger, A. Starodumov, CMS-CR-2006-071

598. D. Martinez, J.A. Hernando, F. Teubert, LHCb Public note, CERN-LHCb-2007-033

599. A. Nikitenko, A. Starodumov, N. Stepanov, arXiv:hep-ph/9907256

600. ATLAS Collaboration, CERN-LHCC-99-15, ATLAS-TDR-15

601. N. Nikitin, S. Sivoklokov, M. Smizanska, D. Tlisov, K. Toms, ATL-COM-PHYS-2006-086

602. N. Nikitin, P. Reznicek, S. Sivoklokov, M. Smizanska, K. Toms, Nucl. Phys. Proc. Suppl. **163**, 147 (2007)

603. H. Boos, T. Mannel, J. Reuter, Phys. Rev. D **70**, 036006 (2004). arXiv:hep-ph/0403085

604. M. Ciuchini, M. Pierini, L. Silvestrini, Phys. Rev. Lett. **95**, 221804 (2005). arXiv:hep-ph/0507290

605. M. Gronau, J. Zupan, Phys. Rev. D **71**, 074017 (2005)

606. B. Aubert et al. (BaBar Collaboration), Phys. Rev. Lett. **87**, 091801 (2001). arXiv:hep-ex/0107013

607. K. Abe et al. (Belle Collaboration), Phys. Rev. Lett. **87**, 091802 (2001). arXiv:hep-ex/0107061

608. B. Aubert et al. (BaBar Collaboration), arXiv:hep-ex/0607107

609. K.-F. Chen et al. (Belle Collaboration), arXiv:hep-ex/0608039

610. B. Aubert et al. (BaBar Collaboration), Phys. Rev. Lett. **87**, 241801 (2001). arXiv:hep-ex/0107049

611. I. Dunietz, H.R. Quinn, A. Snyder, W. Toki, H.J. Lipkin, Phys. Rev. D **43**, 2193 (1991)

612. A. Bondar, T. Gershon, P. Krokovny, Phys. Lett. B **624**, 1 (2005). arXiv:hep-ph/0503174

613. B. Aubert et al. (BaBar Collaboration), Phys. Rev. D **71**, 032005 (2005). arXiv:hep-ex/0411016

614. R. Itoh et al. (Belle Collaboration), Phys. Rev. Lett. **95**, 091601 (2005). arXiv:hep-ex/0504030

615. B. Aubert et al. (BaBar Collaboration), arXiv:hep-ex/0607105

616. P. Krokovny et al. (Belle Collaboration), Phys. Rev. Lett. **97**, 081801 (2006)

617. Y. Grossman, H.R. Quinn, Phys. Rev. D **58**, 017504 (1998). arXiv:hep-ph/9712306

618. B. Aubert et al. (BaBar Collaboration), Phys. Rev. Lett. **95**, 041805 (2005). arXiv:hep-ex/0503049

619. K. Abe et al. (Belle Collaboration), arXiv:hep-ex/0507039

620. B. Aubert et al. (BaBar Collaboration), arXiv:hep-ex/0607106

621. K. Abe (Belle Collaboration), arXiv:hep-ex/0608035

622. B. Aubert et al. (BaBar Collaboration), arXiv:hep-ex/0607097

623. A.E. Snyder, H.R. Quinn, Phys. Rev. D **48**, 2139 (1993)

624. B. Aubert et al. (BaBar Collaboration), arXiv:hep-ex/0608002

625. K. Abe et al. (Belle Collaboration), arXiv:hep-ex/0609003

626. B. Aubert et al. (BaBar Collaboration), arXiv:hep-ex/0408099

627. I.I.Y. Bigi, A.I. Sanda, Phys. Lett. B **211**, 213 (1988)

628. A.B. Carter, A.I. Sanda, Phys. Rev. Lett. **45**, 952 (1980)

629. M. Gronau, Phys. Lett. B **557**, 198 (2003). arXiv:hep-ph/0211282

630. D. Atwood, A. Soni, Phys. Rev. D **71**, 013007 (2005). arXiv:hep-ph/0312100

631. Y. Grossman, A. Soffer, J. Zupan, Phys. Rev. D **72**, 031501 (2005)

632. M. Gronau, D. London, Phys. Lett. B **253**, 483 (1991)

633. M. Gronau, D. Wyler, Phys. Lett. B **265**, 172 (1991)

634. M. Gronau, Phys. Rev. D **58**, 037301 (1998). arXiv:hep-ph/9802315

635. D. Atwood, I. Dunietz, A. Soni, Phys. Rev. Lett. **78**, 3257 (1997). arXiv:hep-ph/9612433

636. D. Atwood, I. Dunietz, A. Soni, Phys. Rev. D **63**, 036005 (2001). arXiv:hep-ph/0008090

637. A. Giri, Y. Grossman, A. Soffer, J. Zupan, Phys. Rev. D **68**, 054018 (2003). arXiv:hep-ph/0303187

638. A. Bondar, in *Proceedings of BINP Special Analysis Meeting on Dalitz*, 24–26 September 2002, unpublished

639. A. Poluektov et al. (Belle Collaboration), Phys. Rev. D **73**, 112009 (2006)

640. B. Aubert et al. (BaBar Collaboration), arXiv:hep-ex/0607104

641. B. Aubert et al. (BaBar Collaboration), Phys. Rev. Lett. **95**, 121802 (2005)

642. H. Muramatsu et al. (CLEO Collaboration), Phys. Rev. Lett. **89**, 251802 (2002) [Erratum: Phys. Rev. Lett. **90**, 059901 (2003)]. arXiv:hep-ex/0207067

643. G.J. Feldman, R.D. Cousins, Phys. Rev. D **57**, 3873 (1998). arXiv:physics/9711021

644. D. Atwood, A. Soni, Phys. Rev. D **68**, 033009 (2003). arXiv:hep-ph/0206045

645. D. Atwood, A. Soni, Phys. Rev. D **68**, 033003 (2003)

646. D. Asner, talk given at the 3rd Workshop on the CKM Unitarity Triangle (CKM2005). ckm2005.ucsd.edu/WG/WG5/thu3/Asner-WG5-S4.pdf

647. B. Kayser, D. London, Phys. Rev. D **61**, 116013 (2000). arXiv:hep-ph/9909561

648. A. Bondar, A. Poluektov, Eur. Phys. J. C **47**, 347 (2006)

649. O. Long, M. Baak, R.N. Cahn, D. Kirkby, Phys. Rev. D **68**, 034010 (2003). arXiv:hep-ex/0303030

650. B. Aubert et al. (BaBar Collaboration), Phys. Rev. D **71**, 112003 (2005). arXiv:hep-ex/0504035

651. B. Aubert et al. (BaBar Collaboration), Phys. Rev. D **73**, 111101 (2006). arXiv:hep-ex/0602049

652. F.J. Ronga et al. (Belle Collaboration), Phys. Rev. D **73**, 092003 (2006). arXiv:hep-ex/0604013

653. I. Dunietz, Phys. Lett. B **427**, 179 (1998). arXiv:hep-ph/9712401

654. O. Deschamps, F. Machefert, S. Monteil, P. Perret, P. Robbe, A. Robert, M.-H. Schune, LHCb Public note, LHCb-2007-046

655. P.F. Harrison, H.R. Quinn (eds.), *The BaBar Physics Book*, SLAC-R-504 (1998), Sect. 6.5

656. M. Patel, LHCb Public note, LHCb-2006-066

657. M. Patel, LHCb Public note, LHCb-2007-043

658. V. Gibson, C. Lazzeroni, J. Libby, LHCb Public note, LHCb-2007-048

659. A. Powell, LHCb Public note, LHCb-2007-004

660. K. Akiba, M. Gandelman, Decays, LHCb Public note, HCb-2007-050

661. J. Rademacker, G. Wilkinson, Phys. Lett. B **647**, 400 (2007). arXiv:hep-ph/0611272

662. S. Cohen, M. Merk, E. Rodrigues, LHCb Public note, LHCb-2007-041

663. R. Fleischer, Nucl. Phys. B **671**, 459 (2003). arXiv:hep-ph/0304027

664. V.V. Gligorov, LHCb Public note, LHCb-2007-044

665. G. Wilkinson, LHCb Public note, LHCb-2005-036

666. S. Amato, M. Gandelman, C. Gobel, L. de Paula, LHCb Public note, LHCb-2007-045

667. V. Abazov (D0 Collaboration), arXiv:hep-ex/0701007

668. V.M. Abazov et al. (D0 Collaboration), Phys. Rev. D **74**, 092001 (2006). arXiv:hep-ex/0609014

669. D. Buskulic et al. (ALEPH Collaboration), Phys. Lett. B **377**, 205 (1996)

670. F. Abe et al. (CDF Collaboration), Phys. Rev. D **59**, 032004 (1999). arXiv:hep-ex/9808003

671. P. Abreu et al. (DELPHI Collaboration), Eur. Phys. J. C **16**, 555 (2000). arXiv:hep-ex/0107077

672. K. Ackerstaff et al. (OPAL Collaboration), Phys. Lett. B **426**, 161 (1998). arXiv:hep-ex/9802002

673. V.M. Abazov et al. (D0 Collaboration), Phys. Rev. Lett. **97**, 241801 (2006). arXiv:hep-ex/0604046

674. A.S. Dighe, I. Dunietz, R. Fleischer, Eur. Phys. J. C **6**, 647 (1999). arXiv:hep-ex/9804253

675. D. Acosta et al. (CDF Collaboration), Phys. Rev. Lett. **94**, 101803 (2005). arXiv:hep-ex/0412057

676. V.M. Abazov et al. (D0 Collaboration), Phys. Rev. Lett. **98**, 121801 (2007). arXiv:hep-ex/0701012

677. A. Abulencia et al. (CDF-Run II Collaboration), Phys. Rev. Lett. **97**, 062003 (2006) [AIP Conf. Proc. **870**, 116 (2006)]. arXiv:hep-ex/0606027

678. Y. Grossman, Y. Nir, G. Raz, Phys. Rev. Lett. **97**, 151801 (2006). arXiv:hep-ph/0605028

679. V.M. Abazov et al. (D0 Collaboration), Phys. Rev. D **76**, 057101 (2007). arXiv:hep-ex/0702030

486

Eur. Phys. J. C (2008) 57: 309–492

680. J. Borel, L. Nicolas, O. Schneider, J. Van Hunen, LHCb Public note, LHCb-2007-017
681. P. Vankov, G. Raven, LHCb Public note, LHCb-2007-055
682. G. Balbi, V.M. Vagnoni, S. Vecchi, LHCb Public note, LHCb-2007-032
683. G. Balbi, S. Vecchi, LHCb Public note, LHCb-2007-056
684. M. Calvi, O. Leroy, M. Musy, LHCb Public note, LHCb-2007-058
685. L. Fernández, EPFL Ph. D. thesis 3613, CERN-THESIS-2006-042
686. L. Fernández, in *Physics at LHC*, Cracow, Poland, LHCb Public note, LHCb-2006-047. Acta Phys. Pol. B **38**, 931 (2007)
687. D. Volyanskyy, J. van Tilburg, LHCb Public note, LHCb-2006-027
688. S. Jimenez-Otero, EPFL PhD thesis 3779, CERN-THESIS-2007-051
689. U. Nierste, arXiv:hep-ph/0406300
690. O. Leroy, F. Muheim, S. Poss, Y. Xie, LHCb Public note, LHCb-2007-029
691. N. Brook, N. Cottingham, R.W. Lambert, F. Muheim, J. Rademacker, P. Szczypka, Y. Xie, LHCb Public note, LHCb-2007-054
692. V.V. Gligorov, J. Rademacker, LHCb Public note, LHCb-2007-053
693. J. Rademacker, Nucl. Instrum. Methods **570**, 525 (2007). arXiv:hep-ex/0502042
694. V. Ciulli et al., CMS NOTE-2006/090
695. CMS Collaboration, The TriDAS project technical design report, vol. 2: Data acquisition and high-level trigger, CERN/LHCC 2002-26, CMS TDR 6.2, 2002
696. CMS Collaboration, CMS physics technical design report, vol. I: Detector performance and software, CERN/LHCC 2006-001, CMS TDR 8.1, 2006
697. I. Dunietz, R. Fleischer, U. Nierste, Phys. Rev. D **63**, 114015 (2001). arXiv:hep-ph/0012219
698. S. Dambach, U. Langenegger, A. Starodumov, Nucl. Instrum. Methods A **569**, 824 (2006). arXiv:hep-ph/0607294
699. A. Starodumov, Z. Xie, B_s decay vertex resolution, CMS NOTE 1997/85
700. ATLAS Collaboration, ATLAS: Detector and physics performance technical design report, vol. 1, CERN-LHCC-99-14
701. A.J. Buras, M. Jamin, P.H. Weisz, Nucl. Phys. B **347**, 491 (1990)
702. M. Beneke, G. Buchalla, C. Greub, A. Lenz, U. Nierste, Phys. Lett. B **459**, 631 (1999). arXiv:hep-ph/9808385
703. M. Beneke, G. Buchalla, A. Lenz, U. Nierste, Phys. Lett. B **576**, 173 (2003). arXiv:hep-ph/0307344
704. M. Ciuchini, E. Franco, V. Lubicz, F. Mescia, C. Tarantino, J. High Energy Phys. **0308**, 031 (2003). arXiv:hep-ph/0308029
705. V. Gimenez, J. Reyes, Nucl. Phys. Proc. Suppl. **94**, 350 (2001). arXiv:hep-lat/0010048
706. S. Hashimoto, K.I. Ishikawa, T. Onogi, M. Sakamoto, N. Tsutsui, N. Yamada, Phys. Rev. D **62**, 114502 (2000). arXiv:hep-lat/0004022
707. S. Aoki et al. (JLQCD Collaboration), Phys. Rev. D **67**, 014506 (2003). arXiv:hep-lat/0208038
708. D. Becirevic, D. Meloni, A. Retico, V. Gimenez, V. Lubicz, G. Martinelli, Eur. Phys. J. C **18**, 157 (2000). arXiv:hep-ph/0006135
709. L. Lellouch, C.J. Lin (UKQCD Collaboration), Phys. Rev. D **64**, 094501 (2001). arXiv:hep-ph/0011086
710. N. Yamada et al. (JLQCD Collaboration), Nucl. Phys. Proc. Suppl. **106**, 397 (2002). arXiv:hep-lat/0110087
711. M. Beneke, G. Buchalla, I. Dunietz, Phys. Rev. D **54**, 4419 (1996). arXiv:hep-ph/9605259
712. A. Lenz, U. Nierste, J. High Energy Phys. **0706**, 072 (2007). arXiv:hep-ph/0612167
713. C. Tarantino, arXiv:hep-ph/0702235
714. Z. Ligeti, M. Papucci, G. Perez, Phys. Rev. Lett. **97**, 101801 (2006). arXiv:hep-ph/0604112
715. P. Ball, R. Fleischer, Eur. Phys. J. C **48**, 413 (2006). arXiv:hep-ph/0604249
716. M. Rescigno, private communication
717. R. Fleischer, Phys. Lett. B **365**, 399 (1996). arXiv:hep-ph/9509204
718. Y. Grossman, M.P. Worah, Phys. Lett. B **395**, 241 (1997). arXiv:hep-ph/9612269
719. R. Fleischer, Int. J. Mod. Phys. A **12**, 2459 (1997). arXiv:hep-ph/9612446
720. M. Ciuchini, E. Franco, G. Martinelli, A. Masiero, L. Silvestrini, Phys. Rev. Lett. **79**, 978 (1997). arXiv:hep-ph/9704274
721. D. London, A. Soni, Phys. Lett. B **407**, 61 (1997). arXiv:hep-ph/9704277
722. G. Buchalla, G. Hiller, Y. Nir, G. Raz, J. High Energy Phys. **0509**, 074 (2005). arXiv:hep-ph/0503151
723. M. Beneke, Phys. Lett. B **620**, 143 (2005). arXiv:hep-ph/0505075
724. H.Y. Cheng, C.K. Chua, A. Soni, Phys. Rev. D **72**, 014006 (2005). arXiv:hep-ph/0502235
725. H.N. Li, S. Mishima, Phys. Rev. D **74**, 094020 (2006). arXiv:hep-ph/0608277
726. H.Y. Cheng, C.K. Chua, A. Soni, Phys. Rev. D **72**, 094003 (2005). arXiv:hep-ph/0506268
727. H.J. Lipkin, Y. Nir, H.R. Quinn, A. Snyder, Phys. Rev. D **44**, 1454 (1991)
728. T. Gershon, M. Hazumi, Phys. Lett. B **596**, 163 (2004). arXiv:hep-ph/0402097
729. Y. Grossman, Z. Ligeti, Y. Nir, H. Quinn, Phys. Rev. D **68**, 015004 (2003). arXiv:hep-ph/0303171
730. K. Abe et al. (Belle Collaboration), arXiv:hep-ex/0208030
731. M. Gronau, J.L. Rosner, Phys. Lett. B **564**, 90 (2003). arXiv:hep-ph/0304178
732. K. Abe et al. (Belle Collaboration), arXiv:hep-ex/0609006
733. M. Gronau, J.L. Rosner, Phys. Rev. D **72**, 094031 (2005). arXiv:hep-ph/0509155
734. B. Aubert et al. (BaBar Collaboration), arXiv:hep-ex/0507016
735. B. Aubert et al. (BaBar Collaboration), arXiv:hep-ex/0607108
736. G. Engelhard, G. Raz, Phys. Rev. D **72**, 114017 (2005). arXiv:hep-ph/0508046
737. G. Engelhard, Y. Nir, G. Raz, Phys. Rev. D **72**, 075013 (2005). arXiv:hep-ph/0505194
738. C.K. Chua, in *The Proceedings of 4th Flavor Physics and CP Violation Conference (FPCP 2006)*, Vancouver, BC, Canada, 9–12 April 2006, p. 008. arXiv:hep-ph/0605301
739. B. Aubert et al. (BaBar Collaboration0, arXiv:hep-ex/0607112
740. M. Ciuchini, M. Pierini, L. Silvestrini, Phys. Rev. D **74**, 051301 (2006). arXiv:hep-ph/0601233
741. M. Ciuchini, M. Pierini, L. Silvestrini, arXiv:hep-ph/0602207
742. M. Gronau, D. Pirjol, A. Soni, J. Zupan, arXiv:hep-ph/0608243
743. B. Grinstein, R.F. Lebed, Phys. Rev. D **53**, 6344 (1996). arXiv:hep-ph/9602218
744. M.J. Savage, M.B. Wise, Phys. Rev. D **39**, 3346 (1989) [Erratum: Phys. Rev. D **40**, 3127 (1989)]
745. L.L. Chau, H.Y. Cheng, W.K. Sze, H. Yao, B. Tseng, Phys. Rev. D **43**, 2176 (1991) [Erratum: Phys. Rev. D **58**, 019902 (1998)]
746. M. Gronau, O.F. Hernandez, D. London, J.L. Rosner, Phys. Rev. D **50**, 4529 (1994). arXiv:hep-ph/9404283
747. M. Gronau, O.F. Hernandez, D. London, J.L. Rosner, Phys. Rev. D **52**, 6356 (1995). arXiv:hep-ph/9504326
748. M. Gronau, O.F. Hernandez, D. London, J.L. Rosner, Phys. Rev. D **52**, 6374 (1995). arXiv:hep-ph/9504327

Eur. Phys. J. C (2008) 57: 309–492

487

749. A.S. Dighe, M. Gronau, J.L. Rosner, Phys. Lett. B **367**, 357 (1996) [Erratum: Phys. Lett. B **377**, 325 (1996)]. arXiv:hep-ph/9509428

750. A.S. Dighe, M. Gronau, J.L. Rosner, Phys. Rev. D **57**, 1783 (1998). arXiv:hep-ph/9709223

751. C.W. Bauer, D. Pirjol, Phys. Lett. B **604**, 183 (2004). arXiv:hep-ph/0408161

752. C.W. Chiang, J.L. Rosner, Phys. Rev. D **65**, 074035 (2002) [Erratum: Phys. Rev. D **68**, 039902 (2003)]. arXiv:hep-ph/0112285

753. C.W. Chiang, M. Gronau, J.L. Rosner, Phys. Rev. D **68**, 074012 (2003). arXiv:hep-ph/0306021

754. C.W. Chiang, M. Gronau, Z. Luo, J.L. Rosner, D.A. Suprun, Phys. Rev. D **69**, 034001 (2004). arXiv:hep-ph/0307395

755. C.W. Chiang, M. Gronau, J.L. Rosner, D.A. Suprun, Phys. Rev. D **70**, 034020 (2004). arXiv:hep-ph/0404073

756. C.W. Chiang, Y.F. Zhou, arXiv:hep-ph/0609128

757. Y.F. Zhou, Y.L. Wu, J.N. Ng, C.Q. Geng, Phys. Rev. D **63**, 054011 (2001). arXiv:hep-ph/0006225

758. X.G. He, Y.K. Hsiao, J.Q. Shi, Y.L. Wu, Y.F. Zhou, Phys. Rev. D **64**, 034002 (2001). arXiv:hep-ph/0011337

759. Y.L. Wu, Y.F. Zhou, Eur. Phys. J. direct C **5**, 014 (2003) [Eur. Phys. J. C **32S1**, 179 (2004)]. arXiv:hep-ph/0210367

760. Y.L. Wu, Y.F. Zhou, Phys. Rev. D **71**, 021701 (2005). arXiv:hep-ph/0409221

761. Y.L. Wu, Y.F. Zhou, Phys. Rev. D **72**, 034037 (2005). arXiv:hep-ph/0503077

762. M. Neubert, J.L. Rosner, Phys. Lett. B **441**, 403 (1998). arXiv:hep-ph/9808493

763. M. Neubert, J.L. Rosner, Phys. Rev. Lett. **81**, 5076 (1998). arXiv:hep-ph/9809311

764. M. Neubert, J. High Energy Phys. **9902**, 014 (1999). arXiv:hep-ph/9812396

765. M. Gronau, D. Pirjol, T.M. Yan, Phys. Rev. D **60**, 034021 (1999) [Erratum: Phys. Rev. D **69**, 119901 (2004)]. arXiv:hep-ph/9810482

766. C.W. Bauer, I.Z. Rothstein, I.W. Stewart, Phys. Rev. D **74**, 034010 (2006). arXiv:hep-ph/0510241

767. M. Gronau, J.L. Rosner, arXiv:hep-ph/0610227

768. X.Q. Hao, X.G. He, X.Q. Li, arXiv:hep-ph/0609264

769. M. Gronau, J.L. Rosner, Phys. Rev. D **58**, 113005 (1998). arXiv:hep-ph/9806348

770. A.J. Buras, R. Fleischer, S. Recksiegel, F. Schwab, Eur. Phys. J. C **45**, 701 (2006). arXiv:hep-ph/0512032

771. R. Fleischer, Phys. Lett. B **459**, 306 (1999). arXiv:hep-ph/9903456

772. R. Fleischer, Eur. Phys. J. C **52**, 267 (2007). arXiv:0705.1121 [hep-ph]

773. R. Fleischer, J. Matias, Phys. Rev. D **61**, 074004 (2000). arXiv:hep-ph/9906274

774. R. Fleischer, J. Matias, Phys. Rev. D **66**, 054009 (2002). arXiv:hep-ph/0204101

775. D. London, J. Matias, J. Virto, Phys. Rev. D **71**, 014024 (2005). arXiv:hep-ph/0410011

776. M. Gronau, Phys. Lett. B **492**, 297 (2000). arXiv:hep-ph/0008292

777. D. Tonelli (CDF Collaboration), PoS **HEP2005**, 258 (2006). arXiv:hep-ex/0512024

778. R. Fleischer, S. Recksiegel, F. Schwab, Eur. Phys. J. C **51**, 55 (2007). arXiv:hep-ph/0702275

779. A.J. Buras, R. Fleischer, S. Recksiegel, F. Schwab, Acta Phys. Pol. B **36**, 2015 (2005). arXiv:hep-ph/0410407

780. A.J. Buras, R. Fleischer, S. Recksiegel, F. Schwab, Nucl. Phys. B **697**, 133 (2004). arXiv:hep-ph/0402112

781. A.J. Buras, R. Fleischer, S. Recksiegel, F. Schwab, Phys. Rev. Lett. **92**, 101804 (2004). arXiv:hep-ph/0312259

782. A. Soni, D.A. Suprun, arXiv:hep-ph/0609089

783. A. Soni, D.A. Suprun, Phys. Lett. B **635**, 330 (2006). arXiv:hep-ph/0511012

784. M. Gronau, J.L. Rosner, J. Zupan, Phys. Rev. D **74**, 093003 (2006). arXiv:hep-ph/0608085

785. M. Gronau, J.L. Rosner, J. Zupan, Phys. Lett. B **596**, 107 (2004). arXiv:hep-ph/0403287

786. M. Gronau, Y. Grossman, J.L. Rosner, Phys. Lett. B **579**, 331 (2004). arXiv:hep-ph/0310020

787. M. Gronau, J.L. Rosner, Phys. Rev. D **71**, 074019 (2005). arXiv:hep-ph/0503131

788. G. Raz, arXiv:hep-ph/0509125

789. M. Gronau, J.L. Rosner, Phys. Rev. D **59**, 113002 (1999). arXiv:hep-ph/9809384

790. H.J. Lipkin, Phys. Lett. B **445**, 403 (1999). arXiv:hep-ph/9810351

791. M. Gronau, J.L. Rosner, Phys. Rev. D **65**, 013004 (2002) [Erratum: Phys. Rev. D **65**, 079901 (2002)]. arXiv:hep-ph/0109238

792. M. Gronau, Y. Grossman, G. Raz, J.L. Rosner, Phys. Lett. B **635**, 207 (2006). arXiv:hep-ph/0601129

793. M. Gronau, Phys. Lett. B **627**, 82 (2005). arXiv:hep-ph/0508047

794. S. Baek, D. London, J. Matias, J. Virto, J. High Energy Phys. **0602**, 027 (2006). arXiv:hep-ph/0511295

795. A.S. Safir, J. High Energy Phys. **0409**, 053 (2004). arXiv:hep-ph/0407015

796. S. Descotes-Genon, J. Matias, J. Virto, Phys. Rev. Lett. **97**, 061801 (2006). arXiv:hep-ph/0603239

797. S. Descotes-Genon, J. Matias, J. Virto, Phys. Rev. D **76**, 074005 (2007). arXiv:0705.0477 [hep-ph]

798. S. Baek, D. London, J. Matias, J. Virto, arXiv:hep-ph/0610109

799. A.J. Buras, L. Silvestrini, Nucl. Phys. B **569**, 3 (2000). arXiv:hep-ph/9812392

800. M. Ciuchini, E. Franco, G. Martinelli, L. Silvestrini, Nucl. Phys. B **501**, 271 (1997). arXiv:hep-ph/9703353

801. M. Ciuchini, E. Franco, G. Martinelli, M. Pierini, L. Silvestrini, Phys. Lett. B **515**, 33 (2001). arXiv:hep-ph/0104126

802. M. Ciuchini, M. Pierini, L. Silvestrini, arXiv:hep-ph/0703137

803. M. Ciuchini et al., in preparation

804. R. Barbieri, A. Strumia, Nucl. Phys. B **508**, 3 (1997). arXiv:hep-ph/9704402

805. A.L. Kagan, M. Neubert, Phys. Rev. D **58**, 094012 (1998). arXiv:hep-ph/9803368

806. S.A. Abel, W.N. Cottingham, I.B. Whittingham, Phys. Rev. D **58**, 073006 (1998). arXiv:hep-ph/9803401

807. A. Kagan, arXiv:hep-ph/9806266

808. R. Fleischer, T. Mannel, Phys. Lett. B **511**, 240 (2001). arXiv:hep-ph/0103121

809. E. Lunghi, D. Wyler, Phys. Lett. B **521**, 320 (2001). arXiv:hep-ph/0109149

810. M.B. Causse, arXiv:hep-ph/0207070

811. G. Hiller, Phys. Rev. D **66**, 071502 (2002). arXiv:hep-ph/0207356

812. S. Khalil, E. Kou, Phys. Rev. D **67**, 055009 (2003). arXiv:hep-ph/0212023

813. S. Baek, Phys. Rev. D **67**, 096004 (2003). arXiv:hep-ph/0301269

814. K. Agashe, C.D. Carone, Phys. Rev. D **68**, 035017 (2003). arXiv:hep-ph/0304229

815. J.F. Cheng, C.S. Huang, X.h. Wu, Phys. Lett. B **585**, 287 (2004). arXiv:hep-ph/0306086

816. D. Chakraverty, E. Gabrielli, K. Huitu, S. Khalil, Phys. Rev. D **68**, 095004 (2003). arXiv:hep-ph/0306076

817. S. Khalil, E. Kou, Phys. Rev. Lett. **91**, 241602 (2003). arXiv:hep-ph/0303214

488

Eur. Phys. J. C (2008) 57: 309–492

818. S. Khalil, E. Kou, in *The Proceedings of 2nd Workshop on the CKM Unitarity Triangle*, Durham, England, 5–9 April 2003, p. WG305. arXiv:hep-ph/0307024

819. J.F. Cheng, C.S. Huang, X.H. Wu, Nucl. Phys. B **701**, 54 (2004). arXiv:hep-ph/0404055

820. S. Khalil, E. Kou, Phys. Rev. D **71**, 114016 (2005). arXiv:hep-ph/0407284

821. E. Gabrielli, K. Huitu, S. Khalil, Nucl. Phys. B **710**, 139 (2005). arXiv:hep-ph/0407291

822. S. Khalil, Mod. Phys. Lett. A **19**, 2745 (2004) [Afr. J. Math. Phys. **1**, 101 (2004)]. arXiv:hep-ph/0411151

823. S. Khalil, Phys. Rev. D **72**, 035007 (2005). arXiv:hep-ph/0505151

824. M. Ciuchini et al., in preparation

825. M. Ciuchini, Nucl. Phys. Proc. Suppl. B **109**, 307 (2002). arXiv:hep-ph/0112133

826. A.L. Kagan, arXiv:hep-ph/0407076

827. M. Endo, S. Mishima, M. Yamaguchi, Phys. Lett. B **609**, 95 (2005). arXiv:hep-ph/0409245

828. J.A. Casas, S. Dimopoulos, Phys. Lett. B **387**, 107 (1996). arXiv:hep-ph/9606237

829. B. Aubert et al. (BaBar Collaboration), arXiv:hep-ex/0508017

830. B. Aubert et al. (BaBar Collaboration), arXiv:hep-ex/0607101

831. B. Aubert et al. (BaBar Collaboration), arXiv:hep-ex/0607096

832. B. Aubert et al. (BaBar Collaboration), Phys. Rev. Lett. **98**, 031801 (2007). arXiv:hep-ex/0609052

833. B. Aubert et al. (BaBar Collaboration), Phys. Rev. Lett. **97**, 171805 (2006). arXiv:hep-ex/0608036

834. M. Raidal, Phys. Rev. Lett. **89**, 231803 (2002). arXiv:hep-ph/0208091

835. S. Amato, J. McCarron, F. Muheim, B. Souza de Paula, Y. Xie, LHCb Public note, LHCb-2007-047

836. Y. Xie, LHCb Public note, LHCb-2007-130

837. A.G. Akeroyd et al., Physics at super-*B* factory, to be posted on hep-ex

838. M. Hazumi, Contribution to ICHEP 2006

839. S. Hashimoto et al., Letter of intent for KEK super *B* factory, KEK-REPORT-2004-4

840. B. Aubert et al. (BaBar Collaboration), Phys. Rev. D **74**, 051106 (2006). arXiv:hep-ex/0607063

841. BaBar Collaboration, Phys. Rev. D **73**, 071102 (2006)

842. B. Aubert et al. (BaBar Collaboration), Phys. Rev. Lett. **98**, 051802 (2007). arXiv:hep-ex/0607109

843. Belle Collaboration, arXiv:hep-ex/0608034

844. B. Aubert et al. (BaBar Collaboration), arXiv:hep-ex/0607098

845. Belle Collaboration, Phys. Rev. Lett. **96**, 171801 (2006)

846. BaBar Collaboration, arXiv:hep-ex/0610073

847. Belle Collaboration, Phys. Rev. Lett. **94**, 221804 (2005)

848. BaBar Collaboration, arXiv:hep-ex/0607057

849. Belle Collaboration, arXiv:hep-ex/0505039

850. A. Datta, D. London, Int. J. Mod. Phys. A **19**, 2505 (2004)

851. D. London, N. Sinha, R. Sinha, Phys. Rev. D **69**, 114013 (2004)

852. C.-D. Lu, Y.-L. Shen, W. Wang, arXiv:hep-ph/0606092

853. BaBar Collaboration, Phys. Rev. D **74**, 031104 (2006)

854. A. Abulencia et al. (CDF Collaboration), Phys. Rev. Lett. **97**, 211802 (2006). arXiv:hep-ex/0607021

855. A. Carbone, J. Nardulli, S. Pennazzi, A. Sarti, V. Vagnoni, LHCb Public note, CERN-LHCb-2007-059

856. O. Leitner, Z.J. Ajaltouni, Nucl. Phys. Proc. Suppl. **174**, 169 (2007). arXiv:hep-ph/0610189

857. G. Buchalla, A.J. Buras, Phys. Rev. D **54**, 6782 (1996). arXiv:hep-ph/9607447

858. A.J. Buras, F. Schwab, S. Uhlig, arXiv:hep-ph/0405132

859. G. Isidori, in *The Proceedings of 4th Flavor Physics and CP Violation Conference (FPCP 2006)*, Vancouver, BC, Canada, 9–12 April 2006, p. 035. arXiv:hep-ph/0606047

860. D. Bryman, A.J. Buras, G. Isidori, L. Littenberg, Int. J. Mod. Phys. A **21**, 487 (2006). arXiv:hep-ph/0505171

861. W.J. Marciano, Z. Parsa, Phys. Rev. D **53**, 1 (1996)

862. F. Mescia, C. Smith, Phys. Rev. D **76**, 034017 (2007). arXiv:0705.2025 [hep-ph]

863. A.J. Buras, M. Gorbahn, U. Haisch, U. Nierste, Phys. Rev. Lett. **95**, 261805 (2005). arXiv:hep-ph/0508165

864. A.J. Buras, M. Gorbahn, U. Haisch, U. Nierste, J. High Energy Phys. **0611**, 002 (2006). arXiv:hep-ph/0603079

865. G. Isidori, F. Mescia, C. Smith, Nucl. Phys. B **718**, 319 (2005). arXiv:hep-ph/0503107

866. A.J. Buras, A. Romanino, L. Silvestrini, Nucl. Phys. B **520**, 3 (1998). arXiv:hep-ph/9712398

867. V.V. Anisimovsky et al. (E949 Collaboration), Phys. Rev. Lett. **93**, 031801 (2004). arXiv:hep-ex/0403036

868. S. Adler et al. (E787 Collaboration), Phys. Rev. Lett. **88**, 041803 (2002). arXiv:hep-ex/0111091

869. S. Adler et al. (E787 Collaboration), Phys. Rev. Lett. **79**, 2204 (1997). arXiv:hep-ex/9708031

870. Y. Grossman, Y. Nir, Phys. Lett. B **398**, 163 (1997). arXiv:hep-ph/9701313

871. G. Buchalla, G. D'Ambrosio, G. Isidori, Nucl. Phys. B **672**, 387 (2003). arXiv:hep-ph/0308008

872. G. Isidori, C. Smith, R. Unterdorfer, Eur. Phys. J. C **36**, 57 (2004). arXiv:hep-ph/0404127

873. U. Haisch, in *Proceedings of KAON International Conference*, Laboratori Nazionali di Frascati dell'INFN, Rome, Italy, 21–25 May 2007. arXiv:0707.3098 [hep-ph]

874. C. Tarantino, in *Proceedings of KAON International Conference*, Laboratori Nazionali di Frascati dell'INFN, Rome, Italy, 21–25 May 2007. arXiv:0706.3436 [hep-ph]

875. C. Smith, in *Proceedings of KAON International Conference*, Laboratori Nazionali di Frascati dell'INFN, Rome, Italy, 21–25 May 2007. arXiv:0707.2309 [hep-ph]

876. J.K. Ahn et al. (E391a Collaboration), arXiv:0712.4164 [hep-ex]

877. A. Alavi-Harati et al. (KTeV Collaboration), Phys. Rev. Lett. **93**, 021805 (2004). arXiv:hep-ex/0309072

878. A. Alavi-Harati et al. (KTeV Collaboration), Phys. Rev. Lett. **84**, 5279 (2000). arXiv:hep-ex/0001006

879. G. Isidori, F. Mescia, P. Paradisi, C. Smith, S. Trine, J. High Energy Phys. **0608**, 064 (2006). arXiv:hep-ph/0604074

880. G. Buchalla, G. Isidori, Phys. Lett. B **440**, 170 (1998). arXiv:hep-ph/9806501

881. G. Isidori, G. Martinelli, P. Turchetti, Phys. Lett. B **633**, 75 (2006). arXiv:hep-lat/0506026

882. A.J. Buras, M.E. Lautenbacher, M. Misiak, M. Munz, Nucl. Phys. B **423**, 349 (1994). arXiv:hep-ph/9402347

883. G. D'Ambrosio, G. Ecker, G. Isidori, J. Portoles, J. High Energy Phys. **9808**, 004 (1998). arXiv:hep-ph/9808289

884. S. Friot, D. Greynat, E. De Rafael, Phys. Lett. B **595**, 301 (2004). arXiv:hep-ph/0404136

885. J.R. Batley et al. (NA48/1 Collaboration), Phys. Lett. B **576**, 43 (2003). arXiv:hep-ex/0309075

886. J.R. Batley et al. (NA48/1 Collaboration), Phys. Lett. B **599**, 197 (2004). arXiv:hep-ex/0409011

887. F. Mescia, C. Smith, S. Trine, J. High Energy Phys. **0608**, 088 (2006). arXiv:hep-ph/0606081

888. M. Gorbahn, U. Haisch, Phys. Rev. Lett. **97**, 122002 (2006). arXiv:hep-ph/0605203

889. G. Isidori, R. Unterdorfer, J. High Energy Phys. **0401**, 009 (2004). arXiv:hep-ph/0311084

890. J.M. Gerard, C. Smith, S. Trine, Nucl. Phys. B **730**, 1 (2005). arXiv:hep-ph/0508189

891. M. Blanke, A.J. Buras, D. Guadagnoli, C. Tarantino, J. High Energy Phys. **0610**, 003 (2006). arXiv:hep-ph/0604057

892. G. Buchalla, A.J. Buras, Phys. Lett. B **333**, 221 (1994). arXiv:hep-ph/9405259

893. A.J. Buras, R. Fleischer, Phys. Rev. D **64**, 115010 (2001). arXiv:hep-ph/0104238

894. Y. Nir, M.P. Worah, Phys. Lett. B **423**, 319 (1998). arXiv:hep-ph/9711215

895. G. Colangelo, G. Isidori, J. High Energy Phys. **9809**, 009 (1998). arXiv:hep-ph/9808487

896. G. Isidori, P. Paradisi, Phys. Rev. D **73**, 055017 (2006). arXiv:hep-ph/0601094

897. T. Moroi, Phys. Lett. B **493**, 366 (2000). arXiv:hep-ph/0007328

898. D. Chang, A. Masiero, H. Murayama, Phys. Rev. D **67**, 075013 (2003). arXiv:hep-ph/0205111

899. P.L. Cho, M. Misiak, D. Wyler, Phys. Rev. D **54**, 3329 (1996). arXiv:hep-ph/9601360

900. S. Davidson, D.C. Bailey, B.A. Campbell, Z. Phys. C **61**, 613 (1994). arXiv:hep-ph/9309310

901. R. Barbier et al., arXiv:hep-ph/9810232

902. Y. Grossman, G. Isidori, H. Murayama, Phys. Lett. B **588**, 74 (2004). arXiv:hep-ph/0311353

903. A. Deandrea, J. Welzel, M. Oertel, J. High Energy Phys. **0410**, 038 (2004). arXiv:hep-ph/0407216

904. N.G. Deshpande, D.K. Ghosh, X.G. He, Phys. Rev. D **70**, 093003 (2004). arXiv:hep-ph/0407021

905. G. Anelli et al., CERN-SPSC-2005-013, SPSC-P-326, 11/06/2005

906. G. Unal (NA48 Collaboration), Frascati Phys. Ser. **21**, 361 (2001). arXiv:hep-ex/0012011

907. http://j-parc.jp/index-e.html

908. http://j-parc.jp/NuclPart/PAC_for_NuclPart.html

909. The J-PARC proposals, including the kaon experiments. Available from http://j-parc.jp/NuclPart/Proposal_0606_e.html

910. I.I.Y. Bigi, Y.L. Dokshitzer, V.A. Khoze, J.H. Kuhn, P.M. Zerwas, Phys. Lett. B **181**, 157 (1986)

911. G. Burdman, E. Golowich, J. Hewett, S. Pakvasa, Phys. Rev. D **66**, 014009 (2002)

912. S. Bianco, F.L. Fabbri, D. Benson, I. Bigi, Riv. Nuovo Cimento **26**(N7), 1 (2003)

913. G. Burdman, I. Shipsey, Annu. Rev. Nucl. Part. Sci. **53**, 431 (2003)

914. A.A. Petrov, eConf **C030603**, MEC05 (2003). arXiv:hep-ph/0311371

915. H.N. Nelson, in *Proceedings of the 19th International Symposium on Photon and Lepton Interactions at High Energy LP99*, ed. by J.A. Jaros, M.E. Peskin. arXiv:hep-ex/9908021

916. A. Datta, D. Kumbhakar, Z. Phys. C **27**, 515 (1985)

917. A.A. Petrov, Phys. Rev. D **56**, 1685 (1997)

918. K. Abe et al. (Belle Collaboration), Phys. Rev. D **72**, 071101 (2005)

919. C. Cawlfield et al.(CLEO Collaboration), Phys. Rev. D **71**, 077101 (2005)

920. B. Aubert et al. (BaBar Collaboration), Phys. Rev. D **70**, 091102 (2004)

921. M. Hosack (FOCUS Collaboration), Fermilab-Thesis-2002-25 (2002)

922. E.M. Aitala et al. (E791 Collaboration), Phys. Rev. Lett. **77**, 2384 (1996)

923. I.I.Y. Bigi, in *Proceedings of the XXXIII International Conference on High Energy Physics*, Berkeley, CA, USA, 1986, SLAC-PUB-4074

924. G. Blaylock, A. Seiden, Y. Nir, Phys. Lett. B **355**, 555 (1995)

925. S. Bergmann, Y. Grossman, Z. Ligeti, Y. Nir, A.A. Petrov, Phys. Lett. B **486**, 418 (2000)

926. L. Zhang et al. (Belle Collaboration), Phys. Rev. Lett. **96**, 151801 (2006)

927. J. Li et al. (Belle Collaboration), Phys. Rev. Lett. **94**, 071801 (2005)

928. J.M. Link et al. (FOCUS Collaboration), Phys. Lett. B **618**, 23 (2005)

929. B. Aubert et al. (BaBar Collaboration), Phys. Rev. Lett. **91**, 171801 (2003)

930. R. Godang et al. (CLEO Collaboration), Phys. Rev. Lett. **84**, 5038 (2000)

931. E.M. Aitala et al. (E791 Collaboration), Phys. Rev. D **57**, 13 (1998)

932. R. Barate et al. (ALEPH Collaboration), Phys. Lett. B **436**, 211 (1998)

933. B. Aubert et al. (BaBar Collaboration), Phys. Rev. Lett. **98**, 211802 (2007)

934. A. Abulencia et al. (CDF Collaboration), Phys. Rev. D **74**, 031109 (2006)

935. P. Spradlin, G. Wilkinson, F. Xing, LHCb Public note, LHCb-2007-049

936. W.M. Yao et al. (Particle Data Group), J. Phys. G **33**, 1 (2006), review by D. Asner on pp. 713–716

937. E.M. Aitala et al. (E791 Collaboration), Phys. Lett. B **403**, 377 (1997)

938. J.M. Link et al. (FOCUS Collaboration), Phys. Lett. B **491**, 232 (2000) [Erratum: Phys. Lett. B **495**, 443 (2000)]

939. B. Aubert et al. (BaBar Collaboration), Phys. Rev. D **71**, 091101 (2005)

940. S. Malvezzi, AIP Conf. Proc. **549**, 569 (2002)

941. S. Kopp et al. (CLEO Collaboration), Phys. Rev. D **63**, 092001 (2001)

942. G. Brandenburg et al. (CLEO Collaboration), Phys. Rev. Lett. **87**, 071802 (2001)

943. D.M. Asner et al. (CLEO Collaboration), Phys. Rev. D **70**, 091101 (2004)

944. D. Cronin-Hennessy et al. (CLEO Collaboration), Phys. Rev. D **72**, 031102 (2005)

945. I.I.Y. Bigi, A.I. Sanda, Camb. Monogr. Part. Phys. Nucl. Phys. Cosmol. **9**, 1 (2000)

946. X.C. Tian et al. (Belle Collaboration), Phys. Rev. Lett. **95**, 231801 (2005)

947. S.A. Dytman et al. (CLEO Collaboration), Phys. Rev. D **64**, 111101 (2001)

948. B. Aubert et al. (BaBar Collaboration), Phys. Rev. Lett. **97**, 221803 (2006)

949. D.M. Asner et al. (CLEO Collaboration), Phys. Rev. D **72**, 012001 (2005)

950. K. Abe et al. (Belle Collaboration), Phys. Rev. Lett. **99**, 131803 (2007)

951. B. Aubert et al. (BaBar Collaboration), Phys. Rev. Lett. **91**, 121801 (2003)

952. K. Abe et al. (Belle Collaboration), arXiv:hep-ex/0308034

953. K. Abe et al. (Belle Collaboration), Phys. Rev. Lett. **88**, 162001 (2002)

954. S.E. Csorna et al. (CLEO Collaboration), Phys. Rev. D **65**, 092001 (2002)

955. J.M. Link et al. (FOCUS Collaboration), Phys. Lett. B **485**, 62 (2000)

956. E.M. Aitala et al. (E791 Collaboration), Phys. Rev. Lett. **83**, 32 (1999)

957. M. Staric et al. (Belle Collaboration), Phys. Rev. Lett. **98**, 211803 (2007)

958. I.I.Y. Bigi, in *Tau Charm Factory Workshop*, Stanford, CA, 23–27 May 1989, UND-HEP-89-BIG01

959. D. Atwood, A.A. Petrov, Phys. Rev. D **71**, 054032 (2005)

960. D.M. Asner, W.M. Sun, Phys. Rev. D **73**, 034024 (2006)

961. D.M. Asner et al. (CLEO Collaboration), Int. J. Mod. Phys. A **21**, 5456 (2006)

962. A.F. Falk, Y. Grossman, Z. Ligeti, A.A. Petrov, Phys. Rev. D **65**, 054034 (2002)

490

Eur. Phys. J. C (2008) 57: 309–492

963. A.F. Falk, Y. Grossman, Z. Ligeti, Y. Nir, A.A. Petrov, Phys. Rev. D **69**, 114021 (2004)
964. I.I.Y. Bigi, N.G. Uraltsev, Nucl. Phys. B **592**, 92 (2001)
965. E. Golowich, S. Pakvasa, A.A. Petrov, arXiv:hep-ph/0610039
966. K. Abe et al. (Belle Collaboration), Phys. Rev. D **73**, 051106 (2006)
967. M. Saigo et al. (Belle Collaboration), Phys. Rev. Lett. **94**, 091601 (2005)
968. F. Buccella, M. Lusignoli, G. Miele, A. Pugliese, P. Santorelli, Phys. Rev. D **51**, 3478 (1995)
969. J.M. Link et al. (FOCUS Collaboration), Phys. Lett. B **622**, 239 (2005)
970. L.M. Sehgal, M. Wanninger, Phys. Rev. D **46**, 1035 (1992) [Erratum: Phys. Rev. D **46**, 5209 (1992)]
971. D. Acosta et al. (CDF Collaboration), Phys. Rev. Lett. **94**, 122001 (2005)
972. G. Burdman, E. Golowich, J.L. Hewett, S. Pakvasa, Phys. Rev. D **52**, 6383 (1995)
973. C. Greub, T. Hurth, M. Misiak, D. Wyler, Phys. Lett. B **382**, 415 (1996)
974. Q. Ho-Kim, X.Y. Pham, Phys. Rev. D **61**, 013008 (2000)
975. S. Prelovsek, D. Wyler, Phys. Lett. B **500**, 304 (2001)
976. S. Fajfer, S. Prelovsek, P. Singer, Phys. Rev. D **64**, 098502 (2001)
977. S. Fajfer, P. Singer, J. Zupan, Eur. Phys. J. C **27**, 201 (2003)
978. Q. He et al. (CLEO Collaboration), Phys. Rev. Lett. **95**, 221802 (2005)
979. B. Aubert (BaBar Collaboration), arXiv:hep-ex/0607051
980. S. Fajfer, S. Prelovsek, arXiv:hep-ph/0610032
981. S. Prelovsek, PhD thesis. arXiv:hep-ph/0010106
982. S. Fajfer, S. Prelovsek, P. Singer, D. Wyler, Phys. Lett. B **487**, 81 (2000)
983. S. Fajfer, S. Prelovsek, P. Singer, Eur. Phys. J. C **6**, 471 (1999)
984. S. Fajfer, S. Prelovsek, P. Singer, Phys. Rev. D **58**, 094038 (1998)
985. T.E. Coan et al. (CLEO Collaboration), Phys. Rev. Lett. **90**, 101801 (2003)
986. J.M. Link et al. (FOCUS Collaboration), Phys. Lett. B **572**, 21 (2003)
987. A. Korn (CDF Collaboration), arXiv:hep-ex/0305054
988. E.M. Aitala et al. (E791 Collaboration), Phys. Lett. B **462**, 401 (1999)
989. K. Kodama et al. (E653 Collaboration), Phys. Lett. B **345**, 85 (1995)
990. A. Freyberger et al. (CLEO Collaboration), Phys. Rev. Lett. **76**, 3065 (1996) [Erratum: Phys. Rev. Lett. **77**, 2147 (1996)]
991. P.L. Frabetti et al. (E687 Collaboration), Phys. Lett. B **398**, 239 (1997)
992. M. Artuso, Int. J, Mod. Phys. A **21**, 1697 (2006) arXiv:hep-ex/0510052
993. D. Asner, arXiv:hep-ex/0410014 (expanded version of review in Eidelman et al., Phys. Lett. B **592**, 1 (2004), pp. 664–667)
994. Y. Grossman, Z. Ligeti, A. Soffer, Phys. Rev. D **67**, 071301 (2003)
995. J.L. Rosner, D.A. Suprun, Phys. Rev. D **68**, 054010 (2003)
996. C. Cawlfield et al. (CLEO Collaboration), Phys. Rev. D **74**, 031108 (2006)
997. A. Bondar, in *The Proceedings of the BINP Special Analysis Meeting on Dalitz Analysis*, 24–26 September, 2002, unpublished
998. A. Bondar, A. Poluektov, in *Proceedings of the CKM 2006 Workshop*
999. B. Grinstein, Phys. Rev. Lett. **71**, 3067 (1993)
1000. D. Silverman, H. Yao, Phys. Rev. D **38**, 214 (1988)
1001. A.G. Akeroyd, Prog. Theor. Phys. **111**, 295 (2004). arXiv:hep-ph/0308260
1002. J.L. Hewett, arXiv:hep-ph/9505246
1003. G. Bonvicini et al. (CLEO Collaboration), Phys. Rev. D **70**, 112004 (2004)
1004. P. Rubin et al. (CLEO Collaboration), Phys. Rev. D **73**, 112005 (2006)
1005. M. Chadha et al. (CLEO Collaboration), Phys. Rev. D **58**, 032002 (1998)
1006. Yu. Alexandrov et al. (BEATRICE Collaboration), Phys. Lett. B **478**, 31 (2000)
1007. A. Heister et al. (ALEPH Collaboration), Phys. Lett. B **528**, 1 (2002)
1008. G. Abbiendi et al. (OPAL Collaboration), Phys. Lett. B **516**, 236 (2001)
1009. M. Acciarri et al. (L3 Collaboration), Phys. Lett. B **396**, 327 (1997)
1010. T.W. Chiu, T.H. Hsieh, J.Y. Lee, P.H. Liu, H.J. Chang, Phys. Lett. B **624**, 31 (2005)
1011. D. Becirevic, P. Boucaud, J.P. Leroy, V. Lubicz, G. Martinelli, F. Mescia, F. Rapuano, Phys. Rev. D **60**, 074501 (1999)
1012. J. Bordes, J. Penarrocha, K. Schilcher, J. High Energy Phys. **0511**, 014 (2005)
1013. S. Narison, arXiv:hep-ph/0202200
1014. D. Ebert, R.N. Faustov, V.O. Galkin, Phys. Lett. B **635**, 93 (2006)
1015. G. Cvetic, C.S. Kim, G.L. Wang, W. Namgung, Phys. Lett. B **596**, 84 (2004)
1016. Z.G. Wang, W.M. Yang, S.L. Wan, Nucl. Phys. A **744**, 156 (2004)
1017. L.A.M. Salcedo, J.P.B. de Melo, D. Hadjmichef, T. Frederico, Braz. J. Phys. **34**, 297 (2004)
1018. J.F. Amundson, J.L. Rosner, M.A. Kelly, N. Horwitz, S.L. Stone, Phys. Rev. D **47**, 3059 (1993)
1019. N.E. Adam et al. (CLEO Collaboration), Phys. Rev. Lett. **97**, 251801 (2006)
1020. M. Ablikim et al. (BES Collaboration), Phys. Lett. B **608**, 24 (2005)
1021. T.E. Coan et al. (CLEO Collaboration), Phys. Rev. Lett. **95**, 181802 (2005)
1022. G.S. Huang et al. (CLEO Collaboration), Phys. Rev. Lett. **95**, 181801 (2005)
1023. Y. Gao, Talk given at ICHEP 2006, Moscow, Russia, August 2006
1024. J.M. Link et al. (FOCUS Collaboration), Phys. Lett. B **535**, 43 (2002)
1025. M.R. Shepherd et al., Phys. Rev. D **74**, 052001 (2006)
1026. S. Fajfer, J. Kamenik, AIP Conf. Proc. **806**, 203 (2006)
1027. G.S. Huang et al. (CLEO Collaboration), Phys. Rev. Lett. **94**, 011802 (2005)
1028. K. Abe et al. (Belle Collaboration), arXiv:hep-ex/0510003
1029. B. Aubert et al. (BaBar Collaboration), arXiv:hep-ex/0607077
1030. S. Stone, in *Heavy Flavours*, ed. by A.J. Buras, M. Lindner (World Scientific, Singapore, 1992)
1031. R.J. Hill, Phys. Rev. D **73**, 014012 (2006)
1032. S. Fajfer, J. Kamenik, Phys. Rev. D **72**, 034029 (2005)
1033. S. Fajfer, J. Kamenik, N. Kosnik, Phys. Rev. D **74**, 034027 (2006)
1034. Q. He et al. (CLEO Collaboration), Phys. Rev. Lett. **95**, 121801 (2005) [Erratum: Phys. Rev. Lett. **96**, 199903 (2006)]
1035. N. Adam et al. (CLEO Collaboration), arXiv:hep-ex/0607079
1036. B.Y. Blok, M.A. Shifman, Sov. J. Nucl. Phys. **45**, 301 (1987) [Yad. Fiz. **45**, 478 (1987)]
1037. H.Y. Cheng, Phys. Lett. B **335**, 428 (1994)
1038. J.L. Rosner, Phys. Rev. D **60**, 114026 (1999)
1039. C.W. Chiang, J.L. Rosner, Phys. Rev. D **65**, 054007 (2002)
1040. C.W. Chiang, Z. Luo, J.L. Rosner, Phys. Rev. D **67**, 014001 (2003)

Eur. Phys. J. C (2008) 57: 309–492

491

1041. Y.L. Wu, M. Zhong, Y.F. Zhou, Eur. Phys. J. C **42**, 391 (2005)

1042. X.Y. Wu, X.G. Yin, D.B. Chen, Y.Q. Guo, Y. Zeng, Mod. Phys. Lett. A **19**, 1623 (2004)

1043. S. Ritt (MEG Collaboration), Nucl. Phys. Proc. Suppl. **162**, 279 (2006)

1044. T. Browder, M. Ciuchini, T. Gershon, M. Hazumi, T. Hurth, Y. Okada, A. Stocchi, arXiv:0710.3799 [hep-ph]

1045. M. Bona et al., INFN/AE-07/2, SLAC-R-856, LAL 07-15. arXiv:0709.0451 [hep-ex]

1046. A.G. Akeroyd et al. (SuperKEKB Physics Working Group), arXiv:hep-ex/0406071

1047. M. Hazumi et al. (SuperKEKB Physics Working Group), in preparation

1048. O. Schneider, in *1st LHCb Collaboration Upgrade Workshop*, January 2007. Available from http://indico.cern.ch/conferenceDisplay.py?confId=8351

1049. G. Wilkinson, in *1st LHCb Collaboration Upgrade Workshop*, January 2007. Available from http://indico.cern.ch/conferenceDisplay.py?confId=8351

1050. E. Gabrielli, G.F. Giudice, B **433**, 3 (1995). [Erratum: Nucl. Phys. B **507**, 549 (1997)]. arXiv:hep-lat/9407029

1051. L. Calibbi, A. Faccia, A. Masiero, S.K. Vempati, Phys. Rev. D **74**, 116002 (2006). arXiv:hep-ph/0605139

1052. T. Goto, Y. Okada, Y. Shimizu, T. Shindou, M. Tanaka, Phys. Rev. D **70**, 035012 (2004). arXiv:hep-ph/0306093

1053. T. Goto, Y. Okada, T. Shindou, M. Tanaka, Phys. Rev. D **77**, 095010 (2008). arXiv:0711.2935 [hep-ph]

1054. PEP-II Conceptual Design Report, SLAC-372, LBL-PUB-5303, CALT-68-1715, UCRL-ID-106426, UC-IIRPA-91-01 (1991)

1055. J. Seeman et al., in *European Particle Accelerator Conference (EPAC 06)*, Edinburgh, Scotland, 26–30 June 2006, SLAC-PUB-12023

1056. S. Kurokawa, E. Kikutani, Nucl. Instrum. Methods A **499**, 1 (2003), and other papers that volume

1057. B. Aubert et al. (BaBar Collaboration), Nucl. Instrum. Methods A **479**, 1 (2002)

1058. A. Abashian, et al. (Belle Collaboration), Nucl. Instrum. Methods A **479**, 117 (2002)

1059. J. Hewett, D. Hitlin (eds.), arXiv:hep-ph/0503261, and references therein

1060. J. Seeman et al., in *Proceedings of the 9th European Particle Accelerator Conference (EPAC 2004)*, Lucerne, 2004

1061. S. Hashimoto (ed.), KEK-REPORT-2004-4,2004

1062. The URL for the Super*B* web site is http://www.pi.infn.it/SuperB/

1063. N. Harnew et al., Nucl. Instrum. Methods A **408**, 137 (1998), also see updates in these proceedings

1064. S. Hashimoto (ed.), KEK-REPORT-2004-4, June 2004

1065. K. Akai, in *10th European Particle Accelerator Conference (EPAC06)*, Edinburgh, UK, 26–30 June 2006, pp. 19–23, KEK-PREPRINT-2006-020, KEK-PREPRINT-2006-20

1066. T. Abe, T. Kageyama, K. Akai, K. Ebihara, H. Sakai, Y. Takeuchi, KEK-PREPRINT-2005-78, KEK, Tsukuba, November 2005. Phys. Rev. Spec. Top. Accel.Beams **9**, 062002 (2006)

1067. T. Kageyama, in *Particles and Nuclei*, Santa Fe, 2005. AIP Conf. Proc. **842**, 1064 (2006)

1068. Y. Takeuchi, T. Abe, T. Kageyama, H. Sakai, in *Particle Accelerator Conference*, Knoxville, May 2005, p. 1195, KEK-PREPRINT-2005-53, PAC-2005-WPAT010

1069. T. Abe, T. Kageyama, Z. Kabeya, T. Kawasumi, T. Nakamura, K. Tsujimoto, K. Tajiri, in *Particle Accelerator Conference*, Knoxville, May 2005, p. 1051, PAC-2005-TPPT007

1070. Y. Suetsugu, K. Kanazawa, K. Shibata, H. Hisamatsu Nucl. Instrum. Methods A **556**, 399 (2006)

1071. Y. Suetsugu et al., Nucl. Instrum. Methods A **554**, 92 (2005)

1072. Y. Suetsugu, K.I. Kanazawa, K. Ohuchi, K. Shibata, M. Shirai, in *Particle Accelerator Conference*, Knoxville, May 2005, p. 3203, PAC-2005-RPPE052

1073. Y. Suetsugu, H. Hisamatsu, K.I. Kanazawa, N. Ohuchi, K. Shibata, M. Shirai, in *Particle Accelerator Conference*, Knoxville, May 2005, p. 3256, PAC-2005-RPPE053

1074. K.I. Kanazawa, H. Fukuma, H. Hisamatsu, Y. Suetsugu, in *Particle Accelerator Conference*, Knoxville, May 2005, p. 1054, PAC-2005-FPAP007

1075. J.W. Flanagan, K. Ohmi, H. Fukuma, S. Hiramatsu, M. Tobiyama, E. Perevedentsev, Phys. Rev. Lett. **94**, 054801 (2005)

1076. T. Suwada et al., KEK-PREPRINT-2006-56, November 2006. Phys. Rev. Spec. Top. Accel. Beams **10**, 073501 (2007)

1077. T. Kamitani et al., in *Particle Accelerator Conference*, Knoxville, May 2005, p. 1233, PAC-2005-TPPT011

1078. N. Ohuchi, Y. Funakoshi, H. Koiso, K. Oide, K. Tsuchiya, in *Particle Accelerator Conference*, Knoxville, May 2005, p. 2470, PAC-2005-MPPT037

1079. K. Ohmi, K. Oide, Phys. Rev. Spec. Top. Accel. Beams **10**, 014401 (2007)

1080. K. Ohmi, K. Oide, E. Perevedentsev, in *10th European Particle Accelerator Conference (EPAC06)*, Edinburgh, UK, June 2006, pp. 616–618

1081. K. Ohmi, Y. Funakoshi, S. Hiramatsu, K. Oide, M. Tobiyama in *10th European Particle Accelerator Conference (EPAC06)*, Edinburgh, UK, June 2006, pp. 619–621

1082. K. Ohmi, M. Tawada, Y. Funakoshi, in *Particle Accelerator Conference*, Knoxville, May 2005, p. 925, KEK-PREPRINT-2005-42, PAC-2005-TPPP004

1083. K. Akai, Y. Morita, in *Particle Accelerator Conference*, Knoxville, May 2005, p. 1129, KEK-PREPRINT-2005-26, PAC-2005-TPPT008

1084. T. Abe et al., arXiv:0706.3248 [physics.ins-det]

1085. M. Tobiyama, J.W. Flanagan, H. Fukuma, S. Kurokawa, K. Ohmi, S.S. Win, Phys. Rev. ST Accel. Beams **9**, 012801 (2006)

1086. R. Antunes Nobrega et al., LHCb TDR 9, CERN/LHCC/2003-30, 2003

1087. I.I.Y. Bigi, A.I. Sanda, Nucl. Phys. B **193**, 85 (1981)

1088. Heavy Flavor Averaging Group, updated Summer 2007. http://www.slac.stanford.edu/xorg/hfag/

1089. F. Muheim, Nucl. Phys. Proc. Suppl. **170**, 317 (2007)

1090. H. Dijkstra, The LHCb upgrade, in *FPCP07*, Bled, Slovenia, May 2007

1091. C. Parkes, The LHCb detector, in *EPS07*, Manchester, UK, July 2007

1092. V. Obraztsov, in *BEACH2006*, Lancaster, UK, July 2006

1093. M.J. Strasser, K.M. Zurek, arXiv:hep-ph/0604261

1094. M.J. Strasser, K.M. Zurek, arXiv:hep-ph/0605193

1095. M.J. Strassler, arXiv:hep-ph/0607160

1096. M. Cvetic, P. Langacker, G. Shiu, Phys. Rev. D **66**, 066004 (2002). arXiv:hep-ph/0205252

1097. N. Arkani-Hamed, S. Dimopoulos, S. Kachru, arXiv:hep-th/0501082

1098. V. Barger, P. Langacker, G. Shaughnessy, New J. Phys. **9**, 333 (2007). arXiv:hep-ph/0702001

1099. C. Parkes, Nucl. Instrum. Methods A **569**, 115 (2006)

1100. M. Ciuchini, E. Franco, D. Guadagnoli, V. Lubicz, M. Pierini, V. Porretti, L. Silvestrini, arXiv:hep-ph/0703204

1101. A. Masiero, M. Piai, A. Romanino, L. Silvestrini, Phys. Rev. D **64**, 075005 (2001). arXiv:hep-ph/0104101

1102. S. Baek, T. Goto, Y. Okada, K.i. Okumura, Phys. Rev. D **63**, 051701 (2001). arXiv:hep-ph/0002141

1103. J. Hisano, Y. Shimizu, Phys. Lett. B **565**, 183 (2003). arXiv:hep-ph/0303071

1104. C.S. Huang, T.J. Li, W. Liao, Nucl. Phys. B **673**, 331 (2003). arXiv:hep-ph/0304130

1105. A.J. Buras, R. Buras, Phys. Lett. B **501**, 223 (2001). arXiv:hep-ph/0008273

1106. W. de Boer, A. Dabelstein, W. Hollik, W. Mosle, U. Schwickerath, Z. Phys. C **75**, 627 (1997). arXiv:hep-ph/9607286

1107. W. de Boer, A. Dabelstein, W. Hollik, W. Mosle, U. Schwickerath, arXiv:hep-ph/9609209

1108. G.C. Cho, K. Hagiwara, Nucl. Phys. B **574**, 623 (2000). arXiv:hep-ph/9912260

1109. Y.M. Cho, I.P. Neupane, Int. J. Mod. Phys. A **18**, 2703 (2003). arXiv:hep-th/0112227

1110. J. Erler, D.M. Pierce, Nucl. Phys. B **526**, 53 (1998). arXiv:hep-ph/9801238

1111. G. Altarelli, F. Caravaglios, G.F. Giudice, P. Gambino, G. Ridolfi, J. High Energy Phys. **0106**, 018 (2001). arXiv:hep-ph/0106029

1112. A. Djouadi, M. Drees, J.L. Kneur, J. High Energy Phys. **0108**, 055 (2001). arXiv:hep-ph/0107316

1113. W. de Boer, M. Huber, C. Sander, D.I. Kazakov, Phys. Lett. B **515**, 283 (2001)

1114. W. de Boer, C. Sander, Phys. Lett. B **585**, 276 (2004). arXiv:hep-ph/0307049

1115. G. Belanger, F. Boudjema, A. Cottrant, A. Pukhov, A. Semenov, Nucl. Phys. B **706**, 411 (2005). arXiv:hep-ph/0407218

1116. J.R. Ellis, K.A. Olive, Y. Santoso, V.C. Spanos, Phys. Rev. D **69**, 095004 (2004). arXiv:hep-ph/0310356

1117. J.R. Ellis, D.V. Nanopoulos, K.A. Olive, Y. Santoso, Phys. Lett. B **633**, 583 (2006). arXiv:hep-ph/0509331

1118. J.R. Ellis, S. Heinemeyer, K.A. Olive, A.M. Weber, G. Weiglein, arXiv:0706.0652 [hep-ph]

1119. E.A. Baltz, P. Gondolo, J. High Energy Phys. **0410**, 052 (2004). arXiv:hep-ph/0407039

1120. B.C. Allanach, Phys. Lett. B **635**, 123 (2006). arXiv:hep-ph/0601089

1121. B.C. Allanach, K. Cranmer, C.G. Lester, A.M. Weber, arXiv:0705.0487 [hep-ph]

1122. O. Buchmueller et al., arXiv:0707.3447 [hep-ph]

1123. M. Carena, S. Heinemeyer, C.E.M. Wagner, G. Weiglein, Eur. Phys. J. C **26**, 601 (2003). arXiv:hep-ph/0202167

1124. M. Carena, S. Heinemeyer, C.E.M. Wagner, G. Weiglein, Eur. Phys. J. C **45**, 797 (2006). arXiv:hep-ph/0511023

1125. S. Schael et al. (LEP Working Group for Higgs boson searches), Eur. Phys. J. C **47**, 547 (2006). arXiv:hep-ex/0602042

1126. A. Abulencia et al. (CDF Collaboration), Phys. Rev. Lett. **96**, 011802 (2006). arXiv:hep-ex/0508051

1127. V.M. Abazov et al. (D0 Collaboration), Phys. Rev. Lett. **95**, 151801 (2005). arXiv:hep-ex/0504018

1128. G.W. Bennett et al. (Muon G-2 Collaboration), Phys. Rev. D **73**, 072003 (2006). arXiv:hep-ex/0602035

1129. B.C. Allanach et al., Eur. Phys. J. C **25**, 113 (2002). arXiv:hep-ph/0202233

1130. R. Barate et al. (LEP Working Group for Higgs boson searches), Phys. Lett. B **565**, 61 (2003). arXiv:hep-ex/0306033

1131. S. Heinemeyer, W. Hollik, G. Weiglein, Phys. Rep. **425**, 265 (2006). arXiv:hep-ph/0412214

1132. J.A. Aguilar-Saavedra et al., Eur. Phys. J. C **46**, 43 (2006). arXiv:hep-ph/0511344

1133. H. Baer, F.E. Paige, S.D. Protopopescu, X. Tata, arXiv:hep-ph/0312045

1134. H. Bachacou, I. Hinchliffe, F.E. Paige, Phys. Rev. D **62**, 015009 (2000). arXiv:hep-ph/9907518

1135. ATLAS Collaboration, ATLAS detector and physics performance technical design report, CERN/LHCC 99-14/15, 1999

1136. B.C. Allanach, C.G. Lester, M.A. Parker, B.R. Webber, J. High Energy Phys. **0009**, 004 (2000). arXiv:hep-ph/0007009

1137. B.K. Gjelsten, E. Lytken, D.J. Miller, P. Osland, G. Polesello, ATLAS internal note ATL-PHYS-2004-007, 2004, published in [1138]

1138. G. Weiglein et al. (LHC/LC Study Group), Phys. Rep. **426**, 47 (2006). arXiv:hep-ph/0410364

1139. J. Hisano, K. Kawagoe, M.M. Nojiri, Phys. Rev. D **68**, 035007 (2003). arXiv:hep-ph/0304214

1140. M.M. Nojiri, G. Polesello, D.R. Tovey, J. High Energy Phys. **0603**, 063 (2006). arXiv:hep-ph/0512204

1141. J. Hisano, K. Kawagoe, M.M. Nojiri, Determination of stop and sbottom sector by LHC and ILC, published in [1142]

1142. G. Belanger, F. Boudjema, A. Pukhov, A. Semenov, Comput. Phys. Commun. **149**, 103 (2002). arXiv:hep-ph/0112278

1143. See contribution by XY, these proceedings

1144. D. Acosta et al., CMS NOTE 2006/134, 2006

1145. J. Allison et al., IEEE Trans. Nucl. Sci. **53**(1), 270–278 (2006)

1146. CMS Collaboration, CERN/LHCC 2006-001, 2006

1147. S. Abdullin et al., arXiv:hep-ph/0605143

1148. S. Heinemeyer, W. Hollik, D. Stockinger, A.M. Weber, G. Weiglein, J. High Energy Phys. **0608**, 052 (2006). arXiv:hep-ph/0604147

1149. S. Heinemeyer, W. Hollik, A.M. Weber, G. Weiglein, arXiv:0710.2972 [hep-ph]

1150. seal.web.cern.ch/seal/snapshot/work-packages/mathlibs/minuit

1151. J.R. Ellis, S. Heinemeyer, K.A. Olive, G. Weiglein, J. High Energy Phys. **0502**, 013 (2005). arXiv:hep-ph/0411216

1152. B.C. Allanach, C.G. Lester, Phys. Rev. D **73**, 015013 (2006). arXiv:hep-ph/0507283

1153. R.R. de Austri, R. Trotta, L. Roszkowski, J. High Energy Phys. **0605**, 002 (2006). arXiv:hep-ph/0602028

1154. J.R. Ellis, S. Heinemeyer, K.A. Olive, G. Weiglein, J. High Energy Phys. **0605**, 005 (2006). arXiv:hep-ph/0602220

1155. B.C. Allanach, C.G. Lester, A.M. Weber, J. High Energy Phys. **0612**, 065 (2006). arXiv:hep-ph/0609295

1156. P. Bechtle, K. Desch, P. Wienemann, Comput. Phys. Commun. **174**, 47 (2006). arXiv:hep-ph/0412012

1157. R. Lafaye, T. Plehn, D. Zerwas, arXiv:hep-ph/0404282

1158. ALEPH Collaboration, Phys. Rep. **427**, 257 (2006). arXiv:hep-ex/0509008

1159. ALEPH Collaboration, arXiv:hep-ex/0511027

1160. M. Grünewald, private communication